

**School of Science and Engineering
Department of Applied Geology**

**The Role of Carbonaceous Material in the Formation of
Macraes Orogenic Gold Deposit, New Zealand**

Si-Yu Hu

**This thesis is presented for the Degree of
Doctor of Philosophy
of
Curtin University**

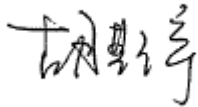
September 2016

Declaration

To the best of my knowledge and belief this thesis contains no material previously published by any other person except where due acknowledgment has been made.

This thesis contains no material which has been accepted for the award of any other degree or diploma in any university.

Si-Yu Hu

A handwritten signature in black ink, appearing to be the Chinese characters '胡斯宇' (Hu Siyu).

Date 07/09/2016

Abstract

Gold is a precious metal and gold deposits are a perennial exploration target. Carbonaceous material (CM) has been observed intimately associated with Au in gold deposits, and has been proposed to play an important role in the formation of gold deposits, in the source, transportation and deposition. For example, CM-associated diagenetic pyrite has been proposed to be the source of Au for gold deposits. Pyrobitumen has been suggested to be the carrier of gold during gold mobilization prior to deposition. In metasediment-hosted gold deposits, CM, which is widespread in mineralized rocks, is closely associated with gold and sulfides. CM is thought to make a direct or indirect contribution to gold precipitation. However, many details of the role that CM plays in gold deposits are poorly understood.

The Macraes gold deposit, hosted by the Otago Schist in the South Island of New Zealand, has a reserve of more than 300 tonnes of gold. Gold in mineralized rocks occurs either in quartz veins or as micro-inclusions in sulfides associated with graphitic microspheres. CM has been suggested to reduce Au-bisulfide complexes in solution directly, or to facilitate the formation of shear zones which then focus fluid flow and Au deposition. However, the role of CM in this deposit is still debated. Archean gold deposits, such as the St. Ives and Wiluna gold deposits in Western Australia, are hosted by, or associated with a black shale unit called the Kapaia Slate, which is rich in CM and sulfides. However, CM in these gold deposits has not yet been characterized in detail. The role of CM in the formation of these deposits was therefore explored via a combination of organic geochemical analysis, cutting-edge petrographic analytical techniques, thermodynamic modelling, and laboratory experiments.

Rock samples collected from the Macraes gold deposit (New Zealand), and the St. Ives and Wiluna gold deposits (Western Australia) were analysed with conventional organic geochemical approaches, such as Rock-Eval analysis, Soxhlet extraction and gas chromatography-mass spectroscopy (GC-MS) (**Chapter 2**). However, results show that CM in those gold deposits is highly mature, to the extent that only limited information can be inferred from the organic geochemical analyses. However, it was

possible to characterize CM in rocks distal and proximal from the Macraes gold deposit with optical microscopy and Raman spectroscopy (**Chapter 3**). Four types of CM were characterized with various thermal maturity and possible origins.

Based on the characterization of CM by Raman spectroscopy in polyframboids, which have been suggested to be the source of Au for the Macraes deposit, synchrotron X-ray fluorescence microscopy (SXRF) and laser ablation inductively coupled plasma mass spectrometry (LA-ICP-MS) were applied to elucidate the role of CM in the source rock (**Chapter 4**). The association between CM, trace elements and sulfides in polyframboids was investigated by characterizing the distribution and concentrations of Au and other trace elements. Zn was found to co-locate with CM, suggesting that Zn was incorporated into polyframboids via the activity of sulfate reducing bacteria. The concentration of Au is positively correlated with that of Zn, implying that Au may be absorbed into polyframboids by a similar process to that of Zn. The distribution of Zn in polyframboids was further investigated using techniques with high spatial resolution, i.e., nanoscale secondary ion mass spectrometry (NanoSIMS) (**Chapter 5**). The distribution of Zn in polyframboids is variable. Therefore, the sequestration of Zn into polyframboids is proposed to occur as a sequence of stages, with mechanisms that depend on the concentrations of key cations, such as Fe and Zn, in solution, during the activity of sulphate-reducing bacteria. The progressive incorporation of Zn into polyframboids may have implications for Zn isotope fractionation process during the fixation of Zn from seawater to sediments, and for the sequestration of Au into polyframboids.

The role of CM during gold deposition was explored with thermodynamic modelling which simulated mineralization processes of the Macraes gold deposit (**Chapter 6**). A combination of thermodynamic modelling, petrographic observations and geochemical data implies a genetic link between CM, sulfide and gold deposition. Modelling results, which successfully replicated the mineral assemblages in mineralized rocks, suggested that gold is deposited from hydrothermal fluids due to the co-deposition of sulfides and graphite. The results have implications for Au deposition mechanisms in other similar gold deposits.

To investigate the transportation of Au by CM, experiments on Au solubility in organic liquids were performed in the laboratory (**Chapter 7**). The work included experiments on gold solubility in pure organic liquids, organic component characterization and analytical method development to quantify gold concentrations in organic liquids following experiments. It is the first time that experiments of Au solubility in single component organic liquids have been performed. New methods were developed to quantify Au concentrations in organic liquids precisely and quickly. Preliminary results showed that dodecanethiol can dissolve a significant amount of Au, implying that this hydrocarbon is capable of transporting gold in ore-forming systems.

To summarize, this PhD project has explored the value of conventional organic geochemistry analyses for CM in Archean gold deposits (Australia) and the Macraes gold deposit (New Zealand), and revealed new aspects of CM characterization in Au deposits via Raman spectroscopy. The long-debated question about the role CM plays during the gold precipitation in gold deposits was assessed via thermodynamic modelling. The project also used laboratory experiments to demonstrate that Au may be transported by organic complexes. The knowledge gained suggests that CM plays both direct and indirect roles in the source, transport and deposition of Au, and has identified key areas for further study that will provide additional valuable information to help the genesis of these deposits to be better understood.

Acknowledgements

Coming to Australia and finishing this PhD project are what I've never thought when I was young, or even when I took the IELTS test. Luckily, I received the scholarships and started this exciting journey which would be one of my great experience in my life. During the four-year PhD study, I've grown up, not only in academic field, but also in life. Now take a look back at this journey, I'm so proud of myself for those efforts to make myself a better person, but, more importantly, I owe thanks to many people for their help and support on this project. This work could not have been performed so well without them. Thanks to you sincerely, whether named here or not.

First of all, I'd like to express my most sincere gratitude and appreciation to my primary supervisor Assoc. Prof. Katy Evans. Thank you for bringing me to this wonderful project, for your kind guidance in all aspects of this project, for passing your wisdom and critical thinking to me. You are always there when I need help, and provide great perspective on my project. At the beginning, I knew little about ore deposits, and the work was not on the right track as expected. Thanks for teaching me the knowledge and bringing me to the wonderful Otago Schist at the beginning, for always encouraging me to improve my self-confidence in this project, for trusting me to explore my own ideas in the final stage. Thanks for your help that I can produce such great results and will be confident to go further in my future career.

My sincere gratitude goes to my co-supervisors, Dr. Kirsten Rempel and Prof. Kliti Grice, and previous co-supervisor, Dr. Jeff Dick. Thank you, Kirsten, for teaching me how to conduct geochemical experiments, for improving my laboratory skills and for providing guidance and constructive suggestions on my project. It's a wonderful experience to be the first person to perform those experiments in the world, which are full of up and downs though. Learning how to face failures is one of most precious presents from this project. I thank Kliti for passing organic geochemistry knowledge to me, always encouraging me and bringing me to WA-OIGC groups where I met lots of great researchers and PhD fellows. I'm grateful to Jeff, who has left Curtin and is teaching English in Thailand, for your efforts in teaching me thermodynamic knowledge, reading and providing constructive comments to my first paper. Your curiosity to science has inspired me in the subsequent PhD study. Many thanks also to the support I have received from the rest of staff and PhD fellows in the Department of Applied Geology. You make my life easier and enjoyable in many ways.

Special thanks must go to Prof. Dave Crow from University of Otago for being a wonderful guide in the field work in the Otago Schist, and for always providing constructive scientific perspective in paper discussion. You have certainly made great contributions to this PhD project.

Thanks also to those researchers who helped during sample analysis. These include Dr. Julien Bourdet (CSIRO) for Raman spectroscopy analysis; Drs. Louise Fisher (CSIRO) and Susan Cumberland (Australian Synchrotron) for the help of SXRF analysis; Drs. Noreen J. Evans and Richard Taylor, and Mr Bradley McDonald for LA-ICP-MS analysis; Assoc. Prof. Matt Kilburn (UWA) and Dr Paul Guagliardo (UWA) for NanoSIMS analysis; Leif Cooper (ChemCentre) for organic component characterization. I also thank Prof. Lorenz Schwark and his organic geochemistry lab of Kiel University for elemental analysis and Rock-Eval analysis; Dr. Dave Patterson for the expertise during the Synchrotron beam time and Dr Chris Ryan for help during Synchrotron data processing; technical staff in Curtin Materials Research Lab for the induction of SEM-EDS analysis, and the Labwest for Au concentration analysis.

It is a great honour to be part of the CSIRO Mineral Resources Flagship Cluster for Organic Geochemistry of Mineral Systems and get to know lots of great people. Thanks are delivered to Drs. Caroline Jaraula and Alex Holman for the help in the organic geochemical laboratory, Aileen Robert, Hendrik Grotheer and other PhD students for the help and discussions. Additional valuable discussions and meaningful advice on this project are attributed to those great researchers, including Prof. Campbell McCuaig (UWA), Prof. Ross Large (University of Tasmania), Assoc. Prof. Paul Greenwood (UWA), Dr. Martijn Woltering (CSIRO), Dr. Weihua Liu (CSIRO), and Dr. Chris Yeats (CSIRO).

I'm lucky to come from a very supportive family who always keep me company through the ups and downs. Mum and Dad, thanks for teaching me how to be a nice person, and for allowing me to make my own decisions and supporting me. Your endless love, encouragement and support always make me feel warm. I can't say thank you enough.

Finally, thanks go to my scholarships of the Chinese Scholarship Council (CSC)-Curtin International Postgraduate Research Scholarship (CIPRS), CSIRO top up scholarship. Thank you for supporting me.

List of publications included as a part of this thesis

This thesis is assembled from two individual chapters, describing experimental work, and four research papers, which have been published in international peer-reviewed journals or were under review at the time of writing of this thesis. The relationships between each chapters are included in the Introduction chapter, and summarized in the final chapter.

The formatting of each chapter within this thesis may appear to vary, and may differ to the published form based on the requirements and formatting guidelines of each individual journal and this thesis. Due to the nature of this thesis as a composite of peer-reviewed manuscripts there is a degree of repetition throughout.

The four research papers are listed below:

Chapter 3

Hu, S., Evans, K., Craw, D., Rempel, K., Bourdet, J., Dick, J., Grice, K., 2015.

Raman characterization of carbonaceous material in the Macraes orogenic gold deposit and metasedimentary host rocks, New Zealand. *Ore Geology Reviews* 70, 80-95 (Impact factor 3.819).

Chapter 4

Hu, S.-Y., Evans, K., Fisher, L., Rempel, K., Craw, D., Evans, N.J., Cumberland, S.,

Robert, A., Grice, K., 2016. Associations between sulfides, carbonaceous material, gold and other trace elements in polyframboids: Implications for the source of orogenic gold deposits, Otago Schist, New Zealand. *Geochimica et Cosmochimica Acta* 180, 197-213 (Impact factor 4.315).

Chapter 5

Hu, S.-Y., Evans, K., Rempel, K., Guagliardo, P., Kilburn, M., Craw, D., Grice, K.

A new look at mixed sphalerite-pyrite framboids and the sequestration of Zn into framboids as a key process of Zn cycling in the ocean. *In revision for resubmission to Geochimica et Cosmochimica Acta.*

Chapter 6

Hu, S.-Y., Evans, K., Craw, D., Rempel, K., Grice, K. Resolving the Role of Carbonaceous Materials in Gold Precipitation in Metasediment-hosted Orogenic Gold Deposits. *Under review, Geology*.

Table of contents

Declaration.....	II
Abstract.....	III
Acknowledgements.....	VI
List of publications included as a part of this thesis	VIII
Table of contents	X
List of figures	XVIII
List of tables.....	XXVI

Chapter 1

Introduction.....	1
1.1 Carbonaceous material (CM).....	1
1.1.1 Introduction of CM.....	1
1.1.2 CM in ore deposits	2
1.1.3 CM in gold deposits	3
1.2 Research areas	5
1.2.1 Geological setting of Otago Schist and Macraes gold deposit, New Zealand	5
1.2.2 CM in the Otago Schist and Macraes gold deposit.....	9
1.2.3 Gold deposits in Western Australia	11
1.3 Thermodynamic modelling.....	12
1.4 Gold solubility in pure organic liquids	12
1.5 Objectives of thesis	13
1.6 Research methods.....	13
1.6.1 Field work.....	13
1.6.2 Laboratory analyses	14

1.7 Thesis structure	15
1.8 References	19

Chapter 2

Applications of conventional organic geochemical methods to samples from three gold deposits.....	28
2.1 Introduction	28
2.1.1 CM and metals	28
2.1.2 CM and Au	30
2.1.3 CM characterization.....	30
2.2 Geological background and sampling	32
2.2.1 St. Ives goldfield	32
2.2.2 Wiluna lode-gold deposits	35
2.2.3 Macraes gold deposit	37
2.3 Methods	39
2.3.1 Element analysis.....	39
2.3.2 Rock-Eval analysis.....	40
2.3.3 GC-MS	40
2.4 Results and discussion.....	42
2.4.1 St. Ives samples	42
2.4.2 Wiluna samples	44
2.4.3 Macraes samples	44
2.5 Conclusions	45
2.6 References	45

Chapter 3

Raman characterization of carbonaceous material in the Macraes orogenic gold deposit and metasedimentary host rocks, New Zealand.....	52
Abstract	53
3.1 Introduction	53
3.2 Geological setting and regional gold mobility	55
3.3 Sampling and analytical methods	58
3.3.1 Sample selection and characterization.....	58
3.3.2 Non-carbonate carbon and gold content analysis.....	58
3.3.3 Petrographic methods.....	59
3.3.4 Raman spectroscopy	59
3.4 Results.....	71
3.4.1 Raman spectra.....	71
3.4.2 The effects of crystal orientation on Raman spectra	72
3.4.4 Chemical and petrographic characterization.....	74
3.5 Discussion	79
3.5.1 CM Raman spectra compared with previous work.....	79
3.5.2 Temperature estimates of CM from Raman spectra.....	81
3.5.3 Possible origins of CM.....	82
3.5.4 Synthesis of relationships between CM and Au in the Otago Schist ..	86
3.6 Conclusions	89
3.7 Acknowledgements	90
3.8 References	90

Chapter 4

Associations between sulfides, carbonaceous material, gold and other trace elements in polyframboids: implications for the source of orogenic gold deposits, Otago Schist, New Zealand.....	98
Abstract	99
4.1 Introduction	99
4.2 Geological Background and Sampling	102
4.3 Methods	104
4.3.1 Sulfur content analyses.....	104
4.3.2 Petrographic methods.....	104
4.3.3 LA-ICP-MS	104
4.3.4 SXRF	105
4.4 Results.....	107
4.4.1 Petrographic features	107
4.4.2 SXRF mapping.....	109
4.4.3 Element concentrations in polyframboids analyzed by LA-ICP-MS	116
4.5 Discussion	122
4.5.1 Association between CM, Au and other elements in polyframboids	122
4.5.2 Mechanism of incorporation of trace elements into polyframboids .	126
4.5.3 Implications for genetic models for ore deposit formation involving metal sources	127
4.6 Conclusions	130
4.7 Acknowledgements.....	131
4.8 References	132

Chapter 5

A new look at mixed sphalerite-pyrite framboids and the sequestration of Zn into framboids as a key process of Zn cycling in the ocean.....	142
Abstract	143
5.1 Introduction	143
5.2 Geological background and sampling	145
5.3 Methods	147
5.4 Results.....	147
5.4.1 Petrographic observations	147
5.4.2 NanoSIMS observations	148
5.5 Discussion	153
5.5.1 Zn and pyrite relationships.....	153
5.5.2 OM and sulfide associations	154
5.5.3 The sequestration of Zn into framboids	155
5.5.4 Implications for Zn isotope fractionation processes.....	157
5.6 Conclusions	159
5.7 Acknowledgements.....	159
5.8 References	160

Chapter 6

Resolving the role of carbonaceous material in gold precipitation in metasediment-hosted orogenic gold deposits.....	166
Abstract	167
6.1 Introduction	167
6.2 Petrographic observations	168
6.3 Samples and methods.....	169

6.4 Results.....	171
6.4.1 Geochemical analyses	172
6.4.2 Thermodynamic modelling	172
6.5 Discussion and conclusions	174
6.5.1 Consistency of rocks with model results	174
6.5.2 Precipitation of sulfides	175
6.5.3 Gold precipitation	176
6.5.4 Implications for other gold deposits.....	177
6.6 Acknowledgments.....	177
6.7 References	177

Chapter 7

Experimental investigations of gold solubility in pure organic liquids.....	181
7.1 Introduction	181
7.2 Experiments of gold solubility in organic liquids	184
7.2.1 Apparatus	184
7.2.2 Experiment design	185
7.3 Analytical method development.....	186
7.3.1 Direct injection into ICP-MS	186
7.3.2 Dry ashing.....	187
7.3.3 Chemical digestion.....	188
7.4 Analysis in organic liquids post-experiment	190
7.4.1 Au concentration quantification.....	190
7.4.2 Organic component characterization.....	192
7.5 Results.....	193
7.5.1 Experiment with dodecanethiol.....	193

7.5.2 Experiment with DBT (organic component characterization)	197
7.6 Discussion	200
7.6.1 The solubility of gold in dodecanethiol	200
7.6.2 The solubility of gold in DBT	201
7.7 Summary	202
7.8 References	202
Chapter 8	
Conclusions	208
8.1 CM in the Macraes gold deposit and the Otago Schist	208
8.2 The role of CM in the formation of gold deposits	209
8.3 Limitations and future work	214
Bibliography	216
Appendix A1 Bulk composition of samples from the Otago Schist and Macraes gold deposit	248
Appendix A2 Sample description of thin sections (the Otago Schist and Macraes gold deposit).....	259
Appendix A3 Sample description on hand specimens (St. Ives and Wiluna gold deposits).....	301
Appendix A4 Results of LA-ICP-MS data quality monitoring.....	309
Appendix B1 Fluid and rock composition used in the model	310
Appendix B2 Sulfur and non-carbonate carbon concentrations from four metasediment-hosted gold deposits	311
Appendix B3 Thermodynamic modelling results.....	315
Appendix C Statements of contribution by others.....	423

Appendix D Permission of copyright from third parties..... 428

List of figures

Figure 1.1 The maturation process (Libes, 2011). MW: molecular weight.	2
Figure 1.2 Geological map of the South Island of New Zealand. The Otago and Alpine Schist comprises parts of metamorphosed Caples and Torlesse terranes sedimentary rocks. Modified from Coombs et al. (1976), Mortimer (1993) and Mortimer (2000).	7
Figure 1.3 Geological map of the Otago Schist, New Zealand, which formed due to the collision of the Torlesse Terrane and the Caples Terrane. The metamorphic grade ranges from prehnite-pumpellyite (P-P) facies on the margins, through pumpellyite-actinolite (P-A) facies, to lower greenschist (G-S) facies on the core of the belt, and to amphibolite facies near the Alpine fault. DMOB – Dun Mountain Opholite Belt. Modified from Mortimer (2000) and Pitcairn et al. (2006).	8
Figure 1.4 Geological map of (A) Otago Schist and (B) Macraes gold deposit (Modified from Pitcairn et al. (2006) and De Ronde et al. (2000). Areas indicated by red boxes or a red line are sampling areas.	9
Figure 1.5 (A) A geological profile through Fiddlers Flat. Metamorphic grade ranges from prehnite-pumpellyite facies to lower greenschist facies. (B) A geological cross section through the Hyde-Macraes shear zone. Modified from Large et al. (2012). The locations of both profiles are indicated in Figure 1.4 A.	11
Figure 2.1 Location of three gold deposits studied in detail in this chapter (highlighted by yellow stars; Modified from Google Maps).	32
Figure 2.2 Geological map of St. Ives goldfield. BLFZ: Boulder–Lefroy Fault Zone; SFZ: Speedway Fault Zone; FT: Foster Thrust; PRF: Playa–Repulse Fault. Modified from Prendergast (2007).	34
Figure 2.3 Geological map of Wiluna lode gold deposit. Modified from Hagemann and Lüders (2003). The area of Wiluna is indicated with a rectangle in the map of lower right corner.	37
Figure 2.4 Flowchart diagram of sample processing.	39

Figure 2.5 Results of Rock-Eval pyrolysis, HI versus OI diagram (I , II ,III represent three types of kerogen (Simoneit and Gize, 2000).....	44
Figure 3.1 Geological map of the Otago Schist in New Zealand (modified from Henne and Craw, 2012 and Pitcairn et al., 2005); the highlighted areas with black boxes are sampling locations, i.e. Lake Hawea, Fliddlers Flat and Golden Bar.....	56
Figure 3.2 The two vibrational modes that may be displayed by single-crystal graphite. E2g is an in-plane optical vibration model and only this model is Raman active (modified from Reich and Thomsen, 2004).	60
Figure 3.3 (A) Raman spectrum of graphite (modified after Wopenka and Pasteris, 1993); (B) Raman spectrum of disordered CM (modified after Wopenka and Pasteris, 1993); (C) Raman spectrum of CM 1 from FF-16; (D) Raman spectrum of CM 2 from FF-12-A; (E) Raman spectrum of CM 3 from TC-01; (F) Raman spectrum of CM 4 from GB-04-A; The numbers in brackets are peak positions/average peak positions (see Figure 3.1) in cm^{-1}	61
Figure 3.4 Plot of (A) $R1=D/G$ (intensity ratio); (B) $R2= D/G$ (width ratio); (C) $R3=(D+D1)/(D+D1+G+D2+D3)$ (area ratio); (D) $R4= S1/(S1+S2+S3)$ (area ratio). These ratios are plotted against the estimated ranked metamorphic grade, from P-P to lower G-S facies (P-P: Prehnite-Pumpellyite facies; P-A: Pumpellyite-Actinolite facies; G-S: Lower Greenschist facies); the error bars shown are one standard deviation, taken from multiple measurements of CM in the same samples.	74
Figure 3.5 Petrographic photomicrographs of CM 1 in framboidal pyrite in lower P-P facies in reflected light (FF-16).	75
Figure 3.6 Petrographic photomicrographs of CM 1 in upper P-P facies (FF-15); (A) backscatter electron (BSE) image of CM 1 and pyrite; (B) reflected light image of CM 1, pyrite and chalcopyrite.....	76
Figure 3.7 Photomicrographs of CM 2 in P-A and G-S facies samples in reflected light and SEM-BSE; (A) Strip-shaped CM 2 and framboidal pyrite in reflected light; (B) Strip-shaped CM 2 and framboidal pyrite in BSE from FF-04, P-A facies; (C) Flaky CM 2 in carbonate veins in BSE from FF-13, P-A facies; (D) Flaky CM 2 elongated parallel the foliation with pyrite and chalcopyrite in reflected light from FF-12-A, G-S facies.	77

- Figure 3.8** Photomicrographs of CM 3 from P-A facies (LH-01); (A) CM 3 grain in reflected light; (B) black bands (dark) consisting of CM 3 in transmitted light; (C) black bands (dotted line) consisting of CM 3 in reflected light. 78
- Figure 3.9** Photomicrographs of CM 4 in reflected light (from GB-04-A, lower G-S facies) in mineralized sheared rock, Golden Bar pit, Macraes mine. (A) Mica-rich shears (dark) surround disrupted fragments of quartz (pale grey). White sulfides, including a large fractured arsenopyrite grain (centre) are scattered through the sheared rock. These sulfides contain particulate and solid solution Au (Large et al. 2012). (B) CM 4 particles are scattered through the sheared rock with the auriferous sulfides. 79
- Figure 3.10** Relationships between CM, Au and As with increasing metamorphic grade in the Otago Schist (P-P: Prehnite-Pumpellyite facies; P-A: Pumpellyite-Actinolite facies; G-S: Lower Greenschist facies; AMP: Amphibolite facies). The first column is the representative Raman spectra of four types of CM from our studies compared to X-ray diffraction and reflectance of CM (after Henne and Craw, 2012; Landis 1971; McKeag and Craw 1989). The second column is the sulfides transformation investigated by Pitcairn et al., (2010). The third column is trace metal concentration variations from Pitcairn et al., (2006) and Large et al., (2012). 80
- Figure 3.11** A comparison of Raman spectra results and FTIR results (The Raman spectrum of crystalline graphite is modified from Wopenka and Pasteris, 1993; FTIR results were investigated by Pitcairn et al., 2005). 86
- Figure 4.1** Geological map of the Otago Schist (Hu et al., 2015; modified after Henne and Craw (2012)). The black square on map is the sampling location. 104
- Figure 4.2** Representative spectra produced by SXRF analysis of FF-16. The original spectra are plotted with the black solid line. Fit spectra calculated by GeoPIXE™ are displayed by the grey dashed line (DA matrix: dynamic matrix). The background, calculated with the Statistics-sensitive Non-linear Iterative peak-clipping (SNIP) algorithm (Ryan et al., 1988, 1990), is shown by the grey solid line. The energy range over which the spectra is fitted is 3–25 keV. Observed trace elements from the bulk sample spectra include Fe, Cu, Zn, As, Rb, Sr and Zr, the K- α lines for which are indicted by black dashed lines. 107

Figure 4.3 Petrographic photomicrographs of polyframboids. (A) Ellipsoidal polyframboids in reflected light, dominated by pyrite framboids and pyrite microcrystals. (B) SEM image of part of the polyframboids shown in A, showing clusters of pyrite framboids, pyrite microcrystals and other sulfides. Typical pyrite framboids have been indicated with dashed lines. (C) Enlarged view of part of the polyframboids in (B) in reflected light, showing carbonaceous material (CM), pyrite (Py) and chalcopyrite (Cpy) (Hu et al., 2015). (D) SEM image of carbonaceous material (CM) in (C) with sphalerite (Sph) and cobaltite (Cob)..... 108

Figure 4.4 SXRF element maps of Sr, Rb, Fe and a combination of Ca (red)-Rb (green)-Fe (blue), showing the variation of those elements in the mapped area and providing an example of the association between polyframboids and the surrounding minerals and matrix. In Sr, Rb and Fe mapping, warm colors represent high concentrations and cool colors represent low concentrations. 110

Figure 4.5 (A) SXRF element map of Zn-Fe, showing the distribution of Zn in polyframboids. Zn concentrations are highest in the red spheroids, with a variable distribution in the polyframboids; (B) Reflected light photomicrograph of part of the same polyframboids. CM occurs as rounded globules which are grey with low reflectivity in reflected light. The hot spot of Zn in (A) corresponds to large patches of CM within the red circles in (B), while lower Zn zones coincide with smaller grains of CM in many cases (Figure 4.3 B). 111

Figure 4.6 (A) The same image shown in Figure 4.5 A but with zones of the variable Zn/Fe ratio in (B) outlined. (B) Compositional data from all pixels were extracted from the map in (A) and plotted as Zn (wt %) versus Fe (wt %) in (B). Each pixel corresponds to a single point on the plot. The color change on the plot is determined by the frequency of a specific Zn/Fe ratio. The brighter and darker colored points represent higher and lower populations of pixels of equivalent Zn/Fe ratios, respectively. The circled regions in (A) correspond to the regions in (B) of equivalent line style, and include all the points with a given range of Zn/Fe. 112

Figure 4.7 (A) Reflected light view of the polyframboids in Figure 4.5 A; (B) SXRF element map of As (red), Zn (green) and Fe (blue) in the same framboid. The concentration of As, which is up to 2.5 wt %, varies in the polyframboids, except for the hot spot coinciding with Co. (C) SXRF element map of Cu (red), Zn (green) and Co (blue) in the same polyframboids; (D) Higher-resolution SXRF element map of

As (red), Co (green) and Zn (blue) for the boxed area shown in (C); (E) Higher-resolution SXRF element map of Zn (pink) and Cu (green) for the same area shown in (D).	113
Figure 4.8 SXRF element map of Zn, the distribution of which coincides with that of CM; A transect x-x' through the polyframboids shows variation in Sr, Rb, Fe, Zn, Ni, Cu, Co, As.	115
Figure 4.9 Petrographic images of polyframboids in reflected light with laser spots (indicated by red circles) in sample FF-16. Laser spots were focused on different textural classes: polyframboid areas (Pf), mixed polyframboid-matrix areas (Pf + Matrix) and matrix areas (Matrix).	117
Figure 4.10 Comparison of different concentrations of trace elements in three different textural classes: polyframboid areas (Pf), mixed polyframboid-matrix areas (Pf + Matrix) and matrix areas (Matrix). The concentration of Au in the matrix areas is below the detection limits. Data is presented in Table 4.1.	118
Figure 4.11 Geochemical plots of data from LA-ICP-MS analysis of polyframboids. (A) Au vs Zn (R^2 (the square of Pearson correlation coefficient) = 0.82); (B) Ag vs Zn ($R^2 = 0.89$); (C) Au vs Ag ($R^2 = 0.90$); (D) Au vs As; (E) Co vs Zn; (F) As vs Zn; (G) Ni vs Zn; (H) Mo vs Zn; (I) Cu vs Zn; (J) Pb vs Zn.	119
Figure 4.12 Schematic diagram of the evolution of one framboid in polyframboids and trace element mobility during the evolution of sulfides in the Otago Schist, modified after Pitcairn et al. (2010) and Large et al. (2007). Stages are labelled with estimated temperatures.	130
Figure 5.1 Geological map of the Otago Schist from Hu et al. (2015). The red rectangle on map is the sampling location.	146
Figure 5.2 Petrographic photomicrograph and SEM images of polyframboids. (A) Reflected light photomicrograph of polyframboid consisting of numerous microcrystals; (B) SEM image of the same polyframboid in (A) with more clear observations of rounded or irregular framboids; (C) Rounded framboids formed partially of hexagonally ordered microcrystals (indicated by the dashed line); (D) Well-organized tiny framboids.	148

- Figure 5.3** The distributions of Fe (as $^{56}\text{Fe}^{32}\text{S}$) and Zn (as $^{65}\text{Zn}^{32}\text{S}$) on microcrystals. Linear element profiles were taken from x to x' (from the center to the boundaries of grains). Element counts were normalized to secondary electron (SE) counts. (A) Pyrite microcrystals with almost homogeneous Zn (type 1). On the profile, both Fe and Zn contents show similar trends. Normalized Zn counts are positively correlated with those of Fe. (B) Pyrite microcrystals with Zn concentrated on the boundaries (type 2). On the profile, Zn has relatively low counts in the center of the grain, but high counts on the boundary where Fe content is relatively low. Dashed lines on the profiles are used to indicate the boundaries of grains. 150
- Figure 5.4** (A) The distributions of Fe and Zn in a single framboid depicted in Figure 5.2 C. (B) Enlarged image of part of (A). The microcrystal circled with the dotted line has a core of pyrite and a rim of sphalerite (type 3), and that with a dashed line is sphalerite (type 4). (C) Normalized counts of Fe and Zn are plotted against each other with sphalerite (Sph) and pyrite (Py) analyses plotting in distinctly different areas. 151
- Figure 5.5** Distributions of CN (as $^{12}\text{C}^{14}\text{N}$) and Fe (as $^{56}\text{Fe}^{32}\text{S}$) in (A) pyrite microcrystals, and (B) pyrite and sphalerite. Part (B) also shows the Zn (as $^{65}\text{Zn}^{32}\text{S}$) distribution. For a pyrite grain (type 2) in (A) and a sphalerite grain (type 4) in (B), linear profiles were taken from x to x' across the grains. Element counts were extracted and normalized to secondary electron (SE) counts, shown on the corresponding graphs. CN index was calculated and presented on the profiles. Dashed lines on the profiles are used to indicate the boundaries of grains in (A) and (B) and “hole” area in (B). 153
- Figure 5.6** A general model of Zn sequestration processes in framboids, as an example of a single microcrystal. (Sph: sphalerite; Py: pyrite; BSR: bacterial sulfate reduction) 157
- Figure 5.7** Zn isotope fractionation steps from seawater to continental margin sediment deposition. (1) Zn isotope in seawater (Zhao et al., 2014); (2) Lighter Zn isotopes is taken up by plankton in the upper seawater (John and Conway, 2014); (3, 4) During the degradation of dead organisms, lighter Zn isotopes are released into seawater (John and Conway, 2014); (5) Heavier Zn isotopes are bound to degrading plankton (John and Conway, 2014); (6) Zn is deposited directly in sediments; (7, 8) Zn fixation in framboids proposed in this study, including sulfide precipitation

during BSR activity and directly incorporated into pyrite; (9) Zn isotope in sediments (Little et al., 2016; Maréchal et al., 2000). (OM: organic matter.) 158

Figure 6.1 Photomicrographs of gold-bearing sulfides from the Macraes deposit in transmitted light (A, C) and BSE (back-scattered electron) imaging (B, D). Pyrite (circled by dashed lines) is surrounded by (A, B) or overprints (C, D) graphitic shears (indicated by dotted lines) which contains fine-grained carbonaceous material (CM) and sulfides, especially arsenopyrite. On the BSE images, pyrite is light grey and arsenopyrite is white..... 169

Figure 6.2 S vs. NCC by mass from four goldfields compared to model results. A vector from unmineralized rock to cell 1 in the model results was used to indicate the modelled trajectory in S vs. NCC space. This vector can be decomposed into two reactions: graphite deposition via reaction 4 (R4), and dominant sulfide deposition (R5/6: plotted as weighted average $S_{\text{model}}:C_{\text{model}2}$ mass ratios from reactions 5 and 6). 172

Figure 6.3 Results of fluid infiltration at 220 °C, 3 kbar. In cell 0, the concentration of solid components represents the amount in unreacted GB-01 and that of aqueous components represents the total amount in unreacted country rock fluid or ore fluid. Results of the fluid infiltration are presented in cells 1–18. (A) Pyrite and pyrrhotite; (B) Arsenopyrite; (C) Au and Au bisulfide species; (D) H₂ in equilibrated fluids and unreacted mixtures; (E) Total graphite (C_{model}), precipitated graphite, CH₄ and CO₂, RE. 174

Figure 7.1 Autoclave used in the experiments (not to scale), with 0.5 mL or 0.5 g organics and 0.01 g gold wire. 185

Figure 7.2 The presence of gold (bright spots) within carbonaceous material (CM, as dark areas) on the razor blade. 188

Figure 7.4 The contents of dissolved Au in dodecanethiol vs. time (days) at 200°C. 194

Figure 7.5 The GC-MS spectra of organic compounds in organic liquids pre-experiment (A) and post-experiment (B) for dodecanethiol..... 195

Figure 7.6 The GC-MS spectra of organic compounds in organic liquids pre-experiment (A) and post-experiment (B) for DBT. 198

Figure 8.1 The role of CM in the formation of Macraes gold deposit. Au and Zn are incorporated into framboids through sulfate reducing bacterial activity, and preserved with CM within framboids in pelites as the source rock. A single microcrystal is taken as an example to show the detailed sequestration processes of Zn into framboids. Au is then released during the transition from framboids to euhedral pyrite, and to pyrrhotite when metamorphic grade increases. Thiols in organic matter generated during catagenesis may be capable of transporting Au. When Au is transported to deposition site, the co-deposition of CM and sulfides drives gold deposition. (CM, carbonaceous material; Sph, sphalerite; Py, pyrite; Aspy, arsenopyrite; Po, pyrrhotite; Q, quartz; P-P, prehnite-pumpellyite; P-A, pumpellyite-actonlite; G-S, greenschist; Amp, amphibolite.)..... 213

List of tables

Table 1.1 Potential roles of CM during ore-forming processes (modified from Leventhal and Giordano (2000).	3
Table 2.1 List of samples, including sample locations, ID and depth.....	35
Table 2.2 A summary of characteristics of three gold deposits (Craw, 2002; Hagemann and Cassidy, 2000; Hagemann and Lüders, 2003; Neumayr et al., 2008).	38
Table 2.3 Elemental analysis and Rock-Eval pyrolysis results of St. Ives, Wiluna and Macraes samples.	43
Table 3.1 Sampling locations, rock type, non-carbonate carbon content, Au content, relevant parameters of Raman spectra of samples investigated.....	65
Table 3.2 Relevant parameters of Raman spectra of selected samples under polarized light and circular polarized light.	68
Table 3.3 Temperature estimates from Raman spectra and metamorphic facies for each CM type.	82
Table 4.1 The concentration of trace elements in the three textural classes investigated: polyframboids (Pf), mixed polyframboids and matrix (Pf + Matrix) and matrix (Matrix). (DL: detection limits; σ : standard deviation; N is the number of analyzed samples.)	120
Table 4.2 The concentration of trace elements in ten analyzed polyframboids (Pf).	121
Table 7.1 Results of chemical digestion with multiple elements in oil standard from a single analysis.....	190
Table 7.2 The concentrations of Au in solutions of each step and the contents of dissolved Au in dodecanethiol.	193
Table 7.3 The chemical components in organic liquids pre- and post-experiment for dodecanethiol.	196
Table 7.4 The chemical components in organic liquids pre- and post-experiment for DBT.....	199

Chapter 1

Introduction

1.1 Carbonaceous material (CM)

1.1.1 Introduction of CM

CM, defined as carbon-rich material containing C-O and/or C-H bonds (Leventhal and Giordano, 2000), is widespread in sedimentary and meta-sedimentary rocks, and commonly originates from two processes (Luque del Villar et al., 1998; Simoneit and Gize, 2000). CM may be precipitated from carbon-bearing hydrothermal fluids, i.e., via mixing of CO₂ and CH₄ (Ohmoto and Kerrick, 1977). CM deposited abiologically is referred as ex-situ (Luque del Villar et al., 1998; Luque et al., 2009). CM deposited along with host sediments without any mobilization after the death of living organisms, is termed in-situ (Leventhal and Giordano, 2000; Simoneit and Gize, 2000).

With increasing metamorphic grade, CM transforms from an amorphous structure to fully crystallized graphite (Landis, 1971) and loses external chemical functional groups at the same time. This process, referred to as graphitization, is governed by temperature (T), duration of metamorphism, the type of host rock and carbon precursor, and, to a lesser extent, pressure (P) (Beysac et al., 2002; Luque del Villar et al., 1998). With burial, the initial CM, kerogen, loses some heteroatoms, where heteroatoms are non-C atoms in the kerogen structure, such as N, S, H and O. The process is known as diagenesis (Simoneit and Gize, 2000). With longer burial time and increasing temperature, kerogen continues to lose heteroatoms, generating hydrogen small chain hydrocarbons, the process of which is known as catagenesis (Simoneit and Gize, 2000). As temperature increases further, CM continues to lose hydrogen and turns into crystalline, graphitic CM; these final changes are known as metagenesis (Leventhal and Giordano, 2000; Simoneit and Gize, 2000). The details of the graphitization process are shown in Figure 1.1.

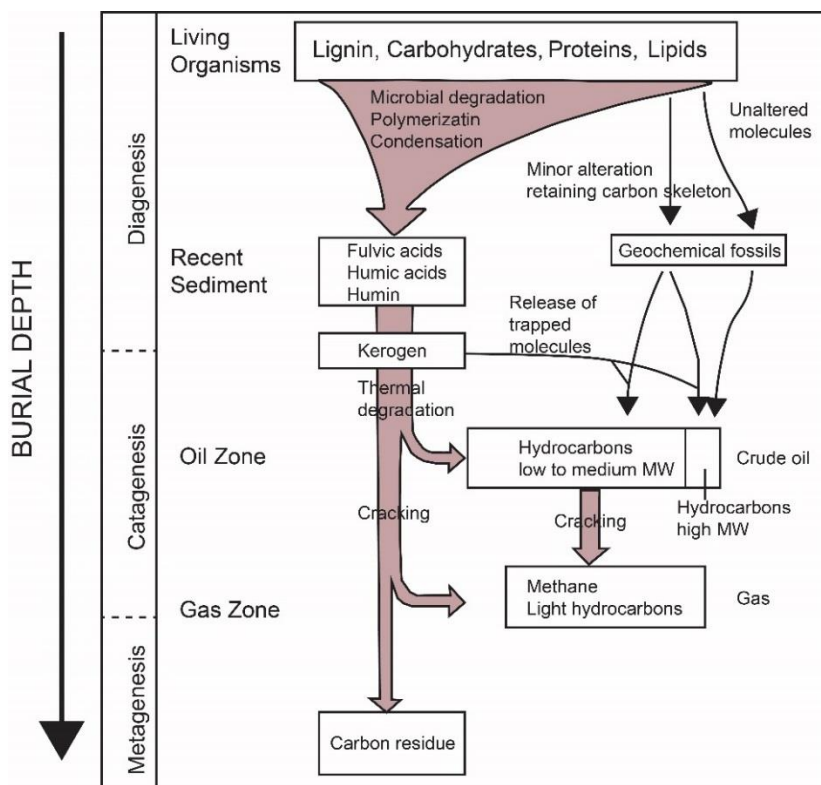


Figure 1.1 The maturation process (Libes, 2011). MW: molecular weight.

1.1.2 CM in ore deposits

The majority of investigations of CM maturation during diagenesis and metamorphism are in the petroleum field of research. However, CM in ore deposits has received increasing attention in recent decades. It is recognized that CM is closely associated with various sedimentary-hosted ore deposits, such as Pb-Zn deposits (Bechtel et al., 1998; Chen et al., 2003; Gize and Barnes, 1994; Spangenberg and Macko, 1998), gold deposits (Bierlein et al., 2001; Craw, 2002; Gatellier and Disnar, 1989), stratiform copper deposits (Ho and Mauk, 1996; Ho et al., 1990; Rieger et al., 2008) and uranium deposits (Landais, 1996; Leventhal et al., 1986; Spirakis, 1996). It is now widely accepted that CM can play an active or passive role in the formation of these ore deposits. CM may act, directly or indirectly, as a source, an aid to transportation, and/or as a facilitator of deposition of metals during the formation of ore deposits. Proposed active roles played by CM during ore forming process are summarized in Table 1.1.

However, it is also possible that CM may play no role or passive role, even if the CM is present in ore deposits (Leventhal and Giordano, 2000).

Table 1.1 Potential roles of CM during ore-forming processes (modified from Leventhal and Giordano (2000)).

Role	Detailed Mechanism
Source	Accumulate metals in source rock from seawaters (for sediment-hosted type).
Mobilization	Metals are mobilized from source rock into carbonic fluids and/or with C-bearing ligands.
Transportation	Metals are transported in C-bearing fluids from the source rocks to the site of deposition.
Deposition	Metals are concentrated and precipitated at the site of deposition through reduction or oxidation reactions.

1.1.3 CM in gold deposits

Gold deposits, not only for gold but other precious metals as well, have long been a favoured exploration target (Tomkins, 2013). Decades of research have demonstrated that CM is intimately associated with gold deposits, with proposed roles in source, transportation and deposition processes (Bierlein et al., 2001; Craw, 2002; Emsbo and Koenig, 2007; Large et al., 2011; Williams-Jones and Migdisov, 2007).

Source

Large et al. (2011) proposed a two-stage model for gold deposit formation based on multiple investigations of Carlin-type and orogenic gold deposits. In the model, gold and other metals are initially concentrated from seawater into diagenetic pyrite through bacterial activity, and then released during the transition of pyrite to pyrrhotite as metamorphic grade increases. Laboratory experiments have demonstrated that bacteria are capable of absorbing Au from sea water and/or precipitating gold by reduction of Au^{3+} from solution to Au^0 (Kashefi et al., 2001; Zhang et al., 1997) or depositing elemental gold on the cell surface (Lengke and Southam, 2006; Lengke and Southam, 2007). However, direct evidence of the processes by which gold is extracted by bacteria from seawater and deposited in sediments as the source of gold deposits is rare.

Transportation

When gold is transported in ore fluids, it is well known to be complexed with sulfide ligands in hydrothermal fluids from 100 to 500 °C, 500 to 1500 bar (Baranova and

Zotov, 1998; Benning and Seward, 1996; Gibert et al., 1998; Renders and Seward, 1989; Seward, 1973; Shenberger and Barnes, 1989; Stefánsson and Seward, 2004) and chloride ligands under conditions of 300 to 600 °C, 500 to 1800 bar (Gammons and Williams-Tones, 1995; Gammons et al., 1997; Henley, 1973; Stefánsson and Seward, 2003; Wood et al., 1987; Zotov et al., 1991). However, the possibility and effectiveness of gold transportation by CM is controversial. In early studies of supergene gold deposits, humic acid and organic-colloids were found capable of transporting gold away from the initial source (Baker, 1978; Freise, 1931; Lungwitz, 1900; Ong et al., 1970). In hydrothermal gold deposits, CM, like bitumen and pyrobitumen, has been proposed to carry gold during the mobilization of gold before precipitation (Zhuang et al., 1999). In the Carlin gold deposits of Nevada, up to 100 ppm Au is found in bitumen, implying that gold may be mobilized by organic fluids (Emsbo and Koenig, 2007; Williams-Jones et al., 2009). However, co-deposition of gold and bitumen from hydrothermal fluids could also account for this observation (Williams-Jones et al., 2009). Laboratory experiments by Williams-Jones and Migdisov (2007) have shown that Au can be dissolved by crude oil up to ppb level, although the actual speciation of the gold is unknown.

Deposition

Gold is closely associated with CM and sulfides in mineralized rocks in some orogenic disseminated gold deposits, such as the Victorian goldfield, Australia (Bierlein et al., 2001), the Macraes gold deposit, New Zealand (Craw, 2002), the Yukon gold deposit in White River area, Canada (MacKenzie et al., 2010), and the Carlin gold deposits in Nevada, United States (Cline et al., 2005). CM may contribute to gold deposition directly or indirectly. CM has been proposed to act as a reductant, which reacts with gold-bisulfide to cause the direct deposition of gold (Cox et al., 1995; McKeag et al., 1989; Radtke and Scheiner, 1970). In addition to any direct role played by CM, sulfidation, which is accompanied with gold precipitation, may be affected by CM, which can act as an electron donor (Cline et al., 2005; Craw, 2002; Craw et al., 2007; Craw et al., 2015). Further, the deposition of CM prior to that of gold may help to facilitate the formation of shear zones, which can focus fluid flow and associated gold precipitation (Upton and Craw, 2008, 2014).

To summarize, knowledge of the source, transportation and deposition mechanisms associated with CM could contribute to exploration for CM-associated gold deposits. Yet even though many studies have been conducted on the role of CM in the formation of CM-associated gold deposits, details of the role of CM are not fully understood. The characterization of CM via organic geochemistry techniques and other state-of-the-art in-situ analysis techniques have the potential to provide new insights into CM composition and is the topic of this thesis.

1.2 Research areas

1.2.1 Geological setting of Otago Schist and Macraes gold deposit, New Zealand

South Island of New Zealand

The South Island of New Zealand is composed of two distinct parts, the Western Province and the East Province (Figure 1.2, Landis and Coombs, 1967). The two parts are separated by a tectonically complex zone referred to as the Median Tectonic Line, which is cut and displaced by the Alpine fault (Landis and Coombs, 1967).

The Western Province, which is thought to have originally formed part of the Gondwana continental block (Cooper, 1975), consists of Paleozoic sedimentary rocks (MacKinnon, 1983) and the Tasman metamorphic belt, which has suffered relative high temperature- low pressure metamorphism. The metamorphic grade ranges from unmetamorphosed, through greenschist facies to amphibolite facies (Landis and Coombs, 1967). The Eastern Province, which includes the Torlesse and coeval terranes and clastic sedimentary rocks, is thought to be the Australian-Antarctic margin of Gondwanaland (Fleming, 1979), and has gone through low temperature-high pressure metamorphism in a region known as the Wakatipu metamorphic belt (Landis and Coombs, 1967). The metamorphism shifted from zeolite facies, through prehnite-pumpellyite, pumpellyite-actinolite facies, and locally lawsonite-albite-chlorite facies, into the greenschist and amphibolite facies (Turnbull et al., 2001).

According to previous studies (Coombs et al., 1976; Mortimer, 1993; Mortimer, 2000), the Eastern Province can be divided into eight units on the basis of lithology, structure and metamorphism (Figure 1.2). These units are the Torlesse Terrane,

Caples Terrane, Otago and Alpine Schist, Marlborough Schist, Dun Mountain Ophiolite Belt, Maitai Terrane, Murihiku Terrane and Brook Street Terrane. The combination of the Marlborough, Alpine and Otago Schists was previously known as the Haast Schist (Mortimer, 2000). The Otago Schist is a metamorphic belt that resulted from the collision of the Torlesse Terrane and the Caples Terrane in a fore-arc region in the later Mesozoic (Mortimer, 1993). Thus, the Otago Schist consists of parts of both terranes. The boundary of the Torlesse Terrane and the Caples Terrane has been overprinted by metamorphism and ductile deformation (Mortimer, 1993). The Torlesse Terrane was deposited during the Carboniferous to Lower Cretaceous according to fossil evidence (MacKinnon, 1983). The lithologies are monotonous quartzofeldspathic greywackes and mudstones, intercalated with minor conglomerate, volcanics, chert and limestone (MacKinnon, 1983). Sandstone and mudstone display graded beds, indicating the sediments are turbidites deposited in a submarine fan environment by gravity flow (MacKinnon, 1983). The Caples Terrane is bounded by the Torlesse terrane and the Dun Mountain ophiolite belt (Figure 1.2). The rocks comprise late Paleozoic to early Mesozoic schistose and non-schistose rocks, including volcanoclastic greywacke and argillite (Bishop et al., 1976; Mortimer, 1993). The Aspiring Terrane, which comprises pelitic schist, greenschist and minor chert and is juxtaposed with the Torlesse and Caples terranes, has been considered as an individual terrane that lies within the Otago Schist (Norris and Craw, 1987). However, Mortimer (1993) and Mortimer and Roser (1992) proposed that the Aspiring terrane is a segregated part of the Torlesse terrane.

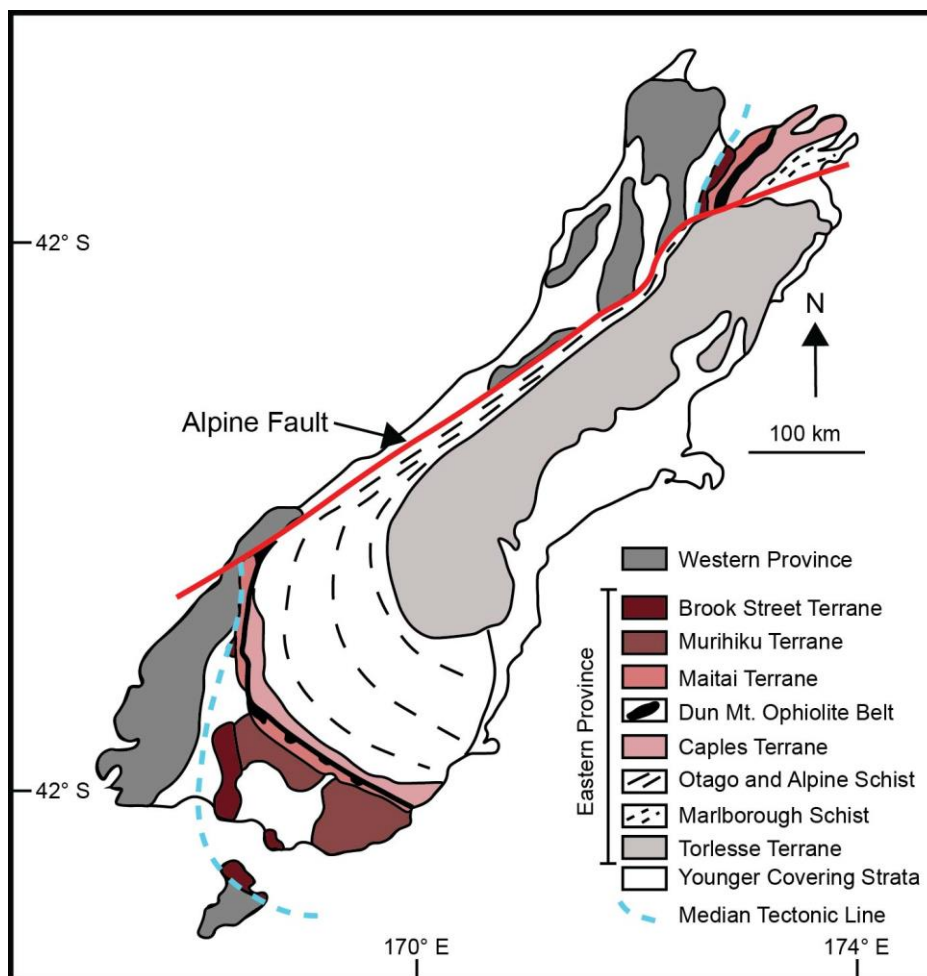


Figure 1.2 Geological map of the South Island of New Zealand. The Otago and Alpine Schist comprise parts of the metamorphosed Caples and Torlesse terranes sedimentary rocks. Modified from Coombs et al. (1976), Mortimer (1993) and Mortimer (2000).

The Otago Schist and the Macraes gold deposit

The protoliths of the Otago Schist rocks are Paleozoic to Mesozoic turbidites, which consist of quartzofeldspathic sandstone and pelites. Regional metamorphism of the Otago area commenced in the Early Jurassic due to the collision of the Torlesse and Caples terranes, and concluded with uplift and cooling through the Cretaceous, resulting in a symmetrical metamorphic belt (Figure 1.3). The metamorphic grade ranges from prehnite-pumpellyite (P-P) facies on the margins, through pumpellyite-actinolite (P-A) facies, to lower greenschist (G-S) facies in the core of the belt (Mortimer, 1993). Amphibolite facies rocks are exposed in the northwest of the main belt (Mortimer, 2000; Pitcairn et al., 2006). Normal faults formed after uplift resulted in the juxtaposition of different metamorphic rocks (Craw, 2002).

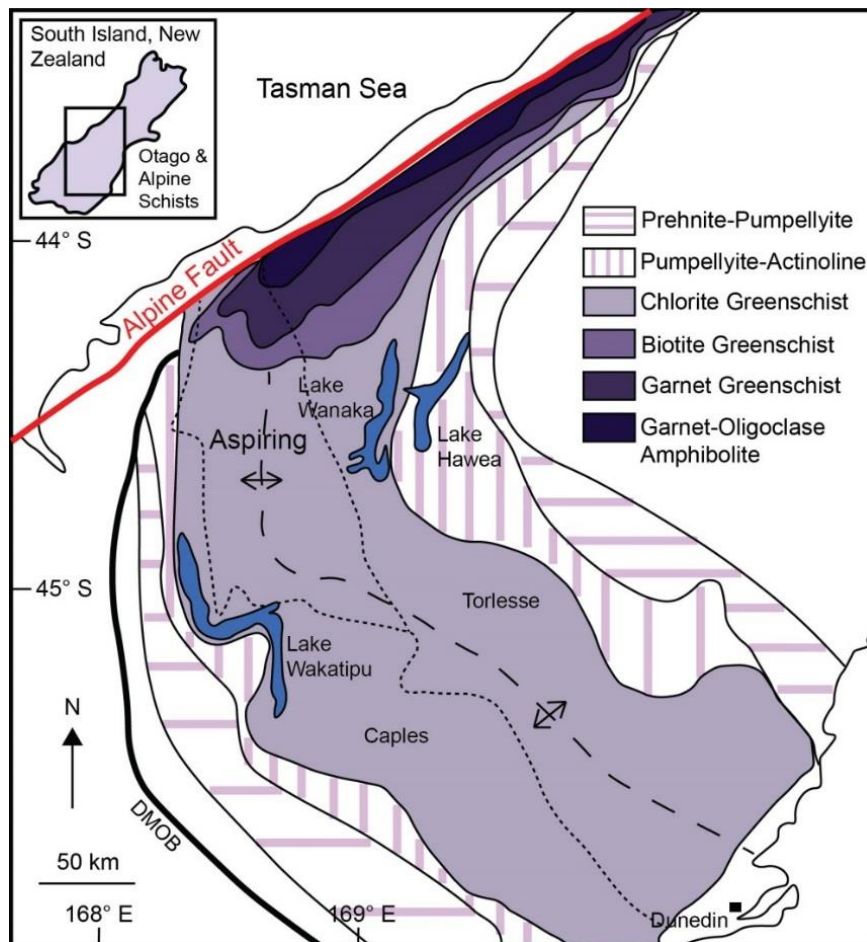


Figure 1.3 Geological map of the Otago Schist, New Zealand, which formed due to the collision of the Torlesse and Caples Terrane. The metamorphic grade ranges from prehnite-pumpellyite (P-P) facies on the margins, through pumpellyite-actinolite (P-A) facies, to lower greenschist (G-S) facies in the core of the belt, and to amphibolite facies near the Alpine fault. DMOB – Dun Mountain Ophiolite Belt. Modified from Mortimer (2000) and Pitcairn et al. (2006).

The Macraes gold deposit is a world-class gold deposit, hosted by the Otago Schist, with a reserve of more than 300 tonnes of gold (Moore and Doyle, 2015).

Mineralization occurred under lower G-S facies conditions (300–350 °C) during brittle-ductile transition. The goldfield occurs in the Hyde-Macraes Shear Zone, which is a thrust structure that has juxtaposed mineralized rocks against unmineralized rocks. Gold occurs within quartz veins or is closely associated with pyrite and arsenopyrite in graphitic schist. The latter is referred to as “intra schist” (Figure 1.4). It is thought that mineralizing fluids, generated at depth during metamorphism, mobilized and transported gold and other metals from P-P facies

source rocks to zones of mineralization (Large et al., 2012; Pitcairn et al., 2014a; Pitcairn et al., 2010; Pitcairn et al., 2006). Diagenetic pyrite in P-P facies rocks has been suggested to be the sink for gold (Large et al., 2012). Gold deposition is thought to be a consequence of the cooling of mineralizing fluid and reduction of Au-bisulfide, resulting in the deposition of sulfides and destabilization of gold-bisulfide (Craw, 1992, 2002).

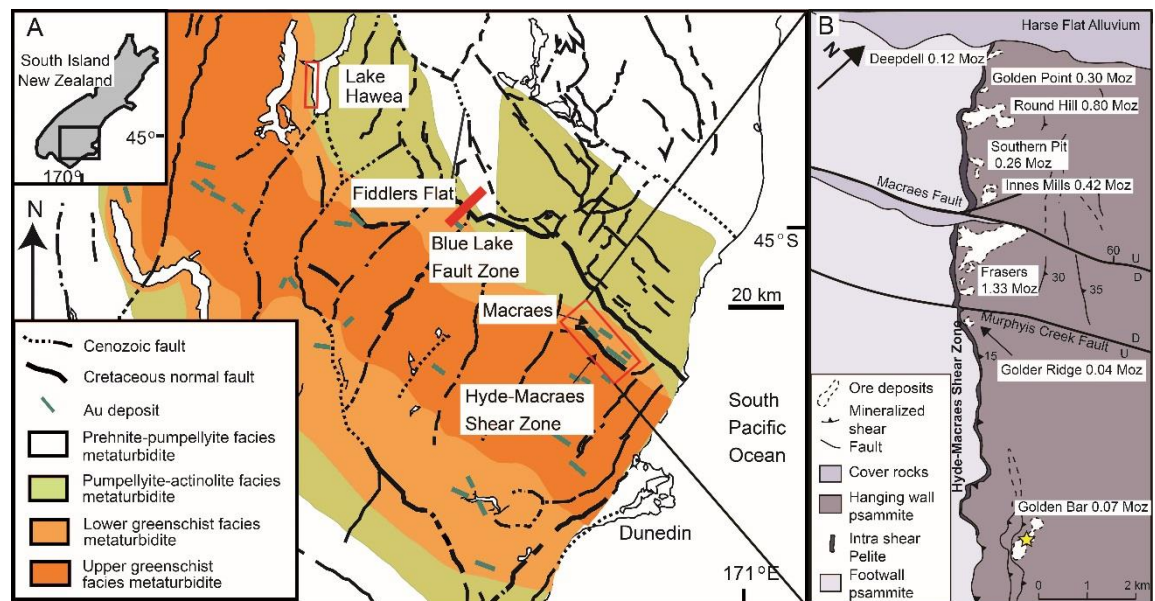


Figure 1.4 Geological map of (A) the Otago Schist and (B) Macraes gold deposit (modified from Pitcairn et al. (2006) and De Ronde et al. (2000)). The red box and red line indicate areas sampled for this study.

1.2.2 CM in the Otago Schist and Macraes gold deposit

CM in Otago Schist

The average non-carbonate carbon (NCC) content in the turbidites of the Otago Schist is less than 0.1 wt % and is around 0.1–0.3 wt % in the host rock of Macraes gold deposits (Craw, 2002; Henne and Craw, 2012). A detailed study of CM in a typical profile through Fiddlers Flat (Figures 1.4, 1.5 A), from P-P facies to lower G-S facies, was conducted by Henne and Craw (2012). This study showed that CM displays various morphologies from lower to higher grade metamorphic rocks. In P-P facies, detrital CM occurs as angular and rounded fragments, less than 50 μm in the longest dimension. In micaceous schists of higher metamorphic grade rocks, i.e., P-A and G-S facies, CM always occurs as coarse-grained graphite ($\sim 100 \mu\text{m}$) and is

associated with quartz veins. Pyrite is often associated with CM, and the content of CM in pyrite-rich micaceous schists is distinctively high (up to 5 wt %). CM porphyroblasts are crystallographically continuous internally with low reflectance. The minimum reflectance is less than 1% whereas the maximum reflectance is up to 8%. CM in P-P facies rock is proposed to have been mobilized by metamorphic fluids and re-deposited in P-A and G-S facies (Henne and Craw, 2012).

CM in the Macraes gold deposit

In mineralized rocks (Figure 1.5 B), the NCC content is much higher than that in unmineralized rocks, with NCC up to 3% (Henne and Craw, 2012). It has been proposed that the CM in the mineralized rocks is in-situ and derived from the pre-metamorphic protolith (McKeag et al., 1989) or deposited via the mixing of CO₂ and CH₄ from hydrothermal fluids (Craw, 2002). Pitcairn et al. (2005) used Fourier Transform Infra-Red spectroscopy (FTIR) to show that that CM in mineralized rocks was precipitated from hydrothermal fluids. In petrographic observations, CM is observed to be closely associated with sulfides and gold (Craw et al., 1999). The contribution of CM to gold mineralization has been proposed to relate to reduction of gold-bearing fluids (Craw et al., 1999; McKeag et al., 1989), controlling the formation of shear zones which will focus fluid flow and cause gold precipitation (Upton and Craw, 2008, 2014), or an indirect role related to the co-deposition of graphite and sulfides (Craw et al., 2015).

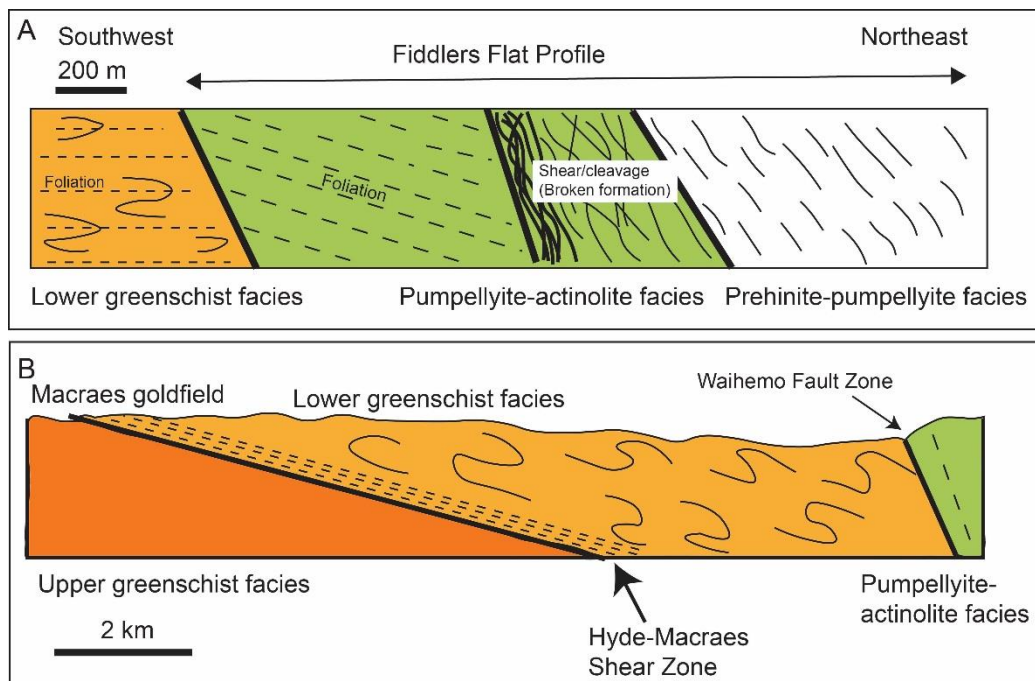


Figure 1.5 (A) A geological profile through Fiddlers Flat. Metamorphic grade ranges from prehnite-pumpellyite facies to lower greenschist facies. (B) A geological cross section through the Hyde-Macraes shear zone. Modified from Large et al. (2012). The locations of both profiles are indicated in Figure 1.4 A.

To summarize, CM is widely preserved in the Otago Schist and Macraes gold deposits, and plays potential roles in the formation of the Macraes gold deposits. Particular areas of interest are: (1) the association of CM with the diagenetic pyrite in P-P facies rocks that are thought to be the source of gold (Large et al., 2012; Pitcairn et al., 2006); and (2) the contribution of the CM that is so abundant in the mineralized rocks to the gold precipitation mechanism.

1.2.3 Gold deposits in Western Australia

The St. Ives goldfield and Wiluna lode-gold deposits are Archean gold deposits, developed in the Norseman-Wiluna belt, Western Australia. They are hosted by, or are associated with the Kapai Slate which comprises sulfidic mudstone and shale. Recent calculations of the amount of Au released by sedimentary pyrite in the Kapai Slate by Gregory et al. (2016) imply that the slate may be the source of a minor amount of the Au found in the St. Ives district. Black shale is always CM-rich. However, the contribution of CM to the formation of the St. Ives and Wiluna gold

deposits is rarely investigated. A small number of samples were collected from the two gold deposits to characterize the host rocks using organic geochemical approaches. Full details of the geological background will be provided in **Chapter 2**.

1.3 Thermodynamic modelling

To test the role of CM during gold precipitation, thermodynamic modelling using the HCh software package (Shvarov and Bastrakov, 1999) was used to simulate mineralization processes that result from fluid-rock interaction. HCh, which uses a free-energy minimization approach, has the capability of calculating the compositions of equilibrated fluids and rocks of interest given the bulk composition of the system at a specified temperature and pressure. The accessible temperature range is 0–1000 °C and pressures can reach up to 500 MPa. Results of fluid-rock interaction calculations made with HCh for open and closed systems have been published previously, e.g., Phillips and Evans (2004), Oliver et al. (2004), Evans et al. (2006), Mernagh and Bierlein (2008), and (Evans, 2010).

1.4 Gold solubility in pure organic liquids

Laboratory investigations are essential to answer the question of whether Au can be transported by CM. Previous investigations of the transportation of gold in hydrothermal fluids have conventionally used experiments of gold solubility in aqueous solutions, e.g., Stefánsson and Seward (2004). It has also been proposed that Au is mobilized and transported by CM (Emsbo and Koenig, 2007). However, few experiments of gold solubility in organic liquids have been conducted, other than an investigation of solubility of gold in crude oil by Williams-Jones and Migdisov (2007). This study suggested that liquid hydrocarbons may be capable of transporting gold, but the composition of crude oil is so complex that the actual gold speciation and gold complexing ligand in the oil could not be determined. Investigation of gold solubility in pure organic liquids, where the gold complexing ligand would be easier to determine, would provide useful contributions to our knowledge of Au solubility and transport. Further details of the background to this work will be provided in **Chapter 7**.

1.5 Objectives of thesis

This PhD project focusses on CM in rocks distal and proximal to the Macraes gold deposit and CM in some samples from the St. Ives and Wiluna gold deposits. The study uses organic geochemical approaches, other cutting-edge petrographic analytical techniques, and thermodynamic simulation. To constrain gold transportation by CM, experiments of gold solubility in organic liquids are performed.

The overarching objective is to elucidate the role played by CM during the formation of gold deposits in terms of source, transportation and deposition.

Specific objectives are to:

- (1) Use techniques developed for organic geochemistry, such as chromatography, to characterize CM, and constrain its maturation, chemical composition and possible origins, for rocks distal and proximal from Macraes gold deposit, and samples from the St. Ives and Wiluna gold deposits in Western Australia;
- (2) Use petrological and inorganic geochemical mapping techniques to understand metal sequestration processes in source rocks and the role of CM in the source of Au and other metals in the Macraes gold deposit;
- (3) Use thermodynamic simulations to better understand the mechanism by which CM might contribute to gold deposition;
- (4) Experimentally evaluate the possibility that gold can be transported by particular organic complexes.

1.6 Research methods

1.6.1 Field work

A two-week geological field excursion was conducted in the Otago Schist, on the South Island of New Zealand. The main task for the trip was to record geological observations and collect samples. A total of 40 samples were collected from a range of metamorphic grades in Fiddlers Flat, Lake Hawea and Golden Bar pit (Figure 1.4 A). In the Fiddlers Flat area, samples were collected from a geological cross section from P-P facies to lower G-S facies rocks. At Lake Hawea, carbonaceous meta-

pelitic samples were collected from P-A facies and lower G-S facies schists.

Unmineralized schists and mineralized graphitic sheared rocks were collected from the Golden Bar pit of the Macraes gold deposit. There are 6 samples from the P-P facies, 18 samples from the P-A facies and 16 samples from the lower G-S facies.

13 samples were collected as drill cores from St. Ives and 2 samples from the Wiluna gold deposits.

Detailed sample descriptions are included in **Appendix A1, A2 and A3**.

1.6.2 Laboratory analyses

Preliminary laboratory analyses include rock cutting and crushing were conducted in the rock and sample preparation laboratory, Department of Applied Geology, Curtin University. Bulk composition analyses were performed by Intertek Genalysis Lab, Perth (**Appendix A1**). Thin section observations were undertaken using a Nikon optical transmitted and reflected light microscope (**Appendix A2**). Scanning electron microscopy (SEM) and energy-dispersive X-ray spectroscopy (EDS) observations were made using a Zeiss Neon 40EsB field-emission gun scanning electron microscope (FEG-SEM) in the Curtin Materials Research Lab and Hitachi Tabletop Microscope TM3030 in the Department of Applied Geology, Curtin University.

Organic geochemical analyses, including non-carbonate carbon removal, sulfur removal, Soxhlet extraction and gas chromatographic-mass spectrometry (GC-MS), were performed at the WA Organic and Isotope Geochemistry Facility (WA-OIGC), Curtin University. Elemental analysis (non-carbonate carbon, total of nitrogen, total of sulfur) and Rock-Eval pyrolysis were undertaken at the Organic Geochemistry Laboratory of Kiel University.

Raman spectroscopy was used to characterize the structure and relative maturity of CM using a Horiba® LabRAM HR Evolution and a Snyapse Visible detector at the Commonwealth Scientific and Industrial Research Organisation (CSIRO).

The distribution and concentration of trace elements and CM in polyframboidal sulfides were determined by synchrotron X-ray fluorescence microscopy (SXRF) at the Australian Synchrotron, laser ablation inductively coupled plasma mass spectrometry (LA-ICP-MS) at John de Laeter Centre, Curtin University and

nanoscale secondary ion mass spectrometry (NanoSIMS) at the Centre for Microscopy, Characterization and Analysis (CMCA), at the University of Western Australia.

Thermodynamic modelling was performed with HCh software at the Department of Applied Geology, Curtin University.

Experiments on gold solubility in organic liquids (dodecanethiol and dibenzothiophene) were conducted at the Curtin Experimental Geochemistry (CEG) facility at the Department of Applied Geology, Curtin University. Gas chromatography-flame ionization detector (GC-FID), gas chromatography-flame photometer detector (GC-FPD), GC-MS were utilized for the characterization of organic compounds of the experimental products at the ChemCentre, Perth. Au concentration analysis was performed with inductively coupled plasma mass spectrometry (ICP-MS) at the Labwest (Perth).

1.7 Thesis structure

This thesis begins with this introduction (**Chapter 1**) that defines CM, reviews the association between CM and ore deposits, in particular the association between CM and gold deposits, the geological background of the Otago schist and the Macraes gold deposit, and highlights scientific questions that this study aims to address.

Chapter 2 describes organic geochemical investigations of samples from the St. Ives and Wiluna gold deposits (Western Australia) and the Macraes gold deposit (New Zealand). **Chapter 3** describes the characterization of CM in distal and proximal rocks in the Macraes gold deposit with a combination of Raman spectroscopy and petrographical observations. This chapter has been published in *Ore Geology Reviews*. **Chapter 4** is devoted to the association between sulfides, CM, Au and other trace elements in polyframboids, which is investigated using SXRF and LA-ICP-MS. The work has been published in *Geochimica et Cosmochimica Acta*.

Chapter 5 is complementary to **Chapter 4** and includes CM mapping and further observations of the framboids from the Otago Schist similar to those described in **Chapter 4** via NanoSIMS. This work is under revision for resubmission to *Geochimica et Cosmochimica Acta*. The role of CM in gold deposition was investigated using thermodynamic modelling and this work is described in **Chapter**

6 which is under review in *Geology*. Finally, an experimental investigation of gold solubility in pure organic liquids is described in **Chapter 7**. The thesis is completed with a summary in **Chapter 8**.

A brief summary of chapters 2, 3, 4, 5, 6 and 7 is presented below:

Chapter 2

CM from orogenic gold deposits had not been characterized by organic geochemical approaches prior to the beginning of this work. These techniques were therefore applied to samples from Macraes gold deposit and St. Ives and Wiluna gold deposits. This chapter describes the detailed geologic background of the two gold deposits in Western Australia and the application of organic geochemistry methods to those samples from three gold deposits. Based on element analysis, samples with the highest NCC content were chosen for Rock-Eval pyrolysis and Soxhlet extraction (pre-treatment for gas chromatographic-mass spectrometry (GC-MS) characterization). However, Rock-Eval pyrolysis results showed that the hydrogen and oxygen index of samples are low. This implies that CM in those samples is highly mature and cannot be further analysed by conventional organic geochemistry techniques.

Chapter 3

Considering that CM cannot provide conventional organic geochemical information (**Chapter 2**), CM is characterized with petrographic and Raman spectroscopic analysis. Four types of CM were identified from rocks of various thermal maturity and origins distal and proximal to Macraes gold deposit. In low metamorphic grade rocks (P-P and P-A facies), CM 1 is low maturity and coexists with pyrite framboids with a sedimentary origin. CM 2, found in P-A facies rocks, is proposed to have deposited from hydrothermal fluids. CM 3, recognized in lower G-S facies, is thought to have been transported in hydrothermal fluids, but only on short length scales. CM 4, which is associated with mineralized rocks, is relatively low maturity and likely to deposit from hydrothermal fluids as well. A number of unresolved questions that relate to gold mineralization are identified, and these are investigated with thermodynamic modelling in **Chapter 6**.

Chapter 4

Diagenetic pyrite in low metamorphic grade rocks (P-P facies) has been suggested to be the source of gold and other metals of the Macraes gold deposit (Large et al., 2012; Pitcairn et al., 2005). **Chapter 4** therefore investigates the association between CM, trace elements and sulfides in the polyframboids described in **Chapter 3**, with the aim of elucidating the role of CM in the source of Au for the Macraes gold deposit. The distribution of trace elements was quantitatively characterized with SXRF and LA-ICP-MS. Results show that trace elements such as Au, Zn, As, Mo, Co, Ni, Cu, Ag and Pb are significantly enriched in the polyframboids. Zn has a similar distribution pattern to that of CM, indicating the absorption of Zn to CM is associated with biological processes. Positive linear relationships were observed between Au and Zn and Ag and Zn. The results suggest that Au and Ag may undergo similar processes and immobilization mechanisms to Zn. The observations are consistent with the previously suggested idea that polyframboids are a potential source of Au for the orogenic gold deposits in the Otago Schist.

Chapter 5

Given the demonstrated co-location of Au and Zn documented in **Chapter 4**, it was decided to investigate the distribution of Zn in polyframboids using techniques with the highest possible spatial resolution. A combination of optical microscopy, SEM and NanoSIMS was utilized to characterize the spatial relationships between Zn, pyrite and organic matter in framboids. The distribution of Zn in framboids is variable. Most microcrystals are pyrite microcrystals with minor Zn contents. Zn is also present as ZnS, co-located with organic matter, on the boundaries of pyrite microcrystals. Interestingly, Zn is also observed in sphalerite microcrystals which sometimes occur as rims around pyrite microcrystals. The occurrence of mixed pyrite-sphalerite framboids is an entirely new discovery. The various distributions of Zn suggest that Zn is sequestered into framboids in different ways, depending on the relative concentrations of Zn and Fe in solution, and that Zn sequestration is associated with sulfide reducing bacteria activity. The progressive incorporation of Zn into framboids may have implications for Zn isotope fractionation process during sequestration from seawater to sediments, and the incorporation of Au into these sediments as the source of Au for Macraes orogenic gold deposits.

Chapter 6

As CM 4 is found closely associated with sulfide in mineralized rocks (**Chapter 3**), thermodynamic modelling was performed to investigate links between reactions involving CM and gold precipitation, based on geochemical data from the Macraes gold deposit (New Zealand), Paleoproterozoic gold deposits in Southern Ghana, the Touquoy Zone deposit in Meguma Terrane (Canada) and the Victorian goldfield (Australia). There is a positive correlation between the weight percent of sulfur and non-carbonate carbon in mineralized samples implying a genetic link between sulfides and CM during mineralization. Results from thermodynamic simulations of the mineralization process, replicate observed relationships between S and NCC and suggest that the coexistence of CM and pyrite is produced by interactions between CO₂ in ore fluids and ferrous minerals in wall rock, with associated consumption of H₂S from hydrothermal fluids. This decrease in H₂S concentration drives destabilization of Au(HS)₂⁻ complexes and promotes the precipitation of Au.

Chapter 7

CM has been proposed to be responsible for the transportation of gold in some cases but experiments investigating the solubility of gold in organic liquids are rare. This chapter describes some laboratory investigations of the solubility of gold in two pure organic liquids, dodecanethiol and dibenzothiophene. Kinetic series of experiments were performed using 0.01g gold wire and 0.5 mL dodecanethiol/ 0.5 g DBT in polytetrafluoroethylene (PTFE)-lined stainless steel vessels. Experiments were performed in a furnace at temperatures up to 150 °C and pressures determined by the liquid-vapour pressure of the liquid. After the experiments, organic species were characterized with GC-FID, GC-FPD and GC-MS. To quantify the gold concentrations in organic liquid, direct injection into ICP-MS, dry ashing and chemical digestion were tested using Au sulfur-free metallo-organic standards and multiple elements in an oil standard. New methods were developed to quantify gold concentration in organic liquids in a precise, quick and inexpensive way. Preliminary results have revealed that a significant amount of Au can be dissolved by dodecanethiol and the reaction may reach equilibrium after 25 days, indicating dodecanethiol may have the capability to complex gold.

1.8 References

- Baker, W., 1978. The role of humic acid in the transport of gold. *Geochimica et Cosmochimica Acta* 42, 645-649.
- Baranova, N., Zotov, A., 1998. Stability of gold sulphide species $\text{AuHS}^0_{(\text{aq})}$ and $\text{Au}(\text{HS})^2^-_{(\text{aq})}$ at 300, 350 °C and 500 bar: experimental study. *Mineralogical Magazine A* 62, 116-117.
- Bechtel, A., Pervaz, M., Püttmann, W., 1998. Role of organic matter and sulphate-reducing bacteria for metal sulphide precipitation in the Bahloul Formation at the Bou Grine Zn/Pb deposit (Tunisia). *Chemical Geology* 144, 1-21.
- Benning, L.G., Seward, T.M., 1996. Hydrosulphide complexing of Au (I) in hydrothermal solutions from 150-400 °C and 500-1500 bar. *Geochimica et Cosmochimica Acta* 60, 1849-1871.
- Beyssac, O., Goffé, B., Chopin, C., Rouzaud, J., 2002. Raman spectra of carbonaceous material in metasediments: a new geothermometer. *Journal of Metamorphic Geology* 20, 859-871.
- Bierlein, F.P., Cartwright, I., McKnight, S., 2001. The role of carbonaceous "indicator" slates in the genesis of lode gold mineralization in the Western Lachlan Orogen, Victoria, Southeastern Australia. *Economic Geology* 96, 431-451.
- Bishop, D., Bradshaw, J., Landis, C., Turnbull, I., 1976. Lithostratigraphy and structure of the Caples terrane of the Humboldt Mountains, New Zealand. *New Zealand Journal of Geology and Geophysics* 19, 827-848.
- Chen, J., Walter, M.R., Logan, G.A., Hinman, M.C., Summons, R.E., 2003. The Paleoproterozoic McArthur River (HYC) Pb/Zn/Ag deposit of northern Australia: organic geochemistry and ore genesis. *Earth and Planetary Science Letters* 210, 467-479.
- Cline, J.S., Hofstra, A.H., Muntean, J.L., Tosdal, R.M., Hickey, K.A., 2005. Carlin-type gold deposits in Nevada: Critical geologic characteristics and viable models. *Economic Geology 100th Anniversary Volume* 100, 451-484.
- Coombs, D., Landis, C., Norris, R., Sinton, J., Borns, D., Craw, D., 1976. The Dun Mountain Ophiolite Belt, New Zealand, its tectonic setting, constitution, and

- origin, with special reference to the southern portion. *American Journal of Science* 276, 561-603.
- Cooper, R., 1975. New Zealand and south-east Australia in the early Paleozoic. *New Zealand Journal of Geology and Geophysics* 18, 1-20.
- Cox, S., Sun, S., Etheridge, M., Wall, V., Potter, T., 1995. Structural and geochemical controls on the development of turbidite-hosted gold quartz vein deposits, Wattle Gully mine, central Victoria, Australia. *Economic Geology* 90, 1722-1746.
- Craw, D., 1992. Fluid evolution, fluid immiscibility and gold deposition during Cretaceous-Recent tectonics and uplift of the Otago and Alpine Schist, New Zealand. *Chemical Geology* 98, 221-236.
- Craw, D., 2002. Geochemistry of late metamorphic hydrothermal alteration and graphitisation of host rock, Macraes gold mine, Otago Schist, New Zealand. *Chemical Geology* 191, 257-275.
- Craw, D., MacKenzie, D., Pitcairn, I., Teagle, D., Norris, R., 2007. Geochemical signatures of mesothermal Au-mineralized late-metamorphic deformation zones, Otago Schist, New Zealand. *Geochemistry: Exploration, Environment, Analysis* 7, 225-232.
- Craw, D., Mortensen, J., MacKenzie, D., Pitcairn, I., 2015. Contrasting geochemistry of orogenic gold deposits in Yukon, Canada and Otago, New Zealand. *Geochemistry: Exploration, Environment, Analysis* 15, 150-166.
- Craw, D., Windle, S., Angus, P., 1999. Gold mineralization without quartz veins in a ductile-brittle shear zone, Macraes Mine, Otago Schist, New Zealand. *Mineralium Deposita* 34, 382-394.
- De Ronde, C.E., Faure, K., Bray, C.J., Whitford, D.J., 2000. Round Hill shear zone-hosted gold deposit, Macraes Flat, Otago, New Zealand: evidence of a magmatic ore fluid. *Economic Geology* 95, 1025-1048.
- Emsbo, P., Koenig, A., 2007. Transport of Au in petroleum: evidence from the northern Carlin trend, Nevada, Digging Deeper, Proceedings of the 9th Biennial SGA Meeting.

- Evans, K., Phillips, G., Powell, R., 2006. Rock-buffering of auriferous fluids in altered rocks associated with the Golden Mile-style mineralization, Kalgoorlie gold field, Western Australia. *Economic Geology* 101, 805-817.
- Evans, K.A., 2010. A test of the viability of fluid–wall rock interaction mechanisms for changes in opaque phase assemblage in metasedimentary rocks in the Kambalda-St. Ives goldfield, Western Australia. *Mineralium Deposita* 45, 207-213.
- Fleming, C.A., 1979. *The geological history of New Zealand and its life*. Auckland University Press.
- Freise, F.W., 1931. The transportation of gold by organic underground solutions. *Economic Geology* 26, 421-431.
- Gammons, C.H., Williams-Tones, A., 1995. The solubility of Au-Au alloy + AgCl in HCl/NaCl solutions at 300° C: New data on the stability of Au (I) chloride complexes in hydrothermal fluids. *Geochimica et Cosmochimica Acta* 59, 3453-3468.
- Gammons, C.H., Yu, Y., Williams-Jones, A., 1997. The disproportionation of gold (I) chloride complexes at 25 to 200 C. *Geochimica et Cosmochimica Acta* 61, 1971-1983.
- Gatellier, J.-P., Disnar, J.-R., 1989. Organic matter and gold-ore association in a hydrothermal deposit, France. *Applied Geochemistry* 4, 143-149.
- Gibert, F., Pascal, M.-L., Pichavant, M., 1998. Gold solubility and speciation in hydrothermal solutions: Experimental study of the stability of hydrosulphide complex of gold (AuHS) at 350 to 450 °C and 500 bars. *Geochimica et Cosmochimica Acta* 62, 2931-2947.
- Gize, A., Barnes, H., 1994. Organic contributions to Mississippi Valley-type lead-zinc genesis—a critical assessment, *Sediment-Hosted Zn-Pb Ores*. Springer, pp. 13-26.
- Gregory, D.D., Large, R.R., Bath, A.B., Steadman, J.A., Wu, S., Danyushevsky, L., Bull, S.W., Holden, P., Ireland, T.R., 2016. Trace Element Content of Pyrite from the Kapaï Slate, St. Ives Gold District, Western Australia. *Economic Geology* 111, 1297-1320.

- Henley, R., 1973. Solubility of gold in hydrothermal chloride solutions. *Chemical Geology* 11, 73-87.
- Henne, A., Craw, D., 2012. Synmetamorphic carbon mobility and graphite enrichment in metaturbidites as a precursor to orogenic gold mineralisation, Otago Schist, New Zealand. *Mineralium Deposita*, 1-17.
- Ho, E.S., Mauk, J.L., 1996. Relationship between organic matter and copper mineralization in the Proterozoic Nonesuch Formation, northern Michigan. *Ore Geology Reviews* 11, 71-87.
- Ho, E.S., Meyers, P.A., Mauk, J.L., 1990. Organic geochemical study of mineralization in the Keweenaw Nonesuch Formation at White Pine, Michigan. *Organic Geochemistry* 16, 229-234.
- Kashefi, K., Tor, J.M., Nevin, K.P., Lovley, D.R., 2001. Reductive precipitation of gold by dissimilatory Fe (III)-reducing bacteria and archaea. *Applied and Environmental Microbiology* 67, 3275-3279.
- Landais, P., 1996. Organic geochemistry of sedimentary uranium ore deposits. *Ore Geology Reviews* 11, 33-51.
- Landis, C., 1971. Graphitization of dispersed carbonaceous material in metamorphic rocks. *Contributions to Mineralogy and Petrology* 30, 34-45.
- Landis, C., Coombs, D., 1967. Metamorphic belts and orogenesis in southern New Zealand. *Tectonophysics* 4, 501-518.
- Large, R., Thomas, H., Craw, D., Henne, A., Henderson, S., 2012. Diagenetic pyrite as a source for metals in orogenic gold deposits, Otago Schist, New Zealand. *New Zealand Journal of Geology and Geophysics* 55, 137-149.
- Large, R.R., Bull, S.W., Maslennikov, V.V., 2011. A carbonaceous sedimentary source-rock model for Carlin-type and orogenic gold deposits. *Economic Geology* 106, 331-358.
- Lengke, M., Southam, G., 2006. Bioaccumulation of gold by sulfate-reducing bacteria cultured in the presence of gold (I)-thiosulfate complex. *Geochimica et Cosmochimica Acta* 70, 3646-3661.

- Lengke, M.F., Southam, G., 2007. The deposition of elemental gold from gold (I)-thiosulfate complexes mediated by sulfate-reducing bacterial conditions. *Economic Geology* 102, 109-126.
- Leventhal, J., Giordano, T., 2000. The nature and roles of organic matter associated with ores and ore-forming systems: An introduction. *Reviews in Economic Geology* 9, 1-26.
- Leventhal, J.S., Daws, T.A., Frye, J.S., 1986. Organic geochemical analysis of sedimentary organic matter associated with uranium. *Applied Geochemistry* 1, 241-247.
- Libes, S., 2011. *Introduction to marine biogeochemistry*. Academic Press.
- Lungwitz, E., 1900. The lixiviation of gold deposits by vegetation. *Engineering and Mining Journal* 69, 500-502.
- Luque del Villar, F.J., Pasteris, J.D., Wopenka, B., Rodas, M., Fernández Barrenechea, J.M., 1998. Natural fluid-deposited graphite: mineralogical characteristics and mechanisms of formation. *American Journal of Science* 298, 471-498.
- Luque, F., Ortega, L., Barrenechea, J.F., Millward, D., Beyssac, O., Huizenga, J.M., 2009. Deposition of highly crystalline graphite from moderate-temperature fluids. *Geology* 37, 275-278.
- MacKenzie, D., Craw, D., Cooley, M., Fleming, A., 2010. Lithochemical localisation of disseminated gold in the White River area, Yukon, Canada. *Mineralium Deposita* 45, 683-705.
- MacKinnon, T.C., 1983. Origin of the Torlesse terrane and coeval rocks, South Island, New Zealand. *Geological Society of America Bulletin* 94, 967-985.
- McKeag, S., Craw, D., Norris, R., 1989. Origin and deposition of a graphitic schist-hosted metamorphogenic Au-W deposit, Macraes, East Otago, New Zealand. *Mineralium Deposita* 24, 124-131.
- Mernagh, T.P., Bierlein, F.P., 2008. Transport and precipitation of gold in Phanerozoic metamorphic terranes from chemical modeling of fluid-rock interaction. *Economic Geology* 103, 1613-1640.

- Moore, J., Doyle, S., 2015. Resource definition in the world-class Macraes gold mine, New Zealand, Proceedings, PACRIM Congress, AusIMM Publication Series, pp. 557-564.
- Mortimer, N., 1993. Jurassic tectonic history of the Otago schist, New Zealand. *Tectonics* 12, 237-244.
- Mortimer, N., 2000. Metamorphic discontinuities in orogenic belts: example of the garnet-biotite-albite zone in the Otago Schist, New Zealand. *International Journal of Earth Sciences* 89, 295-306.
- Mortimer, N., Roser, B., 1992. Geochemical evidence for the position of the Caples–Torlesse boundary in the Otago Schist, New Zealand. *Journal of the Geological Society* 149, 967-977.
- Norris, R., Craw, D., 1987. Aspiring Terrane: an oceanic assemblage from New Zealand and its implications for terrane accretion in the southwest Pacific. *Terrane Accretion and Orogenic Belts*, 169-177.
- Ohmoto, H., Kerrick, D., 1977. Devolatilization equilibria in graphitic systems. *American Journal of Science* 277, 1013-1044.
- Oliver, N.H., Cleverley, J.S., Mark, G., Pollard, P.J., Fu, B., Marshall, L.J., Rubenach, M.J., Williams, P.J., Baker, T., 2004. Modeling the role of sodic alteration in the genesis of iron oxide-copper-gold deposits, Eastern Mount Isa block, Australia. *Economic Geology* 99, 1145-1176.
- Ong, H.L., Swanson, V.E., Bisque, R.E., 1970. Natural organic acids as agents of chemical weathering. *Geological Survey Research*, 130-137.
- Phillips, G., Evans, K., 2004. Role of CO₂ in the formation of gold deposits. *Nature* 429, 860-863.
- Pitcairn, I.K., Craw, D., Teagle, D.A., 2014a. Metabasalts as sources of metals in orogenic gold deposits. *Mineralium Deposita* 50, 1-18.
- Pitcairn, I.K., Olivo, G.R., Teagle, D.A., Craw, D., 2010. Sulfide evolution during prograde metamorphism of the Otago and Alpine schists, New Zealand. *The Canadian Mineralogist* 48, 1267-1295.

- Pitcairn, I.K., Roberts, S., Teagle, D.A., Craw, D., 2005. Detecting hydrothermal graphite deposition during metamorphism and gold mineralization. *Journal of the Geological Society* 162, 429-432.
- Pitcairn, I.K., Teagle, D.A., Craw, D., Olivo, G.R., Kerrich, R., Brewer, T.S., 2006. Sources of metals and fluids in orogenic gold deposits: insights from the Otago and Alpine Schists, New Zealand. *Economic Geology* 101, 1525-1546.
- Radtke, A.S., Scheiner, B.J., 1970. Studies of hydrothermal gold deposition-(pt.) 1, carlin gold deposit, Nevada, the role of carbonaceous materials in gold deposition. *Economic Geology* 65, 87-102.
- Renders, P., Seward, T., 1989. The stability of hydrosulphido- and sulphido-complexes of Au (I) and Ag (I) at 25 °C. *Geochimica et Cosmochimica Acta* 53, 245-253.
- Rieger, A., Schwark, L., Cisternas, M.-E., Miller, H., 2008. Genesis and evolution of Bitumen in Lower Cretaceous lavas and implications for strata-bound copper deposits, North Chile. *Economic Geology* 103, 387-404.
- Seward, T.M., 1973. Thio complexes of gold and the transport of gold in hydrothermal ore solutions. *Geochimica et Cosmochimica Acta* 37, 379-399.
- Shenberger, D., Barnes, H., 1989. Solubility of gold in aqueous sulfide solutions from 150 to 350 C. *Geochimica et Cosmochimica Acta* 53, 269-278.
- Shvarov, Y.V., Bastrakov, E., 1999. HCh: a software package for geochemical equilibrium modelling. User's guide. Australian Geological Survey Organisation. *Science and Resources, Record* 25, 61.
- Simoneit, B., Gize, A., 2000. Analytical techniques for organic matter characterization in ore deposits. *Ore genesis and exploration: the roles of organic matter. Reviews in Economic Geology* 9, 27-61.
- Spangenberg, J.E., Macko, S.A., 1998. Organic geochemistry of the San Vicente zinc-lead district, eastern Pucará Basin, Peru. *Chemical Geology* 146, 1-23.
- Spirakis, C.S., 1996. The roles of organic matter in the formation of uranium deposits in sedimentary rocks. *Ore Geology Reviews* 11, 53-69.

- Stefánsson, A., Seward, T., 2003. Stability of chloridogold (I) complexes in aqueous solutions from 300 to 600 °C and from 500 to 1800 bar. *Geochimica et Cosmochimica Acta* 67, 4559-4576.
- Stefánsson, A., Seward, T., 2004. Gold (I) complexing in aqueous sulphide solutions to 500 °C at 500 bar. *Geochimica et Cosmochimica Acta* 68, 4121-4143.
- Tomkins, A.G., 2013. On the source of orogenic gold. *Geology* 41, 1255-1256.
- Turnbull, I., Mortimer, N., Craw, D., 2001. Textural zones in the Haast Schist—a reappraisal. *New Zealand Journal of Geology and Geophysics* 44, 171-183.
- Upton, P., Craw, D., 2008. Modelling the role of graphite in development of a mineralised mid-crustal shear zone, Macraes mine, New Zealand. *Earth and Planetary Science Letters* 266, 245-255.
- Upton, P., Craw, D., 2014. Modelling of structural and lithological controls on mobility of fluids and gold in orogenic belts, New Zealand. Geological Society, London, Special Publications 402, 231-253.
- Williams-Jones, A., Migdisov, A., 2007. The solubility of gold in crude oil: implications for ore genesis, Proceedings of the 9 th Biennial SGA Meeting, Dublin. Millpress, pp. 765-768.
- Williams-Jones, A.E., Bowell, R.J., Migdisov, A.A., 2009. Gold in solution. *Elements* 5, 281-287.
- Wood, S.A., Crerar, D.A., Borcsik, M.P., 1987. Solubility of the assemblage pyrite-pyrrhotite-magnetite-sphalerite-galena-gold-stibnite-bismuthinite-argen-tite-molybdenite in H₂O-NaCl-CO₂ solutions from 200 °C to 350 °C. *Economic Geology* 82, 1864-1887.
- Zhang, J., Lu, J., Zhai, J., Yang, F., 1997. Simulating experiments on enrichment of gold by bacteria and their geochemical significance. *Chinese Journal of Geochemistry* 16, 369-373.
- Zhuang, H., Lu, J., Fu, J., Ren, C., Zou, D., 1999. Crude oil as carrier of gold: petrological and geochemical evidence from Lannigou gold deposit in southwestern Guizhou, China. *Science in China Series D: Earth Sciences* 42, 216-224.

Zotov, A., Baranova, N., Dar'yina, T., Bannykh, L., 1991. The solubility of gold in aqueous chloride fluids at 350-500 °C and 500-1500 atm: Thermodynamic parameters of AuCl_2 (aq) up to 750 °C and 5000 atm. *Geochemistry International* 28, 63-71.

Chapter 2

Applications of conventional organic geochemical methods to samples from three gold deposits

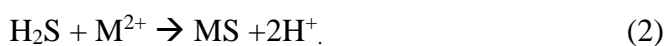
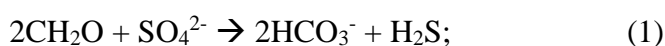
This chapter describes the application of conventional organic geochemical methods to characterize carbonaceous materials (CM) associated with three gold deposits. Gold deposits studied are from the St. Ives goldfield and the Wiluna lode-gold deposits in Western Australia, and the Macraes gold deposit in New Zealand. Methods used include elemental analysis (C, N, S), Rock-Eval analysis and gas chromatography–mass spectrometry (GC-MS), which are common approaches used to determine the maturity and molecular composition of CM in sedimentary rocks. However, due to the high maturity of CM in the studied deposits, where temperatures have exceeded those associated with the oil and gas generation window, results from conventional organic geochemistry techniques provided only limited information.

2.1 Introduction

2.1.1 CM and metals

Conventional organic geochemistry techniques are most often applied to petroleum systems, which contain a high proportion of hydrocarbons, and with maximum temperatures below that of closure of the oil window. However, in recent decades, hydrocarbons in mineral systems have received increasing attention. CM is found in several significant ore deposits and is thought to play roles in the source, transportation and deposition of ore metals (Chen et al., 2003; Gatellier and Disnar, 1989; Holman et al., 2014; Large et al., 2009; Leventhal et al., 1986; Rieger et al., 2008; Williford et al., 2011). Most CM is thought to originate as living organisms, such as Bacteria, Archaea and Eukaryotes, though some occurs as a consequence of abiotic process (Leventhal and Giordano, 2000; Simoneit and Gize, 2000). Those living organisms, as the precursors of CM, have been reported to play an active role in concentrating and precipitating metals (Beveridge, 1988; Greenwood et al., 2013;

Lengke and Southam, 2006; Lengke and Southam, 2007; Pósfai and Dunin-Borkowski, 2006). For example, during the metabolism of organisms, bacterial surfaces serve as nucleation sites for metals, which are termed biologically induced mineralization (Pósfai and Dunin-Borkowski, 2006). The surfaces of bacterial cells, which include carboxyl, phosphate and nitrogenous groups, are commonly characterized by negative charge and can react with positive ions, such as metallic cations, with the consequence that metals are easily adsorbed by bacterial walls (Beveridge, 1988; Greenwood et al., 2013). Sulfate reducing bacteria (SRB), which can precipitate primary sulfides at low temperature in anoxic environments, are particular bacteria that can also generate biogenic H₂S (Grice et al., 2005; Labrenz and Banfield, 2004; Labrenz et al., 2000; Plet et al., 2016; Rickard, 1970). These biogenic processes commonly occur at low temperature, below 80 °C. In addition, SRB have been reported to destabilize gold-thiosulfate complexes (Au(S₂O₃)₂³⁻) so that gold is precipitated on the bacterial cell from solution (Lengke and Southam, 2006; Lengke and Southam, 2007). CM can also facilitate metal deposition in an abiotic way as an electron donor in thermochemical sulfate reduction (TSR). TSR is, however, less efficient than biogenic processes, but is still geologically significant (Machel, 2001). TSR generally happens at a higher temperature, around 100–140 °C (Machel, 2001). Several TSR reactions have been proposed to facilitate the precipitation of metals by Rieger et al. (2008), Chen et al. (2003) and Machel et al. (1995). For example, in the Here's Your Chance (HYC) Pb, Zn and Ag deposit, Chen et al. (2003) suggested that reactions like (1) occur during sulfidation (2).



During TSR processes, CM is oxidized to produce hydrogen sulfide that reacts with metals in hydrothermal brines (Chen et al., 2003).

In addition to these bacterial activities, CM can react with metals to form metal-organic complexes and transport metals to the sites of deposition (Manning and Gize, 1993). In low temperature supergene deposits, metals have been reported to be carried by humic and fulvic acids in aqueous solutions (Baker, 1978; Giordano, 2000; Ong et al., 1970). In hydrothermal deposits, organosulfur ligands have been reported to mobilize and transport metals (Fein and Williams-Jones, 1997; Giordano, 2000; Giordano, 1994). Some metals, such as Fe, Pb and Zn, can be transported by

carboxylate and acetate complexes in certain environments, reviewed by Giordano (2000). In hydrocarbon liquids, ore metals such as V, Zn, Fe, and Ni have been observed to be complexed by porphyrin as metallo-porphyrins (Eckardt et al., 1989; Gize, 1999; Gize and Barnes, 1987; Grice et al., 1996; Grice et al., 1997). These metals may be released into a coexisting aqueous phase as the organic matter becomes thermally mature, e.g., in Mississippi Valley-type deposits (Giordano, 2000).

2.1.2 CM and Au

Gold occurs at high concentrations in black shales equalling at least three times that of the average concentration in continental crust (Bavinton and Keays, 1978; Coveney et al., 1992; Crocket and Kuo, 1979; Large et al., 2011; Wedepohl, 1995). Black shales, which contain abundant CM, have been suggested to be well-endowed not only with gold but with other associated metals, and to act as source of metals for orogenic and Carlin-type sediment-hosted gold deposits (Ketris and Yudovich, 2009; Large et al., 2011). CM in black shales is thought to be responsible for concentration of gold and other trace elements from sea water (Large et al., 2011; Zhang et al., 1997). Further, CM may act as a transport agent for gold (reviewed in **Chapter 7**) and promote the precipitation of gold (reviewed in **Chapter 6**). However, for most CM related gold deposits, detailed organic geochemical information about CM, including molecular composition, which is necessary if we are to understand organic-metal interactions, is still poorly understood. Characterization of CM in those deposits via organic geochemical approaches is, therefore, of great importance for us to reconstruct the depositional environment of CM and recognize the source of CM, its alteration during mineralization, and infer the role of CM in ore-forming processes.

2.1.3 CM characterization

Deposited CM will become highly mature, losing chemical function and becoming crystalline graphite, as temperature increases and given sufficient time (Simoneit and Gize, 2000) (reviewed in **Chapter 1**). During diagenesis, the hydrocarbon skeleton molecules are known as “biomarkers”. These molecules are molecular fossils of

biological compounds and may have suffered molecular alteration since the death of the precursor living organisms (Greenwood et al., 2013; Simoneit and Gize, 2000). Those biomarkers found in ore deposits give us insights into depositional environments, the source of CM, and provide a record of organic-inorganic interactions and CM alteration during the formation of ore deposits (Greenwood et al., 2013; Holman et al., 2014; Peters et al., 2007; Williford et al., 2011).

Conventional organic geochemistry methods, including elemental analysis, Rock-Eval analysis, and GC-MS analysis, which have been used to characterize the hydrocarbon composition and properties of oil and gas, can help us to investigate the CM precursors and evolution in sediments (Greenwood et al., 2013; Holman et al., 2014; Holman et al., 2012; Jaraula et al., 2015; Peters et al., 2005; Simoneit and Gize, 2000). Rock-Eval pyrolysis is a conventional and rapid method used in petroleum research to help to assess the petroleum potential of organic matter in sedimentary rocks (Behar et al., 2001; Hare et al., 2014; Lafargue et al., 1998). GC-MS is another powerful technique; GC can provide very effective separation of many non-polar hydrocarbons while MS can unravel the complexities of hydrocarbon mixtures (Eiserbeck et al., 2012; Simoneit and Gize, 2000).

The research areas discussed here are located in Western Australia and on the South Island of New Zealand (Figure 2.1). In Western Australia, most gold deposits are hosted by Archean rocks, which have contributed about half of the world gold production (Phillips and Groves, 1983; Woodall, 1979). The St. Ives goldfield and the Wiluna lode-gold deposits in Western Australia are hosted by, or associated with, a black shale unit called the Kapaï Slate (McCall, 1970). This spatial association has been used as the basis for the suggestion of a potential association between CM and gold mineralization. In the Macraes gold deposit, which is hosted by the Otago Schist of New Zealand, gold is found disseminated in graphitic schists and it has been proposed that CM in the schist precipitated gold by reducing Au-bisulfide complexes in solution (Craw, 2002; McKeag et al., 1989). In spite of the potentially critical role of CM in these deposits, its organic geochemical characteristics of CM in these gold deposits have received limited attention. In this chapter, organic geochemistry methods are applied to samples from those deposits to help address the characteristics of CM and the possible role played by CM during the formation of gold deposits is discussed.

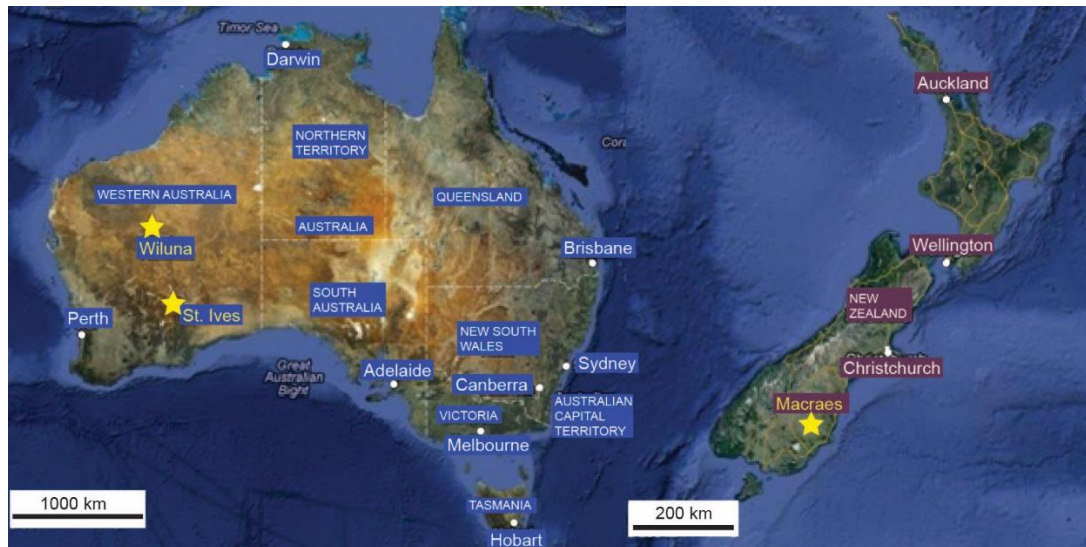


Figure 2.1 Location of the three gold deposits studied in detail in this chapter (highlighted by yellow stars; Modified from Google Maps).

2.2 Geological background and sampling

2.2.1 St. Ives goldfield

The St. Ives goldfield, which has a production up to 300 t to date (Prendergast, 2007), is located in the south of the Norseman-Wiluna greenstone belt in the Eastern Goldfields province of the Yilgarn Craton in Western Australia (Figure 2.2) (Evans, 2010). The deposits developed in the Kambalda corridor, which consists of the Kalgoorlie Group, Black Flag Group, and Merougil Formation (Prendergast, 2007). The Kalgoorlie Group consists of a sequence of metamorphosed Archean komatiite and basalt flows, together with minor interflow sediments (Cox and Ruming, 2004; Roberts and Elias, 1990), including up to 10 m of carbonaceous and sulfidic argillites of the Kapai Slate (Prendergast, 2007). The Black Flag Group represents a sequence of clastic sedimentary rocks and felsic volcanic-volcaniclastic rocks, which is intruded by the differentiated Condenser dolerite, gabbro and peridotite sills (Kendrick et al., 2011; Prendergast, 2007). The Merougil Formation comprises rudites, arenites and minor argillites (Prendergast, 2007). The host rock sequence has been metamorphosed to upper greenschist to lower amphibolite facies (Neumayr et al., 2008).

The mineralization area is constrained by the NNW-trending Boulder-Lefroy Fault Zone (BLFZ) in the east and Speedway Fault Zone (SFZ) in the west and has

undergone four deformation events, that produced gold-bearing shear zones (Figure 2.2) (Prendergast, 2007). D1 produced regional northward-directed thrusts, such as the Foster Thrust (FT). D2, which is a NE-SW compression, caused upright, NNW-trending gently plunging folds, such as the Kambalda anticline. D3, which involved SE-NW compression, generated brittle to ductile transition shear zones, which are associated with gold mineralization. D4 produced NW-trending faults that offset earlier structures.

Gold mineralization occurred at 2.65-2.60 Ga and is hosted by various rocks from the Kalgoorlie Group and Black Flag Group (Kendrick et al., 2011). Wall rocks that are adjacent to faults, shear zones and quartz-carbonate veins have undergone hydrothermal alteration. The hydrothermal fluids have left footprints in the form of veins and disseminated sulfide and oxide minerals, e.g. pyrite-magnetite or pyrrhotite-magnetite assemblages (Evans, 2010; Neumayr et al., 2008). Gold is present in pyrite-rich quartz veins or disseminated in alteration zones. Gold is thought to have been transported by aqueous metamorphic fluids and deposited due to fluid-rock interaction in which Au-bisulfide complexes were destabilized (Evans, 2010).

Samples were collected from drill cores that penetrate the Kapaï Slate. There are 13 samples in total from hole CD16056. The depth of the samples ranges from 224 to 811 m (Table 2.1).

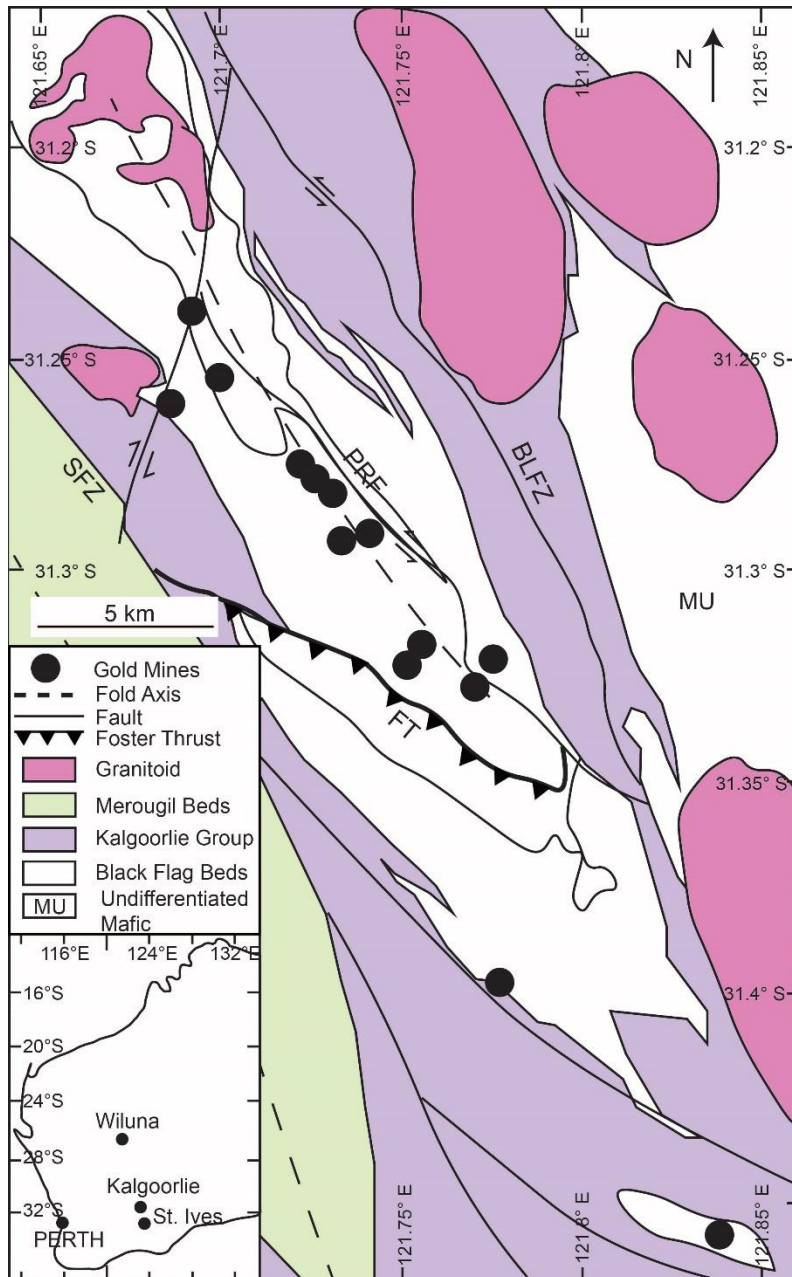


Figure 2.2 Geological map of St. Ives goldfield. BLFZ: Boulder–Lefroy Fault Zone; SFZ: Speedway Fault Zone; FT: Foster Thrust; PRF: Playa–Repulse Fault. Modified from Prendergast (2007).

Table 2.1 List of samples, including sample locations, ID and depth.

Sample Name	Location	Hole_ID	Depth (m)
KS-21	Kambalda WA	CD16056	224.0-224.20
KS-22	Kambalda WA	CD16056	667.90-678.20
KS-23	Kambalda WA	CD16056	684.60-684.80
KS-24	Kambalda WA	CD16056	693.30-693.50
KS-25	Kambalda WA	CD16056	794.00-794.50
KS-26	Kambalda WA	CD16056	796.00-796.30
KS-27	Kambalda WA	CD16056	796.80-797.30
KS-28	Kambalda WA	CD16056	797.60-797.80
KS-29	Kambalda WA	CD16056	798.15-798.40
KS-30	Kambalda WA	CD16056	805.80-806.00
KS-31	Kambalda WA	CD16056	807.50-807.70
KS-32	Kambalda WA	CD16056	810.40-810.60
KS-33	Kambalda WA	CD16056	810.75-810.95

2.2.2 Wiluna lode-gold deposits

The Wiluna lode-gold deposits, which have produced around 150 t Au to date (Hagemann and Cassidy, 2000), are situated in the northernmost part of the Norseman-Wiluna greenstone belt in the Archean Yilgarn Block of Western Australia, about 550 km north of Kalgoorlie (Figure 2.3) (Eilu and Mikucki, 1998; Hagemann and Lüders, 2003). The deposits are hosted by mafic and ultramafic lava flows with interflow sediments (Hagemann et al., 1992). The stratigraphy has been subdivided into an older greenstone series and a younger greenstone series (Hagemann et al., 1992). The older greenstone series consists of flow I, including felsic porphyries, felsic dikes, interflow sedimentary and quartz reefs, flow II, consisting of felsic sill, dolerite units and komatiitic basalt units, and flow III, which contains felsic dikes, dolerite dikes, quartz reef and interflow sedimentary material including siltstone, mudstone and black shale (Hagemann et al., 1992). In contrast to the St. Ives goldfield, which has been metamorphosed to greenschist to amphibolite facies, Wiluna only suffered very low grade metamorphism, up to prehnite-pumpellyite facies (Hagemann et al., 1992).

Mineralization at Wiluna is controlled by the Wiluna strike-slip fault system, which consists of multiple dextral strike-slip faults and multiple displacements with

dominantly brittle deformation. Four sets of structures have been recognized in previous studies (Hagemann et al., 1992). D1 structures are associated with upright folding of the greenstone sequence, during which the rocks were metamorphosed to prehnite-pumpellyite facies. D2 structures are related to regional fracture sets. D3 is associated with the Wiluna strike-slip fault system, which shows a maximum displacement of 1350 m. D3 structures facilitate the mineralization, whereas D4 structures, which accompany emplacement of an east-west dolerite dike, are thought to have formed during a Proterozoic tectonic event.

Mineralization occurred in two stages, according to Hagemann and Cassidy (2000). In stage 1, gold, together with pyrite and arsenopyrite, was finely disseminated in alteration halos in the hanging wall of brittle fault zones. Associated alteration ranges from rutile+chlorite+carbonate to carbonate+chlorite+sericite+fuchsite from distal to proximal zones. Gold is commonly present in arsenopyrite and pyrite as small inclusions. In stage 2, gold was precipitated with stibnite in massive quartz veins and brecciated wall rock, accompanied by accessory arsenopyrite and pyrite. Gold deposition is thought to have resulted from a reduction in the concentration of H₂S in hydrothermal fluids (Hagemann and Lüders, 2003).

Two samples from Wiluna were studied in detail. These samples are sulfidic shales from Albion Downs, Agnew-Wiluna Belt. The samples are from drill cores with drilling IDs of BBW-15 and BBW-18, respectively.

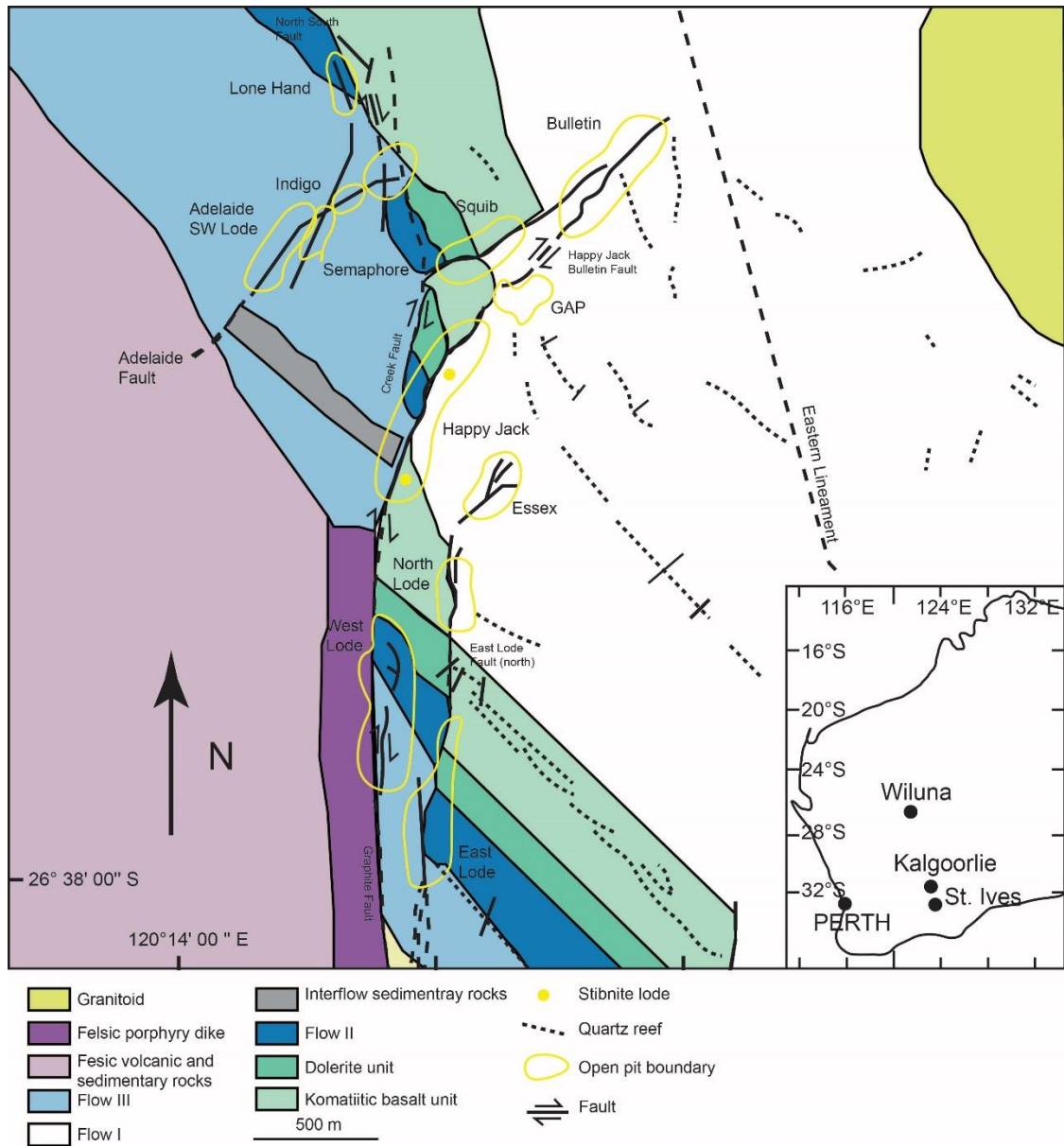


Figure 2.3 Geological map of the Wiluna lode gold deposit. Modified from Hagemann and Lüders (2003).

2.2.3 Macraes gold deposit

The geological background of the Macraes gold deposit was summarised in **Chapter 1** (section 1.2). The features of the three study areas are summarized in Table 2.2.

Table 2.2 A summary of characteristics of three gold deposits (Craw, 2002; Hagemann and Cassidy, 2000; Hagemann and Lüders, 2003; Neumayr et al., 2008).

Au Deposit	Au Province	Mineralization Age	Location	Classification	Host Rock	Metamorphism	Size	Au Grade
St. Ives	Eastern Goldfields Province	Neoproterozoic (2650-2600 Ma)	Western Australia	Orogenic	Meta-komatiite and basalt, Kapii slate	Greenschist facies	265 t	3.42 g/t
Wiluna	Eastern Goldfields Province	Neoproterozoic (minimum ages, 2749±7 Ma)	Western Australia	Orogenic	Meta-volcanic rocks and interflow sediments	Up to prehnite-pumpellyite facies	150 t	
Macraes	Macraes gold deposit	Mesozoic (150-130 Ma)	New Zealand	Orogenic	Meta-turbidites	Lower greenschist facies	300 t	1.6g/t

2.3 Methods

Sample processing included core/rock sampling, powder crushing, organic extraction and characterization (Figure 2.4).

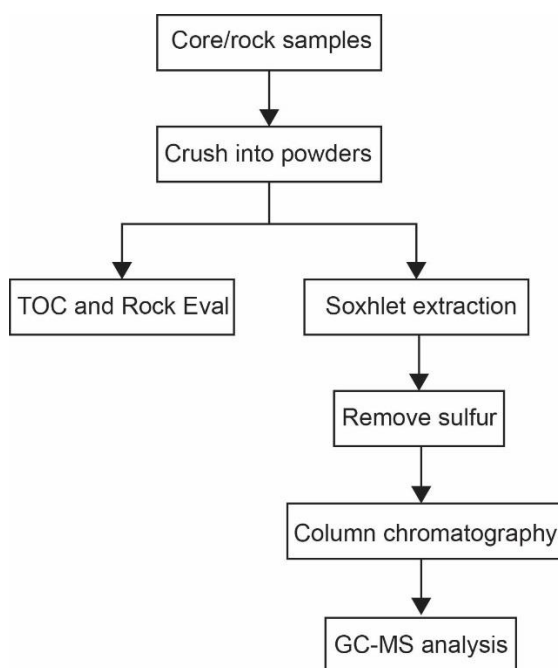


Figure 2.4 Flowchart diagram of sample processing.

2.3.1 Element analysis

Samples were crushed into powder in a tungsten carbide ring mill for non-carbonate carbon (NCC), total nitrogen (TON) and total sulfur (TOS) analysis. Analyses were conducted by Intertek Genalysis Lab (Perth, Australia) and the Organic Geochemistry Laboratory in Kiel University. For analysis at the Intertek Genalysis Lab, samples were treated with dilute acid to remove carbonate, and the residue was analyzed for NCC using infrared spectroscopy. For analysis at the Organic Geochemistry Laboratory of Kiel University, samples were pre-treated with hydrochloride (HCl) to remove the carbonate and the NCC, N and S contents were analyzed with an Elementar III Elemental Analyser without further pre-treatment (Jaraula et al., 2015).

2.3.2 Rock-Eval analysis

Powder samples were analyzed by Rock–Eval using a VINCI Rock-Eval-II+ instrument at the Organic Geochemistry Laboratory of Kiel University (Jaraula et al., 2015). Details of the method are provided in Lüniger and Schwark (2002) and Simoneit and Gize (2000). Briefly, the most NCC-rich bulk dried powder samples are heated in a helium atmosphere. Mobile hydrocarbons are produced during heating, which are quantified by flame-ionisation detection. The S1 detector records mobile or free hydrocarbons which are thermo-vaporizable at 300 °C. These are assumed to give information on hydrocarbons produced during the geological processes such as diagenesis and catagenesis. The S2 detector records hydrocarbon compounds that would be liberated by kerogen produced during deeper burial or some other heating process between 300 and 550 °C. The ratio of the amount of hydrocarbons generated during heating and the total organic carbon represents the hydrogen index (HI) (mg HC/g TOC). During heating, CO₂ is generated from organic matter between 300–390 °C, and is quantified by the S3 detector, and the ratio of the amount of CO₂ released to the total amount of organic carbon represents the oxygen content (OI) (mg CO₂/g TOC). The temperature of maximum yield on S2 is recorded as T_{max} (°C). Therefore, during Rock-Eval pyrolysis, S1, S2, S3 and T_{max} values were measured and corresponding HI and OI values calculated.

2.3.3 GC-MS

Before direct injection of samples into the GC-MS, powder samples need to be pre-treated via Soxhlet extraction to extract the organics and remove sulphur. Sulfur removal is important because sulphur can interfere with the results.

Soxhlet extraction

Powdered samples were accurately weighed into a pre-extracted (DCM (dichloromethane): MeOH (methanol), 9:1) cellulose thimble. Anti-bumping granules were placed in the thimble. The top of the thimble was plugged with pre-extracted glass wool. The extraction was performed using a Soxhlet apparatus, with a mixture of DCM and MeOH (9:1, respectively). The extraction was allowed to proceed for at least 72 hours, or until the solvent was colourless.

Sulfur removal

The dissolved extracts were placed in n-hexane, and copper turnings, which had been activated with HCl and rinsed with MilliQ water, were added. The solutions were left to stand for more than one hour. The n-hexane was removed from the vial along with the copper/extract mixture and filtered through a packed, cleaned Pasteur pipette. The filtered n-hexane was then collected as the “sulphur-free extract”. The copper turnings were rinsed twice with n-hexane and the rinsing solution was filtered. This filtered n-hexane was combined with the sulphur-free extract. The copper turnings were then rinsed twice more with DCM, which was then filtered and combined with the previous aliquots of collected n-hexane. The packed Pasteur pipette was then rinsed with two volumes of DCM, which was combined with the filtered DCM.

Small scale column chromatography (1-20 mg)

Silica gel 60 (0.063-0.200 mm, MERCK) for column chromatography was activated at 120 °C for at least 8 hours, and pre-rinsed with n-hexane prior to use. The extract solutions were added to the top of a small column (5.5 cm x 0.5 cm i.d.) of activated silica gel. The aliphatic hydrocarbon (saturate), aromatic and polar fraction was eluted with n-pentane, 30 % DCM in n-pentane and 1:1 (by volume) DCM:MeOH respectively (Holman et al., 2012). Solvents were then vapored at 60 °C on a sand bath.

GC-MS

Extracts from last step were analysed by GC-MS using a Hewlett Packard (HP) 6890 gas chromatograph (GC) equipped with a DB5-MS column (60 m × 0.25 mm i.d × 0.25 µm film thickness) and coupled to a HP 5973 mass selective detector (Holman et al., 2012; Jaraula et al., 2015). Helium was used as the carrier gas. Saturated hydrocarbons were dissolved in n-hexane and injected into a split-splitless injector in pulsed splitless mode. The GC oven temperature was increased from 40 °C to 310 °C at 3 °C per minute then held for 30 min. Data were acquired in full scan mode from 50 to 500 daltons.

2.4 Results and discussion

2.4.1 St. Ives samples

There were 13 samples from the St. Ives deposits in total. Samples were taken from core CD16056, with the depth ranging from 224 to 811m. The NCC content is relatively high in KS-22 (3.67 wt %), KS-25 (4.98 wt %), KS-26 (9.45 wt %), KS-27 (14.39 wt %), KS-28 (7.61 wt %), which are carbonaceous shale, sulfidic shale, calcite-rich carbonaceous shale, sulfidic shale, and sulfidic shale respectively, as identified from the hand specimen. TON content is commonly low for all the samples. TOS content is relatively high in NCC-rich samples, except the calcite-rich shale KS-26, in which there is no sulfur.

The most NCC-rich samples were selected for Rock-Eval pyrolysis analysis (Table 2.3). Hydrogen index was plotted against oxygen index in a conventional Van Krevelen diagram (Figure 2.5). The HI and OI values are very low, indicating the almost total loss of hydrogen and oxygen from the samples and a high thermal maturity of CM. Therefore, the samples from St. Ives deposits were not suitable for organic extraction and GC-MS analysis because the CM is too refractory to be extracted using the Soxhlet extraction technique.

Table 2.3 Elemental analysis and Rock-Eval pyrolysis results of St. Ives, Wiluna and Macraes samples.

Samples	Depth (m)	NCC (%)	TON (%)	TOS (%)	S1 (mg HC/g Rock)	S2 (mg HC/g Rock)	S3 (mg CO ₂ /g Rock)	T _{max} (°C)	IP	HI	OI
									S1/(S1+S2)	S2/NCC*100 (mg HC/g TOC)	S3/NCC*100 (mg CO ₂ /g TOC)
KS-21	224	0.02	0.005	0.11							
KS-22	805	3.67	0.006	4.06	0.07	0.02	0.69	319	0.78	2	19
KS-23	684	0.05	0.001	0.13							
KS-24	693	0.03	0.004	0.73							
KS-25	796	4.98	0.003	5.9	0.1	0.02	0.71	422	0.83	0	14
KS-26	810.4	9.45	0	0	0.12	0.15	1.16	312	0.46	2	12
KS-27	796.8	14.39	0.004	2.74	0.14	0.04	0.54	360	0.78	0	4
KS-28	797	7.61	0	8.52	0.12	0.01	0.76	X	1	0	10
KS-29	667	0.11	0.005	0.78							
KS-30	807	0.25	0.003	0.62							
KS-31	794	0.54	0	2.32							
KS-32	810.7	0.07	0.002	1.17							
KS-33	798	0.58	0.005	1.49							
AD-01		0.0005			0.0195	0.0141	0.1538	491.3	0.58	X	X
AD-02		1.62			0.0021	0.0053	0.1944	492.6	0.28	0	12
FF-13		2.58			0.06	0.03	0.24	538	0.67	1	9
Notes	X: data is not available; KS: samples from the St. Ives; AD: samples from the Wuluna; FF: samples from the Macraes.										

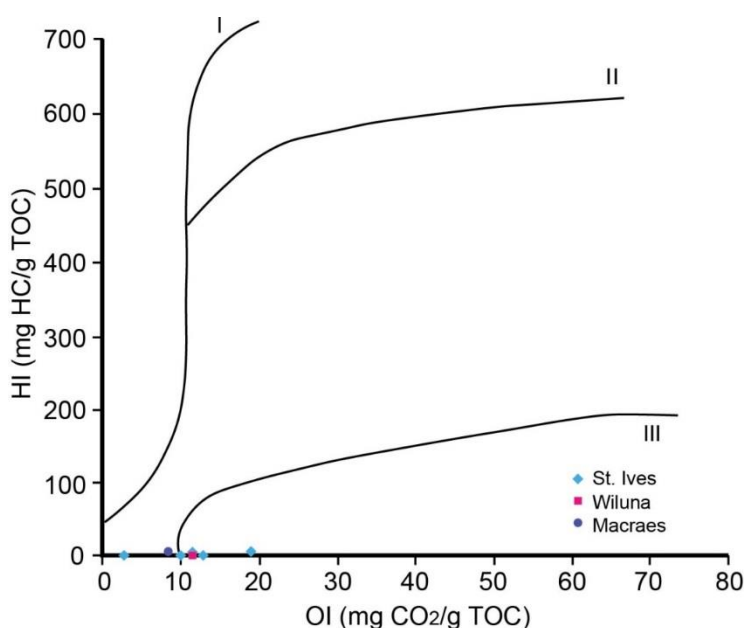


Figure 2.5 Results of Rock-Eval pyrolysis, HI versus OI diagram (I , II ,III represent three types of kerogen (Simoneit and Gize, 2000).

2.4.2 Wiluna samples

The two samples studied in detail are inter-laminated shale with sulfides. However, NCC contents are quite low (less than 2 %) in both samples (Table 2.4). HI and OI are low as well, suggesting that CM in these samples is over mature, that is, the volatile hydrocarbons have been extracted during metamorphism, (Figure 2.5).

Because the metamorphic peak temperature for Wiluna was low (< 300 °C), Soxhlet extraction of CM was attempted in spite of the unpromising Rock-Eval results. Unfortunately, almost no hydrocarbons were extracted by this method and the extracts could not be directly injected into the GC-MS. Thus, no results were obtained via these organic geochemistry methods.

2.4.3 Macraes samples

The NCC contents of samples collected from the Macraes gold deposit and Otago schist are quite low (Table 3.1). Sample FF-13, which has the highest TOC content (2.58 wt %) was selected for Rock-Eval pyrolysis analysis. The Rock-Eval pyrolysis

results show low hydrogen and oxygen indices (Table 2.5). Therefore, this sample, like those from Wiluna and St. Ives, is over-mature and the volatile hydrocarbons used for GC-MS have already been lost during metamorphism (Figure 2.5). Nevertheless, Soxhlet extraction was performed on this sample. However, after removal of sulphur from the extract, there was insufficient CM for analysis by GC-MS.

2.5 Conclusions

Unfortunately, the CM in those three deposits has become so mature that they are not appropriate for conventional organic geochemical analysis. However, this maturity does not preclude a role for the CM in these deposits. Catalytic hydrolysis (HyPy), which can characterize organic components of highly mature materials, like graphite, has been applied to orogenic Au deposits recently (Grotheer et al., 2015; Robert et al., 2016). Other techniques, such as optical microscopy, which can help to identify CM according to its petrographic features, and Raman spectroscopy, which can produce various CM spectra due to the structural information, were used to characterize the CM in this study. The application of Raman spectroscopy and optical microscopy to samples from the Macraes gold deposit is described in **Chapter 3**.

2.6 References

- Baker, W., 1978. The role of humic acid in the transport of gold. *Geochimica et Cosmochimica Acta* 42, 645-649.
- Bavinton, O., Keays, R.R., 1978. Precious metal values from interflow sedimentary rocks from the komatiite sequence at Kambalda, Western Australia. *Geochimica et Cosmochimica Acta* 42, 1151-1163.
- Behar, F., Beaumont, V., Pentead, H.D.B., 2001. Rock-Eval 6 technology: performances and developments. *Oil & Gas Science and Technology* 56, 111-134.

- Beveridge, T., 1988. The bacterial surface: general considerations towards design and function. *Canadian Journal of Microbiology* 34, 363-372.
- Chen, J., Walter, M.R., Logan, G.A., Hinman, M.C., Summons, R.E., 2003. The Paleoproterozoic McArthur River (HYC) Pb/Zn/Ag deposit of northern Australia: organic geochemistry and ore genesis. *Earth and Planetary Science Letters* 210, 467-479.
- Coveney, R.M., Murowchick, J.B., Grauch, R.I., Glascock, M.D., Denison, J.R., 1992. Gold and platinum in shales with evidence against extraterrestrial sources of metals. *Chemical Geology* 99, 101-114.
- Cox, S., Ruming, K., 2004. The St Ives mesothermal gold system, Western Australia—a case of golden aftershocks? *Journal of Structural Geology* 26, 1109-1125.
- Craw, D., 2002. Geochemistry of late metamorphic hydrothermal alteration and graphitisation of host rock, Macraes gold mine, Otago Schist, New Zealand. *Chemical Geology* 191, 257-275.
- Crocket, J., Kuo, H., 1979. Sources for gold, palladium and iridium in deep-sea sediments. *Geochimica et Cosmochimica Acta* 43, 831-842.
- Eckardt, C., Wolf, M., Maxwell, J., 1989. Iron porphyrins in the Permian Kupferschiefer of the lower Rhine Basin, NW Germany. *Organic Geochemistry* 14, 659-666.
- Eilu, P., Mikucki, E.J., 1998. Alteration and primary geochemical dispersion associated with the Bulletin lode-gold deposit, Wiluna, Western Australia. *Journal of Geochemical Exploration* 63, 73-103.
- Eiserbeck, C., Nelson, R.K., Grice, K., Curiale, J., Reddy, C.M., 2012. Comparison of GC-MS, GC-MRM-MS, and GC×GC to characterise higher plant biomarkers in Tertiary oils and rock extracts. *Geochimica et Cosmochimica Acta* 87, 299-322.
- Evans, K.A., 2010. A test of the viability of fluid–wall rock interaction mechanisms for changes in opaque phase assemblage in metasedimentary rocks in the

- Kambalda-St. Ives goldfield, Western Australia. *Mineralium Deposita* 45, 207-213.
- Fein, J.B., Williams-Jones, A., 1997. The role of mercury-organic interactions in the hydrothermal transport of mercury. *Economic Geology* 92, 20-28.
- Gatellier, J.-P., Disnar, J.-R., 1989. Organic matter and gold-ore association in a hydrothermal deposit, France. *Applied Geochemistry* 4, 143-149.
- Giordano, T., 2000. Organic matter as a transport agent in ore-forming systems. *Reviews in Economic Geology* 9, 133-155.
- Giordano, T.H., 1994. Metal transport in ore fluids by organic ligand complexation, Organic acids in geological processes. Springer, pp. 319-354.
- Gize, A.P., 1999. A special issue on Organic matter and ore deposits; interactions, applications, and case studies; introduction. *Economic Geology* 94, 963-965.
- Gize, A.P., Barnes, H., 1987. The organic geochemistry of two Mississippi Valley-type lead-zinc deposits. *Economic Geology* 82, 457-470.
- Greenwood, P., Brocks, J., Grice, K., Schwark, L., Jaraula, C., Dick, J., Evans, K., 2013. Organic geochemistry and mineralogy. I. Characterisation of organic matter associated with metal deposits. *Ore Geology Reviews* 50, 1-27.
- Grice, K., Cao, C., Love, G.D., Böttcher, M.E., Twitchett, R.J., Grosjean, E., Summons, R.E., Turgeon, S.C., Dunning, W., Jin, Y., 2005. Photic zone euxinia during the Permian-Triassic superanoxic event. *Science* 307, 706-709.
- Grice, K., Gibbison, R., Atkinson, J.E., Schwark, L., Eckardt, C.B., Maxwell, J.R., 1996. Maleimides (1H-pyrrole-2, 5-diones) as molecular indicators of anoxygenic photosynthesis in ancient water columns. *Geochimica et Cosmochimica Acta* 60, 3913-3924.
- Grice, K., Schaeffer, P., Schwark, L., Maxwell, J.R., 1997. Changes in palaeoenvironmental conditions during deposition of the Permian Kupferschiefer (Lower Rhine Basin, northwest Germany) inferred from molecular and isotopic compositions of biomarker components. *Organic Geochemistry* 26, 677-690.

- Hagemann, S., Cassidy, K.F., 2000. Archean orogenic lode gold deposits. *Reviews in Economic Geology* 13, 9-68.
- Hagemann, S., Groves, D., Ridley, J., Vearncombe, J.R., 1992. The Archean lode gold deposits at Wiluna, Western Australia; high-level brittle-style mineralization in a strike-slip regime. *Economic Geology* 87, 1022-1053.
- Hagemann, S., Lüders, V., 2003. PTX conditions of hydrothermal fluids and precipitation mechanism of stibnite-gold mineralization at the Wiluna lode-gold deposits, Western Australia: conventional and infrared microthermometric constraints. *Mineralium Deposita* 38, 936-952.
- Hare, A.A., Kuzyk, Z.Z.A., Macdonald, R.W., Sanei, H., Barber, D., Stern, G.A., Wang, F., 2014. Characterization of sedimentary organic matter in recent marine sediments from Hudson Bay, Canada, by Rock-Eval pyrolysis. *Organic Geochemistry* 68, 52-60.
- Holman, A.I., Grice, K., Jaraula, C.M., Schimmelmann, A., 2014. Bitumen II from the Paleoproterozoic Here's Your Chance Pb/Zn/Ag deposit: Implications for the analysis of depositional environment and thermal maturity of hydrothermally-altered sediments. *Geochimica et Cosmochimica Acta* 139, 98-109.
- Holman, A.I., Grice, K., Jaraula, C.M., Schimmelmann, A., Brocks, J.J., 2012. Efficiency of extraction of polycyclic aromatic hydrocarbons from the Paleoproterozoic Here's Your Chance Pb/Zn/Ag ore deposit and implications for a study of Bitumen II. *Organic Geochemistry* 52, 81-87.
- Jaraula, C.M., Schwark, L., Moreau, X., Pickel, W., Bagas, L., Grice, K., 2015. Radiolytic alteration of biopolymers in the Mulga Rock (Australia) uranium deposit. *Applied Geochemistry* 52, 97-108.
- Kendrick, M., Honda, M., Walshe, J., Petersen, K., 2011. Fluid sources and the role of abiogenic-CH₄ in Archean gold mineralization: Constraints from noble gases and halogens. *Precambrian Research* 189, 313-327.
- Ketris, M., Yudovich, Y.E., 2009. Estimations of Clarkes for Carbonaceous biolithes: World averages for trace element contents in black shales and coals. *International Journal of Coal Geology* 78, 135-148.

- Labrenz, M., Banfield, J., 2004. Sulfate-reducing bacteria-dominated biofilms that precipitate ZnS in a subsurface circumneutral-pH mine drainage system. *Microbial Ecology* 47, 205-217.
- Labrenz, M., Druschel, G.K., Thomsen-Ebert, T., Gilbert, B., Welch, S.A., Kemner, K.M., Logan, G.A., Summons, R.E., De Stasio, G., Bond, P.L., 2000. Formation of sphalerite (ZnS) deposits in natural biofilms of sulfate-reducing bacteria. *Science* 290, 1744-1747.
- Lafargue, E., Marquis, F., Pillot, D., 1998. Rock-Eval 6 applications in hydrocarbon exploration, production, and soil contamination studies. *Revue de L'institut Français du Pétrole* 53, 421-437.
- Large, R.R., Bull, S.W., Maslennikov, V.V., 2011. A carbonaceous sedimentary source-rock model for Carlin-type and orogenic gold deposits. *Economic Geology* 106, 331-358.
- Large, R.R., Danyushevsky, L., Hollit, C., Maslennikov, V., Meffre, S., Gilbert, S., Bull, S., Scott, R., Emsbo, P., Thomas, H., 2009. Gold and trace element zonation in pyrite using a laser imaging technique: implications for the timing of gold in orogenic and Carlin-style sediment-hosted deposits. *Economic Geology* 104, 635-668.
- Lengke, M., Southam, G., 2006. Bioaccumulation of gold by sulfate-reducing bacteria cultured in the presence of gold (I)-thiosulfate complex. *Geochimica et Cosmochimica Acta* 70, 3646-3661.
- Lengke, M.F., Southam, G., 2007. The deposition of elemental gold from gold (I)-thiosulfate complexes mediated by sulfate-reducing bacterial conditions. *Economic Geology* 102, 109-126.
- Leventhal, J., Giordano, T., 2000. The nature and roles of organic matter associated with ores and ore-forming systems: An introduction. *Reviews in Economic Geology* 9, 1-26.
- Leventhal, J.S., Daws, T.A., Frye, J.S., 1986. Organic geochemical analysis of sedimentary organic matter associated with uranium. *Applied Geochemistry* 1, 241-247.

- Lüniger, G., Schwark, L., 2002. Characterisation of sedimentary organic matter by bulk and molecular geochemical proxies: an example from Oligocene maar-type Lake Enspel, Germany. *Sedimentary Geology* 148, 275-288.
- Machel, H., 2001. Bacterial and thermochemical sulfate reduction in diagenetic settings—old and new insights. *Sedimentary Geology* 140, 143-175.
- Machel, H.G., Krouse, H.R., Sassen, R., 1995. Products and distinguishing criteria of bacterial and thermochemical sulfate reduction. *Applied Geochemistry* 10, 373-389.
- Manning, D.A., Gize, A.P., 1993. The role of organic matter in ore transport processes, *Organic Geochemistry*. Springer, pp. 547-563.
- McCall, G.J.H., 1970. The Archean succession to the west of Lake Lefroy.
- McKeag, S., Craw, D., Norris, R., 1989. Origin and deposition of a graphitic schist-hosted metamorphogenic Au-W deposit, Macraes, East Otago, New Zealand. *Mineralium Deposita* 24, 124-131.
- Neumayr, P., Walshe, J., Hagemann, S., Petersen, K., Roache, A., Frikken, P., Horn, L., Halley, S., 2008. Oxidized and reduced mineral assemblages in greenstone belt rocks of the St. Ives gold camp, Western Australia: vectors to high-grade ore bodies in Archaean gold deposits? *Mineralium Deposita* 43, 363-371.
- Ong, H.L., Swanson, V.E., Bisque, R.E., 1970. Natural organic acids as agents of chemical weathering. *Geological Survey Research*, 130-137.
- Peters, K.E., Walters, C.C., Moldowan, J.M., 2005. *The biomarker guide*. Cambridge University Press.
- Peters, S.G., Jiazhan, H., Zhiping, L., Chenggui, J., 2007. Sedimentary rock-hosted Au deposits of the Dian–Qian–Gui area, Guizhou, and Yunnan Provinces, and Guangxi District, China. *Ore Geology Reviews* 31, 170-204.
- Phillips, G.N., Groves, D.I., 1983. The nature of Archaean gold - bearing fluids as deduced from gold deposits of Western Australia. *Journal of the Geological Society of Australia* 30, 25-39.

- Plet, C., Grice, K., Pagès, A., Ruebsam, W., Coolen, M., Schwark, L., 2016. Microbially-mediated fossil-bearing carbonate concretions and their significance for palaeoenvironmental reconstructions: A multi-proxy organic and inorganic geochemical appraisal. *Chemical Geology* 426, 95-108.
- Pósfai, M., Dunin-Borkowski, R.E., 2006. Sulfides in biosystems. *Reviews in Mineralogy and Geochemistry* 61, 679-714.
- Prendergast, K., 2007. Application of litho-geochemistry to gold exploration in the St Ives goldfield, Western Australia. *Geochemistry: Exploration, Environment, Analysis* 7, 99-108.
- Rickard, D.T., 1970. The origin of framboids. *Lithos* 3, 269-293.
- Rieger, A., Schwark, L., Cisternas, M.-E., Miller, H., 2008. Genesis and evolution of Bitumen in Lower Cretaceous lavas and implications for strata-bound copper deposits, North Chile. *Economic Geology* 103, 387-404.
- Roberts, D., Elias, M., 1990. Gold deposits of the Kambalda-St Ives region. *Geology of the Mineral Deposits of Australia and Papua New Guinea*, 479-491.
- Simoneit, B., Gize, A., 2000. Analytical techniques for organic matter characterization in ore deposits. *Ore genesis and exploration: the roles of organic matter. Reviews in Economic Geology* 9, 27-61.
- Wedepohl, K.H., 1995. The composition of the continental crust. *Geochimica et Cosmochimica Acta* 59, 1217-1232.
- Williford, K.H., Grice, K., Logan, G.A., Chen, J., Huston, D., 2011. The molecular and isotopic effects of hydrothermal alteration of organic matter in the Paleoproterozoic McArthur River Pb/Zn/Ag ore deposit. *Earth and Planetary Science Letters* 301, 382-392.
- Woodall, R., 1979. Gold-Australia and the world. *Gold mineralization. University of Western Australia*, 1-34.
- Zhang, J., Lu, J., Zhai, J., Yang, F., 1997. Simulating experiments on enrichment of gold by bacteria and their geochemical significance. *Chinese Journal of Geochemistry* 16, 369-373.

Chapter 3

Raman characterization of carbonaceous material in the Macraes orogenic gold deposit and metasedimentary host rocks, New Zealand

This chapter is a published paper in *Ore Geology Reviews*:

Hu, S., Evans, K., Craw, D., Rempel, K., Bourdet, J., Dick, J., Grice, K., 2015.

Raman characterization of carbonaceous material in the Macraes orogenic gold deposit and metasedimentary host rocks, New Zealand. *Ore Geology Reviews* 70, 80-95 (Impact factor 3.819).

Contributions by co-authors

Si-Yu Hu and Katy Evans collected samples. Dave Craw provided assistance on the field trip. Si-Yu Hu performed sample preparation for element concentrations analysis, petrographic observations, and Raman spectroscopy analysis with the help of Julien Bourdet. Si-Yu Hu is the primary author of the manuscript with helpful discussions, suggestions and guidance, from all co-authors. Funds was provided by the CSIRO Organic Geochemistry of Mineral Systems Cluster.

Abstract

Raman spectroscopic and petrographic analyses were performed on samples collected from zones distal and proximal to the Macraes gold deposit in the Otago Schist of New Zealand to characterize the features and possible origins of Carbonaceous Material (CM) and to assess the potential role of CM in the formation of gold deposits. CM is a common component in meta-sedimentary orogenic gold deposits, and it has been proposed that CM contributes to gold mineralization processes, but the details of the mechanisms responsible are not fully understood. Documentation of the origins of the Otago schist CM will improve our understanding of the role of CM in gold deposits.

This work has identified four types of CM of varying thermal maturity and origins from prehnite-pumpellyite grade to lower greenschist grade samples. In prehnite-pumpellyite and pumpellyite-actinolite grade rocks, low-maturity CM 1 coexists with framboidal pyrite, indicating an *in-situ*, sedimentary origin, with a potential association with the source of gold. Low crystallinity CM 2 is also found in low grade samples and is likely to have been deposited from fluids unrelated to gold mobilization. CM 3 is the highest maturity CM recognized. CM 3 is found in samples from the highest metamorphic grades studied (lower greenschist facies), where bands of CM 3 cross cut the foliation, CM 3 is therefore thought to have been transported by fluids, though possibly only at short length scales. CM 4 is less mature than CM 3 and is found in mineralized rocks in association with sulfide minerals and gold. CM 4 is likely to have a depositional origin but its precise role with respect to gold mineralization has not been identified.

3.1 Introduction

Carbonaceous material (CM) is commonly associated with gold in metasediment-hosted orogenic and Carlin-type gold deposits (Bierlein et al., 2001; Cox et al., 1995; Large et al., 2011; Thomas et al., 2011). Detrital CM, especially in organic-matter (OM)-rich shales, can contribute to the sequestration of metals during sediment deposition, and these OM-rich sediments can then act as sources for metals during subsequent metamorphic processes (Large et al., 2012; Large et al., 2011; Peters et

al., 2007; Zhang et al., 1997). During ore deposition, the presence of CM in metasedimentary host rocks may facilitate precipitation of gold from hydrothermal fluids by chemical reduction (Bierlein et al., 2001; Cox et al., 1995; Craw et al., 2010; Goldfarb et al., 2007; Zoheir et al., 2008). Alternatively, CM may be deposited from hydrothermal fluids containing volatile organic compounds during gold deposit formation (Craw, 2002; Gu et al., 2012; Huizenga, 2011; Luque del Villar et al., 1998; Luque et al., 2009; Vallance et al., 2003).

Because of the close associations between CM and gold in metasedimentary terranes, it is important to understand the nature of changes in CM during the transitions that occur with increasing metamorphism and associated fluid migration, and between primary source rocks and gold depositional systems. Metamorphism of detrital CM has been well studied in several metasedimentary belts (Beysac et al., 2002; Beysac et al., 2003b; Landis, 1971; Pasteris and Wopenka, 1991; Rahl et al., 2005). However, links between organic maturation, CM mobility, and regional gold mineralization processes have received less attention.

The texture and structure of CM can be used to assess whether it has been remobilized, and to infer the role of CM in metal mobilization and deposition (Luque del Villar et al., 1998). The usual analytical methods employed to provide structural characterization of CM are quantitative reflectance, X-ray diffraction (XRD), high-resolution transmission electron microscopy (HRTEM) and Raman microspectroscopy (Beysac et al., 2002; Beysac et al., 2003b; Henne and Craw, 2012; Wopenka and Pasteris, 1993). With the advantages of *in-situ* analysis and high resolution data acquisition, Raman microspectroscopy has become increasingly popular (e.g. Beysac et al., 2002; Beysac et al., 2003b; Jehlička et al., 2003; Pasteris and Wopenka, 2003; Quirico et al., 2009; Quirico et al., 2005; Rahl et al., 2005). It has long been observed that Raman spectra are sensitive to changes in crystallinity and structure of CM, which largely depend on temperature during metamorphism. The graphitization is presumed to be an irreversible process (Beysac et al., 2002; Wopenka and Pasteris, 1993). Beysac et al. (2002), Lahfid et al. (2010) and Rahl et al. (2005) found a linear relationship between quantifiable features in the Raman spectra of CM and peak metamorphic temperature, and used this relationship to develop a geothermometer for metamorphic samples, which was calibrated for

temperature ranges of 330 – 650 °C, 200 – 320 °C and 100 – 700 °C by the respective authors. However, few studies have combined the characteristics of Raman spectra with the petrographic features of CM in metamorphic rocks as a means to trace the origins of CM. It is the aim of this paper to use a combination of Raman and petrographic analysis to document the CM transformations that occurred during prograde metamorphism in a metamorphic belt in which Au is thought to have been mobilized by the same regional metamorphic processes (Large et al., 2012). The results are used to quantify the changes that have occurred to the CM within the linked metamorphic and hydrothermal systems.

Gold-bearing rocks used for this study are taken from the vicinity of the world-class Macraes orogenic gold deposit, which is hosted by the Otago Schist in southern New Zealand (Craw, 2002). The gold in this deposit was emplaced by metamorphic-hydrothermal fluids in the latter stages of metamorphism (Craw, 2002), and is thought to have been generated by metamorphism of host metasediments that contained gold accumulated during diagenesis (Large et al., 2012; Pitcairn et al., 2006). There is abundant CM throughout the host rock sequence, from low grade metamorphic schists to the gold deposit itself where hydrothermal enrichment of up to 3 wt% carbon has occurred (Craw, 2002; Henne and Craw, 2012).

3.2 Geological setting and regional gold mobility

The Otago Schist is a Mesozoic metasedimentary belt with a core zone of upper greenschist facies rocks flanked on either side by zones of progressively lower grade rocks (Figure 3.1) (Mortimer, 1993; Mortimer, 2000). The protoliths for the schist belt are Paleozoic to Mesozoic turbidites which were metamorphosed to prehnite-pumpellyite facies in the Jurassic (MacKinnon, 1983; Mortimer, 1993). There is a generally symmetrical regional increase in metamorphic grade of these protolith metaturbidites through pumpellyite-actinolite facies and lower greenschist facies towards the core zone of the schist belt (Figure 3.1) (Mortimer, 1993). The rocks become progressively more recrystallized and foliated through this increase in metamorphic grade, and the schists in the core of the belt have been pervasively recrystallized with several generations of folding and foliation development

(Mortimer, 1993). Amphibolite facies rocks underlie the core upper greenschist facies rocks, and these have been tectonically exposed farther to the northwest of the main belt (Mortimer, 2000; Pitcairn et al., 2006). In detail, the boundaries between metamorphic zones are commonly post-metamorphic structures, especially extensional faults that were initiated in the middle Cretaceous (Figure 3.1) (Deckert et al., 2002; Henne and Craw, 2012).

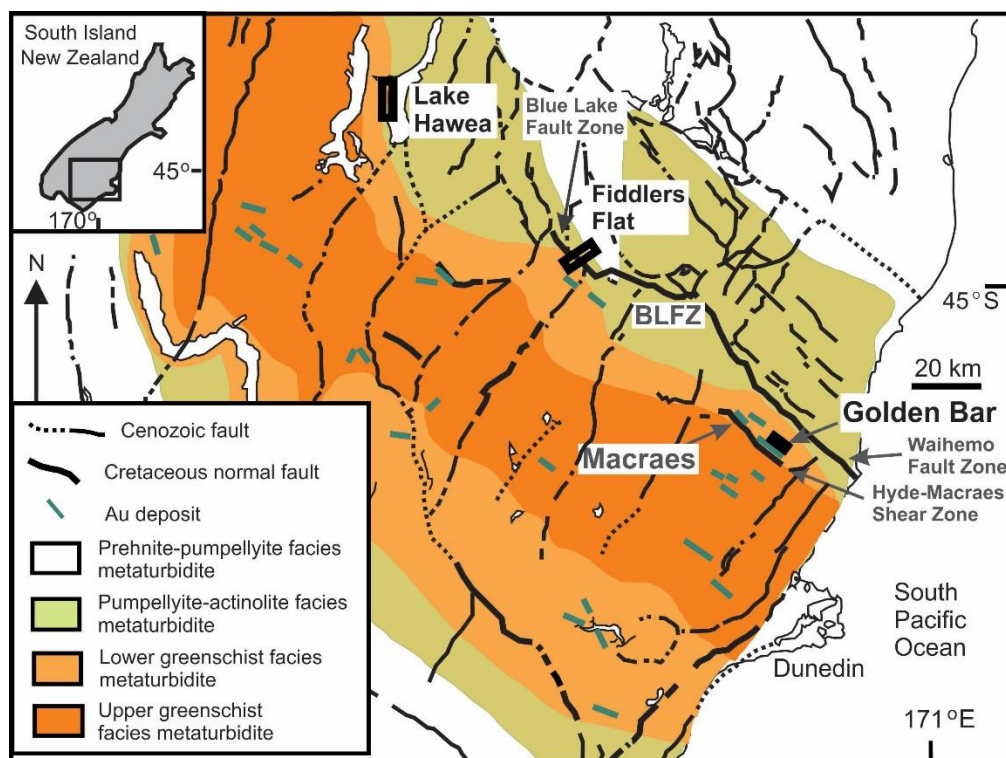


Figure 3.1 Geological map of the Otago Schist in New Zealand (modified from Henne and Craw, 2012 and Pitcairn et al., 2005); the highlighted areas with black boxes are sampling locations, i.e. Lake Hawea, Fiddlers Flat and Golden Bar.

The consistent protolith composition that persists across the whole schist belt has enabled geochemical comparison of metal and metalloid contents at different metamorphic grades, in order to quantify metamorphogenic mobilization of these elements (Pitcairn et al., 2014a; Pitcairn et al., 2010; Pitcairn et al., 2006). Gold and arsenic, in particular, have been demonstrably mobilized on a regional scale during metamorphism, with prominent decreases in contents of these elements in the transition from the lower greenschist facies to amphibolite facies (Pitcairn et al., 2014a; Pitcairn et al., 2006). These elements were initially weakly enriched

compared to the average crustal concentrations, on a regional scale, in diagenetic pyrite in the prehnite- pumpellyite facies protoliths, and prograde metamorphic recrystallization of that pyrite facilitated mobilization of Au and As (Large et al., 2012; Pitcairn et al., 2014a; Pitcairn et al., 2010; Pitcairn et al., 2006). Minor intercalated metabasic layers in the metamorphic pile did not contribute significantly to the amount of mobilized Au, and were local sinks for mobilized As (Pitcairn et al., 2014a). The regional scale metamorphogenic mobilization of Au and As, along with other elements commonly associated with orogenic hydrothermal deposits, such as Sb, W, and Hg, has been responsible for widespread formation of orogenic gold deposits across the schist belt in the late Mesozoic (Mortensen et al., 2010; Pitcairn et al., 2006). A similar regional scale system, in the same rock sequence, was reactivated in the late Cenozoic in rocks northwest of the Otago Schist (Pitcairn et al., 2014a; Pitcairn et al., 2006).

All of the orogenic systems depicted in Figure 3.1 have been mined historically at some stage, but production has been small. However, one such set of historic mines, at Macraes (Figure 3.1), has been developed into a world-class deposit, with more than 9 million ounces gold resource. The Macraes deposit is a mineralized late metamorphic shear zone hosted in lower greenschist facies meta-turbidites. The mineralized shear zone formed during Jurassic-Early Cretaceous uplift through the brittle-ductile transition (Craw, 2002; Craw et al., 1999; Mortensen et al., 2010). The mineralized rocks include a complex array of syndeformational quartz veins and adjacent sheared and hydrothermally altered schists (Craw, 2002; Craw et al., 1999). The total width of the mineralized zone locally exceeds 200 m, with a strike length >30 km, and known down-dip extension in the main mining area of >500 m (Figure 3.1).

Gold is closely associated with metamorphic-hydrothermal pyrite and arsenopyrite, some of which occurs as porphyroblasts in hydrothermally altered rock (Craw, 2002; Henne and Craw, 2012; Large et al., 2012). Early-formed auriferous sulfides were deformed by subsequent shearing, with additional sulfidic mineralization, leading to several generations of sulfide and gold emplacement (Craw et al., 1999; Large et al., 2012). Deposition of abundant hydrothermal CM accompanied all stages of

mineralization, and post-mineralization shearing has remobilized some of that CM (Craw, 2002; Craw et al., 1999; Henne and Craw, 2012).

3.3 Sampling and analytical methods

3.3.1 Sample selection and characterization

A set of samples of metasedimentary rocks from a range of metamorphic grades was obtained from unweathered outcrops at road cuts, river gorges, lake shore, and mine excavations (Figure 3.1). In the Fiddlers Flat area (Figure 3.1), in a section described by Henne and Craw (2012) and Large et al. (2012), a traverse was made across the transition from prehnite-pumpellyite facies to lower greenschist facies schists. At Lake Hawea (Figure 3.1), carbonaceous metapelitic samples were collected from pumpellyite-actinolite facies and lower greenschist facies schists. Graphitic lower greenschist facies host schists proximal to the Macraes gold mine, as well as mineralized graphitic sheared rocks, were collected from the Golden Bar pit, a satellite pit of the main Macraes mine described by Large et al. (2012). A total of 40 samples were collected, with 6 samples from the prehnite-pumpellyite (P-P) facies, 18 samples from the pumpellyite-actinolite (P-A) facies and 16 samples from the lower greenschist (G-S) facies.

3.3.2 Non-carbonate carbon and gold content analysis

Samples were crushed into powder for non-carbonate carbon and gold analyses in a tungsten carbide ring mill. Analyses were conducted by Intertek Genalysis Lab (Perth, Australia). For non-carbonate carbon, samples were treated with dilute acid to remove carbonate, and the residue was analyzed for carbon using infrared spectroscopy. For gold analysis, a lead fire assay preconcentration step was used to separate the gold from the matrix as a pellet, which was then dissolved in dilute aqua regia and analyzed for Au with flame atomic absorption spectrometry. The accuracy of non-carbonate carbon measurements is less than 10%, and that of Au is less than 5%.

3.3.3 Petrographic methods

Petrographic samples were prepared as thin sections for optical microscopy, scanning electron microscopy (SEM), and energy-dispersive X-ray spectroscopy (EDS) to characterize the petrographic features. Thin sections were cut perpendicular to the foliation and parallel to the stretching lineation. Petrographic inspection of the samples was conducted with a Nikon optical transmitted and reflected light microscope. SEM and EDS observations were made using a Zeiss Neon 40EsB field-emission gun scanning electron microscope (FEGSEM) in the Curtin Materials Research Lab of Curtin University (Perth, Australia). For the BSE (back-scattered electron) signal, the energy was 20.00 kV and the working distance was 7.7 mm.

3.3.4 Raman spectroscopy

Raman spectra of carbonaceous material

Two wavelength intervals at 1100 – 1800 cm^{-1} and 2500 – 3100 cm^{-1} have been documented in studies of the Raman spectra of CM, and have been referred to as the first- and the second-order regions respectively (Beysac et al., 2002; Beysac et al., 2003b; Pasteris and Wopenka, 2003; Wopenka and Pasteris, 1993; Yui et al., 1996). In the first-order region, well-organized graphite with D^4_{6h} crystal symmetry ($D^4_{6h} = P6_3/mmc$, hexagonal Brillouin zone) has a detectable E_{2g2} vibration mode at 1580 cm^{-1} in Raman spectra, which is an in-plane mode (Figure 3.2; (Pasteris and Wopenka, 1991; Wopenka and Pasteris, 1993). This single peak is named the “G band,” and splits into two peaks when the CM becomes disordered (Figure 3.3 A & B) (Beysac et al., 2002; Wopenka and Pasteris, 1993). In disordered and poorly-organized CM, the Raman spectra consist of two bands, the G band at 1600 cm^{-1} , and the D band at 1355 cm^{-1} (Figure 3.3 B). The D band is considered to be due to in-plane defects caused by heteroatoms or structural defects (Beysac et al., 2002; Pasteris and Wopenka, 1991; Wopenka and Pasteris, 1993). The D band includes, in addition to the main D peak, an intense single peak (D1) on the left shoulder of the D peak at $\sim 1200 \text{ cm}^{-1}$ (Figure 3.3 C, D & F). The G band includes a wide peak at $\sim 1550 \text{ cm}^{-1}$ on the left shoulder of the main G peak, and this is referred to as the D2 peak (Figure 3.3 C, D & F). D1 has been attributed to vibration modes of polyene-like structures, and D2 is thought to be associated with amorphous carbon (Dippel et al.,

1999; Jawhari et al., 1995). In well-organized CM, an additional D3 peak around 1613 cm^{-1} appears on the right shoulder of the G band (Figure 3.3 B & E).

In the second-order region, the typical peaks for CM in previous studies are located at 2400 , 2700 , 2900 and 3300 cm^{-1} (Figure 3.3A & B) (Beysac et al., 2002; Nemanich and Solin, 1979; Wopenka and Pasteris, 1993). Usually, the peaks in the second-order region are interpreted as overtones ($2 \times 1335\text{ cm}^{-1} \approx 2670\text{ cm}^{-1}$; $2 \times 1600\text{ cm}^{-1} \approx 3207\text{ cm}^{-1}$, and so on) and combination scattering of energy in the low wavenumber region ($1335\text{ cm}^{-1} + 1600\text{ cm}^{-1} \approx 2925\text{ cm}^{-1}$) (Beysac et al., 2002; Beysac et al., 2003b; Wopenka and Pasteris, 1993). Wopenka and Pasteris (1993) stated that the intensity of peaks in the second-order region is a reflection of three-dimensional ordering. Among the second order peaks, S1 (2700 cm^{-1}) has been used to represent the two-dimensional extent of graphitic layers and the three-dimensional ordering of the graphite lattice; this peak splits into two as the graphite lattice changes from dominantly two-dimensional to three-dimensional (Lespade et al., 1984). The S2 (2900 cm^{-1}) peak has been proposed to be a result of C-H bonding, but there is a lack of consensus on this interpretation (Beysac et al., 2002; Tsu et al., 1978).

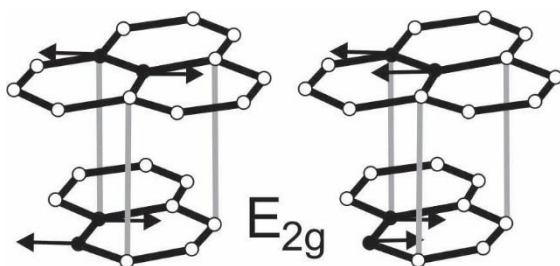


Figure 3.2 The two vibrational modes that may be displayed by single-crystal graphite. E_{2g} is an in-plane optical vibration model and only this model is Raman active (modified from Reich and Thomsen, 2004).

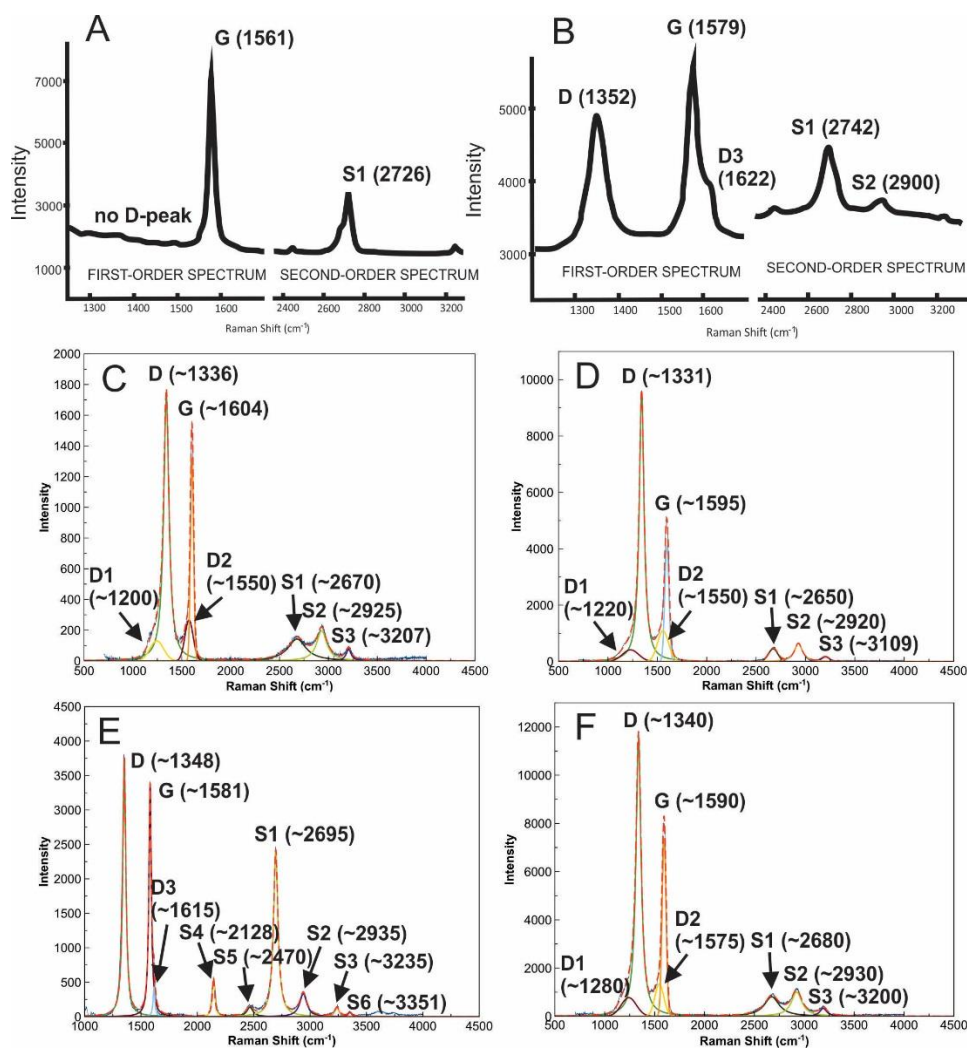


Figure 3.3 (A) Raman spectrum of graphite (modified after Wopenka and Pasteris, 1993); (B) Raman spectrum of disordered CM (modified after Wopenka and Pasteris, 1993); (C) Raman spectrum of CM 1 from FF-16; (D) Raman spectrum of CM 2 from FF-12-A; (E) Raman spectrum of CM 3 from TC-01; (F) Raman spectrum of CM 4 from GB-04-A; The numbers in brackets are peak positions/average peak positions (see Figure 3.1) in cm^{-1} .

Raman methods

Quantitative Raman analysis was carried out on CM in 17 selected samples from various metamorphic grades. The instrument, which is located at the CSIRO laboratories in Bentley, Perth, Australia, is a Horiba® LabRAM HR Evolution using a 600 gr/mm grating and a Synapse Visible detector. The 532 nm incident radiation was produced by a 100 mW Laser Quantum Torus consisting of a continuous wave single frequency diode laser. During the analyses, the laser beam was focused to a

width of about 0.72 μm with a 100X objective. The numeric aperture (NA) of objective was 0.90. The beam was aimed perpendicular to the thin section. Visible damage on the surface of the sample or alteration of the Raman signal were monitored and avoided by adjusting the laser power. Filters decreased the laser power to 0.3 mW on the sample surface. Data were collected in the 700 – 4000 cm^{-1} range to capture the first-order and second-order Raman bands.

The measurements were collected on randomly oriented grains, with a fixed orientation of the polarized laser beam (Table 3.1). 5-10 spectra were acquired for each sample except FF-14 and GB-4-B. Polishing has been reported to induce disorder of CM at the nanometre scale (Beysac et al., 2003b; Pasteris and Chou, 1998). The intensity ratio of D and G peaks is supposed to be sensitive to the polishing, but the width of G peak remains more stable, as determined in investigations by Ammar et al. (2011). Such polishing effects are thought to be of no concern for CM with low degrees of structural order, such as the bulk of those examined for this study (Bonal et al., 2010). However, a few samples may contain CM with sufficient structural order that polishing effects may be significant. To assess the extent of polishing effects, we compared the Raman spectra from polished and unpolished areas of billets that contained low maturity and the highest maturity CM. The intensity ratio of D and G peaks and width of G peak of low maturity CM remained almost unchanged. However, those in high mature CM varied to a minor extent only. Thus, the absence or presence of a polished surface did not induce any significant change in the Raman spectra. It is assumed that polishing effects are negligible in this study.

Additionally, as anisotropic materials may produce pleochroism in Raman spectra (Yoon et al., 2008), the extent to which sample orientation affected the spectra was also investigated. Measurements presented in this study were made with a linearly polarized laser, so measurements made with a circular polarized laser, which is insensitive to crystal orientation, were made to assess the extent to which pleochroism affected the spectra. CM grains from five selected samples covering all metamorphic grades investigated were analyzed in a variety of orientations. The polarization angle of the laser relative to the material was changed by rotation of the sample from 0 to 90° at 15° intervals using a petrographic stage with an analyzer

plate placed in the Raman spectrometer after the edge filter. This procedure was then applied to the same grains using circular polarized light with a quarter wave plate placed in the laser path before reaching the sample (de-polarization of the laser). The averages and the standard deviations of the measured parameters for the various sample orientations were calculated for each set of data (Table 3.2). Uncertainties presented in Table 3.2 are the ratios of one standard deviation to the average value.

Peak positions, widths, relative intensities and areas were obtained by fitting the spectra in “MagicPlot” (Magicplot Systems LLC, Saint Petersburg, Russia). The background was removed manually by creating splines, moving anchor points on the splines to set appropriate fit intervals which contain only baseline without peaks, and fitting. Then a mixed Gaussian-Lorentzian curve-fitting procedure was applied to deconvolute the spectra. Initial Gaussian/Lorentzian curves were first fitted into spectra manually, then fit procedures were run by the software during which the parameters of fit function would vary iteratively to minimize the residual sum of squares. The output parameters are the position of peaks, intensity, full width at half maximum (FWHM) and integrated area. The positions of all the peaks were constrained into a certain range with first-order region between 900 – 2000 cm^{-1} and second-order region between 2300 – 3500 cm^{-1} following studies in Sadezky et al. (2005) and Sforna et al. (2014). The intensity of D3 was restricted to be less than half of the intensity of the G band (Sforna et al., 2014). In the first-order region, spectra were deconvoluted into the primary peaks, the D peak (1330 - 1350 cm^{-1}) and G peak (1580 - 1610 cm^{-1}), and three smaller peaks, the D1 peak (1190 - 1250 cm^{-1}), D2 peak (1500 – 1550 cm^{-1}) and D3 peak (1610 – 1620 cm^{-1}). In the second-order region, the commonly-observed peaks are S1 (2630 – 2700 cm^{-1}), S2 (2900 – 2940 cm^{-1}) and S3 (3190 – 3240 cm^{-1}). However, in some higher metamorphic grade samples, additional S peaks are displayed at wavenumbers of 2128 cm^{-1} (S4), 2470 cm^{-1} (S5), 3351 cm^{-1} (S6) and 3610 cm^{-1} (S7). Typical results of the fits are displayed in Figures 3.3 D to F.

The following ratios were used to characterize the Raman spectra:

$$R1 = I_D/I_G \quad (1)$$

$$R2 = W_D/W_G \quad (2)$$

$$R3 = (A_D + A_{D1}) / (A_D + A_{D1} + A_G + A_{D2} + A_{D3}) \quad (3)$$

$$R4 = A_{S1} / (A_{S1} + A_{S2} + A_{S3}) \quad (4)$$

I_X is the intensity of peak X above the background-corrected baseline, W_X is the width of peak X at half maximum height, and A_X is the integrated area of peak X above the baseline. These ratios are plotted against the estimated ranked metamorphic grade, from P-P to lower G-S facies. Samples from the Fiddlers Flat traverse are ranked by position within the sequence, increasing from northeast to southwest (Figure 3.1). Lake Hawea P-A samples were ranked above the Fiddlers Flat P-A samples, because these samples come from the P-A: lower G-S transition. In the lower G-S facies the Fiddlers Flat samples were ranked the lowest, followed by the Lake Hawea samples and the Golden Bar samples. The Golden Bar samples are from close to the upper G-S: lower G-S transition, so the assignment of the highest ranking to these samples is reasonable. The Lake Hawea samples and the Fiddlers Flat samples come from a similar position relative to the P-P/P-A and P-A/lower G-S boundary, so the assignment of the Lake Hawea samples to the higher ranked metamorphic grade was somewhat arbitrary, but is consistent with the trends in Raman spectral parameters (see below).

Table 3.1 Sampling locations, rock type, non-carbonate carbon content, Au content, relevant parameters of Raman spectra of samples investigated.

Metamorphic Grade	Sample ID	NCC (%)	CM Type	Au (ppm)	Sampling Location	Lithology	Measurement Number	D Position (cm ⁻¹)	D Width (FWHM) (cm ⁻¹)	G Position (cm ⁻¹)	G Width (FWHM) (cm ⁻¹)	R1 Ratio	R2 Ratio	R3 Ratio	R4 Ratio
P-P	FF-16	0.24	CM 1		FF	Meta-pelite	7	1336.68	77.79	1601.34	37.49	0.99	2.08	0.683	0.52
			STD				0.51	1.19	0.59	0.53	0.03	0.06	0.005	0.13	
P-P	FF-16		CM 2		FF	Meta-pelite	1	1329.99	99.78	1601.74	37.45	0.92	2.66	0.71	0.40
P-P	FF-06	0.2	CM 1		FF	Meta-pelite	3	1337.25	89.09	1603.78	37.90	1.08	2.35	0.704	0.45
			STD				0.14	7.76	0.96	2.9	0.31	0.12	0.003	0.03	
P-P	FF-06		CM 2		FF	Meta-pelite	1	1321.59	122.21	1591.56	43.73	0.84	2.79	0.67	0.47
P-P	FF-15	0.11	CM 1		FF	Meta-pelite	1	1337.92	90.14	1615.24	44.22	0.89	2.04	0.68	0.39
			STD												
P-P	FF-15		CM 2		FF	Meta-pelite	3	1328.35	102.55	1599.88	35.81	0.78	2.79	0.68	0.40
			STD				1.73	2.26	2.62	1.99	0.01	0.12	0.02	0.05	
P-A	FF-04		CM 1		FF	Meta-pelite	1	1335.39	133.64	1598.49	58.70	0.64	2.28	0.57	0.31
P-A	FF-04	0.18	CM 2	0.14	FF	Meta-pelite	3	1331.06	105.66	1601.58	41.55	0.73	2.84	0.65	0.41
						STD		4.69	12.13	4.46	3.15	0.05	2.79	0.04	0.11

Metamorphic Grade	Sample ID	NCC (%)	CM Type	Au (ppm)	Sampling Location	Lithology	Measurement Number	D Position (cm ⁻¹)	D Width (FWHM) (cm ⁻¹)	G Position (cm ⁻¹)	G Width (FWHM) (cm ⁻¹)	R1 Ratio	R2 Ratio	R3 Ratio	R4 Ratio
P-A	FF-14	0.33	CM 2	0.02	FF	Meta-pelite	1	1328.51	104.96	1599.60	37.57	0.76	2.79	0.66	0.36
P-A	FF-03	0.31	CM 2	0.03	FF	Meta-pelite	1	1322.26	89.58	1590.57	43.60	0.66	2.05	0.59	0.50
P-A	FF-13	2.58	CM 2		FF	Meta-pelite STD	7	1332.21 0.69	100.76 5.31	1601.08 0.95	35.107 1.80	0.77 0.08	2.87 0.02	0.69 0.02	0.39 0.03
P-A	FF-01	0.1	CM 2		FF	Meta-sandstone STD		1323.41 7.26	97.31 11.89	1588.84 7.54	49.05 4.64	0.66 0.06	1.98 0.22	0.59 0.06	0.34 0.11
P-A	LH-01	0.32	CM 3		LH	Meta-pelite STD		1348.33 0.01	33.98 3.45	1580.85 2.00	28.41 4.59	0.99 0.17	1.20 0.06	0.528 0.005	0.83 0.17
P-A	TC-01	0.45	CM 3		LH	Meta-pelite STD		1350.38 2.53	37.42 6.09	1581.54 0.41	28.29 2.74	1.24 0.17	1.32 0.09	0.59 0.04	0.75 0.04
P-A	TC-02	0.24	CM 3		LH	Meta-pelite STD		1348.22 0.24	39.72 3.78	1583.24 0.65	28.35 1.71	1.70 0.15	1.40 0.11	0.69 0.03	0.81 0.04
G-S	FF-12-A	0.66	CM 2	0.03	FF	Meta-pelite STD		1345.36 0.21	64.14 0.39	1602.14 0.34	48.14 0.44	2.061 0.03	1.33 0.01	0.719 0.005	0.46 0.01

Metamorphic Grade	Sample ID	NCC (%)	CM Type	Au (ppm)	Sampling Location	Lithology	Measurement Number	D Position (cm ⁻¹)	D Width (FWHM) (cm ⁻¹)	G Position (cm ⁻¹)	G Width (FWHM) (cm ⁻¹)	R1 Ratio	R2 Ratio	R3 Ratio	R4 Ratio
G-S	FF-12-B	0.63	CM 2		FF	Meta-pelite		1340.51	57.71	1597.18	48.56	2.15	1.19	0.729	0.46
								1.29	0.46	1.22	1.93	0.16	0.06	0.003	0.01
G-S	LH-03	0.20	CM 3		LH	Meta-pelite		1348.71	31.15	1581.37	30.85	1.08	1.11	0.52	0.76
								0.68	1.30	0.06	3.11	0.24	1.34	0.02	0.04
G-S	GB-01	0.63	CM 3		GB	Meta-pelite		1346.60	31.15	1579.20	27.50	0.98	1.14	0.51	0.76
								0.68	1.30	0.32	1.97	0.18	0.12	0.02	0.10
G-S	GB-04-A	0.4	CM 4	9.17	GB	Meta-pelite		1347.06	56.48	1599.87	50.03	1.68	1.13	0.67	0.50
								1.06	4.13	0.55	1.04	0.13	0.09	0.01	0.04
G-S	GB-04-B	0.42	CM 4	5.37	GB	Meta-pelite		1347.83	33.88	1587.79	24.43	1.39	1.39	0.64	0.37
Notes	* P-P: Prehnite-Pumpellyite facies; P-A: Pumpellyite-Actinolite facies; G-S: Lower Greenschist facies; NCC: Non-Carbonate Carbon; FF: Flddlers Flat; LH: Lake Hawea; GB: Golden Bar pit.														

Table 3.2 Relevant parameters of Raman spectra of selected samples under polarized light and circular polarized light.

Metamorphic Grade	Sample ID	Rotation Angle (°)	D Position (cm ⁻¹)	D Width (FWHM) (cm ⁻¹)	G Position (cm ⁻¹)	G Width (FWHM) (cm ⁻¹)	R1 Ratio	R2 Ratio	R3 Ratio	R4 Ratio
P-P	FF-16	0	1336.4	76.9	1600.4	37.6	1.01	2.05	0.679	0.76
		15	1336.4	78.3	1601.4	37.4	0.99	2.10	0.680	0.47
		30	1336.5	78.8	1601.2	37.0	0.95	2.13	0.676	0.55
		45	1336.3	78.5	1600.9	37.6	0.98	2.09	0.685	0.55
		60	1336.5	78.8	1601.5	37.1	0.99	2.12	0.682	0.41
		75	1336.7	77.5	1601.8	37.2	1.00	2.08	0.686	0.34
		90	1337.8	75.6	1602.2	38.6	1.03	1.96	0.689	0.56
		Average	1336.7	77.8	1601.3	37.5	0.99	2.08	0.682	0.52
	σ	0.5	1.2	0.6	0.5	0.03	0.06	0.004	0.13	
	Uncertainty (%)	0.04	1.50	0.04	1.40	3.03	2.88	0.59	25.00	
	Circular Polarized		1338.7	65.7	1602.0	37.5	1.15	1.75	0.713	0.36
P-A	FF-13	0	1332.7	97.6	1600.1	34.3	0.63	2.84	0.64	0.39
		15	1333.1	93.7	1601.8	32.5	0.61	2.89	0.64	0.34
		30	1331.4	96.1	1599.9	33.4	0.62	2.87	0.64	0.4
		45	1332.1	107.9	1601.1	37.1	0.78	2.91	0.69	0.41
		60	1331.2	103.1	1600.9	36.1	0.75	2.85	0.69	0.38
		75	1332.3	106.3	1601.0	37.2	0.79	2.85	0.68	0.41
		90	1332.7	100.7	1602.7	35.1	0.74	2.87	0.68	0.44
		Average	1332.2	100.8	1601.1	35.1	0.70	2.87	0.67	0.4
	σ	0.7	5.3	0.9	1.8	0.08	0.02	0.02	0.03	
	Uncertainty (%)	0.05	5.27	0.06	5.14	11.42	0.70	2.99	7.50	
	Circular Polarized		1327.8	109.3	1596.8	39.5	0.88	2.77	0.69	0.29

Metamorphic Grade	Sample ID	Rotation Angle (°)	D Position (cm ⁻¹)	D Width (FWHM) (cm ⁻¹)	G Position (cm ⁻¹)	G Width (FWHM) (cm ⁻¹)	R1 Ratio	R2 Ratio	R3 Ratio	R4 Ratio
P-A	TC-02	0	1348.6	38.9	1582.9	25.3	1.65	1.55	0.72	0.74
		15	13478.0	38.3	1582.3	29.4	1.58	1.3	0.67	0.78
		30	1348.4	37.8	1583.1	27.6	1.59	1.37	0.69	0.82
		45	1348.3	38.0	1582.7	28.5	1.61	1.33	0.68	0.86
		60	1348.2	39.2	1584.0	29.1	1.82	1.35	0.7	0.86
		75	1348.0	38.1	1584.0	28.3	1.97	1.35	0.72	0.79
		90	1348.1	47.8	1583.7	30.4	1.68	1.57	0.63	0.83
	Average		1348.2	39.7	1583.2	28.3	1.70	1.40	0.69	0.81
	σ		0.2	3.6	0.6	1.7	0.15	0.11	0.03	0.04
	Uncertainty (%)		0.02	9.00	0.04	6.03	8.82	7.86	4.35	4.94
	Circular Polarized		1348.0	37.6	1583.6	30.6	1.96	1.23	0.74	0.75
G-S	FF-12-A	0	1345.4	63.8	1602.2	47.4	2.05	1.35	2.05	0.45
		15	1345.6	64.1	1602.5	48.3	1.99	1.33	1.99	0.47
		30	1345.1	63.8	1601.9	48.5	2.09	1.31	2.09	0.45
		45	1345.7	64.7	1602.4	47.8	2.06	1.36	2.06	0.48
		60	1345.3	64.0	1601.9	48.5	2.05	1.32	2.05	0.44
		75	1345.4	63.9	1602.4	47.9	2.09	1.33	2.09	0.46
		90	1345.1	64.7	1601.6	48.5	2.07	1.33	2.07	0.46
	Average		1345.4	64.1	1602.1	48.1	2.06	1.33	2.06	0.46
	σ		0.2	0.4	0.34	0.4	0.03	0.01	0.03	0.01
	Uncertainty (%)		0.02	0.62	0.02	0.90	1.46	0.75	1.46	2.17
	Circular Polarized		1344.7	63.8	1601.5	49.2	2.07	1.30	0.717	0.47

Metamorphic Grade	Sample ID	Rotation Angle (°)	D Position (cm ⁻¹)	D Width (FWHM) (cm ⁻¹)	G Position (cm ⁻¹)	G Width (FWHM) (cm ⁻¹)	R1 Ratio	R2 Ratio	R3 Ratio	R4 Ratio
G-S	GB-04-A	0	1348.3	52.5	1599.4	51.1	1.56	1.03	0.65	0.50
		15	1348.8	51.5	1599.7	51.6	1.50	0.99	0.66	0.47
		30	1346.3	53.2	1599.9	49.5	1.80	1.07	0.69	0.47
		45	1346.7	61.5	1599.1	50.4	1.84	1.22	0.67	0.53
		60	1346.0	58.6	1600.7	48.9	1.58	1.20	0.68	0.44
		75	1346.8	56.9	1600.0	49.6	1.77	1.15	0.68	0.56
		90	1346.6	61.1	1600.3	49.0	1.70	1.25	0.68	0.50
		Average		1347.1	56.5	1599.9	50.0	1.68	1.13	0.67
	σ		1.1	4.1	0.6	1.0	0.13	0.09	0.01	0.04
	Uncertainty (%)		0.08	7.30	0.03	2.09	7.74	7.96	1.49	8.00
	Circular Polarized		1348.9	54.3	1599.3	52.5	1.85	1.04	0.67	0.50
<i>Notes</i>	* Data with different rotation angles were analyzed in polarized light; Circular Polarized: the data in the last row of each sample were analyzed in circular polarized light; P-P: Prehnite-Pumpellyite facies; P-A: Pumpellyite-Actinolite facies; G-S: Lower Greenschist facies; σ : standard deviation.									

3.4 Results

3.4.1 Raman spectra

The CM in these samples was divided into four types, designated CM 1–4 herein, based on Raman spectra observations (Figure 3.3). CM 1 is the dominant form of CM in P-P facies samples with a mode (volume concentration) around 5%. CM 2 is present at all metamorphic grades, but is less common in P-P facies (mode \approx 2%) and lower G-S facies (mode \approx 3%) and more abundant in P-A facies (mode \approx 6 – 10%). CM 3 is found in P-A facies (mode \approx 7%) and lower G-S facies (mode \approx 8%), including the host rocks of the Golden Bar pit, and CM 4 (mode \approx 5%) is only observed in mineralized rocks.

CM 1 (see Figure 3.3 C) is characterized by a high intensity, wide (up to 134.69 cm^{-1} FWHM) D band at around $1336.5 \pm 2.4 \text{ cm}^{-1}$ ($n = 4$, n is equal to total sample number) and a relatively low intensity, narrow (up to 52.18 cm^{-1} FWHM) G band at $1604.1 \pm 3.54 \text{ cm}^{-1}$ ($n = 4$). The spectra also display a low intensity, wide (up to 148.04 cm^{-1} FWHM) D1 band and a wide (up to 159.12 cm^{-1} FWHM) D2 band. In the second-order region, the major peaks occur at wavenumbers of 2670 cm^{-1} (S1), 2925 cm^{-1} (S2), and 3207 cm^{-1} (S3) and they are typically present in spectra from low-maturity CM at $2663 \pm 27 \text{ cm}^{-1}$, $2923 \pm 17 \text{ cm}^{-1}$, and $3206 \pm 9 \text{ cm}^{-1}$, respectively ($n = 4$).

The Raman spectra of CM 2 (see Figure 3.3 D) exhibit a relatively low intensity, wide (up to 113.61 cm^{-1}) D peak and high intensity, narrow (up to 48.56 cm^{-1}) G peak. The positions of the D peak and G peak are $1330.67 \pm 7.4 \text{ cm}^{-1}$ ($n = 10$) and $1598.2 \pm 5.1 \text{ cm}^{-1}$ ($n = 10$) respectively. The width of D peak in CM 2, which is around 100 cm^{-1} , is much wider than that in CM 1 which is around 85 cm^{-1} . CM 2 has similarly-located D1 and D2 bands (1210 cm^{-1} and 1550 cm^{-1} respectively) as compared with CM 1, but the D1 band is much wider (up to 180.4 cm^{-1} for CM 2, and up 148.0 cm^{-1} for CM 1). The S peaks for CM 2 are qualitatively indistinguishable from those in CM 1.

The Raman spectra of CM 3 (see Figure 3.3 E), which is found in upper P-A and lower G-S facies, are considerably different from those of CM 1 and CM 2. In the first-order region, both the D and G peaks are relatively narrow, with about 30 cm^{-1}

FWHM. The position of the D band is $1348.4 \pm 1.3 \text{ cm}^{-1}$ ($n = 5$) while that of the G band is $1581.24 \pm 1.45 \text{ cm}^{-1}$ ($n = 5$). The D1 and D2 peaks are found at similar positions to the equivalent peaks in CM 1 and CM 2, but an additional D3 band is observed on the shoulder of the G band at $1615.25 \pm 4.1 \text{ cm}^{-1}$ ($n = 5$). In the second-order region, CM 3 is distinguished by spectra with a very high intensity S1 peak and an additional S5 peak around 2470 cm^{-1} that is not observed in the other samples. Some spectra also have an S4 peak (2128 cm^{-1}), S6 peak (3351 cm^{-1}) and S7 peak (3610 cm^{-1}).

The Raman spectra of CM 4 (see Figure 3.3 F), which is found in the mineralized rocks, are similar to those of CM 1, but the widths of the D and G bands are significantly narrower, with maximum FWHM of 57.14 cm^{-1} and 49.69 cm^{-1} respectively.

3.4.2 The effects of crystal orientation on Raman spectra

Table 3.2 summarises the relationship between crystal orientation and Raman spectra parameters for polarized and circular polarized laser beam measurements. Results for each sample under circular polarized light are independent of orientation, but are somewhat different to measurements made under the polarized light used in the bulk of the measurements. For example, FWHM of the D peak in the P-P sample FF-16 was $77.8 \pm 1.2 \text{ cm}^{-1}$ in polarized light, and 65.7 cm^{-1} in circular polarized light. Under polarized light, the effect of orientation on measured parameters was similar to the expected analytical error for the majority of parameters in most samples. Notable exceptions, with relative uncertainties greater than 10%, are the R4 ratio in CM 1 from FF-16 (25%), R1 in CM 2 from P-A facies sample FF-13 (11%). S4 and S6 peaks, which have highly variable intensity as a function of orientation, were only observed in CM 3. These peaks, therefore, were not considered further.

The effect of crystal orientation is therefore considered to be negligible for most measured parameters, although interpretations based on the R4 ratio, which involves the second order peaks, are treated with caution.

3.4.3 Variation in individual parameters

R1 (Figure 3.4 A)

The ratio of the intensity of the D and G peaks ($R1: I_D/I_G$) decreases from 1 to 0.62 as metamorphic grade increases through P-P facies and into P-A facies. Data for CM 1 and CM 2 overlap for P-P facies samples. R1 then increases sharply from 0.99 (CM 3, P-A) to 2.15 (CM 2, lower G-S). The four highest grade samples, one from Lake Hawea and the three from Golden Bar, then exhibit a drop in R1 to values between 0.98 and 1.66.

R2 (Figure 3.4 B)

R2, the ratio of the width of the D peak to that of the G peak (W_D/W_G) fluctuates without any clear trend from P-P to upper P-A facies, with an average value of 2.5 ± 0.3 ($n = 12$). The higher values in this population are from CM 2 grains (2.78 ± 0.07 , $n = 6$). The R2 of CM 1 grains is 2.32 ± 0.25 ($n = 4$). R2 drops to 1.20 in the upper P-A facies (CM 3). Further increases in grade do not affect R2 significantly. R2 is 1.25 ± 0.11 ($n = 9$) for grains of CM 2, CM 3 and CM 4 from lower G-S and G-S facies.

R3 (Figure 3.4C)

R3, the ratio of the total area of D peaks to the total D and G peak area, drops from 0.71 to 0.53 from P-P to P-A facies, and then increases to 0.69 in CM 3 grains from upper P-A grade samples. R3 values for CM 1 decrease with increasing metamorphic grade from 0.70 to 0.59 with some overlap with CM 2 in P-P grade samples. R3 for CM 2 also decreases with metamorphic grade. CM 2 and CM 3 in samples from the lower G-S facies also exhibit a general decrease with metamorphic grade down to values of 0.51. This trend is not followed by CM 4, which shows values for R3 of 0.66 ± 0.02 ($n = 2$).

R4 (Figure 3.4 D)

R4, the ratio of the S1 peak to the total S peak area, is consistently low at 0.42 ± 0.05 ($n = 16$) for CM 1, CM 2 and CM 4. CM 3 grains provide a significantly different population, in which R4 is 0.78 ± 0.04 ($n = 5$).

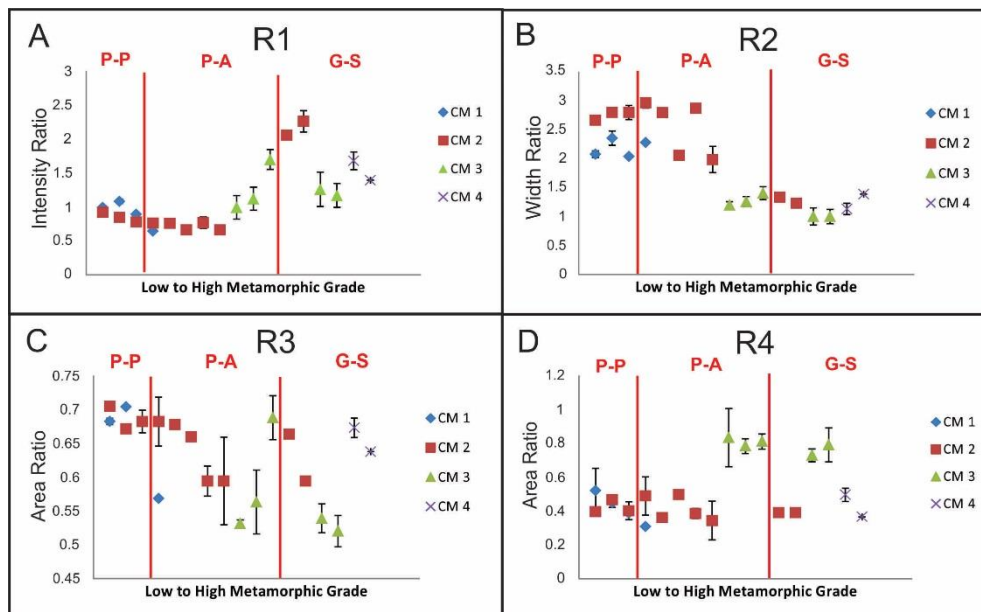


Figure 3.4 Plot of (A) $R1 = D/G$ (intensity ratio); (B) $R2 = D/G$ (width ratio); (C) $R3 = (D+D1)/(D+D1+G+D2+D3)$ (area ratio); (D) $R4 = S1/(S1+S2+S3)$ (area ratio). These ratios are plotted against the estimated ranked metamorphic grade, from P-P to lower G-S facies (P-P: Prehnite-Pumpellyite facies; P-A: Pumpellyite-Actinolite facies; G-S: Lower Greenschist facies); the error bars shown are one standard deviation, taken from multiple measurements of CM in the same samples.

3.4.4 Chemical and petrographic characterization

Bulk rock analysis

The non-carbonate carbon (NCC) content in all samples collected, except for 7 quartz vein-bearing samples, ranges from 0.02% to 2.58%. NCC content is 0.06 – 0.24% ($0.15 \pm 0.07\%$, $n = 5$) in P-P facies samples, 0.04 – 2.58% ($0.34 \pm 0.61\%$, $n = 16$) in P-A facies samples, 0.06 – 0.66% ($0.24 \pm 0.24\%$, $n = 9$) in lower G-S facies samples and 0.4 – 0.63% ($0.48 \pm 0.13\%$, $n = 3$) in mineralized samples.

Gold concentrations were below the detection limit of 0.01 ppm in all P-P facies samples. However, gold was detected in some samples from other metamorphic grades (excluding the samples with Au concentrations below the detection limit), with 0.11 ± 0.04 ppm ($n = 4$) gold in P-A facies samples, 0.03 ± 0.01 ppm ($n = 4$) gold in lower G-S facies samples and 7.3 ± 2.7 ppm ($n = 2$) gold in mineralized samples from the Golden Bar pit.

Petrography

CM 1, as defined by the Raman spectral characteristics has an appearance quite distinct to that of the other CM types. CM 1 is opaque in plane polarized light (ppl) and grey with low reflectivity in reflected light (Figure 3.5). In weakly deformed and folded P-P facies samples, grain shapes are round to sub-rounded with grain sizes ranging from 1 to 10 μm . In pelitic samples, CM 1 is usually intergrown with very fine-grained pyrite and chalcopyrite (about 1 – 5 μm) that occur as framboidal clusters (Figure 3.5 A). The largest cluster observed is about 0.1 x 0.2 mm and is surrounded by quartz, albite, muscovite and stilpnomelane (Figure 3.5 A). Finer-grained CM 1 has a grain size of about 1 μm , which is similar to that of fine-grained pyrite and chalcopyrite (Figure 3.5 B). Both CM 1 and sulfide minerals are sparsely disseminated through the sediment matrix. In more sheared and deformed P-P samples, CM 1 occurs as angular grains with widths of about 10 – 20 μm (Figure 3.6 A & B).

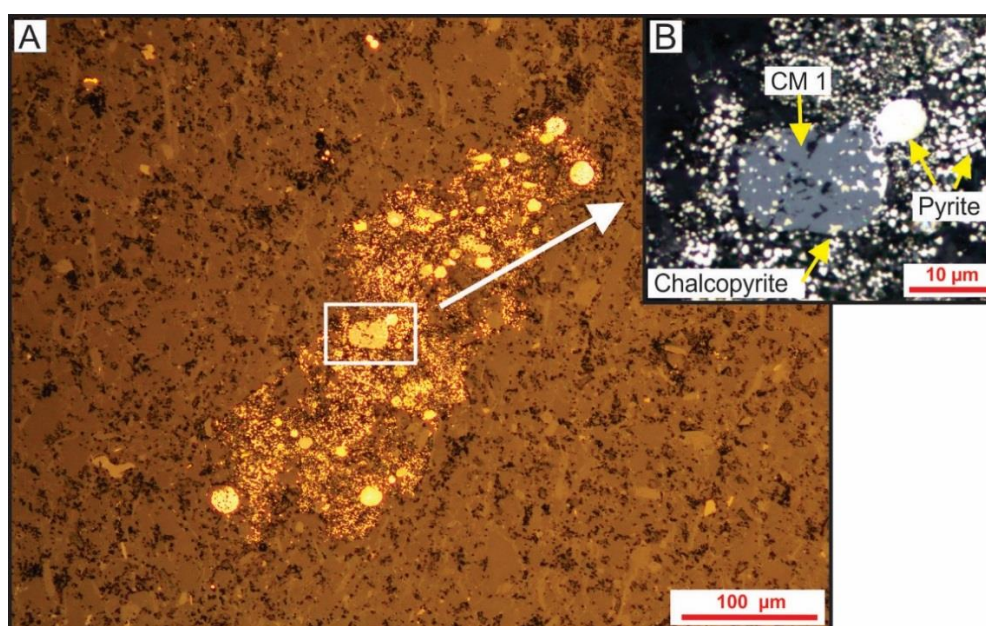


Figure 3.5 Petrographic photomicrographs of CM 1 in framboidal pyrite in lower P-P facies in reflected light (FF-16).

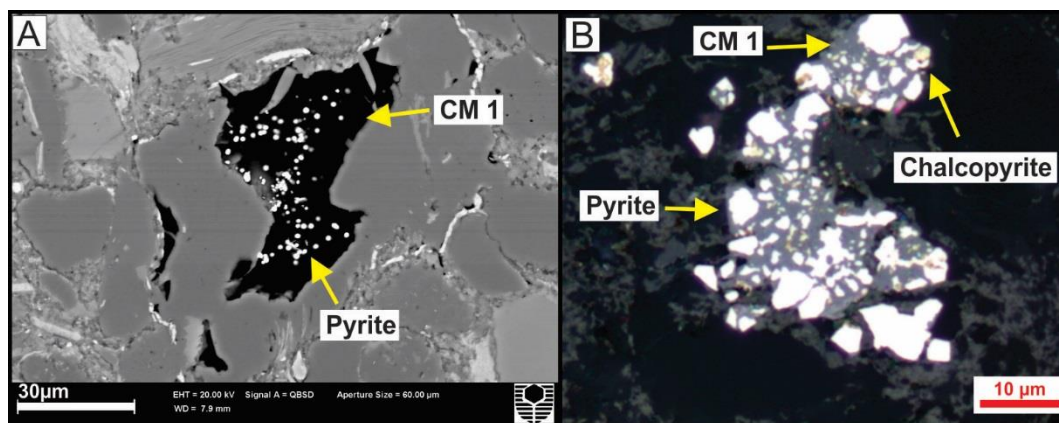


Figure 3.6 Petrographic photomicrographs of CM 1 in upper P-P facies (FF-15); (A) backscatter electron (BSE) image of CM 1 and pyrite; (B) reflected light image of CM 1, pyrite and chalcopyrite.

CM with the Raman spectral characteristics of CM 2 differs in appearance and textural position from CM 1 in a number of ways. This CM appears pale yellow, with low reflectivity, in reflected light. It occurs as short strips or slabs interstitial to other minerals (Figures 3.7 A & B). The lengths of the strips are up to 150 μm . CM 2 has a different association with pyrite to CM1; framboidal pyrite is observed to be sparsely disseminated through CM 2, but does not occur within the sediment matrix as observed for CM 1 samples. Large (100 – 150 μm) flakes of CM 2 are observed in carbonate veins (Figure 3.7 C). In lower G-S facies rocks, bands of black material with high CM 2 content aligned parallel to the foliation are observed throughout the thin sections. In these bands, CM 2 has the same optical properties as above, but it is present as fragments with widths of about 20 μm and lengths of about 40 μm , and is associated with cubic pyrite (Figure 3.7 D).

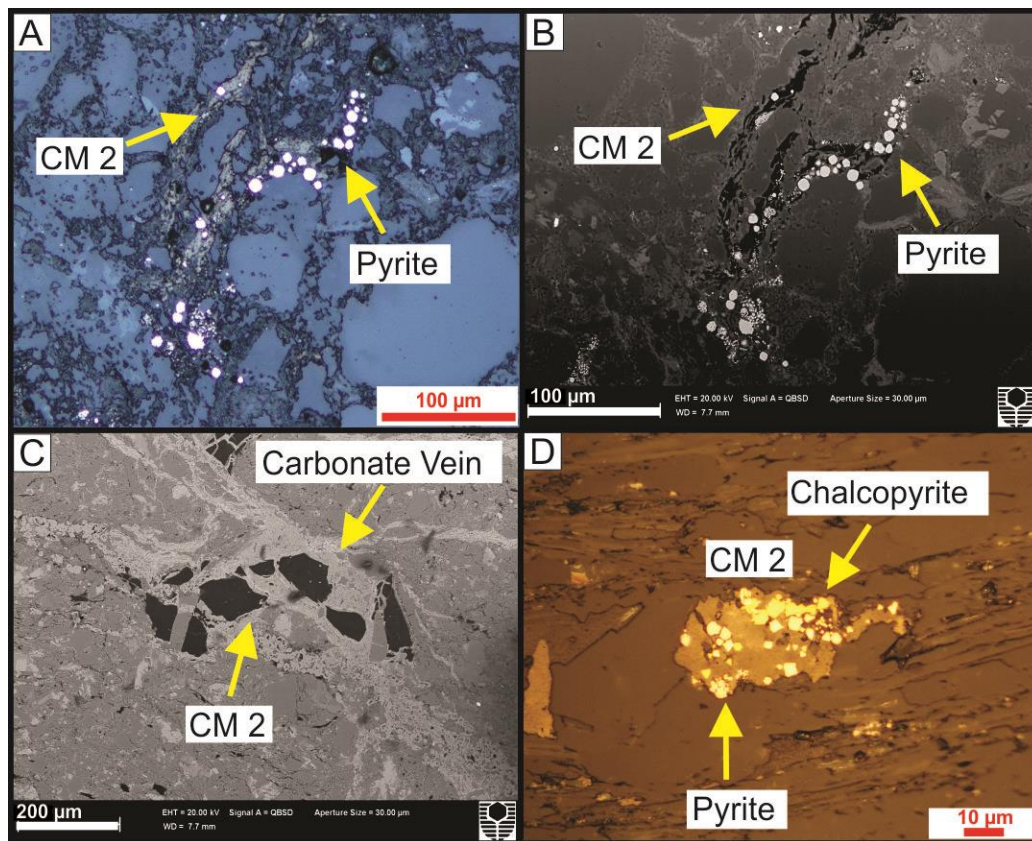


Figure 3.7 Photomicrographs of CM 2 in P-A and G-S facies samples in reflected light and SEM-BSE; (A) Strip-shaped CM 2 and framboidal pyrite in reflected light; (B) Strip-shaped CM 2 and framboidal pyrite in BSE from FF-04, P-A facies; (C) Flaky CM 2 in carbonate veins in BSE from FF-13, P-A facies; (D) Flaky CM 2 elongated parallel the foliation with pyrite and chalcopyrite in reflected light from FF-12-A, G-S facies.

CM with the Raman spectral characteristic defined as CM 3 occurs in samples of P-A facies and lower G-S facies from Lake Hawea and lower G-S facies samples from the host rock at the Golden Bar Pit. This CM is also optically and texturally distinct from the other CM types. CM 3 has a sub-rounded grain shape with an elongate elliptical habit, is less than $4 \times 10 \mu\text{m}$ in size, and is light grey with low reflectivity in reflected light (Figure 3.8 A). In all of the CM 3-bearing samples, the foliation is defined by segregation of the sample into quartz-rich and quartz-poor layers. The quartz-poor layers mainly comprise recrystallized quartz, albite, chlorite and muscovite and are cross cut by black bands (Figure 3.8 A & B). These bands are made up of consistently aligned CM 3 grains (Figure 3.8 C).

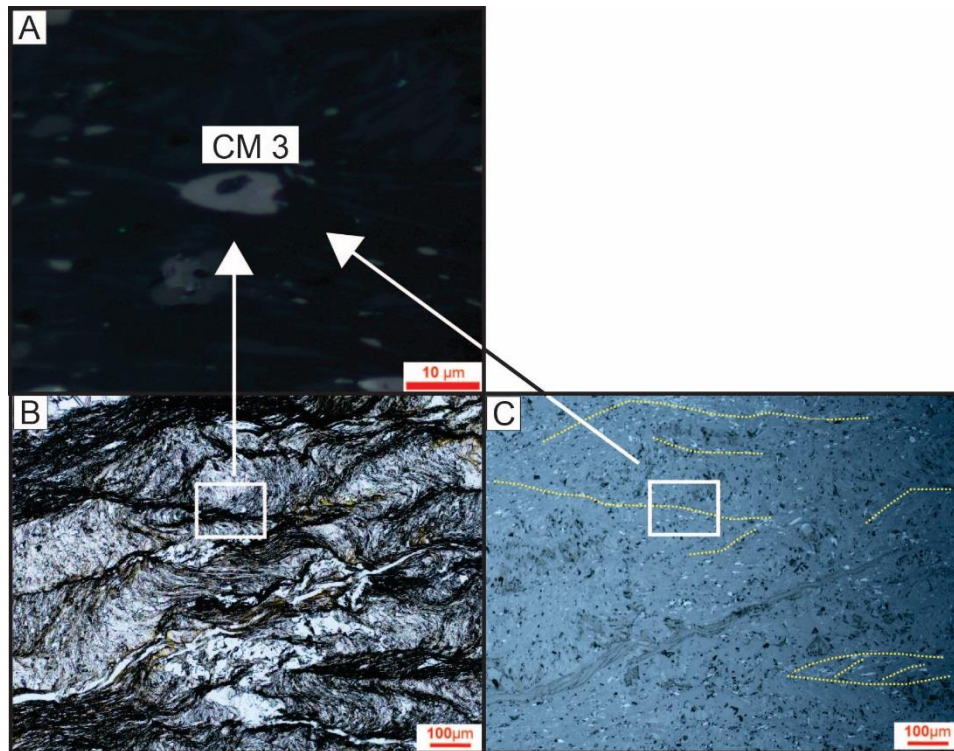


Figure 3.8 Photomicrographs of CM 3 from P-A facies (LH-01); (A) CM 3 grain in reflected light; (B) black bands (dark) consisting of CM 3 in transmitted light; (C) black bands (dotted line) consisting of CM 3 in reflected light.

CM with the Raman spectral characteristics defined to present CM 4 is present in mineralized rocks from Golden Bar pit (Figure 3.9 A). This CM is angular and grey with low reflectivity, and grain size is up to 10 µm in the largest dimension (Figure 3.9 B). Some CM 4 grains are as small as 1 µm in the smallest dimension, and occur in aggregates with pyrite, arsenopyrite, galena and clay minerals. These smaller CM grains are hard to characterize petrographically, but can be analysed without difficulty using the high spatial resolution Raman microscope.

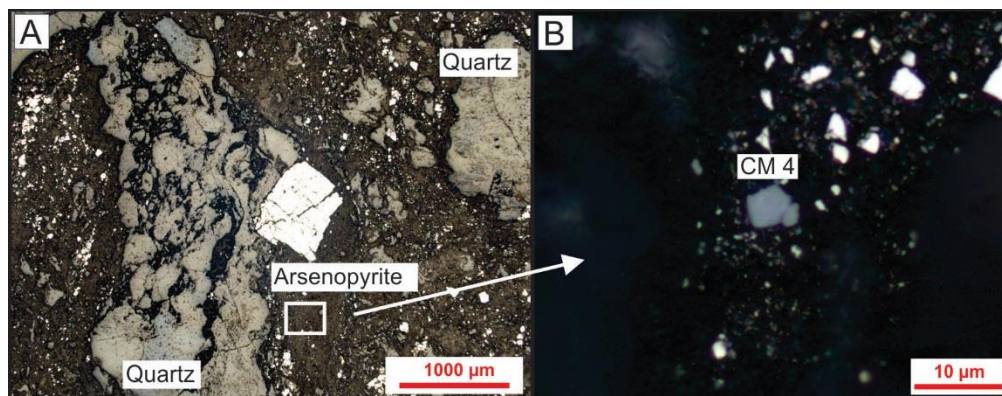


Figure 3.9 Photomicrographs of CM 4 in reflected light (from GB-04-A, lower G-S facies) in mineralized sheared rock, Golden Bar pit, Macraes mine. (A) Mica-rich shears (dark) surround disrupted fragments of quartz (pale grey). White sulfides, including a large fractured arsenopyrite grain (centre) are scattered through the sheared rock. These sulfides contain particulate and solid solution Au (Large et al. 2012). (B) CM 4 particles are scattered through the sheared rock with the auriferous sulfides.

3.5 Discussion

3.5.1 CM Raman spectra compared with previous work

Previous studies have documented decreases in R1, R2 and the widths of the D and G bands of CM with increasing temperature (Beyssac et al., 2002; Wopenka and Pasteris, 1993). These studies were made on samples from G-S facies metamorphic grade and higher. R3 has been observed to decrease with increasing degree of crystallinity, but this trend was not observed in very low maturity CM, where vitrinite reflectance is less than 2.5% (Beyssac et al., 2002; Quirico et al., 2005; Wopenka and Pasteris, 1993). With respect to the S peaks, as crystallite size decreases, S1 is expected to become wider, S2 to become more intense and S3 to be suppressed (Wopenka and Pasteris, 1993). Thus, R4 has been used to estimate the relative crystallite size for well-organized CM (Wopenka and Pasteris, 1993).

From the above, we may infer that low maturity CM should have a high R1, R2 and R3, and a low R4, combined with relatively wide D and G peaks. High maturity CM, on the other hand, should have the opposite characteristics. Spectra from this study exhibit D and G bands with widths that decrease with metamorphic grade, consistent with previous work, and R1 decreases with grade through the P-P facies. However, in contrast to most previous results, R1 shows an overall increase between P-A to lower G-S facies in spectra measured from samples from this study. The observations of R1 trends from this study are, however, consistent with those Quirico et al. (2005) who measured the Raman spectra of coal samples with a vitrinite reflectance of 2 – 7%.

CM 1 and CM 2 have relatively low R4, and high R2 and R3 and wide D and G peaks, consistent with low maturity CM. An exception is seen for one CM 2 sample

taken from the lower G-S facies, but an increase in maturity in CM 2 relative to the one in other CM 2 bearing samples from P-P and P-A facies is expected. An observed alignment with metamorphic foliation and association with cubic rather than framboidal pyrite suggests that this CM 2 likely experienced some degree of metamorphic recrystallization. CM 3 and CM 4 have relatively high R4 and low R2 and R3 compared to CM 1 and CM 2, consistent with a higher degree of maturity for these samples. CM 3 has much higher R4, due to the very high S1 peak, than CM 4, so CM 3 is interpreted to have a higher degree of crystallinity and 3D ordering than CM 4. This relative maturity is consistent with X-ray diffraction and reflectance data from samples of similar grade (Figure 3.10).

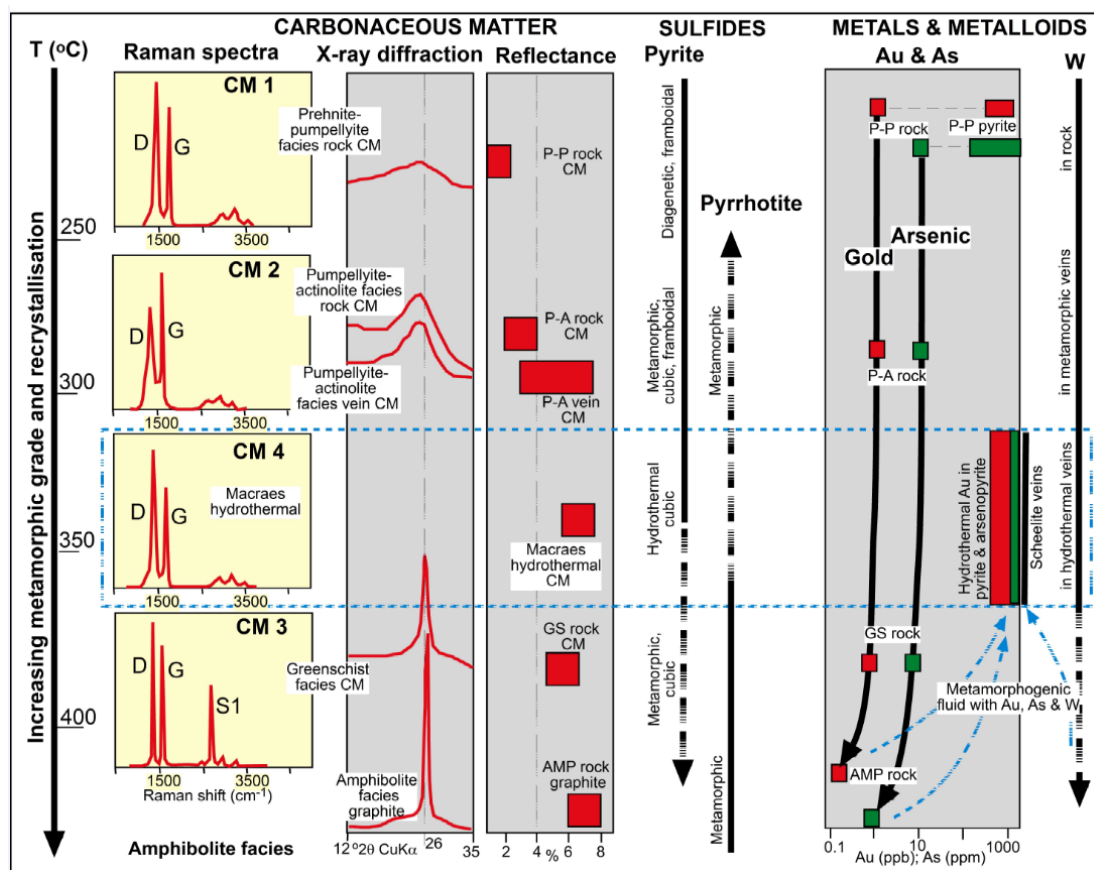


Figure 3.10 Relationships between CM, Au and As with increasing metamorphic grade in the Otago Schist (P-P: Prehnite-Pumpellyite facies; P-A: Pumpellyite-Actinolite facies; G-S: Lower Greenschist facies; AMP: Amphibolite facies). The first column is the representative Raman spectra of four types of CM from our studies compared to X-ray diffraction and reflectance of CM (after Henne and Craw, 2012; Landis 1971; McKeag and Craw 1989). The second column is the sulfides transformation investigated by Pitcairn et al., (2010). The

third column is trace metal concentration variations from Pitcairn et al., (2006) and Large et al., (2012).

3.5.2 Temperature estimates of CM from Raman spectra

A geothermometer for the Raman spectra of carbonaceous material, based on an observed linear correlation between D: G area ratios (equivalent to the R3 ratio in our study) and peak metamorphic temperature has been described (Beysac et al., 2002; Lahfid et al., 2010; Rahl et al., 2005). The equations of Lahfid et al. (2010) and Rahl et al. (2005) both work for low temperature metamorphic rocks, as the former is applicable from 200 – 320 °C and the latter ranges from 100 - 700°C. Both geothermometers have been applied to our rocks used for this study. Results from Rahl et al. (2005) geothermometer, which uses the parameters of the relative intensity and areas of the D and G peaks, were consistent with those from mineral composition-based temperature-pressure estimates (Frey et al., 1991; Mortimer, 2000). However, results from the Lahfid et al. (2010) geothermometer, which only contains the parameter of the relative areas of the D and G peaks, were up to 100 °C higher than previous estimated temperature. The Rahl et al. (2005) thermometer is considered to be more applicable to our study area, as the evolution of Raman spectra in the samples is probably more complex than can be described simply by an area ratio. The equation is as follows:

$$T (^{\circ}\text{C}) = 737.3 + 320.9 R_1 - 1067 R_3 - 80.638 R_1^2. \quad (5)$$

The temperatures obtained from the above equation indicate that $T_{\text{CM}2} \approx T_{\text{CM}1} \ll T_{\text{CM}4} < T_{\text{CM}3}$ (Table 3.3), which is consistent with the relative maturity of CM inferred from the spectra, unsurprisingly, given that both methods use the same ratios. The Raman-derived temperatures (T_{R}) of CM 1 are in agreement with the metamorphic grades which have been estimated from previous studies (Mortimer, 2000). Calculated T_{R} for most CM 2 is lower than the estimated metamorphic temperature ranges (T_{M}), and is the same, within error, for CM 2 in P-P and P-A facies samples. CM 3 has higher values of T_{R} than CM 1, CM 2 and CM 4 in all samples investigated, and T_{R} for CM 3 are at the high end or slightly higher than, estimated ranges for T_{M} . The T_{R} of CM 4 is lower than, but within error of, the estimated metamorphic temperature ranges for the lower G-S facies, and is lower

than T_R for CM 3. The structure of low temperature CM may be affected by other parameters, such as carbon precursor and the duration of metamorphism (Beysac et al., 2003a; Lahfid et al., 2010). However, Beysac et al. (2003a) demonstrated that temperature still plays the key role during the graphitization of CM. Our study was conducted on the basis of this argument.

Table 3.3 Temperature estimates from Raman spectra and metamorphic facies for each CM type.

CM Type	Number of Samples	Metamorphic Grade	Sample Location	T_R (°C)	T_M (°C)
CM 1	3	P-P	Fiddlers Flat	239 ± 8	150 ~ 250
	1	P-A	Fiddlers Flat	304	250 ~ 350
CM 2	3	P-P	Fiddlers Flat	226 ± 12	150 ~ 250
	5	P-A	Fiddlers Flat	237 ± 26	250 ~ 350
	2	Lower G-S	Fiddlers Flat	283 ± 8	350 ~ 450
CM 3	4	P-A	Lake Hawea	388 ± 55	250 ~ 350
	1	Lower G-S	Golden Bar	433	350 ~ 450
CM 4	2	Lower G-S	Golden Bar	339 ± 12	350 ~ 450
Notes	P-P: Prehnite-Pumpellyite; P-A: Pumpellyite-Actinolite; G-S: Lower Greenschist; T_R : Temperature estimated from Raman; T_M : Temperature estimated from metamorphic grade.				

3.5.3 Possible origins of CM

CM 1

Framboidal diagenetic pyrite grows in low-energy environments where the distinctive framboidal texture can be preserved for long periods of time (Love, 1964; Rickard, 1970). Early diagenetic processes have long been known to form framboidal textures through the involvement of organic matter (Chauhan, 1974; Love, 1964; MacLean et al., 2008; Rickard, 1970; Taylor and Macquaker, 2000). Rickard (1970) proposed that framboids form from by pseudomorphism of organic material; clusters of organic globules may be replaced by intermediate monosulphides such as

mackinawite ((Fe,Ni)_{1+x}S) or greigite (Fe₃S₄) and in turn replaced by pyrite microcrysts, creating the framboidal aggregates. The coexistence of framboidal pyrite, inferred to be diagenetic, with low maturity and low temperature CM 1 in lower P-P facies suggests an *in-situ* origin for CM 1.

Chalcopyrite with framboidal texture is also observed in the Fiddler's Flat framboids. Oszczepalski (1999) attributed the presence of framboidal chalcopyrite with relict pyrite cores in the Kupferschiefer to oxidative alteration of diagenetic pyrite framboids by cupriferous fluids; the chalcopyrite associated with framboidal pyrite in this study may have formed through analogous secondary processes. In upper P-P facies samples, the more angular morphology of CM 1 and decreasing association of CM 1 with pyrite may be associated with recrystallization and possible loss of pyrite due to the secondary processes.

CM 2

In previous work on the Mount Isa Basin, short ribbons of carbonaceous material with petrographic characteristics similar to those of CM 2 are considered to result from carbon migration (Glikson et al., 2006; Glikson et al., 2000). In Otago schist samples, some CM 2 is present as flakes in carbonate veins, which is consistent with deposition from a fluid during metamorphism (Luque del Villar et al., 1998). These textures suggest that CM 2 may have been deposited during the passage of carbon-rich fluid through the host rocks.

Though fluid-deposited CM is often documented as well-organized (e.g. Luque et al., 1998), disordered CM, such as the CM 2 described here, can be also deposited from fluids, and such fluid-deposited CM has a spectral signature similar to that of *in-situ* kerogen as a metastable precursor to graphite (Foustoukos, 2012; Luque del Villar et al., 1998; Pasteris and Chou, 1998). The Raman spectra of CM 2 show relatively low crystallinity with low R₂ and R₃ values, comparable to those of kerogen. However, CM 2 in lower G-S facies rocks has higher maturity Raman parameters than CM 2 in P-P and P-A facies samples, which can be attributed to either deposition from higher temperature fluids in the lower G-S rocks, or to metamorphism subsequent to deposition.

Rare framboidal pyrite grains are found sparsely disseminated through CM 2 in sample FF-04. This inclusion of pyrite in CM 2 is quite different to the more intimately intergrown CM 1 – pyrite association described above. Although more commonly attributed to a diagenetic origin, framboidal pyrite has been observed to grow from metal-enriched H₂S-bearing hydrothermal fluids during low-grade regional metamorphism (Scott et al., 2009). Thus, framboidal pyrite associated with CM 2 may have deposited from C and H₂S-bearing hydrothermal fluids.

The above discussion suggests that attribution of an origin to CM requires evaluation of both textural and Raman evidence. The flakes of CM 2 in veins are unambiguously associated, texturally, with fluid-related features, whereas if Raman evidence alone was considered then interpretation of the origin as *in-situ* deposition of CM 2 would be more likely. Detailed studies of CM from Fiddlers Flat by Henne and Craw (2012) demonstrated that CM referred to as graphite in this area was deposited from metamorphic fluids prior to gold mineralization. We propose that CM 2 is similar to the graphite studied by Henne and Craw (2012) (Figure 3.10), and infer that CM 2 was deposited from fluids.

CM 3

According to the Raman results, CM 3 is the highest maturity carbonaceous material examined in this study, and the strikingly high R₄ value and S₁ peak area indicate that CM 3 has high crystallinity. The orientation dependence of the S peaks for CM 3 supports this conclusion; as the grains of CM become larger and better ordered then greater anisotropy is expected (Table 3.2). The black bands that contain CM 3 cross cut the foliation, which suggests that CM 3 has been recrystallized and remobilized during syn- to late metamorphic processes in mainly lower G-S facies rocks (Figure 3.8 A, B & C). CM 3 is, on the basis of Raman spectra results, the most mature CM type observed in this study.

This CM 3 material is assumed to be equivalent to the CM documented by Pitcairn et al. (2005) in unmineralized samples from Lake Hawea taken from the same outcrops as those used for this study, since only one type of CM was observed in these rocks. Interestingly, Fourier Transform IR (FTIR) analyses of the CM studied by Pitcairn et

al. (2005) reveals a sub-graphitized carbon spectra with features attributed to the presence of CH_2+CH_3 and $>\text{C}=\text{O}$ groups (Figure 3.11). These spectral features mitigate against deposition from aqueous fluids because CH and $>\text{C}=\text{O}$ groups are generally thought to be destroyed during fluid-transport (Luque del Villar et al., 1998; Pitcairn et al., 2005). However, it is possible that CM 3 was mobilized only on short length scales (millimetres), possibly within a hydrocarbon-rich or bitumen-like, H_2O -poor fluid. In such a fluid the CH or $>\text{C}=\text{O}$ groups could be retained.

CM 4

CM 4 from mineralized rocks is less-well crystallized than CM 3 that occurs in the immediate host rocks (Figure 3.3 E, F; Table 3.3). On Raman spectral evidence alone, CM 4 could be either fluid-deposited or a remnant of primary CM. However, CM 4 is found only in the mineralized rocks from Golden Bar (GB-04-A & B) that contain abundant of hydrothermal sulfide minerals (Figure 3.9 A, B). This CM material also occurs in hydrothermal veins and mineralized shears, and is interpreted to have been deposited from hydrothermal fluids (Craw, 2002; Henne and Craw, 2012; Pitcairn et al., 2005). The bulk Au contents of the Golden Bar samples are 5.4 and 9.3 ppm respectively, an enrichment of more than 2000 times over background values near 1 ppb (Pitcairn et al., 2006). The estimated formation temperature of CM 4 from Raman spectra is around 339 °C (Table 3.3), which is similar, within error, to the mineralization temperature of 300 - 350 °C (Craw, 2002). Thus it is reasonable to consider a link between CM 4 and gold mineralization (see below).

CM 4 is similar to the kerogen-like CM described by Pitcairn et al. (2005). The FTIR results of Pitcairn et al. (2005) suggest the CM in mineralized rocks has less CH or $>\text{C}=\text{O}$ groups (Figure 3.11) than that in adjacent unmineralized rocks, consistent with a fluid deposition origin. CM 4 is also commonest in the Golden Bar rocks, where significant deposition of fluid-borne CM is thought to have occurred (Craw, 2002). Raman spectra of CM 4 indicate that this material is relatively immature and poorly organized compared to graphite (Figure 3.11), which could argue against the deposition of CM 4 from fluids. However, as for CM 2, there are documented cases of deposition of poorly organized CM from fluids, and in these cases the poorly organized CM is interpreted to be metastable relative to well-organized CM

(Foustoukos, 2012; Luque del Villar et al., 1998; Pasteris and Chou, 1998). However, the estimated temperature of CM 4 is similar to the metamorphic temperature so *in situ* origins cannot be ruled out.

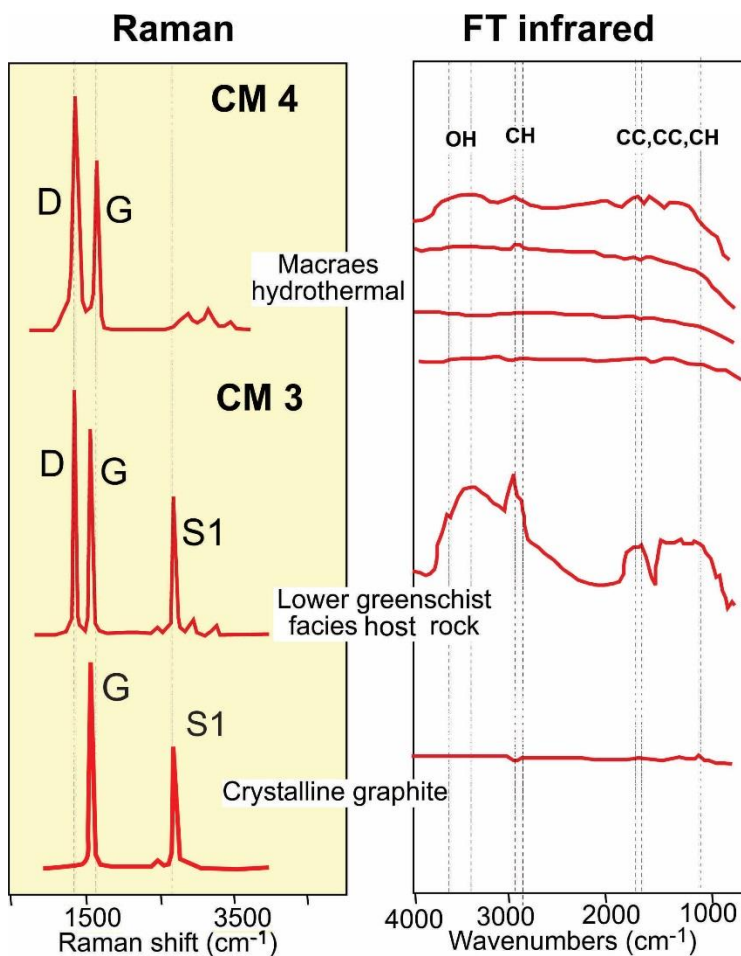


Figure 3.11 A comparison of Raman spectra results and FTIR results (The Raman spectrum of crystalline graphite is modified from Wopenka and Pasteris, 1993; FTIR results were investigated by Pitcairn et al., 2005).

3.5.4 Synthesis of relationships between CM and Au in the Otago Schist

There is a general increase in maturity of CM towards graphite with increasing metamorphic grade in the Otago Schist, from CM 1 to CM 2 to CM 3 (Figure 3.3; Table 3.3). The crystallinity of CM 1 - 3 also increases with metamorphic grade in parallel with the Raman-documented maturation, as indicated by X-ray diffraction and reflectance data (Figure 3.10) (Henne and Craw, 2012; Landis, 1971; McKeag et al., 1989). The principal CM X-ray diffraction peak becomes narrower, and the

optical reflectance becomes progressively higher as metamorphic grade increases (Figure 3.10) (Henne and Craw, 2012). This increase in maturity of CM with metamorphic grade occurred in parallel with mobilization of gold and associated elements from the metamorphic pile (Figure 3.10) (Pitcairn et al., 2010; Pitcairn et al., 2006). Hence, there may be a genetic relationship between CM and gold during the evolution of these rocks.

In P-P facies rocks, CM 1 coexists with framboidal pyrite (Figure 3.5, 3.6). Both CM and pyrite are dispersed through these low grade (P-P) rocks, and are generally in close proximity at the micron to millimetre scale (Figure 3.5, 3.6). This pyrite is of diagenetic origin, and the presence of the reductive organic matter that became CM 1 probably facilitated deposition of that pyrite. At the same time, the combination of authigenic pyrite and CM facilitated localized enrichment of Au within the pyrite (Large et al., 2012; Large et al., 2011). Large et al. (2012) conducted LA-ICP-MS on framboidal pyrite in P-P samples from Fiddlers Flat, and detected 0.5 – 10 ppm Au and 1000 - 8000 ppm As (Figure 3.10) (Large et al., 2012). In terms of implications of framboidal pyrite for gold mineralization, Vilor (1983) proposed that gold is deposited from seawater by interaction with hydrogen sulfide, and is adsorbed by organic detritus. Bacteria are thought to contribute to this process (Zhang et al., 1997). If we assume these processes occurred during formation of the framboidal pyrite in the lowest grade P-P samples, CM 1 may have been associated with the extraction or adsorption of gold from seawater.

The diagenetic pyrite recrystallized to coarser grained pyrite, and ultimately transformed to pyrrhotite during progressive metamorphism to greenschist facies (Figure 3.7, 3.10) (Henne and Craw, 2012; Large et al., 2012; Large et al., 2011). CM 2 and CM 3 were deposited from metamorphic-hydrothermal fluids during this same transition. The scale of mobility of the carbon required to cause the observed localized enrichment of CM in veins is unknown, but may be only millimetres (Figure 3.8 B) (Henne and Craw, 2012). However, associated Au and As contents are very similar in the matrices of P-P, P-A, and lower G-S facies rocks (Table 3.1) (Pitcairn et al., 2006), so there is no evidence to support a link between changes in CM type and gold mobilization. CM 2 is equivalent to the CM referred to as graphite

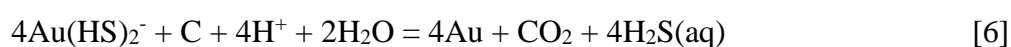
by Henne and Craw (2012), who proposed that this CM was mobilized and deposited prior to gold mobilization and deposition.

Pyrrhotite is the principal sulfide mineral in the amphibolite facies rocks, and both pyrite and pyrrhotite can be present in different rock-types throughout the metamorphic transition from P-P (Figure 3.10) (Pitcairn et al., 2006). Gold and other trace elements were released from pyrite into metamorphic-hydrothermal fluids during upper greenschist facies metamorphism, in the transition to pyrrhotite that was completed by amphibolite facies (Figure 3.10) (Pitcairn et al., 2010; Pitcairn et al., 2006). The metamorphic-hydrothermal fluids that formed CM 3 in late metamorphic shears were undoubtedly related to the gold-bearing fluids generated during prograde metamorphism, but no gold deposition is observed to have coincided with the deposition of CM 3. Instead, gold deposition occurred at slightly lower temperatures, in structurally-controlled fluid flow zones, with the less well crystallized CM 4 (Figure 3.9; Table 3.3).

Previous workers have suggested that CM may have some relationship with deposition of gold and other sulfide minerals in the Victorian gold province of Australia and elsewhere (e.g. Bierlein et al., 2001). Given the clear association between CM 4, sulfide minerals and gold at the Macraes mine, it is necessary to consider if CM 4 is associated with gold deposition at that site. There are potentially four different relationships between CM 4 and gold deposition that need to be considered.

(1) CM 4 is pre-existing *in-situ* CM that reacted with metal-bearing fluid flowing through a primary organic-rich layer (Cox et al., 1995; McKeag et al., 1989).

Deposition of gold and sulfide minerals may have been via formation of gold-organic compounds that were subsequently oxidized to form metallic gold (e.g., Radtke and Scheiner, 1970). Alternatively, CM in host rocks may have acted as a reducing agent for fluid carrying gold as bisulfide complexes, resulting in gold precipitation via a reaction like Equation [6] (Craw, 2002; Craw et al., 2007; Zoheir et al., 2008).



(2) CM 4 was deposited from the mixing of CO₂-rich and organic-rich or methane (CH₄)-rich fluids during deposition of sulfide minerals, and the sulfide mineral deposition facilitated gold deposition within those sulfide grains (e.g., Craw, 2002).

(3) Some CM 4 was precipitated from fluids prior to gold mineralization and caused the deposition of gold *via* mechanisms such as equation [6] (Craw, 2002; Craw et al., 2007).

(4) CM 4 was precipitated from fluids prior to, during, or after, gold mineralization, but had no direct causal role in gold precipitation. In this case, the CM may reflect only the focussing of fluid, rather than have a direct chemical role for CM in gold transport or deposition. For example, the CM may have had only a structural role that focused the hosting shear zone (Upton and Craw, 2008).

The evidence collected in this study, combined with previous work, shows clearly that mineralization-related CM 4 material is different from the CM 3 in host rocks, and that essentially precludes the first of the above scenarios. Our data are as yet insufficient to distinguish among the other three possible scenarios. Further work using additional techniques such as thermodynamic modelling and detailed chemical mapping using synchrotron and laser-ablation techniques are underway to further distinguish among the scenarios outlined above.

3.6 Conclusions

The combination of petrographic analysis and acquisition of Raman spectra revealed four types of carbonaceous material (CM) of varying maturity and origins in the Otago Schist. In P-P and P-A grade rocks, low maturity CM 1 coexists with framboidal pyrite and is proposed to have an *in-situ*, sedimentary origin. This CM may have been involved in sedimentary processes that produced the source of Au for gold deposits in the Otago region. CM 2, which also has low crystallinity, is also found in low grade samples and is interpreted, on the basis of its presence as large flakes in veins, to have been deposited by fluids. At the highest metamorphic grades studied (lower G-S), well organized CM 3 is interpreted to have been deposited from fluids after the peak of deformation because black bands that contain CM 3 cross cut the foliation. Less-well crystallized CM 4 from mineralized rocks is associated with

sulfide minerals, and is interpreted to have a fluid-mediated history although the details are poorly understood.

Based on the above discussion, various carbonaceous materials with different origins may have had different roles in the formation of the gold deposit. Further, the strong association of CM 1 with gold-bearing sulfide minerals suggests that CM may have played a role in pre-concentrating the gold source. CM 4 at the deposit site may have been involved in gold deposition, but in the Otago Schist region, the detailed mechanism of gold deposition is still poorly understood.

3.7 Acknowledgements

Critical reviews by two anonymous reviewers to improve the manuscript significantly are highly appreciated. All the authors acknowledge the support from the CSIRO Mineral Resources Flagship Cluster for Organic Geochemistry of Mineral Systems led by Curtin University and additional support from WA-Organic and Isotope Geochemistry Centre (WA-OIGC), The Institute of Geoscience Research (TIGeR) and Curtin University. S.H. acknowledges the receipt of Chinese Scholarship Council (CSC)-Curtin International Postgraduate Research Scholarship (CIPRS), CSIRO PhD Top-up Scholarship. Additional funding support was provided by Ministry of Business, Innovation and Employment, New Zealand.

3.8 References

- Ammar, M., Charon, E., Rouzaud, J.-N., Aleon, J., Guimbretière, G., Simon, P., 2011. On a reliable structural characterization of polished carbons in meteorites by Raman microspectroscopy. *Spectroscopy Letters* 44, 535-538.
- Beyssac, O., Brunet, F., Petit, J.-P., Goffé, B., Rouzaud, J.-N., 2003a. Experimental study of the microtextural and structural transformations of carbonaceous materials under pressure and temperature. *European Journal of Mineralogy* 15, 937-951.

- Beysac, O., Goffé, B., Chopin, C., Rouzaud, J., 2002. Raman spectra of carbonaceous material in metasediments: a new geothermometer. *Journal of Metamorphic Geology* 20, 859-871.
- Beysac, O., Goffé, B., Petitet, J.-P., Froigneux, E., Moreau, M., Rouzaud, J.-N., 2003b. On the characterization of disordered and heterogeneous carbonaceous materials by Raman spectroscopy. *Spectrochimica Acta Part A: Molecular and Biomolecular Spectroscopy* 59, 2267-2276.
- Bierlein, F.P., Cartwright, I., McKnight, S., 2001. The role of carbonaceous "indicator" slates in the genesis of lode gold mineralization in the Western Lachlan Orogen, Victoria, Southeastern Australia. *Economic Geology* 96, 431-451.
- Bonal, L., Huss, G.R., Krot, A.N., Nagashima, K., 2010. Chondritic lithic clasts in the CB/CH-like meteorite Isheyevo: Fragments of previously unsampled parent bodies. *Geochimica et Cosmochimica Acta* 74, 2500-2522.
- Chauhan, D., 1974. Diagenetic pyrite from the lead-zinc deposits of Zawar, India. *Mineralium Deposita* 9, 69-73.
- Cox, S., Sun, S., Etheridge, M., Wall, V., Potter, T., 1995. Structural and geochemical controls on the development of turbidite-hosted gold quartz vein deposits, Wattle Gully mine, central Victoria, Australia. *Economic Geology* 90, 1722-1746.
- Craw, D., 2002. Geochemistry of late metamorphic hydrothermal alteration and graphitisation of host rock, Macraes gold mine, Otago Schist, New Zealand. *Chemical Geology* 191, 257-275.
- Craw, D., MacKenzie, D., Pitcairn, I., Teagle, D., Norris, R., 2007. Geochemical signatures of mesothermal Au-mineralized late-metamorphic deformation zones, Otago Schist, New Zealand. *Geochemistry: Exploration, Environment, Analysis* 7, 225-232.
- Craw, D., Upton, P., Yu, B.-S., Horton, T., Chen, Y.-G., 2010. Young orogenic gold mineralisation in active collisional mountains, Taiwan. *Mineralium Deposita* 45, 631-646.

- Craw, D., Windle, S., Angus, P., 1999. Gold mineralization without quartz veins in a ductile-brittle shear zone, Macraes Mine, Otago Schist, New Zealand. *Mineralium Deposita* 34, 382-394.
- Deckert, H., Ring, U., Mortimer, N., 2002. Tectonic significance of Cretaceous bivergent extensional shear zones in the Torlesse accretionary wedge, central Otago Schist, New Zealand. *New Zealand Journal of Geology and Geophysics* 45, 537-547.
- Dippel, B., Jander, H., Heintzenberg, J., 1999. NIR FT Raman spectroscopic study of flame soot. *Physical Chemistry Chemical Physics* 1, 4707-4712.
- Foustoukos, D.I., 2012. Metastable equilibrium in the CHO system: Graphite deposition in crustal fluids. *American Mineralogist* 97, 1373-1380.
- Frey, M., Capitani, C.d., Liou, J., 1991. A new petrogenetic grid for low-grade metabasites. *Journal of Metamorphic Geology* 9, 497-509.
- Glikson, M., Golding, S., Southgate, P., 2006. Thermal evolution of the ore-hosting Isa superbasin: Central and northern Lawn Hill platform. *Economic Geology* 101, 1211-1229.
- Glikson, M., Mastalerz, M., Golding, S., McConachie, B., 2000. Metallogenesis and hydrocarbon generation in northern Mount Isa Basin, Australia: implications for ore grade mineralization, Organic Matter and Mineralisation: Thermal Alteration, Hydrocarbon Generation and Role in Metallogenesis. Springer, pp. 149-184.
- Goldfarb, R.J., Hart, C., Davis, G., Groves, D., 2007. East Asian gold: Deciphering the anomaly of Phanerozoic gold in Precambrian cratons. *Economic Geology* 102, 341-345.
- Gu, X., Zhang, Y., Li, B., Dong, S., Xue, C., Fu, S., 2012. Hydrocarbon-and ore-bearing basinal fluids: a possible link between gold mineralization and hydrocarbon accumulation in the Youjiang basin, South China. *Mineralium Deposita*, 1-20.

- Henne, A., Craw, D., 2012. Synmetamorphic carbon mobility and graphite enrichment in metaturbidites as a precursor to orogenic gold mineralisation, Otago Schist, New Zealand. *Mineralium Deposita*, 1-17.
- Huizenga, J.-M., 2011. Thermodynamic modelling of a cooling C–O–H fluid–graphite system: implications for hydrothermal graphite precipitation. *Mineralium Deposita* 46, 23-33.
- Jawhari, T., Roid, A., Casado, J., 1995. Raman spectroscopic characterization of some commercially available carbon black materials. *Carbon* 33, 1561-1565.
- Jehlička, J., Urban, O., Pokorný, J., 2003. Raman spectroscopy of carbon and solid bitumens in sedimentary and metamorphic rocks. *Spectrochimica Acta Part A: Molecular and Biomolecular Spectroscopy* 59, 2341-2352.
- Lahfid, A., Beyssac, O., Deville, E., Negro, F., Chopin, C., Goffé, B., 2010. Evolution of the Raman spectrum of carbonaceous material in low - grade metasediments of the Glarus Alps (Switzerland). *Terra Nova* 22, 354-360.
- Landis, C., 1971. Graphitization of dispersed carbonaceous material in metamorphic rocks. *Contributions to Mineralogy and Petrology* 30, 34-45.
- Large, R., Thomas, H., Craw, D., Henne, A., Henderson, S., 2012. Diagenetic pyrite as a source for metals in orogenic gold deposits, Otago Schist, New Zealand. *New Zealand Journal of Geology and Geophysics* 55, 137-149.
- Large, R.R., Bull, S.W., Maslennikov, V.V., 2011. A carbonaceous sedimentary source-rock model for Carlin-type and orogenic gold deposits. *Economic Geology* 106, 331-358.
- Lespade, P., Marchand, A., Couzi, M., Cruege, F., 1984. Caractérisation de matériaux carbonés par microspectrométrie Raman. *Carbon* 22, 375-385.
- Love, L.G., 1964. Early diagenetic pyrite in fine-grained sediments and the genesis of sulphide ores. *Sedimentology and Ore Genesis*, 11-17.
- Luque del Villar, F.J., Pasteris, J.D., Wopenka, B., Rodas, M., Fernández Barrenechea, J.M., 1998. Natural fluid-deposited graphite: mineralogical characteristics and mechanisms of formation. *American Journal of Science* 298, 471-498.

- Luque, F., Ortega, L., Barrenechea, J.F., Millward, D., Beyssac, O., Huizenga, J.M., 2009. Deposition of highly crystalline graphite from moderate-temperature fluids. *Geology* 37, 275-278.
- MacKinnon, T.C., 1983. Origin of the Torlesse terrane and coeval rocks, South Island, New Zealand. *Geological Society of America Bulletin* 94, 967-985.
- MacLean, L., Tyliczszak, T., Gilbert, P., Zhou, D., Pray, T., Onstott, T., Southam, G., 2008. A high-resolution chemical and structural study of framboidal pyrite formed within a low-temperature bacterial biofilm. *Geobiology* 6, 471-480.
- McKeag, S., Craw, D., Norris, R., 1989. Origin and deposition of a graphitic schist-hosted metamorphogenic Au-W deposit, Macraes, East Otago, New Zealand. *Mineralium Deposita* 24, 124-131.
- Mortensen, J.K., Craw, D., MacKenzie, D.J., Gabites, J.E., Ullrich, T., 2010. Age and origin of orogenic gold mineralization in the Otago Schist Belt, South Island, New Zealand: Constraints from lead isotope and $^{40}\text{Ar}/^{39}\text{Ar}$ dating studies. *Economic Geology* 105, 777-793.
- Mortimer, N., 1993. Jurassic tectonic history of the Otago schist, New Zealand. *Tectonics* 12, 237-244.
- Mortimer, N., 2000. Metamorphic discontinuities in orogenic belts: example of the garnet-biotite-albite zone in the Otago Schist, New Zealand. *International Journal of Earth Sciences* 89, 295-306.
- Nemanich, R., Solin, S., 1979. First- and second-order Raman scattering from finite-size crystals of graphite. *Physical Review B* 20, 392.
- Oszczepalski, S., 1999. Origin of the Kupferschiefer polymetallic mineralization in Poland. *Mineralium Deposita* 34, 599-613.
- Pasteris, J.D., Chou, I., 1998. Fluid-deposited graphitic inclusions in quartz: Comparison between KTB (German Continental Deep-Drilling) core samples and artificially reequilibrated natural inclusions. *Geochimica et Cosmochimica Acta* 62, 109-122.

- Pasteris, J.D., Wopenka, B., 1991. Raman spectra of graphite as indicators of degree of metamorphism. *Canadian Mineralogist* 29, 1-9.
- Pasteris, J.D., Wopenka, B., 2003. Necessary, but not sufficient: Raman identification of disordered carbon as a signature of ancient life. *Astrobiology* 3, 727-738.
- Peters, S.G., Jiazhan, H., Zhiping, L., Chenggui, J., 2007. Sedimentary rock-hosted Au deposits of the Dian–Qian–Gui area, Guizhou, and Yunnan Provinces, and Guangxi District, China. *Ore Geology Reviews* 31, 170-204.
- Pitcairn, I.K., Craw, D., Teagle, D.A., 2014a. Metabasalts as sources of metals in orogenic gold deposits. *Mineralium Deposita* 50, 1-18.
- Pitcairn, I.K., Olivo, G.R., Teagle, D.A., Craw, D., 2010. Sulfide evolution during prograde metamorphism of the Otago and Alpine schists, New Zealand. *The Canadian Mineralogist* 48, 1267-1295.
- Pitcairn, I.K., Roberts, S., Teagle, D.A., Craw, D., 2005. Detecting hydrothermal graphite deposition during metamorphism and gold mineralization. *Journal of the Geological Society* 162, 429-432.
- Pitcairn, I.K., Teagle, D.A., Craw, D., Olivo, G.R., Kerrich, R., Brewer, T.S., 2006. Sources of metals and fluids in orogenic gold deposits: insights from the Otago and Alpine Schists, New Zealand. *Economic Geology* 101, 1525-1546.
- Quirico, E., Montagnac, G., Rouzaud, J.-N., Bonal, L., Bourot-Denise, M., Duber, S., Reynard, B., 2009. Precursor and metamorphic condition effects on Raman spectra of poorly ordered carbonaceous matter in chondrites and coals. *Earth and Planetary Science Letters* 287, 185-193.
- Quirico, E., Rouzaud, J.-N., Bonal, L., Montagnac, G., 2005. Maturation grade of coals as revealed by Raman spectroscopy: Progress and problems. *Spectrochimica Acta Part A: Molecular and Biomolecular Spectroscopy* 61, 2368-2377.
- Radtke, A.S., Scheiner, B.J., 1970. Studies of hydrothermal gold deposition-(pt.) 1, carlin gold deposit, Nevada, the role of carbonaceous materials in gold deposition. *Economic Geology* 65, 87-102.

- Rahl, J.M., Anderson, K.M., Brandon, M.T., Fassoulas, C., 2005. Raman spectroscopic carbonaceous material thermometry of low-grade metamorphic rocks: calibration and application to tectonic exhumation in Crete, Greece. *Earth and Planetary Science Letters* 240, 339-354.
- Rickard, D.T., 1970. The origin of framboids. *Lithos* 3, 269-293.
- Sadezky, A., Muckenhuber, H., Grothe, H., Niessner, R., Pöschl, U., 2005. Raman microspectroscopy of soot and related carbonaceous materials: spectral analysis and structural information. *Carbon* 43, 1731-1742.
- Scott, R.J., Meffre, S., Woodhead, J., Gilbert, S.E., Berry, R.F., Emsbo, P., 2009. Development of framboidal pyrite during diagenesis, low-grade regional metamorphism, and hydrothermal alteration. *Economic Geology* 104, 1143-1168.
- Sforna, M., van Zuilen, M., Philippot, P., 2014. Structural characterization by Raman hyperspectral mapping of organic carbon in the 3.46 billion-year-old Apex chert, Western Australia. *Geochimica et Cosmochimica Acta* 124, 18-33.
- Taylor, K., Macquaker, J., 2000. Early diagenetic pyrite morphology in a mudstone-dominated succession: the Lower Jurassic Cleveland Ironstone Formation, eastern England. *Sedimentary Geology* 131, 77-86.
- Thomas, H.V., Large, R.R., Bull, S.W., Maslennikov, V., Berry, R.F., Fraser, R., Froud, S., Moye, R., 2011. Pyrite and pyrrhotite textures and composition in sediments, laminated quartz veins, and reefs at Bendigo gold mine, Australia: insights for ore genesis. *Economic Geology* 106, 1-31.
- Tsu, R., González H, J., Hernández C, I., 1978. Observation of splitting of the E_{2g} mode and two-phonon spectrum in graphites. *Solid State Communications* 27, 507-510.
- Upton, P., Craw, D., 2008. Modelling the role of graphite in development of a mineralised mid-crustal shear zone, Macraes mine, New Zealand. *Earth and Planetary Science Letters* 266, 245-255.
- Vallance, J., Cathelineau, M., Boiron, M., Fourcade, S., Shepherd, T., Naden, J., 2003. Fluid-rock interactions and the role of late Hercynian aplite intrusion

- in the genesis of the Castromil gold deposit, northern Portugal. *Chemical Geology* 194, 201-224.
- Vilor, N., 1983. Gold in black shales. *Geochemistry International* 20, 167-176.
- Wopenka, B., Pasteris, J.D., 1993. Structural characterization of kerogens to granulite-facies graphite: applicability of Raman microprobe spectroscopy. *The American Mineralogist* 78, 533-557.
- Yoon, D., Moon, H., Son, Y.-W., Samsonidze, G., Park, B.H., Kim, J.B., Lee, Y., Cheong, H., 2008. Strong polarization dependence of double-resonant Raman intensities in graphene. *Nano Letters* 8, 4270-4274.
- Yui, T.F., Huang, E., Xu, J., 1996. Raman spectrum of carbonaceous material: a possible metamorphic grade indicator for low-grade metamorphic rocks. *Journal of Metamorphic Geology* 14, 115-124.
- Zhang, J., Lu, J., Zhai, J., Yang, F., 1997. Simulating experiments on enrichment of gold by bacteria and their geochemical significance. *Chinese Journal of Geochemistry* 16, 369-373.
- Zoheir, B., El-Shazly, A., Helba, H., Khalil, K., Bodnar, R., 2008. Origin and evolution of the Um Egat and Dungash orogenic gold deposits, Egyptian Eastern Desert: evidence from fluid inclusions in quartz. *Economic Geology* 103, 405-424.

Chapter 4

Associations between sulfides, carbonaceous material, gold and other trace elements in polyframboids: implications for the source of orogenic gold deposits, Otago Schist, New Zealand

This chapter is a published paper in *Geochimica et Cosmochimica Acta*.

Hu, S.-Y., Evans, K., Fisher, L., Rempel, K., Craw, D., Evans, N.J., Cumberland, S., Robert, A., Grice, K., 2016. Associations between sulfides, carbonaceous material, gold and other trace elements in polyframboids: Implications for the source of orogenic gold deposits, Otago Schist, New Zealand. *Geochimica et Cosmochimica Acta* 180, 197-213 (Impact factor 4.315).

Contributions by co-authors

Si-Yu Hu and Katy Evans collected samples. Dave Craw provided assistance in the field trip. Si-Yu Hu performed sample preparation for element concentration analysis, petrographic observations, Synchrotron X-ray fluorescence microscopy (SXRF) with the help of Louise Fisher, Katy Evans, Susan Cumberland and Aileen Robert, and laser ablation inductively coupled plasma mass spectrometry (LA-ICP-MS) with the help of Noreen J. Evans and Katy Evans. Si-Yu Hu is the primary author of the manuscript with helpful discussions and guidance from all co-authors. Funds was provided by the CSIRO Organic Geochemistry of Mineral Systems Cluster.

Abstract

Intimately intergrown micron-scale framboidal pyrite, carbonaceous material (CM), chalcopyrite, sphalerite and cobaltite form polyframboids in prehnite-pumpellyite facies rocks of the Otago Schist, New Zealand. This study quantifies the metal contents of these polyframboids using synchrotron X-ray fluorescence (SXRF) and laser ablation inductively coupled plasma spectrometry (LA-ICP-MS). Trace elements Au, Zn, As, Mo, Co, Ni, Cu, Ag and Pb are significantly enriched in the polyframboids. The distribution of Zn most closely follows that of CM, and was probably absorbed into the structure of the polyframboids during biogenic processes. The concentrations of Au and Ag are positively correlated with the Zn concentration in the polyframboids (R^2 of Au-Zn and Ag-Zn are 0.81 and 0.89, respectively.). The concentration of other trace elements, such as As, Co and Cu, which occur adjacent to Zn on elemental maps, show a weak relationship with Zn and may have been incorporated into the polyframboids during later processes. These polyframboids are a probable source for gold and other elements in the orogenic gold mineralization system of the Otago Schist. Metamorphic transformation of the polyframboids may have released the metallic elements into the mineralizing fluid during prograde metamorphism of the schist belt.

4.1 Introduction

Pyrite framboids, present as spherical aggregates of pyrite microcrystals, are commonly found in sedimentary rocks, especially in mudstone or siltstone (Love et al., 1984; Rickard, 1970; Schoonen, 2004; Wilkin and Barnes, 1997). Sometimes, these framboids are clustered as aggregates, termed as “polyframboids” (Love, 1971; Mees and Stoops, 2010). There has been much debate over whether these framboids have biogenic or inorganic origins, and there is evidence for both genetic processes (Donald and Southam, 1999; Love, 1971; Love et al., 1984; Rickard, 1970; Schoonen, 2004; Wilkin and Barnes, 1997). More recently, attention has become focussed on trace element enrichment in framboids, and it has been shown that As, Ni, Co, Pb, Zn, Mo, V and Cd are enriched in polyframboids (Gregory et al., 2015; Large et al., 2011; Large et al., 2009; Large et al., 2007; Scholz and Neumann,

2007). Polyframboids are commonly intimately associated with carbonaceous material (CM), as well as other sulfide minerals such as sphalerite and cobaltite (Large et al., 1999; MacLean et al., 2007; Wilkin et al., 1996). Sphalerite has been recorded to occur as a coating on the CM organic structure, whereas pyrite is found in the interstices of the CM structure, rather than in direct contact with organic surfaces (MacLean et al., 2007; MacLean et al., 2008). Cobaltite has been recorded to occur interstitial to microcrystalline pyrite (Large et al., 1999)

Gold enrichment in polyframboids, in addition to the other elements, has been a major focus of recent research (Gregory et al., 2015; Large et al., 2012; Large et al., 2011; Large et al., 2009; Large et al., 2007). However, it has also been demonstrated that Au is intimately related to CM in organic-rich shale (Bavinton and Keays, 1978; Coveney et al., 1992; Crocket and Kuo, 1979; Kettler et al., 1990; Titley, 1991). These results have led to the hypothesis that recrystallization of polyframboids could be the source for the gold and other elements found in orogenic and Carlin-style sediment-hosted mineralised systems (Large et al., 2011; Large et al., 2009; Pitcairn et al., 2006).

Despite the apparent importance of relationships between sulfides, CM, and trace metals to studies of mineral deposit formation, the details of these inter-relationships are poorly understood because of the fine grain size of polyframboids in potential Au source rocks. Elucidation of these relationships requires analytical techniques with high spatial resolution and low detection limits. Previous studies of trace elements in framboids have used a variety of techniques, such as X-ray and backscatter electron imaging and electron probe microanalysis (EPMA) (Craig et al., 1998; Large et al., 1999; Lowers et al., 2007; MacLean et al., 2007). However, the utility of these results is limited for elements such as Au because of the low concentration of trace elements in the framboids relative to the detection limits of the instruments. More recently, laser ablation inductively coupled plasma mass spectrometry (LA-ICP-MS) and synchrotron X-ray fluorescence microscopy (SXRF) techniques have been applied to sulfide analysis (Large et al., 2009, 2012; Fisher et al., 2014). These techniques have lower detection limits and/or better spatial resolution than the previous techniques, making high precision analysis of these trace elements possible for the first time.

Analysis conducted by LA-ICP-MS can provide quantitative results for trace elements present at very low concentrations (> 0.01 ppm), such as Au, Ag and Pb (Large et al., 2009). However, the spot size of the laser beam is quite large (typically 15 to 75 μm in diameter) so the ability to resolve fine details in the target area is limited (Fisher et al., 2014; Large et al., 2009). SXRF, on the other hand, has the advantage of very high spatial resolution (spot size as low as 2 μm), relatively low detection limits (10–100 ppm for many trace elements), and non-destructive, rapid, quantitative analysis (Ryan et al., 2010a; Ryan et al., 2010b). SXRF using the Maia detector (Ryan et al., 2010a; Ryan et al., 2010b) has therefore been applied to understand the distribution of trace elements and rare phases within geological samples (Dyl et al., 2014; Fisher et al., 2014). An additional advantage to SXRF mapping using the Maia detector and the associated GeoPIXETM spectral deconvolution software is that, rather than limiting the analyses by selecting elements of interest prior to measurement, the elements present can be identified during the spectra fitting processes (Fisher et al., 2014). Further, the technology lends itself to the construction of element maps, which provides a huge amount of textural information. A combination of LA-ICP-MS and SXRF analyses were adopted herein so that both low detection limits and high spatial resolution could be achieved.

In this study, we have quantified the compositions of polyframboids in low grade metasediments (prehnite-pumpellyite facies) from the Otago Schist, New Zealand. We focus on the concentrations and distributions of Au and other metals, and the associations of metals with CM in the polyframboids. We then evaluate the potential for these polyframboids to provide metal sources for ore deposit formation. Our study complements previous work by Large et al. (2012), who used LA-ICP-MS investigations to quantify some metal contents of diagenetic pyrite in these rocks, and Hu et al. (2015) who documented maturation of CM in the same rocks. We extend this previous work with better spatial resolution and lower analytical detection limits of SXRF, and relate our results to genetic models of orogenic gold deposit formation.

4.2 Geological Background and Sampling

The Otago Schist, located on the South Island of New Zealand, is a Paleozoic to Mesozoic turbidite sequence that was metamorphosed and uplifted in the Jurassic and early Cretaceous (Figure 4.1) (MacKinnon, 1983; Mortimer, 1993). Normal faults formed after uplift resulted in the juxtaposition of schists at different metamorphic grades from prehnite-pumpellyite (P-P) facies to upper greenschist (G-S) facies (Mortimer, 2000). The metamorphosed belt is symmetrical with a core zone of upper G-S facies rocks, flanked on either side by zones of progressively lower grade rocks (Figure 4.1) (Mortimer, 1993; Mortimer, 2000). Metamorphic grades range from P-P facies on the margins, through pumpellyite-actinolite (P-A) facies, to lower G-S facies within the core zone of the schist belt (Figure 4.1). The protoliths to the rocks examined here are quartzofeldspathic sandstones and pelites.

Metapsammites and metapelites of the P-P facies and P-A facies mostly lack foliation and preserve bedding (Henne and Craw, 2012). The typical mineral assemblage of metapsammites and metapelites is quartz, albite, muscovite, chlorite, epidote, stilpnomelane, pumpellyite plus prehnite in P-P facies and actinolite in P-A facies (Mortimer, 1993; Mortimer, 2000). Pyrite is the most common sulfide mineral, and framboidal pyrite dominates over cubic pyrite in P-P facies rocks, whereas more cubic pyrite and less framboidal pyrite is present in P-A facies rocks. Framboidal pyrite in P-P facies rocks is of diagenetic origin, whereas there is some evidence that framboidal pyrite in P-A facies rocks has been deposited or modified by metamorphic-hydrothermal fluids (Hu et al., 2015). Rocks become progressively more recrystallized and foliated as metamorphic grade increases, and the schists in the core of the belt have been pervasively recrystallized during several generations of folding and foliation development (Mortimer, 1993).

The Otago Schist belt hosts numerous orogenic gold deposits formed during Mesozoic metamorphism and uplift (Figure 4.1) (Mortensen et al., 2010). The Macraes deposit (Figure 4.1) is the only mine currently in operation in the area, and this world-class deposit has a total Au resource of more than 9 million ounces (~300 tonnes) (Moore and Doyle, 2015). In addition, more than 8 million ounces of placer gold, derived from eroded orogenic gold-bearing vein systems, have been mined in the area (Williams and McKee, 1974). Gold and associated elements (especially As

and Sb) are thought to have been mobilized on a regional scale during metamorphism, based on observations of depletion of these elements in amphibolite facies rocks relative to lower greenschist facies rocks (Pitcairn et al., 2014a; Pitcairn et al., 2006). Diagenetic pyrite in low grade rocks is thought to have provided a source of these elements for the metamorphogenic ore-forming system (Large et al., 2012; Pitcairn et al., 2010; Pitcairn et al., 2006). Metals may have been released into the ore-forming fluids during the recrystallization of framboidal to euhedral pyrite and during the metamorphism-induced transition from pyrite to pyrrhotite (Large et al., 2012; Pitcairn et al., 2010; Pitcairn et al., 2006).

This study focuses on the lowest grade rocks in this ore-forming system, and examines the metal content of the potential source material. Rocks for this study were collected from Fiddlers Flat, north-central Otago (Figure 4.1). This area has a well-exposed and previously documented transition from P-P facies to lower G-S schists that is punctuated by post-metamorphic faults (Henne and Craw, 2012; Hu et al., 2015; Large et al., 2012). Rocks are exposed in a deep river gorge, providing fresh, unoxidized exposures. The SXRF and LA-ICP-MS analyses presented here, along with sulfur content analysis, are of a single P-P sample, FF-16 with. Further details on the samples collected for this work are provided in Hu et al. (2015).

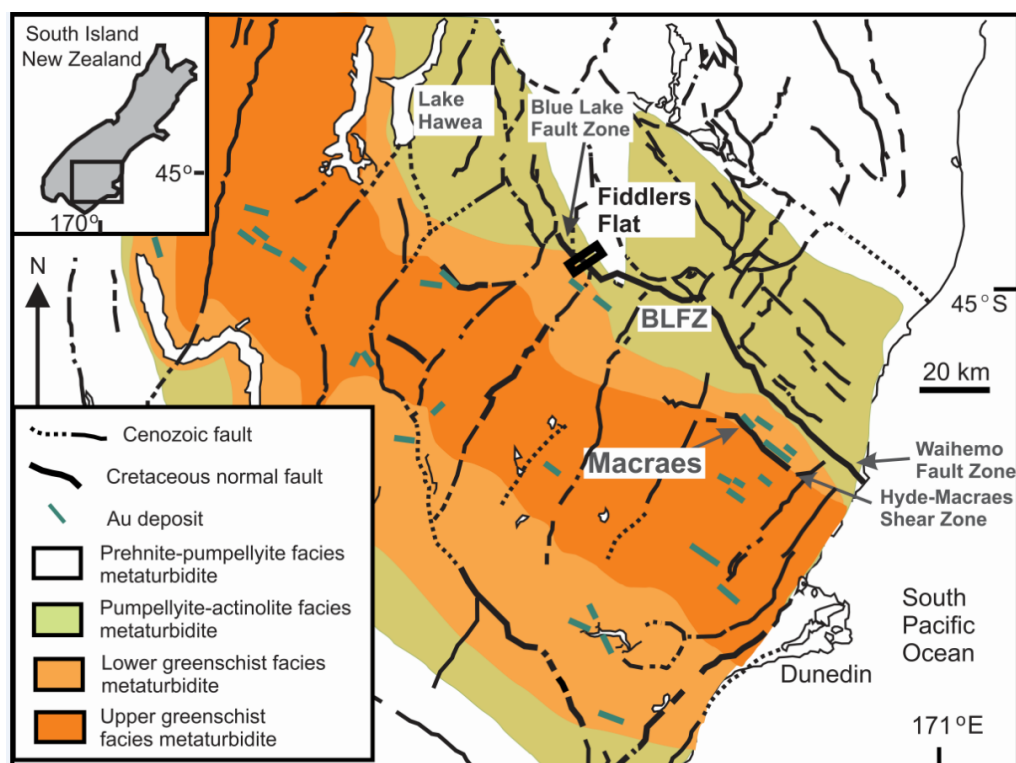


Figure 4.1 Geological map of the Otago Schist (Hu et al., 2015; modified after Henne and Craw (2012)). The black square on map is the sampling location.

4.3 Methods

4.3.1 Sulfur content analyses

Samples were crushed into powder for sulfur (S) in a tungsten carbide ring mill. Analyses were conducted by Intertek Genalysis Lab (Perth, Australia). S contents were obtained by induction furnace heating and infrared spectrometry. The standards used are MA-1b (certified reference gold ore), OD4 (matrix-matched certified reference material) and OREAS 45d (certified ferruginous soil lithogeochem reference material). The S content were determined with a relative uncertainty of less than 10 %, is used as an input for mass balance calculations in the discussion.

4.3.2 Petrographic methods

Billets left after thin section construction were polished for petrographic, SXRF and LA-ICP-MS analysis. Optical microscopy, scanning electron microscopy (SEM) and energy-dispersive X-ray spectroscopy (EDS) were used to characterize the petrographic features. Petrographic inspection of the thin sections and billets was conducted with a Nikon optical transmitted and reflected light microscope. SEM and EDS observations were made using a Tescan Mira3 field emission gun scanning electron microscope (FEG-SEM) with energy-dispersive X-ray spectroscopy (Aztec EDS) in the Curtin Materials Research Lab of Curtin University (Perth, Australia). The energy was 20.00 kV and the working distance was 15 mm. Cu foil and appropriate minerals in an Astimex standard block were used for EDS calibration.

4.3.3 LA-ICP-MS

LA-ICP-MS for in situ trace element analysis of polyframboids was performed on polished billet (FF-16) in the GeoHistory Facility of the John de Laeter Centre, Curtin University, Perth. The billet was used because LA-ICP-MS can easily penetrate a thin section before obtaining adequate counting statistics for low

concentration elements. The analysis utilized a Resonetics RESolution M-50A-LR incorporating a Compex 102 excimer laser, coupled to an Agilent 7700s quadrupole ICP-MS. Following a 20s period of background analysis, samples were spot ablated for 40 s at a 7 Hz repetition rate in an ultrahigh purity He-N₂ atmosphere using a 75 μm beam and laser energy (at the sample surface) of 2.5 J/cm². High purity Ar was employed as the plasma gas. International glass standard GSD-1G was used as the primary standard to calculate elemental concentrations (using ⁵⁷Fe as the internal standard element) and to correct for instrument drift on all elements except Au. G-NIST612 was used as a secondary standard to validate the data, indicating an accuracy of less than 10% for the analysed elements (Ag, As, Co, Cu, Ni, Mo, Pb, Zn, Mn and V). Certified sulfide standard Laflamme Po726 (synthetic pyrrhotite doped with platinum group elements and Au) was utilized as the primary standard for Au calculation. Bonn-NBS-6b was used as a secondary standard and showed a relative uncertainty of less than 5% for Au measurement. For results of data quality monitoring, please refer to Appendix A4. Standard blocks were run every 10 unknowns and the mass spectra were reduced using Iolite (Paton et al., 2011). The Fe contents of ablation spots were determined by the average Fe concentrations of areas next to the spots. The measurements were performed on the MIRA TESCAN Field Emission Gun Scanning Electron Microscope (FEG-SEM) at Curtin University with an Astimex standard block. The precision and accuracy of EDX results were checked by repeat analyse of secondary standards from the block. The relative accuracy of Fe concentration measurement is less than 5%.

4.3.4 SXRF

SXRF was performed on the X-ray fluorescence microscopy (XFM) beamline with the Kirkpatrick-Baez (KB) mirror end-station at the Australian Synchrotron (Fisher et al., 2014; Paterson et al., 2011; Ryan et al., 2013). The technique provides a monochromatic 2 μm beam spot size for energies in the 4–20 keV range (Fisher et al., 2014; Ryan et al., 2013). The XFM beamline is equipped with a Maia 384 large angle detector array and integrated real-time processor, allowing an acquisition of full X-ray spectra with high spatial resolution (2–4 μm per pixel) for images up to 100M pixels (Ryan et al., 2010a; Ryan et al., 2010b).

Analyses were conducted on the polished billet of FF-16. Element mapping was performed over an area of 1.23 mm × 0.876 mm with a beam energy of 18.5 keV, a step size of 2 μm and dwell time of 7.812 ms per 2 μm pixel. Standard foils of Fe, Mn, Pt and YF₃ were analyzed daily to allow calculation of the X-ray flux and monitor energy drift. X-rays may penetrate a significant distance into the sample because of the high energy of the beam. Thus, the concentration from each pixel is an average of the whole volume sampled (Dyl et al., 2014; Fisher et al., 2014; Ryan et al., 2014). Data reduction was performed using the GeoPIXETM software which uses a fundamental parameter model, the Maia detector array efficiency model, and a dynamic analysis (DA) matrix method to deconvolute spectra and create images (Dyl et al., 2014; Fisher et al., 2014; Ryan et al., 1990; Ryan et al., 2005; Ryan et al., 1995). Full spectral data were collected for each pixel and representative spectra were extracted for both the bulk sample and subsequently for specific phases of interest. Yields, used to relate spectral content to element concentration, were integrated for a given matrix or mineral phase, producing a representative total spectrum for the phase (Fisher et al., 2014; Ryan et al., 2010b). Spectra were fitted with elements identified during the peak fitting process (Figure 4.2). Images of the mapped area were then created by DA matrix analysis, which is a matrix transform method allowing decomposition of spectral data into its elemental components (Ryan et al., 2010b). In the element maps produced each pixel has spectral information which the DA matrix converts to quantified elemental concentrations. In this study, the maps of the whole sample were initially produced by fitting the bulk spectra for the sample using a yield file based on the whole rock mineral assemblage. Subsequently, smaller area sub-maps of specific mineral phases with more accurate element concentrations were produced by refitting spectra from the phase of interest with yields calculated for that specific matrix based on the X-ray interaction properties of that mineral phase.

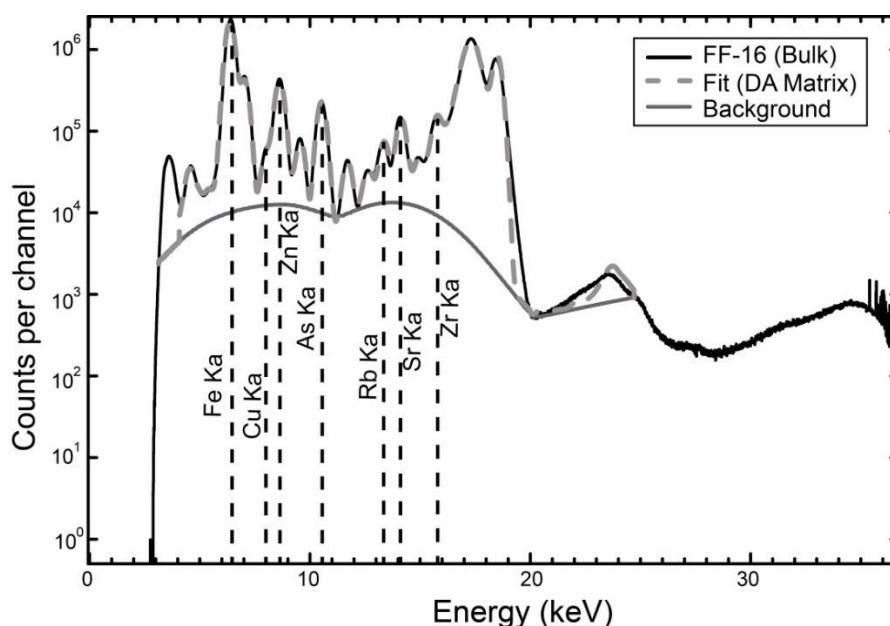


Figure 4.2 Representative spectra produced by SXRf analysis of FF-16. The original spectra are plotted with the black solid line. Fit spectra calculated by GeoPIXE™ are displayed by the grey dashed line (DA matrix: dynamic matrix). The background, calculated with the Statistics-sensitive Non-linear Iterative peak-clipping (SNIP) algorithm (Ryan et al., 1988, 1990), is shown by the grey solid line. The energy range over which the spectra is fitted is 3–25 keV. Observed trace elements from the bulk sample spectra include Fe, Cu, Zn, As, Rb, Sr and Zr, the K- α lines for which are indicated by black dashed lines.

4.4 Results

4.4.1 Petrographic features

Sample FF-16 is metapelitic and preserves relict bedding structures. Sedimentary clasts include quartz, albite, muscovite, and stilpnomelane with a small amount of chlorite and epidote. Prehnite and pumpellyite were not observed by optical microscopy in this section. Clasts are fine-grained with sizes up to 50 μm . The matrix is mainly finer-grained quartz, feldspar, CM and clay minerals. The bulk sulfur content is 0.08 wt %, which is typical of rocks in this metamorphic sequence.

Polyframboids, which are typically 100–300 μm across, are scattered through the rock and commonly occur as clusters, with sulfide microcrystals impinging on each other (Figure 4.3 A & B.). The polyframboids are ellipsoidal in shape, with the long axis sub-parallel to bedding in the host rocks. The polyframboids are dominated by

pyrite framboids and pyrite microcrystals with a mode (volume concentration) of pyrite around 90%. The size of single pyrite microcrystal is usually less than 1 μm across (Figure 4.3 A& B). Other sulfide minerals, including sphalerite, chalcopyrite and cobaltite, are intergrown with the pyrite microcrystals and scattered through the polyframboids (Figure 4.3 C& D). Irregularly shaped fragments of CM are grey with low reflectivity in reflected light. CM, ranging in size from 1 to 10 μm (Figure 4.3 C& D) (Hu et al., 2015), occurs in intimate contact with pyrite microcrystals within the polyframboids. EDS on these CM grains gives Zn and S peaks, so very fine-grained sphalerite is inferred to be associated with the CM. Chalcopyrite and cobaltite are, in places, intergrown with CM/sphalerite (Figure 4. 3 C& D).

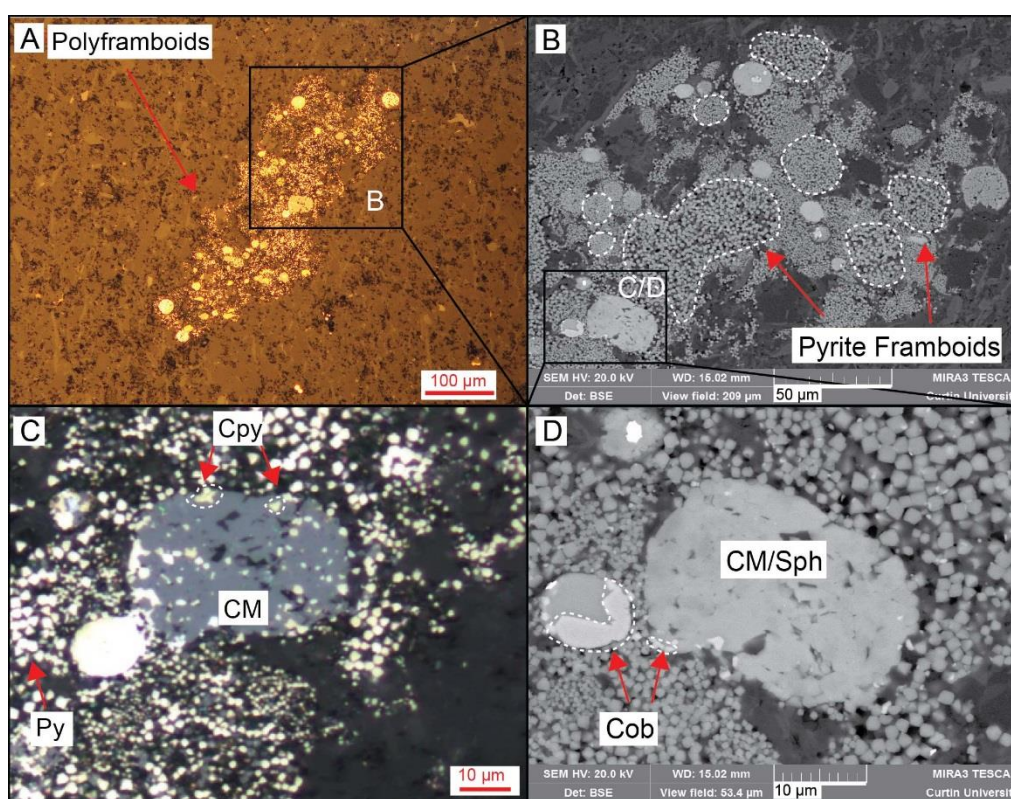


Figure 4.3 Petrographic photomicrographs of polyframboids. (A) Ellipsoidal polyframboids in reflected light, dominated by pyrite framboids and pyrite microcrystals. (B) SEM image of part of the polyframboids shown in A, showing clusters of pyrite framboids, pyrite microcrystals and other sulfides. Typical pyrite framboids have been indicated with dashed lines. (C) Enlarged view of part of the polyframboids in (B) in reflected light, showing carbonaceous material (CM), pyrite (Py) and chalcopyrite (Cpy) (Hu et al., 2015). (D) SEM image of carbonaceous material (CM) in (C) with sphalerite (Sph) and cobaltite (Cob).

4.4.2 SXRF mapping

The SXRF elemental maps processed from the bulk sample spectra, including polyframboids, surrounding minerals and matrix, are presented as a composite of the individual Ca, Sr, Rb and Fe maps (Figure 4.4). Within the map area of 1.23 mm × 0.876 mm, considerable variation is seen in element concentrations within the polyframboids, surrounding minerals and matrix. Fe is most abundant in the polyframboids and shows variable concentrations in the clasts and matrix. Elongate Fe-rich minerals within the clasts in Figure 4.4 are identified as stilpnomelane. Quartz veins, identified in transmitted light, are present adjacent to the polyframboids and contain low concentrations of Sr and Rb. Sr is present in high concentrations in clasts and veins, and occurs as hot spots in the polyframboids, whereas Rb shows more variability in the clasts, matrix and veins. The distribution of fine-grained calcic minerals such as prehnite and pumpellyite, which are difficult to identify using optical microscopy, can be inferred from Ca-rich spots. The abundance of Ca and Rb in the surrounding minerals and matrix is consistent with the mineral assemblage muscovite, albite, chlorite, prehnite and pumpellyite. Grains with high Ca and Fe are epidote. Quartz, present in the clasts, is depleted in Ca, Sr, Rb and Fe and appears as dark areas in the matrix in Figure 4.4. No measurable Au was detected by SXRF, due to the very low concentration of < 0.5 ppm as compared to the approximate 100 ppm Au detection limit for this sample.

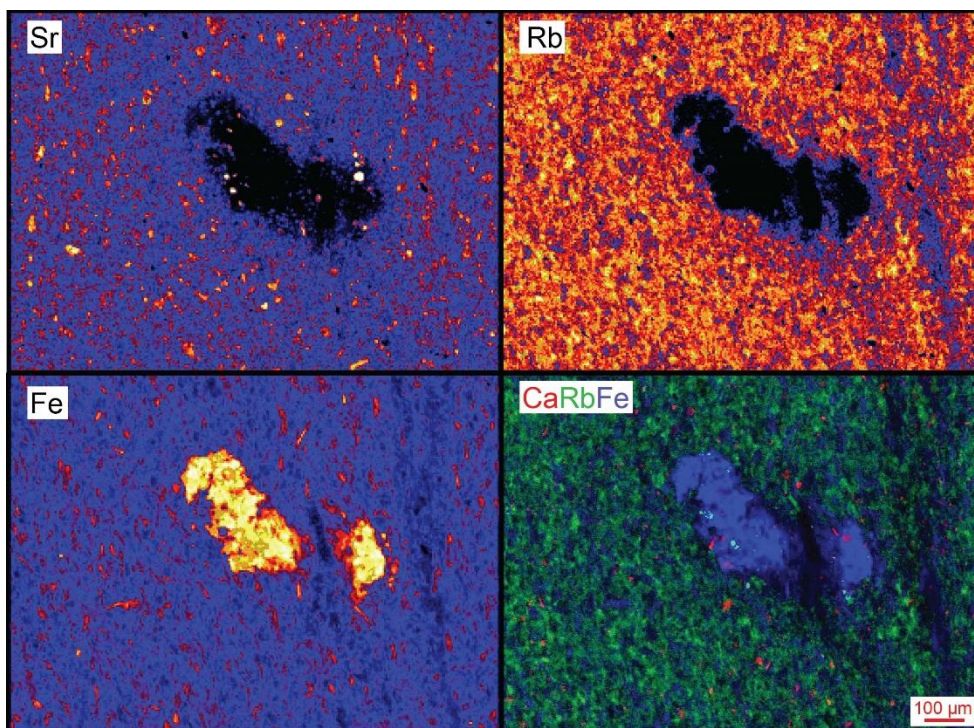


Figure 4.4 SXRf element maps of Sr, Rb, Fe and a combination of Ca (red)-Rb (green)-Fe (blue), showing the variation of those elements in the mapped area and providing an example of the association between polyframboids and the surrounding minerals and matrix. In Sr, Rb and Fe mapping, warm colors represent high concentrations and cool colors represent low concentrations.

Zn distribution in polyframboids

Spectra for one of the polyframboids were extracted and refitted using the average chemical composition of these polyframboids. New element maps for the selected polyframboids were produced. Figure 4.5 A is a map of Zn (red) and Fe (blue) distribution. Fe shows variable and inhomogeneous distribution in the polyframboids. Zn concentrations, which are taken to be a proxy for sphalerite, vary across the polyframboids, with high-Zn zones displayed as red spheroids. The distribution of sphalerite closely mirrors the distribution of CM seen in reflected light (Figure 4.5 B). Raman spectroscopy indicates that this CM comprises low maturity carbonaceous material (Hu et al., 2015).

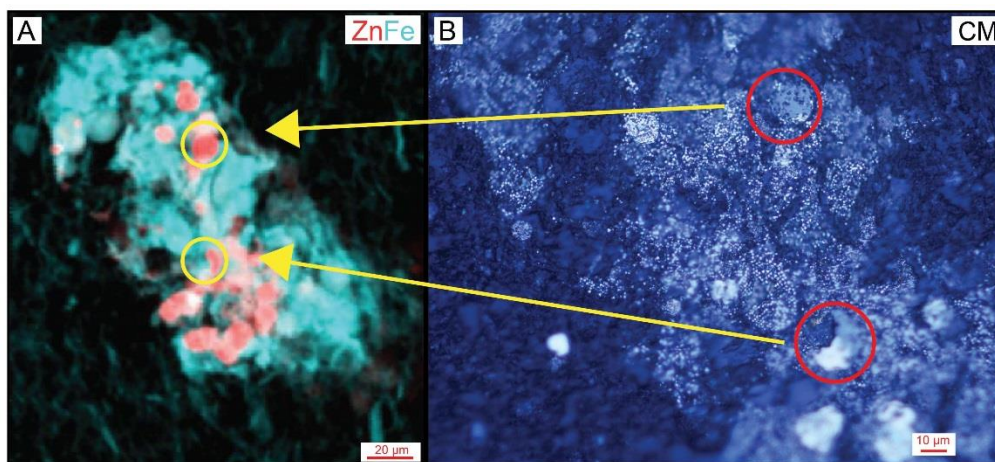


Figure 4.5 (A) SXRf element map of Zn-Fe, showing the distribution of Zn in polyframboids. Zn concentrations are highest in the red spheroids, with a variable distribution in the polyframboids; (B) Reflected light photomicrograph of part of the same polyframboids. CM occurs as rounded globules which are grey with low reflectivity in reflected light. The hot spot of Zn in (A) corresponds to large patches of CM within the red circles in (B), while lower Zn zones coincide with smaller grains of CM in many cases (Figure 4.3 B).

The relationship between Zn and Fe in the map shown in Figure 4.5 was further assessed by considering the relative concentration of these elements, using the GeoPIXE feature that allows the concentration of elements in any pixel to be plotted and related to its spatial location (Figure 4.6). This feature enables elemental relationships to be plotted so that points from different user-specified spatial locations can be distinguished. For example, the highest Zn concentrations, which are plotted in a cloud surrounded by a thick solid line in Figure 4.6 B, are found in areas surrounded by a thick solid line in Figure 4.6 A. The polyframboids are characterized by variable enrichment of Zn relative to Fe; these areas are delineated by solid lines, dashed lines and dotted lines with decreasing Zn concentration. It is important to note that element concentrations calculated from SXRf mapping are average concentrations for volumes that are 2 x 2 microns on the surface, but with a depth equal to the beam penetration depth of several microns. The measured apparent concentration of elements from mineral grains less than several microns in thickness will therefore be lower than expected from those minerals due to dilution from surrounding grains. For example, the measured concentration of Zn and Fe (Figure

4.6) in sphalerite and pyrite, respectively, will be less than 68.8 wt % and 46.67 wt % if the volume of analysis is not 100% sphalerite or pyrite. On Figure 4.6, Zn concentration ranges from 1 to 25 wt % and shows a negative relationship with Fe concentration. The most Zn-rich area, dominated by sphalerite and a small amount of microcrystalline pyrite, outlined by a heavy solid line in Figure 4.6 A, has a composition of 25 wt % Zn and 17 wt % Fe. Outside this area, Zn content drops from 25 wt % to 5 wt %, with a corresponding increase in Fe content (Figure 4.6 B). The concentration of Zn decreases gradually from the boundary of the polyframboids towards the matrix. Two trends are seen on Figure 4.6 B; a mixing line between matrix (low Fe, low Zn) and the polyframboids (high Fe, moderate Zn), and a mixing trend between sphalerite (high Zn, moderate Fe) and other parts of the polyframboids. The most Fe-rich areas, limited by dashed line, are consistent with the observed position of pyrite microcrystals, and the most Zn-rich areas are, in many cases, co-located with the CM identified by Raman spectroscopy.

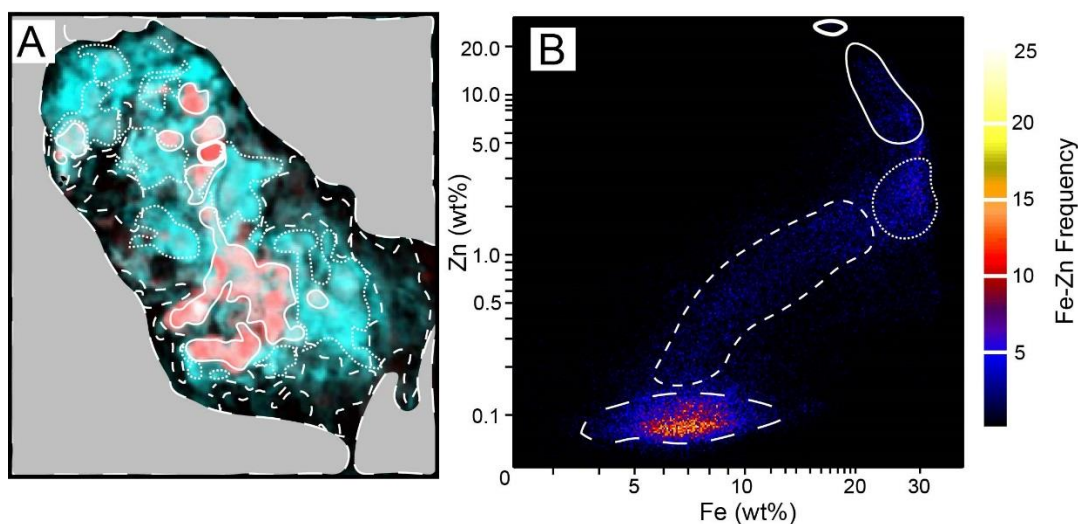


Figure 4.6 (A) The same image shown in Figure 4.5 A but with zones of the variable Zn/Fe ratio in (B) outlined. (B) Compositional data from all pixels were extracted from the map in (A) and plotted as Zn (wt %) versus Fe (wt %) in (B). Each pixel corresponds to a single point on the plot. The color change on the plot is determined by the frequency of a specific Zn/Fe ratio. The brighter and darker colored points represent higher and lower populations of pixels of equivalent Zn/Fe ratios, respectively. The circled regions in (A) correspond to the regions in (B) of equivalent line style, and include all the points with a given range of Zn/Fe.

The association between other trace elements with CM in polyframboids

The distributions of Zn and CM in polyframboids are similar, so the nature of the association between other elements and Zn provides an indication of the relationship between these elements and CM. The use of Zn as a proxy for CM is useful, because CM is not measured directly by LA-ICP-MS or SXRF (Figure 4.7, 4.8). Arsenic is locally abundant (> 6 wt %), but has no obvious relationship with Zn (Figure 4.7 B). Other areas of the polyframboids contain lower As concentrations (up to 2.5 wt %). The distributions of Co and As coincide due to the presence of cobaltite, surrounding or adjacent to Zn (Figure 4.7 D). Cu is locally enriched, and occasionally coincident with or adjacent to Zn (Figure 4.7 C & E).

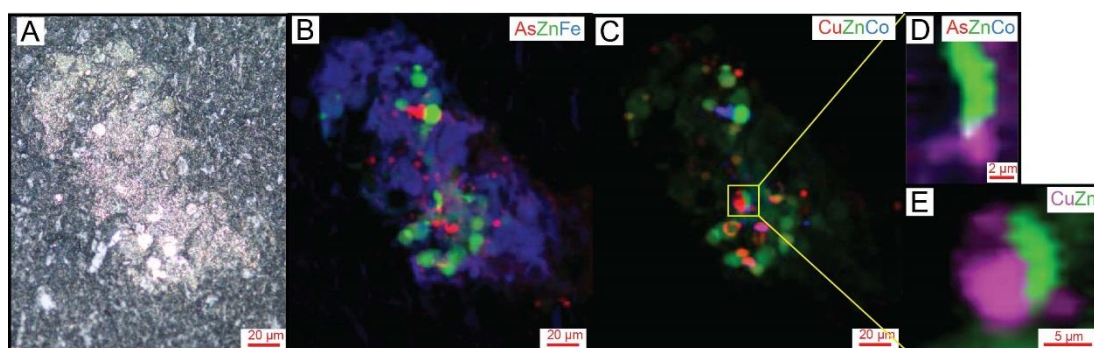


Figure 4.7 (A) Reflected light view of the polyframboids in Figure 4.5 A; (B) SXRF element map of As (red), Zn (green) and Fe (blue) in the same framboid. The concentration of As, which is up to 2.5 wt %, varies in the polyframboids, except for the hot spot coinciding with Co. (C) SXRF element map of Cu (red), Zn (green) and Co (blue) in the same polyframboids; (D) Higher-resolution SXRF element map of As (red), Co (green) and Zn (blue) for the boxed area shown in (C); (E) Higher-resolution SXRF element map of Zn (pink) and Cu (green) for the same area shown in (D).

Element concentrations on a transect (x-x') across the polyframboids in Figure 4.5 A illustrate the variations in Sr, Rb, Fe, Zn, Ni, Cu, Co, and As (Figure 4.8). Analyses were averaged to give points at 10 μm spacing along a 100 μm transect (Figure 4.8). Sr and Rb are more concentrated in the matrix than in the polyframboids, which is consistent with petrographic observations, except for the high Sr concentration of 0.2 wt % in the middle of the polyframboids which is similar to the Sr content in the matrix and may represent a fissure in the polyframboids. Fe, with a concentration range of 5–30 wt%, shows a distinct enrichment due to the present of pyrite, but

decreases to 15 wt % in the center of the polyframboids (700–900 μm in Figure 4.8). Zn concentrations in the polyframboids range from 1–5 wt % in the pyrite microcrystal-rich areas and up to 25 wt % in the CM-rich areas. The Zn-rich area coincides with the low Fe concentration area. The concentration of Ni is up to 0.3 wt %. Cu concentration ranges from 0.2 to 1.4 wt %. The spatial location of one of the Cu peaks is close to that of Zn peak, but does not overlap. Co and As concentrations coincide across on the transect, with averages in Co and As around 0.06 wt % and 0.15 wt %, respectively, across the polyframboids, but reaching up to 4.5 wt % and 6.5 wt %, respectively, in the phase identified as cobaltite optically and with EDS. There is an offset between the position of enrichment of Ni, Cu, Co and As with that of Zn; the position of the former is around 750 μm whereas the latter is around 820 μm (dashed lines on Figure 4.8).

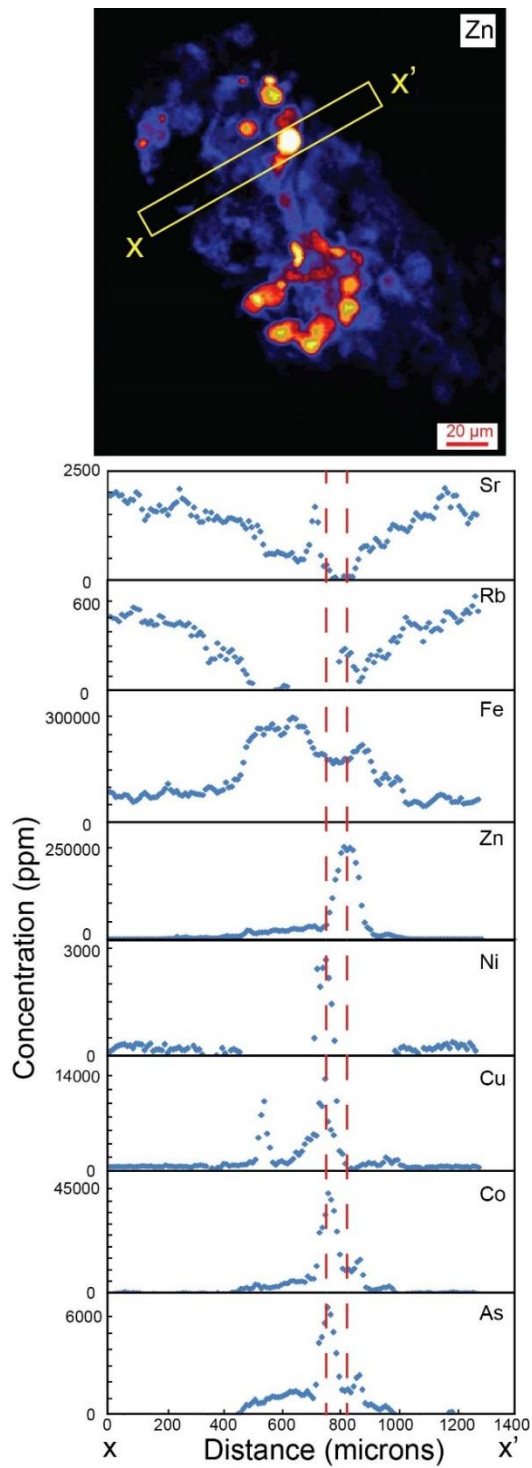


Figure 4.8 SXRf element map of Zn, the distribution of which coincides with that of CM; A transect x-x' though the polyframboids shows variation in Sr, Rb, Fe, Zn, Ni, Cu, Co, As.

4.4.3 Element concentrations in polyframboids analyzed by LA-ICP-MS

Laser analyses were performed on three textural types within the section: polyframboid areas with concentrated microcrystals; mixed polyframboid-matrix areas with less concentrated microcrystals, and matrix (Figure 4.9, 4.10, Table 4.1). The concentrations of Au, Ag, As, Co, Cu, Ni, Mo, Pb, Zn decrease progressively from the polyframboids to the matrix (Figure 4.10, Table 4.1). In particular, Au content has an average of 0.56 ± 0.31 ppm ($n=10$, n is the number of analyses) in the polyframboids, only 0.044 ppm in the polyframboid-matrix areas and is below the detection limits in the matrix. V and Mn, on the other hand, are depleted in the polyframboids relative to the matrix. The results from LA-ICP-MS are consistent with those from SXRF, for those elements above the detection limits of SXRF.

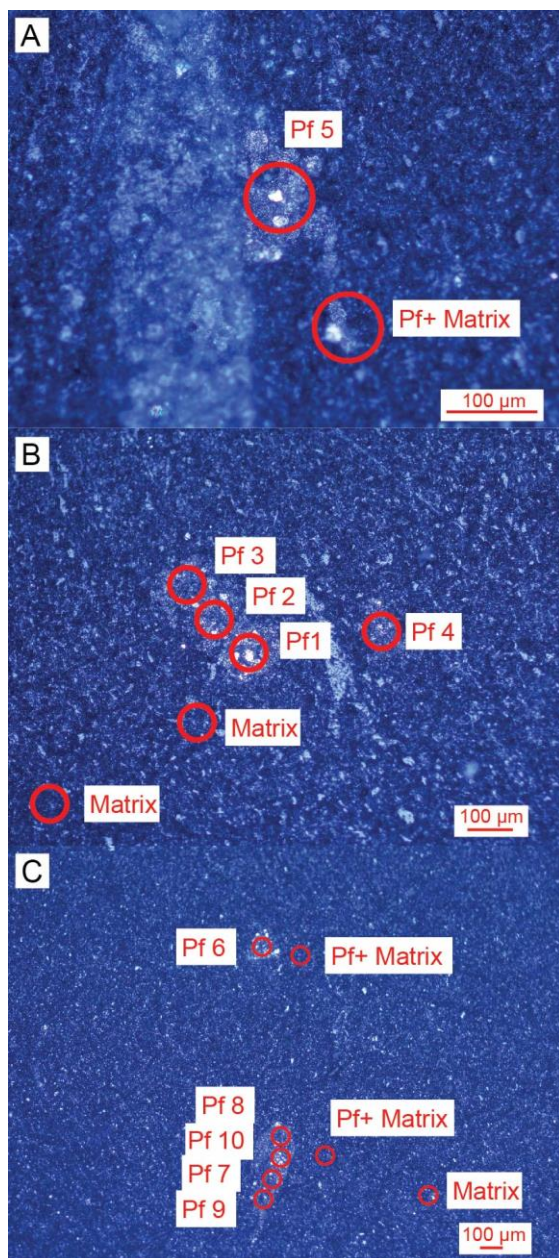


Figure 4.9 Petrographic images of polyframboids in reflected light with laser spots (indicated by red circles) in sample FF-16. Laser spots were focused on different textural classes: polyframboid areas (Pf), mixed polyframboid-matrix areas (Pf + Matrix) and matrix areas (Matrix).

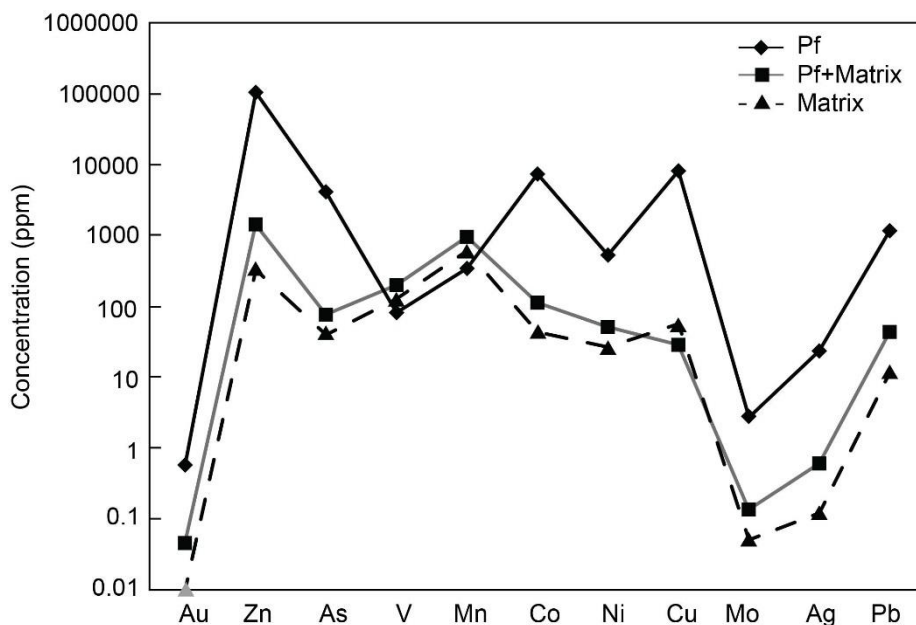


Figure 4.10 Comparison of different concentrations of trace elements in three different textural classes: polyframoid areas (Pf), mixed polyframoid-matrix areas (Pf + Matrix) and matrix areas (Matrix). The concentration of Au in the matrix areas is below the detection limits. Data is presented in Table 4.1.

From the results of 10 analyses in the polyframoids, Zn, As, Cu, Co and Pb are dominant with Zn up to 22.7 wt %, As up to 0.9 wt %, Cu up to 2.86 wt %, Co up to 1.6 wt % and Pb up to 0.3 wt % (Figure 4.11, Table 4.2). The concentration of Au, which is of low level, is up to 1.1 ppm whereas most are less than 1 ppm. Au shows a positive correlation with Zn (Figure 4.11 A). Silver concentrations are 22.5 ± 12.4 ppm and there is a positive relationship between Ag and Zn (Figure 4.11 B). Au and Ag are also positively related (Figure 4.11 C), which is unsurprising given their mutual position correlation with Zn. Au-As and As-Zn show only weak relationships (Figure 4.11 D & F). As and Co are weakly correlated with Zn (Figure 4.11 E & F). The Ni content in polyframoids varies between 374 and 1000 ppm (Figure 4.11 G). The correlation between Ni and Zn is also weak, similar to that between As and Zn (Figure 4.11 F & G). The concentration of Mo is relatively low at less than 4.3 ppm; Mo is not correlated with Zn (Figure 4.11 H).

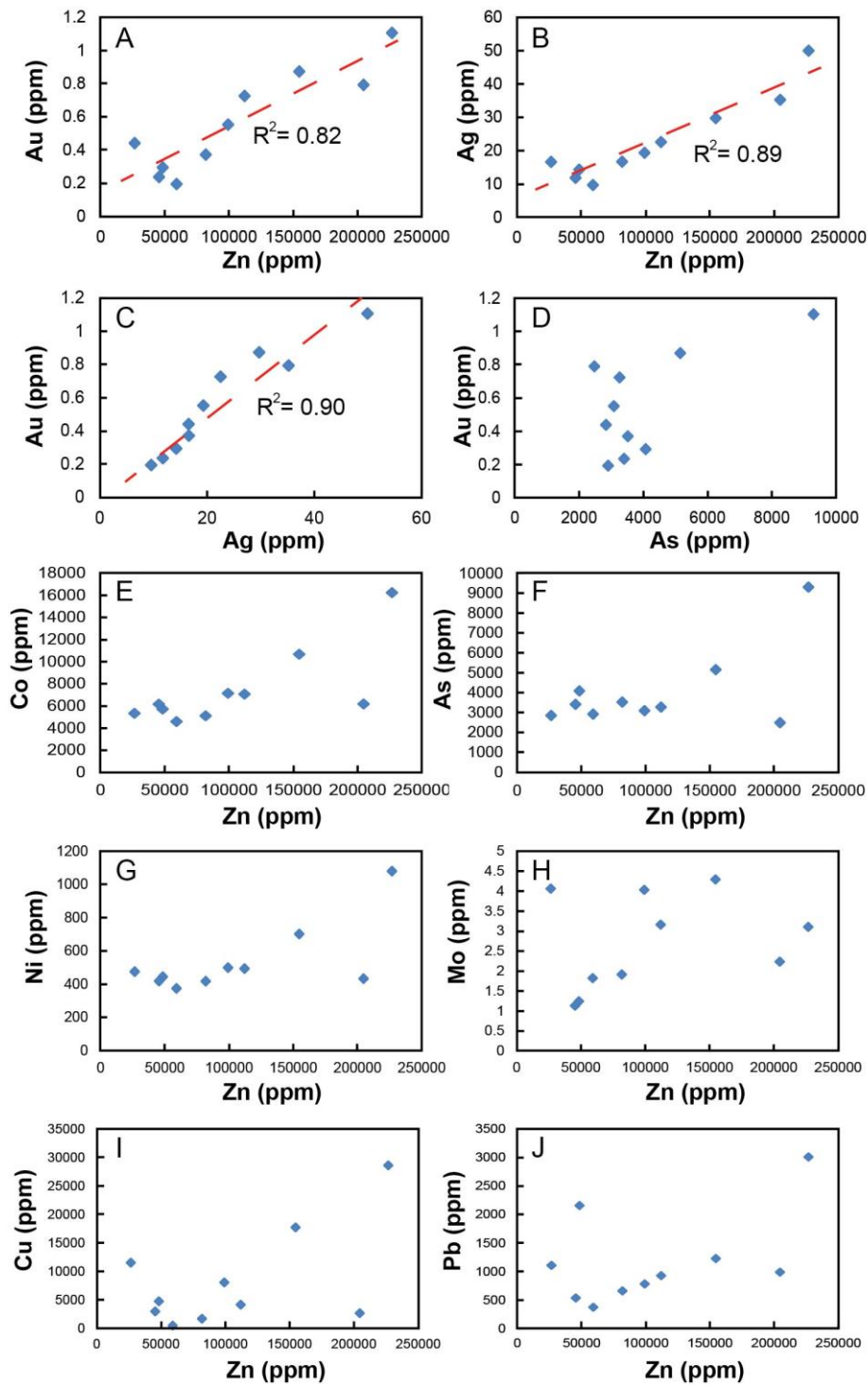


Figure 4.11 Geochemical plots of data from LA-ICP-MS analysis of polyframboids. (A) Au vs Zn (R^2 (the square of Pearson correlation coefficient) = 0.82); (B) Ag vs Zn ($R^2 = 0.89$); (C) Au vs Ag ($R^2 = 0.90$); (D) Au vs As; (E) Co vs Zn; (F) As vs Zn; (G) Ni vs Zn; (H) Mo vs Zn; (I) Cu vs Zn; (J) Pb vs Zn.

Table 4.1 The concentration of trace elements in the three textural classes investigated: polyframboids (Pf), mixed polyframboids and matrix (Pf + Matrix) and matrix (Matrix). (DL: detection limits; σ : standard deviation; N is the number of analyzed samples.)

FF-16	Au ppm	Zn ppm	As ppm	V ppm	Mn ppm	Co ppm	Ni ppm	Cu ppm	Mo ppm	Ag ppm	Pb ppm
Pf	0.56	105942	4003.5	81.9	345.4	7417.2	533.3	8233.6	2.7	22.5	1179.2
σ (N=10)	0.3	69003.13	2005.9	19.6	133.9	3530.9	211.8	8867.3	1.2	12.4	809.6
Pf+Matrix	0.044	1419.5	75.4	195.7	943.3	110.3	50	28	0.13	0.59	42.8
σ (N=3)	0	1925.4	74.7	34.9	205	115.4	7.7	14.3	0.14	0.8	39.3
Matrix	<DL	328	39.7	128.1	610.3	43.4	26.6	56.6	0.05	0.12	11.7
σ (N=3)	<DL	232.5	26.8	9.2	34.1	28.1	1.9	13.7	0.03	0.04	4.2

Table 4.2 The concentration of trace elements in ten analyzed polyframoids (Pf).

FF-16	Au ppm	Zn ppm	As ppm	V ppm	Mn ppm	Co ppm	Ni ppm	Cu ppm	Mo ppm	Ag ppm	Pb ppm	Fe Internal
Pf 1	1.104	226900	9300	116.3	585.0	16230	1080	28600	3.10	49.90	3010	0.267
Pf 2	0.293	48500	4075	83.7	309.1	5710	444	4710	1.24	14.25	2160	0.267
Pf 3	0.370	81900	3520	83.0	374.9	5100	417	1660	1.91	16.61	662	0.267
Pf 4	0.235	45550	3405	80.8	254.0	6151	418	2940	1.13	11.76	538	0.267
Pf 5	0.791	204700	2480	66.2	255.0	6180	432	2630	2.23	35.19	992	0.230
Pf 6	0.724	112100	3265	45.1	178.6	7070	493	4130	3.16	22.5.0	930	0.270
Pf 7	0.551	99300	3088	84.2	308.0	7140	499	8020	4.03	19.29	784	0.255
Pf 8	0.193	59200	2909	82.6	335.8	4591	374	446	1.82	9.60	376	0.255
Pf 9	0.439	26570	2843	105.1	573.0	5330	475	11500	4.06	16.56	1110	0.255
Pf 10	0.871	154700	5150	71.6	280.2	10670	701	17700	4.29	29.7	1230	0.255

4.5 Discussion

4.5.1 Association between CM, Au and other elements in polyframboids

Polyframboids in this study mainly comprise a composite of CM, pyrite framboids and various microcrystalline sulfides, including pyrite, sphalerite, cobaltite and chalcopyrite. This type of polyframboids has not often been previously reported (Degens et al., 1972; Large et al., 1999; MacLean et al., 2007). Different trace elements show distinctly different distributions in relation to the distribution of the CM in the polyframboids. CM and Zn (present as sphalerite) are mostly co-located in the polyframboids, and LA-ICP-MS data record a positive correlation between Au and Zn, and Ag and Zn. It is therefore inferred that Au, Ag and Zn are dominantly co-located in the CM. Other trace elements are dominantly hosted by pyrite and other sulfides. As and Co are most likely hosted by cobaltite, and Cu is hosted by chalcopyrite that occurs adjacent to sphalerite and CM. Chalcopyrite is texturally later than the sphalerite. These observations are consistent with LA-ICP-MS data, which show a lack of correlation between As, Co, Ni, Cu and Pb with Zn and Au (Figure 4.8). Mo, on the other hand, does not appear to be co-located with any of the other trace elements, or occur preferentially in any of the phases analyzed.

To explain the distribution of the trace elements, it is necessary to consider the development of polyframboids and associated mineral intergrowths. The polyframboids investigated in this study, which are dominated by pyrite framboids, are thought to have a similar formation history to framboidal pyrite. Early researchers proposed that framboidal pyrite is produced by replacement of a pre-existing spherical organic structure (Rickard, 1970). However, subsequent studies of experimentally synthesised framboids and field observations suggest that additional processes contribute towards the formation of framboidal pyrite: (1) the nucleation and growth of iron monosulfides (FeS) as precursors; (2) the conversion of monosulfides to pyrite; and (3) the growth of pyrite (Ohfuji and Rickard, 2005; Schoonen, 2004; Wilkin and Barnes, 1997). The polyframboidal textural with smaller pyrite framboids and pyrite microcrystals may form from the splitting of large framboids into smaller grains (Love, 1971). It has been confirmed that individual pyrite crystals in framboidal pyrite are often associated with CM (Folk, 2005; Love, 1967; Love et al., 1984). For example, single pyrite microcrystals have been found to

be coated by nanobacterial cells (25–40 nm), and associated with decaying CM (Folk, 2005). MacLean et al. (2008) confirmed that framboids formed within an organic carbon matrix, which defines the framboidal structure. This carbon matrix provides an organic template for the growth of framboidal pyrite. Sulfate-reducing bacteria are thought to play a role during the formation of iron monosulfides, but also contribute during the conversion of monosulfides to pyrite by supplying H_2S or releasing an organic sulfur compound that acts as an electron acceptor, facilitating formation of FeS_2 on cell surfaces (Donald and Southam, 1999; Fortin et al., 1994; Grice et al., 2005; Jaraula et al., 2013; Melendez et al., 2013; Nabbefeld et al., 2010; Schoonen and Barnes, 1991).

Fine grained ZnS has been observed to occur as a coating on CM by MacLean et al. (2007), which explains the co-location of Zn with low maturity CM found in this study. DNA evidence in MacLean et al. (2007) suggests that the growth of ZnS on biofilms is induced by the activity of sulfate-reducing bacteria. This assumption is supported by experiments under laboratory conditions, and by observations of natural systems (Awid-Pascual et al., 2015; Labrenz et al., 2000; Moreau et al., 2001). FeS, the monosulfide phase that is thought to form the precursor of pyrite in polyframboids, has also been demonstrated to be bacterially precipitated (Watson and Ellwood, 1994; Watson et al., 1995). The results of theoretical models are also consistent with the formation of metal-sulfide aggregates during sulfate reduction (Druschel et al., 2002). ZnS is thought to precipitate prior to FeS because Zn^{2+} has faster water exchange reaction kinetics than Fe^{2+} (Morse and Luther, 1999). Thus, coexisting ZnS and CM in polyframboids in this study are proposed to have been produced by sulfate-reducing bacteria prior to the formation of other sulfides.

Zn has the same distribution as CM in polyframboids in most cases, so the association between the distributions of other trace elements and Zn can be used to infer the distribution relationships between other trace elements and CM. This slightly convoluted process is necessary because CM is not mapped directly on either the synchrotron XRF and carbon is not analyzed quantitatively by the LA-ICP-MS method.

The geochemical data reveals a positive correlation between Au, Ag and Zn. The Au-Ag relationship has not been previously reported. It therefore seems likely that Au

and Ag are both concentrated with Zn within the CM associated with the polyframboids. Experiments show that bacteria are capable of absorbing Au from sea water and/or precipitating gold by reduction of Au^{3+} from solution to Au^0 (Kashefi et al., 2001; Zhang et al., 1997) or depositing elemental gold at the cell surface (Lengke and Southam, 2006; Lengke and Southam, 2007). As Zn is most likely a product of the activity of sulfate-reducing bacteria, we postulate that Au and Ag are absorbed together into the organic structure at the same time as Zn and that the absorption is linked to the activity of sulfate-reducing bacteria. Other workers have recorded associations between Au and As in arsenian pyrite (Large et al., 2012; Large et al., 2009; Reich et al., 2005), in contrast to the trends observed in this study. However, the Reich et al. (2005) data set is derived from a wide range of pyrite-forming environments, including sediment basins and hydrothermal ore deposits, so it may be that the relationship is environment-dependent.

As and Co each have weak linear relationships with Zn, while As is strongly correlated with Co. The As-Co association is attributed to the presence of cobaltite. As is seldom co-located with Zn, though cobaltite is immediately adjacent to the high Zn concentrations (Figure 4.7), suggesting that Co-As minerals such as cobaltite may form within the organic template (Large et al., 1999). However, the imperfect correlation between As and Co may indicate that As is also located in pyrite as solid solutions (Reich et al., 2005). Previous studies claim that the monosulfide precursor (FeS) of pyrite (FeS_2) is capable of concentrating As and Co from the solutions, and that As and Co are released from Fe-sulfides form cobaltite during the transition from FeS to FeS_2 (Large et al., 1999; Watson et al., 1995; Wilkin and Barnes, 1997). This proposal is consistent with the spatial and textural relationships observed here. The relationship between Ni and Zn is similar to that observed between As and Zn so a similar mechanism to that proposed for As and Co may apply to Ni which may be hosted by pyrite (Watson et al., 1995).

The highest Cu concentrations are only weakly spatially co-located with Zn-rich areas in most cases, though in one instance sphalerite is observed to be replaced by chalcopyrite (Figure 4.7 E). The relationship between Cu and Zn concentrations has some similarity to that for observed for As-Zn and Co-Zn, so Cu may have been incorporated into the polyframboids via similar mechanisms to those proposed for As

and Co. Indeed, Cu can be absorbed by FeS from aqueous solutions, though less Cu is incorporated into FeS by this mechanism compared with Co (Watson et al., 1995). Thus, Cu could be absorbed into FeS and expelled to form chalcopyrite during FeS-pyrite conversion, or deposited as chalcopyrite directly during the replacement of sphalerite (Barton Jr and Bethke, 1987; Bente and Doering, 1993). The trends of Pb versus Zn are similar to that of Cu versus Zn, indicating that Pb underwent a similar history to Cu.

Mo shows no systematic relationship with Zn. Mo may therefore be unaffected by the activity of sulfate-reducing bacteria and may be incorporated into the polyframboidal structure by solid solution after, or during, pyrite formation (Algeo and Maynard, 2004).

To summarise, the trace elements in polyframboids can be divided into three groups:

(1) Zn, hosted by sphalerite and associated with CM, was probably incorporated into the solid phases via sulfate reducing bacterial activity prior to the formation of FeS. Au and Ag, which exhibit a positive correlation with Zn, were probably absorbed onto the CM by a similar mechanism.

(2) As, Co, Cu, Ni, Pb have a weak association with Zn, and thus with CM. These elements are therefore proposed to have been absorbed into the precursor monosulfide from solution, rather than via a process involving the CM directly. Cobaltite may have formed when As and Co were released during the transition of FeS to FeS₂. Chalcopyrite may have formed by the same mechanism, but later than the cobaltite, or it may have formed directly from solution via the replacement of sphalerite.

(3) Mo has no spatial or concentration relationship with Zn and it is therefore likely that incorporation of Mo into pyrite occurred without the direct contribution from CM or bacterial activity.

4.5.2 Mechanism of incorporation of trace elements into polyframboids

It is commonly agreed that metastable FeS is the precursor of pyrite (Schoonen and Barnes, 1991) and that this phase could be produced by sulfate-reducing bacteria on the bacterial cell surface (Donald and Southam, 1999; Fortin et al., 1994). FeS then transforms into pyrite via sulfur addition or iron loss (Rickard and Luther, 1997; Wilkin and Barnes, 1997). During this process, sulfate-reducing bacteria can utilize sulfate as a terminal electron acceptor to produce hydrogen sulfide (Schoonen, 2004). Donald and Southam (1999) and Grimes et al. (2001) pointed out that FeS₂ forms on the bacterial cell surface under experimental conditions. Pyrite can grow directly from FeS-undersaturated solutions via a mechanism in which S-S bonds are formed on the surface of a growing pyrite crystal (Schoonen, 2004).

The behavior of trace element incorporation into polyframboids is complicated and the systematics proposed by different researchers varies. Watson et al. (1995) proposed, on the basis of experiments, that FeS absorbs trace elements, such as Co, Ni, Cu, Pb from solution; Co is strongly absorbed into FeS while Cu displayed only weak absorption. The observation regarding Cu is consistent with the results of Scholz and Neuman (2007). Further, Large et al. (1999) claimed that cobaltite interstitial to the framboidal pyrite formed due to the release of As and Co during the transition of monosulfide precursors to pyrite. In contrast, Morse and Luther (1999) suggested that Pb and Zn, with faster water exchange reaction kinetics than Fe²⁺, probably precipitated as MeS, where Me is Pb or Zn, prior to FeS formation, and that Co, As, Mo and Ni are later incorporated into pyrite. The proposed precipitation of ZnS is consistent with the results of Scholz and Neumann (2007), who found that Zn was poorly accommodated in pyrite.

In agreement with previous work, we postulate that the first stage of sulfide deposition is the formation of ZnS deposits on bacteria cell surfaces via the activity of sulfate reducing bacteria. During this process, Au and Ag are also absorbed on the cell surface. The precipitation of sphalerite and CM produce a template for the structure of polyframboids. FeS, the precursor of pyrite, is deposited within the organic template and incorporates some trace elements, such as As, Co, Cu, Ni, Pb, from aqueous solutions. The transformation from FeS to FeS₂ is facilitated via bacteria and may involve the incorporation of additional sulfur. Co and some of As

were probably released during this transition to produce cobaltite. Mo is likely taken up by pyrite, however, the incorporation of As, Co, Cu and Ni into pyrite appears partial, given the presence of cobaltite and chalcopyrite.

4.5.3 Implications for genetic models for ore deposit formation involving metal sources

There is a clear textural change from framboidal pyrite to euhedral pyrite in the host rocks of sediment-hosted orogenic gold deposits (Large et al., 2009). During this recrystallization process, Au and other trace elements can be released into fluids (Large et al., 2012; Large et al., 2007). The polyframboids in this study, comprising aggregates of framboidal pyrite, could have undergone these same textural changes as metamorphic grade increased. In the Otago Schist, the volume fraction of CM within polyframboids has been observed to decrease at higher metamorphic grades (Hu et al., 2015). It is therefore possible that CM-associated elements like Au and Ag are released during the recrystallization of polyframboids and associated oxidation of CM, and may have been incorporated into euhedral pyrite. Alternatively, Au and Ag could have been mobilized by fluids, but the metals have different solubilities and partition differently into pyrite so the proportions retained in pyrite and transported in fluids would differ (Gammons and Barnes, 1989; Henley, 1973; Seward, 1973). Other trace elements, like As and Ni, are thought to transfer easily from polyframboids to euhedral pyrite (Large et al., 2011). Sphalerite and chalcopyrite, which are commonly associated with pyrite in lower G-S rocks (Pitcairn et al., 2010), may retain Zn and Cu in the rocks (Large et al., 2012).

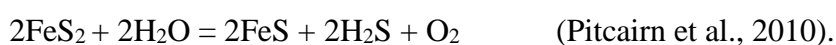
Metals in the Macraes gold deposit are thought to have been transported in fluids generated during metamorphism at the greenschist to amphibolite transition (Pitcairn et al., 2006). Evidence from previous studies indicates that low grade metamorphic rocks in the Otago Schist could be the source of those metals (Large et al., 2012; Pitcairn et al., 2014a; Pitcairn et al., 2006). Owing to their trace element enrichments, polyframboids have been proposed to be the metal fertilizer (Large et al., 2012). On the basis of the evidence provided here, however, the CM in polyframboids may be the carrier of both Au and Ag.

Simple mass balance calculations were performed to assess the possibility that Au and Ag in the Macraes gold deposit can be feasibly sourced from CM in polyframboids. The concentration of non-carbonate carbon in P-P facies rocks is around 0.15 wt % (data is from in Hu et al., 2015). If 10% of this CM in the host rocks was deposited from fluids (Hu et al., 2015), then CM associated with polyframboids in P-P rocks is estimated to be 0.13 wt % of the total rock mass. The best estimates of Au and Ag in CM are 0.56 ppm and 22.5 ppm, respectively. Hence, bulk rock concentrations are 0.00076 ppm Au and 0.03 ppm Ag in P-P rocks. If there is a 50% loss of metals during leaching, transport and deposition, then around 300 km³ of rocks similar to FF-16 could provide sufficient Au and Ag for the Macraes gold deposit, which contains approximate 300 t Au and 30 t Ag (estimated from Large et al. (2012) and Moore and Doyle (2015)). This Au endowment is found across a 30 km strike length (Pitcairn et al., 2006), so processing of a 2 km-wide and 5 km-thick sequence of sediment through the Au-releasing reaction would produce sufficient Au and Ag.

The mass balance constraints for As are also of interest. The concentration of S in FF-16 is 0.08 wt%. As the mode of pyrite is around 90% in polyframboids, and the S concentration in sphalerite, cobaltite and chalcopyrite is lower than that in pyrite, more than 90% of S is assumed to be associated with pyrite. The minimum concentration of pyrite in rocks is calculated as 0.27 wt %. The minimum concentration of polyframboids in rocks is, therefore, calculated as 0.3 wt %. The As concentration is 4000 ppm in polyframboids, giving a maximum of 12 ppm As in P-P rocks, which is close to the reported concentration of 8.258 ppm As (Pitcairn et al., 2014b). The As from only 20 km³ P-P rocks could therefore provide the estimated As content of the Macraes gold deposit, which is around 300,000 t As (estimated from Craw et al. (2015) and Moore and Doyle (2015)). Thus, derivation of Au and As from the sediments is consistent with preliminary mass balance constraints. A similar conclusion was reached by Large et al. (2012).

The evolution of pyrite in the Otago Schist involves a transition from polyframboids, through the composite pyrite which displays euhedral and polyframboidal morphologies, to euhedral pyrite (Figure 4.12) (Pitcairn et al., 2010). The concentration of Au measured by Pitcairn et al. (2006) and Pitcairn et al. (2010) is

slightly higher in euhedral pyrite (up to 110 ppm) in lower G-S facies than in polyframboids (up to 90 ppm) in P-P facies. However, in this study, the Au concentration in the polyframboids is around 1.2 ppm (Figure 4.11), which is similar to the results of Large et al. (2012). Thus, we infer that Au was transferred from CM in the polyframboids to euhedral pyrite as metamorphic grade increased. In the lower G-S facies rocks, pyrite is replaced by pyrrhotite at sub-greenschist facies (Pitcairn et al., 2010). This pyrrhotite does not contain detectable levels of Au, Ag or As (Pitcairn et al., 2010). If Au is transferred from CM to euhedral pyrite during low-grade metamorphism, then Au could be released from pyrite into fluids during the metamorphic transition of pyrite to pyrrhotite via



H₂S released during this reaction could form Au-bisulfide complexes with Au (Tomkins, 2010; Sun et al., 2013). Such complexes are proposed to carry Au in Au-bearing fluids (Benning and Seward, 1996; Emsbo et al., 2003; Evans et al., 2006; Tomkins, 2013). Then, Au could have been transported as Au-bisulfide complexes in fluids to the Macraes area and deposited via processes that may have involved CM from the host rock (Craw, 2002; Craw et al., 2007; Hu et al., 2015; McKeag et al., 1989).

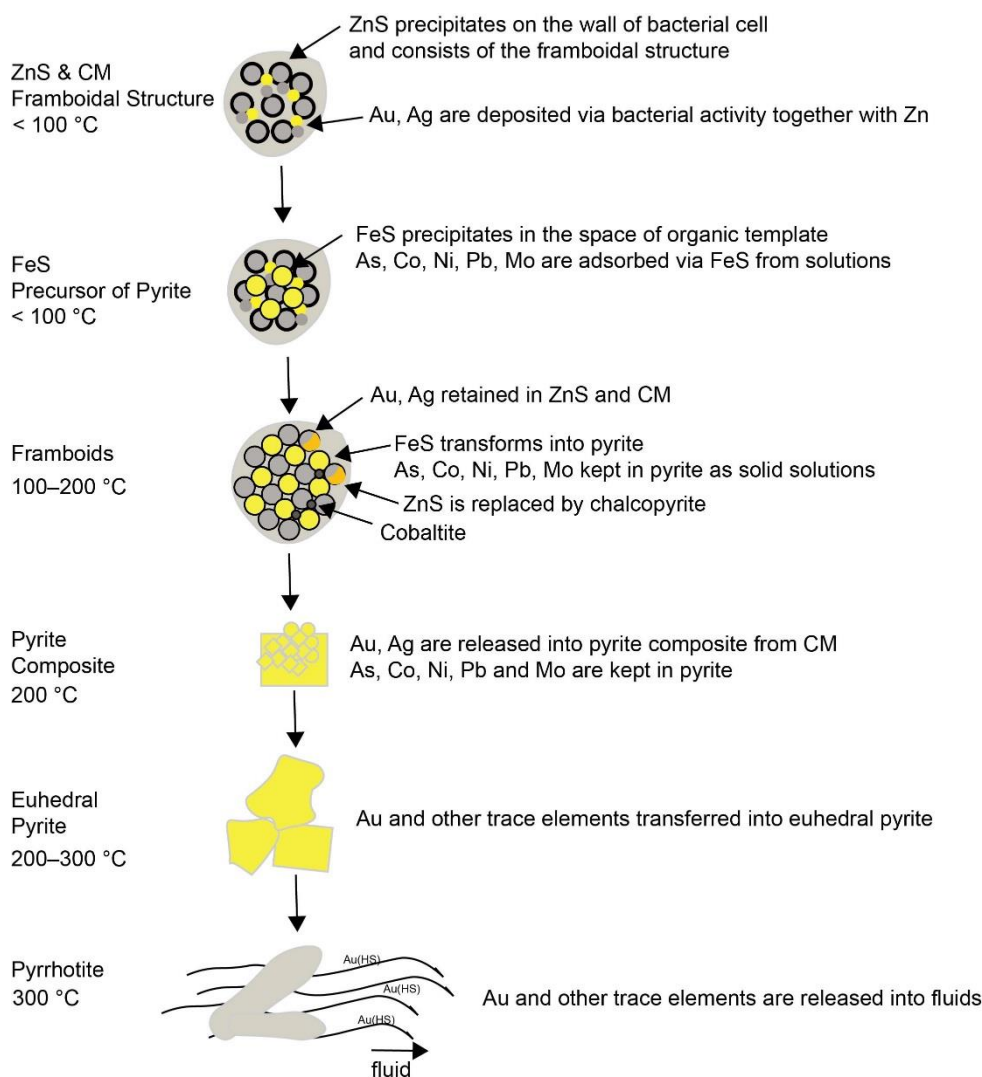


Figure 4.12 Schematic diagram of the evolution of one framboid in polyframboids and trace element mobility during the evolution of sulfides in the Otago Schist, modified after Pitcairn et al. (2010) and Large et al. (2007). Stages are labelled with estimated temperatures.

4.6 Conclusions

In this study, we examined the association between sulfides, CM and trace elements in polyframboids. Petrographic observations and SXRF mapping indicate that Zn and CM are co-located. It is likely that this coexistence is the consequence of sulfate-reducing bacterial activities. Low concentrations of Au and Ag, detected by LA-ICP-MS, are found to have a positive correlation with Zn, suggesting Au and Ag may also have been absorbed by bacteria from sea water during the deposition of sphalerite and CM. This process, which occurred prior to the formation of FeS, produces an

organic template for the structure of polyframboids. FeS is then deposited within the organic template and transformed into FeS₂ via sulfate-reducing bacteria activity. Other trace elements, such as As, Co, Cu, Ni, Pb and Mo, which are not co-located with Zn, may have been incorporated into sulfide phases during these processes.

CM associated elements like Au and Ag are postulated to be released from CM and incorporated into euhedral pyrite during the transition from polyframboids to euhedral pyrite, and further released from pyrite into fluids during the transition from pyrite to pyrrhotite. Other trace elements, not sourced from CM, may simply mobilize from polyframboids to euhedral pyrite, then into fluids during the pyrite-pyrrhotite transition. Mass balance calculations indicate that Au and Ag carried by CM and As hosted by polyframboids from 120 km³ P-P rocks could have provided sufficient Au, Ag and As for the Macraes gold deposit. The calculation results are consistent with previous proposals that the low grade metamorphic rocks of the Otago Schist are the source of metals for the Macraes gold deposit.

4.7 Acknowledgements

All the authors acknowledge the support from the CSIRO Mineral Resources Flagship Cluster for Organic Geochemistry of Mineral Systems led by Curtin University and additional support from WA-Organic and Isotope Geochemistry Centre (WA-OIGC), The Institute of Geoscience Research (TIGeR) and Curtin University. Additional funding support was provided by Ministry of Business, Innovation and Employment, New Zealand.

SXRF work was undertaken on the X-ray fluorescence microscopy beam line at the Australian Synchrotron, Victoria, Australia (Proposal 7823). We also thank Dr. Dave Patterson for the expertise during the beam time and Dr Chris Ryan for help during data processing. This work was supported by the Multi-modal Australian ScienceS Imaging and Visualisation Environment (MASSIVE) (www.massive.org.au). LA-ICP-MS work was performed at the John de Laeter Centre, Curtin University, Perth, with the help of Mr Bradley McDonald and Dr Richard Taylor. Dr. Marc Norman, Prof. Weidong Sun, Prof. Dima Kamenetsky and an anonymous reviewer are thanked for editorial handling and perceptive reviews that improved the manuscript.

S.H. acknowledges the receipt of Chinese Scholarship Council (CSC)-Curtin International Postgraduate Research Scholarship (CIPRS), CSIRO PhD Top-up Scholarship.

4.8 References

- Algeo, T.J., Maynard, J.B., 2004. Trace-element behavior and redox facies in core shales of Upper Pennsylvanian Kansas-type cyclothems. *Chemical Geology* 206, 289-318.
- Awid-Pascual, R., Kamenetsky, V.S., Goemann, K., Allen, N., Noble, T.L., Lottermoser, B.G., Rodemann, T., 2015. The evolution of authigenic Zn-Pb-Fe-bearing phases in the Grieves Siding peat, western Tasmania. *Contributions to Mineralogy and Petrology* 170, 1-16.
- Barton Jr, P., Bethke, P.M., 1987. Chalcopyrite disease in sphalerite: Pathology and epidemiology. *American Mineralogist* 72, 451-467.
- Bavinton, O., Keays, R.R., 1978. Precious metal values from interflow sedimentary rocks from the komatiite sequence at Kambalda, Western Australia. *Geochimica et Cosmochimica Acta* 42, 1151-1163.
- Benning, L.G., Seward, T.M., 1996. Hydrosulphide complexing of Au (I) in hydrothermal solutions from 150-400 °C and 500-1500 bar. *Geochimica et Cosmochimica Acta* 60, 1849-1871.
- Bente, K., Doering, T., 1993. Solid-state diffusion in sphalerites: An experimental verification of the chalcopyrite disease'. *European Journal of Mineralogy* 5, 465-478.
- Coveney, R.M., Murowchick, J.B., Grauch, R.I., Glascock, M.D., Denison, J.R., 1992. Gold and platinum in shales with evidence against extraterrestrial sources of metals. *Chemical Geology* 99, 101-114.
- Craig, J., Vokes, F., Solberg, T., 1998. Pyrite: physical and chemical textures. *Mineralium Deposita* 34, 82-101.

- Craw, D., 2002. Geochemistry of late metamorphic hydrothermal alteration and graphitisation of host rock, Macraes gold mine, Otago Schist, New Zealand. *Chemical Geology* 191, 257-275.
- Craw, D., MacKenzie, D., Pitcairn, I., Teagle, D., Norris, R., 2007. Geochemical signatures of mesothermal Au-mineralized late-metamorphic deformation zones, Otago Schist, New Zealand. *Geochemistry: Exploration, Environment, Analysis* 7, 225-232.
- Craw, D., Mortensen, J., MacKenzie, D., Pitcairn, I., 2015. Contrasting geochemistry of orogenic gold deposits in Yukon, Canada and Otago, New Zealand. *Geochemistry: Exploration, Environment, Analysis* 15, 150-166.
- Crocket, J., Kuo, H., 1979. Sources for gold, palladium and iridium in deep-sea sediments. *Geochimica et Cosmochimica Acta* 43, 831-842.
- Degens, E., Okada, H., Honjo, S., Hathaway, J., 1972. Microcrystalline sphalerite in resin globules suspended in Lake Kivu, East Africa. *Mineralium Deposita* 7, 1-12.
- Donald, R., Southam, G., 1999. Low temperature anaerobic bacterial diagenesis of ferrous monosulfide to pyrite. *Geochimica et Cosmochimica Acta* 63, 2019-2023.
- Druschel, G., Labrenz, M., Thomsen-Ebert, T., Fowle, D., Banfield, J., 2002. Geochemical modeling of ZnS in biofilms: An example of ore depositional processes. *Economic Geology* 97, 1319-1329.
- Dyl, K.A., Cleverley, J.S., Bland, P.A., Ryan, C.G., Fisher, L.A., Hough, R.M., 2014. Quantified, whole section trace element mapping of carbonaceous chondrites by Synchrotron X-ray Fluorescence Microscopy: 1. CV meteorites. *Geochimica et Cosmochimica Acta* 134, 100-119.
- Emsbo, P., Hofstra, A.H., Lauha, E.A., Griffin, G.L., Hutchinson, R.W., 2003. Origin of high-grade gold ore, source of ore fluid components, and genesis of the Meikle and neighboring Carlin-type deposits, northern Carlin Trend, Nevada. *Economic Geology* 98, 1069-1105.

- Evans, K., Phillips, G., Powell, R., 2006. Rock-buffering of auriferous fluids in altered rocks associated with the Golden Mile-style mineralization, Kalgoorlie gold field, Western Australia. *Economic Geology* 101, 805-817.
- Fisher, L.A., Fougereuse, D., Cleverley, J.S., Ryan, C.G., Micklethwaite, S., Halfpenny, A., Hough, R.M., Gee, M., Paterson, D., Howard, D.L., 2014. Quantified, multi-scale X-ray fluorescence element mapping using the Maia detector array: application to mineral deposit studies. *Mineralium Deposita*, 1-10.
- Folk, R.L., 2005. Nannobacteria and the formation of framboidal pyrite: Textural evidence. *Journal of Earth System Science* 114, 369-374.
- Fortin, D., Southam, G., Beveridge, T., 1994. Nickel sulfide, iron-nickel sulfide and iron sulfide precipitation by a newly isolated *Desulfotomaculum* species and its relation to nickel resistance. *FEMS Microbiology Ecology* 14, 121-132.
- Gammons, C.H., Barnes, H., 1989. The solubility of Ag_2S in near-neutral aqueous sulfide solutions at 25 to 300 °C. *Geochimica et Cosmochimica Acta* 53, 279-290.
- Gregory, D.D., Large, R.R., Halpin, J.A., Baturina, E.L., Lyons, T.W., Wu, S., Danyushevsky, L., Sack, P.J., Chappaz, A., Maslennikov, V.V., 2015. Trace element content of sedimentary pyrite in black shales. *Economic Geology* 110, 1389-1410.
- Grice, K., Cao, C., Love, G.D., Böttcher, M.E., Twitchett, R.J., Grosjean, E., Summons, R.E., Turgeon, S.C., Dunning, W., Jin, Y., 2005. Photic zone euxinia during the Permian-Triassic superanoxic event. *Science* 307, 706-709.
- Grimes, S.T., Brock, F., Rickard, D., Davies, K.L., Edwards, D., Briggs, D.E., Parkes, R.J., 2001. Understanding fossilization: Experimental pyritization of plants. *Geology* 29, 123-126.
- Henley, R., 1973. Solubility of gold in hydrothermal chloride solutions. *Chemical Geology* 11, 73-87.

- Henne, A., Craw, D., 2012. Synmetamorphic carbon mobility and graphite enrichment in metaturbidites as a precursor to orogenic gold mineralisation, Otago Schist, New Zealand. *Mineralium Deposita*, 1-17.
- Hu, S., Evans, K., Craw, D., Rempel, K., Bourdet, J., Dick, J., Grice, K., 2015. Raman characterization of carbonaceous material in the Macraes orogenic gold deposit and metasedimentary host rocks, New Zealand. *Ore Geology Reviews* 70, 80-95.
- Jaraula, C.M., Grice, K., Twitchett, R.J., Böttcher, M.E., LeMetayer, P., Dastidar, A.G., Opazo, L.F., 2013. Elevated pCO₂ leading to Late Triassic extinction, persistent photic zone euxinia, and rising sea levels. *Geology* 41, 955-958.
- Kashefi, K., Tor, J.M., Nevin, K.P., Lovley, D.R., 2001. Reductive precipitation of gold by dissimilatory Fe (III)-reducing bacteria and archaea. *Applied and Environmental Microbiology* 67, 3275-3279.
- Kettler, R.M., Waldo, G.S., Penner-Hahn, J.E., Meyers, P.A., Kesler, S.E., 1990. Sulfidation of organic matter associated with gold mineralization, Pueblo Viejo, Dominican Republic. *Applied Geochemistry* 5, 237-248.
- Labrenz, M., Druschel, G.K., Thomsen-Ebert, T., Gilbert, B., Welch, S.A., Kemner, K.M., Logan, G.A., Summons, R.E., De Stasio, G., Bond, P.L., 2000. Formation of sphalerite (ZnS) deposits in natural biofilms of sulfate-reducing bacteria. *Science* 290, 1744-1747.
- Large, D., Sawlowicz, Z., Spratt, J., 1999. A cobaltite-framboidal pyrite association from the Kupferschiefer; possible implications for trace element behaviour during the earliest stages of diagenesis. *Mineralogical Magazine* 63, 353-361.
- Large, R., Thomas, H., Craw, D., Henne, A., Henderson, S., 2012. Diagenetic pyrite as a source for metals in orogenic gold deposits, Otago Schist, New Zealand. *New Zealand Journal of Geology and Geophysics* 55, 137-149.
- Large, R.R., Bull, S.W., Maslennikov, V.V., 2011. A carbonaceous sedimentary source-rock model for Carlin-type and orogenic gold deposits. *Economic Geology* 106, 331-358.

- Large, R.R., Danyushevsky, L., Hollit, C., Maslennikov, V., Meffre, S., Gilbert, S., Bull, S., Scott, R., Emsbo, P., Thomas, H., 2009. Gold and trace element zonation in pyrite using a laser imaging technique: implications for the timing of gold in orogenic and Carlin-style sediment-hosted deposits. *Economic Geology* 104, 635-668.
- Large, R.R., Maslennikov, V.V., Robert, F., Danyushevsky, L.V., Chang, Z., 2007. Multistage sedimentary and metamorphic origin of pyrite and gold in the giant Sukhoi Log deposit, Lena gold province, Russia. *Economic Geology* 102, 1233-1267.
- Lengke, M., Southam, G., 2006. Bioaccumulation of gold by sulfate-reducing bacteria cultured in the presence of gold (I)-thiosulfate complex. *Geochimica et Cosmochimica Acta* 70, 3646-3661.
- Lengke, M.F., Southam, G., 2007. The deposition of elemental gold from gold (I)-thiosulfate complexes mediated by sulfate-reducing bacterial conditions. *Economic Geology* 102, 109-126.
- Love, L., 1967. Early diagenetic iron sulphide in recent sediments of the Wash (England). *Sedimentology* 9, 327-352.
- Love, L.G., 1971. Early diagenetic polyframboidal pyrite, primary and redeposited, from the Wenlockian Denbigh Grit Group, Conway, North Wales, UK. *Journal of Sedimentary Research* 41, 1038-1044.
- Love, L.G., Al-Kaisy, A.T., Brockley, H., 1984. Mineral and organic material in matrices and coatings of framboidal pyrite from Pennsylvanian sediments, England. *Journal of Sedimentary Research* 54, 869-876.
- Lowers, H.A., Breit, G.N., Foster, A.L., Whitney, J., Yount, J., Uddin, M.N., Muneem, A.A., 2007. Arsenic incorporation into authigenic pyrite, Bengal Basin sediment, Bangladesh. *Geochimica et Cosmochimica Acta* 71, 2699-2717.
- MacKinnon, T.C., 1983. Origin of the Torlesse terrane and coeval rocks, South Island, New Zealand. *Geological Society of America Bulletin* 94, 967-985.

- MacLean, L., Pray, T., Onstott, T., Brodie, E., Hazen, T., Southam, G., 2007. Mineralogical, chemical and biological characterization of an anaerobic biofilm collected from a borehole in a deep gold mine in South Africa. *Geomicrobiology Journal* 24, 491-504.
- MacLean, L., Tyliczszak, T., Gilbert, P., Zhou, D., Pray, T., Onstott, T., Southam, G., 2008. A high - resolution chemical and structural study of framboidal pyrite formed within a low - temperature bacterial biofilm. *Geobiology* 6, 471-480.
- McKeag, S., Craw, D., Norris, R., 1989. Origin and deposition of a graphitic schist-hosted metamorphogenic Au-W deposit, Macraes, East Otago, New Zealand. *Mineralium deposita* 24, 124-131.
- Mees, F., Stoops, G., 2010. Sulphuric and sulphidic materials. Interpretation of micromorphological features of soils and regoliths. Elsevier, Amsterdam, 543-568.
- Melendez, I., Grice, K., Schwark, L., 2013. Exceptional preservation of Palaeozoic steroids in a diagenetic continuum. *Scientific Reports* 3, 2768.
- Moore, J., Doyle, S., 2015. Resource definition in the world-class Macraes gold mine, New Zealand, Proceedings, PACRIM Congress, AusIMM Publ Series, pp. 557-564.
- Moreau, J., Webb, R., Banfield, J., 2001. The mineralogy and microstructure of sedimentary zinc sulfides formed by bacterial sulfate reduction, AGU Fall Meeting Abstracts, p. 0124.
- Morse, J., Luther, G., 1999. Chemical influences on trace metal-sulfide interactions in anoxic sediments. *Geochimica et Cosmochimica Acta* 63, 3373-3378.
- Mortensen, J.K., Craw, D., MacKenzie, D.J., Gabites, J.E., Ullrich, T., 2010. Age and origin of orogenic gold mineralization in the Otago Schist Belt, South Island, New Zealand: Constraints from lead isotope and $^{40}\text{Ar}/^{39}\text{Ar}$ dating studies. *Economic Geology* 105, 777-793.
- Mortimer, N., 1993. Jurassic tectonic history of the Otago schist, New Zealand. *Tectonics* 12, 237-244.

- Mortimer, N., 2000. Metamorphic discontinuities in orogenic belts: example of the garnet-biotite-albite zone in the Otago Schist, New Zealand. *International Journal of Earth Sciences* 89, 295-306.
- Nabbefeld, B., Grice, K., Schimmelmann, A., Sauer, P.E., Böttcher, M.E., Twitchett, R., 2010. Significance of δD kerogen, $\delta^{13}C$ kerogen and $\delta^{34}S$ pyrite from several Permian/Triassic (P/Tr) sections. *Earth and Planetary Science Letters* 295, 21-29.
- Ohfuji, H., Rickard, D., 2005. Experimental syntheses of framboids—a review. *Earth-Science Reviews* 71, 147-170.
- Paterson, D., De Jonge, M., Howard, D., Lewis, W., McKinlay, J., Starritt, A., Kusel, M., Ryan, C., Kirkham, R., Moorhead, G., 2011. The X-ray fluorescence microscopy beamline at the Australian Synchrotron, The 10th International Conference on X-ray Microscopy. AIP Publishing, pp. 219-222.
- Paton, C., Hellstrom, J., Paul, B., Woodhead, J., Hergt, J., 2011. Iolite: Freeware for the visualisation and processing of mass spectrometric data. *Journal of Analytical Atomic Spectrometry* 26, 2508-2518.
- Pitcairn, I.K., Craw, D., Teagle, D.A., 2014a. Metabasalts as sources of metals in orogenic gold deposits. *Mineralium Deposita* 50, 1-18.
- Pitcairn, I.K., Craw, D., Teagle, D.A., 2014b. The gold conveyor belt: Large-scale gold mobility in an active orogen. *Ore Geology Reviews* 62, 129-142.
- Pitcairn, I.K., Olivo, G.R., Teagle, D.A., Craw, D., 2010. Sulfide evolution during prograde metamorphism of the Otago and Alpine schists, New Zealand. *The Canadian Mineralogist* 48, 1267-1295.
- Pitcairn, I.K., Teagle, D.A., Craw, D., Olivo, G.R., Kerrich, R., Brewer, T.S., 2006. Sources of metals and fluids in orogenic gold deposits: insights from the Otago and Alpine Schists, New Zealand. *Economic Geology* 101, 1525-1546.
- Reich, M., Kesler, S.E., Utsunomiya, S., Palenik, C.S., Chryssoulis, S.L., Ewing, R.C., 2005. Solubility of gold in arsenian pyrite. *Geochimica et Cosmochimica Acta* 69, 2781-2796.

- Rickard, D., Luther, G.W., 1997. Kinetics of pyrite formation by the H₂S oxidation of iron (II) monosulfide in aqueous solutions between 25 and 125 °C: the mechanism. *Geochimica et Cosmochimica Acta* 61, 135-147.
- Rickard, D.T., 1970. The origin of framboids. *Lithos* 3, 269-293.
- Ryan, C., Cousens, D., Sie, S., Griffin, W., Suter, G., Clayton, E., 1990. Quantitative PIXE microanalysis of geological material using the CSIRO proton microprobe. *Nuclear Instruments and Methods in Physics Research Section B: Beam Interactions with Materials and Atoms* 47, 55-71.
- Ryan, C., Etschmann, B., Vogt, S., Maser, J., Harland, C., Van Achtenbergh, E., Legnini, D., 2005. Nuclear microprobe–synchrotron synergy: Towards integrated quantitative real-time elemental imaging using PIXE and SXRF. *Nuclear Instruments and Methods in Physics Research Section B: Beam Interactions with Materials and Atoms* 231, 183-188.
- Ryan, C., Jamieson, D., Churms, C., Pilcher, J., 1995. A new method for on-line true-elemental imaging using PIXE and the proton microprobe. *Nuclear Instruments and Methods in Physics Research Section B: Beam Interactions with Materials and Atoms* 104, 157-165.
- Ryan, C., Kirkham, R., Hough, R., Moorhead, G., Siddons, D., De Jonge, M., Paterson, D., De Geronimo, G., Howard, D., Cleverley, J., 2010a. Elemental X-ray imaging using the Maia detector array: The benefits and challenges of large solid-angle. *Nuclear Instruments and Methods in Physics Research Section A: Accelerators, Spectrometers, Detectors and Associated Equipment* 619, 37-43.
- Ryan, C., Siddons, D., Kirkham, R., Dunn, P., Kuczewski, A., Moorhead, G., De Geronimo, G., Paterson, D., De Jonge, M., Hough, R., 2010b. The new Maia detector system: methods for high definition trace element imaging of natural material, *X-ray Optics and Microanalysis: Proceedings of the 20th International Congress*. AIP Publishing, pp. 9-17.
- Ryan, C., Siddons, D., Kirkham, R., Li, Z., de Jonge, M., Paterson, D., Cleverley, J., Kuczewski, A., Dunn, P., Jensen, M., 2013. The Maia detector array and x-ray fluorescence imaging system: Locating rare precious metal phases in

- complex samples, SPIE Optical Engineering+ Applications. International Society for Optics and Photonics, pp. 88510Q-88510Q-88511.
- Ryan, C., Siddons, D., Kirkham, R., Li, Z., de Jonge, M., Paterson, D., Kuczewski, A., Howard, D., Dunn, P., Falkenberg, G., 2014. MAIA X-ray fluorescence imaging: capturing detail in complex natural samples, *Journal of Physics: Conference Series*. IOP Publishing, p. 012002.
- Scholz, F., Neumann, T., 2007. Trace element diagenesis in pyrite-rich sediments of the Achterwasser lagoon, SW Baltic Sea. *Marine Chemistry* 107, 516-532.
- Schoonen, M., Barnes, H., 1991. Reactions forming pyrite and marcasite from solution: I. Nucleation of FeS₂ below 100 °C. *Geochimica et Cosmochimica Acta* 55, 1495-1504.
- Schoonen, M.A., 2004. Mechanisms of sedimentary pyrite formation. *Geological Society of America Special Papers* 379, 117-134.
- Seward, T.M., 1973. Thio complexes of gold and the transport of gold in hydrothermal ore solutions. *Geochimica et Cosmochimica Acta* 37, 379-399.
- Titley, S.R., 1991. Phanerozoic ocean cycles and sedimentary-rock-hosted gold ores. *Geology* 19, 645-648.
- Tomkins, A.G., 2013. On the source of orogenic gold. *Geology* 41, 1255-1256.
- Watson, J., Ellwood, D., 1994. Biomagnetic separation and extraction process for heavy metals from solution. *Minerals Engineering* 7, 1017-1028.
- Watson, J., Ellwood, D., Deng, Q., Mikhalovsky, S., Hayter, C., Evans, J., 1995. Heavy metal adsorption on bacterially produced FeS. *Minerals Engineering* 8, 1097-1108.
- Wilkin, R., Barnes, H., 1997. Formation processes of framboidal pyrite. *Geochimica et Cosmochimica Acta* 61, 323-339.
- Wilkin, R., Barnes, H., Brantley, S., 1996. The size distribution of framboidal pyrite in modern sediments: an indicator of redox conditions. *Geochimica et Cosmochimica Acta* 60, 3897-3912.

Williams, G.J., McKee, T.J., 1974. Economic geology of New Zealand: the TJ McKee memorial volume. Australasian Institute of Mining and Metallurgy.

Zhang, J., Lu, J., Zhai, J., Yang, F., 1997. Simulating experiments on enrichment of gold by bacteria and their geochemical significance. Chinese Journal of Geochemistry 16, 369-373.

Chapter 5

A new look at mixed sphalerite-pyrite framboids and the sequestration of Zn into framboids as a key process of Zn cycling in the ocean

This chapter is a manuscript which is in revision for re-submission to *Geochimica et Cosmochimica Acta*.

Hu, S.-Y., Evans, K., Rempel, K., Guagliardo, P., Kilburn, M., Craw, D., Grice, K.

A new look at mixed sphalerite-pyrite framboids and the sequestration of Zn into framboids as a key process of Zn cycling in the ocean. *In revision for re-submission to Geochimica et Cosmochimica Acta.*

Contributions by co-authors

Samples were collected by Si-Yu Hu and Katy Evans with the assistance of Dave Craw in the field. Si-Yu Hu performed sample preparation, petrographic observations, and nanoscale secondary ion mass spectrometry (NanoSIMS) with the help of Paul Guagliardo, Matt Kilburn. Manuscript was prepared by Si-Yu Hu with insightful discussions with Katy Evans and Kirsten Rempel, and contributions from other co-authors. Funds was provided by the CSIRO Organic Geochemistry of Mineral Systems Cluster.

Abstract

Zinc (Zn) is an important micronutrient in the ocean, and the fixation of Zn into organic, trace element-rich sediments is an important contribution to Zn cycling in the ocean. Framboids are considered to be the primary host for Zn in such settings. However, the sequestration of Zn into framboids is not fully understood, though the mechanism of sequestration affects Zn isotope fractionation, which is used as a record of Zn cycling. In this study, optical microscopy, scanning electron microscopy (SEM) and nanoscale secondary ion mass spectrometry (NanoSIMS) are utilized to characterize, on the sub-micron scale, the association between Zn, pyrite and organic matter in framboids from pelites of the Otago Schist, New Zealand. The distribution of Zn in framboids is variable. Most pyrite microcrystals include minor amounts of Zn. However, Zn is also observed to co-locate with organic matter, which occur on the boundaries of pyrite microcrystals. Finally, Zn is found as single sphalerite microcrystals or sphalerite rims around pyrite microcrystals within individual framboids. This texture has not been recorded before, to our knowledge. This distribution pattern suggests that, as a result of bacterial activity, Zn is sequestered into framboids in variable quantities, depending on the relative concentrations of Zn and Fe in solution. At higher Zn concentrations, individual microcrystals of sphalerite may deposit directly onto organic matter. Additional deposition of Zn from solution can then result in the development of a framework of sphalerite around the margins of a single microcrystal, infilled with pyrite cores. At low Zn/Fe ratios, Zn may be incorporated into pyrite as nanoparticles or as solid solutions, resulting in a more homogeneous distribution of Zn in the framboids. The whole process is proposed to relate to sulfate-reducing bacterial activity, which provides reduced sulfur. The sequence of events that sequesters Zn into framboids may affect progressive Zn isotope fractionation from seawater to continental margin sediments.

5.1 Introduction

Framboids are spheroidal aggregates consisting of microcrystals of sulfide minerals and are commonly observed in sedimentary rocks (Hu et al., 2016; Ohfuji and Rickard, 2005). Often associated with organic matter (OM), framboids have been

suggested to result from bacterial sulfate reduction (BSR) (Grice et al., 2005; Love, 1971; Love et al., 1984; MacLean et al., 2008; Plet et al., 2016; Wacey et al., 2015). Framboids can also be synthesized abiotically (Berner, 1969; Schoonen, 2004; Wilkin and Barnes, 1997), reviewed by Ohfuji and Rickard (2005). The term “framboids” is usually taken to be synonymous with the term “framboidal pyrite” because the overwhelming majority of framboids are composed of pyrite microcrystals (Gregory et al., 2015; Love, 1971). However, in recent decades, other sulfides, such as cobaltite, chalcopyrite and sphalerite, have been observed in framboids (Bawden et al., 2003; Hu et al., 2016; Kucha et al., 2010; Large et al., 2001; Large et al., 1999; MacLean et al., 2007).

Zn is a widespread trace element and an essential micronutrient in the ocean (Conway and John, 2015; John and Conway, 2014). studies have demonstrated that seawater preferentially concentrates heavy $\delta^{66}\text{Zn}$, while organic, trace element-rich continental margin sediments are sinks for light $\delta^{66}\text{Zn}$, suggesting that Zn isotope fractionation may occur during Zn fixation in those settings (Little et al., 2014; Little et al., 2016; Zhao et al., 2014). Framboids are common in such sediments and are thought to be the primary host for Zn and other trace elements in sediments (Hu et al., 2016; Large et al., 2014; Ohfuji and Rickard, 2005). Hence, an understanding of Zn sequestration processes into framboids, the details of which are not fully understood, is necessary to account for Zn isotope fractionation during sediment deposition.

The distribution of Zn in framboids has been shown to be variable by previous studies, and the details of Zn behavior during incorporation into framboids are not well understood. Zn occurs as solid solution in pyrite (Huerta-Diaz and Morse, 1992; Tribovillard et al., 2006) or sphalerite inclusions in framboids (Berner et al., 2013; Gregory et al., 2015). Zn has been inferred to be incorporated into pyrite as a substitution for Fe (Huerta-Diaz and Morse, 1992), after absorption on the surface of mackinawite (FeS), the precursor to pyrite (Morse and Arakaki, 1993), or directly precipitated as sphalerite. Sphalerite has been found co-located with OM within pyrite framboids (Hu et al., 2016; MacLean et al., 2007), implying that as well as Fe, Zn may be sequestered into framboids by biological activity. These findings indicate a broad continuum of Zn distribution and incorporation mechanisms. Thus, to

improve our understanding of the processes that incorporate Zn into framboids, it is of significance to explore the spatial relationships between Zn, pyrite and OM within framboids.

A variety of techniques have been previously applied to characterize framboids, such as X-ray and backscatter electron imaging and electron probe microanalysis (EPMA) (Hu et al., 2016; Large et al., 1999; Lowers et al., 2007; MacLean et al., 2007).

However, due to the small size of the microcrystals within framboids, these conventional techniques tend to lack the spatial resolution necessary to provide detailed information (Wacey et al., 2015). Nanoscale secondary ion mass spectrometry (NanoSIMS) can determine the distribution of trace elements in situ with submicron resolution relatively quickly (Kilburn and Clode, 2014).

Additionally, NanoSIMS is able to map the distribution of nitrogen (N) and carbon (C), which are key elements involved in biological processes (Kilburn and Wacey, 2011). These light elements are difficult to locate with many other techniques, but their distribution is a valuable indication of the location of OM that occurs as a precursor to framboids, and thus provides information on the role of bacteria in framboid growth (Wacey et al., 2015).

In this study, optical microscopy, SEM and NanoSIMS were utilized to characterize framboids in low metamorphic grade metasediments (prehnite-pumpellyite facies) from the Otago Schist, New Zealand. NanoSIMS element mapping was performed to determine element distribution within framboids. The distributions of metals (Zn, Fe) and OM (C, N) are compared to determine the spatial relationships between Zn, pyrite and OM, and constrain the processes via which Zn is incorporated into framboids.

5.2 Geological background and sampling

The Otago Schist is a Paleozoic to Mesozoic turbidite sequence comprising quartzofeldspathic psammite and pelites, developed in a continental margin setting (Craw, 2002; MacKinnon, 1983). These schists were metamorphosed during the collision of the Caples and Torlesse Terranes (Mortimer, 2000), and uplifted to form a symmetrical metamorphosed belt. The belt comprises a core zone of upper

greenschist facies rocks flanked on either side by zones of progressively lower grade rocks (Figure 5.1) (Mortimer, 1993; Mortimer, 2000). The metamorphic grade increases from prehnite-pumpellyite (P-P) facies on the margins, moving through pumpellyite-actinolite (P-A) facies to upper greenschist (G-S) facies within the core zone of the schist belt (Figure 5.1). The rocks become progressively more recrystallized and foliated through this increase in metamorphic grade, and the schists in the core of the belt have been pervasively recrystallized with several generations of folding and foliation development (Mortimer, 1993). The primary mineral assemblage of rocks in P-P facies is quartz, albite, muscovite, chlorite, epidote, stilpnomelane, pumpellyite and prehnite. Framboids, thought to be the source of Au for orogenic gold deposits in the Otago Schist, are commonly observed in P-P facies rocks and enriched in trace elements (Hu et al., 2016; Large et al., 2012; Pitcairn et al., 2006).

The sample (FF-16) for this study were collected from P-P facies rocks at Fiddlers Flat (Figure 5.1). Details of the sampling locations have been described by Hu et al. (2016).

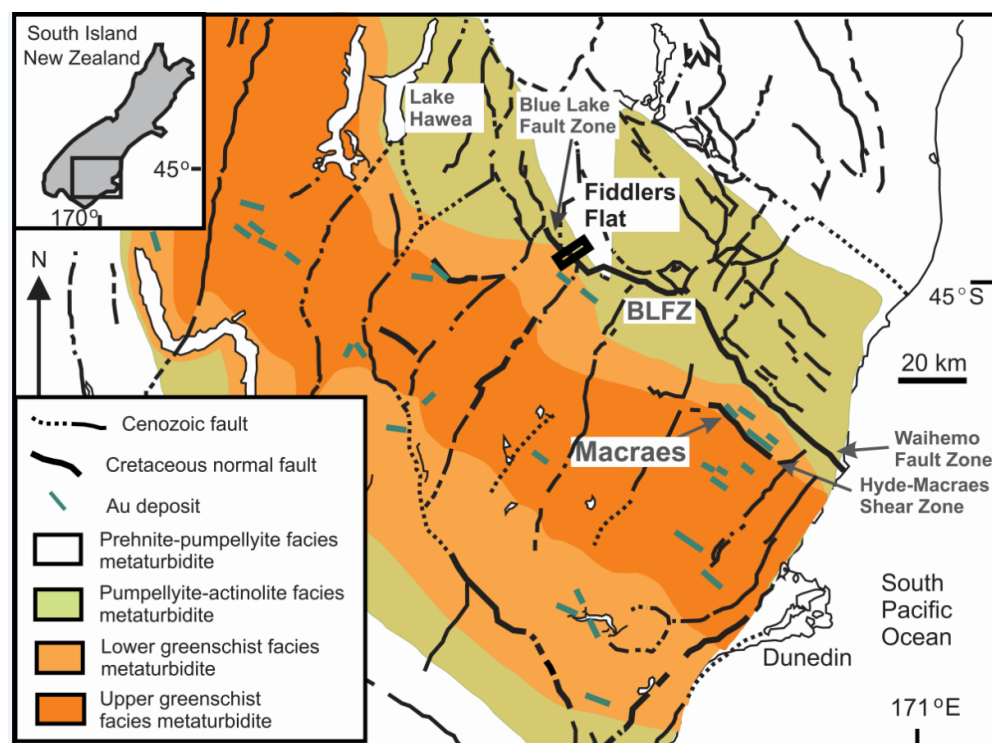


Figure 5.1 Geological map of the Otago Schist from Hu et al. (2015). The red rectangle on map is the sampling location.

5.3 Methods

Samples were cut to form billets and the fresh surfaces were polished. Mineral assemblages were characterized with transmitted and reflected light, and framboids were further characterized with optical microscopy, scanning electron microscopy with X-ray microanalysis (SEM-EDS) at the Department of Applied Geology, Curtin University (Perth, Australia).

Elemental mapping was performed with a Cameca NanoSIMS 50 at the Centre for Microscopy, Characterization and Analysis (CMCA), at the University of Western Australia. Circular areas of about 8 mm in diameter and containing framboids were cut from the billets, embedded in one-inch resin mounts, polished, and coated with silver at high voltage for conductivity. Measurements were performed with a Cs^+ primary beam, with a spot size of approximately 100 nm, an impact energy of 16 keV, and a beam current of approximately 2 pA. The instrument was operated in multicollector mode with simultaneous detection of $^{12}\text{C}_2^-$, $^{12}\text{C}^{14}\text{N}^-$, $^{56}\text{Fe}^{32}\text{S}^+$ and $^{65}\text{Zn}^{32}\text{S}^+$ from the same analysis region. Prior to imaging, a 500 pA primary Cs^+ current of $> 2 \times 10^{17}$ ions/cm² was used to presputter in order to remove surface contamination and implant Cs^+ ions to reach a steady-state of ion emission. Secondary ion images were obtained by rastering the primary ion beam with areas of $8 \times 8 - 45 \times 45 \mu\text{m}^2$, resolution of 256×256 pixels and dwell times of 45–250 ms per pixel. Element counts were collected quantitatively.

The data were processed with OpenMIMS software developed by the National Resource for Imaging Mass Spectrometry, Harvard University. Counts of elements are positively correlated to the element concentrations. Counts of each element from each grain were extracted and normalized to their respective secondary electron (SE) counts to remove anomalies caused by topography.

5.4 Results

5.4.1 Petrographic observations

Framboids occur in clusters of smaller framboids typically $200 \times 50 \mu\text{m}$ in size (Figure 5.2). The larger composite framboids are referred to here as polyframboids. The sizes of individual framboids within the polyframboids range from ~ 10 to $30 \mu\text{m}$

in diameter and are rounded, elliptical or irregular in shape. Framboids are surrounded by quartz, albite, muscovite and stilpnomelane. The dominant microcrystals within the framboids are pyrite, which is euhedral and pale yellow in reflected light (Figure 5.2 A). Sphalerite microcrystals, which are euhedral and grey in reflected light, are intergrown with pyrite in some framboids. More detailed SEM observations reveal that the single microcrystals within the framboids vary from euhedral cubic or octahedral to sub-rounded (Figure 5.2 B& C). In some cases, microcrystals are distributed in an ordered fashion, with hexagonal or pseudo-hexagonal symmetry (Figure 5.2 C), or, in other cases, present as apparently randomly distributed aggregates of crystals. Small framboids of less than 10 μm , were most commonly well-organized of hexagonal symmetry (Figure 5.2 D). Compositions of microcrystals, analyzed with semi-quantitative EDS analysis on the SEM range from variably zinc-rich pyrite (~40 wt % Fe, ~50 wt % S and up to 10 wt % Zn), or sphalerite with minor Fe (~60 wt % Zn, ~30 wt % S and up to 10 wt % Fe).

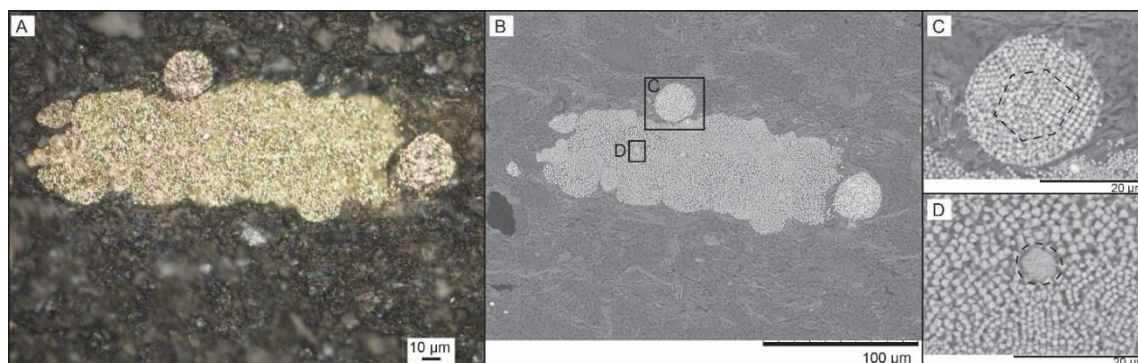


Figure 5.2 Petrographic photomicrograph and SEM images of polyframboids. (A) Reflected light photomicrograph of polyframboid consisting of numerous microcrystals; (B) SEM image of the same polyframboid in (A) with more clear observations of rounded or irregular framboids; (C) Rounded framboids formed partially of hexagonally ordered microcrystals (indicated by the dashed line); (D) Well-organized tiny framboids.

5.4.2 NanoSIMS observations

Fe and Zn mapping

Four types of microcrystals with differing Fe and Zn concentrations were recognized within the framboids and described as follows.

Type 1: Pyrite microcrystals with homogeneous Zn

Pyrite, characterized by high counts of Fe (as $^{56}\text{Fe}^{32}\text{S}$) and minor Zn (as $^{65}\text{Zn}^{32}\text{S}$), is the dominant microcrystal type in these framboids (Figure 5.3 A). The distribution of Zn is homogeneous within grains. Individual microcrystals are irregular to sub-rounded with sizes of 1–2 μm . On an element profile across a microcrystal, Fe and Zn contents show similar trends (Figure 5.3 A). Normalized Zn counts were plotted against those for Fe, and display a positive correlation in these microcrystals.

Type 2: Pyrite microcrystals with Zn concentrated on boundaries

Type 2 microcrystals have a similar shape to type 1 and are characterized by high Fe and low Zn contents, similar to type 1. However, instead of the homogeneous element distribution found in the type 1 microcrystals, Zn counts are higher at the boundaries relative to inside the grain (Figure 5.3 B). On an element profile across type 2 microcrystal, Zn counts are consistently low in the center of the grain, and high on the boundary where Fe counts are relatively low (Figure 5.3 B).

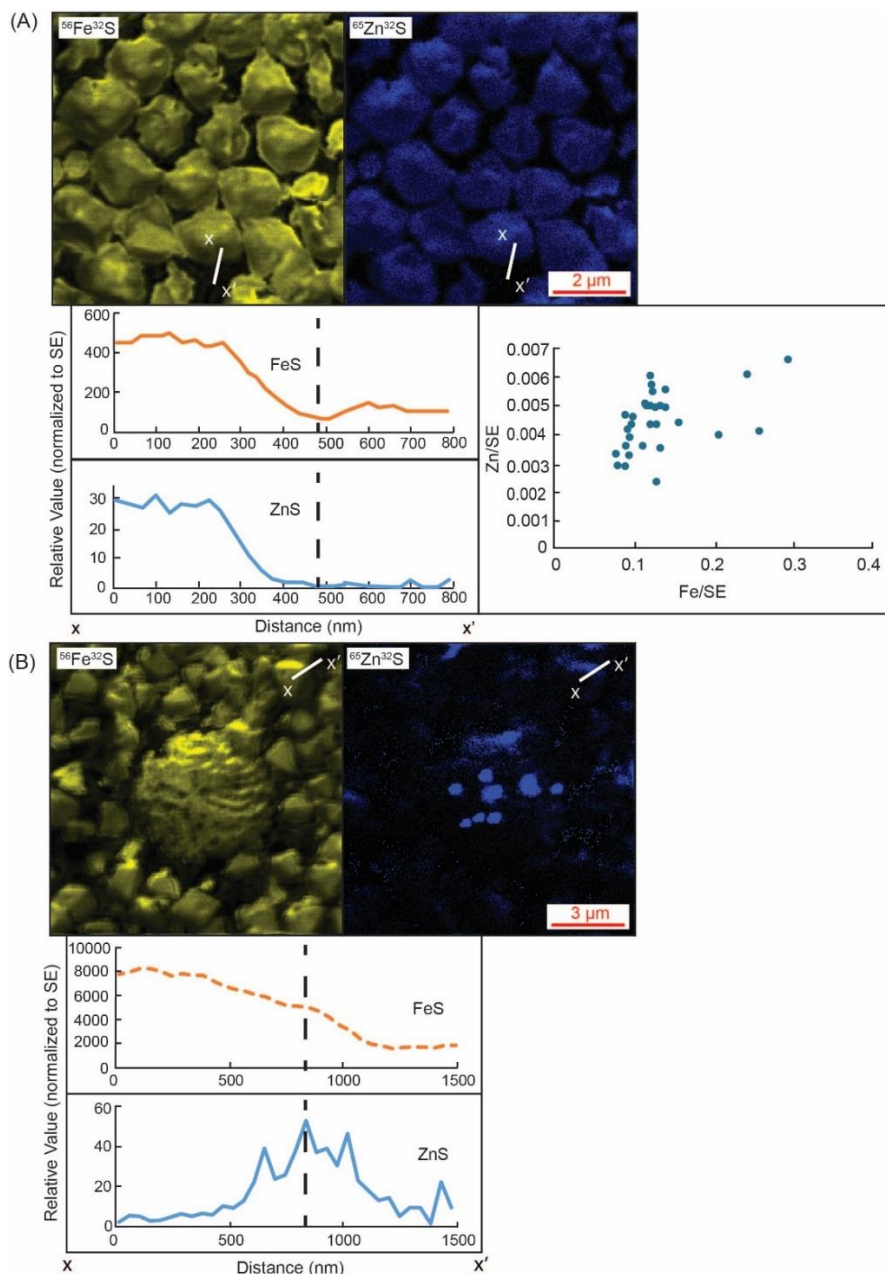


Figure 5.3 The distributions of Fe (as $^{56}\text{Fe}^{32}\text{S}$) and Zn (as $^{65}\text{Zn}^{32}\text{S}$) on microcrystals. Linear element profiles were taken from x to x' (from the center to the boundaries of grains). Element counts were normalized to secondary electron (SE) counts. (A) Pyrite microcrystals with almost homogeneous Zn (type 1). On the profile, both Fe and Zn contents show similar trends. Normalized Zn counts are positively correlated with those of Fe. (B) Pyrite microcrystals with Zn concentrated on the boundaries (type 2). On the profile, Zn has relatively low counts in the center of the grain, but high counts on the boundary where Fe content is relatively low. Dashed lines on the profiles are used to indicate the boundaries of grains.

Type 3: Microcrystals with intergrown pyrite and sphalerite

Pyrite and sphalerite are observed coexisting in some framboids (Figure 5.4 A). In this type, microcrystals display an octahedral shape with cores of pyrite and rims of sphalerite (Figure 5.4 B). The diameter of an entire type 3 microcrystal is around 1 μm , whereas that of the inner pyrite core varies from 0.06 to 0.6 μm . Plots of SE-normalized Zn against Fe reveal well-delineated groups of data with both high and low Zn/Fe ratios, which correspond to sphalerite and pyrite respectively (Figure 5.4 C).

Type 4: Sphalerite microcrystals

In framboids that contain the type 3 composite pyrite-sphalerite microcrystals, sphalerite also occurs as individual crystals distinguished by high Zn counts. The sphalerite microcrystals are otherwise similar to adjacent pyrite microcrystals (Figure 5.4 B) in that the two minerals have similar crystal shape and size (around 1 μm). There is no easily recognizable pattern to the distribution of pyrite and sphalerite, so they are taken to be randomly distributed.

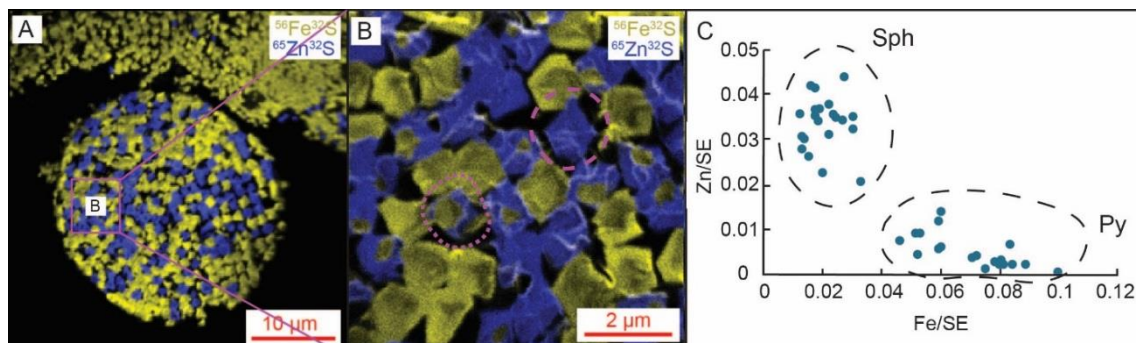


Figure 5.4 (A) The distributions of Fe and Zn in a single framboid depicted in Figure 5.2 C. (B) Enlarged image of part of (A). The microcrystal circled with the dotted line has a core of pyrite and a rim of sphalerite (type 3), and that with a dashed line is sphalerite (type 4). (C) Normalized counts of Fe and Zn are plotted against each other with sphalerite (Sph) and pyrite (Py) analyses plotting in distinctly different areas.

Distribution of OM

OM-pyrite relationships

Carbon-nitrogen (CN, as $^{12}\text{C}^{14}\text{N}$) mapping reveals that CN is concentrated on the boundaries of pyrite microcrystals, in ring-like zone (Figure 5.5 A). CN index, calculated as count ratio of CN/ (CN+Fe+Zn), is used to represent, semi-quantitatively, the relative concentration of CN relative to that of other elements. A line profile through type 2 microcrystal shows high Fe with low Zn, CN and carbon (C_2 , as $^{12}\text{C}_2^-$) contents within the crystal. The concentrations of CN are higher on both boundaries than inside the grain, and the boundaries are highlighted by high CN index. C_2 follows a similar trend to CN, but the correlation between those two is weak. Counts of Zn are generally low in the C- and CN-rich areas, but Zn counts are highest at one of the grain boundaries, co-located with a peak in CN concentration.

OM-sphalerite relationships

Sphalerite (type 4 microcrystal) is characterized by high Zn and CN contents, with minor Fe and C_2 (Figure 5.5 B). On the profile, Zn, Fe and CN have similar trends with wide, superimposed peaks. The concentration of Zn is high relative to that of Fe, but there is almost no Zn or Fe in the middle of the grain, which corresponds to a hole in the grain. The concentration of CN is relatively high across the grain, and there are non-zero counts at the position of the hole where the CN index is the highest. The contents of Zn, Fe and CN are low on one side of the “hole” and high on the other side. The carbon counts are generally low with a small peak on the boundary.

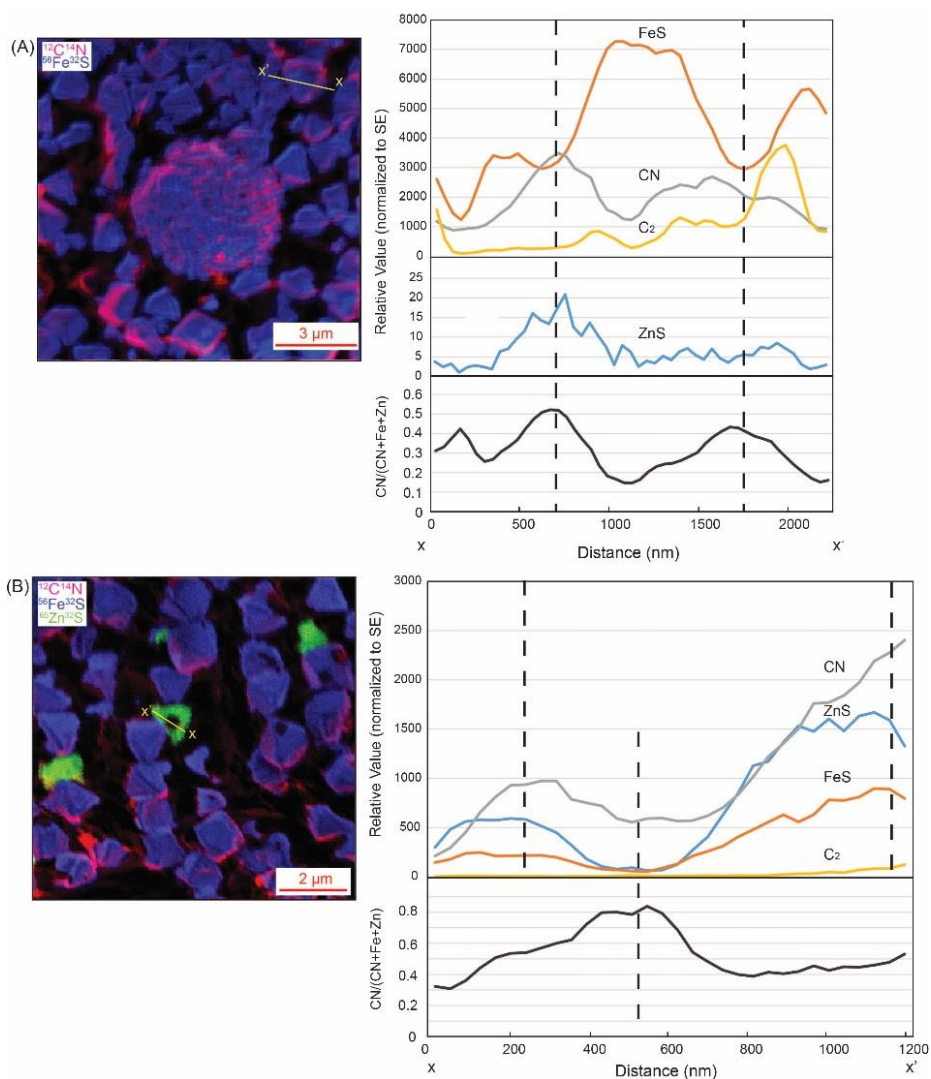


Figure 5.5 Distributions of CN (as $^{12}\text{C}^{14}\text{N}$) and Fe (as $^{56}\text{Fe}^{32}\text{S}$) in (A) pyrite microcrystals, and (B) pyrite and sphalerite. Part (B) also shows the Zn (as $^{65}\text{Zn}^{32}\text{S}$) distribution. For a pyrite grain (type 2) in (A) and a sphalerite grain (type 4) in (B), linear profiles were taken from x to x' across the grains. Element counts were extracted and normalized to secondary electron (SE) counts, shown on the corresponding graphs. CN index was calculated and presented on the profiles. Dashed lines on the profiles are used to indicate the boundaries of grains in (A) and (B) and “hole” area in (B).

5.5 Discussion

5.5.1 Zn and pyrite relationships

In this study, Zn has highly variable abundances in framboids and is closely associated with pyrite in four distinct types of microcrystal. There four types of

microcrystal can be used to interpret the process via which Zn is incorporated into the framboids during diagenesis. Type 1 and 2 both involve pyrite microcrystals with minor Zn, which correspond to Zn-rich pyrite with up to 10 wt % Zn observed using SEM. In type 1, Zn occurs in low concentrations in pyrite framboids. Diagenetic pyrite is thought to be the host for trace elements, including Zn, and Zn may be incorporated into pyrite as nanoparticles or as solid solutions (Deditius et al., 2011; Large et al., 2014), either of which is consistent with the positive correlation of Zn-Fe concentrations (Figure 5.3 A). In type 2 microcrystals, minor Zn is concentrated on the boundaries of pyrite grains. In types 3 and 4, pyrite microcrystals are intergrown with or coexist with sphalerite, respectively, within a single framboid. As discussed above, inclusion of sphalerite in pyrite framboids has been recorded by other workers (Berner et al., 2013; Gregory et al., 2015). However, descriptions of the type 3 and 4 framboids are, to the best of our knowledge, presented here for the first time.

The zonation of Zn or sphalerite around pyrite in type 2 and 3 microcrystals is of particular relevance to the understanding of Zn fixation in framboids. Although Zn has been proposed to be incorporated into the pyrite phase directly (Huerta-Diaz and Morse, 1992), recent studies on sedimentary pyrite show that Zn generally occurs as sphalerite microinclusion in pyrite (Gregory et al., 2015; Large et al., 2014). As noted by Morse and Luther (1999), pyrite deposition after sphalerite crystal formation is consistent with what is known of water exchange reaction kinetics. These authors suggested that Zn, which has faster H₂O exchange reaction kinetics than Fe, precipitates prior to FeS, the precursor of pyrite, during sulfidic sediment deposition. If kinetics were the principal control on the distribution of Fe and Zn sulfides, then the relative distribution of the two minerals in type 3 grains, where sphalerite occurs on the margins of pyrite, would not be expected, unless pyrite is deposited within sphalerite framework.

5.5.2 OM and sulfide associations

C₂ and CN have similar distributions on profiles through pyrite and sphalerite microcrystals, but CN tends to have higher count rates than C₂ (Figure 5.5). CN, represented by ¹²C¹⁴N, indicates the co-occurrence of C and N, and the C and N

signals have been inferred to record OM in other biogeoscientific studies (Kilburn and Wacey, 2011; Wacey et al., 2015). Given that CN is more indicative of OM than C₂, and has higher count rates and therefore higher signal:noise, CN was used to represent OM in this study, consistent with the strategy employed by other workers (Wacey et al., 2010; Wacey et al., 2015). The location of CN, concentrated on the boundaries of pyrite (Figure 5.5 A), is consistent with the observations of Donald and Southam (1999), MacLean et al. (2008) and Wacey et al. (2015), who all recorded single pyrite microcrystals enclosed by OM, and the interpretation that pyrite grows within biofilms or an organic matrix as the result of bacterial activity. Zn can also have high concentrations on the boundaries of pyrite, co-locating with CN in Figure 5.5 A. This indicates that Zn may be deposited in-situ with OM during sulfate-reducing bacterial activity, a proposal that is consistent with the previous results by Labrenz et al. (2000), Moreau et al. (2004), Yoon et al. (2012) and Hu et al. (2016). On the sphalerite microcrystal element profile (Figure 5.5 B), the distribution of CN is similar to that of Zn and Fe, indicating that CN may deposit together with Zn and Fe. CN is characterized by relatively higher counts where there is almost no Zn and Fe, implying that the organic matrix can be preserved at prehnite-pumpellyite facies without sulfide mineralization.

5.5.3 The sequestration of Zn into framboids

Based on observations documented here, the proposed progressive incorporation of Zn into framboids is illustrated in Figure 5.6. Pyrite framboids have been thought to be produced from sulfide created by sulfate reducing bacteria using OM as an electron source (Donald and Southam, 1999; Machel, 2001; Schoonen, 2004). In this case, OM present in mixed sphalerite-pyrite framboids would provide a record of sulfate reducing bacterial activity (Bawden et al., 2003; Kucha et al., 2010; Labrenz et al., 2000).

We propose that sphalerite is initially deposited directly on the bacterial cell during bacterial activity as type 4 before iron sulfide deposition, when Zn is present in sufficient concentrations in the aqueous solution present during diagenesis, e.g. modified seawater. This mechanism is consistent with experimental results by Labrenz et al. (2000) and observations in Hu et al. (2016). When Zn concentrations

in solution are reduced, Zn may be deposited on OM directly instead of a well crystallized sphalerite, while pyrite or its precursor (mackinawite) is then precipitated within the OM framework as type 2 microcrystals (MacLean et al., 2008; Wacey et al., 2015). More Zn in the solution would be accumulated into OM continuously until sphalerite is formed, which may result in the formation of type 3 microcrystals where pyrite is enclosed by sphalerite as a single microcrystal. When most of Zn is consumed, pyrite or mackinawite may be precipitated directly, with low concentrations of Zn incorporated into pyrite as type 1 microcrystals via adsorption on the growth surfaces of pyrite or its precursor (Morse and Arakaki, 1993). It is noted that mackinawite has been suggested to be the primary products of bacterial activity and that this phase transforms later to pyrite (Donald and Southam, 1999). The relationships between the transformation of mackinawite to pyrite and sphalerite deposition is unknown, but need not to be specified for the purpose of the discussion presented here.

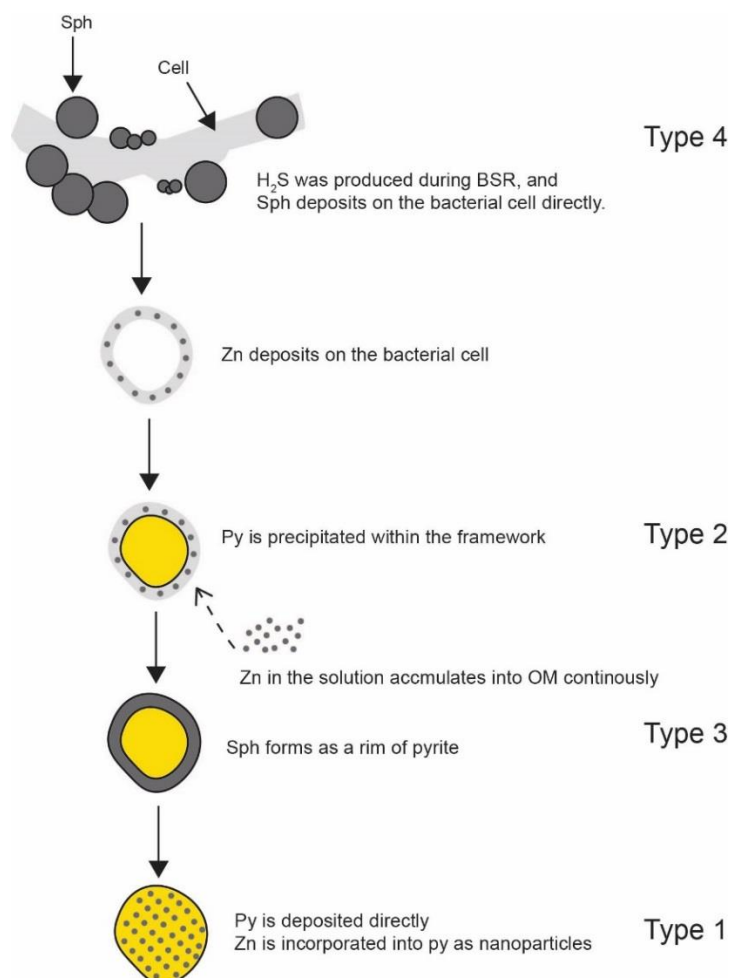


Figure 5.6 A general model of Zn sequestration processes in framboids, as an example of a single microcrystal. (Sph: sphalerite; Py: pyrite; BSR: bacterial sulfate reduction)

5.5.4 Implications for Zn isotope fractionation processes

In this study, new observations of the coexistence of sphalerite and pyrite microcrystals were made as a consequence of an investigation of the spatial relationships between Zn, pyrite and OM in framboids. The different types of Zn incorporation in framboids may occur during different stages of Zn sequestration into the framboids, dependent on the concentrations of Zn and Fe in solutions. Therefore, the observation of co-location of sphalerite and OM in polyframboids reported by Hu et al. (2016) corresponds to an early stage of framboids evolution. The ubiquitous presence of OM suggests that the entire process is linked to bacterial activity, such as that represented by equations (1, 2), and is consistent with the results of other workers (MacLean et al., 2007; MacLean et al., 2008; Wacey et al., 2015).



The presence of Zn in framboids also has implications for Zn isotope fractionation during the deposition of marine sediments. As reported in recent studies, organic, trace element-rich continental margin sediments are sinks for light $\delta^{66}\text{Zn}$ (as low as ~ -0.40 ‰), in contrast to heavy $\delta^{66}\text{Zn}$ in seawaters ($\sim +0.53$ ‰) (Little et al., 2014; Little et al., 2016; Zhao et al., 2014). To understand the processes involved in this fractionation, an assumption of route taken by Zn from seawaters to sedimentary rocks is required, which has been summarized in Figure 5.7. Critical processes include the cycling of Zn through living organisms, deposition directly in sediments, and incorporation of Zn into framboids. Previous studies have noted that lighter Zn isotopes tend to be taken up by plankton in the upper seawater with $\Delta\delta^{66}\text{Zn}$ around 0.8 ‰) (John and Conway, 2014; John et al., 2007). During the degradation of dead organisms, lighter Zn isotopes are released into seawater ($\Delta\delta^{66}\text{Zn} \sim -0.27$ ‰) and heavier Zn isotopes are retained by the degrading plankton ($\Delta\delta^{66}\text{Zn} \sim 0.32$ ‰) (John and Conway, 2014), which may be deposited directly in sediments. However,

measurements of Zn concentrations in framboids and matrix respectively (Hu et al., 2016), suggests that Zn in framboids can account for up to 90% of Zn in sediments. In this case, the sequestration of Zn from the seawater into framboids is would be the overall control on Zn isotope fractionation processes. The fixation of Zn in framboids is likely the result of a combination of two processes: sulfide precipitation during BSR activity and direct incorporation into pyrite. The precipitation of ZnS has been proposed to preferentially incorporate lighter Zn isotopes relative to that in the parent solution ($\Delta\delta^{66}\text{Zn} \sim -0.4\text{‰}$) (Archer et al., 2004; Fujii et al., 2011). Because Zn isotope fractionation has been recorded during biological process (Cloquet et al., 2008; John et al., 2007), and sulfate-reducing bacteria are thought to play a more important role than simply providing H_2S (Schoonen, 2004), Zn isotope may be fractionated during BSR activity, however, no data for the extent of this fractionation is currently available. The incorporation of Zn into pyrite may induce isotope fractionation as well, but again, little is known of the magnitude of this fractionation. The light Zn isotopes in sphalerite, and the likely dominance of the Zn budget by Zn sequestration into framboids, which is consistent with the light Zn isotope signature of continental margin sediments (Little et al., 2016; Maréchal et al., 2000), provides a strong motivation for further studies into Zn isotope fractionation during BSR and framboids formation, and into the implications of the fractionation for current nutrient cycling models.

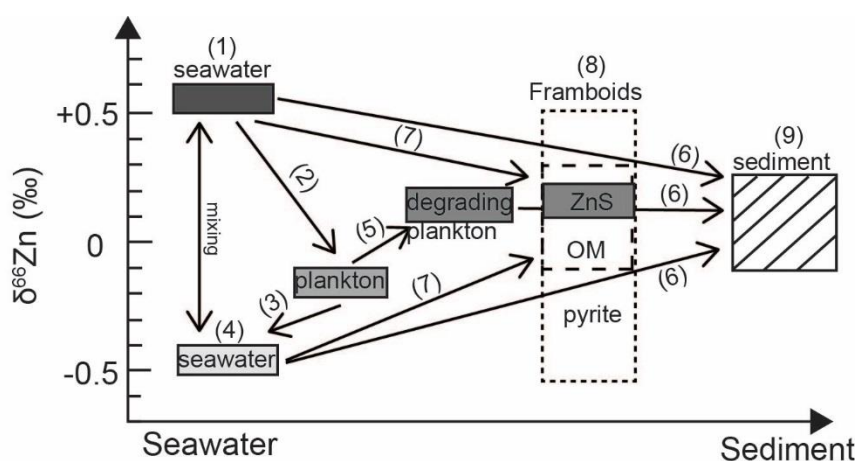


Figure 5.7 Zn isotope fractionation steps from seawater to continental margin sediment deposition. (1) Zn isotope in seawater (Zhao et al., 2014); (2) Lighter Zn isotopes is taken up by plankton in the upper seawater (John and Conway, 2014); (3, 4) During the degradation of dead organisms, lighter Zn isotopes are released into seawater (John and Conway, 2014);

(5) Heavier Zn isotopes are bound to degrading plankton (John and Conway, 2014); (6) Zn is deposited directly in sediments; (7, 8) Zn fixation in framboids proposed in this study, including sulfide precipitation during BSR activity and directly incorporated into pyrite; (9) Zn isotope in sediments (Little et al., 2016; Maréchal et al., 2000). (OM: organic matter.)

5.6 Conclusions

The abundance of Zn is highly variable in framboids and NanoSIMS analysis revealed four types of microcrystals in the pelites of the Otago Schist, New Zealand. Most microcrystals are pyrite microcrystals with high Fe concentrations and minor homogeneous distributed Zn. However, some pyrite microcrystals were observed with co-located Zn-OM boundaries. Zn also occurs as previously unrecorded sphalerite microcrystals which have a similar crystal shape and size to those of pyrite microcrystals, or sphalerite rims around pyrite core within single framboids. The difference distributions of Zn in framboids may be a record of progressive incorporation of Zn into framboids, as a consequences of sulfate reducing bacteria activity with dependence on the Zn/Fe ratio of co-existing seawater or modified seawater. Better constraints on the extent of Zn isotope fractionation are required to quantify the extent to which this process affects the fractionation Zn isotopes during sequestration into sediments.

5.7 Acknowledgements

All the authors acknowledge the support from the CSIRO Mineral Resources Flagship Cluster for Organic Geochemistry of Mineral Systems led by Curtin University and additional support from WA-Organic and Isotope Geochemistry Centre (WA-OIGC), The Institute of Geoscience Research (TIGeR) and Curtin University. S.H. acknowledges the receipt of Chinese Scholarship Council (CSC)-Curtin International Postgraduate Research Scholarship (CIPRS), CSIRO PhD Top-up Scholarship. Additional funding support was provided by Ministry of Business, Innovation and Employment, New Zealand.

5.8 References

- Archer, C., Vance, D. and Butler, I., 2004. Abiotic Zn isotope fractionations associated with ZnS precipitation. *Geochimica et Cosmochimica Acta* 66, A325.
- Bawden, T.M., Einaudi, M.T., Bostick, B.C., Meibom, A., Wooden, J., Norby, J.W., Orobona, M.J., Chamberlain, C.P., 2003. Extreme ³⁴S depletions in ZnS at the Mike gold deposit, Carlin Trend, Nevada: Evidence for bacteriogenic supergene sphalerite. *Geology* 31, 913-916.
- Berner, R.A., 1969. The synthesis of framboidal pyrite. *Economic Geology* 64, 383-384.
- Berner, Z.A., Puchelt, H., Noeltner, T., Kramar, U., 2013. Pyrite geochemistry in the Toarcian Posidonia Shale of south-west Germany: Evidence for contrasting trace - element patterns of diagenetic and syngenetic pyrites. *Sedimentology* 60, 548-573.
- Cloquet, C., Carignan, J., Lehmann, M.F., Vanhaecke, F., 2008. Variation in the isotopic composition of zinc in the natural environment and the use of zinc isotopes in biogeosciences: a review. *Analytical and Bioanalytical Chemistry* 390, 451-463.
- Conway, T.M., John, S.G., 2015. The cycling of iron, zinc and cadmium in the North East Pacific Ocean—Insights from stable isotopes. *Geochimica et Cosmochimica Acta* 164, 262-283.
- Craw, D., 2002. Geochemistry of late metamorphic hydrothermal alteration and graphitisation of host rock, Macraes gold mine, Otago Schist, New Zealand. *Chemical Geology* 191, 257-275.
- Deditius, A.P., Utsunomiya, S., Reich, M., Kesler, S.E., Ewing, R.C., Hough, R., Walshe, J., 2011. Trace metal nanoparticles in pyrite. *Ore Geology Reviews* 42, 32-46.
- Donald, R., Southam, G., 1999. Low temperature anaerobic bacterial diagenesis of ferrous monosulfide to pyrite. *Geochimica et Cosmochimica Acta* 63, 2019-2023.

- Fujii, T., Moynier, F., Pons, M.-L., Albarède, F., 2011. The origin of Zn isotope fractionation in sulfides. *Geochimica et Cosmochimica Acta* 75, 7632-7643.
- Gregory, D.D., Large, R.R., Halpin, J.A., Baturina, E.L., Lyons, T.W., Wu, S., Danyushevsky, L., Sack, P.J., Chappaz, A., Maslennikov, V.V., 2015. Trace element content of sedimentary pyrite in black shales. *Economic Geology* 110, 1389-1410.
- Grice, K., Cao, C., Love, G.D., Böttcher, M.E., Twitchett, R.J., Grosjean, E., Summons, R.E., Turgeon, S.C., Dunning, W., Jin, Y., 2005. Photic zone euxinia during the Permian-Triassic superanoxic event. *Science* 307, 706-709.
- Hu, S.-Y., Evans, K., Fisher, L., Rempel, K., Craw, D., Evans, N.J., Cumberland, S., Robert, A., Grice, K., 2016. Associations between sulfides, carbonaceous material, gold and other trace elements in polyframboids: Implications for the source of orogenic gold deposits, Otago Schist, New Zealand. *Geochimica et Cosmochimica Acta* 180, 197-213.
- Huerta-Diaz, M.A., Morse, J.W., 1992. Pyritization of trace metals in anoxic marine sediments. *Geochimica et Cosmochimica Acta* 56, 2681-2702.
- John, S.G., Conway, T.M., 2014. A role for scavenging in the marine biogeochemical cycling of zinc and zinc isotopes. *Earth and Planetary Science Letters* 394, 159-167.
- John, S.G., Geis, R.W., Saito, M.A., Boyle, E.A., 2007. Zinc isotope fractionation during high-affinity and low-affinity zinc transport by the marine diatom *Thalassiosira oceanica*. *Limnology and Oceanography* 52, 2710-2714.
- Kilburn, M.R., Clode, P.L., 2014. Elemental and isotopic imaging of biological samples using NanoSIMS. *Electron Microscopy: Methods and Protocols*, 733-755.
- Kilburn, M.R., Wacey, D., 2011. Elemental and isotopic analysis by NanoSIMS: insights for the study of stromatolites and early life on Earth, *Stromatolites: interaction of microbes with sediments*. Springer, pp. 463-493.

- Kucha, H., Schroll, E., Raith, J., Halas, S., 2010. Microbial sphalerite formation in carbonate-hosted Zn-Pb ores, Bleiberg, Austria: Micro-to nanotextural and sulfur isotope evidence. *Economic Geology* 105, 1005-1023.
- Labrenz, M., Druschel, G.K., Thomsen-Ebert, T., Gilbert, B., Welch, S.A., Kemner, K.M., Logan, G.A., Summons, R.E., De Stasio, G., Bond, P.L., 2000. Formation of sphalerite (ZnS) deposits in natural biofilms of sulfate-reducing bacteria. *Science* 290, 1744-1747.
- Large, D., Fortey, N., Milodowski, A., Christy, A., Dodd, J., 2001. Petrographic observations of iron, copper, and zinc sulfides in freshwater canal sediment. *Journal of Sedimentary Research* 71, 61-69.
- Large, D., Sawlowicz, Z., Spratt, J., 1999. A cobaltite-framboidal pyrite association from the Kupferschiefer; possible implications for trace element behaviour during the earliest stages of diagenesis. *Mineralogical Magazine* 63, 353-361.
- Large, R., Thomas, H., Craw, D., Henne, A., Henderson, S., 2012. Diagenetic pyrite as a source for metals in orogenic gold deposits, Otago Schist, New Zealand. *New Zealand Journal of Geology and Geophysics* 55, 137-149.
- Large, R.R., Halpin, J.A., Danyushevsky, L.V., Maslennikov, V.V., Bull, S.W., Long, J.A., Gregory, D.D., Lounejeva, E., Lyons, T.W., Sack, P.J., 2014. Trace element content of sedimentary pyrite as a new proxy for deep-time ocean-atmosphere evolution. *Earth and Planetary Science Letters* 389, 209-220.
- Little, S., Vance, D., Walker-Brown, C., Landing, W., 2014. The oceanic mass balance of copper and zinc isotopes, investigated by analysis of their inputs, and outputs to ferromanganese oxide sediments. *Geochimica et Cosmochimica Acta* 125, 673-693.
- Little, S.H., Vance, D., McManus, J., Severmann, S., 2016. Key role of continental margin sediments in the oceanic mass balance of Zn and Zn isotopes. *Geology* 44, 207-210.
- Love, L.G., 1971. Early diagenetic polyframboidal pyrite, primary and redeposited, from the Wenlockian Denbigh Grit Group, Conway, North Wales, UK. *Journal of Sedimentary Research* 41, 1038-1044.

- Love, L.G., Al-Kaisy, A.T., Brockley, H., 1984. Mineral and organic material in matrices and coatings of framboidal pyrite from Pennsylvanian sediments, England. *Journal of Sedimentary Research* 54, 869-876.
- Lowers, H.A., Breit, G.N., Foster, A.L., Whitney, J., Yount, J., Uddin, M.N., Muneem, A.A., 2007. Arsenic incorporation into authigenic pyrite, Bengal Basin sediment, Bangladesh. *Geochimica et Cosmochimica Acta* 71, 2699-2717.
- Machel, H., 2001. Bacterial and thermochemical sulfate reduction in diagenetic settings—old and new insights. *Sedimentary Geology* 140, 143-175.
- MacKinnon, T.C., 1983. Origin of the Torlesse terrane and coeval rocks, South Island, New Zealand. *Geological Society of America Bulletin* 94, 967-985.
- MacLean, L., Pray, T., Onstott, T., Brodie, E., Hazen, T., Southam, G., 2007. Mineralogical, chemical and biological characterization of an anaerobic biofilm collected from a borehole in a deep gold mine in South Africa. *Geomicrobiology Journal* 24, 491-504.
- MacLean, L., Tyliczszak, T., Gilbert, P., Zhou, D., Pray, T., Onstott, T., Southam, G., 2008. A high - resolution chemical and structural study of framboidal pyrite formed within a low - temperature bacterial biofilm. *Geobiology* 6, 471-480.
- Maréchal, C.N., Nicolas, E., Douchet, C., Albarède, F., 2000. Abundance of zinc isotopes as a marine biogeochemical tracer. *Geochemistry, Geophysics, Geosystems* 1.
- Moreau, J.W., Webb, R.I., Banfield, J.F., 2004. Ultrastructure, aggregation-state, and crystal growth of biogenic nanocrystalline sphalerite and wurtzite. *American Mineralogist* 89, 950-960.
- Morse, J., Luther, G., 1999. Chemical influences on trace metal-sulfide interactions in anoxic sediments. *Geochimica et Cosmochimica Acta* 63, 3373-3378.
- Morse, J.W., Arakaki, T., 1993. Adsorption and coprecipitation of divalent metals with mackinawite (FeS). *Geochimica et Cosmochimica Acta* 57, 3635-3640.

- Mortimer, N., 1993. Jurassic tectonic history of the Otago schist, New Zealand. *Tectonics* 12, 237-244.
- Mortimer, N., 2000. Metamorphic discontinuities in orogenic belts: example of the garnet–biotite–albite zone in the Otago Schist, New Zealand. *International journal of earth sciences* 89, 295-306.
- Ohfuji, H., Rickard, D., 2005. Experimental syntheses of framboids—a review. *Earth-Science Reviews* 71, 147-170.
- Pitcairn, I.K., Teagle, D.A., Craw, D., Olivo, G.R., Kerrich, R., Brewer, T.S., 2006. Sources of metals and fluids in orogenic gold deposits: insights from the Otago and Alpine Schists, New Zealand. *Economic Geology* 101, 1525-1546.
- Plet, C., Grice, K., Pagès, A., Ruebsam, W., Coolen, M., Schwark, L., 2016. Microbially-mediated fossil-bearing carbonate concretions and their significance for palaeoenvironmental reconstructions: A multi-proxy organic and inorganic geochemical appraisal. *Chemical Geology* 426, 95-108.
- Schoonen, M.A., 2004. Mechanisms of sedimentary pyrite formation. *Geological Society of America Special Papers* 379, 117-134.
- Tribovillard, N., Algeo, T.J., Lyons, T., Riboulleau, A., 2006. Trace metals as paleoredox and paleoproductivity proxies: an update. *Chemical Geology* 232, 12-32.
- Wacey, D., Gleeson, D., Kilburn, M., 2010. Microbialite taphonomy and biogenicity: new insights from NanoSIMS. *Geobiology* 8, 403-416.
- Wacey, D., Kilburn, M.R., Saunders, M., Cliff, J.B., Kong, C., Liu, A.G., Matthews, J.J., Brasier, M.D., 2015. Uncovering framboidal pyrite biogenicity using nano-scale CN_{org} mapping. *Geology* 43, 27-30.
- Wilkin, R., Barnes, H., 1997. Formation processes of framboidal pyrite. *Geochimica et Cosmochimica Acta* 61, 323-339.
- Yoon, S.-j., Yáñez, C., Bruns, M.A., Martínez-Villegas, N., Martínez, C.E., 2012. Natural zinc enrichment in peatlands: biogeochemistry of ZnS formation. *Geochimica et Cosmochimica Acta* 84, 165-176.

Zhao, Y., Vance, D., Abouchami, W., De Baar, H., 2014. Biogeochemical cycling of zinc and its isotopes in the Southern Ocean. *Geochimica et Cosmochimica Acta* 125, 653-672.

Chapter 6

Resolving the role of carbonaceous material in gold precipitation in metasediment-hosted orogenic gold deposits

This chapter is a manuscript which is under review in *Geology*.

Hu, S.-Y., Evans, K., Craw, D., Rempel, K., Grice, K. Resolving the Role of Carbonaceous Materials in Gold Precipitation in Metasediment-hosted Orogenic Gold Deposits. Under review, *Geology*.

Contributions by co-authors

Samples were collected by Si-Yu Hu and Katy Evans with the assistance of Dave Craw in the field. Thermodynamic modelling was performed by Si-Yu Hu with the supervision of Katy Evans. A large dataset of sulfur and non-carbonate carbon concentrations was provided by Dave Craw. Si-Yu Hu prepared the manuscript with the discussions, suggestions and guidance from all co-authors. Funds was provided by the CSIRO Organic Geochemistry of Mineral Systems Cluster.

Abstract

Carbonaceous material (CM) is commonly associated with gold and sulfides in metasediment-hosted orogenic gold deposits. The role of CM in Au deposition is controversial; CM has been proposed to contribute to gold deposition by reducing Au bisulfide complexes, or by facilitating sulfidation, which destabilizes Au bisulfide complexes with resultant Au deposition. Integration of petrographic observations, thermodynamic models with geochemical data from metasediment-hosted orogenic gold deposits in New Zealand, Australia, Canada and West Africa reveals genetic links between sulfides, CM and mineralization. The results are consistent with the coexistence of CM and pyrite as a consequence of their co-deposition from hydrothermal fluids, with a minor proportion of CM originally in-situ in the host rocks. Au is deposited when pyrite and CM deposition decreases H₂S concentration in hydrothermal fluids, destabilizing Au(HS)₂⁻ complexes. Most of the CM in gold deposits is proposed to form from reaction between CO₂ and CH₄ in infiltrating fluids. These findings are applicable to similar deposits worldwide.

6.1 Introduction

Metasediment-hosted orogenic gold deposits such as the Victorian goldfields of Australia (Bierlein et al., 2001), the Macraes gold deposit of New Zealand (Craw, 2002), and the Paleoproterozoic gold deposits of West Africa (Křibek et al., 2015) are some of the world's largest. Ore fluids are low salinity, CO₂ rich, often CH₄-bearing and near-neutral, but the source of ore fluids and metals is controversial (Berge, 2011; De Ronde et al., 2000; Goldfarb and Groves, 2015). Recent research suggests that gold is sourced from organic, pyrite-rich sediments, and that fluids are generated during the lower greenschist (G-S) to amphibolite facies transition (Hu et al., 2016; Large et al., 2011; Pitcairn et al., 2006; Thomas et al., 2011; Tomkins, 2010, 2013). Mineralization commonly occurs in shear zones at pressures of 1–3 kbar and temperatures of 200–400 °C. In auriferous zones, carbonaceous material (CM) is widespread and spatially associated with gold and sulfides (Berge, 2011; Bierlein et al., 2001; Hu et al., 2015; Křibek et al., 2015; MacKenzie et al., 2010). CM may be in-situ, derived from organic matter that was deposited along with the sediments and matured during metamorphism (Berge, 2011; Bierlein et al., 2001).

Alternatively, CM may be deposited from hydrothermal fluids (Křibek et al., 2015; Pitcairn et al., 2005). (CM has long been thought to directly or indirectly contribute to gold deposition, but details of the role of CM are not well understood. Possible roles for CM were summarized by Hu et al. (2015):

(1) In-situ CM, a reductant, reacts with Au-rich fluid to cause gold precipitation via reaction (1);

$4\text{Au}(\text{HS})_2^- (\text{aq}) + \text{C}(\text{s}) + 4\text{H}^+ (\text{aq}) + 2\text{H}_2\text{O}(\text{l}) = 4\text{Au}(\text{s}) + \text{CO}_2(\text{aq}) + 8\text{H}_2\text{S}(\text{aq})$. (1) (e.g. Cox et al., 1995);

(2) CM was remobilized during metamorphism, but prior to mineralization, and acts as a reductant in a similar way to reaction (1);

(3) Hydrothermal CM is precipitated from fluids simultaneously with sulfides via reaction (2), and the loss of sulfur from solution drives gold deposition via destabilization of Au-sulfide complexes in solution, summarized as:

$4\text{FeS}(\text{s}) + 4\text{H}_2\text{S}(\text{aq}) + \text{CO}_2(\text{aq}) = 4\text{FeS}_2(\text{s}) + \text{C}(\text{s}) + 2\text{H}_2\text{O}(\text{l}) + 2\text{H}_2(\text{aq})$. (2) (e.g. Craw, 2002);

(4) Presence of CM plays a physical rather than a chemical role in Au precipitation by facilitating the formation of shear zones that focus fluid flow (e.g. Upton and Craw, 2008).

In this study we combine thermodynamic modelling using the HCh software package (Shvarov and Bastrakov, 1999) with new petrographic observations and geochemical analyses of samples from the Macraes gold deposit, and with published geochemical data from similar gold deposits, to test the hypotheses above. We use Macraes as the primary example because it provides an extensive dataset and abundant CM in mineralized rocks (Craw, 2002). However, the results are relevant to other similar gold deposits where CM is ubiquitous, e.g., Křibek et al. (2015).

6.2 Petrographic observations

In the Macraes deposit, CM, sulfide and Au are spatially associated in mineralized rocks. The CM is dominantly hydrothermal graphite introduced during mineralization, although some metamorphosed CM also occurs in the host rocks

(Craw, 2002; Henne and Craw, 2012; Hu et al., 2015; Petrie et al., 2005; Pitcairn et al., 2005). Gold occurs primarily as micro-scale inclusions in sulfides (Petrie et al., 2005). Auriferous sulfides are often texturally synchronous with or post-formation of graphitic microshears which include fine grained CM and sulfides (Figure 6.1) (Craw, 2002; Upton and Craw, 2008).

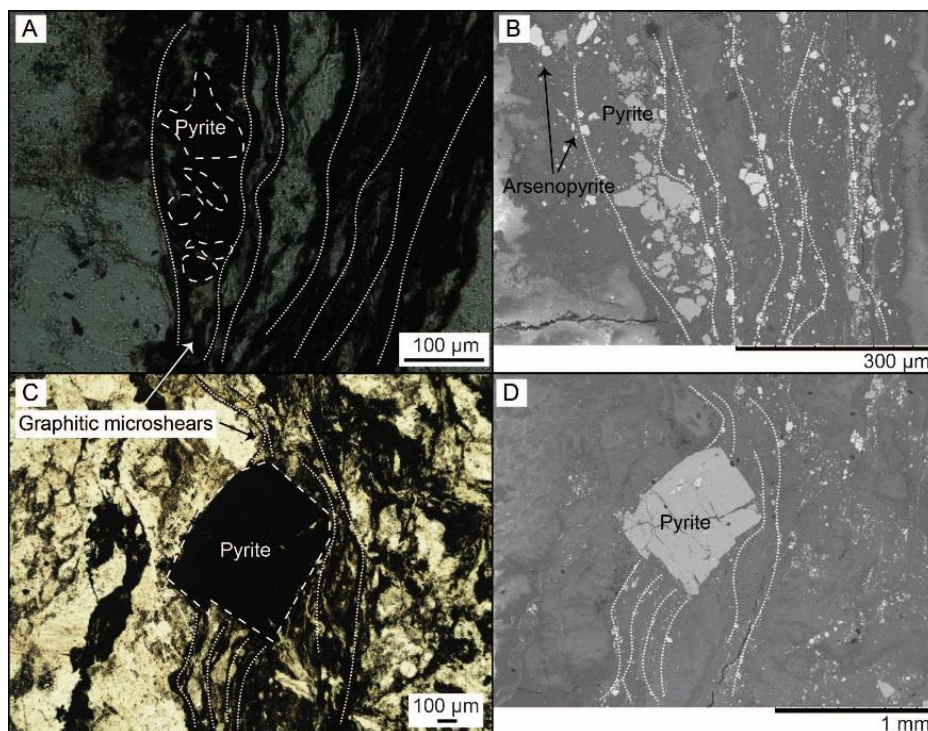


Figure 6.1 Photomicrographs of gold-bearing sulfides from the Macraes deposit in transmitted light (A, C) and BSE (back-scattered electron) imaging (B, D). Pyrite (circled by dashed lines) is surrounded by (A, B) or overprints (C, D) graphitic shears (indicated by dotted lines) which contains fine-grained carbonaceous material (CM) and sulfides, especially arsenopyrite. On the BSE images, pyrite is light grey and arsenopyrite is white.

6.3 Samples and methods

New sulfur (S) and non-carbonate carbon (NCC) data were obtained from mineralized rocks from the Golden Bar pit in the Macraes deposit. Methods were described in (Hu et al., 2016; Hu et al., 2015). Additional S and NCC data for Macraes deposit samples were collected using X-ray fluorescence at the University of Otago, with representative data published in Craw (2002) and Petrie et al. (2005). Extant S and NCC data were obtained from Phanerozoic deposits of the Victorian

goldfield (Australia), the Phanerozoic Touquoy Zone deposit (Meguma Terrane, Canada), and several Paleoproterozoic deposits (West Africa) (Bierlein et al., 2001; Bierlein and Smith, 2003; Křibek et al., 2015, respectively). All the data are included in Appendix B2.

The HCh program coupled with the Unitherm database was used for thermodynamic modeling (Shvarov and Bastrakov, 1999). Bulk compositions used in the modelling were derived from Otago Schist and Golden Bar pit samples (Hu et al., 2015). The chemical components of the systems investigated are Al_2O_3 -CaO-CuO-K₂O-FeO-MgO-Na₂O-SiO₂-ZnO-Au-As-C-CO₂-S-H₂O. The conceptual model was designed to simulate infiltration of ore fluids generated by underlying metasediments into lower G-S facies rocks, which has been proposed to apply to the Macraes deposit and other similar CM-rich gold deposits (Large et al., 2011; Pitcairn et al., 2006).

Production of the ore fluid by equilibration of metamorphic fluids with a sedimentary host rock at depth was simulated in an initial model cell in which an H₂O-rich fluid (fluid 1) was equilibrated with a graphite- and Au-bearing rock at 500°C and 5 kbar. The rock composition was that of a CM-rich sample (FF-13) from the prehnite-pumpellyite facies thought to be typical of the source rocks (Hu et al., 2016). Magnetite and pyrrhotite were set in excess in this initial cell to simulate fluid production under $f\text{O}_2 - f\text{S}_2$ conditions representative of the greenschist-amphibolite transition. Details of fluid 1 and FF-13 rock compositions are provided in Appendix B1.

Subsequent model cells were designed to simulate spatial variation in fluid-rock interaction during ore fluid infiltration into lower G-S metasediments. The composition of these rocks was based on that of a Golden Bar pit sample (GB-01; Appendix B1). In the model, the ore fluid infiltrates a notional cell containing GB-01 at 3 kbar and a specified mineralization temperature (T_{\min}). After equilibration of the ore fluid with the rock in that cell at T_{\min} , the fluid was passed on to the next cell at the same pressure and at T_{\min} , where it was equilibrated and passed on again. The first cell of this model, where the ore fluids are added to the host rock at T_{\min} , simulates the addition of channelized fluid to a host rock with which the fluid is not in thermal or chemical equilibrium. The subsequent cells simulate slower pervasive isothermal and isobaric infiltration of the fluid into the surrounding country rock.

Infiltration was investigated at 160 to 400 °C, to assess the effects of fluid infiltration at different levels in the crust.

The time integrated fluid:rock ratio for each simulation was 1:1 by mass. To assess the effect of different instantaneous fluid:rock ratios, variations from 0.05 to 1 were tested. So, for example, 10 fluid infiltration increments with an instantaneous fluid:rock ratio of 0.1 were compared to 20 fluid infiltration increments with an instantaneous fluid:rock ratio of 0.05. The change in number of increments did not produce any significant change in the results (Appendix B3). Phase separation was not modelled because evidence of phase separation is not observed at Macraes (De Ronde et al., 2000).

The results for 18 cells are presented here because this number was sufficient to reproduce the mineralogical zoning observed in the field. Note that the bulk composition of GB-01 was set such that a small amount of fluid was present within the country rock (fluid:rock = 0.025 by mass) prior to ore fluid infiltration.

Equilibration between the ore fluid and the country rock thus involves mixing between the country rock fluid and the infiltrating fluid, as well as reaction between the infiltrating fluid and the country rock. It was therefore necessary to include this country rock fluid in calculations of species concentration changes during reaction. Changes in species concentrations were calculated for each cell by comparing the concentrations of the species of interest in the unreacted mixture with those in the equilibrated products.

CM abundance is reported as NCC for natural samples and C_{model} for modelled graphite. In reality, CM in natural samples is not pure graphite, but a complex mixture of C-O-H compounds that are difficult to characterize and impossible, currently, to model. Representation of CM by graphite in the model introduces uncertainty, but first order trends are considered robust because features of the natural samples are replicated satisfactorily by the model. Whole rock sulfur concentration is referred to as S for natural samples and S_{model} for modelling results.

6.4 Results

6.4.1 Geochemical analyses

S versus NCC by mass for unmineralized and mineralized samples from four goldfields is shown in Figure 6.2. In unmineralized rocks, the S and NCC contents are generally low, i.e. less than 1 wt%. The data in mineralized rocks show considerable scatter, but the S and NCC contents range to values several times higher than those in unmineralized rocks.

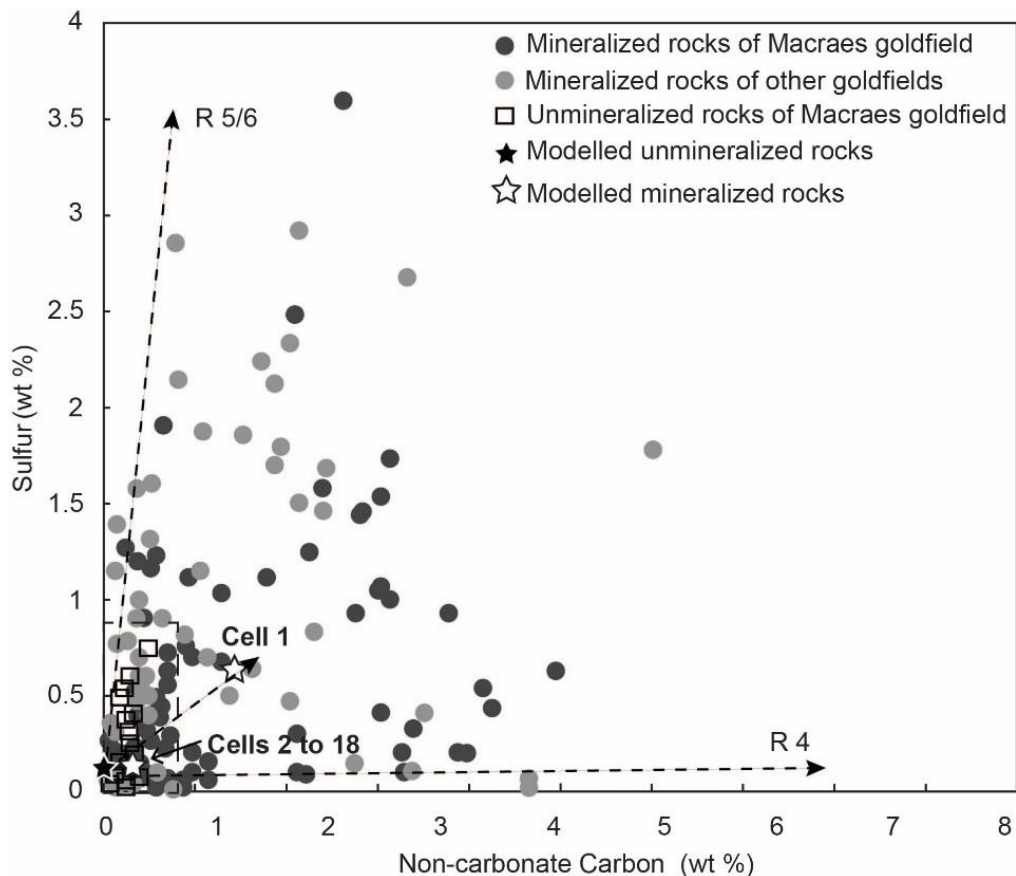


Figure 6.2 S vs. NCC by mass from four goldfields compared to model results. A vector from unmineralized rock to cell 1 in the model results was used to indicate the modelled trajectory in S vs. NCC space. This vector can be decomposed into two reactions: graphite deposition via reaction 4 (R4), and dominant sulfide deposition (R5/6: plotted as weighted average $S_{\text{model}}:C_{\text{model}2}$ mass ratios from reactions 5 and 6).

6.4.2 Thermodynamic modelling

Calculated mineral assemblages of the mineralized rock are consistent with those observed in the field, comprising graphite, quartz, pyrite, arsenopyrite, calcite, siderite, muscovite, epidote, chlorite and albite. Infiltration at different temperatures produced assemblages compatible with known phase stability fields (Appendix B3). The co-existence of pyrite and arsenopyrite occurs at a low temperature, e.g. 280 °C. Typical model results for 220 °C, 3 kbar are shown in Figure 6.3.

Deposition of Au, sulfides and graphite occurs in all cells, but primarily in the first infiltration cell. Pyrrhotite is present in the unaltered model host rock, whereas pyrite is the dominant sulfide throughout the mineralization (Figure 6.3 A). Arsenopyrite occurs in the unaltered model host rock, and modes increase in the outer margins of the pyrite-rich zone (Figure 6.3 B). Au precipitation is accompanied by a decrease in the concentration of Au bisulfide complexes (Figure 6.3 C).

The H₂ concentration in equilibrated model fluids decreases in cell 1 and increases slightly in the following cells, however, the concentration in each cell is always less than that in unreacted mixtures (Figure 6.3 D). This means that H₂, in small amounts, is consumed during the deposition of pyrite.

The concentration of graphite (C_{model}) is the total of graphite present in the unreacted rock plus precipitated graphite (Figure 6.3 E). Precipitated graphite forms the larger proportion of C_{model} , particularly in the first infiltration cell. Infiltrated CO₂ forms carbonates and is also involved in redox reactions, resulting in graphite deposition. Inspection of the mineral modes allows deduction of the amount of CO₂ that is reduced to form graphite (as CO_{2, RE}) via

$$\text{CO}_{2, \text{RE(aq)}} = \text{CO}_{2, \text{total loss(aq)}} - \text{CO}_{2, \text{carbonates(aq)}}. \quad (3)$$

Graphite precipitation is also accompanied by a decrease in the CH₄ concentration in the fluid, with a greater decrease in CO_{2, RE} than in CH₄ (Figure 6.3 E). The decreases in CO_{2, RE} and CH₄ concentrations account for 51–53 % and 47–49 % of precipitated graphite, respectively. Model results at higher and lower temperatures show the same features (Appendix B3).

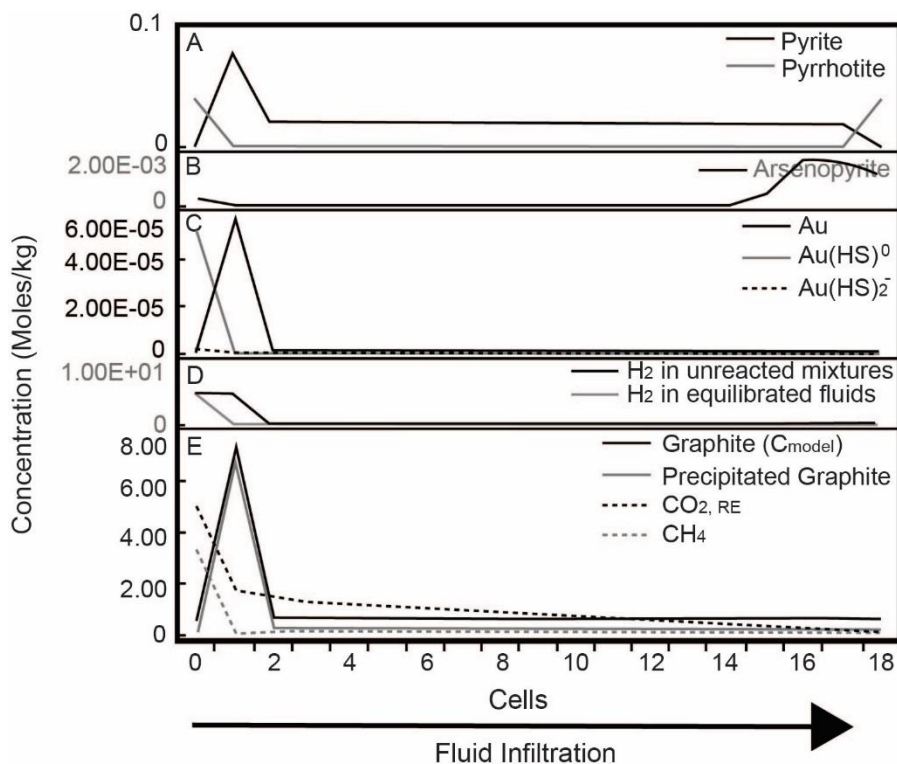


Figure 6.3 Results of fluid infiltration at 220 °C, 3 kbar. In cell 0, the concentration of solid components represents the amount in unreacted GB-01 and that of aqueous components represents the total amount in unreacted country rock fluid or ore fluid. Results of the fluid infiltration are presented in cells 1–18. (A) Pyrite and pyrrhotite; (B) Arsenopyrite; (C) Au and Au bisulfide species; (D) H₂ in equilibrated fluids and unreacted mixtures; € Total graphite (C_{model}), precipitated graphite, CH₄ and CO_{2, RE}.

6.5 Discussion and conclusions

6.5.1 Consistency of rocks with model results

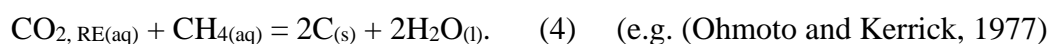
In the natural samples, one of the most obvious geochemical changes during mineralization is the increase in S and NCC contents, which is replicated in the model (Figures 6.1, 6.2). The model simulates infiltration of an ore fluid of constant composition, resulting in the co-deposition of graphite and sulfides consistent with observations of syn-depositional pyrite and graphitic microspheres. However, in natural systems, mineralization is caused by infiltration of multiple fluids with different compositions rather than a monotonous single fluid infiltration event. Thus, later infiltration of S-rich, C-poor fluids is invoked to explain the late pyrite that

overprints graphitic microshears, and increases the S and NCC contents of mineralized rocks. Arsenopyrite distribution is broadly consistent with the model results, with arsenopyrite present peripheral to pyrite (Figure 6.1). However, some arsenopyrite occurs with late pyrite in the core of graphitic microshears, and is attributed, like the late pyrite, to post Au deposition fluid flow.

6.5.2 Precipitation of sulfides

The modelled co-precipitation of Au, sulfides and graphite is consistent with CM-Au relationships, i.e. hypotheses (2), (3) and (4). To distinguish between these three hypotheses, it is necessary to explore links between the electron transfer processes that form pyrite, graphite and Au from aqueous Au^+ in Au bisulfide, C^{4+} in $\text{CO}_{2, \text{RE}}$, C^{4-} in CH_4 , and from S^{2-} in bisulfide and H_2S .

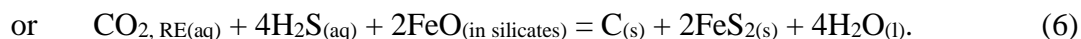
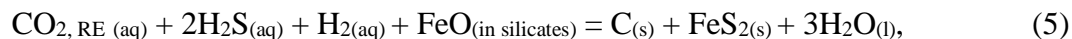
The most obvious change in fluid composition during fluid infiltration is a drop in $\text{CO}_{2, \text{RE}}$ and CH_4 concentrations that coincides with graphite deposition. Transfer of electrons between $\text{CO}_{2, \text{RE}}$ and CH_4 forms water and graphite via reaction (4):



This reaction accounts for 94–98% of precipitated graphite, with >90% of the CO_2 and CH_4 carried into the host rock by the ore fluids. However, the drop in $\text{CO}_{2, \text{RE}}$ concentration is larger than that of CH_4 , indicating that more $\text{CO}_{2, \text{RE}}$ than CH_4 is involved in the fluid:rock reaction. 2–6% of the graphite that formed by $\text{CO}_{2, \text{RE}}$ consumption is not balanced by CH_4 consumption and requires additional electrons. To investigate the electron transfer processes that formed this additional graphite, the precipitated graphite was split into two components: C_{model1} , graphite that can be accounted for by reaction (4), and C_{model2} , extra graphite that cannot be accounted for by reaction (4).

Formation of pyrite from H_2S in solution requires an electron acceptor, because divalent S^{2-} must lose electrons to form monovalent S^- in pyrite. In light of the $\text{CO}_{2, \text{RE}} - \text{CH}_4$ imbalance discussed above, $\text{CO}_{2, \text{RE}}$ is a possible electron acceptor in the modelled system. The $\text{S}_{\text{model}}:\text{C}_{\text{model2}}$ ratio is calculated, because if $\text{CO}_{2, \text{RE}}$ provides the electron acceptor for H_2S -hosted sulfur, then pyrite and C_{model2} should be correlated. The $\text{S}_{\text{model}}:\text{C}_{\text{model2}}$ mass ratio is 6 in cell 1 and 10 in following cells, which

corresponds to molar ratios of 2 and 4, respectively. The electron exchange between $\text{CO}_{2, \text{RE}}$ and H_2S , with intermittent involvement of H_2 , can be written as



A vector from the unmineralized rock to cell 1 is used to represent the increase in S_{model} and C_{model} contents through mineralization (Figure 6.2). This can be decomposed into two sub-vectors: one produces increasing C_{model} contents, driven by graphite deposition from reaction (4). The second produces high $S_{\text{model}}:C_{\text{model}}$ ratios via sulfide deposition (reactions 5, 6).

In natural systems, a combination of reactions such as (4) to (6) acted during time-integrated fluid flow to produce the observed S and NCC concentrations and petrography. Thus, the scattered data could be caused by a continuum between rocks in which reactions such as (5) and (6) dominated sulfide deposition and those in which reactions such as (4) dominated graphite deposition. Fluid infiltration during different periods, along with pre-metamorphic sulfide and CM in the natural rocks, would also increase S and NCC concentrations, so scattered natural data are expected. Meanwhile, the co-existence of pyrite and graphitic microspheres could result from overlap between sulfide-dominant and graphite-dominant deposition during fluid infiltration of different periods. Note that, although the model uses a sediment-derived ore fluid consistent with previous work (Large et al., 2011; Tomkins, 2013) and produces results consistent with observations, alternative sources of fluid, such as magmatic fluids, are not eliminated by the model.

6.5.3 Gold precipitation

The model results suggest that the coexistence of CM and pyrite, often observed in natural samples, may be a consequence of their co-deposition from fluids, with a minor proportion of CM originally in-situ in the host rocks. Deposition of pyrite and CM in the model is accompanied by gold precipitation (Figure 6.3 C). Au in the model is transported by the gold bisulfide complexes $\text{Au}(\text{HS})^0$ and $\text{Au}(\text{HS})_2^-$. Decrease of H_2S in the ore fluid drives destabilization of Au bisulfide complexes and causes gold precipitation (e.g. (Seward, 1973)).

6.5.4 Implications for other gold deposits

To summarize, most CM is proposed to be of hydrothermal origin, and the first order role for CM involves electron transfer in which fluid-borne CO₂ acts as an electron acceptor. This enables pyrite deposition with a consequent decrease in dissolved H₂S concentrations and the destabilization of aqueous gold bisulfide complexes. The results presented here are broadly applicable to many other orogenic gold deposits around the world (references above), although details, such as the spatial relationships and relative modes of arsenopyrite, and the inferred importance of fluid immiscibility, may vary. Some gold deposits such as the Carlin gold deposits in United States and Telfer gold deposits in Australia display a similar close association between gold, CM and sulfides in mineralized rocks (Cline et al., 2005; Goellnicht et al., 1989). The host rocks are carbonate-rich, so decarbonation may provide an additional source of CO₂ (Cline et al., 2005). Processes described herein may imply a similar role for CM for some gold deposition in these deposits, although additional processes may have been involved as well.

6.6 Acknowledgments

All authors acknowledge the CSIRO Flagship Collaboration Fund Cluster for Organic Geochemistry of Mineral Systems led by Curtin University and additional support from WA-Organic and Isotope Geochemistry Centre (WA-OIGC), The Institute of Geoscience Research (TIGeR), Oceanagold Corporation and Ministry of Business, Innovation and Employment, New Zealand. S.H. acknowledges the receipt of Chinese Scholarship Council (CSC)-Curtin International Postgraduate Research Scholarship (CIPRS), CSIRO Top-up Scholarship. Prof. Campbell McCuaig is thanked for helpful discussions.

6.7 References

Berge, J., 2011. Paleoproterozoic, turbidite-hosted, gold deposits of the Ashanti gold belt (Ghana, West Africa): Comparative analysis of turbidite-hosted gold deposits and an updated genetic model. *Ore Geology Reviews* 39, 91-100.

- Bierlein, F.P., Cartwright, I., McKnight, S., 2001. The role of carbonaceous "indicator" slates in the genesis of lode gold mineralization in the Western Lachlan Orogen, Victoria, Southeastern Australia. *Economic Geology* 96, 431-451.
- Bierlein, F.P., Smith, P.K., 2003. The Touquoy Zone deposit: an example of "unusual" orogenic gold mineralisation in the Meguma Terrane, Nova Scotia, Canada. *Canadian Journal of Earth Sciences* 40, 447-466.
- Cline, J.S., Hofstra, A.H., Muntean, J.L., Tosdal, R.M., Hickey, K.A., 2005. Carlin-type gold deposits in Nevada: critical geologic characteristics and viable models. *Economic Geology 100th Anniversary Volume* 100, 451-484.
- Cox, S., Sun, S., Etheridge, M., Wall, V., Potter, T., 1995. Structural and geochemical controls on the development of turbidite-hosted gold quartz vein deposits, Wattle Gully mine, central Victoria, Australia. *Economic Geology* 90, 1722-1746.
- Craw, D., 2002. Geochemistry of late metamorphic hydrothermal alteration and graphitisation of host rock, Macraes gold mine, Otago Schist, New Zealand. *Chemical Geology* 191, 257-275.
- De Ronde, C.E., Faure, K., Bray, C.J., Whitford, D.J., 2000. Round Hill shear zone-hosted gold deposit, Macraes Flat, Otago, New Zealand: Evidence of a magmatic ore fluid. *Economic Geology* 95, 1025-1048.
- Goellnicht, N., Groves, D., McNaughton, N., Dimo, G., 1989. An epigenetic origin for the Telfer gold deposit. Western Australia: *Economic Geology Monograph* 6, 151-167.
- Goldfarb, R.J., Groves, D.I., 2015. Orogenic gold: Common or evolving fluid and metal sources through time. *Lithos* 233, 2-26.
- Henne, A., Craw, D., 2012. Synmetamorphic carbon mobility and graphite enrichment in metaturbidites as a precursor to orogenic gold mineralisation, Otago Schist, New Zealand. *Mineralium Deposita*, 1-17.
- Hu, S.-Y., Evans, K., Fisher, L., Rempel, K., Craw, D., Evans, N.J., Cumberland, S., Robert, A., Grice, K., 2016. Associations between sulfides, carbonaceous

- material, gold and other trace elements in polyframboids: Implications for the source of orogenic gold deposits, Otago Schist, New Zealand. *Geochimica et Cosmochimica Acta* 180, 197-213.
- Hu, S., Evans, K., Craw, D., Rempel, K., Bourdet, J., Dick, J., Grice, K., 2015. Raman characterization of carbonaceous material in the Macraes orogenic gold deposit and metasedimentary host rocks, New Zealand. *Ore Geology Reviews* 70, 80-95.
- Křibek, B., Sýkorová, I., Machovič, V., Knésl, I., Laufek, F., Zachariáš, J., 2015. The origin and hydrothermal mobilization of carbonaceous matter associated with Paleoproterozoic orogenic-type gold deposits of West Africa. *Precambrian Research* 270, 300-317.
- Large, R.R., Bull, S.W., Maslennikov, V.V., 2011. A carbonaceous sedimentary source-rock model for Carlin-type and orogenic gold deposits. *Economic Geology* 106, 331-358.
- MacKenzie, D., Craw, D., Cooley, M., Fleming, A., 2010. Lithogeochemical localisation of disseminated gold in the White River area, Yukon, Canada. *Mineralium Deposita* 45, 683-705.
- Ohmoto, H., Kerrick, D., 1977. Devolatilization equilibria in graphitic systems. *American Journal of Science* 277, 1013-1044.
- Petrie, B., Craw, D., Ryan, C., 2005. Geological controls on refractory ore in an orogenic gold deposit, Macraes mine, New Zealand. *Mineralium Deposita* 40, 45-58.
- Pitcairn, I.K., Roberts, S., Teagle, D.A., Craw, D., 2005. Detecting hydrothermal graphite deposition during metamorphism and gold mineralization. *Journal of the Geological Society* 162, 429-432.
- Pitcairn, I.K., Teagle, D.A., Craw, D., Olivo, G.R., Kerrich, R., Brewer, T.S., 2006. Sources of metals and fluids in orogenic gold deposits: Insights from the Otago and Alpine Schists, New Zealand. *Economic Geology* 101, 1525-1546.
- Seward, T.M., 1973. Thio complexes of gold and the transport of gold in hydrothermal ore solutions. *Geochimica et Cosmochimica Acta* 37, 379-399.

- Shvarov, Y.V., Bastrakov, E., 1999. HCh: a software package for geochemical equilibrium modelling. User's guide. Australian Geological Survey Organisation. Science and Resources, Record 25, 61.
- Thomas, H.V., Large, R.R., Bull, S.W., Maslennikov, V., Berry, R.F., Fraser, R., Froud, S., Moye, R., 2011. Pyrite and pyrrhotite textures and composition in sediments, laminated quartz veins, and reefs at Bendigo gold mine, Australia: insights for ore genesis. *Economic Geology* 106, 1-31.
- Tomkins, A.G., 2010. Windows of metamorphic sulfur liberation in the crust: implications for gold deposit genesis. *Geochimica et Cosmochimica Acta* 74, 3246-3259.
- Tomkins, A.G., 2013. On the source of orogenic gold. *Geology* 41, 1255-1256.
- Upton, P., Craw, D., 2008. Modelling the role of graphite in development of a mineralised mid-crustal shear zone, Macraes mine, New Zealand. *Earth and Planetary Science Letters* 266, 245-255.

Chapter 7

Experimental investigations of gold solubility in pure organic liquids

This chapter describes laboratory work investigating gold solubility in organic liquids, which includes experiments on gold solubility in pure organic liquids, organic component characterization, and analytical method development to quantify gold concentrations in organic liquids following experiments. It is the first time that gold solubility experiments have been carried out in pure organic liquids, as the majority of previous work has focussed on aqueous solutions, with a single study on Au in crude oil (Williams-Jones and Migdisov, 2007). Development of a precise, quick, and inexpensive method to quantify gold concentrations in organic liquids is a time-consuming and painstaking process, but this chapter presents a workable method that may be used by future researchers. Preliminary results have shown that a significant amount of gold can be dissolved in dodecanethiol, indicating that this organic liquid may be capable of transporting gold in ore-forming systems.

7.1 Introduction

Gold has very low average concentrations (2.5 ppb) in Earth's crust (Wedepohl, 1995) and therefore economic deposits require processes that are very efficient at extracting, transporting and depositing the metal. It is commonly known that gold can be transported by aqueous crustal fluids and concentrated as ores at specific environmental conditions during the formation of gold deposits (Bateman and Hagemann, 2004; Evans et al., 2006; Tomkins, 2013). To understand the mechanisms of mobilization, transportation and deposition of gold during ore-forming processes, investigations of the solubility and stability of gold in hydrothermal solutions have been conducted for decades (Gammons and Barnes, 1989; Gammons and Williams-Tones, 1995; Henley, 1973; Renders and Seward, 1989; Seward, 1973; Shenberger and Barnes, 1989; Stefánsson and Seward, 2003;

Stefánsson and Seward, 2004). From experiments on gold solubility in aqueous solutions, gold is known to form complexes with hydrosulfide ligands (Baranova and Zotov, 1998; Benning and Seward, 1996; Gibert et al., 1998; Hayashi and Ohmoto, 1991; Loucks and Mavrogenes, 1999; Pan and Wood, 1994; Renders and Seward, 1989; Seward, 1973; Shenberger and Barnes, 1989; Stefánsson and Seward, 2004; Zotov et al., 1991) and chloride ligands (Frank et al., 2002; Gammons and Williams-Tones, 1995; Henley, 1973; Stefánsson and Seward, 2003; Wood et al., 1987; Zotov et al., 1991). The $\text{Au}_2(\text{HS})_2\text{S}^{2-}$ ligand predominates in alkaline solutions whereas $\text{Au}(\text{HS})_2^-$ dominates in neutral pH solutions (Seward, 1973; Stefánsson and Seward, 2004). $\text{Au}(\text{HS})^0$ occurs in acidic solutions (Stefánsson and Seward, 2004). AuCl_2^- is an important chloride ligand responsible for gold transportation (Stefánsson and Seward, 2003; Zotov et al., 1991), however gold chloride is less stable than Au bisulfides in most situations relevant to hydrothermal ore deposition formation (Hayashi and Ohmoto, 1991). Ore deposits may also form at pressure-temperature conditions in which water vapour is present, and aqueous fluids in the vapour state can also transport metals. Gas mixtures such as $\text{HCl-H}_2\text{O}$ and $\text{H}_2\text{S-H}_2\text{O}$ have been proposed to dissolve ppb levels of gold (Archibald et al., 2001; Zevin et al., 2007, 2011). The vapour-transport model has been applied to model gold ore-forming processes related to vapour-bearing magmatic hydrothermal systems (Williams-Jones et al., 2009; Zevin et al., 2007).

In addition to aqueous liquids and vapours, organic species have been found to transport gold in natural environments (Baker, 1978; Emsbo and Koenig, 2007; Freise, 1931; Lungwitz, 1900; Ong et al., 1970; Radtke and Scheiner, 1970; Zhuang et al., 1999). This process was first proposed by Lungwitz (1900), who found that gold was transported by some unknown vegetable-decomposition product in tropical streams. In alluvial gold deposits, humic acid plays an active role in the transportation of gold by binding Au as a humic acid-stabilized colloid (Baker, 1978; Freise, 1931; Ong et al., 1970; Seeley and Senden, 1994). In hydrothermal gold deposits, Radtke and Scheiner (1970) found that fine-grained amorphous carbon is capable of adsorbing gold chloride or gold cyanide complexes from solution. Pyrobitumen in the Lannigou gold deposit (Carlin-type) in Guizhou, China, was thought to be the carrier of gold during the mobilization of gold before precipitation (Zhuang et al., 1999). In the Carlin-type deposits of Nevada, up to 100 ppm Au has

been detected in bitumen, implying that gold may be mobilized by organic fluids (Emsbo and Koenig, 2007). Almost no data on gold solubility in organic liquids is available, with the exception of an investigation of the solubility of gold in crude oil by Williams-Jones and Migdisov (2007). That study measured ppb levels of gold dissolved in crude oil, indicating that liquid hydrocarbons may be capable of transporting gold. However, the composition of crude oil is complex and the actual gold speciation and gold complexing ligand in the oil is unknown. Thus, the investigation of gold solubility in organic liquids, which is of great significance to understand gold transportation mechanisms, is still poorly understood.

The lack of experimental investigations of gold solubility in organic liquids may be attributed to the complexity of crude oil and the techniques available for quantifying dissolved gold in organic liquids. Conventional methods for analysis of the concentration of trace elements, including Au, in aqueous solutions include instrumental neutron activation analysis (INAA) (Archibald et al., 2001; Zezin et al., 2007) or inductively coupled plasma mass spectrometry (ICP-MS), in which the solutions are introduced directly (Benning and Seward, 1996). However, direct injection of organic liquids into the ICP-MS will cause overloading of the plasma, and graphitization of organics on the cones or the torch of the ICP spectrometer (Ortega et al., 2013). With the development of techniques such as micro-nebulized spray chambers, automated systems have been used in ICP-MS for the analysis of organic liquids (BOTTO, 2002). PremiSolv™ ICP solvent (Conostan, USA) is a good dilutant for ICP analysis of trace elements in oil and other organic fluids, and has been widely applied to dilute oil samples before direct injection into ICP-MS in recent years, e.g., Pulles et al. (2012) and Butler et al. (2014). Alternatively, INAA has been applied to determine the concentration of Au in organic liquids (Williams-Jones and Migdisov, 2007), however, due to the high cost and limited accessibility in Australia, INAA was not the best choice in this study. Dry ashing and chemical digestion of organic liquids are other traditional methods to determine the concentrations of trace elements in organic liquids (Ortega et al., 2013), which cost less and can be done in a standard wet chemistry lab, as compared to the other techniques referred to above. Dry ashing is a common method and can be applied to large numbers of samples, but it is time-consuming and difficult to ensure that no Au volatilises during the ashing process. Chemical decomposition with strong acids has

been used recently as a sample pre-treatment method for trace element analysis, and has been successfully applied to elements such as V, Ni, As and Mn (Ortega et al., 2013).

While the analytical techniques for trace elements outlined above are required to determine whether gold is transported in an organic liquid, characterization of the organics following experiments is also important in determining which organic component is responsible for complexing gold. Gas chromatography (GC), which is used to separate mixtures into components of different molecular weights, coupled with a flame ionization detector (FID) or mass spectrometry (MS) detector, is commonly employed for the analysis of organic compounds (Simoneit and Gize, 2000; Wang et al., 1994). GC-FID is particularly sensitive to hydrocarbons, but not to water, sulfur or nitrogen. GC coupled with a flame photometer detector (FPD) has been developed for sulfur-containing compounds (Buffington and Wilson, 1987). Thus, these techniques are useful for organic characterization in this study. In this study, we have performed experimental investigations of the solubility of gold in two pure organic liquids at 150 °C. They are dodecanethiol and dibenzothiophene (DBT), because they are common component in crude oil and the thiol in these components can provide sulfur which is capable of complexing Au in aqueous solutions (Hopkins and Smith, 1954; Hughes et al., 1995; Seward, 1973). We also explored the suitability of various analytical methods for quantifying gold concentrations in organic liquids, such as direct injection into ICP-MS and indirect injection into ICP-MS with pre-treatment of dry ashing and chemical digestion to quantify the gold concentration in organic liquids. Finally, we applied GC-FID/FPD/MS to characterize the organics after the solubility experiments.

7.2 Experiments of gold solubility in organic liquids

7.2.1 Apparatus

Solubility experiments in previous studies, particularly those in aqueous solution, have commonly been conducted in titanium autoclaves (Archibald et al., 2001; Miedaner et al., 2005) or gold-lined steel vessels (Wood et al., 1987), which are suitable for the higher temperatures of interest relevant to water-dominated

hydrothermal ore systems. As organic liquids are more common to lower-temperature ore systems, and indeed decompose to form bitumen and graphite at elevated temperatures, low-temperature apparatus was more suitable for this study (Williams-Jones and Migdisov, 2007). These experiments were designed to be conducted in 45 mL polytetrafluoroethylene (PTFE)-lined stainless steel vessels (Figure 7.1). This apparatus can resist temperatures up to 250 °C and pressures up to 124 bar. Further chemical digestion of organic liquids after experiments can be performed in the same apparatus, which reduces potential loss of trace metals and other experimental error.

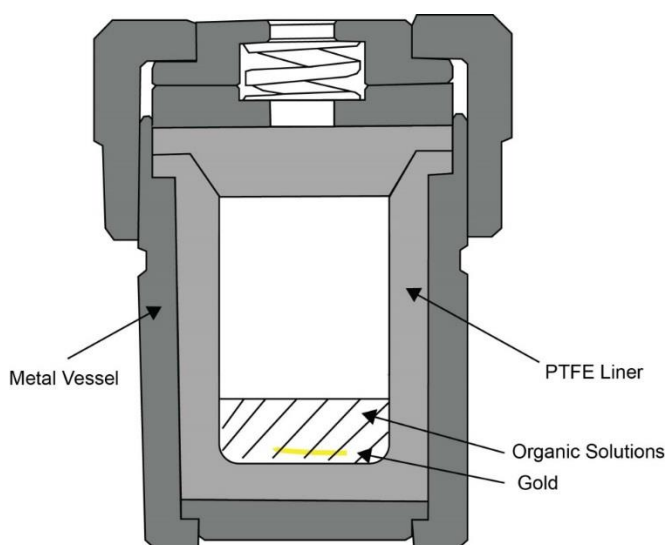


Figure 7.1 Autoclave used in the experiments (not to scale), with 0.5 mL or 0.5 g organics and 0.01 g gold wire.

7.2.2 Experiment design

Alkane thiols (e.g., dodecanethiol, 99%) and dibenzothiophene (DBT, 99%), which are common in petroleum systems, were chosen as target organic liquids and were provided by Sigma-Aldrich and Alfa Aesar. Autoclaves were pre-tested with pure water to ensure that they sealed correctly and no leakage would occur during experiments. All equipment was cleaned with acetone to remove potential organic contamination, then with 10% nitric acid and ultra-pure water (Milli-Q water) to remove any trace metals present before each experiment. A series of experiments designed to explore the kinetics of gold dissolution in the chosen organic liquids was conducted with 0.01 g gold wire and 0.5 g dodecanethiol/ DBT in the PTFE-lined

autoclaves (Figure 7.1). These experiments are referred to below as the “kinetic series”. Experiments were performed in a furnace at temperatures up to 150 °C and pressures determined by the liquid-vapour pressure of the liquid. Seven autoclaves were placed in the furnace at the beginning of the experiment, and one autoclave was quenched to room temperature by immersing the autoclave in cold water every five days. An extra blank was prepared with the same amount of organic liquids as for the Au-bearing experiments but without the Au wire. This experiment was taken out of the furnace along with the last autoclave. All autoclaves were opened at the same time at room temperature. The gold wires were removed with clean forceps and rinsed with acetone. The rinsing solutions were then returned to the autoclaves, where the organic mixtures were further processed with the aim of chemical oxidation of the organic liquids to facilitate analysis (described below). The kinetics series on dodecanethiol were performed as part of the method development. Both dodecanethiol and DBT were tested for stability of the organic compounds during extended periods at elevated temperature. A single kinetics series was performed on dodecanethiol to gain preliminary information on Au solubility in this compound.

7.3 Analytical method development

A number of different methods to obtain Au concentrations in the product organic liquids were tried.

7.3.1 Direct injection into ICP-MS

Direct injection into ICP-MS was tested with a pure dodecanethiol kinetic series. Solutions were diluted 10 x with PremiSolve™ ICP solvent and directly injected into ICP-MS. However, carbonaceous material produced from graphitization of organics was found to precipitate on the cones, clogging and contaminating the instrument, so no further analyses were performed. The dodecanethiol matrix proved not to dissolve completely in the PremiSolve™ ICP solvent, and direct injection into the ICP-MS could not be used for our samples, thus other techniques were pursued.

7.3.2 Dry ashing

This method was tested with Au sulfur-free metallo-organic standards (1000 ppm Au, purchased from VHG, Canada). 0.5 g of standard, weighed with an electronic balance to ± 0.001 , were placed in three cleaned silicate tubes. Silica wool was used to plug the opening of tubes and reduce the escape of volatile elements. The tubes were placed in the furnace, heated to 200 °C for the first 20 minutes to eliminate any potential build-up of combustible gases, then heated to 800 °C for 1–2 hours to volatilize all organic matter. After ashing, only gold and residual ash was left in the tubes. The tubes were then filled with pure aqua regia (ultra-pure HCl: ultra-pure HNO₃ = 3:1 by volume) for 12 hours, ensuring that the silica wool was immersed, in order to dissolve the gold. Aqua regia solutions were then analyzed with ICP-MS by LabWest (Perth). The precision estimate of the analysis is $\pm 1\%$ relative error, and detection limit is 0.05 ug/L. However, the recovery of gold for this method was only around 60~65%.

To test the hypothesis that gold may have escaped along with volatilized carbonaceous materials during the ashing process, additional experiments were performed to collect the volatilized carbonaceous material. 0.3 g of Au standard was placed in an open ceramic crucible overlain by a surgical-grade stainless steel razor blade to act as a substrate for volatilized material, then heated to 350°C. After carbonaceous materials were collected, the razor blade was observed using low-vacuum scanning electron microscopy (SEM) on a Hitachi Tabletop Scanning Electron Microscope TM3030. The results are shown in Figure 7.2. Fined grained carbonaceous material is present as dark area on the blade (Figure 7.2A). Gold particles, observed as bright spots in the image, are spatially distributed within the carbonaceous material on the blade (Figure 7.2B). The sizes of gold particles are up to 10 μm . The coexistence of gold and carbonaceous material suggests that gold has been transferred by volatilized carbonaceous material from the standard to the blade; in other words, organic gases are capable of transporting gold. Therefore, dry ashing is not the best option to determine the concentration of gold in organic liquids.

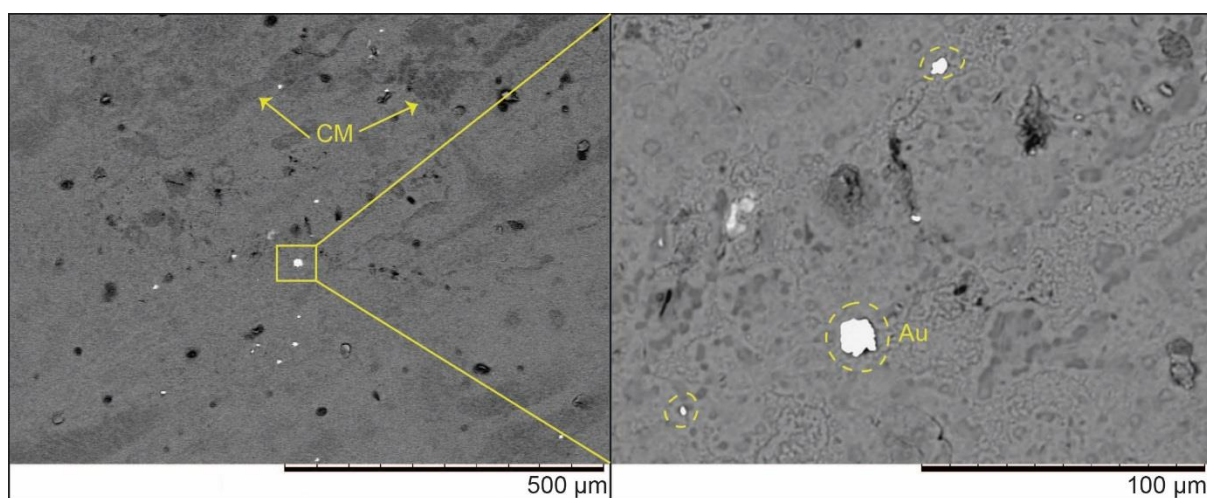


Figure 7.2 The presence of gold (bright spots) within carbonaceous material (CM, as dark areas) on the razor blade.

7.3.3 Chemical digestion

Chemical digestion with Au standard

This method, based on that of Ortega et al. (2013), was tested with an Au sulfur-free metallo-organic standard (1000 ppm Au, VHG, Canada) in the PTFE-lined steel vessels described above. The digestion procedure was as follows:

(1) 0.5 g aliquots of standard were weighed and transferred into five PTFE-lined vessels. 12 mL ultra-pure HNO₃ and 4 mL ultra-pure H₂O₂ were added to each vessel using clean pipettes. Vessels were sealed, placed in a furnace at 200 °C for 24 hours, then naturally cooled to room temperature and opened. Solutions, which were colourless and homogenous, were collected in plastic vials, diluted with ultra-pure water and labelled as *Solution 1*.

(2) 24 mL of freshly-prepared aqua regia was used to rinse each PTFE liner ten times to collect any remaining gold precipitated on the liner walls. Aqua regia was allowed to soak in the liners for several minutes between each rinse. The rinse solutions (*Solution 2*), were collected in new plastic vials and diluted with ultra-pure water.

(3) An additional 12 mL of fresh aqua regia was added to the vessels, which were returned to the furnace for another 24 hours at 100 °C to collect possible gold precipitated on the caps of liners. Vessels were cooled to room temperature and *Solution 3* was transferred into new plastic vials and diluted.

(4) All solutions were analysed with ICP-MS at LabWest, Western Australia.

This method was tried several times with combinations of steps (1) and (2) or steps (1) and (3). The gold recovery was low, at around 65–75% of the standard concentration. A complete set of steps (1) to (3) was then performed, which resulted in more thorough leaching of gold from the liners, but recovery was still less than 80%. It was later discovered that the Au sulfur-free metallo-organic standard had destabilized, precipitating gold particles, which accounted for the low recoveries.

Instability of Au sulfur-free metallo-organic standard

About three months after purchase of the standard, gold particles were observed floating in the standard and precipitated on the bottom of the container. When an aliquot of standard was transferred into a beaker and shaken, gold was observed precipitating from the liquid, thus the solution was not homogeneous. Another aliquot of standard was analysed by LabWest via an ashing method. 1 mL of the standard was added to 1 g silica flour in a porcelain crucible, then slowly heated to 450 °C in a furnace and ashed for 2 hours. The residue was then dissolved in aqua regia, made to volume, diluted and analysed by ICP-MS. The Au concentration in the ashing result is 700 ppm, as compared to the 1000 ppm as labelled on the standard.

Hence, the organic-Au standard, which is critical for assessing the error in the experimental method, seems to be problematic and results in low gold recovery for the methods attempted. The standard producer (VHG) has reformulated a new standard which overcomes the issues experienced.

Chemical digestion with multiple elements in oil standard

The chemical digestion method described above was tested again with an oil standard containing 12 elements (100 ppm, CONOSTAN, Canada), but omitting Au. The procedure followed the tests that used the Au metallo-organic standard. Results from LabWest showed that the recovery of certain elements, including Cu, Ni, Pb and Ti, was near 100% (Table 7.1). As Cu and Au have similar chemical speciation behaviour, this result suggests that this method can be applied to quantify Au concentration in organic liquids after experiments.

Table 7.1 Results of chemical digestion with multiple elements in oil standard from a single analysis.

Elements	Measured concentrations after chemical digestion (ppm)	Expected concentration (ppm)	Recovery (%)
Al	9.67	9.51	101.68
Cu	11.04	9.51	116.08
Ni	12.17	9.51	127.97
Pb	9.02	9.51	94.84
Ti	9.84	9.51	103.47

7.4 Analysis in organic liquids post-experiment

7.4.1 Au concentration quantification

Au contents were quantified by ICP-MS in LabWest in aqueous solutions after chemical digestions of organic liquids.

Chemical digestion

A kinetic series was performed using dodecanethiol as the organic liquid. On opening the autoclaves, it could be seen that the organic liquid has changed progressively towards a solid state with increasing heating time (Figure 7.3). During heating process, the colour of the organics changed from light yellow to dark brown.

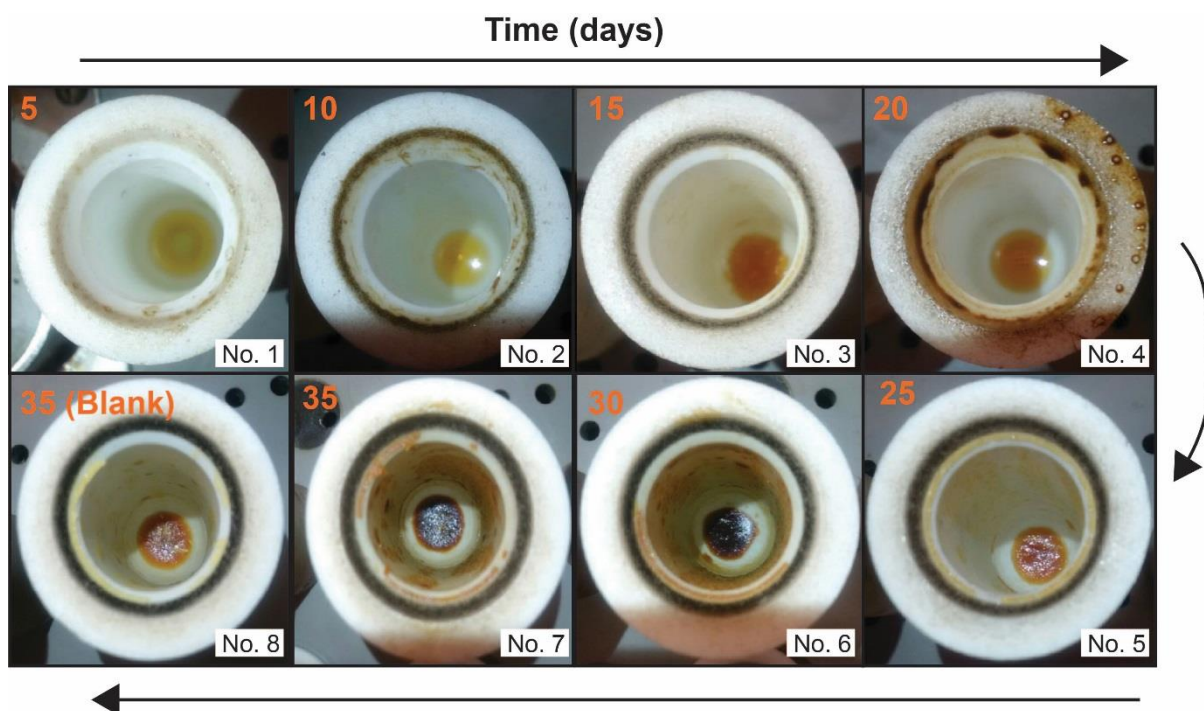


Figure 7.3 Photographs of the experimental products of the kinetic series, showing the change in colour and viscosity of the organic products with time.

Organic liquids were digested with 12 ml HNO_3 and 4 ml H_2O_2 , following the digestion procedure of the metallo-organic Au standard. 4 ml aliquots of H_2O_2 were first added into each liner, with no visible reaction. When 12 ml aliquots of HNO_3 were then added into the No. 1 and 2 liners, immediate and unexpectedly vigorous digestion resulted. Rapid expulsion of gas led to foaming of the solutions, which partly overflowed from the liners. For the remaining liners, the 12 mL of HNO_3 was added slowly, in aliquots of 3 mL at one-hour intervals. Some foaming inevitably occurred, but the overflow was greatly reduced. Subsequent digestions continued following the described methods, but with gradual addition of the HNO_3 .

ICP-MS analysis

Aqueous solutions as productions of chemical digestion of organic liquids post-experiment were injected into ICP-MS to quantify Au concentrations in LabWest. The analysis was performed with a Perkin Elmer Nexion 300 ICP-MS through a

pneumatic nebulizer and a chilled cyclonic spray chamber. The nebulizer gas flow rates are 0.9 L/min. The detection limit for Au concentration is 0.05 $\mu\text{g/L}$.

7.4.2 Organic component characterization

Organic liquids were checked by GC-FPD and GC-FID initially, and then characterized by GC-MS at ChemCentre, Perth.

GC-FPD

Organics were analysed with GC-FPD using an Agilent 6890 gas chromatograph coupled to a Flame Photometric Detector. Organics were directly injected into a split-splitless injector in pulsed split mode (2 μL injection, 4:1 split). A HP-1 column (Agilent Technologies, 30 m length, 0.25 mm i.d., 0.25 μm film thickness) was used with H_2 as the carrier gas (2.0 mL/min). The GC oven temperature was held at 35°C for 3 minutes, then increased to 320°C at 15°C min^{-1} then held for 7 minutes.

GC-FID

Organics were analysed with GC-FID using an Agilent 6890 gas chromatograph coupled to a Flame Ionisation Detector. The instrument conditions are the same to that of GC-FPD.

GC-MS

Solutions were analysed with GC-MS using an Agilent 6890 gas chromatograph coupled to an Agilent 5975 mass selective detector. Samples were directly injected into a split-splitless injector in pulsed splitless mode. A HP5-MS column (Agilent Technologies, 30 m length, 0.25 mm i.d., 0.25 μm film thickness) was used with He as the carrier gas. The GC oven temperature was held at 35°C for 5 minutes, then increased to 320°C at 15°C min^{-1} then held for 7 minutes. Data were acquired in full scan mode (m/z 39–450).

7.5 Results

7.5.1 Experiment with dodecanethiol

Concentrations of dissolved gold in dodecanethiol

The concentration of dissolved Au in dodecanethiol ranges from 0.008 ppm to 0.25 ppm (Table 7.2). Sample No.8 is a blank (no Au added) for comparison. Dissolved Au in sample No. 1 (5 days) is the lowest, with a concentration similar to that of No. 8. There should be no Au in the blank (No. 8). The small amount of Au in the blank suggests that a thoroughly clean of those liners is needed, and that few Au was dissolved in the first five days. The highest Au concentrations are 0.25 ppm and 0.23 ppm in samples No. 4 (25 days) and No. 7 (35 days) respectively. However, Au content in sample No. 6 is lower than that in No. 5 and No. 7. Au may have been lost during the chemical digestion process when the forming of solutions overflowed from the liner. The concentration of dissolved Au in dodecanethiol was plotted against time (days) on a logarithmic scale (Figure 7.4). In general, the concentration of Au increases over time, and appears to have reached a potential equilibrium or steady state after about 25 days. However, owing to potential gold loss during the digestion when the solution foamed and overflowed, these results represent minimum solubilities and equilibrium may have been attained earlier.

Table 7.2 The concentrations of Au in solutions of each step and the contents of dissolved Au in dodecanethiol.

Sample Number	Time (days)	Dodec (g)	Solution 1 (mL)	Conc (ug/L)	Solution 2 (mL)	Conc (ug/L)	Dissolved Au (ug)	Conc dissolved Au in dodec (ppm)
1	5	0.53	30	0.09	37.5	0.05	0.0046	0.0087
2	10	0.50	30	2.05	41	0.64	0.0877	0.1752
3	15	0.53	29.5	0.99	37	0.15	0.0348	0.065
4	20	0.53	30	0.68	37	0.13	0.0252	0.0475
5	25	0.49	30	3.89	44.5	0.22	0.1265	0.2556
6	30	0.51	30	0.8	36.5	1.1	0.0641	0.1260
7	35	0.52	29.5	2.52	38.5	1.28	0.1236	0.2373
8	35	0.52	30	0.09	41	0.1	0.0068	0.0130
(BLANK)								
<i>Notes</i> Dodec: dodecanethiol; Conc: concentration								

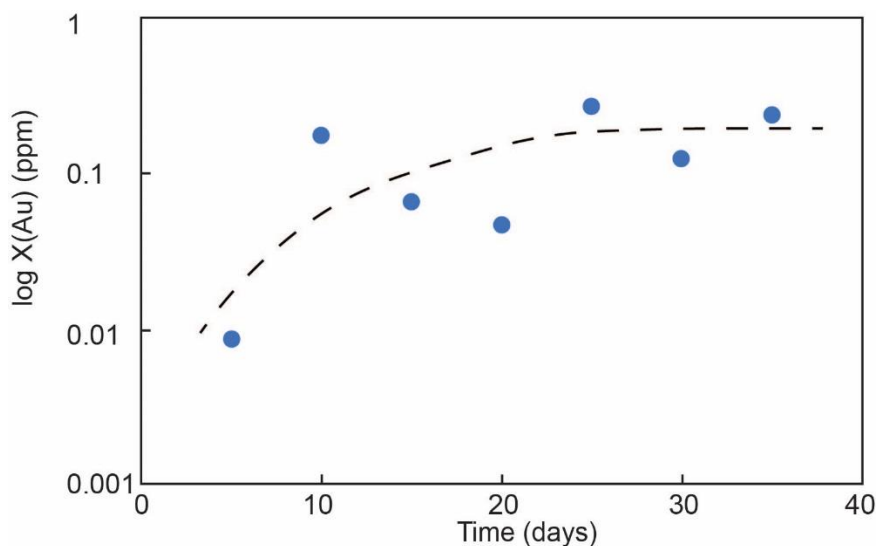


Figure 7.4 The contents of dissolved Au in dodecanethiol vs. time (days) at 200°C.

Organic component characterization

Figure 7.5 shows the spectra of chemical components in dodecanethiol before and after a kinetic experiment with dodecanethiol. Peak areas indicate the relative proportion of organic compounds. The dominant composition of ‘pure’ dodecanethiol that has not undergone heating (Figure 7.5, Table 7.3), is 1-dodecanethiol with minor dodecane, 1,1'-thiobis-dodecane and didodecyl disulfide. After the experiments (Figure 7.5, Table 7.2), the compositions were similar, but the relative proportions of 1,1'-thiobis-dodecane and didodecyl disulfide had increased.

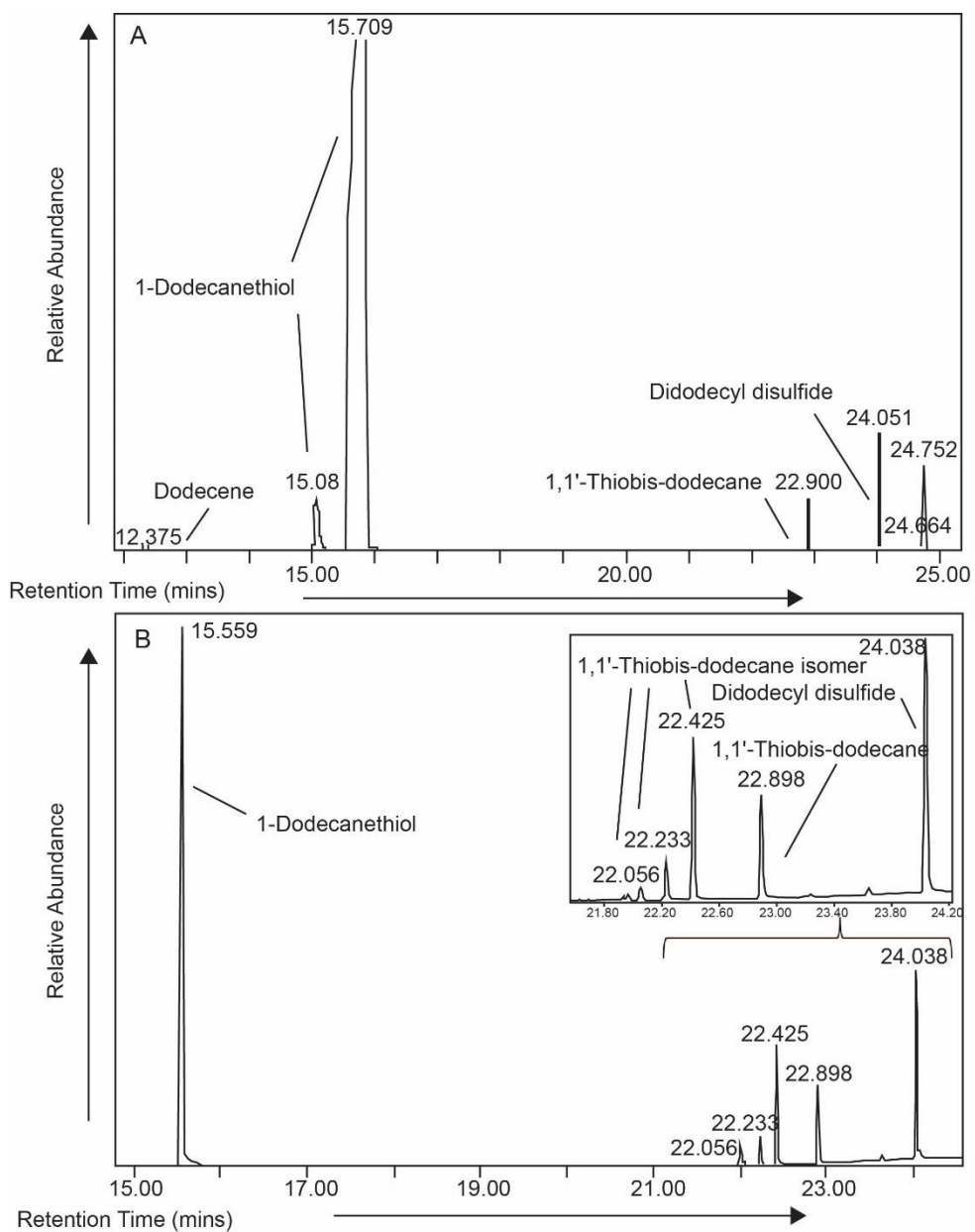


Figure 7.5 The GC-MS spectra of organic compounds in organic liquids pre-experiment (A) and post-experiment (B) for dodecanethiol.

Table 7.3 The chemical components in organic liquids pre- and post-experiment for dodecanethiol.

14B0044/003 - Pure Dodecanethiol		
Peak Retention Time (mins)	Peak Area	Tentative compound ID
12.291	2.59E+06 (0.05%)	1-Dodecene
12.375	2.35E+06 (0.04%)	Dodecane
15.039	6.34E+07 (1.21%)	1-Dodecanethiol
15.081	8.96E+07 (1.71%)	1-Dodecanethiol
15.709	4.82E+09 (92.01%)	1-Dodecanethiol
22.9	4.18E+07 (0.08%)	1,1'-Thiobis-dodecane
24.051	1.08E+08 (2.05%)	Didodecyl disulfide
24.664	1.18E+07 (0.23%)	unknown compound
24.752	1.00E+08 (1.91%)	unknown compound
14B0044/004 - Dodecanethiol + Au		
Peak Retention Time (mins)	Peak Area	Tentative compound ID
15.559	9.60E+07 (56.90%)	1-Dodecanethiol
21.937	4.43E+05 (0.26%)	1,1'-Thiobis-dodecane isomer * (extra ion fragments m/z=285, 299)
21.972	8.04E+05 (0.48%)	1,1'-Thiobis-dodecane isomer * (extra ion fragments m/z=271, 313)
22.056	1.68E+06 (1.00%)	1,1'-Thiobis-dodecane isomer * (extra ion fragments m/z=257, 327)
22.233	4.69E+06 (2.78%)	1,1'-Thiobis-dodecane isomer * (extra ion fragments m/z=243, 341)
22.425	1.93E+07 (11.42%)	1,1'-Thiobis-dodecane isomer * (extra ion fragments m/z=229)
22.898	1.24E+07 (7.38%)	1,1'-Thiobis-dodecane
24.038	3.34E+07 (19.78%)	Didodecyl disulfide

7.5.2 Experiment with DBT (organic component characterization)

Figure 7.6 and Table 7.4 show the organic compounds in pre-experiment and post-experiment dibenzothiophene (DBT). The dominant composition of 'pure' DBT (99%) that has not undergone heating is DBT with minor toluene and biphenyl. In the liquids after the experiments, the composition has changed significantly. The majority of the organic liquid is DBT without toluene but with 4-hydroxy-4-methyl-2-pentanone, and also dodecanethiol and its by-products.

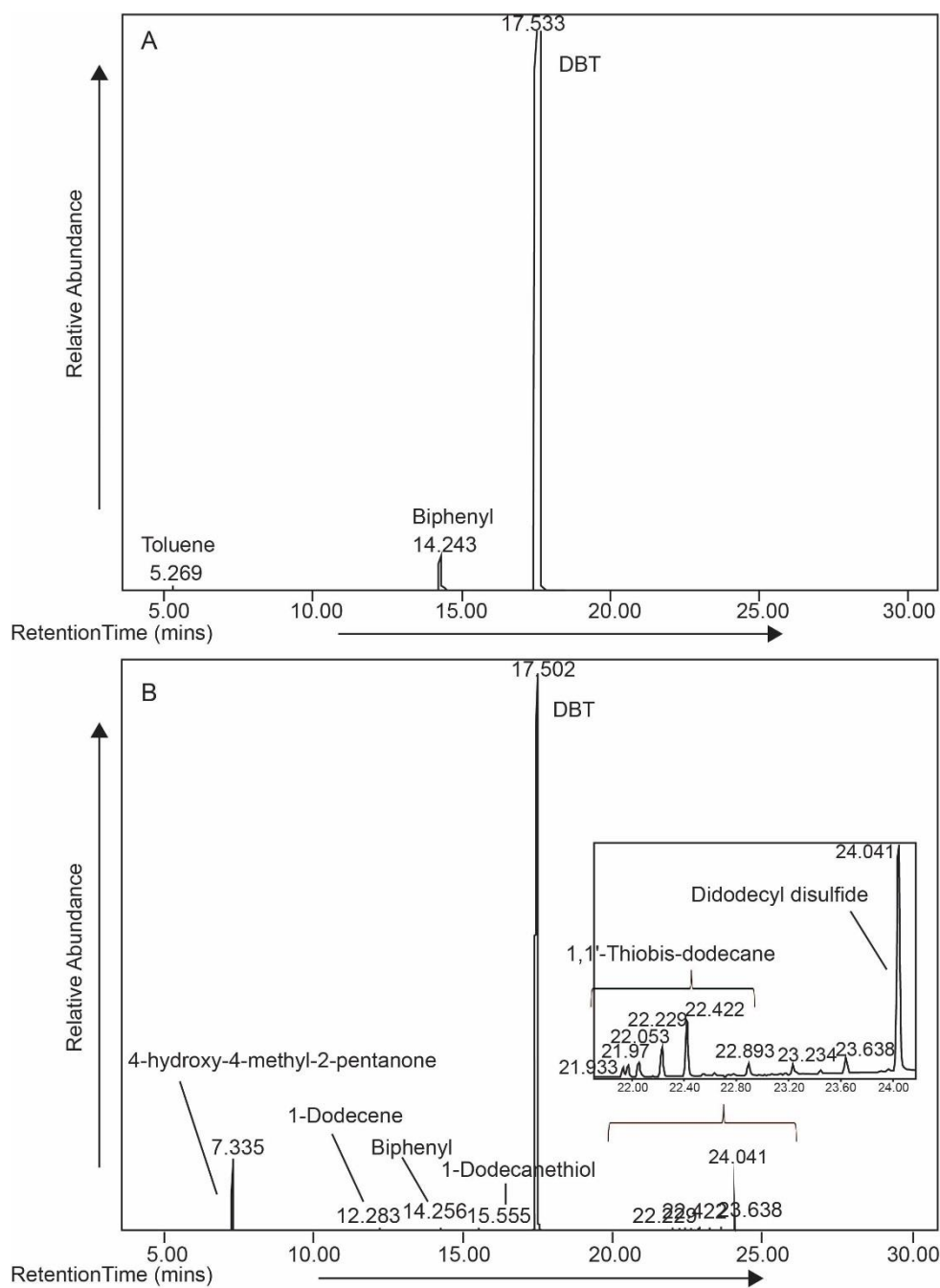


Figure 7.6 The GC-MS spectra of organic compounds in organic liquids pre-experiment (A) and post-experiment (B) for DBT.

Table 7.4 The chemical components in organic liquids pre- and post-experiment for DBT.

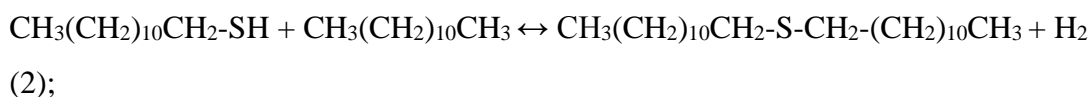
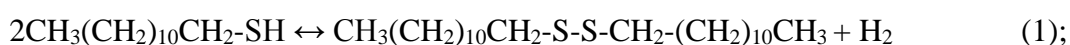
14B0044/001 - Pure DBT		
Peak Retention Time (mins)	Peak Area	Tentative compound ID
5.269	4.29E+06 (0.14%)	Toluene
14.243	3.02E+07 (0.96%)	Biphenyl
17.533	3.11E+09 (98.90%)	Dibenzothiophene
14B0044/002 - DBT+Au		
Peak Retention Time (mins)	Peak Area	Tentative compound ID
7.335	8.98E+07 (5.47%)	4-hydroxy-4-methyl-2-pentanone
12.283	2.79E+06 (0.17%)	1-Dodecene
14.256	4.33E+06 (0.26%)	Biphenyl
15.555	2.43E+06 (0.15%)	1-Dodecanethiol
17.502	1.47E+09 (89.69%)	Dibenzothiophene
21.933	1.66E+06 (0.10%)	1,1'-Thiobis-dodecane isomer * (extra ion fragments m/z=285, 299)
21.97	1.96E+06 (0.12%)	1,1'-Thiobis-dodecane isomer * (extra ion fragments m/z=271, 313)
22.053	2.81E+06 (0.17%)	1,1'-Thiobis-dodecane isomer * (extra ion fragments m/z=257, 327)
22.229	4.83E+06 (0.29%)	1,1'-Thiobis-dodecane isomer * (extra ion fragments m/z=243, 341)
22.422	8.98E+06 (0.55%)	1,1'-Thiobis-dodecane isomer * (extra ion fragments m/z=229)
22.893	2.33E+06 (0.14%)	1,1'-Thiobis-dodecane
23.234	1.87E+06 (0.11%)	unknown
23.638	2.77E+06 (0.17%)	Benzo[b]naphtho[1,2-d]thiophene (?) + Didodecyl disulfide *
24.041	4.26E+07 (2.60%)	Didodecyl disulfide

7.6 Discussion

7.6.1 The solubility of gold in dodecanethiol

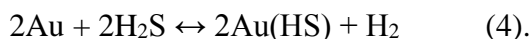
The results suggest that there is a significant concentration of Au dissolved in dodecanethiol and that the concentration of dissolved Au, with some exceptions, increase over time towards a consistent equilibrium concentration (Figure 7.4). There is almost no Au dissolved in dodecanethiol in the early stages, e.g. sample No. 8. However, these concentrations represent minimum solubilities of gold in dodecanethiol, as some Au may have been lost during the digestion process. Varying degrees of overflow of foaming solutions from the liners may contribute to fluctuations in the data. Nonetheless, the data indicate that up to 0.25 ppm Au can be dissolved in dodecanethiol at 200°C. In comparison, the solubility of gold in crude oil has been reported to range from 2 ppb at 100 °C to 20 ppb at 200 °C in the experiments of Williams-Jones and Migdisov (2007). This difference is likely due to the chemical complexity of crude oil. Crude oil may contain dodecanethiol or other thiol compounds, but in smaller, unknown fractions. Our experiment indicates that dodecanethiol can dissolve more gold than crude oil. Hence, it is proposed that dodecanethiol may act as a medium transport agent for Au.

Compared with the organic components in unreacted solutions, organic products contain relatively higher proportions of 1,1'-thiobis-dodecane and didodecyl disulfide, and lower proportions of dodecanethiol. This suggests that dodecanethiol may be aggregated into thiobis-dodecane and didodecyl disulphide during heating via following reactions (1), (2) and (3):



It is interesting to speculate on the speciation of Au dissolved in dodecanethiol. One possibility is that Au complexes directly with the thiol functional group in the dodecanethiol. However, it is worth considering that Au has been proved to be complexed with sulfides as Au bisulfide, e.g. $\text{Au}(\text{HS})^0$ (Stefánsson and Seward,

2004). Reaction (4) may, therefore, be proposed to occur when H₂S is produced in reaction (3).



Alternatively, it is possible that Au was mobilized as nano-particles. It has been reported that dodecanethiol-capped Au nanoparticles can be synthesized with the contribution of tannic acid under experimental conditions, and Au is mobilized by the formation of Au-S bonds (Zhang et al., 2013) (Figure 7.7). Thus, there is also possibility that Au could be attached to thiol group of dodecanethiol as a nano-particle via (5).



To distinguish this two mechanisms, Synchrotron X-ray Absorption Spectroscopy can be applied to figure out the chemical speciation of organic-Au complexes in the future.

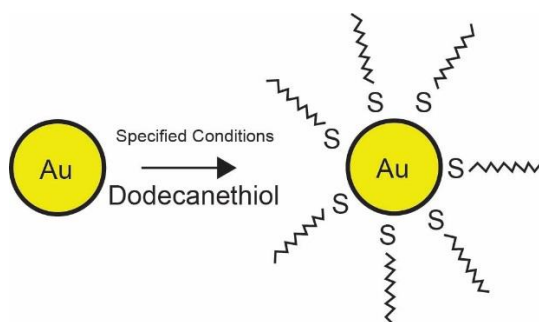
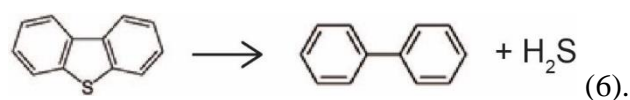


Figure 7.7 Schematic diagram of the synthesis of a dodecanethiol-capped Au nanoparticle from Au and dodecanethiol (Zhang et al., 2013).

7.6.2 The solubility of gold in DBT

The presence of dodecanethiol in post-heating DBT may occur due to the breakdown of DBT rings as both dodecanethiol and DBT have the same number of C and S atoms. Thus, the occurrence of thiobis-dodecane and didodecyl disulphide may be caused by reactions (1), (2) and (3) above with a consequent presence of sulfur in the liquids. However, contamination from previous dodecanethiol experiments cannot be ruled out, although strenuous efforts to clean the vessels were made. In addition, sulfur may be produced during the transition from DBT to biphenyl via (6).



However, there is no gold concentration data for the DBT experiments, as the analytical method was not sufficiently developed in time. The solubility of gold in DBT therefore needs more work in the future.

7.7 Summary

Though reproducible results have not yet been obtained from these experiments, which represent three years of development work, significant progress has been made. A relatively quick and inexpensive method to quantify gold concentrations of organic liquids was developed, and the dissolution of at least 0.25 ppm Au in dodecanethiol is a significant result. A concentration of this magnitude strongly suggests that thiol-bearing organic liquids such as dodecanethiol may act as transport agent for Au in ore-forming systems. In addition, the detection of gold transported by volatilized carbonaceous materials during dry ashing is of significance and suggests that organic vapour could contribute to gold mobilization in ore systems.

However, the Au-organic complexes responsible for transporting Au are still poorly understood and we have no idea about the behaviour of other organics. To achieve better results in the future, three key issues need to be addressed. Firstly, if liners are used for experiments with different organics, they need to be cleaned thoroughly before use. Second, a blank of dodecanethiol/ DBT or other organic liquid which goes through the experiments without gold is needed and the organic composition should be analysed to compare with that of the experimental products. Last but not least, to avoid Au loss, chemical digestion of the experimental products must be tested prior to the digestion.

7.8 References

- Archibald, S., Migdisov, A.A., Williams-Jones, A., 2001. The stability of Au-chloride complexes in water vapor at elevated temperatures and pressures. *Geochimica et Cosmochimica Acta* 65, 4413-4423.

- Baker, W., 1978. The role of humic acid in the transport of gold. *Geochimica et Cosmochimica Acta* 42, 645-649.
- Baranova, N., Zotov, A., 1998. Stability of gold sulphide species $\text{AuHS}^0_{(\text{aq})}$ and $\text{Au}(\text{HS})_2^-_{(\text{aq})}$ at 300, 350 °C and 500 bar: experimental study. *Mineralogical Magazine A* 62, 116-117.
- Bateman, R., Hagemann, S., 2004. Gold mineralisation throughout about 45 Ma of Archaean orogenesis: protracted flux of gold in the Golden Mile, Yilgarn craton, Western Australia. *Mineralium Deposita* 39, 536-559.
- Benning, L.G., Seward, T.M., 1996. Hydrosulphide complexing of Au (I) in hydrothermal solutions from 150-400 °C and 500-1500 bar. *Geochimica et Cosmochimica Acta* 60, 1849-1871.
- Botto, R.I., 2002. Trace element analysis of petroleum naphthas and tars using direct injection ICP-MS. *Canadian Journal of Analytical Sciences and Spectroscopy* 47, 1-12.
- Buffington, R., Wilson, M.K., 1987. *Detectors for gas chromatography: a practical primer*. Hewlett-Packard.
- Butler, O.T., Cairns, W.R., Cook, J.M., Davidson, C.M., 2014. 2013 Atomic spectrometry update—A review of advances in environmental analysis. *Journal of Analytical Atomic Spectrometry* 29, 17-50.
- Emsbo, P., Koenig, A., 2007. Transport of Au in petroleum: evidence from the northern Carlin trend, Nevada, Digging Deeper, Proceedings of the 9th Biennial SGA Meeting.
- Evans, K., Phillips, G., Powell, R., 2006. Rock-buffering of auriferous fluids in altered rocks associated with the Golden Mile-style mineralization, Kalgoorlie gold field, Western Australia. *Economic Geology* 101, 805-817.
- Frank, M.R., Candela, P.A., Piccoli, P.M., Glascock, M.D., 2002. Gold solubility, speciation, and partitioning as a function of HCl in the brine-silicate melt-metallic gold system at 800 °C and 100 MPa. *Geochimica et Cosmochimica Acta* 66, 3719-3732.

- Freise, F.W., 1931. The transportation of gold by organic underground solutions. *Economic Geology* 26, 421-431.
- Gammons, C.H., Barnes, H., 1989. The solubility of Ag_2S in near-neutral aqueous sulfide solutions at 25 to 300 °C. *Geochimica et Cosmochimica Acta* 53, 279-290.
- Gammons, C.H., Williams-Tones, A., 1995. The solubility of Au-Ag alloy + AgCl in HCl/NaCl solutions at 300 °C: New data on the stability of Au (1) chloride complexes in hydrothermal fluids. *Geochimica et Cosmochimica Acta* 59, 3453-3468.
- Gibert, F., Pascal, M.-L., Pichavant, M., 1998. Gold solubility and speciation in hydrothermal solutions: Experimental study of the stability of hydrosulphide complex of gold (AuHS) at 350 to 450 °C and 500 bars. *Geochimica et Cosmochimica Acta* 62, 2931-2947.
- Hayashi, K.-i., Ohmoto, H., 1991. Solubility of gold in NaCl- and H_2S -bearing aqueous solutions at 250-350 °C. *Geochimica et Cosmochimica Acta* 55, 2111-2126.
- Henley, R., 1973. Solubility of gold in hydrothermal chloride solutions. *Chemical Geology* 11, 73-87.
- Hopkins, R.L., Smith, H., 1954. Extraction and recovery of thiols from petroleum distillates. *Analytical Chemistry* 26, 206-207.
- Hughes, W.B., Holba, A.G., Dzou, L.I., 1995. The ratios of dibenzothiophene to phenanthrene and pristane to phytane as indicators of depositional environment and lithology of petroleum source rocks. *Geochimica et Cosmochimica Acta* 59, 3581-3598.
- Loucks, R.R., Mavrogenes, J.A., 1999. Gold solubility in supercritical hydrothermal brines measured in synthetic fluid inclusions. *Science* 284, 2159-2163.
- Lungwitz, E., 1900. The lixiviation of gold deposits by vegetation. *Engineering and Mining Journal* 69, 500-502.

- Miedaner, M., Migdisov, A., Williams-Jones, A., 2005. Solubility of metallic mercury in octane, dodecane and toluene at temperatures between 100 °C and 200 °C. *Geochimica et Cosmochimica Acta* 69, 5511-5516.
- Ong, H.L., Swanson, V.E., Bisque, R.E., 1970. Natural organic acids as agents of chemical weathering. *Geological Survey Research*, 130-137.
- Ortega, G.S., Pécheyran, C., Hudin, G., Marosits, E., Donard, O.F., 2013. Different approaches of crude oil mineralisation for trace metal analysis by ICPMS. *Microchemical Journal* 106, 250-254.
- Pan, P., Wood, S., 1994. Solubility of Pt and Pd sulfides and Au metal in aqueous bisulfide solutions. *Mineralium Deposita* 29, 373-390.
- Pulles, T., van der Gon, H.D., Appelman, W., Verheul, M., 2012. Emission factors for heavy metals from diesel and petrol used in European vehicles. *Atmospheric Environment* 61, 641-651.
- Radtke, A.S., Scheiner, B.J., 1970. Studies of hydrothermal gold deposition-(pt.) 1, carlin gold deposit, nevada, the role of carbonaceous materials in gold deposition. *Economic Geology* 65, 87-102.
- Renders, P., Seward, T., 1989. The stability of hydrosulphido- and sulphido-complexes of Au (I) and Ag (I) at 25 °C. *Geochimica et Cosmochimica Acta* 53, 245-253.
- Seeley, J.B., Senden, T.J., 1994. Alluvial gold in Kalimantan, Indonesia: A colloidal origin? *Journal of Geochemical Exploration* 50, 457-478.
- Seward, T.M., 1973. Thio complexes of gold and the transport of gold in hydrothermal ore solutions. *Geochimica et Cosmochimica Acta* 37, 379-399.
- Shenberger, D., Barnes, H., 1989. Solubility of gold in aqueous sulfide solutions from 150 to 350 C. *Geochimica et Cosmochimica Acta* 53, 269-278.
- Simoneit, B., Gize, A., 2000. Analytical techniques for organic matter characterization in ore deposits. *Ore genesis and exploration: The roles of organic matter. Reviews in Economic Geology* 9, 27-61.

- Stefánsson, A., Seward, T., 2003. Stability of chloridogold (I) complexes in aqueous solutions from 300 to 600 °C and from 500 to 1800 bar. *Geochimica et Cosmochimica Acta* 67, 4559-4576.
- Stefánsson, A., Seward, T., 2004. Gold (I) complexing in aqueous sulphide solutions to 500 °C at 500 bar. *Geochimica et Cosmochimica Acta* 68, 4121-4143.
- Tomkins, A.G., 2013. On the source of orogenic gold. *Geology* 41, 1255-1256.
- Wang, Z., Fingas, M., Li, K., 1994. Fractionation of a light crude oil and identification and quantitation of aliphatic, aromatic, and biomarker compounds by GC-FID and GC-MS, part II. *Journal of chromatographic Science* 32, 367-382.
- Wedepohl, K.H., 1995. The composition of the continental crust. *Geochimica et cosmochimica Acta* 59, 1217-1232.
- Williams-Jones, A., Migdisov, A., 2007. The solubility of gold in crude oil: implications for ore genesis, Proceedings of the 9 th Biennial SGA Meeting, Dublin. Millpress, pp. 765-768.
- Williams-Jones, A.E., Bowell, R.J., Migdisov, A.A., 2009. Gold in solution. *Elements* 5, 281-287.
- Wood, S.A., Crerar, D.A., Borcsik, M.P., 1987. Solubility of the assemblage pyrite-pyrrhotite-magnetite-sphalerite-galena-gold-stibnite-bismuthinite-argen-tite-molybdenite in H₂O-NaCl-CO₂ solutions from 200 °C to 350 °C. *Economic Geology* 82, 1864-1887.
- Zein, D.Y., Migdisov, A.A., Williams-Jones, A.E., 2007. The solubility of gold in hydrogen sulfide gas: An experimental study. *Geochimica et Cosmochimica Acta* 71, 3070-3081.
- Zein, D.Y., Migdisov, A.A., Williams-Jones, A.E., 2011. The solubility of gold in H₂O-H₂S vapour at elevated temperature and pressure. *Geochimica et Cosmochimica Acta* 75, 5140-5153.
- Zhang, H., Goikolea, E., Garitaonandia, J.S., Ortega, D., Saito, K., Suzuki, K., 2013. A two-step process for preparation of dodecanethiol-capped Au nanoparticles

with room-temperature spontaneous magnetization. *New Journal of Chemistry* 37, 2628-2631.

Zhuang, H., Lu, J., Fu, J., Ren, C., Zou, D., 1999. Crude oil as carrier of gold: petrological and geochemical evidence from Lannigou gold deposit in southwestern Guizhou, China. *Science in China Series D: Earth Sciences* 42, 216-224.

Zotov, A., Baranova, N., Dar'yina, T., Bannykh, L., 1991. The solubility of gold in aqueous chloride fluids at 350-500 °C and 500-1500 atm: Thermodynamic parameters of AuCl_2 (aq) up to 750 °C and 5000 atm. *Geochemistry International* 28, 63-71.

Chapter 8

Conclusions

This PhD project has explored new aspects of the role CM plays in the formation of gold deposits, in terms of source, transportation and deposition, and the possibility of organic geochemical characterisation of CM from the St. Ives and Wiluna gold deposits (Western Australia) and the Macraes gold deposit (New Zealand). Although the characterization of CM via conventional organic geochemical approaches shows that CM in these gold deposits is highly mature (**Chapter 2**), petrographic observations, other cutting-edge analytical techniques, and thermodynamic modelling enable the characterization of CM and interpretation of its possible contribution to gold deposit formation. The mechanisms via which Au may be transported by CM have been assessed by laboratory investigations. This project provides the first evidence:

- that in-situ CM directly contributes to Au incorporation into polyframboids which may provide the source of Au for the Macraes gold deposit,
- that at least some CM in mineralized rocks is most likely hydrothermally deposited and contributes to Au precipitation indirectly,
- and that dodecanethiol, which can dissolve a significant amount of Au, may transport Au in hydrothermal systems.

8.1 CM in the Macraes gold deposit and the Otago Schist

Four types of CM in rocks distal and proximal to Macraes gold deposit were characterized with Raman spectroscopy and petrographic observations (**Chapter 3**). CM 1 occurs in prehnite-pumpellyite (P-P) facies and pumpellyite-actinolite (P-A) facies rocks and is observed associated with sulfides in polyframboids. Raman spectra of CM suggest it is of relatively low maturity. Therefore, CM 1 may have an in-situ origin, for example, from the degradation of sulfate reducing bacteria, which produce polyframboids using the remanent CM as a framework. CM 2 has relative low maturity and is present as large flakes in carbonate veins in P-A facies and greenschist (G-S) facies rock. Thus, CM 2 is proposed to deposit from carbonic-rich

hydrothermal fluids. CM 3 is well-organized and occurs in the host rock of Macraes gold deposit. This material is interpreted to have been deposited from fluids but transport distances may have been short, of the order of mm. CM 4, observed in graphitic schist of mineralized rocks, is intimately associated with sulfides and gold. This type of CM is less well-crystallized, and may have a fluid-mediated history.

8.2 The role of CM in the formation of gold deposits

Source

The presence of low maturity CM 1 in polyframboids in pelitic rocks suggests that the formation of polyframboids results from sulfate reducing bacteria (SRB) activity (**Chapter 3**). NanoSIMS mapping shows that the nature of Zn-incorporation in polyframboids is variable, but in most cases Zn is co-located with CM 1 (**Chapter 4 & 5**). Zn is proposed to be sequestered into polyframboids at various stages of the framboid growth, with the precise nature of the incorporation depending on the relative concentrations of Zn and Fe in seawater (Figure 8.1). Individual sphalerite microcrystals may deposit directly on CM when Zn is present in high concentrations relative to Fe in solution. When the contents of Zn in solution are less, Zn may be sorbed or adsorbed directly on CM and mature to form the sphalerite-CM framework gradually with pyrite microcrystals filling in the framework. Zn may also be incorporated into pyrite microcrystals as solid solutions when the Zn/Fe ratio is low in solution. All these processes are linked to SRB activity, because the SRB produce the CM and reduce sulfate in solution to sulfide in sphalerite, pyrite and pyrite precursors.

Although there is no direct observation of a relationship between Au and CM 1 in polyframboids, concentrations of trace elements quantified by LA-ICP-MS show a positive correlation between Au and Zn, implying that Au may be incorporated into polyframboids in the same way as Zn, i.e. via SRB activity. Mass balance calculations suggest that CM 1-associated Au in polyframboids of P-P rocks of the Otago Schist can provide sufficient Au for Macraes orogenic gold deposits.

It is, therefore, postulated that, in the marine bottom waters, when polyframboids are formed during SRB activity, Au and Zn are immobilized by the bacteria from

seawater and deposited directly on the bacterial cell wall (Figure 8.1). When the bacteria are degraded, Au and Zn are preserved with CM 1 within framboids in pelites as the source of Au for orogenic gold deposits.

Mobilization and transportation

When metamorphic grade increases, polyframboids recrystallize into euhedral pyrite. At this time Au is released from CM 1 and incorporated into euhedral pyrite (Figure 8.1). The increased temperature may also trigger the generation of mobilized organic matter in pelite. CM 2 may be mobilized and deposited during this process, or introduced from rocks elsewhere by externally derived carbonic fluids. Au may be transported by thiols in carbonic fluids derived from organic matter, because thiols may be capable of transporting Au, as demonstrated in laboratory experiments (**Chapter 7**). Preliminary results from experiments of Au solubility in organic liquids show that dodecanethiol can dissolve at least 0.25 ppm Au at 200 °C, which is sufficient to indicate that thiol-bearing organic liquids may act as a transport agent for Au in ore-forming system.

During the transition from greenschist to amphibolite facies, euhedral pyrite is replaced by pyrrhotite. Au is released into fluids during this process, and carried as Au bisulfides in aqueous solutions to the Au deposition site. This process is consistent with results produced in the thermodynamic simulation (**Chapter 6**, Figure 8.1).

Precipitation

CM 3 in the host rock and CM 4 in mineralized rock of Macraes gold deposit are thought to have a fluid origin (**Chapter 3**). CM 4 is closely associated with sulfides and gold in graphitic microshears. Thermodynamic modelling, simulating the mineralization process at Macraes, suggests that most CM is precipitated from fluids (**Chapter 6**). Textural evidence suggests that sulphide growth was synchronous with, or post formation of, graphite microshears in rocks. The variable relationships between sulfides and CM in the microshears are attributed to alternation between sulfide-dominated deposition and graphite-dominated deposition during different

periods of fluid flow. Co-deposition of sulfides and graphite causes a decrease in H_2S in ore fluids, which drives the destabilization of Au bisulfides and results in gold precipitation in mineralization zones (**Chapter 6**, Figure 8.1). The results are broadly applicable to many other orogenic gold deposits around the world, such as the Victorian goldfield (Australia).

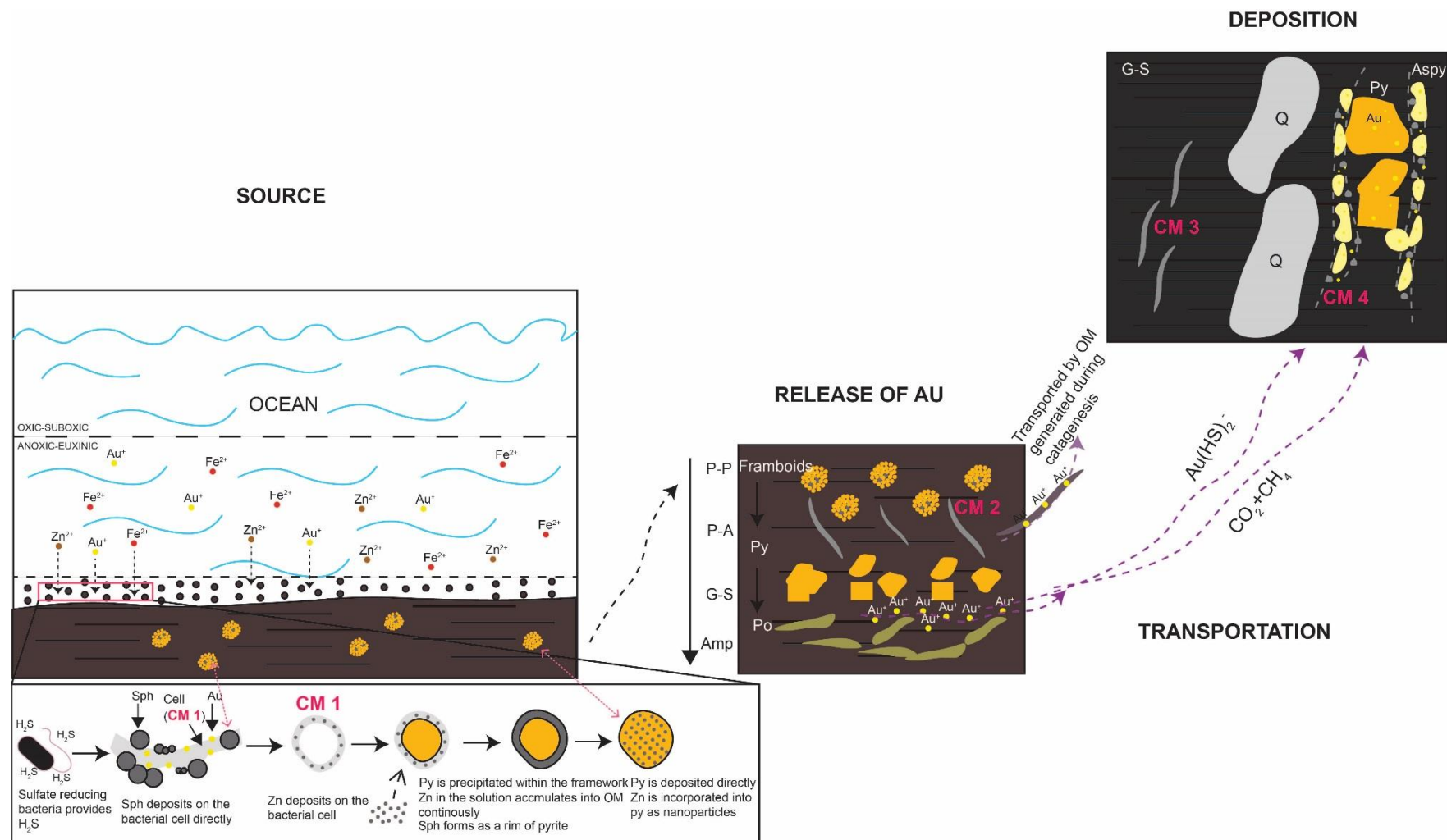


Figure 8.1 The role of CM in the formation of Macraes gold deposit. Au and Zn are incorporated into framboids through sulfate reducing bacterial activity, and preserved with CM 1 within framboids in pelites as the source rock of Au. A single microcrystal is taken as an example to show the detailed sequestration processes of Zn into framboids. Au is then released into hydrothermal fluids during the transition from framboids to euhedral pyrite, and to pyrrhotite when metamorphic grade increases. Thiols in organic matter which is generated during the catagenesis may be capable of transporting Au. When Au is transported to deposition site, the co-deposition of CM and sulfides drives gold precipitation. (CM, carbonaceous material; Sph, sphalerite; Py, pyrite; Aspy, arsenopyrite; Po, pyrrhotite; Q, quartz; P-P, prehnite-pumpellyite; P-A, pumpellyite-actonlite; G-S, greenschist; Amp, amphibolite.)

8.3 Limitations and future work

The results of this work indicate the varied and complex roles played by CM in the formation of Au deposits. In many aspects of the project, however, it was only possible to begin to define the question that must be answered if a comprehensive understanding of the role of CM is to be achieved. Recommended further work includes:

- Further characterisation of organic components in gold deposits

To understand the role of CM in gold deposits better, the characterization of the CM component, in terms of the molecular structure and chemical composition, and the exploration of organic-metal interactions in mineral systems, are necessary. In this project, CM in the three gold deposits is so mature that conventional organic geochemical analysis could only provide very limited information. However, this maturity does not preclude the analysis of biomarkers by novel organic geochemical techniques. An innovative experimental approach, hydropyrolysis (HyPy), has been developed and applied to characterize highly mature CM in CM-rich gold deposits by Grotheer et al. (2015) and Robert et al. (2016). This approach can promote the liberation of hydrocarbons which are covalently-bound to the host kerogen (Robert et al., 2016). The released biomarkers can be characterized by GC-MS and used to reveal the relationship between CM and minerals (Robert et al., 2016). HyPy is, therefore, a useful tool to characterize highly mature CM in gold deposits in the future.

- To quantify Au concentrations and characterize CM in the source rock

In the source rock, Au is proposed to be incorporated into polyframboids directly during SRB activity, but the investigation of the association between Au and CM in the source rock was only made possible by the use of Zn as a linking chemical variable. The distribution or concentrations relationship between Au and CM could not be analysed directly, because the concentration of Au in polyframboids is below the detection limits of SXRF and NanoSIMS, and the CM concentrations cannot be quantified by LA-ICP-MS. In the future, it may be possible to determine the

distribution of Au and CM by other state-of-art analytical techniques which have much lower detection limits of the elements of interest. Additionally, the chemical and molecular characteristics of CM in polyframboids has not been characterized because of the low total organic carbon content in the whole rock. Large quantities of samples from P-P facies rock of the Otago Schist may be analysed in the future to extract useful organic geochemical information.

- Further investigations of Au solubility in organic liquids

The preliminary results of the experiments of Au solubility in organic liquids are very significant, however, satisfactorily reproducible results have not yet been obtained. The challenge of this work is to quantify the Au concentrations in organic liquids. The chemical digestion can oxidize the organic liquids into aqueous solutions effectively. However, exothermic reactions during the digestion can cause foaming of the solutions, which overflow from the liners with associated Au loss. Therefore, in future experiments, development of the digestion process may further improve the reproducibility of the results. In addition, the organic complexes responsible for Au transportation are still unknown. Blank experiments on dodecanethiol/ DBT or other organic liquid without gold are recommended. The organic composition of experimental products involving Au or not can be compared to figure out the possible organic responsible for complexing Au. It may be possible to investigate the speciation of organic-Au complexes by synchrotron X-ray absorption spectroscopy. Last but not least, as we still have no idea about the behaviour of other organics, experiments involved with other types of organic liquids can be performed in the future.

Bibliography

A

- Algeo, T.J., Maynard, J.B., 2004. Trace-element behavior and redox facies in core shales of Upper Pennsylvanian Kansas-type cyclothems. *Chemical Geology* 206, 289-318.
- Ammar, M., Charon, E., Rouzaud, J.-N., Aleon, J., Guimbretière, G., Simon, P., 2011. On a reliable structural characterization of polished carbons in meteorites by Raman microspectroscopy. *Spectroscopy Letters* 44, 535-538.
- Archer, C., Vance, D. and Butler, I., 2004. Abiotic Zn isotope fractionations associated with ZnS precipitation. *Geochimica et Cosmochimica Acta* 66, A325.
- Archibald, S., Migdisov, A.A., Williams-Jones, A., 2001. The stability of Au-chloride complexes in water vapor at elevated temperatures and pressures. *Geochimica et Cosmochimica Acta* 65, 4413-4423.
- Awid-Pascual, R., Kamenetsky, V.S., Goemann, K., Allen, N., Noble, T.L., Lottermoser, B.G., Rodemann, T., 2015. The evolution of authigenic Zn–Pb–Fe-bearing phases in the Grieves Siding peat, western Tasmania. *Contributions to Mineralogy and Petrology* 170, 1-16.

B

- Baker, W., 1978. The role of humic acid in the transport of gold. *Geochimica et Cosmochimica Acta* 42, 645-649.
- Baranova, N., Zotov, A., 1998. Stability of gold sulphide species $\text{AuHS}^0_{(\text{aq})}$ and $\text{Au}(\text{HS})^2^-_{(\text{aq})}$ at 300, 350 °C and 500 bar: experimental study. *Mineralogical Magazine A* 62, 116-117.
- Barker, S.L., Hickey, K.A., Cline, J.S., Dipple, G.M., Kilburn, M.R., Vaughan, J.R., Longo, A.A., 2009. Uncloaking invisible gold: use of nanoSIMS to evaluate gold, trace elements, and sulfur isotopes in pyrite from Carlin-type gold deposits. *Economic Geology* 104, 897-904.

- Barton Jr, P., Bethke, P.M., 1987. Chalcopyrite disease in sphalerite: Pathology and epidemiology. *American Mineralogist* 72, 451-467.
- Bateman, R., Hagemann, S., 2004. Gold mineralisation throughout about 45 Ma of Archaean orogenesis: protracted flux of gold in the Golden Mile, Yilgarn craton, Western Australia. *Mineralium Deposita* 39, 536-559.
- Bavinton, O., Keays, R.R., 1978. Precious metal values from interflow sedimentary rocks from the komatiite sequence at Kambalda, Western Australia. *Geochimica et Cosmochimica Acta* 42, 1151-1163.
- Bawden, T.M., Einaudi, M.T., Bostick, B.C., Meibom, A., Wooden, J., Norby, J.W., Orobona, M.J., Chamberlain, C.P., 2003. Extreme 34S depletions in ZnS at the Mike gold deposit, Carlin Trend, Nevada: Evidence for bacteriogenic supergene sphalerite. *Geology* 31, 913-916.
- Bechtel, A., Pervaz, M., Püttmann, W., 1998. Role of organic matter and sulphate-reducing bacteria for metal sulphide precipitation in the Bahloul Formation at the Bou Grine Zn/Pb deposit (Tunisia). *Chemical Geology* 144, 1-21.
- Behar, F., Beaumont, V., Pentead, H.D.B., 2001. Rock-Eval 6 technology: performances and developments. *Oil & Gas Science and Technology* 56, 111-134.
- Benning, L.G., Seward, T.M., 1996. Hydrosulphide complexing of Au (I) in hydrothermal solutions from 150-400 °C and 500-1500 bar. *Geochimica et Cosmochimica Acta* 60, 1849-1871.
- Bente, K., Doering, T., 1993. Solid-state diffusion in sphalerites: An experimental verification of the chalcopyrite disease'. *European Journal of Mineralogy* 5, 465-478.
- Berge, J., 2011. Paleoproterozoic, turbidite-hosted, gold deposits of the Ashanti gold belt (Ghana, West Africa): Comparative analysis of turbidite-hosted gold deposits and an updated genetic model. *Ore Geology Reviews* 39, 91-100.
- Berner, R.A., 1969. The synthesis of framboidal pyrite. *Economic Geology* 64, 383-384.

- Berner, Z.A., Puchelt, H., Noeltner, T., Kramar, U., 2013. Pyrite geochemistry in the Toarcian Posidonia Shale of south - west Germany: Evidence for contrasting trace - element patterns of diagenetic and syngenetic pyrites. *Sedimentology* 60, 548-573.
- Beveridge, T., 1988. The bacterial surface: general considerations towards design and function. *Canadian Journal of Microbiology* 34, 363-372.
- Beyssac, O., Brunet, F., Petitet, J.-P., Goffé, B., Rouzaud, J.-N., 2003a. Experimental study of the microtextural and structural transformations of carbonaceous materials under pressure and temperature. *European Journal of Mineralogy* 15, 937-951.
- Beyssac, O., Goffé, B., Chopin, C., Rouzaud, J., 2002. Raman spectra of carbonaceous material in metasediments: a new geothermometer. *Journal of Metamorphic Geology* 20, 859-871.
- Beyssac, O., Goffé, B., Petitet, J.-P., Froigneux, E., Moreau, M., Rouzaud, J.-N., 2003b. On the characterization of disordered and heterogeneous carbonaceous materials by Raman spectroscopy. *Spectrochimica Acta Part A: Molecular and Biomolecular Spectroscopy* 59, 2267-2276.
- Bierlein, F.P., Cartwright, I., McKnight, S., 2001. The role of carbonaceous "indicator" slates in the genesis of lode gold mineralization in the Western Lachlan Orogen, Victoria, Southeastern Australia. *Economic Geology* 96, 431-451.
- Bierlein, F.P., Smith, P.K., 2003. The Touquoy Zone deposit: an example of "unusual" orogenic gold mineralisation in the Meguma Terrane, Nova Scotia, Canada. *Canadian Journal of Earth Sciences* 40, 447-466.
- Bishop, D., Bradshaw, J., Landis, C., Turnbull, I., 1976. Lithostratigraphy and structure of the Caples terrane of the Humboldt Mountains, New Zealand. *New Zealand Journal of Geology and Geophysics* 19, 827-848.
- Bonal, L., Huss, G.R., Krot, A.N., Nagashima, K., 2010. Chondritic lithic clasts in the CB/CH-like meteorite Isheyevo: Fragments of previously unsampled parent bodies. *Geochimica et Cosmochimica Acta* 74, 2500-2522.

Botto, R.I., 2002. Trace element analysis of petroleum naphthas and tars using direct injection ICP-MS. *Canadian Journal of Analytical Sciences and Spectroscopy* 47, 1-12.

Buffington, R., Wilson, M.K., 1987. *Detectors for gas chromatography: A practical primer*. Hewlett-Packard.

Butler, O.T., Cairns, W.R., Cook, J.M., Davidson, C.M., 2014. 2013 Atomic spectrometry update—A review of advances in environmental analysis. *Journal of Analytical Atomic Spectrometry* 29, 17-50.

C

Chauhan, D., 1974. Diagenetic pyrite from the lead-zinc deposits of Zawar, India. *Mineralium Deposita* 9, 69-73.

Chen, J., Walter, M.R., Logan, G.A., Hinman, M.C., Summons, R.E., 2003. The Paleoproterozoic McArthur River (HYC) Pb/Zn/Ag deposit of northern Australia: organic geochemistry and ore genesis. *Earth and Planetary Science Letters* 210, 467-479.

Cline, J.S., Hofstra, A.H., Muntean, J.L., Tosdal, R.M., Hickey, K.A., 2005. Carlin-type gold deposits in Nevada: Critical geologic characteristics and viable models. *Economic Geology 100th Anniversary Volume* 100, 451-484.

Cloquet, C., Carignan, J., Lehmann, M.F., Vanhaecke, F., 2008. Variation in the isotopic composition of zinc in the natural environment and the use of zinc isotopes in biogeosciences: a review. *Analytical and Bioanalytical Chemistry* 390, 451-463.

Conway, T.M., John, S.G., 2015. The cycling of iron, zinc and cadmium in the North East Pacific Ocean—Insights from stable isotopes. *Geochimica et Cosmochimica Acta* 164, 262-283.

Coombs, D., Landis, C., Norris, R., Sinton, J., Borns, D., Craw, D., 1976. The Dun Mountain Ophiolite Belt, New Zealand, its tectonic setting, constitution, and origin, with special reference to the southern portion. *American Journal of Science* 276, 561-603.

- Cooper, R., 1975. New Zealand and south-east Australia in the early Paleozoic. *New Zealand Journal of Geology and Geophysics* 18, 1-20.
- Coveney, R.M., Murowchick, J.B., Grauch, R.I., Glascock, M.D., Denison, J.R., 1992. Gold and platinum in shales with evidence against extraterrestrial sources of metals. *Chemical Geology* 99, 101-114.
- Cox, S., Ruming, K., 2004. The St Ives mesothermal gold system, Western Australia—a case of golden aftershocks? *Journal of Structural Geology* 26, 1109-1125.
- Cox, S., Sun, S., Etheridge, M., Wall, V., Potter, T., 1995. Structural and geochemical controls on the development of turbidite-hosted gold quartz vein deposits, Wattle Gully mine, central Victoria, Australia. *Economic Geology* 90, 1722-1746.
- Craig, J., Vokes, F., Solberg, T., 1998. Pyrite: physical and chemical textures. *Mineralium Deposita* 34, 82-101.
- Craw, D., 1992. Fluid evolution, fluid immiscibility and gold deposition during Cretaceous-Recent tectonics and uplift of the Otago and Alpine Schist, New Zealand. *Chemical Geology* 98, 221-236.
- Craw, D., 2002. Geochemistry of late metamorphic hydrothermal alteration and graphitisation of host rock, Macraes gold mine, Otago Schist, New Zealand. *Chemical Geology* 191, 257-275.
- Craw, D., Burridge, C., Waters, J., 2007. Geological and biological evidence for drainage reorientation during uplift of alluvial basins, central Otago, New Zealand. *New Zealand Journal of Geology and Geophysics* 50, 367-376.
- Craw, D., MacKenzie, D., Pitcairn, I., Teagle, D., Norris, R., 2007. Geochemical signatures of mesothermal Au-mineralized late-metamorphic deformation zones, Otago Schist, New Zealand. *Geochemistry: Exploration, Environment, Analysis* 7, 225-232.
- Craw, D., Mortensen, J., MacKenzie, D., Pitcairn, I., 2015. Contrasting geochemistry of orogenic gold deposits in Yukon, Canada and Otago, New Zealand. *Geochemistry: Exploration, Environment, Analysis* 15, 150-166.

Craw, D., Upton, P., Yu, B.-S., Horton, T., Chen, Y.-G., 2010. Young orogenic gold mineralisation in active collisional mountains, Taiwan. *Mineralium Deposita* 45, 631-646.

Craw, D., Windle, S., Angus, P., 1999. Gold mineralization without quartz veins in a ductile-brittle shear zone, Macraes Mine, Otago Schist, New Zealand. *Mineralium Deposita* 34, 382-394.

Crocket, J., Kuo, H., 1979. Sources for gold, palladium and iridium in deep-sea sediments. *Geochimica et Cosmochimica Acta* 43, 831-842.

D

De Ronde, C.E., Faure, K., Bray, C.J., Whitford, D.J., 2000. Round Hill shear zone-hosted gold deposit, Macraes Flat, Otago, New Zealand: evidence of a magmatic ore fluid. *Economic Geology* 95, 1025-1048.

Deckert, H., Ring, U., Mortimer, N., 2002. Tectonic significance of Cretaceous bivergent extensional shear zones in the Torlesse accretionary wedge, central Otago Schist, New Zealand. *New Zealand Journal of Geology and Geophysics* 45, 537-547.

Deditius, A.P., Utsunomiya, S., Reich, M., Kesler, S.E., Ewing, R.C., Hough, R., Walshe, J., 2011. Trace metal nanoparticles in pyrite. *Ore Geology Reviews* 42, 32-46.

Degens, E., Okada, H., Honjo, S., Hathaway, J., 1972. Microcrystalline sphalerite in resin globules suspended in Lake Kivu, East Africa. *Mineralium Deposita* 7, 1-12.

Dippel, B., Jander, H., Heintzenberg, J., 1999. NIR FT Raman spectroscopic study of flame soot. *Physical Chemistry Chemical Physics* 1, 4707-4712.

Donald, R., Southam, G., 1999. Low temperature anaerobic bacterial diagenesis of ferrous monosulfide to pyrite. *Geochimica et Cosmochimica Acta* 63, 2019-2023.

Druschel, G., Labrenz, M., Thomsen-Ebert, T., Fowle, D., Banfield, J., 2002. Geochemical modeling of ZnS in biofilms: An example of ore depositional processes. *Economic Geology* 97, 1319-1329.

Dyl, K.A., Cleverley, J.S., Bland, P.A., Ryan, C.G., Fisher, L.A., Hough, R.M., 2014. Quantified, whole section trace element mapping of carbonaceous chondrites by Synchrotron X-ray Fluorescence Microscopy: 1. CV meteorites. *Geochimica et Cosmochimica Acta* 134, 100-119.

E

Eckardt, C., Wolf, M., Maxwell, J., 1989. Iron porphyrins in the Permian Kupferschiefer of the lower Rhine Basin, NW Germany. *Organic Geochemistry* 14, 659-666.

Eilu, P., Mikucki, E.J., 1998. Alteration and primary geochemical dispersion associated with the Bulletin lode-gold deposit, Wiluna, Western Australia. *Journal of Geochemical Exploration* 63, 73-103.

Eiserbeck, C., Nelson, R.K., Grice, K., Curiale, J., Reddy, C.M., 2012. Comparison of GC-MS, GC-MRM-MS, and GC×GC to characterise higher plant biomarkers in Tertiary oils and rock extracts. *Geochimica et Cosmochimica Acta* 87, 299-322.

Emsbo, P., Hofstra, A.H., Lauha, E.A., Griffin, G.L., Hutchinson, R.W., 2003. Origin of high-grade gold ore, source of ore fluid components, and genesis of the Meikle and neighboring Carlin-type deposits, northern Carlin trend, Nevada. *Economic Geology* 98, 1069-1105.

Emsbo, P., Koenig, A., 2007. Transport of Au in petroleum: evidence from the northern Carlin trend, Nevada, Digging Deeper, Proceedings of the 9th Biennial SGA Meeting.

Evans, K., Phillips, G., Powell, R., 2006. Rock-buffering of auriferous fluids in altered rocks associated with the Golden Mile-style mineralization, Kalgoorlie gold field, Western Australia. *Economic Geology* 101, 805-817.

Evans, K.A., 2010. A test of the viability of fluid–wall rock interaction mechanisms for changes in opaque phase assemblage in metasedimentary rocks in the Kambalda-St. Ives goldfield, Western Australia. *Mineralium Deposita* 45, 207-213.

F

- Fein, J.B., Williams-Jones, A., 1997. The role of mercury-organic interactions in the hydrothermal transport of mercury. *Economic Geology* 92, 20-28.
- Fisher, L.A., Fougereuse, D., Cleverley, J.S., Ryan, C.G., Micklethwaite, S., Halfpenny, A., Hough, R.M., Gee, M., Paterson, D., Howard, D.L., 2014. Quantified, multi-scale X-ray fluorescence element mapping using the Maia detector array: application to mineral deposit studies. *Mineralium Deposita*, 1-10.
- Fleming, C.A., 1979. *The geological history of New Zealand and its life*. Auckland University Press.
- Folk, R.L., 2005. Nannobacteria and the formation of framboidal pyrite: Textural evidence. *Journal of Earth System Science* 114, 369-374.
- Fortin, D., Southam, G., Beveridge, T., 1994. Nickel sulfide, iron-nickel sulfide and iron sulfide precipitation by a newly isolated *Desulfotomaculum* species and its relation to nickel resistance. *FEMS Microbiology Ecology* 14, 121-132.
- Foustoukos, D.I., 2012. Metastable equilibrium in the CHO system: Graphite deposition in crustal fluids. *American Mineralogist* 97, 1373-1380.
- Frank, M.R., Candela, P.A., Piccoli, P.M., Glascock, M.D., 2002. Gold solubility, speciation, and partitioning as a function of HCl in the brine-silicate melt-metallic gold system at 800 °C and 100 MPa. *Geochimica et Cosmochimica Acta* 66, 3719-3732.
- Freise, F.W., 1931. The transportation of gold by organic underground solutions. *Economic Geology* 26, 421-431.
- Frey, M., Capitani, C.d., Liou, J., 1991. A new petrogenetic grid for low - grade metabasites. *Journal of Metamorphic Geology* 9, 497-509.
- Fujii, T., Moynier, F., Pons, M.-L., Albarède, F., 2011. The origin of Zn isotope fractionation in sulfides. *Geochimica et Cosmochimica Acta* 75, 7632-7643.

G

- Gaboury, D., 2013. Does gold in orogenic deposits come from pyrite in deeply buried carbon-rich sediments? : Insight from volatiles in fluid inclusions. *Geology* 41, 1207-1210.
- Gammons, C.H., Barnes, H., 1989. The solubility of Ag_2S in near-neutral aqueous sulfide solutions at 25 to 300 °C. *Geochimica et Cosmochimica Acta* 53, 279-290.
- Gammons, C.H., Williams-Tones, A., 1995. The solubility of Au-Ag alloy + AgCl in HCl/NaCl solutions at 300 °C: New data on the stability of Au (I) chloride complexes in hydrothermal fluids. *Geochimica et Cosmochimica Acta* 59, 3453-3468.
- Gammons, C.H., Yu, Y., Williams-Jones, A., 1997. The disproportionation of gold (I) chloride complexes at 25 to 200° C. *Geochimica et Cosmochimica Acta* 61, 1971-1983.
- Gatellier, J.-P., Disnar, J.-R., 1989. Organic matter and gold-ore association in a hydrothermal deposit, France. *Applied Geochemistry* 4, 143-149.
- Gibert, F., Pascal, M.-L., Pichavant, M., 1998. Gold solubility and speciation in hydrothermal solutions: Experimental study of the stability of hydrosulphide complex of gold (AuHS) at 350 to 450 °C and 500 bars. *Geochimica et Cosmochimica Acta* 62, 2931-2947.
- Giordano, T., 2000. Organic matter as a transport agent in ore-forming systems. *Reviews in Economic Geology* 9, 133-155.
- Giordano, T.H., 1994. Metal transport in ore fluids by organic ligand complexation, Organic acids in geological processes. Springer, pp. 319-354.
- Gize, A., Barnes, H., 1994. Organic contributions to Mississippi Valley-type lead-zinc genesis—a critical assessment, *Sediment-Hosted Zn-Pb Ores*. Springer, pp. 13-26.
- Gize, A.P., 1999. A special issue on Organic matter and ore deposits; interactions, applications, and case studies; introduction. *Economic Geology* 94, 963-965.

- Gize, A.P., Barnes, H., 1987. The organic geochemistry of two Mississippi Valley-type lead-zinc deposits. *Economic Geology* 82, 457-470.
- Glikson, M., Golding, S., Southgate, P., 2006. Thermal evolution of the ore-hosting Isa superbasin: Central and northern Lawn Hill platform. *Economic Geology* 101, 1211-1229.
- Glikson, M., Mastalerz, M., Golding, S., McConachie, B., 2000. Metallogenesis and hydrocarbon generation in northern Mount Isa Basin, Australia: implications for ore grade mineralization, *Organic Matter and Mineralisation: Thermal Alteration, Hydrocarbon Generation and Role in Metallogenesis*. Springer, pp. 149-184.
- Goellnicht, N., Groves, D., McNaughton, N., Dimo, G., 1989. An epigenetic origin for the Telfer gold deposit. *Western Australia: Economic Geology Monograph* 6, 151-167.
- Goldfarb, R.J., Groves, D.I., 2015. Orogenic gold: common or evolving fluid and metal sources through time. *Lithos* 233, 2-26.
- Goldfarb, R.J., Hart, C., Davis, G., Groves, D., 2007. East Asian gold: Deciphering the anomaly of Phanerozoic gold in Precambrian cratons. *Economic Geology* 102, 341-345.
- Greenwood, P., Brocks, J., Grice, K., Schwark, L., Jaraula, C., Dick, J., Evans, K., 2013. Organic geochemistry and mineralogy. I. Characterisation of organic matter associated with metal deposits. *Ore Geology Reviews* 50, 1-27.
- Gregory, D., Meffre, S., Large, R., 2014. Comparison of metal enrichment in pyrite framboids from a metal-enriched and metal-poor estuary. *American Mineralogist* 99, 633-644.
- Gregory, D.D., Large, R.R., Bath, A.B., Steadman, J.A., Wu, S., Danyushevsky, L., Bull, S.W., Holden, P., Ireland, T.R., 2016. Trace Element Content of Pyrite from the Kapaï Slate, St. Ives Gold District, Western Australia. *Economic Geology* 111, 1297-1320.
- Gregory, D.D., Large, R.R., Halpin, J.A., Baturina, E.L., Lyons, T.W., Wu, S., Danyushevsky, L., Sack, P.J., Chappaz, A., Maslennikov, V.V., 2015. Trace

element content of sedimentary pyrite in black shales. *Economic Geology* 110, 1389-1410.

- Grice, K., Cao, C., Love, G.D., Böttcher, M.E., Twitchett, R.J., Grosjean, E., Summons, R.E., Turgeon, S.C., Dunning, W., Jin, Y., 2005. Photic zone euxinia during the Permian-Triassic superanoxic event. *Science* 307, 706-709.
- Grice, K., Gibbison, R., Atkinson, J.E., Schwark, L., Eckardt, C.B., Maxwell, J.R., 1996. Maleimides (1H-pyrrole-2, 5-diones) as molecular indicators of anoxygenic photosynthesis in ancient water columns. *Geochimica et Cosmochimica Acta* 60, 3913-3924.
- Grice, K., Schaeffer, P., Schwark, L., Maxwell, J.R., 1997. Changes in palaeoenvironmental conditions during deposition of the Permian Kupferschiefer (Lower Rhine Basin, northwest Germany) inferred from molecular and isotopic compositions of biomarker components. *Organic Geochemistry* 26, 677-690.
- Grimes, S.T., Brock, F., Rickard, D., Davies, K.L., Edwards, D., Briggs, D.E., Parkes, R.J., 2001. Understanding fossilization: experimental pyritization of plants. *Geology* 29, 123-126.
- Gu, X., Zhang, Y., Li, B., Dong, S., Xue, C., Fu, S., 2012. Hydrocarbon-and ore-bearing basinal fluids: a possible link between gold mineralization and hydrocarbon accumulation in the Youjiang basin, South China. *Mineralium Deposita*, 1-20.

H

- Hagemann, S., Cassidy, K.F., 2000. Archean orogenic lode gold deposits. *Reviews in Economic Geology* 13, 9-68.
- Hagemann, S., Groves, D., Ridley, J., Vearncombe, J.R., 1992. The Archean lode gold deposits at Wiluna, Western Australia; high-level brittle-style mineralization in a strike-slip regime. *Economic Geology* 87, 1022-1053.
- Hagemann, S., Lüders, V., 2003. PTX conditions of hydrothermal fluids and precipitation mechanism of stibnite-gold mineralization at the Wiluna lode-

- gold deposits, Western Australia: conventional and infrared microthermometric constraints. *Mineralium Deposita* 38, 936-952.
- Hare, A.A., Kuzyk, Z.Z.A., Macdonald, R.W., Sanei, H., Barber, D., Stern, G.A., Wang, F., 2014. Characterization of sedimentary organic matter in recent marine sediments from Hudson Bay, Canada, by Rock-Eval pyrolysis. *Organic Geochemistry* 68, 52-60.
- Hayashi, K.-i., Ohmoto, H., 1991. Solubility of gold in NaCl- and H₂S-bearing aqueous solutions at 250-350 °C. *Geochimica et Cosmochimica Acta* 55, 2111-2126.
- Henley, R., 1973. Solubility of gold in hydrothermal chloride solutions. *Chemical Geology* 11, 73-87.
- Henne, A., Craw, D., 2012. Synmetamorphic carbon mobility and graphite enrichment in metaturbidites as a precursor to orogenic gold mineralisation, Otago Schist, New Zealand. *Mineralium Deposita*, 1-17.
- Ho, E.S., Mauk, J.L., 1996. Relationship between organic matter and copper mineralization in the Proterozoic Nonesuch Formation, northern Michigan. *Ore Geology Reviews* 11, 71-87.
- Ho, E.S., Meyers, P.A., Mauk, J.L., 1990. Organic geochemical study of mineralization in the Keweenaw Nonesuch Formation at White Pine, Michigan. *Organic Geochemistry* 16, 229-234.
- Hodkiewicz, P., Groves, D., Davidson, G., Weinberg, R., Hagemann, S., 2009. Influence of structural setting on sulphur isotopes in Archean orogenic gold deposits, Eastern Goldfields Province, Yilgarn, Western Australia. *Mineralium Deposita* 44, 129-150.
- Holman, A.I., Grice, K., Jaraula, C.M., Schimmelmann, A., 2014. Bitumen II from the Paleoproterozoic Here's Your Chance Pb/Zn/Ag deposit: Implications for the analysis of depositional environment and thermal maturity of hydrothermally-altered sediments. *Geochimica et Cosmochimica Acta* 139, 98-109.

- Holman, A.I., Grice, K., Jaraula, C.M., Schimmelmann, A., Brocks, J.J., 2012. Efficiency of extraction of polycyclic aromatic hydrocarbons from the Paleoproterozoic Here's Your Chance Pb/Zn/Ag ore deposit and implications for a study of Bitumen II. *Organic Geochemistry* 52, 81-87.
- Hopkins, R.L., Smith, H., 1954. Extraction and recovery of thiols from petroleum distillates. *Analytical Chemistry* 26, 206-207.
- Hu, S., Evans, K., Craw, D., Rempel, K., Bourdet, J., Dick, J., Grice, K., 2015. Raman characterization of carbonaceous material in the Macraes orogenic gold deposit and metasedimentary host rocks, New Zealand. *Ore Geology Reviews* 70, 80-95.
- Hu, S.-Y., Evans, K., Fisher, L., Rempel, K., Craw, D., Evans, N.J., Cumberland, S., Robert, A., Grice, K., 2016. Associations between sulfides, carbonaceous material, gold and other trace elements in polyframboids: Implications for the source of orogenic gold deposits, Otago Schist, New Zealand. *Geochimica et Cosmochimica Acta* 180, 197-213.
- Huerta-Diaz, M.A., Morse, J.W., 1992. Pyritization of trace metals in anoxic marine sediments. *Geochimica et Cosmochimica Acta* 56, 2681-2702.
- Hughes, W.B., Holba, A.G., Dzou, L.I., 1995. The ratios of dibenzothiophene to phenanthrene and pristane to phytane as indicators of depositional environment and lithology of petroleum source rocks. *Geochimica et Cosmochimica Acta* 59, 3581-3598.
- Huizenga, J.-M., 2011. Thermodynamic modelling of a cooling C-O-H fluid-graphite system: implications for hydrothermal graphite precipitation. *Mineralium Deposita* 46, 23-33.

I**J**

- Jaraula, C.M., Grice, K., Twitchett, R.J., Böttcher, M.E., LeMetayer, P., Dastidar, A.G., Opazo, L.F., 2013. Elevated pCO₂ leading to Late Triassic extinction, persistent photic zone euxinia, and rising sea levels. *Geology* 41, 955-958.

- Jaraula, C.M., Schwark, L., Moreau, X., Pickel, W., Bagas, L., Grice, K., 2015. Radiolytic alteration of biopolymers in the Mulga Rock (Australia) uranium deposit. *Applied Geochemistry* 52, 97-108.
- Jawhari, T., Roid, A., Casado, J., 1995. Raman spectroscopic characterization of some commercially available carbon black materials. *Carbon* 33, 1561-1565.
- Jehlička, J., Urban, O., Pokorný, J., 2003. Raman spectroscopy of carbon and solid bitumens in sedimentary and metamorphic rocks. *Spectrochimica Acta Part A: Molecular and Biomolecular Spectroscopy* 59, 2341-2352.
- John, S.G., Conway, T.M., 2014. A role for scavenging in the marine biogeochemical cycling of zinc and zinc isotopes. *Earth and Planetary Science Letters* 394, 159-167.
- John, S.G., Geis, R.W., Saito, M.A., Boyle, E.A., 2007. Zinc isotope fractionation during high-affinity and low-affinity zinc transport by the marine diatom *Thalassiosira oceanica*. *Limnology and Oceanography* 52, 2710-2714.
- K**
- Kashefi, K., Tor, J.M., Nevin, K.P., Lovley, D.R., 2001. Reductive precipitation of gold by dissimilatory Fe (III)-reducing bacteria and archaea. *Applied and Environmental Microbiology* 67, 3275-3279.
- Kendrick, M., Honda, M., Walshe, J., Petersen, K., 2011. Fluid sources and the role of abiogenic-CH₄ in Archean gold mineralization: Constraints from noble gases and halogens. *Precambrian Research* 189, 313-327.
- Ketris, M., Yudovich, Y.E., 2009. Estimations of Clarkes for Carbonaceous biolithes: World averages for trace element contents in black shales and coals. *International Journal of Coal Geology* 78, 135-148.
- Kettler, R.M., Waldo, G.S., Penner-Hahn, J.E., Meyers, P.A., Kesler, S.E., 1990. Sulfidation of organic matter associated with gold mineralization, Pueblo Viejo, Dominican Republic. *Applied Geochemistry* 5, 237-248.
- Kilburn, M.R., Clode, P.L., 2014. Elemental and isotopic imaging of biological samples using NanoSIMS. *Electron Microscopy: Methods and Protocols*, 733-755.

- Kilburn, M.R., Wacey, D., 2011. Elemental and isotopic analysis by NanoSIMS: insights for the study of stromatolites and early life on Earth, *Stromatolites: interaction of microbes with sediments*. Springer, pp. 463-493.
- Křibek, B., Sýkorová, I., Machovič, V., Knésl, I., Laufek, F., Zachariáš, J., 2015. The origin and hydrothermal mobilization of carbonaceous matter associated with Paleoproterozoic orogenic-type gold deposits of West Africa. *Precambrian Research* 270, 300-317.
- Kucha, H., Schroll, E., Raith, J., Halas, S., 2010. Microbial sphalerite formation in carbonate-hosted Zn-Pb ores, Bleiberg, Austria: Micro-to nanotextural and sulfur isotope evidence. *Economic Geology* 105, 1005-1023.
- L**
- Labrenz, M., Banfield, J., 2004. Sulfate-reducing bacteria-dominated biofilms that precipitate ZnS in a subsurface circumneutral-pH mine drainage system. *Microbial Ecology* 47, 205-217.
- Labrenz, M., Druschel, G.K., Thomsen-Ebert, T., Gilbert, B., Welch, S.A., Kemner, K.M., Logan, G.A., Summons, R.E., De Stasio, G., Bond, P.L., 2000. Formation of sphalerite (ZnS) deposits in natural biofilms of sulfate-reducing bacteria. *Science* 290, 1744-1747.
- Lafargue, E., Marquis, F., Pillot, D., 1998. Rock-Eval 6 applications in hydrocarbon exploration, production, and soil contamination studies. *Revue de L'institut Français du Pétrole* 53, 421-437.
- Lahfid, A., Beyssac, O., Deville, E., Negro, F., Chopin, C., Goffe, B., 2010. Evolution of the Raman spectrum of carbonaceous material in low-grade metasediments of the Glarus Alps (Switzerland). *Terra Nova* 22, 354-360.
- Landais, P., 1996. Organic geochemistry of sedimentary uranium ore deposits. *Ore Geology Reviews* 11, 33-51.
- Landis, C., 1971. Graphitization of dispersed carbonaceous material in metamorphic rocks. *Contributions to Mineralogy and Petrology* 30, 34-45.
- Landis, C., Coombs, D., 1967. Metamorphic belts and orogenesis in southern New Zealand. *Tectonophysics* 4, 501-518.

- Large, D., Fortey, N., Milodowski, A., Christy, A., Dodd, J., 2001. Petrographic observations of iron, copper, and zinc sulfides in freshwater canal sediment. *Journal of Sedimentary Research* 71, 61-69.
- Large, D., Sawlowicz, Z., Spratt, J., 1999. A cobaltite-framboidal pyrite association from the Kupferschiefer; possible implications for trace element behaviour during the earliest stages of diagenesis. *Mineralogical Magazine* 63, 353-361.
- Large, R., Thomas, H., Craw, D., Henne, A., Henderson, S., 2012. Diagenetic pyrite as a source for metals in orogenic gold deposits, Otago Schist, New Zealand. *New Zealand Journal of Geology and Geophysics* 55, 137-149.
- Large, R.R., Bull, S.W., Maslennikov, V.V., 2011. A carbonaceous sedimentary source-rock model for Carlin-type and orogenic gold deposits. *Economic Geology* 106, 331-358.
- Large, R.R., Danyushevsky, L., Hollit, C., Maslennikov, V., Meffre, S., Gilbert, S., Bull, S., Scott, R., Emsbo, P., Thomas, H., 2009. Gold and trace element zonation in pyrite using a laser imaging technique: implications for the timing of gold in orogenic and Carlin-style sediment-hosted deposits. *Economic Geology* 104, 635-668.
- Large, R.R., Halpin, J.A., Danyushevsky, L.V., Maslennikov, V.V., Bull, S.W., Long, J.A., Gregory, D.D., Lounejeva, E., Lyons, T.W., Sack, P.J., 2014. Trace element content of sedimentary pyrite as a new proxy for deep-time ocean-atmosphere evolution. *Earth and Planetary Science Letters* 389, 209-220.
- Large, R.R., Maslennikov, V.V., Robert, F., Danyushevsky, L.V., Chang, Z., 2007. Multistage sedimentary and metamorphic origin of pyrite and gold in the giant Sukhoi Log deposit, Lena gold province, Russia. *Economic Geology* 102, 1233-1267.
- Lengke, M., Southam, G., 2006. Bioaccumulation of gold by sulfate-reducing bacteria cultured in the presence of gold (I)-thiosulfate complex. *Geochimica et Cosmochimica Acta* 70, 3646-3661.

- Lengke, M.F., Southam, G., 2007. The deposition of elemental gold from gold (I)-thiosulfate complexes mediated by sulfate-reducing bacterial conditions. *Economic Geology* 102, 109-126.
- Lespade, P., Marchand, A., Couzi, M., Cruege, F., 1984. Caracterisation de materiaux carbonés par microspectrometrie Raman. *Carbon* 22, 375-385.
- Leventhal, J., Giordano, T., 2000. The nature and roles of organic matter associated with ores and ore-forming systems: An introduction. *Reviews in Economic Geology* 9, 1-26.
- Leventhal, J.S., Daws, T.A., Frye, J.S., 1986. Organic geochemical analysis of sedimentary organic matter associated with uranium. *Applied Geochemistry* 1, 241-247.
- Libes, S., 2011. *Introduction to marine biogeochemistry*. Academic Press.
- Little, S., Vance, D., Walker-Brown, C., Landing, W., 2014. The oceanic mass balance of copper and zinc isotopes, investigated by analysis of their inputs, and outputs to ferromanganese oxide sediments. *Geochimica et Cosmochimica Acta* 125, 673-693.
- Little, S.H., Vance, D., Lyons, T.W., McManus, J., 2015. Controls on trace metal authigenic enrichment in reducing sediments: Insights from modern oxygen-deficient settings. *American Journal of Science* 315, 77-119.
- Little, S.H., Vance, D., McManus, J., Severmann, S., 2016. Key role of continental margin sediments in the oceanic mass balance of Zn and Zn isotopes. *Geology* 44, 207-210.
- Loucks, R.R., Mavrogenes, J.A., 1999. Gold solubility in supercritical hydrothermal brines measured in synthetic fluid inclusions. *Science* 284, 2159-2163.
- Love, L., 1967. Early diagenetic iron sulphide in recent sediments of the Wash (England). *Sedimentology* 9, 327-352.
- Love, L.G., 1964. Early diagenetic pyrite in fine-grained sediments and the genesis of sulphide ores. *Sedimentology and Ore Genesis*, 11-17.

- Love, L.G., 1971. Early diagenetic polyframboidal pyrite, primary and redeposited, from the Wenlockian Denbigh Grit Group, Conway, North Wales, UK. *Journal of Sedimentary Research* 41, 1038-1044.
- Love, L.G., Al-Kaisy, A.T., Brockley, H., 1984. Mineral and organic material in matrices and coatings of framboidal pyrite from Pennsylvanian sediments, England. *Journal of Sedimentary Research* 54, 869-876.
- Lowers, H.A., Breit, G.N., Foster, A.L., Whitney, J., Yount, J., Uddin, M.N., Muneem, A.A., 2007. Arsenic incorporation into authigenic pyrite, Bengal Basin sediment, Bangladesh. *Geochimica et Cosmochimica Acta* 71, 2699-2717.
- Lungwitz, E., 1900. The lixiviation of gold deposits by vegetation. *Engineering and Mining Journal* 69, 500-502.
- Lüniger, G., Schwark, L., 2002. Characterisation of sedimentary organic matter by bulk and molecular geochemical proxies: an example from Oligocene maar-type Lake Enspel, Germany. *Sedimentary Geology* 148, 275-288.
- Luque del Villar, F.J., Pasteris, J.D., Wopenka, B., Rodas, M., Fernández Barrenechea, J.M., 1998. Natural fluid-deposited graphite: mineralogical characteristics and mechanisms of formation. *American Journal of Science* 298, 471-498.
- Luque, F., Ortega, L., Barrenechea, J.F., Millward, D., Beyssac, O., Huizenga, J.M., 2009. Deposition of highly crystalline graphite from moderate-temperature fluids. *Geology* 37, 275-278.

M

- Machel, H., 2001. Bacterial and thermochemical sulfate reduction in diagenetic settings—old and new insights. *Sedimentary Geology* 140, 143-175.
- Machel, H.G., Krouse, H.R., Sassen, R., 1995. Products and distinguishing criteria of bacterial and thermochemical sulfate reduction. *Applied Geochemistry* 10, 373-389.

- MacKenzie, D., Craw, D., Cooley, M., Fleming, A., 2010. Lithogeochemical localisation of disseminated gold in the White River area, Yukon, Canada. *Mineralium Deposita* 45, 683-705.
- MacKinnon, T.C., 1983. Origin of the Torlesse terrane and coeval rocks, South Island, New Zealand. *Geological Society of America Bulletin* 94, 967-985.
- MacLean, L., Pray, T., Onstott, T., Brodie, E., Hazen, T., Southam, G., 2007. Mineralogical, chemical and biological characterization of an anaerobic biofilm collected from a borehole in a deep gold mine in South Africa. *Geomicrobiology Journal* 24, 491-504.
- MacLean, L., Tyliczszak, T., Gilbert, P., Zhou, D., Pray, T., Onstott, T., Southam, G., 2008. A high - resolution chemical and structural study of framboidal pyrite formed within a low - temperature bacterial biofilm. *Geobiology* 6, 471-480.
- Manning, D.A., Gize, A.P., 1993. The role of organic matter in ore transport processes, *Organic Geochemistry*. Springer, pp. 547-563.
- Maréchal, C.N., Nicolas, E., Douchet, C., Albarède, F., 2000. Abundance of zinc isotopes as a marine biogeochemical tracer. *Geochemistry, Geophysics, Geosystems* 1.
- McCall, G.J.H., 1970. The Archean succession to the west of Lake Lefroy.
- McKeag, S., Craw, D., 1989. Contrasting fluids in gold-bearing quartz vein systems formed progressively in a rising metamorphic belt; Otago Schist, New Zealand. *Economic Geology* 84, 22-33.
- McKeag, S., Craw, D., Norris, R., 1989. Origin and deposition of a graphitic schist-hosted metamorphogenic Au-W deposit, Macraes, East Otago, New Zealand. *Mineralium Deposita* 24, 124-131.
- Mees, F., Stoops, G., 2010. Sulphuric and sulphidic materials. Interpretation of micromorphological features of soils and regoliths. Elsevier, Amsterdam, 543-568.
- Melendez, I., Grice, K., Schwark, L., 2013. Exceptional preservation of Palaeozoic steroids in a diagenetic continuum. *Scientific Reports* 3, 2768

- Mernagh, T.P., Bierlein, F.P., 2008. Transport and precipitation of gold in Phanerozoic metamorphic terranes from chemical modeling of fluid-rock interaction. *Economic Geology* 103, 1613-1640.
- Miedaner, M., Migdisov, A., Williams-Jones, A., 2005. Solubility of metallic mercury in octane, dodecane and toluene at temperatures between 100 °C and 200 °C. *Geochimica et Cosmochimica Acta* 69, 5511-5516.
- Miller, J., Blewett, R., Tunjic, J., Connors, K., 2010. The role of early formed structures on the development of the world class St Ives Goldfield, Yilgarn, WA. *Precambrian Research* 183, 292-315.
- Moore, J., Doyle, S., 2015. Resource definition in the world-class Macraes gold mine, New Zealand, Proceedings, PACRIM Congress, AusIMM Publ Series, pp. 557-564.
- Moreau, J., Webb, R., Banfield, J., 2001. The mineralogy and microstructure of sedimentary zinc sulfides formed by bacterial sulfate reduction, AGU Fall Meeting Abstracts, p. 0124.
- Moreau, J.W., Webb, R.I., Banfield, J.F., 2004. Ultrastructure, aggregation-state, and crystal growth of biogenic nanocrystalline sphalerite and wurtzite. *American Mineralogist* 89, 950-960.
- Morse, J., Luther, G., 1999. Chemical influences on trace metal-sulfide interactions in anoxic sediments. *Geochimica et Cosmochimica Acta* 63, 3373-3378.
- Morse, J.W., Arakaki, T., 1993. Adsorption and coprecipitation of divalent metals with mackinawite (FeS). *Geochimica et Cosmochimica Acta* 57, 3635-3640.
- Mortensen, J.K., Craw, D., MacKenzie, D.J., Gabites, J.E., Ullrich, T., 2010. Age and origin of orogenic gold mineralization in the Otago Schist Belt, South Island, New Zealand: Constraints from lead isotope and $^{40}\text{Ar}/^{39}\text{Ar}$ dating studies. *Economic Geology* 105, 777-793.
- Mortimer, N., 1993. Jurassic tectonic history of the Otago schist, New Zealand. *Tectonics* 12, 237-244.

- Mortimer, N., 2000. Metamorphic discontinuities in orogenic belts: example of the garnet-biotite-albite zone in the Otago Schist, New Zealand. *International Journal of Earth Sciences* 89, 295-306.
- Mortimer, N., 2003. A provisional structural thickness map of the Otago Schist, New Zealand. *American Journal of Science* 303, 603-621.
- Mortimer, N., Roser, B., 1992. Geochemical evidence for the position of the Caples–Torlesse boundary in the Otago Schist, New Zealand. *Journal of the Geological Society* 149, 967-977.
- N**
- Nabbefeld, B., Grice, K., Schimmelmann, A., Sauer, P.E., Böttcher, M.E., Twitchett, R., 2010. Significance of δD kerogen, $\delta^{13}\text{C}$ kerogen and $\delta^{34}\text{S}$ pyrite from several Permian/Triassic (P/Tr) sections. *Earth and Planetary Science Letters* 295, 21-29.
- Nemanich, R., Solin, S., 1979. First- and second-order Raman scattering from finite-size crystals of graphite. *Physical Review B* 20, 392.
- Neumayr, P., Walshe, J., Hagemann, S., Petersen, K., Roache, A., Frikken, P., Horn, L., Halley, S., 2008. Oxidized and reduced mineral assemblages in greenstone belt rocks of the St. Ives gold camp, Western Australia: vectors to high-grade ore bodies in Archaean gold deposits? *Mineralium Deposita* 43, 363-371.
- Nguyen, P., Donaldson, J., Ellery, S., 1998. Revenge gold deposit, Kambalda. *Geology of Australian and Papua New Guinean Mineral Deposits*, 233-238.
- Norris, R., Craw, D., 1987. Aspiring Terrane: an oceanic assemblage from New Zealand and its implications for terrane accretion in the southwest Pacific. *Terrane Accretion and Orogenic Belts*, 169-177.

O

- Ohfuji, H., Rickard, D., 2005. Experimental syntheses of framboids—a review. *Earth-Science Reviews* 71, 147-170.

- Ohmoto, H., Kerrick, D., 1977. Devolatilization equilibria in graphitic systems. *American Journal of Science* 277, 1013-1044.
- Oliver, N.H., Cleverley, J.S., Mark, G., Pollard, P.J., Fu, B., Marshall, L.J., Rubenach, M.J., Williams, P.J., Baker, T., 2004. Modeling the role of sodic alteration in the genesis of iron oxide-copper-gold deposits, Eastern Mount Isa block, Australia. *Economic Geology* 99, 1145-1176.
- Ong, H.L., Swanson, V.E., Bisque, R.E., 1970. Natural organic acids as agents of chemical weathering. *Geological Survey Research*, 130-137.
- Ortega, G.S., Pécheyran, C., Hudin, G., Marosits, E., Donard, O.F., 2013. Different approaches of crude oil mineralisation for trace metal analysis by ICPMS. *Microchemical Journal* 106, 250-254.
- Oszczepalski, S., 1999. Origin of the Kupferschiefer polymetallic mineralization in Poland. *Mineralium Deposita* 34, 599-613.
- P**
- Pan, P., Wood, S., 1994. Solubility of Pt and Pd sulfides and Au metal in aqueous bisulfide solutions. *Mineralium Deposita* 29, 373-390.
- Pasteris, J.D., Chou, I., 1998. Fluid-deposited graphitic inclusions in quartz: Comparison between KTB (German Continental Deep-Drilling) core samples and artificially reequilibrated natural inclusions. *Geochimica et Cosmochimica Acta* 62, 109-122.
- Pasteris, J.D., Wopenka, B., 1991. Raman-spectra of graphite as indicators of degree of metamorphism. *Canadian Mineralogist* 29, 1-9.
- Pasteris, J.D., Wopenka, B., 2003. Necessary, but not sufficient: Raman identification of disordered carbon as a signature of ancient life. *Astrobiology* 3, 727-738.
- Paterson, D., De Jonge, M., Howard, D., Lewis, W., McKinlay, J., Starritt, A., Kusel, M., Ryan, C., Kirkham, R., Moorhead, G., 2011. The X-ray Fluorescence Microscopy Beamline at the Australian Synchrotron, The 10th international conference on X-ray microscopy. AIP Publishing, pp. 219-222.

- Paton, C., Hellstrom, J., Paul, B., Woodhead, J., Hergt, J., 2011. Iolite: Freeware for the visualisation and processing of mass spectrometric data. *Journal of Analytical Atomic Spectrometry* 26, 2508-2518.
- Peters, K.E., Walters, C.C., Moldowan, J.M., 2005. *The biomarker guide*. Cambridge University Press.
- Peters, S.G., Jiazhan, H., Zhiping, L., Chenggui, J., 2007. Sedimentary rock-hosted Au deposits of the Dian-Qian-Gui area, Guizhou, and Yunnan Provinces, and Guangxi District, China. *Ore Geology Reviews* 31, 170-204.
- Petrie, B., Craw, D., Ryan, C., 2005. Geological controls on refractory ore in an orogenic gold deposit, Macraes mine, New Zealand. *Mineralium Deposita* 40, 45-58.
- Phillips, G., Evans, K., 2004. Role of CO₂ in the formation of gold deposits. *Nature* 429, 860-863.
- Phillips, G.N., Groves, D.I., 1983. The nature of Archaean gold-bearing fluids as deduced from gold deposits of Western Australia. *Journal of the Geological Society of Australia* 30, 25-39.
- Pitcairn, I.K., Craw, D., Teagle, D.A., 2014a. Metabasalts as sources of metals in orogenic gold deposits. *Mineralium Deposita* 50, 1-18.
- Pitcairn, I.K., Craw, D., Teagle, D.A., 2014b. The gold conveyor belt: Large-scale gold mobility in an active orogen. *Ore Geology Reviews* 62, 129-142.
- Pitcairn, I.K., Olivo, G.R., Teagle, D.A., Craw, D., 2010. Sulfide evolution during prograde metamorphism of the Otago and Alpine schists, New Zealand. *The Canadian Mineralogist* 48, 1267-1295.
- Pitcairn, I.K., Roberts, S., Teagle, D.A., Craw, D., 2005. Detecting hydrothermal graphite deposition during metamorphism and gold mineralization. *Journal of the Geological Society* 162, 429-432.
- Pitcairn, I.K., Teagle, D.A., Craw, D., Olivo, G.R., Kerrich, R., Brewer, T.S., 2006. Sources of metals and fluids in orogenic gold deposits: insights from the Otago and Alpine Schists, New Zealand. *Economic Geology* 101, 1525-1546.

- Plet, C., Grice, K., Pagès, A., Ruebsam, W., Coolen, M., Schwark, L., 2016. Microbially-mediated fossil-bearing carbonate concretions and their significance for palaeoenvironmental reconstructions: A multi-proxy organic and inorganic geochemical appraisal. *Chemical Geology* 426, 95-108.
- Pósfai, M., Dunin-Borkowski, R.E., 2006. Sulfides in biosystems. *Reviews in Mineralogy and Geochemistry* 61, 679-714.
- Prendergast, K., 2007. Application of lithogeochemistry to gold exploration in the St Ives goldfield, Western Australia. *Geochemistry: Exploration, Environment, Analysis* 7, 99-108.
- Pulles, T., van der Gon, H.D., Appelman, W., Verheul, M., 2012. Emission factors for heavy metals from diesel and petrol used in European vehicles. *Atmospheric Environment* 61, 641-651.
- Q**
- Quirico, E., Montagnac, G., Rouzaud, J.-N., Bonal, L., Bourot-Denise, M., Duber, S., Reynard, B., 2009. Precursor and metamorphic condition effects on Raman spectra of poorly ordered carbonaceous matter in chondrites and coals. *Earth and Planetary Science Letters* 287, 185-193.
- Quirico, E., Rouzaud, J.-N., Bonal, L., Montagnac, G., 2005. Maturation grade of coals as revealed by Raman spectroscopy: Progress and problems. *Spectrochimica Acta Part A: Molecular and Biomolecular Spectroscopy* 61, 2368-2377.
- R**
- Radtke, A.S., Scheiner, B.J., 1970. Studies of hydrothermal gold deposition-(pt.) 1, carlin gold deposit, Nevada, the role of carbonaceous materials in gold deposition. *Economic Geology* 65, 87-102.
- Rahl, J.M., Anderson, K.M., Brandon, M.T., Fassoulas, C., 2005. Raman spectroscopic carbonaceous material thermometry of low-grade metamorphic rocks: calibration and application to tectonic exhumation in Crete, Greece. *Earth and Planetary Science Letters* 240, 339-354.

- Reich, M., Kesler, S.E., Utsunomiya, S., Palenik, C.S., Chryssoulis, S.L., Ewing, R.C., 2005. Solubility of gold in arsenian pyrite. *Geochimica et Cosmochimica Acta* 69, 2781-2796.
- Reich, S., Thomsen, C., 2004. Raman spectroscopy of graphite. *Philosophical Transactions of the Royal Society of London. Series A: Mathematical, Physical and Engineering Sciences* 362, 2271-2288.
- Renders, P., Seward, T., 1989. The stability of hydrosulphido- and sulphido-complexes of Au (I) and Ag (I) at 25 °C. *Geochimica et Cosmochimica Acta* 53, 245-253.
- Rickard, D., Luther, G.W., 1997. Kinetics of pyrite formation by the H₂S oxidation of iron (II) monosulfide in aqueous solutions between 25 and 125 °C: the mechanism. *Geochimica et Cosmochimica Acta* 61, 135-147.
- Rickard, D.T., 1970. The origin of framboids. *Lithos* 3, 269-293.
- Rieger, A., Schwark, L., Cisternas, M.-E., Miller, H., 2008. Genesis and evolution of Bitumen in Lower Cretaceous lavas and implications for strata-bound copper deposits, North Chile. *Economic Geology* 103, 387-404.
- Roberts, D., Elias, M., 1990. Gold deposits of the Kambalda-St Ives region. *Geology of the Mineral Deposits of Australia and Papua New Guinea*, 479-491.
- Ryan, C., Clayton, E., Griffin, W., Sie, S., Cousens, D., 1988. SNIP, a statistics-sensitive background treatment for the quantitative analysis of PIXE spectra in geoscience applications. *Nuclear Instruments and Methods in Physics Research Section B: Beam Interactions with Materials and Atoms* 34, 396-402.
- Ryan, C., Cousens, D., Sie, S., Griffin, W., Suter, G., Clayton, E., 1990. Quantitative pxe microanalysis of geological material using the CSIRO proton microprobe. *Nuclear Instruments and Methods in Physics Research Section B: Beam Interactions with Materials and Atoms* 47, 55-71.
- Ryan, C., Etschmann, B., Vogt, S., Maser, J., Harland, C., Van Acherbergh, E., Legnini, D., 2005. Nuclear microprobe-synchrotron synergy: Towards integrated quantitative real-time elemental imaging using PIXE and SXRF.

Nuclear Instruments and Methods in Physics Research Section B: Beam Interactions with Materials and Atoms 231, 183-188.

Ryan, C., Jamieson, D., Churms, C., Pilcher, J., 1995. A new method for on-line true-elemental imaging using PIXE and the proton microprobe. Nuclear Instruments and Methods in Physics Research Section B: Beam Interactions with Materials and Atoms 104, 157-165.

Ryan, C., Kirkham, R., Hough, R., Moorhead, G., Siddons, D., De Jonge, M., Paterson, D., De Geronimo, G., Howard, D., Cleverley, J., 2010a. Elemental X-ray imaging using the Maia detector array: The benefits and challenges of large solid-angle. Nuclear Instruments and Methods in Physics Research Section A: Accelerators, Spectrometers, Detectors and Associated Equipment 619, 37-43.

Ryan, C., Siddons, D., Kirkham, R., Dunn, P., Kuczewski, A., Moorhead, G., De Geronimo, G., Paterson, D., De Jonge, M., Hough, R., 2010b. The new Maia detector system: methods for high definition trace element imaging of natural material, Proceedings of the 20th International Congress. AIP Publishing, pp. 9-17.

Ryan, C., Siddons, D., Kirkham, R., Li, Z., de Jonge, M., Paterson, D., Cleverley, J., Kuczewski, A., Dunn, P., Jensen, M., 2013. The Maia detector array and x-ray fluorescence imaging system: locating rare precious metal phases in complex samples, SPIE Optical Engineering+ Applications. International Society for Optics and Photonics, pp. 88510Q-88510Q-88511.

Ryan, C., Siddons, D., Kirkham, R., Li, Z., de Jonge, M., Paterson, D., Kuczewski, A., Howard, D., Dunn, P., Falkenberg, G., 2014. Maia X-ray fluorescence imaging: capturing detail in complex natural samples, Journal of Physics: Conference Series. IOP Publishing, p. 012002.

S

Sadezky, A., Muckenhuber, H., Grothe, H., Niessner, R., Pöschl, U., 2005. Raman microspectroscopy of soot and related carbonaceous materials: spectral analysis and structural information. Carbon 43, 1731-1742.

- Scholz, F., Neumann, T., 2007. Trace element diagenesis in pyrite-rich sediments of the Achterwasser lagoon, SW Baltic Sea. *Marine Chemistry* 107, 516-532.
- Schoonen, M., Barnes, H., 1991. Reactions forming pyrite and marcasite from solution: I. Nucleation of FeS₂ below 100 °C. *Geochimica et Cosmochimica Acta* 55, 1495-1504.
- Schoonen, M.A., 2004. Mechanisms of sedimentary pyrite formation. *Geological Society of America Special Papers* 379, 117-134.
- Scott, R.J., Meffre, S., Woodhead, J., Gilbert, S.E., Berry, R.F., Emsbo, P., 2009. Development of framboidal pyrite during diagenesis, low-grade regional metamorphism, and hydrothermal alteration. *Economic Geology* 104, 1143-1168.
- Seeley, J.B., Senden, T.J., 1994. Alluvial gold in Kalimantan, Indonesia: A colloidal origin? *Journal of Geochemical Exploration* 50, 457-478.
- Seward, T.M., 1973. Thio complexes of gold and the transport of gold in hydrothermal ore solutions. *Geochimica et Cosmochimica Acta* 37, 379-399.
- Sforna, M., van Zuilen, M., Philippot, P., 2014. Structural characterization by Raman hyperspectral mapping of organic carbon in the 3.46 billion-year-old Apex chert, Western Australia. *Geochimica et Cosmochimica Acta* 124, 18-33.
- Shenberger, D., Barnes, H., 1989. Solubility of gold in aqueous sulfide solutions from 150 to 350 °C. *Geochimica et Cosmochimica Acta* 53, 269-278.
- Shvarov, Y.V., Bastrakov, E., 1999. HCh: a software package for geochemical equilibrium modelling. User's guide. Australian Geological Survey Organisation. *Science and Resources, Record* 25, 61.
- Simoneit, B., Gize, A., 2000. Analytical techniques for organic matter characterization in ore deposits. *Ore genesis and exploration: the roles of organic matter. Reviews in Economic Geology* 9, 27-61.
- Spangenberg, J.E., Macko, S.A., 1998. Organic geochemistry of the San Vicente zinc-lead district, eastern Pucará Basin, Peru. *Chemical Geology* 146, 1-23.
- Spirakis, C.S., 1996. The roles of organic matter in the formation of uranium deposits in sedimentary rocks. *Ore Geology Reviews* 11, 53-69.

- Stefánsson, A., Seward, T., 2003. Stability of chloridogold (I) complexes in aqueous solutions from 300 to 600 °C and from 500 to 1800 bar. *Geochimica et Cosmochimica Acta* 67, 4559-4576.
- Stefánsson, A., Seward, T., 2004. Gold (I) complexing in aqueous sulphide solutions to 500 °C at 500 bar. *Geochimica et Cosmochimica Acta* 68, 4121-4143.
- Sun, W., Li, S., Yang, X., Ling, M., Ding, X., Duan, L.A., Zhan, M., Zhang, H., Fan, W., 2013. Large-scale gold mineralization in eastern China induced by an Early Cretaceous clockwise change in Pacific plate motions. *International Geology Review* 55, 311-321.
- T**
- Taylor, K., Macquaker, J., 2000. Early diagenetic pyrite morphology in a mudstone-dominated succession: the Lower Jurassic Cleveland Ironstone Formation, eastern England. *Sedimentary Geology* 131, 77-86.
- Thomas, H.V., Large, R.R., Bull, S.W., Maslennikov, V., Berry, R.F., Fraser, R., Froud, S., Moye, R., 2011. Pyrite and pyrrhotite textures and composition in sediments, laminated quartz veins, and reefs at Bendigo gold mine, Australia: insights for ore genesis. *Economic Geology* 106, 1-31.
- Titley, S.R., 1991. Phanerozoic ocean cycles and sedimentary-rock-hosted gold ores. *Geology* 19, 645-648.
- Tomkins, A.G., 2010. Windows of metamorphic sulfur liberation in the crust: implications for gold deposit genesis. *Geochimica et Cosmochimica Acta* 74, 3246-3259.
- Tomkins, A.G., 2013. On the source of orogenic gold. *Geology* 41, 1255-1256.
- Tribouillard, N., Algeo, T.J., Lyons, T., Riboulleau, A., 2006. Trace metals as paleoredox and paleoproductivity proxies: an update. *Chemical Geology* 232, 12-32.
- Tsu, R., González H, J., Hernández C, I., 1978. Observation of splitting of the E_{2g} mode and two-phonon spectrum in graphites. *Solid State Communications* 27, 507-510.

Turnbull, I., Mortimer, N., Craw, D., 2001. Textural zones in the Haast Schist—a reappraisal. *New Zealand Journal of Geology and Geophysics* 44, 171-183.

U

Upton, P., Craw, D., 2008. Modelling the role of graphite in development of a mineralised mid-crustal shear zone, Macraes mine, New Zealand. *Earth and Planetary Science Letters* 266, 245-255.

Upton, P., Craw, D., 2014. Modelling of structural and lithological controls on mobility of fluids and gold in orogenic belts, New Zealand. Geological Society, London, Special Publications 402, 231-253.

V

Vallance, J., Cathelineau, M., Boiron, M., Fourcade, S., Shepherd, T., Naden, J., 2003. Fluid–rock interactions and the role of late Hercynian aplite intrusion in the genesis of the Castromil gold deposit, northern Portugal. *Chemical Geology* 194, 201-224.

Vilor, N., 1983. Gold in black shales. *Geochemistry International* 20, 167-176.

W

Wacey, D., Gleeson, D., Kilburn, M., 2010. Microbialite taphonomy and biogenicity: new insights from NanoSIMS. *Geobiology* 8, 403-416.

Wacey, D., Kilburn, M.R., Saunders, M., Cliff, J.B., Kong, C., Liu, A.G., Matthews, J.J., Brasier, M.D., 2015. Uncovering framboidal pyrite biogenicity using nano-scale CN_{org} mapping. *Geology* 43, 27-30.

Wang, Z., Fingas, M., Li, K., 1994. Fractionation of a light crude oil and identification and quantitation of aliphatic, aromatic, and biomarker compounds by GC-FID and GC-MS, part II. *Journal of chromatographic Science* 32, 367-382.

Watson, J., Ellwood, D., 1994. Biomagnetic separation and extraction process for heavy metals from solution. *Minerals Engineering* 7, 1017-1028.

- Watson, J., Ellwood, D., Deng, Q., Mikhalovsky, S., Hayter, C., Evans, J., 1995. Heavy metal adsorption on bacterially produced FeS. *Minerals Engineering* 8, 1097-1108.
- Wedepohl, K.H., 1995. The composition of the continental crust. *Geochimica et Cosmochimica Acta* 59, 1217-1232.
- Wilkin, R., Barnes, H., 1997. Formation processes of framboidal pyrite. *Geochimica et Cosmochimica Acta* 61, 323-339.
- Wilkin, R., Barnes, H., Brantley, S., 1996. The size distribution of framboidal pyrite in modern sediments: An indicator of redox conditions. *Geochimica et Cosmochimica Acta* 60, 3897-3912.
- Williams, G.J., McKee, T.J., 1974. Economic geology of New Zealand: the TJ McKee memorial volume. Australasian Institute of Mining and metallurgy.
- Williams-Jones, A., Migdisov, A., 2007. The solubility of gold in crude oil: implications for ore genesis, Proceedings of the 9th Biennial SGA Meeting, Dublin. Millpress, pp. 765-768.
- Williams-Jones, A.E., Bowell, R.J., Migdisov, A.A., 2009. Gold in solution. *Elements* 5, 281-287.
- Williford, K.H., Grice, K., Logan, G.A., Chen, J., Huston, D., 2011. The molecular and isotopic effects of hydrothermal alteration of organic matter in the Paleoproterozoic McArthur River Pb/Zn/Ag ore deposit. *Earth and Planetary Science Letters* 301, 382-392.
- Wood, S.A., Crerar, D.A., Borcsik, M.P., 1987. Solubility of the assemblage pyrite-pyrrhotite-magnetite-sphalerite-galena-gold-stibnite-bismuthinite-argentite-molybdenite in H₂O-NaCl-CO₂ solutions from 200 °C to 350 °C. *Economic Geology* 82, 1864-1887.
- Woodall, R., 1979. Gold-Australia and the world. Gold mineralization. University of Western Australia, 1-34.
- Wopenka, B., Pasteris, J.D., 1993. Structural characterization of kerogens to granulite-facies graphite: applicability of Raman microprobe spectroscopy. *The American Mineralogist* 78, 533-557.

X**Y**

Yoon, D., Moon, H., Son, Y.-W., Samsonidze, G., Park, B.H., Kim, J.B., Lee, Y., Cheong, H., 2008. Strong polarization dependence of double-resonant Raman intensities in graphene. *Nano Letters* 8, 4270-4274.

Yoon, S.-j., Yáñez, C., Bruns, M.A., Martínez-Villegas, N., Martínez, C.E., 2012. Natural zinc enrichment in peatlands: biogeochemistry of ZnS formation. *Geochimica et Cosmochimica Acta* 84, 165-176.

Yui, T.F., Huang, E., Xu, J., 1996. Raman spectrum of carbonaceous material: a possible metamorphic grade indicator for low-grade metamorphic rocks. *Journal of Metamorphic Geology* 14, 115-124.

Z

Zezein, D.Y., Migdisov, A.A., Williams-Jones, A.E., 2007. The solubility of gold in hydrogen sulfide gas: An experimental study. *Geochimica et Cosmochimica Acta* 71, 3070-3081.

Zezein, D.Y., Migdisov, A.A., Williams-Jones, A.E., 2011. The solubility of gold in H₂O-H₂S vapour at elevated temperature and pressure. *Geochimica et Cosmochimica Acta* 75, 5140-5153.

Zhang, H., Goikolea, E., Garitaonandia, J.S., Ortega, D., Saito, K., Suzuki, K., 2013. A two-step process for preparation of dodecanethiol-capped Au nanoparticles with room-temperature spontaneous magnetization. *New Journal of Chemistry* 37, 2628-2631.

Zhang, J., Lu, J., Zhai, J., Yang, F., 1997. Simulating experiments on enrichment of gold by bacteria and their geochemical significance. *Chinese Journal of Geochemistry* 16, 369-373.

Zhao, Y., Vance, D., Abouchami, W., De Baar, H., 2014. Biogeochemical cycling of zinc and its isotopes in the Southern Ocean. *Geochimica et Cosmochimica Acta* 125, 653-672.

Zhuang, H., Lu, J., Fu, J., Ren, C., Zou, D., 1999. Crude oil as carrier of gold: petrological and geochemical evidence from Lannigou gold deposit in

southwestern Guizhou, China. Science in China Series D: Earth Sciences 42, 216-224.

Zoheir, B., El-Shazly, A., Helba, H., Khalil, K., Bodnar, R., 2008. Origin and evolution of the Um Egat and Dungash orogenic gold deposits, Egyptian Eastern Desert: evidence from fluid inclusions in quartz. Economic Geology 103, 405-424.

Zotov, A., Baranova, N., Dar'yina, T., Bannykh, L., 1991. The solubility of gold in aqueous chloride fluids at 350-500 °C and 500-1500 atm: Thermodynamic parameters of AuCl₂ (aq) up to 750 °C and 5000 atm. Geochemistry International 28, 63-71.

Every reasonable effort has been made to acknowledge the owners of copyright material. I would be pleased to hear from any copyright owner who has been omitted or incorrectly acknowledged.

Appendix A1 Bulk composition of samples from the Otago Schist and Macraes gold deposit

Elements	Au	Al ₂ O ₃	As	BaO	C	CaO	Cl	Co	Cr ₂ O ₃	Cu	Fe	FeO
Units	ppm	%	%	%	%	%	%	%	%	%	%	%
Detection limit	0.01	0.01	0.001	0.005	0.01	0.01	0.002	0.001	0.005	0.001	0.01	0.05
Method	FA25/AA	FB1/XRF	FB1/XRF	FB1/XRF	/CSA	FB1/XRF	FB1/XRF	FB1/XRF	FB1/XRF	FB1/XRF	FB1/XRF	AD71/VOL
Sample numbers												
FF-01	X	13.63	0.001	0.051	0.11	0.24	X	0.003	X	0.001	1.32	1.42
FF-02	X	12.88	0.002	0.035	0.15	0.8	0.002	0.002	X	X	2.64	
FF-03-A	X	17.82	0.001	0.088	0.4	0.35	X	0.002	0.006	0.002	2.9	3.13
FF-03-B	0.03	17.85	0.001	0.08	0.31	0.35	X	0.002	0.006	0.002	2.93	
FF-04	0.14	17.37	0.001	0.072	0.22	1.59	X	0.002	0.006	0.003	3.9	
FF-05	X	11.74	0.001	0.036	0.39	2.51	0.002	0.005	X	X	1.98	
FF-06	X	17.15	0.001	0.075	0.21	1.9	0.002	0.003	0.007	0.003	3.86	4.2
FF-07	X	11.81	0.001	0.038	0.18	1.58	X	0.005	X	X	1.89	2.1
FF-08	X	16.41	0.001	0.101	0.1	2.06	0.003	0.003	X	0.002	3.13	3.21
FF-09	X	17.99	X	0.077	0.16	2.59	0.002	0.002	0.008	0.003	4.28	4.61
FF-10	X	14.18	0.001	0.045	0.09	1.3	X	0.013	0.005	0.001	2.87	
FF-11	0.01	18.92	0.002	0.066	0.21	1.16	X	0.002	0.009	0.002	4.49	5.31

Elements	Au	Al2O3	As	BaO	C	CaO	Cl	Co	Cr2O3	Cu	Fe	FeO
Units	ppm	%	%	%	%	%	%	%	%	%	%	%
Detection limit	0.01	0.01	0.001	0.005	0.01	0.01	0.002	0.001	0.005	0.001	0.01	0.05
Method	FA25/AA	FB1/XRF	FB1/XRF	FB1/XRF	/CSA	FB1/XRF	FB1/XRF	FB1/XRF	FB1/XRF	FB1/XRF	FB1/XRF	AD71/VOL
Sample numbers												
FF-12-A	0.03	16.61	0.002	0.067	0.66	0.34	0.002	0.002	0.005	0.001	3.19	3.73
FF-12-B	X	17.44	0.002	0.068	0.63	0.31	X	0.002	0.006	0.001	3.32	3.91
FF-13	X	12.25	0.003	0.034	3.75	9.34	0.003	0.003	X	0.001	7.97	
FF-14	0.02	17.16	0.001	0.087	0.33	0.28	0.002	0.003	0.005	0.001	2.93	3.04
FF-15	I/S	16.1	0.001	0.072	0.12	1.64	0.002	0.004	0.005	0.003	3.41	3.7
FF-16	X	18.51	0.001	0.077	0.24	1.92	0.002	0.003	0.008	0.005	5.03	5.53
FF-17	0.1	13.93	0.001	0.066	0.07	1.72	X	0.002	X	0.001	2.71	2.62
FF-18	0.04	6.32	0.001	0.01	1.16	5.86	X	0.004	X	X	1.33	
LH-01	I/S	23.08	0.001	0.089	0.32	1.57	X	0.004	0.012	0.004	6.58	
LH-02-A	X	15.74	0.001	0.073	0.05	3.36	X	0.003	X	0.001	3.03	2.52
LH-02-B	0.15	14.47	0.001	0.063	0.06	2.84	X	0.003	X	0.001	2.81	
LH-03-A	X	14.34	0.001	0.056	0.33	3.27	X	0.003	0.009	0.002	4.12	4.29
LH-03-B	0.03	15.42	0.001	0.062	0.22	2.11	X	0.002	0.008	0.003	3.67	3.63
LH-04	X	2.94	0.001	X	0.03	0.11	X	0.01	X	X	0.69	

Elements	Au	Al2O3	As	BaO	C	CaO	Cl	Co	Cr2O3	Cu	Fe	FeO
Units	ppm	%	%	%	%	%	%	%	%	%	%	%
Detection limit	0.01	0.01	0.001	0.005	0.01	0.01	0.002	0.001	0.005	0.001	0.01	0.05
Method	FA25/AA	FB1/XRF	FB1/XRF	FB1/XRF	/CSA	FB1/XRF	FB1/XRF	FB1/XRF	FB1/XRF	FB1/XRF	FB1/XRF	AD71/VOL
Sample numbers												
LH-05-A	X	12.1	0.001	0.035	0.51	3.34	X	0.002	X	0.003	1.89	2.01
LH-05-B	0.03	14.67	0.001	0.061	0.11	1.43	X	0.003	X	0.001	2.08	2.32
LH-06-A	X	13.97	0.001	0.062	0.28	2.69	0.002	0.003	0.007	X	2.43	2.44
LH-06-B	X	14.65	0.001	0.064	0.27	2.76	X	0.003	X	0.001	2.48	2.5
LH-07-A	X	14.84	0.001	0.057	0.18	1.73	X	0.002	0.015	0.001	3.5	
LH-07-B	X	3.49	0.002	X	0.48	1.86	X	0.003	X	X	0.81	1.11
TC-01	I/S	20.58	0.001	0.116	0.45	1.69	X	0.003	0.009	0.003	5.17	
TC-02	X	17.76	0.002	0.067	0.24	1.24	0.002	0.002	0.007	0.002	4.34	
GB-01	X	18.48	0.002	0.059	0.63	0.42	X	0.006	0.007	0.001	3.87	
GB-02	X	16.32	0.002	0.036	0.21	1.34	X	0.003	0.008	0.001	5.14	5.63
GB-03	0.25	2.96	0.229	X	0.48	2.31	X	0.007	X	X	0.24	0.14
GB-04-A	9.17	12.79	2.107	0.053	0.4	0.47	0.002	0.003	0.006	0.001	3.42	
GB-04-B	5.37	15.66	1.248	0.06	0.92	1.64	0.002	0.005	0.007	0.002	2.83	
BLANK 1		0.24	0.002	X	0.03	0.07	0.002	0.004	X	X	0.08	
BLANK 2		0.26	0.002	X	0.04	0.04	0.003	0.005	X	X	0.06	

Elements	Au	Al2O3	As	BaO	C	CaO	Cl	Co	Cr2O3	Cu	Fe	FeO
Units	ppm	%	%	%	%	%	%	%	%	%	%	%
Detection limit	0.01	0.01	0.001	0.005	0.01	0.01	0.002	0.001	0.005	0.001	0.01	0.05
Method	FA25/AA	FB1/XRF	FB1/XRF	FB1/XRF	/CSA	FB1/XRF	FB1/XRF	FB1/XRF	FB1/XRF	FB1/XRF	FB1/XRF	AD71/VOL
Sample numbers												
BLANK 3		0.32	0.002	X	0.04	0.07	0.003	0.005	X	X	0.08	
BLANK 4		0.35	0.002	X	0.03	0.1	X	0.005	X	X	0.11	
BLANK 5		0.62	0.002	X	0.03	0.06	0.002	0.008	X	X	0.21	
BLANK 6		0.02	0.002	X	0.03	X	0.003	0.017	X	X	X	

Elements	Hg	K2O	LOI	MgO	MnO	C-Acinsol	Na2O	Ni	P	Pb	S	S
Units	ppb	%	%	%	%	%	%	%	%	%	%	%
Detection limit	1	0.01	0.01	0.01	0.01	0.01	0.01	0.001	0.001	0.001	0.01	0.001
Method	HG1/CV	FB1/XRF	/TGA	FB1/XRF	FB1/XRF	C71/CSA	FB1/XRF	FB1/XRF	FB1/XRF	FB1/XRF	/CSA	FB1/XRF
Sample numbers												
FF-01	161	2	2.22	0.71	0.02	0.1	2.6	0.001	0.039	0.002	0.03	0.007
FF-02	166	1.09	2.02	1.14	0.04	0.08	3.67	0.001	0.08	0.001	0.03	0.006
FF-03-A	237	3.25	3.23	1.33	0.04	0.4	2.09	0.001	0.059	0.003	0.03	0.009

Elements	Hg	K2O	LOI	MgO	MnO	C-Acinsol	Na2O	Ni	P	Pb	S	S
Units	ppb	%	%	%	%	%	%	%	%	%	%	%
Detection limit	1	0.01	0.01	0.01	0.01	0.01	0.01	0.001	0.001	0.001	0.01	0.001
Method	HG1/CV	FB1/XRF	/TGA	FB1/XRF	FB1/XRF	C71/CSA	FB1/XRF	FB1/XRF	FB1/XRF	FB1/XRF	/CSA	FB1/XRF
Sample numbers												
FF-03-B	255	3.14	3.06	1.36	0.04	0.31	2.33	0.001	0.062	0.003	0.03	0.007
FF-04	108	3.37	3.1	2.09	0.08	0.18	2.68	0.002	0.069	0.004	0.07	0.043
FF-05	32	1.31	2.57	0.94	0.06	0.07	3.65	X	0.034	0.001	0.03	0.01
FF-06	62	3.5	2.84	2.15	0.08	0.2	2.58	0.002	0.123	0.006	0.06	0.038
FF-07	59	1.5	1.67	0.88	0.05	0.06	3.56	X	0.045	0.002	0.05	0.03
FF-08	49	3.4	2	2.01	0.06	0.07	3.52	0.002	0.088	0.004	0.02	0.002
FF-09	73	3.8	3	2.48	0.08	0.16	2.9	0.003	0.079	0.004	0.03	0.009
FF-10	78	1.66	1.91	1.33	0.07	0.04	4.36	0.001	0.049	X	0.03	0.008
FF-11	77	2.68	2.94	2.18	0.1	0.2	3.74	0.003	0.086	0.003	0.02	0.003
FF-12-A	68	2.58	2.96	1.4	0.06	0.66	3.11	0.002	0.064	0.005	0.03	0.009
FF-12-B	76	2.75	3.09	1.46	0.06	0.63	3.18	0.001	0.07	0.005	0.03	0.012
FF-13	264	1.31	12.58	2.3	0.29	2.58	1.57	0.002	0.953	0.001	0.07	0.04
FF-14	347	3.29	3.18	1.34	0.04	0.33	1.87	0.001	0.05	0.002	0.03	0.006
FF-15	88	3.14	2.29	2.02	0.06	0.11	3.09	0.002	0.087	0.004	0.07	0.043

Elements	Hg	K2O	LOI	MgO	MnO	C-Acinsol	Na2O	Ni	P	Pb	S	S
Units	ppb	%	%	%	%	%	%	%	%	%	%	%
Detection limit	1	0.01	0.01	0.01	0.01	0.01	0.01	0.001	0.001	0.001	0.01	0.001
Method	HG1/CV	FB1/XRF	/TGA	FB1/XRF	FB1/XRF	C71/CSA	FB1/XRF	FB1/XRF	FB1/XRF	FB1/XRF	/CSA	FB1/XRF
Sample numbers												
FF-16	87	3.8	3.45	2.51	0.1	0.24	2.06	0.003	0.077	0.005	0.08	0.055
FF-17	18	2.24	1.52	1.25	0.06	0.05	3.71	0.001	0.049	0.003	0.02	0.002
FF-18	24	0.49	5.14	0.76	0.06	0.03	2.28	X	0.015	0.001	0.03	0.01
LH-01	53	4.98	4.23	3	0.14	0.32	2	0.004	0.078	0.006	0.02	0.001
LH-02-A	35	2.65	1.73	1.62	0.07	0.05	3.31	0.001	0.053	0.004	0.02	X
LH-02-B	30	2.22	1.51	1.48	0.07	0.06	3.5	0.001	0.05	0.005	0.03	0.008
LH-03-A	14	2.36	2.77	2.25	0.1	0.18	2.55	0.003	0.087	0.004	0.07	0.038
LH-03-B	11	2.5	2.2	1.92	0.07	0.22	3.38	0.001	0.068	0.003	0.12	0.061
LH-04	6	0.23	0.28	0.31	0.02	0.03	1.12	X	0.016	X	0.02	X
LH-05-A	12	1.31	2.23	0.7	0.06	0.04	4.63	0.001	0.047	0.005	0.29	0.211
LH-05-B	10	2.27	1.62	0.99	0.05	0.06	4.82	X	0.047	0.003	0.04	0.017
LH-06-A	7	2.09	2.25	1.32	0.06	0.07	3.78	0.002	0.043	0.003	0.03	0.008
LH-06-B	4	2.12	2.22	1.35	0.06	0.07	4.04	0.001	0.044	0.003	0.03	0.007
LH-07-A	18	2.66	2.14	1.75	0.07	0.18	3.06	0.004	0.067	0.004	0.03	0.009

Elements	Hg	K2O	LOI	MgO	MnO	C-Acinsol	Na2O	Ni	P	Pb	S	S
Units	ppb	%	%	%	%	%	%	%	%	%	%	%
Detection limit	1	0.01	0.01	0.01	0.01	0.01	0.01	0.001	0.001	0.001	0.01	0.001
Method	HG1/CV	FB1/XRF	/TGA	FB1/XRF	FB1/XRF	C71/CSA	FB1/XRF	FB1/XRF	FB1/XRF	FB1/XRF	/CSA	FB1/XRF
Sample numbers												
LH-07-B	8	0.04	1.73	0.35	0.03	0.02	1.65	X	0.007	0.003	0.02	0.007
TC-01	21	5.29	3.72	2.13	0.09	0.45	1.91	0.002	0.088	0.005	0.02	X
TC-02	19	3.25	2.87	1.83	0.09	0.24	2.93	0.001	0.071	0.004	0.03	0.008
GB-01	36	2.67	3.34	1.85	0.06	0.63	4.4	0.001	0.078	0.003	0.13	0.095
GB-02	23	1.27	3.47	2.97	0.11	0.06	4.21	0.003	0.109	0.002	0.05	0.026
GB-03	21	0.06	1.91	0.05	0.03	0.02	1.65	X	0.012	X	0.16	0.116
GB-04-A	1039	3.85	5.01	1.01	0.01	0.4	0.68	0.002	0.043	0.01	2.19	2.071
GB-04-B	622	3.73	5.5	1.45	0.03	0.42	2.03	0.002	0.05	0.006	1.31	1.304
BLANK 1		0.03	0.15	0.06	X		X	X	0.014	X	0.02	0.004
BLANK 2		0.03	0.15	0.04	X		X	X	0.007	X	0.03	0.002
BLANK 3		0.04	0.17	0.07	X		X	X	0.017	X	0.02	0.002
BLANK 4		0.04	0.2	0.07	X		X	X	0.03	X	0.02	0.003
BLANK 5		0.07	0.23	0.12	X		0.02	X	0.01	X	0.02	0.003
BLANK 6		X	0.09	X	X		X	X	0.001	X	0.02	X

Elements	SiO2	Sn	Sr	TIC	TiO2	Total	V2O5	Zn	Zr
Units	%	%	%	%	%	%	%	%	%
Detection limit	0.01	0.001	0.001	0.01	0.01	0.01	0.005	0.001	0.001
Method	FB1/XRF	FB1/XRF	FB1/XRF	C72/CSA	FB1/XRF	FB1/XRF	FB1/XRF	FB1/XRF	FB1/XRF
Sample numbers									
FF-01	75.91	X	0.014	UA	0.48	99.91	0.009	0.002	0.023
FF-02	73.57	X	0.022	0.07	0.45	99.74	0.01	0.003	0.018
FF-03-A	66.67	X	0.016	UA	0.7	99.96	0.017	0.008	0.027
FF-03-B	66.66	X	0.014	UA	0.69	100	0.017	0.007	0.025
FF-04	63.07	X	0.02	0.04	0.75	100.02	0.021	0.011	0.015
FF-05	73.48	X	0.026	0.27	0.36	99.64	0.007	0.004	0.02
FF-06	63.2	X	0.028	UA	0.74	100.14	0.02	0.011	0.018
FF-07	75.16	X	0.025	0.12	0.6	99.81	0.009	0.004	0.064
FF-08	65.19	X	0.061	UA	0.63	100.22	0.016	0.007	0.021
FF-09	59.8	X	0.037	UA	0.83	99.98	0.024	0.011	0.016
FF-10	69.66	0.002	0.018	0.05	0.57	99.4	0.013	0.005	0.018
FF-11	60.58	0.002	0.013	UA	0.84	99.94	0.022	0.01	0.018
FF-12-A	67.24	X	0.014	UA	0.64	99.82	0.016	0.007	0.022
FF-12-B	65.49	X	0.013	UA	0.67	99.52	0.017	0.007	0.022

Elements	SiO2	Sn	Sr	TIC	TiO2	Total	V2O5	Zn	Zr
Units	%	%	%	%	%	%	%	%	%
Detection limit	0.01	0.001	0.001	0.01	0.01	0.01	0.005	0.001	0.001
Method	FB1/XRF	FB1/XRF	FB1/XRF	C72/CSA	FB1/XRF	FB1/XRF	FB1/XRF	FB1/XRF	FB1/XRF
Sample numbers									
FF-13	45.75	X	0.053	1.17	0.49	99.66	0.014	0.011	0.016
FF-14	67.3	0.002	0.009	UA	0.64	99.59	0.015	0.009	0.018
FF-15	65.3	0.002	0.031	UA	0.68	99.58	0.016	0.009	0.021
FF-16	59.12	0.002	0.027	UA	0.87	99.93	0.024	0.013	0.013
FF-17	70.84	X	0.025	0.02	0.56	99.97	0.015	0.005	0.019
FF-18	76.46	X	0.027	1.13	0.09	99.45	X	0.003	0.002
LH-01	50.23	X	0.019	UA	1.14	100.19	0.031	0.015	0.019
LH-02-A	66.31	0.002	0.04	UA	0.59	100.01	0.014	0.007	0.02
LH-02-B	69.32	0.002	0.036	UA	0.54	100.25	0.013	0.007	0.019
LH-03-A	64.98	X	0.032	0.15	0.73	99.62	0.021	0.009	0.015
LH-03-B	66.3	0.002	0.031	UA	0.62	100.11	0.019	0.008	0.016
LH-04	93.54	X	X	UA	0.03	99.62	X	0.001	X
LH-05-A	72.02	X	0.025	0.47	0.34	99.68	0.007	0.005	0.015
LH-05-B	70.65	X	0.021	0.05	0.49	100.23	0.009	0.005	0.021

Elements	SiO2	Sn	Sr	TIC	TiO2	Total	V2O5	Zn	Zr
Units	%	%	%	%	%	%	%	%	%
Detection limit	0.01	0.001	0.001	0.01	0.01	0.01	0.005	0.001	0.001
Method	FB1/XRF	FB1/XRF	FB1/XRF	C72/CSA	FB1/XRF	FB1/XRF	FB1/XRF	FB1/XRF	FB1/XRF
Sample numbers									
LH-06-A	69.83	0.002	0.035	0.21	0.47	100.19	0.011	0.006	0.014
LH-06-B	68.7	0.002	0.037	0.2	0.49	100.21	0.011	0.006	0.015
LH-07-A	67.82	X	0.019	UA	0.6	99.99	0.019	0.008	0.019
LH-07-B	89.42	X	0.002	0.46	X	99.76	X	0.002	X
TC-01	55.62	0.002	0.023	UA	0.95	99.82	0.024	0.012	0.022
TC-02	62.56	0.002	0.017	UA	0.79	99.85	0.019	0.01	0.018
GB-01	61.92	X	0.007	UA	0.85	99.86	0.019	0.01	0.028
GB-02	62.23	0.002	0.008	0.15	0.9	100.56	0.025	0.01	0.016
GB-03	89.9	X	0.029	0.46	0.08	99.67	X	X	X
GB-04-A	68.98	0.002	0.007	UA	0.57	101.26	0.018	0.007	0.013
GB-04-B	63.26	X	0.014	0.06	0.59	99.85	0.017	0.006	0.015
BLANK 1	99.02	X	X		0.02	99.74	X	X	X
BLANK 2	98.71	X	X		0.01	99.35	X	X	X
BLANK 3	98.54	X	X		0.02	99.37	X	X	X

Elements	SiO2	Sn	Sr	TIC	TiO2	Total	V2O5	Zn	Zr
Units	%	%	%	%	%	%	%	%	%
Detection limit	0.01	0.001	0.001	0.01	0.01	0.01	0.005	0.001	0.001
Method	FB1/XRF	FB1/XRF	FB1/XRF	C72/CSA	FB1/XRF	FB1/XRF	FB1/XRF	FB1/XRF	FB1/XRF
Sample numbers									
BLANK 4	98.36	X	X		0.02	99.37	X	X	X
BLANK 5	97.86	X	X		0.03	99.34	X	X	X
BLANK 6	99.58	X	X		0.02	99.75	X	X	0.002
Legend	X: less then detection limit; UA: unable to Assay.								
Notes	TIC not analysed for when difference between total C and C-Acinsol is 0.01 or less.								
Method code description	/CSA: Induction Furnace Analysed by Infrared Spectrometry; /TGA: No digestion or other pre-treatment undertaken. Analysed by Thermal Gravimetric Analyser; AD71/VOL: Client Specified Digestion or Extraction. Analysed by Volumetric Technique; C71/CSA: Digestion by hot acid(s) and Induction Furnace Analysed by Infrared Spectrometry; C72/CSA: Digestion by hot acid(s) Analysed by Infrared Spectrometry; FA25/AA: 25g Lead collection fire assay. Analysed by Flame Atomic Absorption Spectrometry; FB1/XRF: Fused Disk preparation for XRF analysis Analysed by XRF Spectrometry; HG1/CV: Low temperature Perchloric acid digest specific for Mercury. Analysed by Cold Vapour Generation Atomic Absorption Spectrometry.								
This work was performed by Intertek Genalysis Perth.									

Appendix A2 Sample description of thin sections (the Otago Schist and Macraes gold deposit)

FIDDLERS FLAT

Prehnite-pumpellyite (P-P) facies

Meta-pelite: FF-16, FF-06, FF-09

Petrographic description

This type of samples has relict psammitic texture and relict bedding structure, and consists of fine-grained clasts and cements. Clasts, which are up to 0.05 mm, range from sub-angular to sub-rounded. The main minerals are quartz, albite, muscovite, and stilpnomelane with a small amount of chlorite, apatite, epidote, zircon and pyrite. The cements are mainly very fine grained minerals, e.g. quartz, feldspar clay minerals, and carbonaceous materials (CM). Some meta-pelite is cut by thin quartz veins as well. The following describes the typical features of common clasts.

Quartz is colourless, transparent and angular to sub-rounded with cracks and inclusions on the surface, low relief in plane polarized light (ppl) and white-grey 1st order in cross polarized light (xpl). Some quartz shows embayed texture or sieve texture with apatite, quartz and pyrite inclusions. Quartz size is usually less than 0.05 mm and the mode is approximately 20%.

Albite is also colourless, transparent and sub-angular to sub-rounded, low relief in ppl and white-grey 1st order in xpl. Polysynthetic twinning is sometimes present in thin sections, which is the typical feature of albite. The dirty appearance of some albite grains indicates kaolinization and sericitization occurred. Grainsize is up to 0.05 mm and the albite mode is about 10%.

Muscovite is tabular, colourless, transparent, low relief in ppl. Cleavages can hardly be observed and muscovite is present in the space between other minerals, displaying up to blue 2nd order interference colour in xpl. Most grains have suffered strong

deformation. Some probably co-grew with chlorite. The length of muscovite is about 0.05 mm and the mode is 13 %.

Stilpnomelane is brownish and has a platy habit. It looks quite similar with biotite and is easy to get confused with it. However, biotite usually isn't present at low metamorphic grade and the observation results from secondary electron microscope (SEM) and energy-dispersive spectroscopy (EDS) are consistent with identification of this mineral as stilpnomelane. Stilpnomelane is known to be a typical mineral in the Otago Schist. A faint cleavage, moderate relief in ppl and 1st order yellow or orange in xpl can be observed clearly. This mineral is elongated and fills in the interspace of other minerals. The length along the long axis is up to 0.08 mm and the mode is about 13 %.

Chlorite is pale green, transparent, irregular shaped or bladed, and displays weak pleochroism from transparent to pale green. The highest interference colour in xpl is the first order of yellow but most of the times it appears as inky anomalous 1st order blue. Chlorite sometimes coexists with muscovite or as a replacement of stilpnomelane. Scattered grains are less than 0.05 mm and a mode of 5%.

Epidote is colourless, transparent, anhedral, and has very high relief. The interference colour is up to 2nd order of blue-green. Grain size is about 0.01–0.05 mm and the mode is about 5%.

Apatite is colourless, low relief, tiny and stumpy. Sometimes it is present as inclusions in quartz. The interference colour is grey to black 1st order. Grain size is up to 0.02 mm and the mode is approximately 2%.

Zircon is colourless, transparent but it has very high relief and 3rd to 4th order interference colour, allowing easy identification. The size is about 0.01 mm and the mode is less than 3%.

Pyrite is the main composition of framboids in P-P facies. Framboids is opaque in ppl but bright yellow in reflected light. The single size of pyrite is less than 0.001 mm and the size of framboidal aggregates is up to 0.01–0.15 mm. The mode of framboids is about 3%. Some grains are closely associated with CM.

Chalcopyrite, appearing bright yellow and strong reflectivity in reflected light, sometimes coexists with pyrite and CM. Chalcopyrite grain size is less than 0.001

mm and the tiny grains of chalcopyrite and pyrite form together as framboidal aggregates. The mode of chalcopyrite is about 3%.

The cements are mainly CM, very fine grained and smashed minerals, e.g. quartz, feldspar and clay minerals. Most cement is quartz and feldspar, a small amount of feldspar has suffered sericitization. Clay minerals are very fine-grained, brownish, and irregular, filling in the interspace of clasts. Cement's mode is about 20%.

Among the cements, there are two types of CM in samples. The dominated one (CM 1) is opaque in ppl and grey with low reflectivity in reflected light, which is always rounded or sub-rounded. CM 1 is mainly present in framboidal aggregates as mentioned above. The size of CM 1 is less than 0.02 mm and the mode is about 5%. The second type (CM 2) is also opaque in ppl but light yellow with very low reflectivity in reflected light. It is present interstitial to other minerals as spots or short strips. The mode is up to 3%.

Quartz veins are made up of lots of fine-grained quartz crystals which are less than 0.05 mm. Quartz veins sometimes cut cross each other. The mode is about 3%.

Typical features

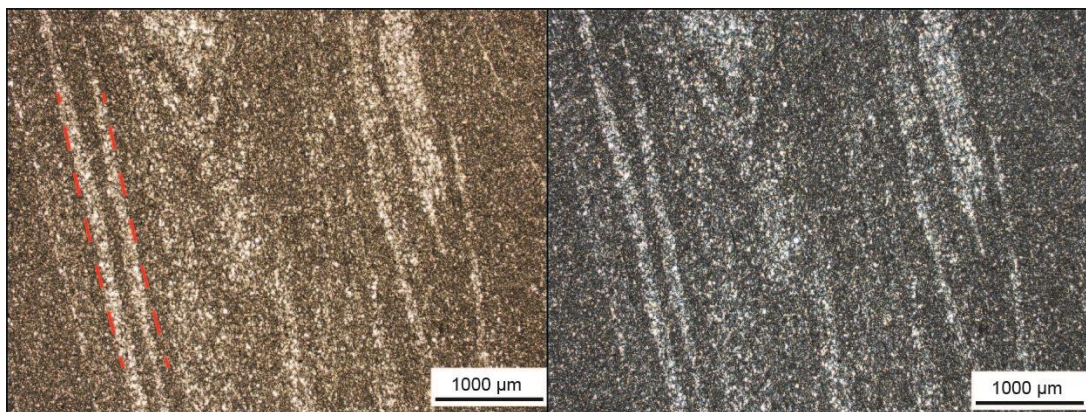
- A. Relict psammitic texture and relict bedding structure;
- B. Sieve texture of quartz with inclusions of quartz, apatite and pyrite;
- C. Muscovite is strongly deformed and coexists with chlorite and stilpnomelane;
- D. Framboidal aggregates of pyrite and chalcopyrite coexist with CM 1;
- E. CM are present as strips (CM 2) or rounded grey spots (CM 1) with sulfide minerals in the interspace between clasts;
- F. Kaolinization and sericitization on albite;
- G. Quartz veins cut through the rocks.

Interpretation

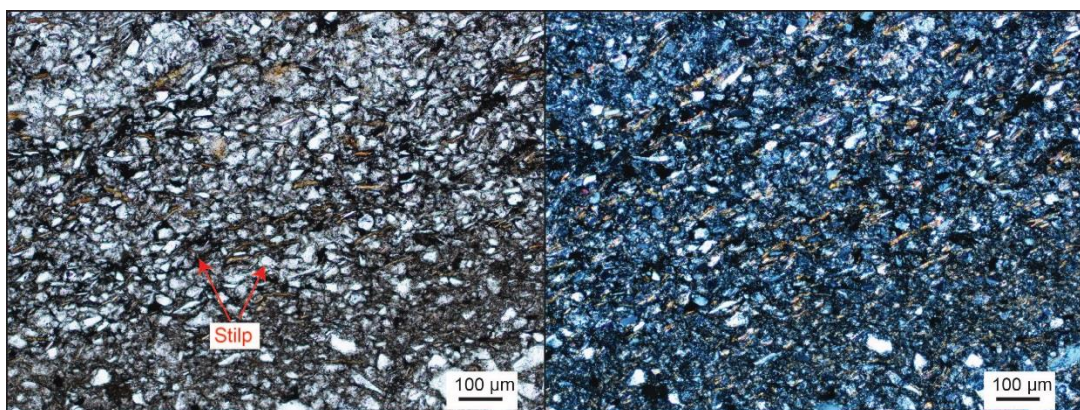
1. Deformation of muscovite may suffer from metamorphism;
2. Quartz veins may result from hydrothermal fluid.

Evolutionary history

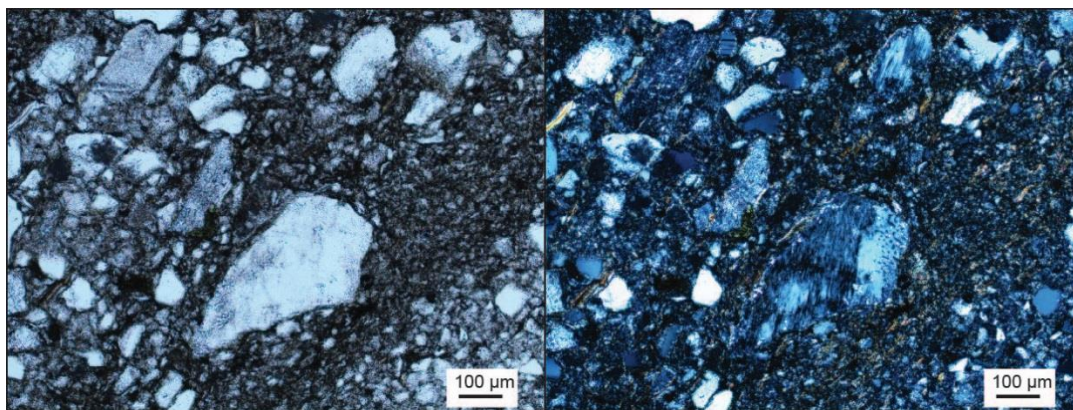
Minerals	Sedimentary	Diagenetic	Metamorphic	Hydrothermal
Quartz				
Albite				
Muscovite				?
Stilpnomelane				?
Chlorite				
Epidote				
Apatite				
Zircon				
Pyrite				?
CM 1				
CM 2				
Quartz veins				

Petrographic photomicrographs

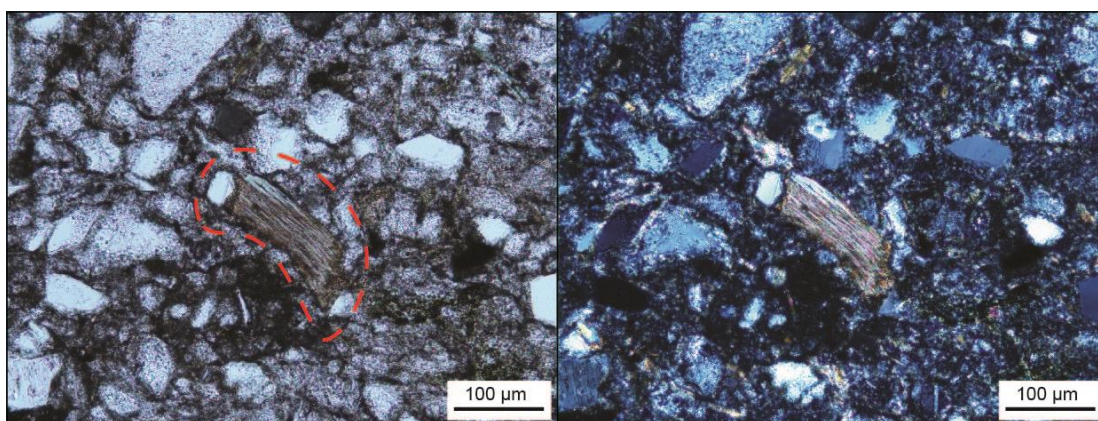
* Blastobedding structure in ppl (left) and xpl (right) (from FF-16).



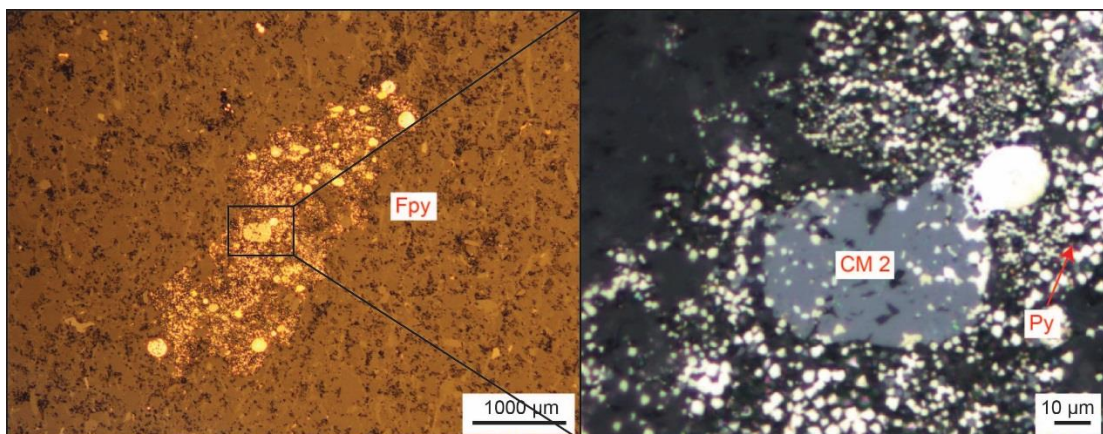
* Blastopsammitic texture and stilpnomelane (Stilp) in ppl (left) and xpl (right) (from FF-06).



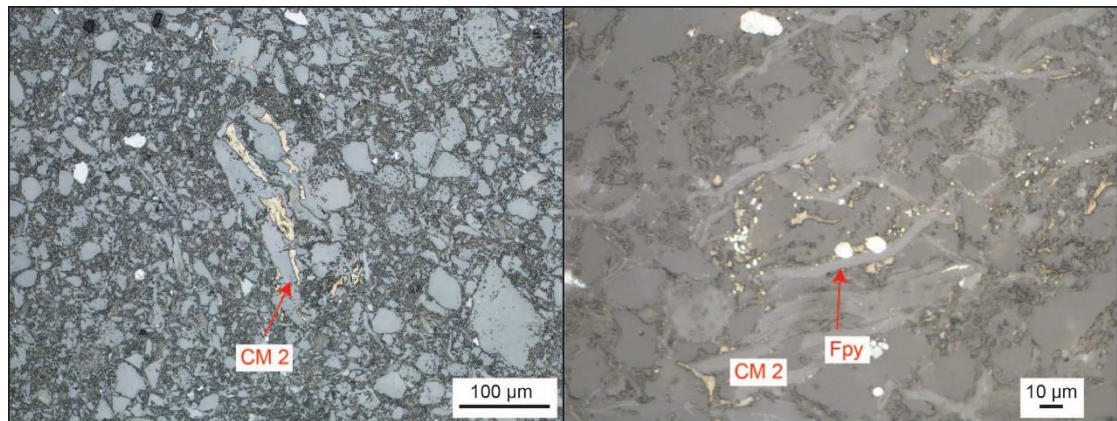
* Twinning of albite in ppl (left) and xpl (right) (from FF-06).



* Muscovite in ppl (left) and xpl (right) (from FF-06).



* Framboidal pyrite in reflected light (left) and CM 1 associated with sulfides within framboids (reflected light, right) (from FF-16).



* CM 2 and its coexistence with framboidal pyrite (Fpy) in reflected light (from FF-06).

Meta-sandstone: FF-15, FF-07

Petrographic description

These two samples have relict psammitic texture and quite weak relict bedding structure. They are made up of clasts and cements, but the clasts are larger than those in pelite. Clasts, which are sub-angular to rounded and up to 0.15 mm, are mainly quartz, albite, muscovite and stilpnomelane with associated minerals being chlorite, apatite, epidote, pyrite and zircon. The cements are made up of very fine grained quartz, feldspar minerals and clay minerals. FF-15 contains coexisting CM and pyrite. FF-17 is cut by thin quartz veins. The following describes the typical features of common minerals.

Quartz is colourless, transparent and angular to sub-rounded with low relief in ppl and white-grey 1st order colours in xpl. It has cracks and inclusions which are apatite and pyrite, resulting in sieve texture. Sometimes aggregates of quartz grains show equiangular grain boundary junctions. Quartz grainsize is usually less than 0.15 mm and the mode is approximately 25%.

Albite is also colourless with some looking dirty on the surface, transparent and sub-angular to sub-rounded, low relief and white-grey 1st order colours in xpl. Clear polysynthetic twinning can be observed in xpl. Sometimes albite is surrounded with sericite. Grainsize is up to 0.15 mm and the albite mode is about 15%.

Muscovite is colourless, transparent, low relief, and strip shape or platy. It has suffered strong deformation and is found in the space between quartz and feldspar with up to blue 2nd order interference colour in xpl. It is about 0.05 mm and the mode of 12%.

Stilpnomelane is brownish and has a tabulate shape, similar to muscovite. A faint cleavage, moderate relief and 1st order orange colours are diagnostic in thin section. Stilpnomelane fills in the interspace between other minerals and coexists with muscovite as a replacement for muscovite. The length along the long axis is up to 0.2 mm and the mode is about 9%.

Chlorite is pale green, transparent, irregular shaped or bladed with weak pleochroism from transparent to pale green in ppl. The interference colour is inky anomalous 1st order blue in xpl. Grainsize is less than 0.08 mm and a mode of 5%.

Epidote is colourless, transparent, anhedral, and has very high relief. The interference colour is up to 2nd order blue-green. Grain size is about 0.1 mm and the mode is about 4%.

Apatite is colourless, low relief and stumpy. Sometimes it is present as inclusions in quartz. The interference colour is grey to black 1st order colours. Grain size is up to 0.05 mm and the mode is approximately 2%.

Zircon is colourless and transparent with very high relief and blue-green 3rd order interference colour, allowing easy identification. The size is about 0.01 mm and the mode is less than 1%.

Pyrite, which is framboidal or cubic in shape, is opaque in ppl but bright yellow in reflected light. Pyrite framboids are more common in FF-15 where it is associated with CM. The size of framboids is about 0.01 mm. Cubic and euhedral pyrite occurs in both samples. Grain size is about 0.01–0.02 mm and the mode is approximately 3%.

Chalcopyrite, which is tiny and less than 0.001 mm, is bright yellow with strong reflectivity in reflected light. It always grew with pyrite and CM in framboids. The mode is about 1%.

The cements comprise CM and very fine grained minerals, e.g. quartz, feldspar, and clay minerals. Clay minerals are very fine grained, brown and fill in the space between clasts. The cement mode is about 20%.

In the matrix, CM 1 and CM 2 both occur in rocks. CM 1 is grey and anhedral in reflected light and closely associated with framboidal aggregates. The size is less than 0.025 mm and mode is about 5%. CM 2 is present as shorts strips and light yellow with very low reflectivity in reflected light. Cubic, anhedral pyrite is observed inside it. The mode is up to 6%.

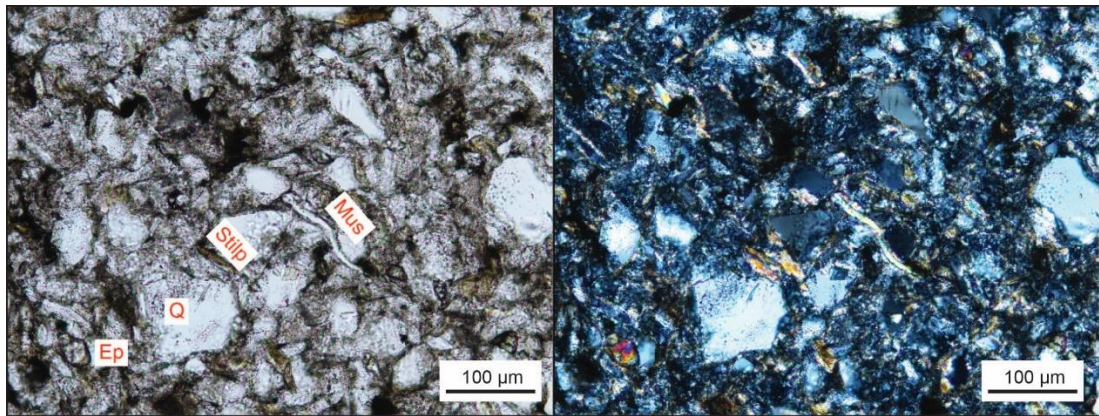
Quartz veins are made up of lots of fine-grained quartz crystals and cut across the whole thin section. The single quartz size is less than 0.1 mm and the mode is about 3%.

Typical features

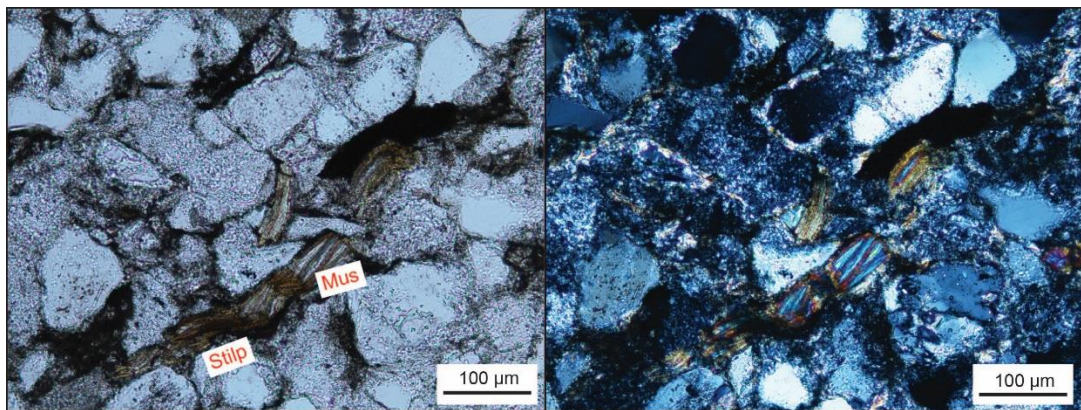
- A. Relict psammitic texture and weak relict bedding structure;
- B. Sieve textured quartz with inclusions of quartz, apatite and pyrite;
- C. Aggregates of quartz grains with equiangular grain junctions;
- D. Muscovite is strongly deformed and coexists with chlorite and stilpnomelane;
- E. Cubic and pyrite framboids coexists with CM 2;
- F. Quartz veins cut through the rocks.

Evolutionary history

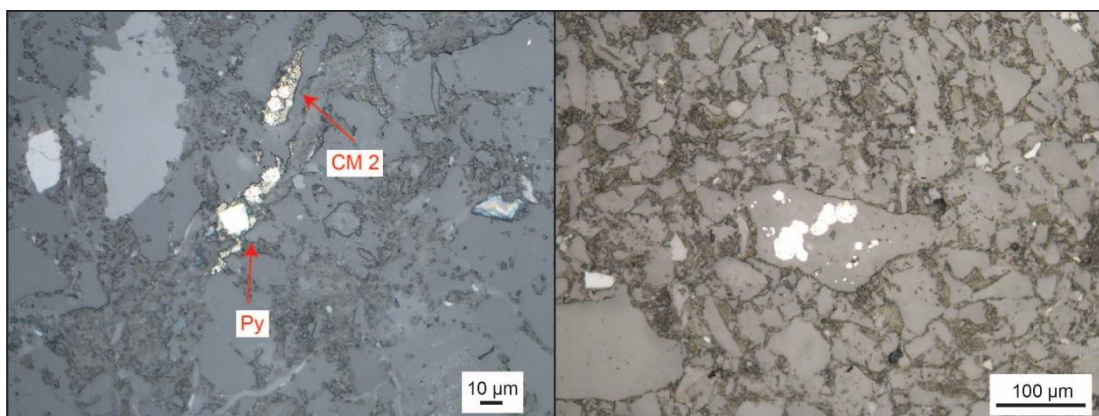
Minerals	Sedimentary	Diagenetic	Metamorphic	Hydrothermal
Quartz				
Albite				
Muscovite				?
Stilpnomelane				?
Chlorite				
Epidote				
Apatite				
Zircon				
Pyrite				?
CM 1				
CM 2				
Quartz veins				

Petrographic photomicrographs

* Relict psammitic texture in ppl (left) and xpl (right) (Q: quartz; Stilp: stilpnomelane; Ep: epidote; Mus: muscovite) (from FF-15).



* Replacement of stilpnomelane (Stilp) by muscovite (Mus) in xpl (left) and ppl (right) (from FF-07).



* CM 2 and its coexistence with framboidal pyrite in reflected light (left); pyrite inclusions in quartz in reflected light (right) (from FF-15).

Pumpellyite-actinolite (P-A) facies**Meta-pelite: FF-04, FF-14, FF-03-A, FF-03-B*****Petrographic description***

These samples have relict psammitic texture but without the relict bedding structure which is common in metapelite of the P-P facies. Metapelite samples consist of fine-grained clasts and finer-grained cements. Clasts are sub-angular to sub-rounded and grains size is up to 0.08 mm. The main minerals are quartz, albite, muscovite, epidote and associated minerals are chlorite, actinolite, stilpnomelane, apatite, zircon and pyrite. The cements are made up of very fine grained minerals, such as quartz, feldspar and clay minerals and carbonaceous material. The following describes typical features of common clasts.

Quartz is colourless, transparent, and angular to sub-rounded with low relief in ppl and 1st order grey in xpl. Epidote, apatite, quartz and muscovite are present as inclusions, giving a sieve-textured appearance. Grainsize is often less than 0.08 mm and the mode is 20%.

Albite is colourless, transparent and sub-angular to sub-rounded, with low relief in ppl and 1st order white-grey in xpl. Common polysynthetic twinning is the diagnostic feature of albite. Some grains appear dirty as a result of kaolinization and sericitization. Cracked grains are common. Grain size is up to 0.07 mm and the mode is about 14%.

Muscovite is tabular or elongate, colourless, transparent, low relief in ppl and up to 2nd order blue in xpl. Most muscovite grains suffered deformation and occur as elongate grains in the interspace of other clasts. Sometimes muscovite co-exists with chlorite. The length of muscovite grains in the long dimension is about 0.07 mm and the mode is 10%.

Epidote is colourless, transparent, anhedral, and has very high relief. The interference colour is up to 2nd order blue-green. Epidote is present as single crystals and aggregates. Single crystal size is less than 0.01 mm and the size of aggregates is up to 0.05 mm. The mode is about 10%.

Actinolite is greenish, irregularly shaped, medium relief and 2nd yellow order interference colour. Cleavages couldn't be observed. The size is about 0.05–0.08 mm and the mode is 8%.

Chlorite is pale green, transparent, irregular shaped or bladed, and displays weak pleochroism from transparent to pale green. The highest interference colour in xpl is first order yellow or inky anomalous blue. Chlorite sometimes cogs with muscovite or stilpnomelane and is often deformed. Chlorite is generally interstitial to other minerals. The grain size is less than 0.05 mm and the mode is 5%.

Stilpnomelane is brownish and elongated but the degree of elongation and absolute grain length is less than the stilpnomelane in P-P facies rocks. The interference colours are up to first order orange in xpl. The length of the long axis is up to 0.03 mm and the mode is about 5%.

Apatite is colourless, low relief, tiny, irregular shaped or stumpy sometimes. It is present as porphyroblasts or inclusions in quartz. Interference colours are 1st order very dark grey to grey. Grain size is up to 0.02 mm and the mode is approximately 2%.

Zircon is colourless and transparent but has very high relief and blue-green 3rd order interference colour, allowing easy identification. The size is about 0.01 mm and the mode is less than 3%.

Pyrite is opaque in ppl but bright yellow in reflected light. Cubic or framboidal pyrite is present in these samples, with a greater proportion in FF-04. Cubic pyrite is sometimes twinned and framboidal pyrite is always associated with CM. The size of cubic or irregular shaped pyrite is about 0.02 mm and the size of framboidal aggregates can be up to 0.015 mm. The mode of pyrite is approximately 4%.

Chalcopyrite, always coexisting with pyrite and CM, appears bright yellow and strong reflectivity in reflected light. Grain size is less than 0.001 mm and chalcopyrite and pyrite form framboidal aggregates together. The mode of chalcopyrite is about 2%.

The cements are mainly CM, very fine grained quartz and feldspar minerals and clay minerals. Clay minerals are very fine-grained, brownish coloured, occurs as irregular patches in between clasts. The cement mode is about 12%.

CM 1 and 2 are also observed in samples, which are quite similar to CM in P-P facies. CM 1 is grey to dark grey, rounded or sub-rounded and strongly associated with tiny pyrite which consist the framboidal aggregates. CM 1 mostly occurs in FF-04 and the mode is about 2%. CM 2 is present as shorts strips and light yellow with very low reflectivity in reflected light. In some samples, framboidal pyrite is intergrown with CM 2. The mode of CM 2 is up to 4%.

Samples are also cut by quartz and carbonate veins. Quartz veins are made up of lots of either fine-grained quartz crystals which are less than 0.001 mm or large quartz crystals which are about 0.1 mm. The mode of quartz veins is around 3%. The carbonate veins mainly consist of calcite, which is colourless and transparent. Calcite has two sets of perfect cleavages of 60° and exhibit very high order creamy interference colours. Sometimes quartz veins grow inside carbonate veins.

Typical features

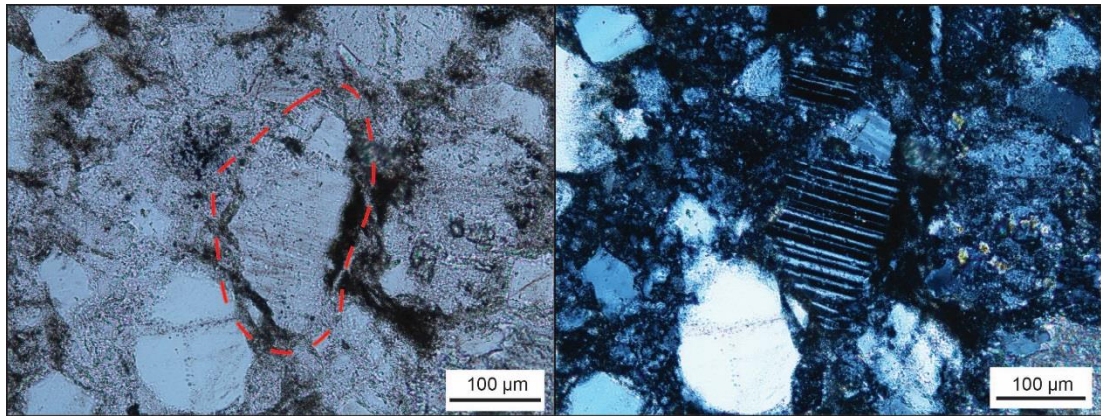
- A. Relict psammitic texture;
- B. Sieve textured quartz with inclusions of epidote, apatite, quartz and muscovite;
- C. Kaolinization and sericitization on albite;
- D. Muscovite is strongly deformed and coexists with chlorite and stilpnomelane;
- E. Cubic and framboidal pyrite coexists with CM;
- F. CM 2 are present as elongate patches in the interspace between clasts and rounded blobs with framboidal pyrite;
- G. Quartz veins and carbonate veins cut through the rocks.

Evolutionary history

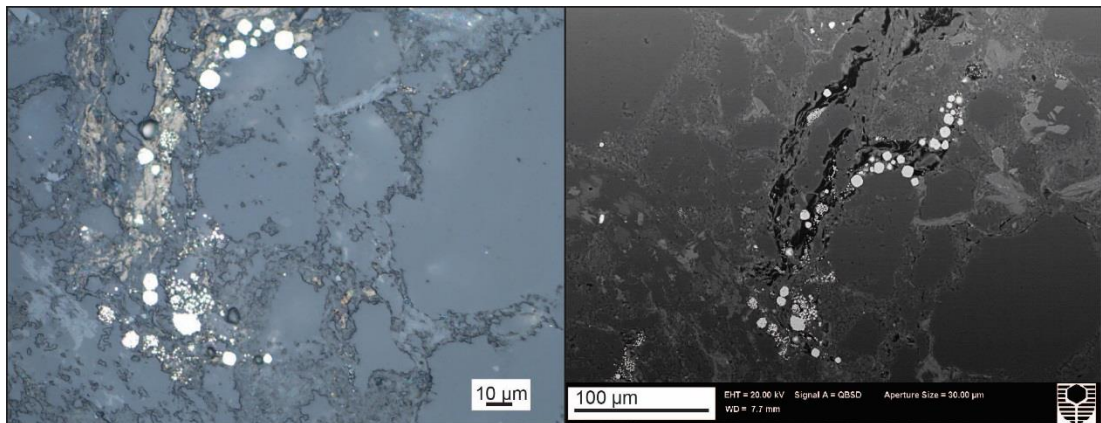
Minerals	Sedimentary	Diagenetic	Metamorphic	Hydrothermal
Quartz				
Albite				
Muscovite				?
Epidote				
Actinolite				
Chlorite				
Stilpnomelane				?
Apatite		?		
Zircon				

Pyrite				?
CM 1				
CM 2				
Quartz veins				
Carbonate veins				

Petrographic photomicrographs



* Polysynthetic twinning of albite in ppl (left) and xpl (right) (from FF-04).



* Framboidal pyrite coexist with CM 2 in reflected light (left) and backscattered electron (BSE) images (from FF-04).

Carbonaceous pelite: FF-13

Petrographic description

This sample, which contains abundant of CM, is referred as a carbonaceous pelite. The mineral assemblage is similar to that in other pelite samples, comprising quartz, albite, clay minerals, carbonate minerals and very fine grained cement.

Quartz is colourless, transparent, and sub-angular to angular, low relief and with 1st order white-grey birefringence. Some quartz contains inclusions of cubic pyrite.

Quartz grain size is 0.1–0.2 mm and the mode is about 8%.

Albite is colourless, transparent, and sub-angular to angular with a slight brownish dirty colour on from alteration and kaolinization. Twinning cannot be observed but this mineral can be identified as albite with SEM and EDS. The size is up to 0.1–0.2 mm and the mode is about 7%.

CM 2 is widespread in this sample and is consistent with the high carbon content from bulk composition analysis and SEM-EDS results. CM 2 is opaque in ppl and yellow with low reflectivity in xpl. The shape of CM 2 is amorphous. Some CM 2 forms elongated grains, and occurs interstitial to silicate minerals, the texture may reflect migration of CM. Some grains are up to 0.1 mm and are strongly associated with carbonate veins. The mode of CM is about 10%.

Most pyrite is present as inclusions in quartz where it occurs as euhedral pyrite with cubic shape or as anhedral pyrite. Pyrite is opaque in transmitted light but bright yellow in reflected light. A small amount of pyrite is associated with CM 2. The size of pyrite is less than 0.03 mm and the mode is about 5%.

The carbonate veins mainly consist of calcite aggregates, which are colourless and transparent. Carbonate is spread widely in the sample and two sets of cleavages and very high order creamy interference colours are observed. The mode of carbonate veins is about 20%.

Typical features

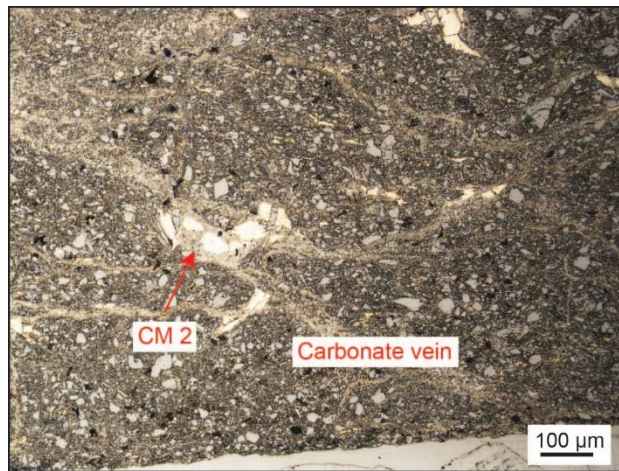
- A. There is large amount of CM 2 and very fine-grained material;
- B. Some pyrite is associated with CM 2;
- C. CM 2 is closely associated with carbonate veins.

Interpretation

1. CM 2 is supposed to deposit from carbonic bearing hydrothermal fluids.

Evolutionary history

Minerals	Sedimentary	Diagenetic	Metamorphic	Hydrothermal
Quartz				
Albite				
Pyrite				?
Carbonate Veins				
CM 2				
Quartz Veins				

Petrographic photomicrographs

* CM 2 occurs with carbonate vein in reflected light (from FF-13)

Meta-sandstone: FF-05, FF-02, FF-01***Petrographic description***

Meta-sandstone in P-A facies has larger grains than that at lower grades and more quartz and feldspar. These samples still have relict psammitic texture and a weak relict bedding structure, and comprise clasts and cements. Clasts, which are up to 0.2 mm and sub-angular to sub-rounded, are made up of quartz, albite, muscovite, chlorite, stilpnomelane, epidote, actinolite with small amount associated accessory minerals, such as apatite, titanite, zircon and pyrite. The cement consists of CM, quartz, feldspar and clays. Samples are penetrated by carbonate veins and quartz veins, especially FF-02 and FF-05. The following is a description of the typical features of common clasts.

Quartz is colourless, transparent, and angular to sub-rounded with low relief in ppl and first order white-grey birefringence in xpl. Sometimes quartz has inclusions of apatite, pyrite, quartz and muscovite which give the grains a sieve-like texture. Quartz aggregates are made of lots of small quartz grains with equiangular grain junctions. The larger quartz grains are usually less than 0.2 mm and the quartz aggregates are about 0.1–0.15 mm. The quartz mode is approximately 30%.

Albite is colourless, transparent and sub-angular to sub-rounded, with low relief in ppl and 1st order white-grey in xpl. Polysynthetic twinning is the feature of albite. Twin lamellae sometimes wedge out within grains or appear kinked. Kaolinization and sericitization gives albite a slightly dirty appearance in ppl and altered areas are 1st order orange in xpl. Some albite is surrounded with sericite, which also occurs as inclusions in albite. Albite grain size is up to 0.2 mm and the albite mode is about 15%.

Muscovite is colourless, transparent, low relief, and tabulate or elongate shaped. It always appears to have been deformed slightly and displays interference colour up to 2nd order blue in xpl. Muscovite is sometimes present as tabulate but most of it occurs as deformed laths interstitial to quartz and albite. Muscovite grains also coexist with chlorite. The typical grain size is about 0.05 mm and the muscovite mode is 8%.

Chlorite is pale green, transparent, irregular shaped or bladed with weak pleochroism from transparent to pale green in ppl. Interference colour are 1st order yellow or anomalous inky blue in xpl. In some parts, chlorite coexists with or gets replaced by muscovite and stilpnomelane. Chlorite grain size is about 0.05 mm and the chlorite mode is 8%.

Stilpnomelane is brownish and lath shaped, with 1st order orange interference colour and with generally quite similar appearance to biotite. Cleavages are rarely observed and most stilpnomelane occurs interstitially to other minerals. Chlorite is replaced by stilpnomelane in some cases. The length of the long axis of grains is about 0.02–0.03 mm and the stilpnomelane mode is about 8%.

Epidote is colourless, transparent, diamond or irregularly shaped with very high relief and up to high 3rd order birefringence. The size of the mineral is about 0.05 mm to 0.1 mm. The mode of scattered epidote is about 5%.

Actinolite is greenish, irregularly shaped, with medium relief and 2nd orange interference colour. One set of cleavage can be observed. Grain size is about 0.05–0.08 mm and the mode is around 3%.

Apatite is colourless, tiny and stumpy. The interference colour is 1st order grey to black. Grain size is less than 0.08 mm. The mode is approximately 3%.

Titanite is colourless, transparent, irregularly shaped with very high relief and 3rd order blue-green interference colour. The grain size is about 0.05 mm and the mode is around 3%.

Zircon is colourless, transparent with very high relief and 3rd order orange to red interference colour. Grain size is about 0.08 mm and the mode is less than 2%.

Pyrite is opaque in transmitted light and bright yellow in reflected light. It appears as cubic crystals or irregular shaped grains. Grain size is up to 0.05 mm and the mode is about 1%.

The cements, which make up a smaller proportion in samples than those in meta-pelite of P-A facies, are mainly CM, clay minerals, and very fine grained minerals, e.g. quartz and feldspar. Clay minerals are very fine grained, brownish and occur interstitial to larger clasts. The cement mode is about 10%.

CM 2 is opaque in ppl and light yellow with very low reflectivity in xpl. It occurs as spotty patches which are about 0.01 mm or short elongate tabular grains interstitial to clasts whose long side is about 0.015 mm. The mode is about 4%.

Samples are cut through by quartz veins or carbonate veins. Quartz veins are made up of lots of fine-grained quartz crystals which are about 0.05 mm and penetrate the whole thin section. Carbonate veins mainly consist of calcite aggregates, which are colourless and transparent. Two sets of perfect cleavages and very high order creamy interference colours are observed. The mode of veins is about 4%.

Typical features

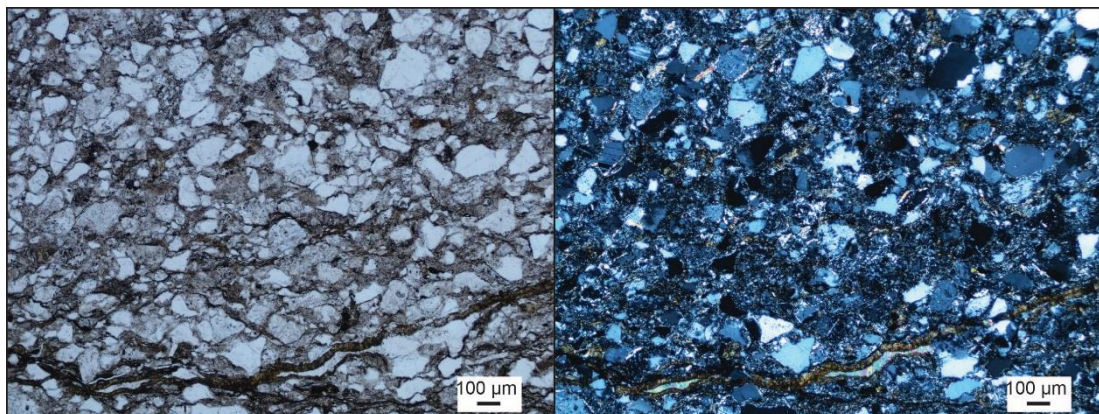
A. Relict psammitic texture;

- B. Sieve textured quartz with inclusions of apatite, pyrite, quartz and muscovite;
- C. Quartz aggregates with equiangular grain junctions;
- D. Kinked and wedged out polysynthetic twinning in albite
- E. Kaolinization and sericitization on albite;
- F. Muscovite is strongly deformed and coexists with chlorite and stilpnomelane;
- G. CM 2 is present as lath-shaped patches interstitial to other clasts;
- H. Quartz veins and carbonate veins cut through samples.

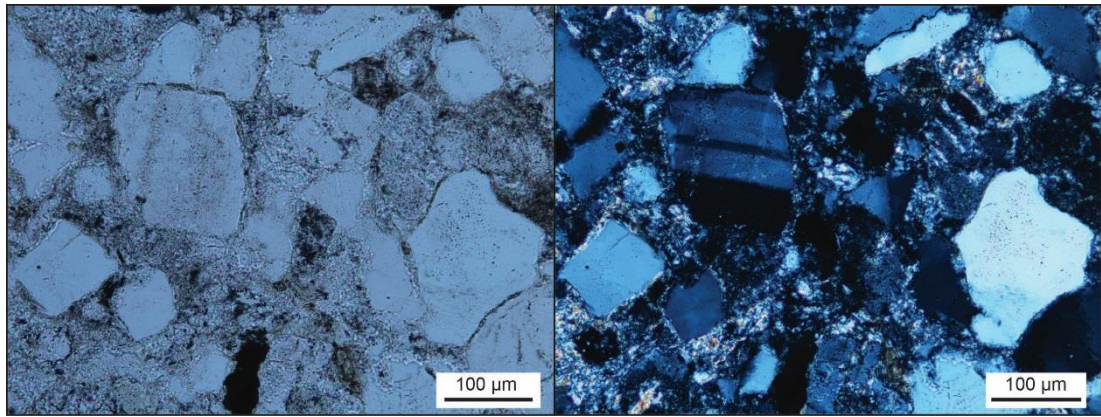
Evolutionary history

Minerals	Sedimentary	Diagenetic	Metamorphic	Hydrothermal
Quartz				
Albite				
Muscovite				?
Chlorite				
Stilpnomelane				?
Epidote				
Actinolite				
Apatite	?	?		
Titanite				
Zircon				
Pyrite			?	?
CM 2				
Quartz veins				
Carbonate veins				

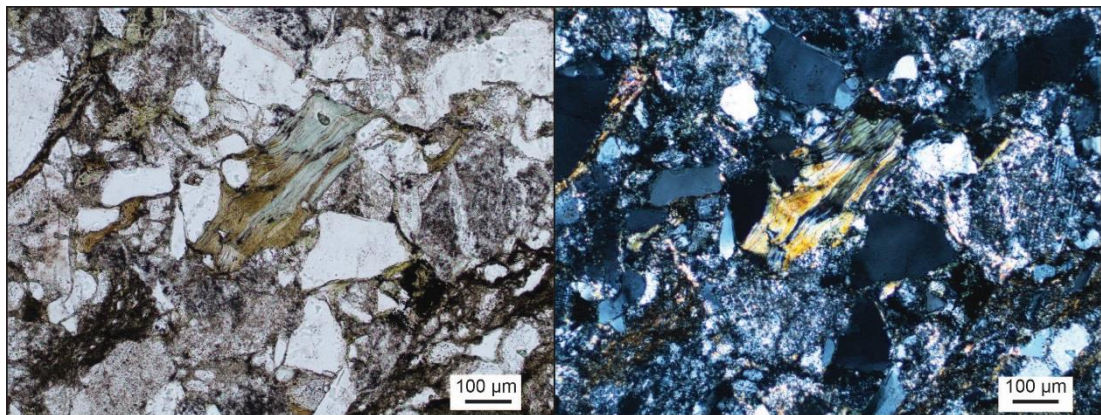
Petrographic photomicrographs



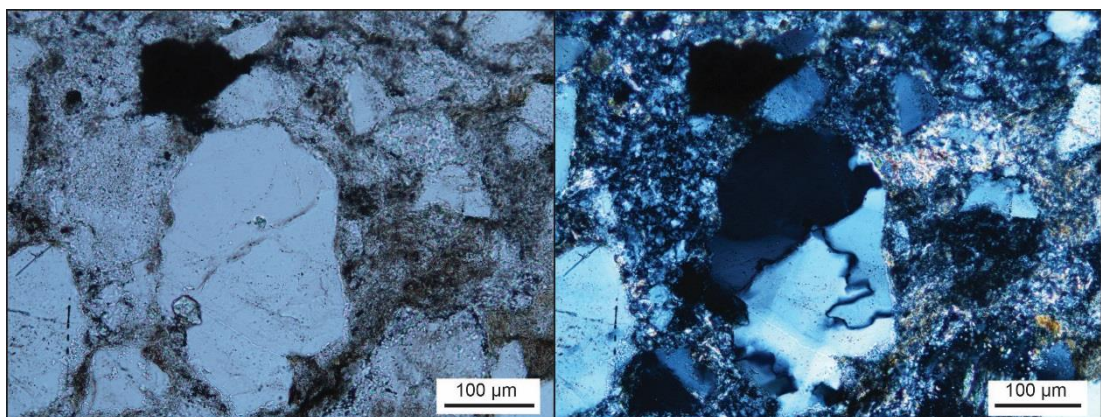
* Blastopsammitic texture in ppl (left) and xpl (right) (from FF-01).



* Twinning of Albite with alteration in some parts and sericitization in matrix in ppl (left) and xpl (right) (from FF-01).



* Replacement of chlorite by muscovite in ppl (left) and xpl (right) (from FF-02).



* Quartz aggregates in ppl (left) and xpl (right), may be resulted from pressure resolution (from FF-01).

Sub-greenschist

Meta-sandstone: FF-10, FF-17 (Quartz-augen schist)

Petrographic description

These samples are metamorphosed to sub-greenschist facies, which occurs between actinolite-pumpellyite facies and greenschist facies. The samples have a weak schistose structure but also retain obvious bedding structure. On the microscale, they exhibit augen structures and weak lepidoblastic textures. Relict bedding structures are defined by variations in the mode of quartz, and lepidoblastic textures involved large amounts of platy minerals, such as muscovite, sericite and chlorite. The quartz-dominated bedding consists of fine grained quartz aggregates, muscovite, chlorite, sericite and epidote. The less quartz-rich beds blastobedding consists of finer-grained minerals with a small amount of quartz, chlorite, sericite and epidote. Augen structures are mostly formed by quartz and albite.

Quartz is colourless, transparent, with elongate or augen shape with low relief in ppl and 1st order white-grey interference in xpl. Quartz also contains apatite, pyrite and quartz inclusions which are always aligned to the foliation. Quartz has pressure shadows which contain chlorite and/or muscovite. The length along the long axis is up to 0.5 mm and the mode is about 40%.

Albite is also colourless, transparent, with elongate or augen shape and a slight brownish colour caused by kaolinization and other alteration. Polysynthetic twinning can easily be observed in xpl. The direction of long axis of albite is aligned with the weak foliation. The grain size is up to 0.2 mm and the mode is about 15%.

The aligned minerals forming the foliation are mainly muscovite, chlorite and some fine-grained clay minerals.

Muscovite is colourless, transparent, low relief and present as needle-shaped or fibrous crystals. It always coexists with chlorite. The interference colour is up to 2nd order blue. The mode of muscovite is about 15%.

Chlorite is greenish, transparent, low relief and present as needle-shaped or fibrous crystals. It always coexists with muscovite. It has 1st order grey or inky anomalous. The chlorite mode is 10%.

Some clay minerals are light brownish to dark and irregularly shaped, some of which have suffered sericitization. The mode is about 10%.

Other minerals, including epidote, apatite, zircon and pyrite, are sporadically distributed in thin section with a total quantity of 15%.

Epidote is colourless, transparent, irregular, high relief with very high interference colour up to 2nd order blue-green. The scattered epidote is about 0.05–0.1 mm and mode of 4%.

Apatite is colourless, tiny and irregular or elongate. The interference colour is 1st order grey to black. Apatite always appears as inclusions in quartz or albite. Grain size is approximately 0.02–0.05 mm and the mode is 2%.

Titanite is colourless, transparent, irregular, very high relief and 3rd orange order interference colour. The size is about 0.05 mm and the mode is 2%.

Siderite is opaque in transmitted light but bright yellow in reflected light. It always coexists with rutile.

Rutile is dark reddish brown in transmitted light but bright yellow in reflected light. It always coexists with siderite. The grain size of siderite plus rutile assemblage is about 0.1 mm and the mode is around 3%.

Zircon is colourless, transparent with very high relief and high interference colour. Zircon is about 0.03–0.05 mm and the mode is less than 1%.

Pyrite mostly occurs as euhedral pyrite with cubic shaped crystals but may also be anhedral. Pyrite is opaque in transmitted light but bright yellow in reflected light. Some grains are associated with carbonate veins. Pyrite grain size is about 0.01 mm and the mode is about 3%.

CM in these two samples is rare, but CM 2 is present (less than 2%).

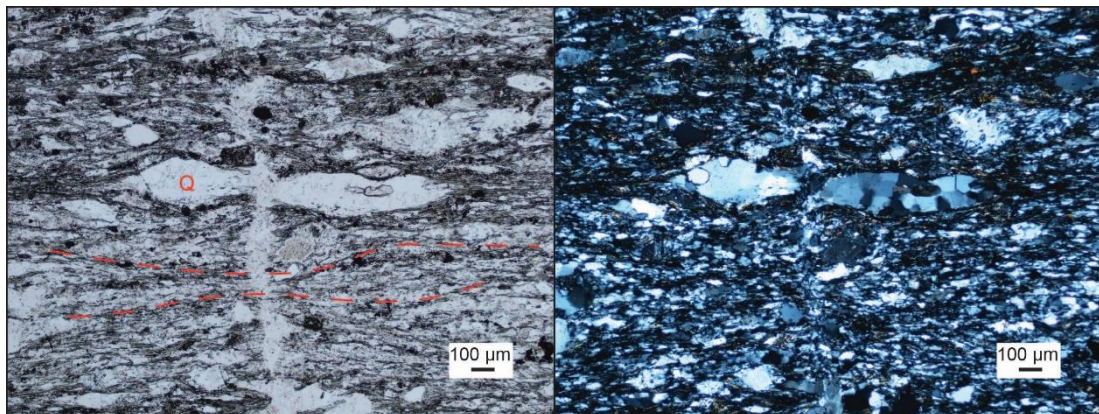
Veins are mainly quartz veins and carbonate. The quartz veins, made up of quartz aggregates, cross cut the whole foliation, Grain size of single crystal is less than 0.1 mm. The carbonate veins mainly consist of calcite, which is colourless and transparent. It is spread widely in samples and two sets of cleavages and very high order creamy interference colours are present.

Typical features

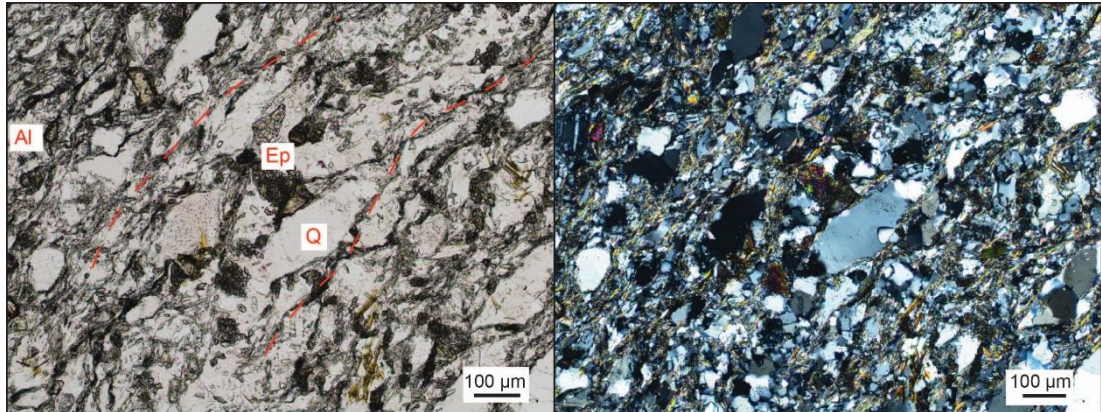
- A. Macro structure: weak schistose structure and obvious relict bedding structure;
 Micro structure: clear augen structure and weak lepidoblastic texture;
- B. The augen-shaped minerals, quartz and albite, are aligned with the foliation;
- C. Pressure shadow structures around quartz that host micas;
- D. The coexistence of muscovite and chlorite;
- E. The coexistence of rutile and siderite;
- F. Cubic or anhedral pyrite which is associated with CM 2;

Evolutionary history

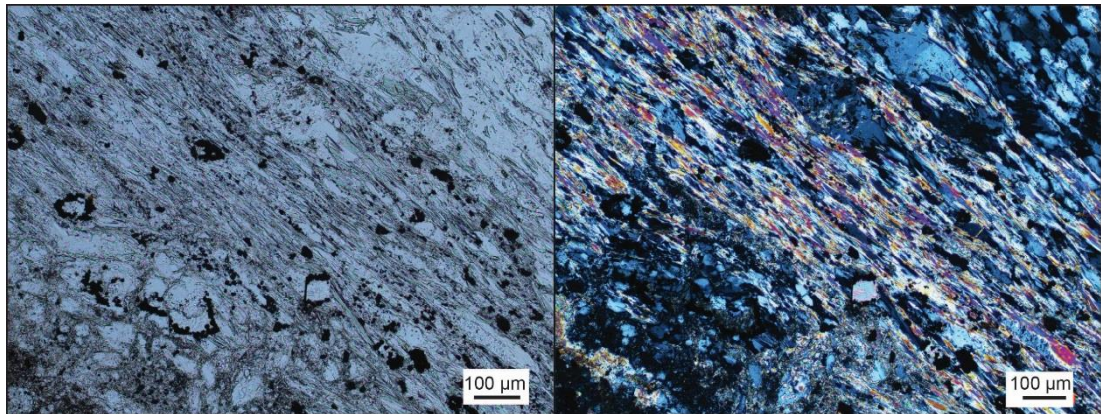
Minerals	Sedimentary	Diagenetic	Metamorphic	Hydrothermal
Quartz				
Albite				
Muscovite				?
Chlorite				?
Epidote				
Apatite				
Zircon				
Siderite				?
Rutile				?
Pyrite				?
Carbonate Veins				
Quartz Veins				
CM 2				

Petrographic photomicrographs

* Weak schistose structure and augen structure in ppl (left) and xpl (right) (Q: quartz) (from FF-10) .



* Weak schistose structure and augen structure in ppl (left) and xpl (right) (Q: quartz; Ab: albite; Ep: epidote) (from FF-17).



* Lepidoblastic texture in some parts in ppl (left) and xpl (right) (from FF-10).

Greenschist

Meta-pelite: FF-11, FF-12-A, FF-12-B (Chlorite Schist)

Petrographic description

These samples, which belong to greenschist facies, exhibit obvious schistose structure and lepidoblastic textures while in some parts retaining a relict bedding structure. The relict bedding structure is defined by a slight difference in the content of quartz and very fine-grained materials, suggesting that the protolith is fine-grained clastic sedimentary rock with micro bedding structure (less than 0.08 mm). The lepidoblastic texture contains interbedded black bands, which consist of very fine-

grained smashed materials, CM and fine-grained platy minerals, such as muscovite, sericite and chlorite. The band structure and aligned lamellar minerals are interleaved with elongated quartz, albite and muscovite and epidote, which are approximately 0.05–0.1 mm. Some quartz and feldspar grains occur as augen-shapes with muscovite grains in the pressure shadows structure.

Quartz is colourless, transparent, elongated or augen shaped with cracks and inclusions. It is present as low relief and has 1st order white-grey birefringence. Some quartz contains apatite, pyrite and quartz-felspathic inclusions which are always aligned to the foliation. Sometimes quartz displays undulate extinction. The length of the long axis of single crystal quartz grains is up to 0.05 mm and the length of smaller grains in quartz aggregates ranges from 0.1–0.15 mm. The quartz mode is about 20%. The direction of long axis of quartz augen is always aligned with foliation.

Albite often co-grows with quartz in thin sections and has a similar shape, size, colour and other identification features with quartz. However, the presence of polysynthetic twinning distinguishes albite and observation with SEM and EDS confirmed twinned grains to be albite. The grain size of albite is up to 0.05 mm and the mode is 5%. The long axis of albite augen is aligned with the foliation.

Epidote is colourless, transparent, and irregular, with high relief and interference colours up to 2nd–3rd order interference colours. The grain size is about 0.05 mm the mode is about 5%.

Apatite is colourless, tiny and irregular or elongated, and always appears as inclusions in other minerals. The interference colour is 1st order grey to black. Apatite is approximately 0.02–0.05 mm and the mode is 3%.

Zircon is colourless, transparent with very high relief and 3rd blue-green interference colours. It is about 0.03–0.05 mm and less than 2%.

Muscovite occurs in patches, is colourless, transparent, low relief, and augen shaped with weak cleavages. Interference colour is up to 2nd order blue in xpl. In some muscovite, the orientation of cleavages is perpendicular to the foliation. It is sometimes replaced by chlorite which is colourless, transparent, low relief but also

low interference colour of 1st inky-grey. Muscovite is about 0.08 mm and the mode is around 5%.

The aligned minerals forming the foliation are mainly muscovite, chlorite and some clay minerals.

Muscovite is colourless, transparent, low relief and present as needle-shaped or fibrous crystals. It always coexists with chlorite. The interference colour is up to 2nd order blue-green. Grain size is less than 0.08 mm and the mode is about 20%.

Chlorite is pale green, transparent, low relief and present as needle-shaped or fibrous shape. It always coexists with muscovite. It has low interference colour, as 1st order grey or inky anomalous. Grain size is less than 0.08 mm and the mode is 20%.

Some clay minerals are light brownish to dark, irregular and some have been altered into sericitization. The mode is about 5%.

Pyrite mostly appears as cubic or euhedral pyrite but a small amount looks like framboidal pyrite, which is quite unusual at this metamorphic grade. Some pyrite is closely related with CM. It is less than 0.01 mm and about 3%.

Chalcopyrite is anhedral, opaque in transmitted light but much brighter yellow than pyrite in reflected light. It is found as “framboidal” shaped grains, coexisting with CM. The size is about 0.01 mm and the mode is about 1%.

Galena is cubic or anhedral, opaque in ppl and light white in reflected light. It coexists with pyrite, chalcopyrite and carbonaceous minerals. The size is about 0.01 mm and the mode is about 1%.

CM 2 is present in these samples, as described at low metamorphic grade. It is opaque in ppl and light yellow with low reflectivity in xpl. It appears as relatively large fragments (~0.1 mm) include in quartz or as smaller fragments (~0.03–0.05 mm) spread along the black bands with other very fine-grained minerals which are regarded as smashed materials. The mode is about 5%.

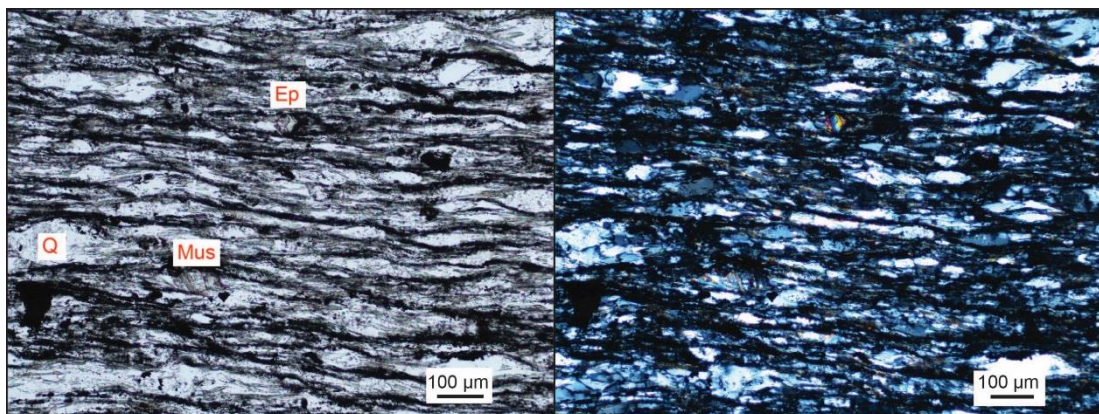
The carbonate veins mainly consist of calcite, which is colourless and transparent. Two sets of perfect cleavages of 60° and very high order creamy interference colours are present.

Typical features

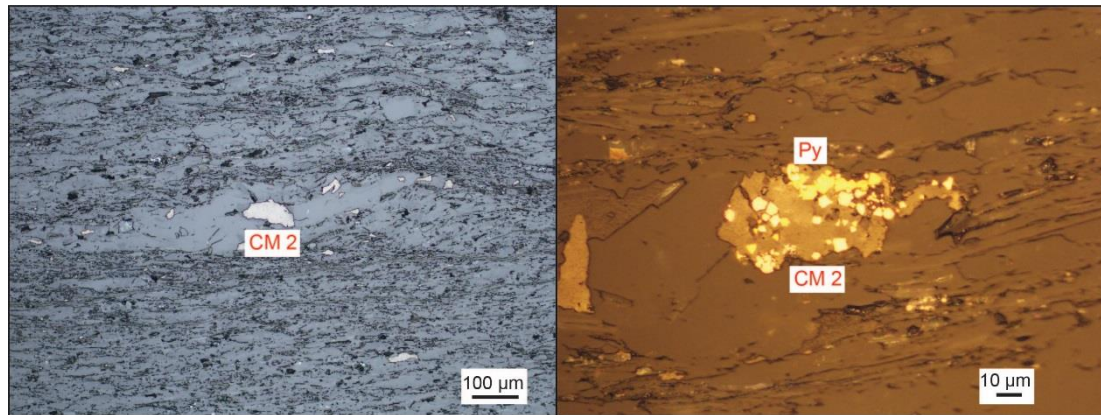
- A. Schistose structure and lepidoblastic texture with some parts displaying relict bedding structure;
- B. Aligned lamellar minerals, quartz/feldspar/muscovite patches which are present as augen structure and with pressure shadow;
- C. The coexistence of muscovite and chlorite;
- D. Augen minerals are aligned with foliation;
- E. Quartz displaying undulate extinction;
- F. Sulfide minerals (pyrite, chalcopyrite and galena) coexisting with Cm 2.

Evolutionary history

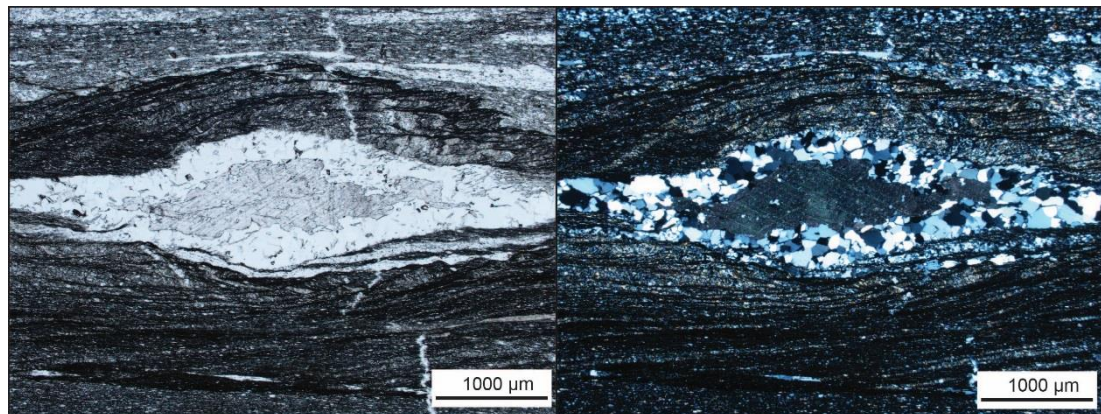
Minerals	Sedimentary	Diagenetic	Metamorphic	Hydrothermal
Quartz				
Albite				
Muscovite				?
Chlorite				?
Epidote				
Apatite				
Zircon				
Pyrite			?	?
Chalcopyrite			?	
Galena			?	
Carbonate Veins				
Quartz Veins				
CM 2				

Petrographic photomicrographs

* Augen structure with quartz aggregates (Q), muscovite (Mus) and epidote (Ep) grains filling in the interspace of minerals in ppl (left) and xpl (right) (from FF-12-B).



* Sulfide minerals coexists with CM 2 in reflected light (from FF-12-B).



* Quartz veins and calcite veins in ppl (left) and xpl (right) (from FF-11).

LAKE HAWEA

Pumpellyite-actinolite (P-A) facies

Meta-pelite: LH-01

Petrographic description

This sample, which belongs to P-A facies, is present as obvious relict bedding structure and schistose structure. Relict bedding structure results from the different content of quartz, consisting of quartz-dominated layer and platy minerals-dominated layer. In quartz-dominated layer, there are large quantities of recrystallized quartz,

albite and other associated minerals, like chlorite and apatite. Platy minerals-dominated layer is made up of platy minerals, such as chlorite, muscovite, and black bands. Other associated minerals, such as apatite, titanite and epidote, tend to overlay other minerals. The whole sample is little bit folded in some parts. Some black bands cross cut the foliation. Quartz veins went through samples along the foliation and get folded as well in some parts. There are also several quartz aggregates patches with pressure shadows.

Quartz, which consist quartz aggregates patch, is colourless, transparent, elongated or augen shaped with cracks and inclusions. It is present as low relief and has 1st order white grey birefringence. Quartz has pressure shadow with muscovite or chlorite in both terminals. Elongated quartz patch size is usually up to 0.1–0.15 mm and the quartz mode is about 12%. The direction of long axis of quartz augen is aligned with foliation.

Albite often co-grows with quartz in thin sections and has the similar features with quartz. But albite has polysynthetic twinning sometimes as the diagnostic features. The grain size is around 0.1 mm and the mode is about 8%. The long axis of albite is aligned with the foliation.

Platy minerals are mainly muscovite and chlorite.

Muscovite is colourless, transparent, low relief and present as needle-shaped or fibrous crystals. It always coexists with chlorite. The interference colour is up to 2nd blue. Grain size is less than 0.1 mm and the mode is about 30%.

Chlorite is pale greenish, transparent, low relief and present as needle-shaped or fibrous shaped. It always coexists with muscovite. It has low interference colour, as 1st order grey. The long length of crystals is less than 0.1 mm and the mode is about 25%.

Carbonaceous mineral is opaque and mixed with other fine-grained minerals forming black bands in ppl and appears grey, elliptical shape in reflected light. Grain size is less than 0.01 mm and aligned with the foliation. The mode is less than 5%.

Other associated minerals will be apatite, epidote and tiny pyrite.

Apatite is colourless, tiny and irregular or elongated, and sometimes appears as inclusions in other minerals. The interference colour is 1st order grey to black.

Apatite is approximately 0.02–0.05 mm and the mode is 3%.

Epidote is colourless, transparent, and irregular, with high relief and interference colours up to 2nd order orange to blue. The grainsize is about 0.05 mm the mode is about 8%.

Tiny Pyrite appears as anhedral along black bands. It looks opaque in ppl and bright yellow in reflected light. The size is about 0.001 mm and the mode is about 1%.

CM 3 occurs in black bands which cross cut the foliation. The CM has a sub-rounded grain shape with an elongate elliptical habit, is less than 4 x 10 µm in size, and is light grey with low reflectivity in reflected light.

The quartz veins, made up of quartz aggregates, cross cut the whole foliation and some have been altered to boudinage structure. The singly crystal is around 0.1 mm and the mode of quartz veins is about 8%.

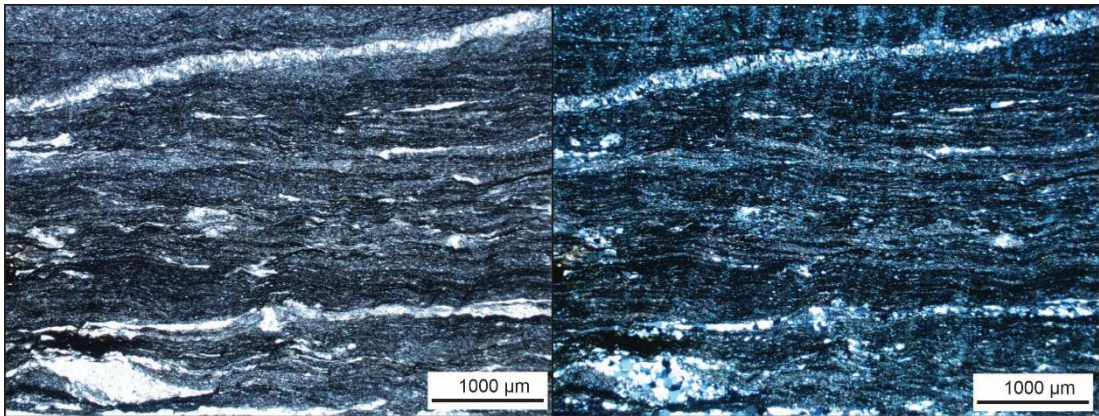
Typical features

- A. Relict bedding structure with quartz-dominated layer and platy minerals-dominated layer;
- B. Schistose structure formed by platy minerals;
- C. Fold structure;
- D. Some black bands which contains CM 3 cross cut the foliation;
- E. Quartz patches forming augen structure with pressure shadow.

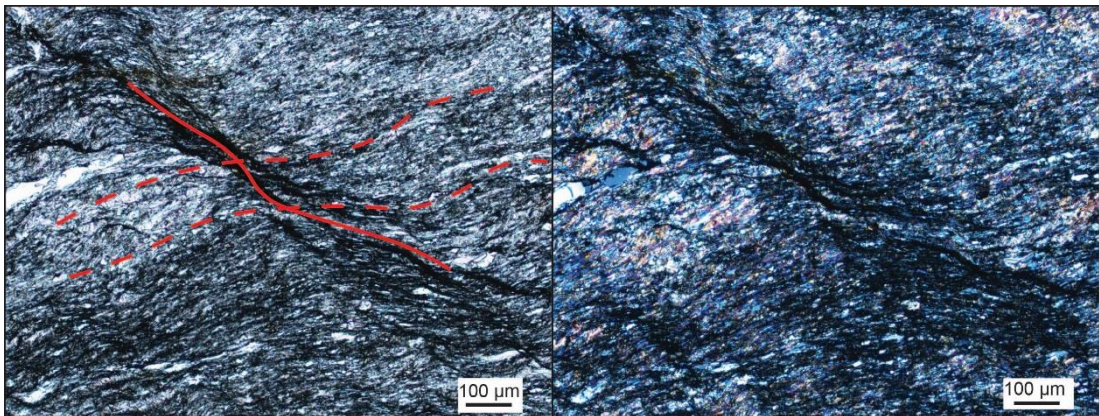
Evolutionary history

Minerals	Sedimentary	Diagenetic	Metamorphic	Hydrothermal
Muscovite				
Chlorite				
CM 3				?
Quartz				
Albite				
Epidote				
Apatite				
Pyrite			?	?
Quartz Veins				

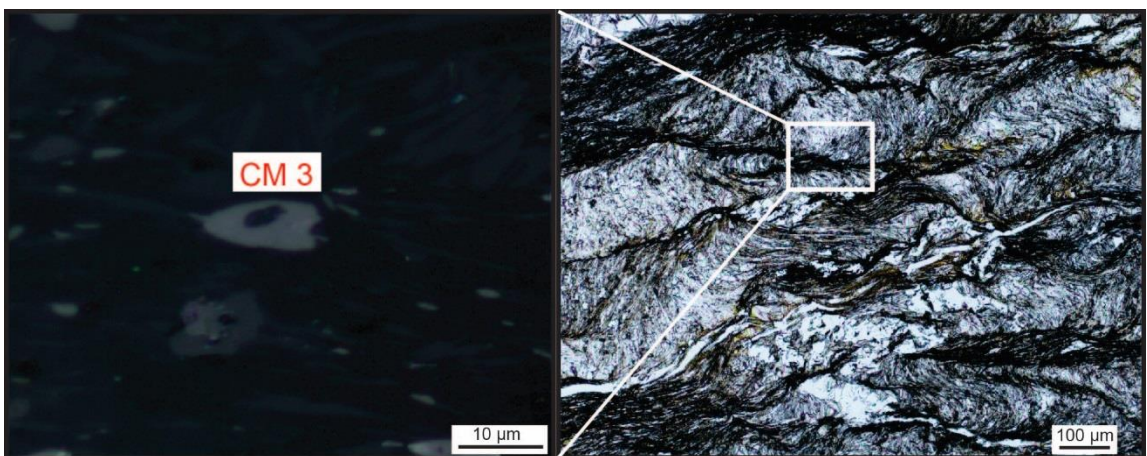
Petrographic photomicrographs



* Relict bedding structure in ppl (left) and xpl (right).



* The folded foliation is cross cut by black bands in ppl (left) and xpl (right).



* CM 3 occurs in black bands in reflected light (left) and ppl (right).

Meta sandstone: LH-02-A, B, LH-07-A***Petrographic description***

Those samples are mainly relict bedding structure and schistosity structure with some parts retaining slight augen structure. Relict bedding structure results from different quartz content of each layer. The quartz-dominated bedding consists of quartz aggregates and a small amount of chlorite, apatite and epidote. The quartz-less bedding is made up of black bands, chlorite, muscovite, apatite, titanite and epidote. Schistosity structure is formed by those platy minerals. There are some quartz, feldspar aggregates and muscovite ellipsoid patches forming augen structure with pressure shadows. And quartz veins go through samples along the foliation and get folded as well in some parts. While there is graphitic dust overlaying on most minerals in same samples, it containing some carbon observed with reflected light and other very fin-grained minerals. The dust is quite similar with the composition of black bands.

Quartz is colourless, transparent, elongated or augen shape, present as low relief and has white-grey 1st order birefringence. The aggregates have pressure shadows ended by platy minerals, such as muscovite and chlorite. Elongated single quartz size is usually up to 0.1 mm while the aggregates will be 0.2–0.4 mm. The mode of quartz is about 27%.

Albite often co-grows with quartz in thin sections and has the similar features with quartz, except for the polysynthetic twinning. The single albite size is about 0.1 mm and the mode is 8%. The long axis is aligned with foliation.

Platy minerals contain muscovite and chlorite.

Muscovite is colourless, transparent, low relief and present as needle-shaped or fibrous shaped. It gets some deformation in some parts. The interference colour is up to 2nd order blue. The length of long axis is less than 0.1 mm and the mode is about 25%.

Chlorite is pale greenish, transparent, low relief and present as needle-shaped or fibrous shaped. It always coexists with muscovite. It has low interference colour, as 1st order grey or inky anomalous birefringence. The size is less than 0.05 mm and the mode is 20%.

Other associated minerals will be apatite, titanite, epidote and pyrite.

Epidote is colourless, transparent, irregular, high relief and high interference colour up to 2nd blue-green. The size is about 0.05 mm and it distributes sporadically. The mode is about 3%.

Apatite is colourless, irregular and medium relief. The interference colour is grey to black 1st order interference colours. It widely spread in samples and the size is about 0.08–0.1 mm. The mode is about 2%.

Titanite is pale brownish, transparent, irregular, very high relief and 3rd blue birefringence. The size is about 0.08–0.1 mm and the mode is 5%.

Black band consists of very fine grained minerals and CM 3. CM 3 is opaque, amorphous in ppl and grey in reflected light. It appears as discontinuous line along the foliation. The mode of black band is about 5%.

The quartz veins, made up of quartz aggregates, cross cut the whole foliation and some got deformed as well. The single crystal is less than 0.05 mm and the mode of veins is about 5%.

Typical features

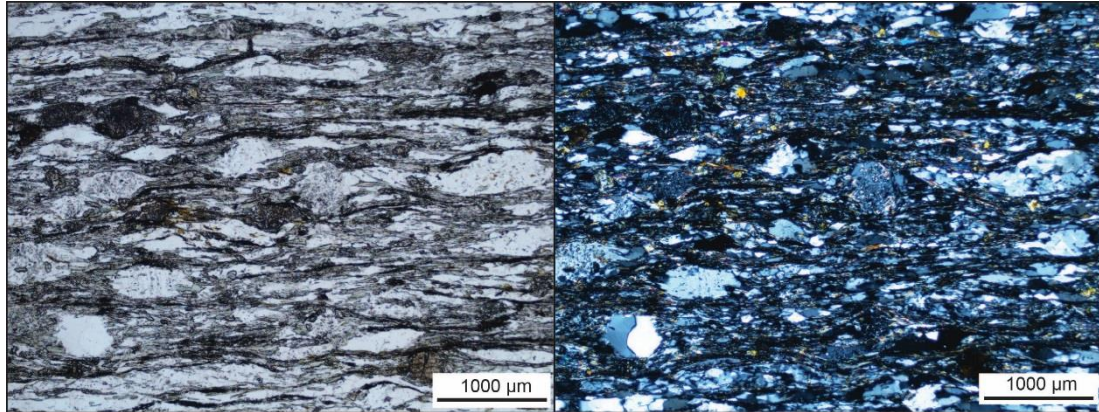
- A. Relict bedding structure with quartz-dominated layer and platy minerals-dominated layer;
- B. Schistose structure formed by platy minerals;
- C. Fold structure;
- D. Quartz patches forming augen structure with pressure shadows.

Evolutionary history

Minerals	Sedimentary	Diagenetic	Metamorphic	Hydrothermal
Muscovite				
Chlorite				
CM 3				?
Quartz				
Albite				
Epidote				
Apatite				
Titanite				
Pyrite			?	

Quartz Veins				
--------------	--	--	--	--

Petrographic photomicrographs



* Augen structure and black bands in ppl (left) and xpl (right) (from LH-02-A).

Greenschist

Metapelite: LH-03-A, B, LH-05-B, LH-06-A, B

Petrographic description

Those samples are schistosity structure with platy minerals such as muscovite, chlorite and relict bedding structure with quartz, feldspar patches. Other associated minerals are apatite, titanite, epidote and pyrite, some of which widely spread in samples. In some parts, quartz, feldspar aggregates and muscovite ellipsoid grains forming augen structure with pressure shadow structure. Black bands get darker than lower greenschist samples. The graphitic dust overlaying other minerals in several samples could be the mixture of very fine-grained materials and CM. Quartz veins and carbonate veins go through samples along the foliation and get folded as well in some parts.

Quartz is colourless, transparent, elongated or augen shaped with cracks and inclusions. It is present as low relief and has white-grey 1st order birefringence. The aggregates have pressure shadows ended by platy minerals, such as muscovite and chlorite. Elongated single quartz size is usually less than 0.1 mm while the aggregates will be 0.2–0.4 mm. The mode of quartz is about 25%.

Albite often co-grows with quartz in thin sections and has the similar features with quartz, except for the polysynthetic twinning. The single albite size is less than 0.05 mm and the mode is 8%. The long axis is aligned with foliation.

Platy minerals contain muscovite and chlorite.

Muscovite is colourless, transparent, low relief and present as needle-shaped or fibrous crystals. It is present some deformation in some parts and usually coexists with chlorite. The interference colour is up to 2nd order blue. The long axis is around 0.2 mm and the mode is about 15%.

Chlorite is pale greenish, transparent, low relief and present as needle-shaped or fibrous crystals. It always coexists with muscovite. It has low interference colour, as 1st order grey. Grain size is up to 0.2 mm and the mode is 15%.

Other associated minerals are apatite, titanite, and epidote.

Epidote is colourless, transparent, irregular, high relief and very high interference colour which is up to 2nd blue-green. The size is about 0.05 mm and it distributes sporadically. The mode is about 3%.

Apatite is colourless, irregular and medium relief. The interference colour is grey to black 1st order birefringence. The size is about 0.08–0.1 mm and the mode is about 4%, quite less than ones in P-A facies.

Titanite is pale brownish, transparent, irregular, very high relief and high interference colour which is up to 3rd blue-green. The size is about 0.08–0.1 mm and the mode is about 4%.

Pyrite is anhedral or as a stump line, opaque in ppl but bright yellow in reflected light. Some looks quite closely associated with CM. Grain size is about 0.03–0.05 mm and the mode is about 4%.

CM 3 is observed in samples, which is opaque, amorphous in xpl and grey and spotted in reflected light. It forms the black bands with other fine grained minerals and coexists with pyrite sometimes. Grain size is about 0.001 mm and the mode is about 4%.

The quartz veins are made up of quartz aggregates, cross cut or go along the foliation. Sequences can be inferred from them. Single crystal is angular and grain size is about 0.1 mm. The mode of quartz veins is around 8%.

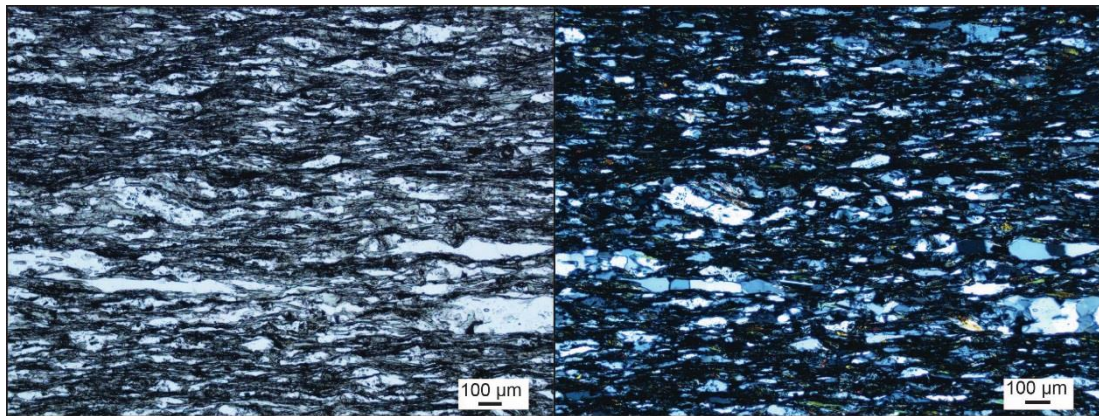
The carbonate veins mainly consist of calcite, which is colourless and transparent. Two sets of perfect cleavages of 60° and very high order creamy interference colours are present. The mode is about 10%.

Typical features

- A. Schistosity structure formed by platy minerals;
- B. Relict bedding structure with quartz, feldspar patches;
- C. Fold structure;
- D. Augen structure formed by quartz, feldspar and muscovite ellipsoid patches;
- E. Black bands consists of fine-grained CM 3;

Evolutionary history

Minerals	Sedimentary	Diagenetic	Metamorphic	Hydrothermal
Muscovite				
Chlorite				
Quartz				
Albite				
Epidote				
Apatite				
Pyrite			?	
CM 3				?
Quartz Veins				
Carbonate Veins				

Petrographic photomicrographs

* Augen structure with quartz-feldspathic and muscovite ellipsoid grains in ppl (left) and xpl (right) (from LH-03-A).

GOLDEN BAR PIT**Greenschist****Metapelite: GB-01, GB-02-A, B (Mus-Chl Schist)***Petrographic description*

These samples have schistosity structure with platy minerals such as muscovite and chlorite which is intergrown with black bands. Schistosity structure is segregated by quartz and albite aggregates. Flaky chlorite is also involved in the segregation. Quartz, albite and muscovite form the augen structure with pressure shadow structure in some parts. Black bands are aligned with the foliation, consisting of very fine grained minerals and carbonaceous minerals. Muscovite gets deformed in the space of black bands. Associated minerals are mainly apatite, titanite, which is quite abundant in samples of Golden Bar, and epidote. Later sulfide minerals, like chalcopyrite, arsenopyrite and pyrite are observed in some samples. There is also some graphitic dust coating on other minerals in some samples which may have similar composition with black bands. Quartz veins and carbonate veins go through samples along the foliation and get folded as well in some parts.

Quartz is colourless, transparent, augen shaped with cracks and inclusions. It is present as low relief and has 1st order white-grey birefringence. Grain size of single

crystals is more than 0.1 mm and the mode is about 20%. The direction of long axis of quartz is always aligned with foliation.

Albite often co-grows with quartz in thin sections and has similar features with quartz, except for the polysynthetic twinning. The grain size of albite is around 0.1 mm and the mode is 10%. The long axis of albite is aligned with the foliation.

Muscovite is colourless, transparent, low relief and present as needle-shaped or fibrous crystals. It gets some deformation co-grows with chlorite. The interference colour is up to 2nd blue. The length of long axis is about 0.15–0.2 mm and the mode is about 20%.

Chlorite is pale greenish, transparent, low relief and present as needle-shaped or fibrous crystals. It always coexists with muscovite. It has low interference colour, as 1st order grey or inky anomalous. The length of grain is about 0.15 mm and the mode is 15%.

Other associated minerals are apatite, titanite and epidote, which always overlay other minerals.

Epidote is colourless, transparent, irregular, high relief and 2nd order blue-green interference colour. The size is about 0.05 mm and it is distributed sporadically. The mode is about 3%.

Apatite is colourless, irregular and medium relief. The interference colour is grey to black 1st order. The size is about 0.08–0.1 mm and the mode is about 5%, quite less than ones in P-A facies.

Titanite is pale brownish, transparent, irregular, very high relief and 3rd order blue interference colour. The size is about 0.08–0.1 mm and the mode is around 5%.

Pyrite is cubic, opaque in transmitted light but bright yellow in reflected light. Some looks quite closely associated with CM. Grain size of single pyrite is less than 0.1 mm and the mode is about 5%.

Chalcopyrite is anhedral, opaque in transmitted light but much brighter yellow than pyrite in reflected light. It is always present with blue-purple tarnish and fractures. Grain size is about 0.08–0.1 mm and the mode is about 3%.

Arsenopyrite is anhedral, opaque in transmitted light and lighter yellow than pyrite in reflected light. It always grows together with pyrite. Grain size of single crystal is about 0.05 mm and the mode is about 3%.

The thin quartz veins, which are about 0.01 mm width and made up of quartz aggregates, go along the foliation. The single crystal size is less than 0.005 mm and the mode is about 3%.

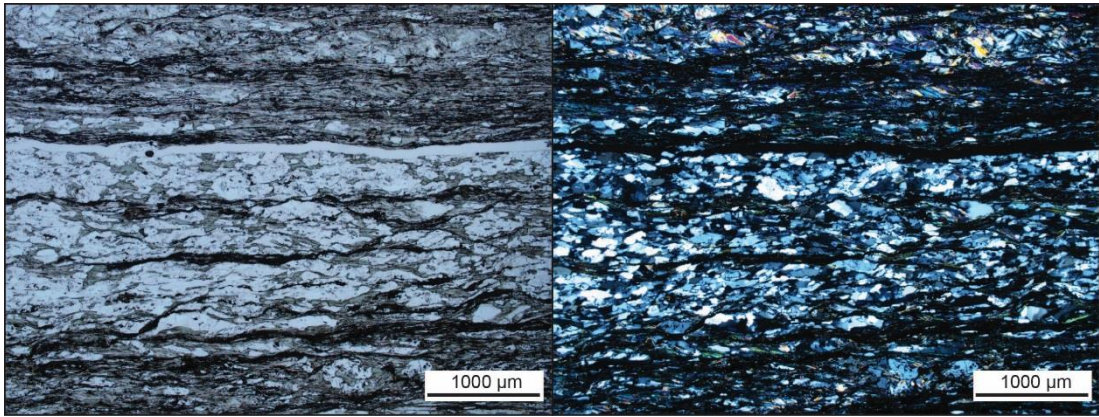
The carbonate veins mainly consist of calcite, which is colourless and transparent. Two sets of cleavages and creamy interference colour are present. The mode is about 3%.

Typical features

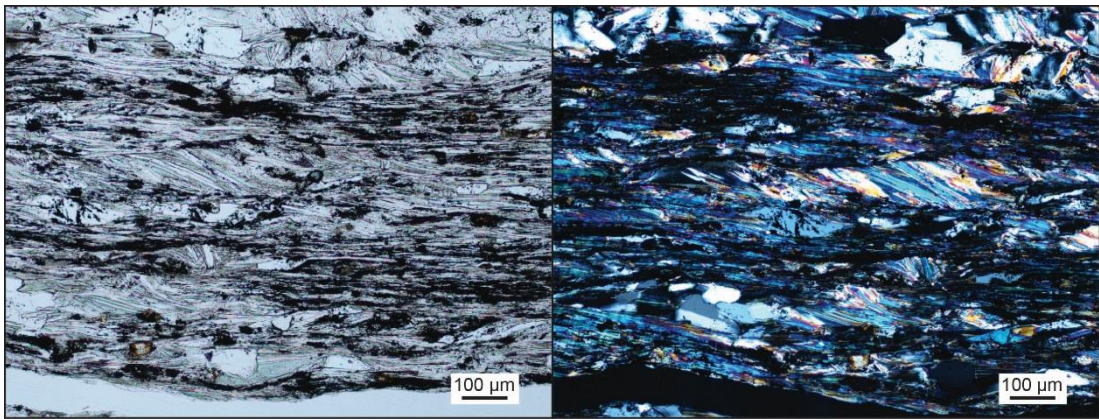
- A. Schistosity structure formed by platy minerals;
- B. Black bands are aligned with the foliation.

Evolutionary history

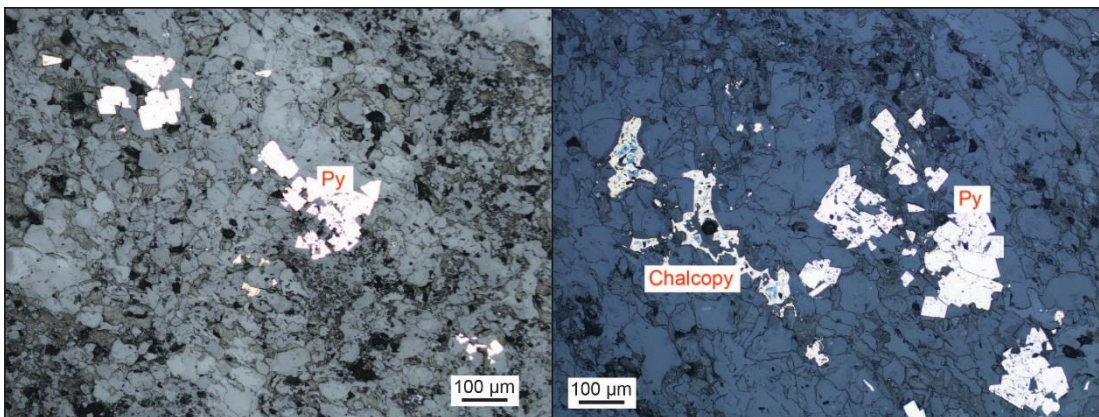
Minerals	Sedimentary	Diagenetic	Metamorphic	Hydrothermal
Muscovite				
Chlorite				
Quartz				
Albite				
Epidote				
Apatite				
Pyrite			?	
Chalcopyrite			?	
Arsenopyrite			?	
Quartz Veins				
Carbonate Veins				

Petrographic photomicrographs

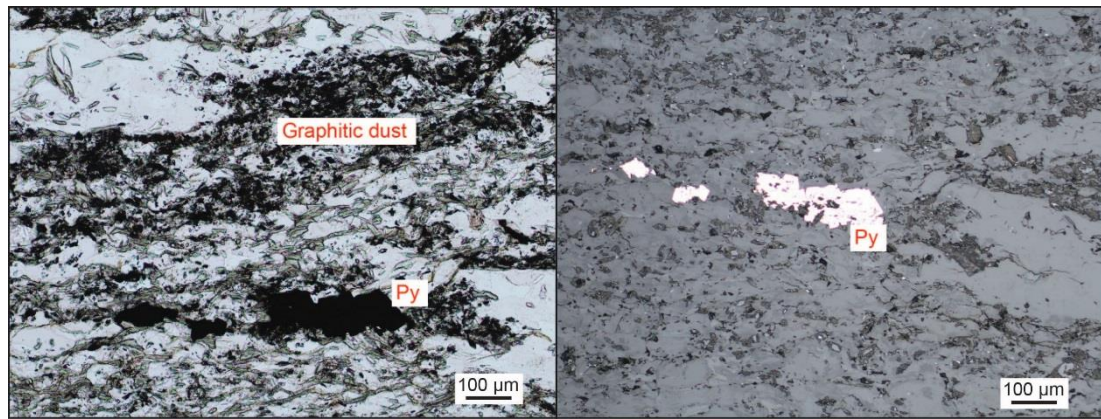
* Schistosity structure and quartz and albite aggregation in ppl (left) and xpl (right) (from GB-01).



* Deformed Muscovite as ellipsoid patches in ppl (left) and xpl (right) (from GB-01).



* Coexisting of pyrite (Py) and chalcopyrite (Chalcopy) in reflected light (from GB-02-B).



* Graphitic dust and pyrite in segregations in xpl (left) and reflected light (right) (from GB-02-A).

Mineralized rock: GB-04-A

Petrographic description

This sample has been mineralized by the alternation of hydrothermal fluids, and consists of quartz (20%), sulfide minerals (20%), graphitic microspheres (50%) and fine-grained matrix (10%).

Sulfide minerals are chalcopyrite, arsenopyrite and pyrite.

Pyrite is cubic, opaque in transmitted light but bright yellow in reflected light. Some looks quite closely associated with CM. Grain size ranges from very tiny to 0.5 mm and the mode is about 5%.

Chalcopyrite is anhedral, opaque in transmitted light but much brighter yellow than pyrite in reflected light. It is always present with blue-purple tarnish and fractures. Grain size is about 0.1 mm and the mode is about 2%.

Arsenopyrite is anhedral, opaque in transmitted light and lighter yellow than pyrite in reflected light. It always grows together with pyrite. Grain size is about 0.1 mm and the mode is about 3%.

The graphitic microspheres include fine grained pyrite, arsenopyrite, CM 4 and rutile.

CM 4 is very fine-grained that it can't be observed visibly in reflected light, it can be identified by Raman spectroscopy and the spectrums suggest that the CM is of relative high mature. The mode of CM is about 10%.

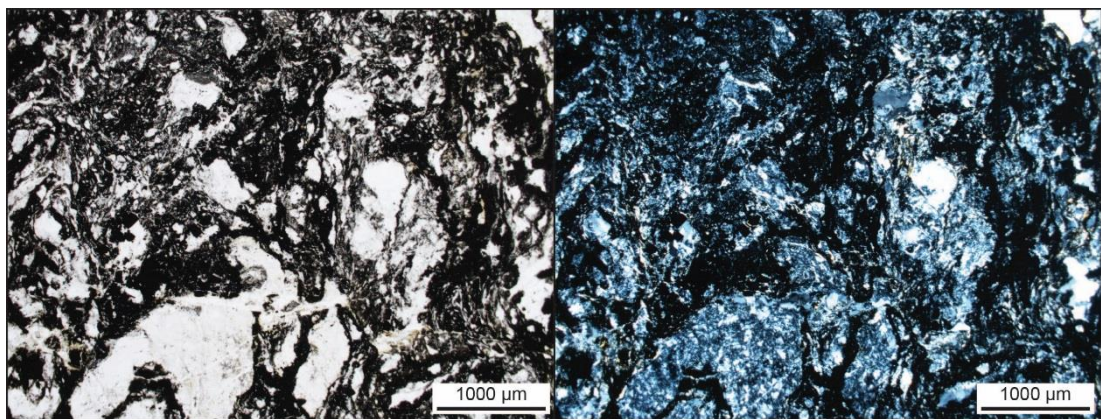
Typical features

A. Pyrite, chalcopyrite and arsenopyrite are abundant in samples;

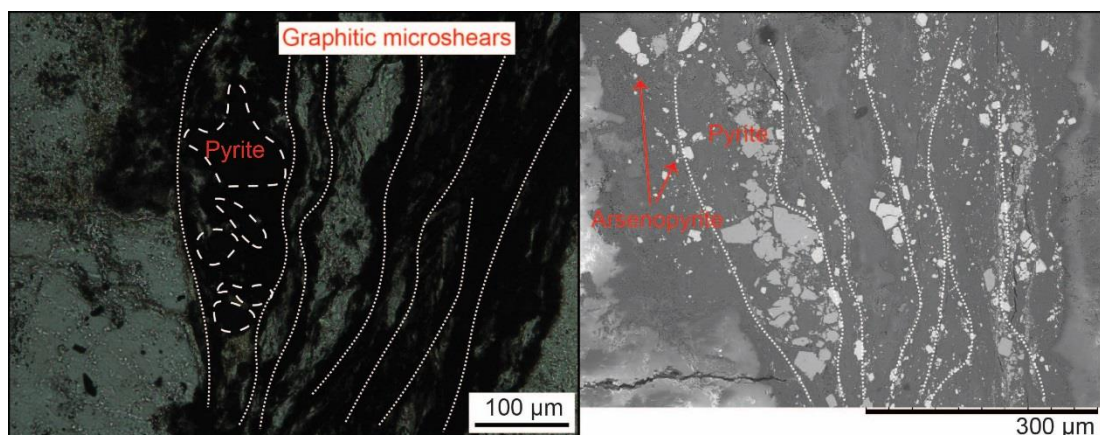
B: Sulfides are closely associated with graphitic microshears.

Evolutionary history

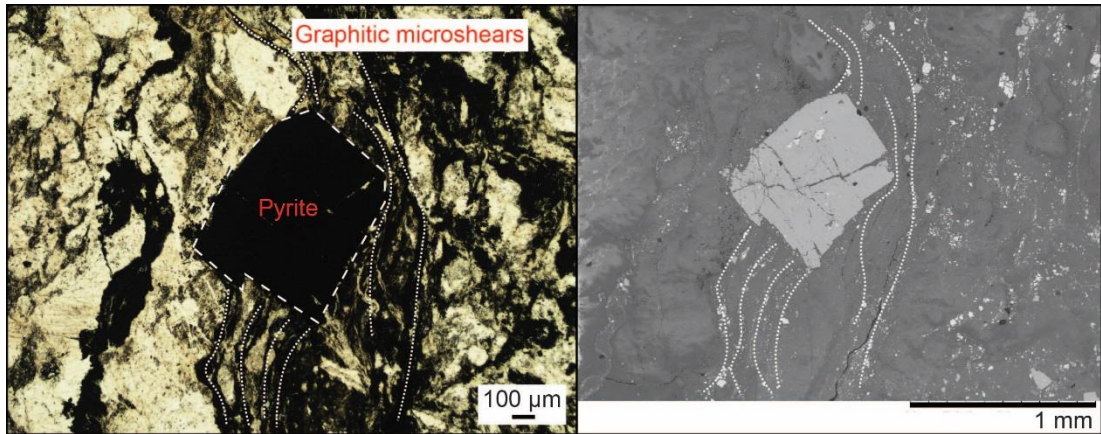
Minerals	Sedimentary	Diagenetic	Metamorphic	Hydrothermal
Pyrite				
Chalcopyrite				
Arsenopyrite				
CM 4				
Quartz Aggregates				
Calcite Aggregates				

Petrographic photomicrographs

* * * Overview of fine grained minerals, quartz-feldspathic minerals and calcite aggregates in ppl (left) and xpl (right).



* Pyrite is surrounded by graphitic microspheres, which includes arsenopyrite, CM 4 and pyrite in ppl (left) and BSE image (right).



* Pyrite overprints graphitic microspheres in ppl (left) and BSE image (right).

Appendix A3 Sample description on hand specimens (St. Ives and Wiluna gold deposits)

ST. IVES

KS-21 Brecciated dolerite

The sample is dark grey, massive structure, heterogeneous (the colour and granule of rock differ), inequigranular, fine grained to medium grained texture, consisting of dolerite, breccia and detrital minerals. The dolerite is made up of plagioclase (15%), pyroxene (25%), chlorite (10%), biotite (5%) and cryptocrystalline matrix (30%). Plagioclase is ivory, euhedral lath-shaped, glassy luster. Pyroxene is dark, stumpy, glassy luster and cleavages cannot be seen. Chlorite is light-green, xenomorphic granular, glassy luster and mainly altered from pyroxene subsequent to crystallisation. Biotite is dark brown, tabular, vitreous luster with cleavage, with some developed in the fractures. Alteration features include brecciation (6%), detrital minerals (5%), veins (2%), and pyrite forming subsequent to crystallisation. The breccia is grey, angular to subangular, matrix supported and some of the clasts are separated and staggered by fractures and faults filled with calcite and biotite. The size of the biggest clast is 1.5 x 2.5cm. The detrital mineral consists of plagioclase, quartz and dark-coloured minerals in the veins and fractures. The veins are dispersing and nearly straight line, white, filled with calcite. The pyrite is pale brass-yellow, cubic and metallic luster, size of 1*1 mm or smaller, and the mode is about 2%.

KS-22 Carbonaceous shale

The sample is light grey to dark grey, layered structure, heterogeneous with the interbedding by different content of carbon materials, fine grained texture and consisting of ore minerals, gangue mineral and wall rock. Ore minerals, also called sulphide minerals, are pyrrhotite (20%), pyrite (5%), and chalcopyrite (5%). Pyrrhotite is pale brass-yellow, metallic luster, disseminated with brown tarnish. The colour shallows from the centre to the around. Pyrite is light brass-yellow, metallic luster, forming with pyrrhotite. Chalcopyrite is brass yellow, metallic luster,

distributing sporadically. The gangue mineral is calcite which is white to grey and two sets of perfect cleavages can be seen. The mode of calcite is 8%. The wall rock is mainly organic matter, the proportion of which is about 60%. The veins are dispersing, S or W or V shaped, white and filled with calcite, about 2%. Besides, the wall rock displays dark and light grey interbedding, indicating different contents of carbon in the different layers.

KS-23 Meta-dolerite

The sample is grey, massive structure, inequigranular texture, and consisting of sulphide minerals (15%), biotite (10%), pale minerals (35%), and other dark minerals (35%). Sulphide minerals such as pyrrhotite display as fine particles, filling in the veins discontinuously. Biotite is dark brown, about 0.1*0.2cm but without good shape and some develop in the fractures. Pale minerals are ivory, granular or aggregate, 0.2*0.3cm or smaller and may be quartz or andalusite, which will be observed further. Other dark minerals are grey and the composition remains to be observed. The rock is also filled with pale veins, the size of which is about 1.5*0.3cm or smaller and 5%.

KS-24 Sulfide-rich dolerite

The sample is grey, massive structure, fine grained texture, and heterogeneous with some part containing sulphide minerals but other places don't contain. The rock is made up of sulphide minerals (35%), biotite (8%), quartz (5%), pale minerals (20%) and dark minerals (32%). Sulphide minerals are brass and fill in the fractures as stringer veins in fine particles. Biotite is dark brown, also fill in the fractures as fine particles. Quartz is coarse grained, colourless and transparent, oily luster, size of which is 2.5*1.5 and 0.5*0.5cm and is associated with serpentinization. The serpentine is light green, stringy, with a waxy luster and altered from minerals containing Mg in hydrothermal metasomatism in later periods. Pale minerals are ivory, and may be quartz or andalusite, which will be observed further. Other dark minerals are grey and the composition remains to be observed. The rock is also filled with stringer veins, containing sulphite minerals, biotite and calcite. The angle

between the vein and long edge of the core is 10° . KS-24 is similar to KS-23, but it has more sulphide minerals and less pale minerals in the fractures.

KS-25 Sulfide shale

The sample is grey with brassy-coloured sulphides, and a mesh-vein or laminated structure. The rock consists of sulphides minerals (48%), gangue mineral (10%) and the wall rock (42%). Sulphide minerals are pyrrhotite (30%), pyrite (10%), and chalcopyrite (8%). Pyrrhotite is pinky-brass, metallic luster, and occurs in interlaminated vein. The fracture is conchoidal and some pyrrhotite is in veins or disseminated. Pyrite is light brass-yellow, metallic luster, distributed sporadically, but is generally associated with pyrrhotite. Some pyrite of has a yellowish-brown tarnish. Chalcopyrite is brass yellow, metallic luster, distributed around or through the pyrrhotite and shows a colourful tarnish. The gangue mineral is calcite, which is white to light grey, fill in the veins and some grows around the pyrrhotite. The wall rock is dark grey and the composition is organic matter. The veins, made up of calcite and sulphite minerals, deform as folds, which may result from the deformation subsequence to rock formation. The angle between the vein and long edge of the core is 30° .

KS-26 Calcite-rich carbonaceous shale

The sample is dark-light grey, laminated structure, consisting of sulphides minerals (25%), gangue minerals (20%) and the wall rock (55%). Sulphide minerals are pyrrhotite (15%), pyrite (8%), and chalcopyrite (2%). Pyrrhotite is pale brass-yellow, develops in interlaminated veins or water drop shape, metallic luster, disseminated with brown tarnish. Pyrite is light brass-yellow, metallic luster, and one set of cleavages can be seen. Chalcopyrite is brass yellow, metallic luster, disseminated among pyrrhotite and calcite. Gangue minerals is made up of calcite (15%) and unidentified green mineral (5%). Calcite is white to grey, disseminated among wall rock. The green mineral, which will be further investigated in thin section, is dark green, fine grained, earthy luster, and looks like coating on other minerals. The angle between the vein and long edge of the core is 40° .

KS-27 Sulfide shale

The sample is grey with brassy-coloured sulphides, laminated structure, consisting of sulphides minerals (35%), gangue minerals (10%) and the wall rock (55%). Sulphide minerals are pyrrhotite (30%) and pyrite (5%). Pyrrhotite is pale brass-yellow, metallic luster, disseminated with brown tarnish, and some occurs in interlaminated veins. Pyrite is light brass-yellow, metallic luster, distributing sporadically, most of which is paragenesis with pyrrhotite. Calcite, as the gangue mineral, is white, occurs as the veins and some grows around the pyrrhotite. The veins are vertical or horizontal in the core. The vertical vein is almost 1cm from the surface of the core.

KS-28 Sulfide shale

The sample is dark grey, pelitic texture, laminated structure, and consisting of sulfide minerals (30%), gangue mineral (15%) and organic matter. Sulfide minerals are pyrrhotite (20%), pyrite (5%), and chalcopyrite (5%). Pyrrhotite is pale brass-yellow, metallic luster with colourful tarnish. Pyrite is light brass-yellow, metallic luster and some grow as cube in wall rock. Chalcopyrite is brass yellow, metallic luster, distributing sporadically, and intergrown with pyrrhotite. Calcite, as the gangue mineral, is white to grey, disseminated among wall rock and grows with pyrrhotite. Some perform as stringer veins which are irregular and discontinuous.

KS-29 Sulfide-rich dolerite

The sample is light grey, fine grained, inequigranular texture, massive structure, and consisting of sulfide minerals (25%), dark minerals (10%), pale minerals (25%), and cryptocrystalline matrix (40%). Sulfide minerals consist of pyrrhotite (18%) and pyrite (7%). Some, about 15%, develop in fractures or disseminated in the matrix and some may forms as aggregates also containing quartz, plagioclase and dark minerals such as biotite, about 0.5*0.6cm~0.6*1.0cm, with mode of about 10%. Dark minerals are black, stumpy or granular, glassy luster and may be pyroxene or amphibole. Pale minerals, which may be quartz and andalusite, occurs ivory, granular or aggregate. The size is around 0.2*0.3cm.

KS-30 Sulfide-rich dolerite

The sample is light grey, inequigranular, porphyritic texture, massive structure, and consisting of dark mineral (10%), sulfide minerals (20%), chlorite (5%), calcite (5%), pale minerals (20%), and cryptocrystalline matrix (40%). Dark mineral is black, sub-rounded to rounded, 0.1*0.2cm~0.5*0.3cm, and will be observed further. Sulfide minerals are pyrrhotite (16%), chalcopyrite (2%), and pyrite (2%). Pyrrhotite is pale brass-yellow, disseminated in matrix with dark brown tarnish. Some is associated with calcite. Pyrite is light brass-yellow, metallic luster, developed in fractures. Chalcopyrite is brass yellow, metallic luster, laminated in matrix. Chlorite is grass-green, glassy luster, and displays as coating on other minerals. Calcite is white to grey, two sets of perfect cleavages, disseminated in matrix and grows with pyrrhotite. Pale minerals, which may be quartz and andalusite, occurs ivory, granular or aggregate. The size is around 0.2*0.3cm. Besides, the rock suffered severe chloritization and serpentinized.

KS-31 Carbonaceous shale

The sample is dark grey, pelitic texture, laminated structure, and consisting of sulfide minerals (25%), gangue mineral (5%) and wall rock (70%). Sulfide minerals are made up of pyrrhotite, pyrite, and chalcopyrite. Pyrrhotite is pale brass-yellow, metallic luster, and grows in veins or aggregated. Pyrite is light brass-yellow, metallic luster, associated with pyrrhotite. Chalcopyrite is brass yellow, metallic luster, distributed around or intergrown with pyrrhotite and has a colourful tarnish. The three ore minerals grow together in yellowish patches. Calcite, as the gangue mineral, is white, disseminated among wall rock and grows with ore minerals as veins. Those veins show as wave-shaped suffered from deformation subsequent to rock formation.

KS-32 Carbonaceous shale

The sample is light-dark grey, pelitic texture, laminated structure, heterogeneous with the interbedding by different content of organic matter, and consisting of sulfide minerals (10%), biotite (8%), gangue minerals (12%) and wall rock (80%). Sulfide

minerals are made up of pyrrhotite (8%) and pyrite (2%). Pyrrhotite is pale brass-yellow, metallic luster, and grows in fractures. Pyrite is light brass-yellow, metallic luster, associated with pyrrhotite. . The gangue minerals are calcite (8%), in which two sets of cleavage can be seen and quartz (4%), which is colourless and transparent, oily luster. In some parts, pyrrhotite grows along or around the calcite and they form irregular stringer veins, which are also wave-shaped, together. And the angle between the vein and long edge of the core is about 60°.

KS-33 Dolerite

The sample is light grey, fine grained and massive texture, heterogeneous with network veins, and consisting of dark mineral (10%), biotite (5%), sulphide mineral (5%), serpentine (2%), green mineral (10%), pale minerals (15%) and cryptocrystalline matrix (58%). Dark mineral is black, sub-rounded to rounded, 0.1*0.2cm, and will be observed further. Biotite, dark brown, foliated, growing in the fractures and one set of perfect cleavages can be seen. Pyrrhotite, as the sulfide mineral, is pale brass-yellow, metallic luster, and granular in pale minerals. Serpentine is light green, stringy, waxy luster, and occurs near the other alteration minerals. Green mineral, forming after alteration, develop between the area of two veins consisting of biotite and dark minerals. Pale minerals, as wave-shaped veins, may be composed of calcite and quartz, about 1 mm~4 mm, and some has been dislocated by fault. This rock has suffered severe alteration.

WILUNA

AD-01 Sulfide shale

The sample is dark grey, pelitic texture, laminated structure, and consisting of sulfide minerals (35%), black ore minerals (5%), gangue minerals (6%) and wall rock (54%). Sulfide minerals are made up of pyrrhotite (20%), pyrite (10%), and chalcopyrite (5%). Pyrrhotite is pale brass, metallic luster, and brown tarnish. Pyrite is light brass-yellow, metallic luster, forming together with pyrrhotite. Chalcopyrite is brass yellow, metallic luster, distributing sporadically or with pyrrhotite. Black ore minerals are fine particles, black, strong metallic luster and distribute sporadically.

Most of the ore minerals develop in the fractures or pores. The gangue minerals are calcite (3%) and chlorite (3%). Calcite is white and disseminated among wall rock. Chlorite is dark green, earthy luster and layering. The composition of wall rock is organic matter. The whole rock has suffered severe alteration, making ore minerals uneven distribution.

AD-02 Sulfide shale

The sample is grey-light grey, fine grained, massive structure, and consisting of sulfide minerals (38%), gangue minerals (25%) and wall rock (40%). Sulfide minerals are made up of pyrrhotite (20%), pyrite (10%), and chalcopyrite (8%). Pyrrhotite is pale brass, metallic luster, and brown tarnish. Pyrite is light brass-yellow, metallic luster, forming together with pyrrhotite. Chalcopyrite is brass yellow, metallic luster, distributing sporadically or with pyrrhotite. Some of sulfide minerals show some oxidation with the colour of red. The gangue minerals are calcite (7%) and chlorite (18%). Calcite is white and develops as veins. Chlorite is grass-green, earthy luster and layering. The composition of wall rock is organic matter with light grey colour. The whole rock has suffered severe hydrothermal alteration and deformation resulting in layers as folds.



Figure A3.1 Photos of St. Ives samples.

Appendix A4 Results of LA-ICP-MS data quality monitoring

Reference standard: S_Po726; Tested standard: S_Bonn-NBS-6b										
Element	Au									
Measured Concentration (ppm)	11.6									
δ	0.38									
Original Concentration (ppm)	11.3									
δ	0.3									
Analysis number = 4; Internal standard element: ^{56}Fe (concentration: 59%); δ : standard deviation.										
Reference standard:GSD-1G; Tested standard: G-NIST612										
Element	Zn	As	V	Mn	Co	Ni	Cu	Mo	Ag	Pb
Measured Concentration (ppm)	39.43	18.8	41.67	41.2	36.69	39.79	40.59	39.09	22.96	41.64
δ	0.64	1.7	0.52	0.69	0.38	0.91	0.84	0.82	0.26	0.63
Original Concentration (ppm)	39.1	35.7	38.8	38.7	35.5	38.8	37.8	37.4	22	38.57
δ	8	14	8	2	4	0.2	6	4	0.3	0.2
Analysis number =9; Internal standard element: ^{28}Si (concentration: 33.7%); δ : standard deviation.										

Appendix B1 Fluid and rock composition used in the model

Table B1 Fluid and rock composition used in the model

Component	GB-01 (wt %)	FF-13 (wt %)	Fluid 1 (wt %)
H ₂ O	2.58	0	70
Al ₂ O ₃	19.45	14.28	0
As	0.002	0.003	0
Au	0	Excess	0
C	0.10	5.83	0
CaO	0.43	10.89	0
Fe ₂ O ₃	0.54	0.93	0
FeO	3.31	8.36	0
K ₂ O	2.75	1.53	0
MgO	1.91	2.68	0
MnO	0.06	0.34	0
Na ₂ O	4.54	1.83	0
SiO ₂	63.93	53.33	0
Fe ₃ O ₄	0	0	Excess
FeS	0.37	0	Excess
ZnO	0.01	0	0
FeS ₂	0	0	30

Appendix B2 Sulfur and non-carbonate carbon concentrations from four metasediment-hosted gold deposits

Table B2-1 New sulfur (S) and non-carbonate carbon (NCC) concentrations of samples from Macraes gold deposit.

S (wt %)	NCC (wt %)	S (wt %)	NCC (wt %)	S (wt %)	NCC (wt %)
Mineralized					
0.17	0.21	0.71	0.2	0.27	0.41
0.13	0.21	0.37	0.23	0.63	0.56
0.11	0.27	0.2	0.24	0.76	0.72
0.1	0.24	0.6	0.17	0.68	1.03
0.1	0.24	0.98	0.15	0.15	0.33
0.11	0.17	0.29	0.41	0.4	0.35
0.11	0.15	0.19	0.31	0.91	0.32
0.15	0.2	1.85	0.34	0.3	0.59
0.19	0.19	0.57	0.1	0.71	0.77
0.12	0.19	0.14	0.06	0.21	0.1
0.21	0.17	0.18	0.12	1.9	0.51
0.1	0.27	0.51	0.19	0.35	0.19
0.24	0.25	0.68	0.19	0.51	0.17
0.86	0.28	0.11	0.15	0.1	0.79
0.12	0.35	0.42	0.16	0.17	0.16
0.17	0.21	0.29	0.25	0.32	0.22
0.16	0.13	0.28	0.14	0.64	0.23
0.13	0.13	1.3	0.14	0.31	0.2
0.45	0.13	0.21	0.2	0.16	0.12
0.13	0.2	1.2	0.26	0.2	0.14
0.35	0.14	0.28	0.21	1.45	2.27
0.58	0.17	0.42	0.23	1.73	2.52
0.66	0.14	0.24	0.25	0.1	0.5
0.61	0.17	0.33	0.16	0.18	0.17
0.44	0.12	1.12	0.74	0.14	0.14
0.46	0.34	0.72	0.56	0.2	3.2
0.21	0.13	0.31	0.33	0.13	0.63
0.98	0.26	1.27	0.2	0.16	0.02
0.44	0.15	0.52	0.27	2.19	0.4
0.23	0.17	0.2	0.75	1.31	0.42
1.2	0.3	0.15	0.92	1.25	0.21
0.4	0.48	0.1	0.36	0.18	0.23
0.26	0.02	0.13	0.16	0.46	0.47

S (wt %)	NCC (wt %)	S (wt %)	NCC (wt %)	S (wt %)	NCC (wt %)
0.13	0.13	0.22	0.55		
0.12	0.18	1.17	0.41		
0.16	0.2	0.5	0.42		
2.24	0.19	1.11	1.44		
0.11	0.07				

S (wt %)	NCC (wt %)	S (wt %)	NCC (wt %)	S (wt %)	NCC (wt %)
Unmineralized					
0.045	0.18	0.53	0.16	0.05	0.23
0.035	0.17	0.17	0.27	0.09	0.2
0.75	0.38	0.4	0.25	0.19	0.21
0.16	0.19	0.5	0.15	0.045	0.2
0.59	0.24	0.25	0.23	0.09	0.1
0.06	0.15	0.08	0.08	0.08	0.1
0.05	0.12	0.035	0.17	0.19	0.18
0.07	0.07	0.14	0.2	0.29	0.23
0.1	0.14	0.19	0.11	0.24	0.24
0.37	0.19	0.13	0.2		

Table B2-2 Published sulfur (S) and non-carbonate carbon (NCC) concentrations of mineralized samples from several Paleoproterozoic deposits from West Africa, Phanerozoic deposits from the Victorian goldfield, Australia, the Phanerozoic Touquoy Zone deposit, Meguma Terrane, Canada, and the Phanerozoic Macraes gold deposit (Bierlein et al., 2001; Bierlein and Smith, 2003; Craw, 2002; Petrie et al., 2005; Křibek et al., 2015).

Western African Gold Deposits		Victorian Goldfield		Touquoy Gold Deposit		Macraes Gold Deposit	
S (wt %)	NCC (wt %)	S (wt %)	NCC (wt %)	S (wt %)	NCC (wt %)	S (wt %)	NCC (wt %)
2.12	1.52	0.824	1.84	0.1	0.5	0.75	0.38
1.51	1.71	1.792	4.9	0.4	0.4	0.16	0.19
2.34	1.65	0.076	0.22	0.5	0.3	0.59	0.24
2.92	1.72	0.108	2.74	0.7	0.9	0.53	0.16
2.25	1.39	0.544	0.29	1	0.3	0.17	0.27
0.77	0.11	0.344	0.065	1.4	0.1	0.4	0.25
1.15	0.07	0.024	0.095	0.3	0.1	0.5	0.15
0.02	0.6	0.804	0.72	0.8	0.2	0.25	0.23
0.47	1.67	0.288	0.29	0.6	0.4	0.19	0.21
0.65	1.29	0.404	2.84	0.6	0.3	0.1	0.14
0.5	1.1	2.148	0.68	0.9	0.5	0.14	0.2
1.89	0.87	0.036	0.005	1.6	0.4	0.19	0.11
1.15	0.87	1.572	0.28	0.9	0.3	0.19	0.18
1.7	1.54	0.032	0.28	1.3	0.4	0.29	0.23
0.02	3.77	0.036	0.02	0.7	0.3	0.24	0.24
1.79	1.54			0.5	0.4	0.37	0.19
0.06	3.77					0.13	0.2
1.47	1.94					2.48	1.68
1.85	1.22					3.6	2.11
1.69	1.98					1.58	1.92
0.15	2.2					0.33	2.74
2.68	2.71					0.42	2.44
2.86	0.65					1.07	2.44
						0.93	2.23
						1.23	0.45
						0.43	3.45
						0.53	3.37
						0.63	3.98
						0.92	3.05
						0.1	2.66
						1.05	2.45
						1.54	2.44
						0.2	3.15
						1.46	2.29

Western African Gold Deposits		Victorian Goldfield		Touquoy Gold Deposit		Macraes Gold Deposit	
S (wt %)	NCC (wt %)	S (wt %)	NCC (wt %)	S (wt %)	NCC (wt %)	S (wt %)	NCC (wt %)
						1	2.54
						0.1	1.69
						0.1	1.79
						1.24	1.81
						0.3	1.7
						0.2	2.64

Appendix B3 Thermodynamic modelling results

Table B3-1 Results of modelled fluid infiltration from 160 to 400 °C.

		Formula:	Au	C	SiO ₂	Fe ₃ O ₄	FeS ₂	Fe ₈ S ₇	ZnS	FeAsS	CaCO ₃	FeCO ₃
		Type:	(s)	(s)	(s)	(s)	(s)	(s)	(s)	(s)	(s)	(s)
Cell	T (°C)	P (bar)	Gold	Graphite	Quartz	Magnetite	Pyrite	Pyrrhotite	Sphalerite	Arsenopyrite	Calcite	Siderite
Ore fluids	500	5000	0	0	0	0	0	0	0	0	0	0
1	400	3000	7.31E-06	1.52E-01	3.92E-01	1.43E-02	0	1.43E-02	1.53E-04	1.35E-05	7.49E-03	0
2	400	3000	2.47E-07	1.05E-02	3.80E-01	1.71E-02	0	4.46E-03	1.54E-04	2.79E-05	7.49E-03	0
3	400	3000	1.85E-07	1.32E-02	3.77E-01	1.59E-02	0	4.32E-03	1.54E-04	2.69E-05	0	0
4	400	3000	2.13E-07	1.36E-02	3.73E-01	1.59E-02	0	4.38E-03	1.54E-04	2.68E-05	0	0
5	400	3000	3.53E-07	1.57E-02	3.86E-01	1.71E-02	0	4.69E-03	1.54E-04	2.63E-05	0	0
6	400	3000	3.02E-08	1.26E-02	3.98E-01	1.73E-02	0	3.95E-03	1.53E-04	2.77E-05	0	0
7	400	3000	3.06E-09	1.17E-02	3.98E-01	1.73E-02	0	3.89E-03	1.53E-04	2.79E-05	0	0
8	400	3000	1.22E-09	1.14E-02	3.98E-01	1.73E-02	0	3.89E-03	1.53E-04	2.79E-05	0	0
9	400	3000	7.32E-10	1.11E-02	3.98E-01	1.73E-02	0	3.89E-03	1.53E-04	2.80E-05	0	0
10	400	3000	5.34E-10	1.09E-02	3.98E-01	1.73E-02	0	3.89E-03	1.53E-04	2.79E-05	0	0
11	400	3000	4.37E-10	1.07E-02	3.98E-01	1.73E-02	0	3.89E-03	1.53E-04	2.79E-05	0	0
12	400	3000	3.83E-10	1.05E-02	3.98E-01	1.73E-02	0	3.89E-03	1.53E-04	2.79E-05	0	0
13	400	3000	3.49E-10	1.03E-02	3.98E-01	1.73E-02	0	3.89E-03	1.53E-04	2.79E-05	0	0
14	400	3000	3.28E-10	1.01E-02	3.98E-01	1.73E-02	0	3.89E-03	1.53E-04	2.79E-05	0	0
15	400	3000	3.13E-10	9.85E-03	3.98E-01	1.73E-02	0	3.89E-03	1.53E-04	2.78E-05	0	0
16	400	3000	3.03E-10	9.62E-03	3.98E-01	1.73E-02	0	3.89E-03	1.53E-04	2.78E-05	0	0
17	400	3000	2.95E-10	9.39E-03	3.98E-01	1.73E-02	0	3.89E-03	1.53E-04	2.78E-05	0	0
18	400	3000	2.89E-10	9.16E-03	3.98E-01	1.73E-02	0	3.89E-03	1.53E-04	2.78E-05	0	0

		Formula:	Au	C	SiO2	Fe3O4	FeS2	Fe.877S	ZnS	FeAsS	CaCO3	FeCO3
		Type:	(s)	(s)	(s)	(s)	(s)	(s)	(s)	(s)	(s)	(s)
Cell	T (°C)	P (bar)	Gold	Graphite	Quartz	Magnetite	Pyrite	Pyrrhotite	Sphalerite	Arsenopyrite	Calcite	Siderite
Ore fluids	500	5000	0	0	0	0	0	0	0	0	0	0
1	370	3000	7.83E-06	2.20E-01	4.00E-01	1.38E-02	0	1.59E-02	1.53E-04	0	7.49E-03	0
2	370	3000	1.20E-07	1.32E-02	3.79E-01	1.72E-02	0	4.21E-03	1.54E-04	2.13E-05	7.49E-03	0
3	370	3000	1.35E-07	1.32E-02	3.77E-01	1.72E-02	0	4.25E-03	1.54E-04	2.87E-05	7.49E-03	0
4	370	3000	1.34E-07	1.54E-02	3.67E-01	1.65E-02	0	4.25E-03	1.54E-04	2.61E-05	0	0
5	370	3000	1.32E-07	1.57E-02	3.97E-01	1.72E-02	0	4.24E-03	1.53E-04	2.65E-05	0	0
6	370	3000	5.77E-09	1.37E-02	3.98E-01	1.73E-02	0	3.90E-03	1.53E-04	2.89E-05	0	0
7	370	3000	1.34E-09	1.32E-02	3.98E-01	1.73E-02	0	3.89E-03	1.53E-04	2.92E-05	0	0
8	370	3000	6.86E-10	1.30E-02	3.98E-01	1.73E-02	0	3.89E-03	1.53E-04	2.93E-05	0	0
9	370	3000	4.80E-10	1.27E-02	3.98E-01	1.73E-02	0	3.89E-03	1.53E-04	2.93E-05	0	0
10	370	3000	3.93E-10	1.25E-02	3.98E-01	1.73E-02	0	3.89E-03	1.53E-04	2.93E-05	0	0
11	370	3000	3.51E-10	1.22E-02	3.98E-01	1.73E-02	0	3.89E-03	1.53E-04	2.93E-05	0	0
12	370	3000	3.27E-10	1.19E-02	3.98E-01	1.73E-02	0	3.89E-03	1.53E-04	2.92E-05	0	0
13	370	3000	3.14E-10	1.16E-02	3.98E-01	1.73E-02	0	3.89E-03	1.53E-04	2.92E-05	0	0
14	370	3000	3.06E-10	1.12E-02	3.98E-01	1.73E-02	0	3.89E-03	1.53E-04	2.91E-05	0	0
15	370	3000	3.01E-10	1.09E-02	3.98E-01	1.73E-02	0	3.89E-03	1.53E-04	2.91E-05	0	0
16	370	3000	2.97E-10	1.05E-02	3.98E-01	1.73E-02	0	3.89E-03	1.53E-04	2.90E-05	0	0
17	370	3000	2.94E-10	1.01E-02	3.98E-01	1.73E-02	0	3.89E-03	1.53E-04	2.89E-05	0	0
18	370	3000	2.91E-10	9.67E-03	3.98E-01	1.73E-02	0	3.89E-03	1.53E-04	2.88E-05	0	0
Ore fluids	500	5000	0	0	0	0	0	0	0	0	0	0
1	340	3000	8.14E-06	2.47E-01	4.14E-01	1.35E-02	0	1.69E-02	1.54E-04	0	7.49E-03	0
2	340	3000	4.78E-08	1.48E-02	3.77E-01	1.73E-02	0	4.06E-03	1.54E-04	0	7.49E-03	0
3	340	3000	5.74E-08	1.49E-02	3.73E-01	1.72E-02	0	4.08E-03	1.54E-04	1.41E-05	7.49E-03	0

		Formula:	Au	C	SiO2	Fe3O4	FeS2	Fe.877S	ZnS	FeAsS	CaCO3	FeCO3
		Type:	(s)	(s)	(s)	(s)	(s)	(s)	(s)	(s)	(s)	(s)
Cell	T (°C)	P (bar)	Gold	Graphite	Quartz	Magnetite	Pyrite	Pyrrhotite	Sphalerite	Arsenopyrite	Calcite	Siderite
4	340	3000	6.13E-08	1.59E-02	3.61E-01	1.67E-02	0	4.09E-03	1.54E-04	2.42E-05	0	0
5	340	3000	5.39E-08	1.58E-02	3.96E-01	1.72E-02	0	4.05E-03	1.54E-04	2.55E-05	0	0
6	340	3000	3.55E-09	1.49E-02	3.98E-01	1.73E-02	0	3.89E-03	1.53E-04	3.06E-05	0	0
7	340	3000	8.50E-10	1.47E-02	3.98E-01	1.73E-02	0	3.88E-03	1.53E-04	3.16E-05	0	0
8	340	3000	4.47E-10	1.45E-02	3.98E-01	1.73E-02	0	3.88E-03	1.53E-04	3.19E-05	0	0
9	340	3000	3.25E-10	1.44E-02	3.98E-01	1.73E-02	0	3.88E-03	1.53E-04	3.20E-05	0	0
10	340	3000	2.77E-10	1.42E-02	3.98E-01	1.73E-02	0	3.88E-03	1.53E-04	3.20E-05	0	0
11	340	3000	2.57E-10	1.40E-02	3.98E-01	1.73E-02	0	3.88E-03	1.53E-04	3.20E-05	0	0
12	340	3000	2.50E-10	1.38E-02	3.98E-01	1.73E-02	0	3.88E-03	1.53E-04	3.20E-05	0	0
13	340	3000	2.48E-10	1.35E-02	3.98E-01	1.73E-02	0	3.88E-03	1.53E-04	3.20E-05	0	0
14	340	3000	2.51E-10	1.31E-02	3.98E-01	1.73E-02	0	3.88E-03	1.53E-04	3.19E-05	0	0
15	340	3000	2.55E-10	1.27E-02	3.98E-01	1.73E-02	0	3.88E-03	1.54E-04	3.18E-05	0	0
16	340	3000	2.60E-10	1.22E-02	3.98E-01	1.73E-02	0	3.88E-03	1.54E-04	3.17E-05	0	0
17	340	3000	2.64E-10	1.16E-02	3.98E-01	1.73E-02	0	3.88E-03	1.54E-04	3.15E-05	0	0
18	340	3000	2.66E-10	1.10E-02	3.98E-01	1.73E-02	0	3.88E-03	1.54E-04	3.13E-05	0	0
Ore fluids	500	5000	0	0	0	0	0	0	0	0	0	0
1	310	3000	8.29E-06	2.56E-01	4.36E-01	1.33E-02	0	1.75E-02	1.54E-04	0	7.49E-03	0
2	310	3000	1.66E-08	1.54E-02	3.72E-01	1.73E-02	0	3.98E-03	1.54E-04	0	7.49E-03	0
3	310	3000	2.19E-08	1.55E-02	3.64E-01	1.73E-02	0	4.00E-03	1.54E-04	0	7.49E-03	0
4	310	3000	2.33E-08	1.59E-02	3.54E-01	1.68E-02	0	4.00E-03	1.54E-04	0	0	0
5	310	3000	1.76E-08	1.57E-02	3.95E-01	1.73E-02	0	3.98E-03	1.54E-04	0	0	0
6	310	3000	1.77E-09	1.54E-02	3.98E-01	1.73E-02	0	3.90E-03	1.53E-04	2.35E-05	0	0
7	310	3000	4.58E-10	1.53E-02	3.98E-01	1.73E-02	0	3.88E-03	1.53E-04	3.56E-05	0	0

Formula:		Au	C	SiO2	Fe3O4	FeS2	Fe.877S	ZnS	FeAsS	CaCO3	FeCO3	
Type:		(s)	(s)	(s)	(s)	(s)	(s)	(s)	(s)	(s)	(s)	
Cell	T (°C)	P (bar)	Gold	Graphite	Quartz	Magnetite	Pyrite	Pyrrhotite	Sphalerite	Arsenopyrite	Calcite	Siderite
8	310	3000	2.46E-10	1.53E-02	3.98E-01	1.73E-02	0	3.88E-03	1.54E-04	3.62E-05	0	0
9	310	3000	1.81E-10	1.52E-02	3.98E-01	1.73E-02	0	3.88E-03	1.54E-04	3.65E-05	0	0
10	310	3000	1.57E-10	1.52E-02	3.98E-01	1.73E-02	0	3.88E-03	1.54E-04	3.67E-05	0	0
11	310	3000	1.49E-10	1.51E-02	3.98E-01	1.73E-02	0	3.88E-03	1.54E-04	3.69E-05	0	0
12	310	3000	1.48E-10	1.50E-02	3.98E-01	1.73E-02	0	3.88E-03	1.54E-04	3.70E-05	0	0
13	310	3000	1.52E-10	1.49E-02	3.98E-01	1.73E-02	0	3.88E-03	1.54E-04	3.71E-05	0	0
14	310	3000	1.59E-10	1.47E-02	3.98E-01	1.73E-02	0	3.88E-03	1.54E-04	3.72E-05	0	0
15	310	3000	1.68E-10	1.45E-02	3.98E-01	1.73E-02	0	3.88E-03	1.54E-04	3.72E-05	0	0
16	310	3000	1.80E-10	1.41E-02	3.98E-01	1.73E-02	0	3.88E-03	1.54E-04	3.72E-05	0	0
17	310	3000	1.93E-10	1.36E-02	3.98E-01	1.73E-02	0	3.88E-03	1.54E-04	3.71E-05	0	0
18	310	3000	2.07E-10	1.29E-02	3.98E-01	1.73E-02	0	3.88E-03	1.54E-04	3.68E-05	0	0
Ore fluids	500	5000	0	0	0	0	0	0	0	0	0	0
1	280	3000	8.35E-06	2.63E-01	4.64E-01	1.55E-02	8.88E-03	0	1.54E-04	0	7.49E-03	0
2	280	3000	4.40E-09	1.66E-02	3.63E-01	1.78E-02	1.97E-03	0	1.54E-04	0	7.49E-03	0
3	280	3000	7.13E-09	1.66E-02	3.50E-01	1.78E-02	1.98E-03	0	1.54E-04	0	7.49E-03	0
4	280	3000	6.57E-09	1.67E-02	3.50E-01	1.75E-02	1.97E-03	0	1.54E-04	0	0	0
5	280	3000	4.26E-09	1.66E-02	3.94E-01	1.78E-02	1.97E-03	0	1.54E-04	0	0	0
6	280	3000	5.88E-10	1.65E-02	3.98E-01	1.78E-02	1.96E-03	0	1.54E-04	0	0	0
7	280	3000	1.48E-10	1.65E-02	3.98E-01	1.78E-02	1.96E-03	0	1.54E-04	0	0	0
8	280	3000	6.57E-11	1.65E-02	3.98E-01	1.78E-02	1.95E-03	0	1.54E-04	4.57E-06	0	0
9	280	3000	7.87E-11	1.55E-02	3.98E-01	1.73E-02	0	3.87E-03	1.54E-04	4.59E-05	0	0
10	280	3000	7.92E-11	1.54E-02	3.98E-01	1.73E-02	0	3.87E-03	1.54E-04	4.53E-05	0	0
11	280	3000	7.68E-11	1.54E-02	3.98E-01	1.73E-02	0	3.87E-03	1.54E-04	4.57E-05	0	0

		Formula:	Au	C	SiO2	Fe3O4	FeS2	Fe.877S	ZnS	FeAsS	CaCO3	FeCO3
		Type:	(s)	(s)	(s)	(s)	(s)	(s)	(s)	(s)	(s)	(s)
Cell	T (°C)	P (bar)	Gold	Graphite	Quartz	Magnetite	Pyrite	Pyrrhotite	Sphalerite	Arsenopyrite	Calcite	Siderite
12	280	3000	7.84E-11	1.54E-02	3.98E-01	1.73E-02	0	3.87E-03	1.54E-04	4.61E-05	0	0
13	280	3000	8.28E-11	1.53E-02	3.98E-01	1.73E-02	0	3.87E-03	1.54E-04	4.65E-05	0	0
14	280	3000	8.98E-11	1.52E-02	3.98E-01	1.73E-02	0	3.87E-03	1.54E-04	4.69E-05	0	0
15	280	3000	9.97E-11	1.51E-02	3.98E-01	1.73E-02	0	3.87E-03	1.54E-04	4.73E-05	0	0
16	280	3000	1.13E-10	1.48E-02	3.98E-01	1.73E-02	0	3.87E-03	1.54E-04	4.77E-05	0	0
17	280	3000	1.31E-10	1.43E-02	3.98E-01	1.73E-02	0	3.87E-03	1.54E-04	4.79E-05	0	0
18	280	3000	1.53E-10	1.31E-02	3.98E-01	1.73E-02	0	3.87E-03	1.54E-04	4.72E-05	0	0
Ore fluids	500	5000	0	0	0	0	0	0	0	0	0	0
1	250	3000	8.37E-06	2.64E-01	4.96E-01	1.55E-02	8.95E-03	0	1.54E-04	0	7.48E-03	0
2	250	3000	6.09E-10	1.66E-02	3.48E-01	1.78E-02	1.96E-03	0	1.54E-04	0	7.49E-03	0
3	250	3000	8.28E-10	1.66E-02	3.35E-01	1.78E-02	1.96E-03	0	1.54E-04	0	7.48E-03	0
4	250	3000	5.55E-10	1.66E-02	3.50E-01	1.77E-02	1.96E-03	0	1.54E-04	0	0	0
5	250	3000	3.40E-10	1.66E-02	3.93E-01	1.78E-02	1.96E-03	0	1.54E-04	0	0	0
6	250	3000	6.75E-11	1.66E-02	3.98E-01	1.78E-02	1.96E-03	0	1.54E-04	0	0	0
7	250	3000	2.04E-11	1.66E-02	3.98E-01	1.78E-02	1.96E-03	0	1.54E-04	0	0	0
8	250	3000	9.95E-12	1.66E-02	3.98E-01	1.78E-02	1.96E-03	0	1.54E-04	0	0	0
9	250	3000	6.40E-12	1.66E-02	3.98E-01	1.78E-02	1.96E-03	0	1.54E-04	0	0	0
10	250	3000	5.02E-12	1.66E-02	3.98E-01	1.78E-02	1.96E-03	0	1.54E-04	0	0	0
11	250	3000	4.58E-12	1.65E-02	3.98E-01	1.78E-02	1.96E-03	0	1.54E-04	0	0	0
12	250	3000	4.68E-12	1.65E-02	3.98E-01	1.78E-02	1.96E-03	0	1.54E-04	0	0	0
13	250	3000	5.18E-12	1.65E-02	3.98E-01	1.78E-02	1.93E-03	0	1.54E-04	5.43E-05	0	0
14	250	3000	6.16E-12	1.64E-02	3.98E-01	1.78E-02	1.91E-03	0	1.54E-04	1.00E-04	0	0
15	250	3000	7.92E-12	1.63E-02	3.98E-01	1.78E-02	1.91E-03	0	1.54E-04	9.83E-05	0	0

Formula:		Au	C	SiO2	Fe3O4	FeS2	Fe.877S	ZnS	FeAsS	CaCO3	FeCO3	
Type:		(s)	(s)	(s)	(s)	(s)	(s)	(s)	(s)	(s)	(s)	
Cell	T (°C)	P (bar)	Gold	Graphite	Quartz	Magnetite	Pyrite	Pyrrhotite	Sphalerite	Arsenopyrite	Calcite	Siderite
16	250	3000	1.12E-11	1.61E-02	3.98E-01	1.78E-02	1.91E-03	0	1.54E-04	9.53E-05	0	0
17	250	3000	4.79E-11	1.47E-02	3.98E-01	1.73E-02	0	3.84E-03	1.54E-04	7.73E-05	0	0
18	250	3000	1.05E-10	1.21E-02	3.98E-01	1.73E-02	0	3.85E-03	1.54E-04	6.61E-05	0	0
Ore fluids	500	5000	0	0	0	0	0	0	0	0	0	0
1	220	3000	8.38E-06	2.64E-01	5.18E-01	1.55E-02	8.97E-03	0	1.54E-04	0	7.47E-03	0
2	220	3000	5.79E-11	1.66E-02	3.33E-01	1.78E-02	1.96E-03	0	1.54E-04	0	7.48E-03	0
3	220	3000	5.92E-11	1.66E-02	3.29E-01	1.78E-02	1.96E-03	0	1.54E-04	0	7.47E-03	0
4	220	3000	3.39E-11	1.66E-02	3.51E-01	1.78E-02	1.96E-03	0	1.54E-04	0	0	0
5	220	3000	1.87E-11	1.66E-02	3.91E-01	1.78E-02	1.96E-03	0	1.54E-04	0	0	0
6	220	3000	5.00E-12	1.66E-02	3.98E-01	1.78E-02	1.96E-03	0	1.54E-04	0	0	0
7	220	3000	1.94E-12	1.66E-02	3.98E-01	1.78E-02	1.96E-03	0	1.54E-04	0	0	0
8	220	3000	1.10E-12	1.66E-02	3.98E-01	1.78E-02	1.96E-03	0	1.54E-04	0	0	0
9	220	3000	8.08E-13	1.66E-02	3.98E-01	1.78E-02	1.96E-03	0	1.54E-04	0	0	0
10	220	3000	7.14E-13	1.66E-02	3.98E-01	1.78E-02	1.96E-03	0	1.54E-04	0	0	0
11	220	3000	7.19E-13	1.66E-02	3.98E-01	1.78E-02	1.96E-03	0	1.54E-04	0	0	0
12	220	3000	7.92E-13	1.66E-02	3.98E-01	1.78E-02	1.96E-03	0	1.54E-04	0	0	0
13	220	3000	9.33E-13	1.66E-02	3.98E-01	1.78E-02	1.96E-03	0	1.54E-04	0	0	0
14	220	3000	1.16E-12	1.66E-02	3.98E-01	1.78E-02	1.96E-03	0	1.54E-04	0	0	0
15	220	3000	1.55E-12	1.66E-02	3.98E-01	1.78E-02	1.96E-03	0	1.54E-04	0	0	0
16	220	3000	2.22E-12	1.64E-02	3.98E-01	1.78E-02	1.90E-03	0	1.54E-04	1.22E-04	0	0
17	220	3000	3.88E-12	1.61E-02	3.98E-01	1.77E-02	1.85E-03	0	1.54E-04	2.22E-04	0	0
18	220	3000	1.57E-11	1.29E-02	3.98E-01	1.72E-02	0	3.75E-03	1.54E-04	1.56E-04	0	0
Ore fluids	500	5000	0	0	0	0	0	0	0	0	0	0

		Formula:	Au	C	SiO2	Fe3O4	FeS2	Fe.877S	ZnS	FeAsS	CaCO3	FeCO3
		Type:	(s)	(s)	(s)	(s)	(s)	(s)	(s)	(s)	(s)	(s)
Cell	T (°C)	P (bar)	Gold	Graphite	Quartz	Magnetite	Pyrite	Pyrrhotite	Sphalerite	Arsenopyrite	Calcite	Siderite
1	190	3000	8.38E-06	2.64E-01	5.23E-01	1.55E-02	8.97E-03	0	1.54E-04	0	7.44E-03	0
2	190	3000	2.93E-12	1.66E-02	3.29E-01	1.78E-02	1.96E-03	0	1.54E-04	0	7.47E-03	0
3	190	3000	2.63E-12	1.62E-02	3.28E-01	1.70E-02	1.96E-03	0	1.54E-04	0	7.42E-03	2.42E-03
4	190	3000	1.45E-12	1.56E-02	3.51E-01	1.58E-02	1.96E-03	0	1.54E-04	0	0	5.90E-03
5	190	3000	7.06E-13	1.66E-02	3.91E-01	1.78E-02	1.96E-03	0	1.54E-04	0	0	0
6	190	3000	2.39E-13	1.66E-02	3.98E-01	1.78E-02	1.96E-03	0	1.54E-04	0	0	0
7	190	3000	1.31E-13	1.66E-02	3.98E-01	1.78E-02	1.96E-03	0	1.54E-04	0	0	0
8	190	3000	9.79E-14	1.66E-02	3.98E-01	1.78E-02	1.96E-03	0	1.54E-04	0	0	0
9	190	3000	9.03E-14	1.66E-02	3.98E-01	1.78E-02	1.96E-03	0	1.54E-04	0	0	0
10	190	3000	9.49E-14	1.66E-02	3.98E-01	1.78E-02	1.96E-03	0	1.54E-04	0	0	0
11	190	3000	1.08E-13	1.66E-02	3.98E-01	1.78E-02	1.96E-03	0	1.54E-04	0	0	0
12	190	3000	1.30E-13	1.66E-02	3.98E-01	1.78E-02	1.96E-03	0	1.54E-04	0	0	0
13	190	3000	1.63E-13	1.66E-02	3.98E-01	1.78E-02	1.96E-03	0	1.54E-04	0	0	0
14	190	3000	2.18E-13	1.66E-02	3.98E-01	1.78E-02	1.96E-03	0	1.54E-04	0	0	0
15	190	3000	3.16E-13	1.66E-02	3.98E-01	1.78E-02	1.96E-03	0	1.54E-04	0	0	0
16	190	3000	5.51E-13	1.65E-02	3.98E-01	1.78E-02	1.96E-03	0	1.54E-04	0	0	0
17	190	3000	1.89E-12	1.51E-02	3.98E-01	1.76E-02	1.72E-03	0	1.54E-04	4.68E-04	0	0
18	190	3000	4.00E-12	2.08E-03	3.98E-01	1.71E-02	0	3.86E-03	1.54E-04	5.07E-05	0	0
Ore fluids	500	5000	0	0	0	0	0	0	0	0	0	0
1	160	3000	8.38E-06	2.56E-01	5.24E-01	5.60E-05	8.98E-03	0	1.54E-04	0	7.42E-03	4.62E-02
2	160	3000	1.64E-13	1.48E-02	3.29E-01	1.43E-02	1.96E-03	0	1.54E-04	0	7.46E-03	1.05E-02
3	160	3000	1.94E-13	1.48E-02	3.28E-01	1.43E-02	1.96E-03	0	1.54E-04	0	7.41E-03	1.06E-02
4	160	3000	1.22E-13	1.55E-02	3.51E-01	1.57E-02	1.96E-03	0	1.54E-04	0	0	6.37E-03

		Formula:	Au	C	SiO2	Fe3O4	FeS2	Fe.877S	ZnS	FeAsS	CaCO3	FeCO3
		Type:	(s)	(s)	(s)	(s)	(s)	(s)	(s)	(s)	(s)	(s)
Cell	T (°C)	P (bar)	Gold	Graphite	Quartz	Magnetite	Pyrite	Pyrrhotite	Sphalerite	Arsenopyrite	Calcite	Siderite
5	160	3000	6.16E-14	1.66E-02	3.92E-01	1.78E-02	1.96E-03	0	1.54E-04	0	0	0
6	160	3000	2.95E-14	1.66E-02	3.98E-01	1.78E-02	1.96E-03	0	1.54E-04	0	0	0
7	160	3000	2.65E-14	1.66E-02	3.98E-01	1.78E-02	1.96E-03	0	1.54E-04	0	0	0
8	160	3000	3.18E-14	1.66E-02	3.98E-01	1.78E-02	1.96E-03	0	1.54E-04	0	0	0
9	160	3000	4.72E-14	1.66E-02	3.98E-01	1.78E-02	1.96E-03	0	1.54E-04	0	0	0
10	160	3000	1.07E-13	1.66E-02	3.98E-01	1.77E-02	1.96E-03	0	1.54E-04	0	0	0
11	160	3000	4.38E-13	7.29E-03	3.98E-01	1.70E-02	0	3.58E-03	1.54E-04	3.33E-04	0	0
12	160	3000	1.82E-13	1.16E-03	3.98E-01	1.71E-02	0	3.89E-03	1.54E-04	2.73E-05	0	0
13	160	3000	6.72E-14	1.13E-03	3.98E-01	1.72E-02	0	3.89E-03	1.54E-04	2.69E-05	0	0
14	160	3000	3.86E-14	1.13E-03	3.98E-01	1.72E-02	0	3.89E-03	1.54E-04	2.68E-05	0	0
15	160	3000	2.62E-14	1.12E-03	3.98E-01	1.72E-02	0	3.89E-03	1.54E-04	2.67E-05	0	0
16	160	3000	1.93E-14	1.12E-03	3.98E-01	1.72E-02	0	3.89E-03	1.54E-04	2.67E-05	0	0
17	160	3000	1.51E-14	1.11E-03	3.98E-01	1.72E-02	0	3.89E-03	1.54E-04	2.67E-05	0	0
18	160	3000	1.22E-14	1.11E-03	3.98E-01	1.72E-02	0	3.89E-03	1.54E-04	2.67E-05	0	0

		Formula:	KAl3Si3 O10(OH) 2	Ca2Al3Si 3O12(OH))	Ca2FeAl2 Si3O12O H	Mg4.5Al3 Si2.5O10(OH)8	Na(AlSi3 O8)	H2O	H+	OH-	CO3--	HCO3-
		Type:	(s)	(s)	(s)	(s)	(s)	(a)	(a)	(a)	(a)	(a)
Cell	T (°C)	P(bar)	Muscovit e	Zoisite	Epidote	Chlorite	Albite	H2O	H+	OH-	CO3--	HCO3-
Ore fluids	500	5000	0	0	0	0	0	4.86E+00	1.66E-08	2.62E-03	3.42E-05	9.52E-03
1	400	3000	6.34E-02	0	0	1.02E-02	1.49E-01	5.17E+00	1.23E-08	6.95E-04	7.47E-05	2.31E-02
2	400	3000	6.53E-02	0	0	1.02E-02	1.43E-01	5.21E+00	1.51E-08	5.30E-04	3.88E-05	1.71E-02

		Formula:	KAl ₃ Si ₃ O ₁₀ (OH) ₂	Ca ₂ Al ₃ Si ₃ O ₁₂ (OH)	Ca ₂ FeAl ₂ Si ₃ O ₁₂ O _H	Mg _{4.5} Al ₃ Si _{2.5} O ₁₀ (OH) ₈	Na(AlSi ₃ O ₈)	H ₂ O	H ⁺	OH ⁻	CO ₃ ⁻⁻	HCO ₃ ⁻
		Type:	(s)	(s)	(s)	(s)	(s)	(a)	(a)	(a)	(a)	(a)
Cell	T (°C)	P(bar)	Muscovite	Zoisite	Epidote	Chlorite	Albite	H ₂ O	H ⁺	OH ⁻	CO ₃ ⁻⁻	HCO ₃ ⁻
3	400	3000	6.28E-02	0	3.74E-03	1.02E-02	1.43E-01	5.24E+00	1.85E-08	4.04E-04	2.06E-05	1.29E-02
4	400	3000	6.23E-02	0	3.74E-03	1.02E-02	1.45E-01	5.28E+00	2.61E-08	2.59E-04	7.46E-06	8.22E-03
5	400	3000	5.75E-02	3.74E-03	0	1.02E-02	1.45E-01	5.30E+00	2.81E-07	2.42E-05	6.52E-08	7.73E-04
6	400	3000	5.67E-02	3.74E-03	0	1.02E-02	1.42E-01	5.32E+00	1.81E-06	4.42E-06	2.44E-09	1.36E-04
7	400	3000	5.67E-02	3.74E-03	0	1.02E-02	1.42E-01	5.34E+00	3.38E-06	2.52E-06	8.06E-10	7.50E-05
8	400	3000	5.67E-02	3.74E-03	0	1.02E-02	1.42E-01	5.35E+00	4.81E-06	1.85E-06	4.33E-10	5.32E-05
9	400	3000	5.67E-02	3.74E-03	0	1.02E-02	1.42E-01	5.37E+00	6.08E-06	1.52E-06	2.87E-10	4.21E-05
10	400	3000	5.67E-02	3.74E-03	0	1.02E-02	1.42E-01	5.38E+00	7.22E-06	1.32E-06	2.14E-10	3.53E-05
11	400	3000	5.67E-02	3.74E-03	0	1.02E-02	1.42E-01	5.40E+00	8.24E-06	1.19E-06	1.71E-10	3.07E-05
12	400	3000	5.67E-02	3.74E-03	0	1.02E-02	1.42E-01	5.41E+00	9.15E-06	1.10E-06	1.43E-10	2.74E-05
13	400	3000	5.67E-02	3.74E-03	0	1.02E-02	1.42E-01	5.43E+00	9.98E-06	1.04E-06	1.23E-10	2.48E-05
14	400	3000	5.67E-02	3.74E-03	0	1.02E-02	1.42E-01	5.44E+00	1.07E-05	9.86E-07	1.09E-10	2.28E-05
15	400	3000	5.67E-02	3.74E-03	0	1.02E-02	1.42E-01	5.45E+00	1.14E-05	9.48E-07	9.82E-11	2.11E-05
16	400	3000	5.67E-02	3.74E-03	0	1.02E-02	1.42E-01	5.47E+00	1.21E-05	9.17E-07	8.96E-11	1.97E-05
17	400	3000	5.67E-02	3.74E-03	0	1.02E-02	1.42E-01	5.48E+00	1.27E-05	8.93E-07	8.25E-11	1.84E-05
18	400	3000	5.67E-02	3.74E-03	0	1.02E-02	1.42E-01	5.49E+00	1.32E-05	8.73E-07	7.67E-11	1.74E-05
Ore fluids	500	5000	0	0	0	0	0	4.86E+00	1.66E-08	2.62E-03	3.42E-05	9.52E-03
1	370	3000	6.46E-02	0	0	1.02E-02	1.45E-01	5.28E+00	1.67E-08	4.62E-04	9.31E-05	2.69E-02
2	370	3000	6.51E-02	0	0	1.02E-02	1.44E-01	5.32E+00	2.00E-08	3.61E-04	5.02E-05	2.01E-02
3	370	3000	6.47E-02	0	0	1.02E-02	1.45E-01	5.36E+00	2.70E-08	2.43E-04	1.95E-05	1.30E-02
4	370	3000	6.02E-02	1.80E-03	1.94E-03	1.02E-02	1.49E-01	5.40E+00	4.66E-08	1.22E-04	4.27E-06	6.61E-03
5	370	3000	5.67E-02	3.74E-03	0	1.02E-02	1.42E-01	5.42E+00	8.72E-07	7.64E-06	1.92E-08	4.10E-04

			Formula:	KAl ₃ Si ₃ O ₁₀ (OH) ₂	Ca ₂ Al ₃ Si ₃ O ₁₂ (OH) ₂	Ca ₂ FeAl ₂ Si ₃ O ₁₂ O _H	Mg _{4.5} Al ₃ Si _{2.5} O ₁₀ (OH) ₈	Na(AlSi ₃ O ₈)	H ₂ O	H ⁺	OH ⁻	CO ₃ ⁻⁻	HCO ₃ ⁻
			Type:	(s)	(s)	(s)	(s)	(s)	(a)	(a)	(a)	(a)	(a)
Cell	T (°C)	P(bar)	Muscovite	Zoisite	Epidote	Chlorite	Albite	H ₂ O	H ⁺	OH ⁻	CO ₃ ⁻⁻	HCO ₃ ⁻	
6	370	3000	5.67E-02	3.74E-03	0	1.02E-02	1.42E-01	5.43E+00	2.66E-06	2.76E-06	2.61E-09	1.42E-04	
7	370	3000	5.67E-02	3.74E-03	0	1.02E-02	1.42E-01	5.45E+00	4.37E-06	1.77E-06	1.05E-09	8.62E-05	
8	370	3000	5.67E-02	3.74E-03	0	1.02E-02	1.42E-01	5.47E+00	5.88E-06	1.37E-06	6.10E-10	6.30E-05	
9	370	3000	5.67E-02	3.74E-03	0	1.02E-02	1.42E-01	5.49E+00	7.21E-06	1.15E-06	4.18E-10	5.03E-05	
10	370	3000	5.67E-02	3.74E-03	0	1.02E-02	1.42E-01	5.51E+00	8.38E-06	1.02E-06	3.16E-10	4.21E-05	
11	370	3000	5.67E-02	3.74E-03	0	1.02E-02	1.42E-01	5.52E+00	9.43E-06	9.34E-07	2.53E-10	3.63E-05	
12	370	3000	5.67E-02	3.74E-03	0	1.02E-02	1.42E-01	5.54E+00	1.04E-05	8.72E-07	2.11E-10	3.19E-05	
13	370	3000	5.67E-02	3.74E-03	0	1.02E-02	1.42E-01	5.56E+00	1.12E-05	8.26E-07	1.80E-10	2.85E-05	
14	370	3000	5.67E-02	3.74E-03	0	1.02E-02	1.42E-01	5.57E+00	1.20E-05	7.92E-07	1.57E-10	2.56E-05	
15	370	3000	5.67E-02	3.74E-03	0	1.02E-02	1.42E-01	5.59E+00	1.27E-05	7.65E-07	1.39E-10	2.33E-05	
16	370	3000	5.67E-02	3.74E-03	0	1.02E-02	1.42E-01	5.60E+00	1.33E-05	7.44E-07	1.25E-10	2.12E-05	
17	370	3000	5.67E-02	3.74E-03	0	1.02E-02	1.42E-01	5.62E+00	1.39E-05	7.27E-07	1.13E-10	1.94E-05	
18	370	3000	5.67E-02	3.74E-03	0	1.02E-02	1.42E-01	5.63E+00	1.44E-05	7.14E-07	1.02E-10	1.78E-05	
Ore fluids	500	5000	0	0	0	0	0	4.86E+00	1.66E-08	2.62E-03	3.42E-05	9.52E-03	
1	340	3000	6.67E-02	0	0	1.02E-02	1.39E-01	5.33E+00	2.50E-08	2.59E-04	1.03E-04	3.08E-02	
2	340	3000	6.47E-02	0	0	1.02E-02	1.45E-01	5.37E+00	2.96E-08	2.07E-04	5.82E-05	2.34E-02	
3	340	3000	6.41E-02	0	0	1.02E-02	1.47E-01	5.41E+00	3.97E-08	1.41E-04	2.33E-05	1.53E-02	
4	340	3000	5.92E-02	2.04E-03	1.70E-03	1.02E-02	1.52E-01	5.45E+00	7.19E-08	6.76E-05	4.69E-06	7.55E-03	
5	340	3000	5.67E-02	3.74E-03	0	1.02E-02	1.43E-01	5.47E+00	9.16E-07	6.12E-06	4.42E-08	6.86E-04	
6	340	3000	5.67E-02	3.74E-03	0	1.02E-02	1.42E-01	5.49E+00	2.78E-06	2.22E-06	5.94E-09	2.35E-04	
7	340	3000	5.67E-02	3.74E-03	0	1.02E-02	1.42E-01	5.51E+00	4.56E-06	1.42E-06	2.36E-09	1.41E-04	

		Formula:	KAl ₃ Si ₃ O ₁₀ (OH) ₂	Ca ₂ Al ₃ Si ₃ O ₁₂ (OH)	Ca ₂ FeAl ₂ Si ₃ O ₁₂ O _H	Mg _{4.5} Al ₃ Si _{2.5} O ₁₀ (OH) ₈	Na(AlSi ₃ O ₈)	H ₂ O	H ⁺	OH ⁻	CO ₃ ⁻⁻	HCO ₃ ⁻
		Type:	(s)	(s)	(s)	(s)	(s)	(a)	(a)	(a)	(a)	(a)
Cell	T (°C)	P(bar)	Muscovite	Zoisite	Epidote	Chlorite	Albite	H ₂ O	H ⁺	OH ⁻	CO ₃ ⁻⁻	HCO ₃ ⁻
8	340	3000	5.67E-02	3.74E-03	0	1.02E-02	1.42E-01	5.53E+00	6.13E-06	1.10E-06	1.35E-09	1.02E-04
9	340	3000	5.67E-02	3.74E-03	0	1.02E-02	1.42E-01	5.55E+00	7.49E-06	9.26E-07	9.11E-10	8.00E-05
10	340	3000	5.67E-02	3.74E-03	0	1.02E-02	1.42E-01	5.57E+00	8.68E-06	8.23E-07	6.77E-10	6.58E-05
11	340	3000	5.67E-02	3.74E-03	0	1.02E-02	1.42E-01	5.59E+00	9.73E-06	7.55E-07	5.32E-10	5.56E-05
12	340	3000	5.67E-02	3.74E-03	0	1.02E-02	1.42E-01	5.61E+00	1.07E-05	7.08E-07	4.34E-10	4.78E-05
13	340	3000	5.67E-02	3.74E-03	0	1.02E-02	1.42E-01	5.63E+00	1.15E-05	6.73E-07	3.61E-10	4.14E-05
14	340	3000	5.67E-02	3.74E-03	0	1.02E-02	1.42E-01	5.64E+00	1.22E-05	6.47E-07	3.06E-10	3.61E-05
15	340	3000	5.67E-02	3.74E-03	0	1.02E-02	1.42E-01	5.66E+00	1.29E-05	6.27E-07	2.61E-10	3.15E-05
16	340	3000	5.67E-02	3.74E-03	0	1.02E-02	1.42E-01	5.68E+00	1.35E-05	6.11E-07	2.25E-10	2.75E-05
17	340	3000	5.67E-02	3.74E-03	0	1.02E-02	1.42E-01	5.70E+00	1.41E-05	5.98E-07	1.94E-10	2.40E-05
18	340	3000	5.67E-02	3.74E-03	0	1.02E-02	1.42E-01	5.71E+00	1.46E-05	5.88E-07	1.67E-10	2.09E-05
Ore fluids	500	5000	0	0	0	0	0	4.86E+00	1.66E-08	2.62E-03	3.42E-05	9.52E-03
1	310	3000	7.01E-02	0	0	1.02E-02	1.29E-01	5.34E+00	3.94E-08	1.31E-04	1.09E-04	3.52E-02
2	310	3000	6.39E-02	0	0	1.02E-02	1.47E-01	5.39E+00	4.65E-08	1.05E-04	6.37E-05	2.72E-02
3	310	3000	6.27E-02	0	0	1.02E-02	1.51E-01	5.43E+00	6.42E-08	6.98E-05	2.48E-05	1.77E-02
4	310	3000	5.79E-02	2.37E-03	1.37E-03	1.02E-02	1.55E-01	5.47E+00	1.24E-07	3.14E-05	4.49E-06	8.38E-03
5	310	3000	5.67E-02	3.75E-03	0	1.02E-02	1.43E-01	5.48E+00	1.03E-06	4.27E-06	9.37E-08	1.15E-03
6	310	3000	5.67E-02	3.74E-03	0	1.02E-02	1.42E-01	5.50E+00	2.89E-06	1.66E-06	1.44E-08	4.23E-04
7	310	3000	5.67E-02	3.74E-03	0	1.02E-02	1.42E-01	5.52E+00	4.65E-06	1.08E-06	5.91E-09	2.58E-04
8	310	3000	5.67E-02	3.74E-03	0	1.02E-02	1.42E-01	5.55E+00	6.18E-06	8.45E-07	3.43E-09	1.87E-04
9	310	3000	5.67E-02	3.74E-03	0	1.02E-02	1.42E-01	5.57E+00	7.49E-06	7.20E-07	2.34E-09	1.47E-04
10	310	3000	5.67E-02	3.74E-03	0	1.02E-02	1.42E-01	5.59E+00	8.62E-06	6.45E-07	1.75E-09	1.20E-04

		Formula:	KAl ₃ Si ₃ O ₁₀ (OH) ₂	Ca ₂ Al ₃ Si ₃ O ₁₂ (OH)	Ca ₂ FeAl ₂ Si ₃ O ₁₂ O _H	Mg _{4.5} Al ₃ Si _{2.5} O ₁₀ (OH) ₈	Na(AlSi ₃ O ₈)	H ₂ O	H ⁺	OH ⁻	CO ₃ ⁻⁻	HCO ₃ ⁻
		Type:	(s)	(s)	(s)	(s)	(s)	(a)	(a)	(a)	(a)	(a)
Cell	T (°C)	P(bar)	Muscovite	Zoisite	Epidote	Chlorite	Albite	H ₂ O	H ⁺	OH ⁻	CO ₃ ⁻⁻	HCO ₃ ⁻
11	310	3000	5.67E-02	3.74E-03	0	1.02E-02	1.42E-01	5.61E+00	9.60E-06	5.96E-07	1.37E-09	1.01E-04
12	310	3000	5.67E-02	3.74E-03	0	1.02E-02	1.42E-01	5.63E+00	1.05E-05	5.61E-07	1.11E-09	8.54E-05
13	310	3000	5.67E-02	3.74E-03	0	1.02E-02	1.42E-01	5.65E+00	1.12E-05	5.37E-07	9.11E-10	7.27E-05
14	310	3000	5.67E-02	3.74E-03	0	1.02E-02	1.42E-01	5.67E+00	1.19E-05	5.18E-07	7.55E-10	6.17E-05
15	310	3000	5.67E-02	3.74E-03	0	1.02E-02	1.42E-01	5.69E+00	1.25E-05	5.04E-07	6.25E-10	5.21E-05
16	310	3000	5.67E-02	3.74E-03	0	1.02E-02	1.42E-01	5.71E+00	1.31E-05	4.93E-07	5.14E-10	4.34E-05
17	310	3000	5.67E-02	3.74E-03	0	1.02E-02	1.42E-01	5.73E+00	1.36E-05	4.84E-07	4.18E-10	3.56E-05
18	310	3000	5.67E-02	3.74E-03	0	1.02E-02	1.42E-01	5.75E+00	1.41E-05	4.78E-07	3.34E-10	2.86E-05
Ore fluids	500	5000	0	0	0	0	0	4.86E+00	1.66E-08	2.62E-03	3.42E-05	9.52E-03
1	280	3000	7.47E-02	0	0	1.02E-02	1.15E-01	5.35E+00	5.73E-08	6.42E-05	1.21E-04	4.00E-02
2	280	3000	6.25E-02	0	0	1.02E-02	1.51E-01	5.40E+00	6.89E-08	5.14E-05	7.07E-05	3.11E-02
3	280	3000	6.04E-02	0	0	1.02E-02	1.58E-01	5.44E+00	1.03E-07	3.16E-05	2.43E-05	1.95E-02
4	280	3000	5.70E-02	2.75E-03	1.00E-03	1.02E-02	1.58E-01	5.48E+00	2.06E-07	1.39E-05	4.26E-06	9.11E-03
5	280	3000	5.67E-02	3.75E-03	0	1.02E-02	1.43E-01	5.50E+00	1.15E-06	2.73E-06	1.81E-07	1.80E-03
6	280	3000	5.67E-02	3.74E-03	0	1.02E-02	1.42E-01	5.52E+00	2.88E-06	1.18E-06	3.38E-08	7.26E-04
7	280	3000	5.67E-02	3.74E-03	0	1.02E-02	1.42E-01	5.54E+00	4.47E-06	7.96E-07	1.46E-08	4.49E-04
8	280	3000	5.67E-02	3.74E-03	0	1.02E-02	1.42E-01	5.56E+00	5.81E-06	6.34E-07	8.63E-09	3.24E-04
9	280	3000	5.67E-02	3.74E-03	0	1.02E-02	1.42E-01	5.59E+00	6.93E-06	5.48E-07	5.96E-09	2.54E-04
10	280	3000	5.67E-02	3.74E-03	0	1.02E-02	1.42E-01	5.61E+00	7.89E-06	4.95E-07	4.46E-09	2.07E-04
11	280	3000	5.67E-02	3.74E-03	0	1.02E-02	1.42E-01	5.63E+00	8.70E-06	4.61E-07	3.48E-09	1.71E-04
12	280	3000	5.67E-02	3.74E-03	0	1.02E-02	1.42E-01	5.65E+00	9.40E-06	4.37E-07	2.78E-09	1.42E-04

		Formula:	KAl ₃ Si ₃ O ₁₀ (OH) ₂	Ca ₂ Al ₃ Si ₃ O ₁₂ (OH)	Ca ₂ FeAl ₂ Si ₃ O ₁₂ O _H	Mg _{4.5} Al ₃ Si _{2.5} O ₁₀ (OH) ₈	Na(AlSi ₃ O ₈)	H ₂ O	H ⁺	OH ⁻	CO ₃ ⁻⁻	HCO ₃ ⁻
		Type:	(s)	(s)	(s)	(s)	(s)	(a)	(a)	(a)	(a)	(a)
Cell	T (°C)	P(bar)	Muscovite	Zoisite	Epidote	Chlorite	Albite	H ₂ O	H ⁺	OH ⁻	CO ₃ ⁻⁻	HCO ₃ ⁻
13	280	3000	5.67E-02	3.74E-03	0	1.02E-02	1.42E-01	5.67E+00	1.00E-05	4.19E-07	2.23E-09	1.17E-04
14	280	3000	5.67E-02	3.74E-03	0	1.02E-02	1.42E-01	5.69E+00	1.05E-05	4.07E-07	1.78E-09	9.51E-05
15	280	3000	5.67E-02	3.74E-03	0	1.02E-02	1.42E-01	5.72E+00	1.10E-05	3.97E-07	1.39E-09	7.55E-05
16	280	3000	5.67E-02	3.74E-03	0	1.02E-02	1.42E-01	5.74E+00	1.14E-05	3.90E-07	1.05E-09	5.74E-05
17	280	3000	5.67E-02	3.74E-03	0	1.02E-02	1.42E-01	5.76E+00	1.18E-05	3.84E-07	7.47E-10	4.10E-05
18	280	3000	5.67E-02	3.74E-03	0	1.02E-02	1.42E-01	5.78E+00	1.22E-05	3.80E-07	4.83E-10	2.66E-05
Ore fluids	500	5000	0	0	0	0	0	4.86E+00	1.66E-08	2.62E-03	3.42E-05	9.52E-03
1	250	3000	8.00E-02	0	0	1.02E-02	9.90E-02	5.36E+00	8.38E-08	2.88E-05	1.31E-04	4.55E-02
2	250	3000	6.00E-02	0	0	1.02E-02	1.59E-01	5.40E+00	1.09E-07	2.15E-05	6.97E-05	3.49E-02
3	250	3000	5.78E-02	0	0	1.02E-02	1.65E-01	5.44E+00	1.85E-07	1.18E-05	1.99E-05	2.06E-02
4	250	3000	5.67E-02	3.34E-03	4.06E-04	1.02E-02	1.58E-01	5.49E+00	3.66E-07	5.35E-06	3.79E-06	1.00E-02
5	250	3000	5.67E-02	3.75E-03	0	1.02E-02	1.44E-01	5.50E+00	1.36E-06	1.53E-06	3.29E-07	2.86E-03
6	250	3000	5.67E-02	3.74E-03	0	1.02E-02	1.42E-01	5.52E+00	2.87E-06	7.76E-07	8.44E-08	1.36E-03
7	250	3000	5.67E-02	3.74E-03	0	1.02E-02	1.42E-01	5.55E+00	4.19E-06	5.54E-07	4.10E-08	8.89E-04
8	250	3000	5.67E-02	3.74E-03	0	1.02E-02	1.42E-01	5.57E+00	5.27E-06	4.56E-07	2.59E-08	6.62E-04
9	250	3000	5.67E-02	3.74E-03	0	1.02E-02	1.42E-01	5.59E+00	6.14E-06	4.02E-07	1.84E-08	5.23E-04
10	250	3000	5.67E-02	3.74E-03	0	1.02E-02	1.42E-01	5.61E+00	6.86E-06	3.69E-07	1.40E-08	4.23E-04
11	250	3000	5.67E-02	3.74E-03	0	1.02E-02	1.42E-01	5.64E+00	7.46E-06	3.48E-07	1.10E-08	3.46E-04
12	250	3000	5.67E-02	3.74E-03	0	1.02E-02	1.42E-01	5.66E+00	7.97E-06	3.33E-07	8.65E-09	2.81E-04
13	250	3000	5.67E-02	3.74E-03	0	1.02E-02	1.42E-01	5.68E+00	8.40E-06	3.22E-07	6.78E-09	2.24E-04
14	250	3000	5.67E-02	3.74E-03	0	1.02E-02	1.42E-01	5.71E+00	8.77E-06	3.14E-07	5.17E-09	1.73E-04
15	250	3000	5.67E-02	3.74E-03	0	1.02E-02	1.42E-01	5.73E+00	9.09E-06	3.09E-07	3.73E-09	1.25E-04

		Formula:	KAl ₃ Si ₃ O ₁₀ (OH) ₂	Ca ₂ Al ₃ Si ₃ O ₁₂ (OH)	Ca ₂ FeAl ₂ Si ₃ O ₁₂ O _H	Mg _{4.5} Al ₃ Si _{2.5} O ₁₀ (OH) ₈	Na(AlSi ₃ O ₈)	H ₂ O	H ⁺	OH ⁻	CO ₃ ⁻⁻	HCO ₃ ⁻
		Type:	(s)	(s)	(s)	(s)	(s)	(a)	(a)	(a)	(a)	(a)
Cell	T (°C)	P(bar)	Muscovite	Zoisite	Epidote	Chlorite	Albite	H ₂ O	H ⁺	OH ⁻	CO ₃ ⁻⁻	HCO ₃ ⁻
16	250	3000	5.67E-02	3.74E-03	0	1.02E-02	1.42E-01	5.75E+00	9.37E-06	3.05E-07	2.40E-09	8.08E-05
17	250	3000	5.67E-02	3.74E-03	0	1.02E-02	1.42E-01	5.77E+00	9.62E-06	3.01E-07	1.32E-09	4.43E-05
18	250	3000	5.67E-02	3.74E-03	0	1.02E-02	1.42E-01	5.79E+00	9.83E-06	2.99E-07	4.65E-10	1.56E-05
Ore fluids	500	5000	0	0	0	0	0	4.86E+00	1.66E-08	2.62E-03	3.42E-05	9.52E-03
1	220	3000	8.35E-02	0	0	1.02E-02	8.86E-02	5.36E+00	1.29E-07	1.13E-05	1.26E-04	5.02E-02
2	220	3000	5.75E-02	0	0	1.02E-02	1.66E-01	5.40E+00	1.86E-07	7.66E-06	5.90E-05	3.74E-02
3	220	3000	5.69E-02	0	0	1.02E-02	1.68E-01	5.45E+00	3.36E-07	3.97E-06	1.55E-05	2.15E-02
4	220	3000	5.67E-02	3.75E-03	0	1.02E-02	1.58E-01	5.49E+00	6.51E-07	1.88E-06	3.21E-06	1.08E-02
5	220	3000	5.67E-02	3.77E-03	0	1.02E-02	1.44E-01	5.51E+00	1.67E-06	7.61E-07	5.40E-07	4.32E-03
6	220	3000	5.67E-02	3.74E-03	0	1.02E-02	1.42E-01	5.53E+00	2.87E-06	4.68E-07	2.02E-07	2.49E-03
7	220	3000	5.67E-02	3.74E-03	0	1.02E-02	1.42E-01	5.55E+00	3.85E-06	3.63E-07	1.16E-07	1.77E-03
8	220	3000	5.67E-02	3.74E-03	0	1.02E-02	1.42E-01	5.57E+00	4.62E-06	3.13E-07	8.04E-08	1.38E-03
9	220	3000	5.67E-02	3.74E-03	0	1.02E-02	1.42E-01	5.59E+00	5.22E-06	2.85E-07	6.10E-08	1.12E-03
10	220	3000	5.67E-02	3.74E-03	0	1.02E-02	1.42E-01	5.62E+00	5.70E-06	2.67E-07	4.85E-08	9.30E-04
11	220	3000	5.67E-02	3.74E-03	0	1.02E-02	1.42E-01	5.64E+00	6.09E-06	2.56E-07	3.92E-08	7.71E-04
12	220	3000	5.67E-02	3.74E-03	0	1.02E-02	1.42E-01	5.66E+00	6.41E-06	2.48E-07	3.18E-08	6.34E-04
13	220	3000	5.67E-02	3.74E-03	0	1.02E-02	1.42E-01	5.68E+00	6.68E-06	2.43E-07	2.54E-08	5.09E-04
14	220	3000	5.67E-02	3.74E-03	0	1.02E-02	1.42E-01	5.71E+00	6.90E-06	2.39E-07	1.96E-08	3.94E-04
15	220	3000	5.67E-02	3.74E-03	0	1.02E-02	1.42E-01	5.73E+00	7.09E-06	2.36E-07	1.42E-08	2.84E-04
16	220	3000	5.67E-02	3.74E-03	0	1.02E-02	1.42E-01	5.75E+00	7.25E-06	2.35E-07	9.11E-09	1.81E-04
17	220	3000	5.67E-02	3.74E-03	0	1.02E-02	1.42E-01	5.78E+00	7.38E-06	2.34E-07	4.22E-09	8.32E-05
18	220	3000	5.67E-02	3.74E-03	0	1.02E-02	1.42E-01	5.79E+00	7.47E-06	2.34E-07	6.05E-10	1.18E-05

		Formula:	KAl ₃ Si ₃ O ₁₀ (OH) ₂	Ca ₂ Al ₃ Si ₃ O ₁₂ (OH) ₂	Ca ₂ FeAl ₂ Si ₃ O ₁₂ O _H	Mg _{4.5} Al ₃ Si _{2.5} O ₁₀ (OH) ₈	Na(AlSi ₃ O ₈)	H ₂ O	H ⁺	OH ⁻	CO ₃ ⁻⁻	HCO ₃ ⁻
		Type:	(s)	(s)	(s)	(s)	(s)	(a)	(a)	(a)	(a)	(a)
Cell	T (°C)	P(bar)	Muscovite	Zoisite	Epidote	Chlorite	Albite	H ₂ O	H ⁺	OH ⁻	CO ₃ ⁻⁻	HCO ₃ ⁻
Ore fluids	500	5000	0	0	0	0	0	4.86E+00	1.66E-08	2.62E-03	3.42E-05	9.52E-03
1	190	3000	8.44E-02	0	0	1.02E-02	8.59E-02	5.36E+00	2.15E-07	3.70E-06	1.05E-04	5.36E-02
2	190	3000	5.68E-02	0	0	1.02E-02	1.69E-01	5.40E+00	3.23E-07	2.42E-06	4.63E-05	3.93E-02
3	190	3000	5.67E-02	0	0	1.02E-02	1.69E-01	5.45E+00	5.82E-07	1.27E-06	1.22E-05	2.24E-02
4	190	3000	5.67E-02	3.75E-03	0	1.02E-02	1.58E-01	5.49E+00	1.07E-06	6.44E-07	2.80E-06	1.15E-02
5	190	3000	5.67E-02	3.81E-03	0	1.02E-02	1.44E-01	5.52E+00	2.00E-06	3.54E-07	8.39E-07	6.12E-03
6	190	3000	5.67E-02	3.74E-03	0	1.02E-02	1.42E-01	5.54E+00	2.78E-06	2.66E-07	4.60E-07	4.26E-03
7	190	3000	5.67E-02	3.74E-03	0	1.02E-02	1.42E-01	5.56E+00	3.37E-06	2.28E-07	3.18E-07	3.32E-03
8	190	3000	5.67E-02	3.74E-03	0	1.02E-02	1.42E-01	5.58E+00	3.81E-06	2.08E-07	2.45E-07	2.71E-03
9	190	3000	5.67E-02	3.74E-03	0	1.02E-02	1.42E-01	5.60E+00	4.15E-06	1.96E-07	1.98E-07	2.26E-03
10	190	3000	5.67E-02	3.74E-03	0	1.02E-02	1.42E-01	5.63E+00	4.40E-06	1.89E-07	1.64E-07	1.90E-03
11	190	3000	5.67E-02	3.74E-03	0	1.02E-02	1.42E-01	5.65E+00	4.60E-06	1.85E-07	1.36E-07	1.57E-03
12	190	3000	5.67E-02	3.74E-03	0	1.02E-02	1.42E-01	5.67E+00	4.76E-06	1.83E-07	1.11E-07	1.28E-03
13	190	3000	5.67E-02	3.74E-03	0	1.02E-02	1.42E-01	5.69E+00	4.88E-06	1.81E-07	8.78E-08	1.00E-03
14	190	3000	5.67E-02	3.74E-03	0	1.02E-02	1.42E-01	5.72E+00	4.98E-06	1.80E-07	6.55E-08	7.39E-04
15	190	3000	5.67E-02	3.74E-03	0	1.02E-02	1.42E-01	5.74E+00	5.06E-06	1.80E-07	4.35E-08	4.83E-04
16	190	3000	5.67E-02	3.74E-03	0	1.02E-02	1.42E-01	5.76E+00	5.11E-06	1.81E-07	2.13E-08	2.32E-04
17	190	3000	5.67E-02	3.74E-03	0	1.02E-02	1.42E-01	5.78E+00	5.11E-06	1.83E-07	1.36E-09	1.44E-05
18	190	3000	5.67E-02	3.74E-03	0	1.02E-02	1.42E-01	5.78E+00	5.11E-06	1.85E-07	9.16E-11	9.47E-07
Ore fluids	500	5000	0	0	0	0	0	4.86E+00	1.66E-08	2.62E-03	3.42E-05	9.52E-03
1	160	3000	8.45E-02	0	0	1.02E-02	8.57E-02	5.40E+00	1.69E-07	2.29E-06	1.73E-04	5.62E-02

		Formula:	KAl ₃ Si ₃ O ₁₀ (OH) ₂	Ca ₂ Al ₃ Si ₃ O ₁₂ (OH)	Ca ₂ FeAl ₂ Si ₃ O ₁₂ O _H	Mg _{4.5} Al ₃ Si _{2.5} O ₁₀ (OH) ₈	Na(AlSi ₃ O ₈)	H ₂ O	H ⁺	OH ⁻	CO ₃ ⁻⁻	HCO ₃ ⁻
		Type:	(s)	(s)	(s)	(s)	(s)	(a)	(a)	(a)	(a)	(a)
Cell	T (°C)	P(bar)	Muscovite	Zoisite	Epidote	Chlorite	Albite	H ₂ O	H ⁺	OH ⁻	CO ₃ ⁻⁻	HCO ₃ ⁻
2	160	3000	5.67E-02	0	0	1.02E-02	1.69E-01	5.45E+00	2.31E-07	1.66E-06	8.39E-05	4.09E-02
3	160	3000	5.67E-02	0	0	1.02E-02	1.69E-01	5.50E+00	3.90E-07	9.37E-07	2.39E-05	2.33E-02
4	160	3000	5.67E-02	3.71E-03	0	1.02E-02	1.58E-01	5.55E+00	7.10E-07	4.85E-07	5.75E-06	1.21E-02
5	160	3000	5.67E-02	3.87E-03	0	1.02E-02	1.44E-01	5.57E+00	1.28E-06	2.76E-07	1.81E-06	6.56E-03
6	160	3000	5.67E-02	3.74E-03	0	1.02E-02	1.42E-01	5.59E+00	1.71E-06	2.16E-07	9.70E-07	4.30E-03
7	160	3000	5.67E-02	3.74E-03	0	1.02E-02	1.42E-01	5.61E+00	2.01E-06	1.90E-07	6.04E-07	2.93E-03
8	160	3000	5.67E-02	3.74E-03	0	1.02E-02	1.42E-01	5.63E+00	2.22E-06	1.77E-07	3.79E-07	1.91E-03
9	160	3000	5.67E-02	3.74E-03	0	1.02E-02	1.42E-01	5.65E+00	2.36E-06	1.71E-07	2.06E-07	1.04E-03
10	160	3000	5.67E-02	3.74E-03	0	1.02E-02	1.42E-01	5.68E+00	2.45E-06	1.69E-07	5.30E-08	2.65E-04
11	160	3000	5.67E-02	3.74E-03	0	1.02E-02	1.42E-01	5.68E+00	2.48E-06	1.70E-07	1.56E-10	7.50E-07
12	160	3000	5.67E-02	3.74E-03	0	1.02E-02	1.42E-01	5.69E+00	2.59E-06	1.65E-07	5.29E-11	2.57E-07
13	160	3000	5.67E-02	3.74E-03	0	1.02E-02	1.42E-01	5.69E+00	2.69E-06	1.60E-07	3.08E-11	1.51E-07
14	160	3000	5.67E-02	3.74E-03	0	1.02E-02	1.42E-01	5.69E+00	2.77E-06	1.56E-07	2.14E-11	1.05E-07
15	160	3000	5.67E-02	3.74E-03	0	1.02E-02	1.42E-01	5.69E+00	2.84E-06	1.54E-07	1.63E-11	8.01E-08
16	160	3000	5.67E-02	3.74E-03	0	1.02E-02	1.42E-01	5.69E+00	2.90E-06	1.51E-07	1.31E-11	6.43E-08
17	160	3000	5.67E-02	3.74E-03	0	1.02E-02	1.42E-01	5.69E+00	2.95E-06	1.50E-07	1.10E-11	5.36E-08
18	160	3000	5.67E-02	3.74E-03	0	1.02E-02	1.42E-01	5.69E+00	2.99E-06	1.48E-07	9.40E-12	4.57E-08

		Formula:	H2CO3	H3SiO4-	H4SiO4	H3AsO3	HAsO3--	As2S4--	HAs2S4-	O2	H2	H2S
		Type:	(a)	(a)	(a)	(a)	(a)	(a)	(a)	(a)	(a)	(a)
Cell	T (°C)	P(bar)	H2CO3 (aq)	H3SiO4-	H4SiO4 (aq)	H3AsO3 (aq)	HAsO3--	As2S4--	HAs2S4-	O2 (aq)	H2 (aq)	H2S (aq)
Ore fluids	500	5000	2.80E-01	1.82E-02	1.17E-02	4.00E-05	2.95E-08	1.18E-08	1.62E-10	3.31E-28	4.77E-03	6.95E-03
1	400	3000	1.82E-01	2.36E-03	4.34E-03	5.32E-05	2.52E-08	6.05E-09	6.94E-11	8.55E-33	7.18E-04	1.20E-03
2	400	3000	1.76E-01	1.83E-03	4.39E-03	5.21E-05	1.32E-08	3.03E-09	4.98E-11	8.26E-33	7.37E-04	1.21E-03
3	400	3000	1.75E-01	1.41E-03	4.43E-03	5.18E-05	7.05E-09	1.58E-09	3.72E-11	8.17E-33	7.48E-04	1.22E-03
4	400	3000	1.74E-01	9.20E-04	4.47E-03	5.17E-05	2.56E-09	5.67E-10	2.36E-11	8.11E-33	7.57E-04	1.22E-03
5	400	3000	1.76E-01	8.61E-05	4.49E-03	5.22E-05	2.23E-11	4.97E-12	2.23E-12	8.18E-33	7.59E-04	1.23E-03
6	400	3000	1.72E-01	1.54E-05	4.49E-03	5.12E-05	8.38E-13	1.81E-13	3.80E-13	8.03E-33	7.70E-04	1.23E-03
7	400	3000	1.67E-01	8.69E-06	4.50E-03	5.00E-05	2.78E-13	5.82E-14	2.02E-13	7.82E-33	7.85E-04	1.23E-03
8	400	3000	1.62E-01	6.34E-06	4.50E-03	4.88E-05	1.50E-13	3.02E-14	1.38E-13	7.61E-33	8.00E-04	1.23E-03
9	400	3000	1.57E-01	5.16E-06	4.50E-03	4.75E-05	1.00E-13	1.94E-14	1.06E-13	7.40E-33	8.16E-04	1.23E-03
10	400	3000	1.53E-01	4.46E-06	4.51E-03	4.63E-05	7.49E-14	1.40E-14	8.55E-14	7.19E-33	8.32E-04	1.23E-03
11	400	3000	1.48E-01	4.00E-06	4.51E-03	4.50E-05	6.01E-14	1.08E-14	7.17E-14	6.98E-33	8.49E-04	1.23E-03
12	400	3000	1.43E-01	3.68E-06	4.51E-03	4.38E-05	5.05E-14	8.70E-15	6.17E-14	6.77E-33	8.66E-04	1.23E-03
13	400	3000	1.39E-01	3.44E-06	4.51E-03	4.26E-05	4.38E-14	7.26E-15	5.39E-14	6.57E-33	8.84E-04	1.23E-03
14	400	3000	1.34E-01	3.26E-06	4.51E-03	4.14E-05	3.89E-14	6.19E-15	4.77E-14	6.38E-33	9.02E-04	1.23E-03
15	400	3000	1.30E-01	3.12E-06	4.51E-03	4.03E-05	3.52E-14	5.38E-15	4.25E-14	6.18E-33	9.21E-04	1.23E-03
16	400	3000	1.26E-01	3.00E-06	4.51E-03	3.91E-05	3.23E-14	4.73E-15	3.82E-14	6.00E-33	9.40E-04	1.23E-03
17	400	3000	1.21E-01	2.91E-06	4.51E-03	3.80E-05	2.99E-14	4.21E-15	3.45E-14	5.81E-33	9.59E-04	1.23E-03
18	400	3000	1.17E-01	2.83E-06	4.51E-03	3.70E-05	2.79E-14	3.77E-15	3.13E-14	5.63E-33	9.79E-04	1.23E-03
Ore fluids	500	5000	2.80E-01	1.82E-02	1.17E-02	4.00E-05	2.95E-08	1.18E-08	1.62E-10	3.31E-28	4.77E-03	6.95E-03
1	370	3000	1.42E-01	1.46E-03	3.63E-03	6.67E-05	2.26E-08	4.20E-09	6.65E-11	2.23E-34	2.73E-04	6.43E-04
2	370	3000	1.37E-01	1.16E-03	3.68E-03	7.21E-05	1.37E-08	2.68E-09	5.91E-11	2.13E-34	2.82E-04	6.46E-04
3	370	3000	1.31E-01	7.92E-04	3.72E-03	7.01E-05	5.39E-09	9.96E-10	3.68E-11	2.04E-34	2.90E-04	6.48E-04

		Formula:	H2CO3	H3SiO4-	H4SiO4	H3AsO3	HAsO3--	As2S4--	HAs2S4-	O2	H2	H2S
		Type:	(a)	(a)	(a)	(a)	(a)	(a)	(a)	(a)	(a)	(a)
Cell	T (°C)	P(bar)	H2CO3 (aq)	H3SiO4-	H4SiO4 (aq)	H3AsO3 (aq)	HAsO3--	As2S4--	HAs2S4-	O2 (aq)	H2 (aq)	H2S (aq)
4	370	3000	1.32E-01	4.07E-04	3.76E-03	7.07E-05	1.18E-09	2.18E-10	1.88E-11	2.05E-34	2.92E-04	6.53E-04
5	370	3000	1.33E-01	2.50E-05	3.76E-03	7.09E-05	5.29E-12	9.79E-13	1.16E-12	2.06E-34	2.93E-04	6.55E-04
6	370	3000	1.28E-01	8.91E-06	3.77E-03	6.87E-05	7.23E-13	1.28E-13	3.83E-13	1.99E-34	3.00E-04	6.55E-04
7	370	3000	1.22E-01	5.66E-06	3.77E-03	6.62E-05	2.95E-13	4.93E-14	2.22E-13	1.91E-34	3.08E-04	6.54E-04
8	370	3000	1.17E-01	4.34E-06	3.78E-03	6.36E-05	1.72E-13	2.71E-14	1.54E-13	1.82E-34	3.17E-04	6.54E-04
9	370	3000	1.11E-01	3.64E-06	3.78E-03	6.10E-05	1.19E-13	1.76E-14	1.16E-13	1.74E-34	3.27E-04	6.53E-04
10	370	3000	1.05E-01	3.21E-06	3.79E-03	5.84E-05	9.05E-14	1.26E-14	9.18E-14	1.65E-34	3.37E-04	6.52E-04
11	370	3000	9.99E-02	2.92E-06	3.79E-03	5.58E-05	7.31E-14	9.52E-15	7.47E-14	1.57E-34	3.48E-04	6.51E-04
12	370	3000	9.45E-02	2.71E-06	3.80E-03	5.32E-05	6.14E-14	7.48E-15	6.19E-14	1.49E-34	3.59E-04	6.49E-04
13	370	3000	8.93E-02	2.56E-06	3.80E-03	5.08E-05	5.30E-14	6.03E-15	5.19E-14	1.41E-34	3.71E-04	6.48E-04
14	370	3000	8.43E-02	2.44E-06	3.80E-03	4.83E-05	4.67E-14	4.95E-15	4.39E-14	1.33E-34	3.84E-04	6.47E-04
15	370	3000	7.94E-02	2.35E-06	3.80E-03	4.60E-05	4.17E-14	4.12E-15	3.74E-14	1.26E-34	3.97E-04	6.45E-04
16	370	3000	7.47E-02	2.27E-06	3.80E-03	4.37E-05	3.77E-14	3.46E-15	3.19E-14	1.19E-34	4.11E-04	6.43E-04
17	370	3000	7.02E-02	2.21E-06	3.81E-03	4.14E-05	3.44E-14	2.93E-15	2.73E-14	1.12E-34	4.26E-04	6.41E-04
18	370	3000	6.59E-02	2.16E-06	3.81E-03	3.93E-05	3.15E-14	2.49E-15	2.35E-14	1.05E-34	4.41E-04	6.39E-04
Ore fluids	500	5000	2.80E-01	1.82E-02	1.17E-02	4.00E-05	2.95E-08	1.18E-08	1.62E-10	3.31E-28	4.77E-03	6.95E-03
1	340	3000	1.22E-01	7.61E-04	2.95E-03	6.67E-05	1.25E-08	1.52E-09	3.80E-11	4.65E-36	9.05E-05	3.28E-04
2	340	3000	1.16E-01	6.16E-04	2.98E-03	9.34E-05	1.04E-08	1.71E-09	5.77E-11	4.42E-36	9.37E-05	3.30E-04
3	340	3000	1.12E-01	4.27E-04	3.02E-03	1.06E-04	4.90E-09	8.92E-10	4.95E-11	4.23E-36	9.67E-05	3.31E-04
4	340	3000	1.15E-01	2.09E-04	3.05E-03	1.08E-04	9.83E-10	1.82E-10	2.50E-11	4.32E-36	9.66E-05	3.34E-04
5	340	3000	1.16E-01	1.86E-05	3.05E-03	1.10E-04	9.24E-12	1.73E-12	2.28E-12	4.39E-36	9.63E-05	3.35E-04
6	340	3000	1.11E-01	6.66E-06	3.06E-03	1.06E-04	1.25E-12	2.22E-13	7.42E-13	4.21E-36	9.89E-05	3.35E-04
7	340	3000	1.05E-01	4.22E-06	3.07E-03	1.01E-04	5.01E-13	8.31E-14	4.18E-13	3.98E-36	1.02E-04	3.34E-04

		Formula:	H2CO3	H3SiO4-	H4SiO4	H3AsO3	HAsO3--	As2S4--	HAs2S4-	O2	H2	H2S
		Type:	(a)	(a)	(a)	(a)	(a)	(a)	(a)	(a)	(a)	(a)
Cell	T (°C)	P(bar)	H2CO3 (aq)	H3SiO4-	H4SiO4 (aq)	H3AsO3 (aq)	HAsO3--	As2S4--	HAs2S4-	O2 (aq)	H2 (aq)	H2S (aq)
8	340	3000	9.87E-02	3.25E-06	3.07E-03	9.56E-05	2.89E-13	4.44E-14	2.81E-13	3.75E-36	1.06E-04	3.34E-04
9	340	3000	9.22E-02	2.73E-06	3.08E-03	9.03E-05	1.98E-13	2.79E-14	2.05E-13	3.51E-36	1.11E-04	3.33E-04
10	340	3000	8.58E-02	2.42E-06	3.08E-03	8.50E-05	1.49E-13	1.92E-14	1.56E-13	3.27E-36	1.15E-04	3.32E-04
11	340	3000	7.94E-02	2.21E-06	3.09E-03	7.97E-05	1.18E-13	1.39E-14	1.22E-13	3.03E-36	1.20E-04	3.31E-04
12	340	3000	7.31E-02	2.06E-06	3.09E-03	7.44E-05	9.79E-14	1.04E-14	9.57E-14	2.79E-36	1.26E-04	3.30E-04
13	340	3000	6.70E-02	1.95E-06	3.10E-03	6.91E-05	8.28E-14	7.93E-15	7.56E-14	2.56E-36	1.32E-04	3.28E-04
14	340	3000	6.10E-02	1.86E-06	3.10E-03	6.39E-05	7.11E-14	6.09E-15	5.97E-14	2.34E-36	1.40E-04	3.27E-04
15	340	3000	5.52E-02	1.80E-06	3.11E-03	5.88E-05	6.18E-14	4.69E-15	4.69E-14	2.12E-36	1.47E-04	3.25E-04
16	340	3000	4.97E-02	1.75E-06	3.11E-03	5.38E-05	5.40E-14	3.62E-15	3.67E-14	1.91E-36	1.56E-04	3.23E-04
17	340	3000	4.44E-02	1.70E-06	3.11E-03	4.90E-05	4.74E-14	2.78E-15	2.85E-14	1.71E-36	1.66E-04	3.21E-04
18	340	3000	3.95E-02	1.67E-06	3.11E-03	4.45E-05	4.17E-14	2.13E-15	2.20E-14	1.53E-36	1.76E-04	3.18E-04
Ore fluids	500	5000	2.80E-01	1.82E-02	1.17E-02	4.00E-05	2.95E-08	1.18E-08	1.62E-10	3.31E-28	4.77E-03	6.95E-03
1	310	3000	1.09E-01	3.60E-04	2.33E-03	6.67E-05	6.08E-09	4.87E-10	2.08E-11	6.99E-38	2.69E-05	1.59E-04
2	310	3000	1.05E-01	2.94E-04	2.36E-03	9.34E-05	5.15E-09	5.61E-10	3.19E-11	6.69E-38	2.78E-05	1.60E-04
3	310	3000	1.03E-01	1.99E-04	2.39E-03	1.20E-04	2.63E-09	3.60E-10	3.44E-11	6.54E-38	2.84E-05	1.61E-04
4	310	3000	1.08E-01	9.12E-05	2.42E-03	1.47E-04	5.53E-10	9.30E-11	2.34E-11	6.84E-38	2.80E-05	1.62E-04
5	310	3000	1.10E-01	1.22E-05	2.42E-03	1.74E-04	1.34E-11	2.68E-12	4.41E-12	6.98E-38	2.78E-05	1.63E-04
6	310	3000	1.05E-01	4.69E-06	2.42E-03	1.77E-04	2.19E-12	4.37E-13	1.72E-12	6.70E-38	2.86E-05	1.63E-04
7	310	3000	9.91E-02	3.03E-06	2.43E-03	1.68E-04	9.09E-13	1.68E-13	9.77E-13	6.31E-38	2.97E-05	1.63E-04
8	310	3000	9.24E-02	2.36E-06	2.43E-03	1.58E-04	5.33E-13	9.07E-14	6.56E-13	5.89E-38	3.09E-05	1.62E-04
9	310	3000	8.56E-02	2.00E-06	2.44E-03	1.49E-04	3.69E-13	5.71E-14	4.75E-13	5.46E-38	3.23E-05	1.62E-04
10	310	3000	7.87E-02	1.79E-06	2.45E-03	1.38E-04	2.79E-13	3.90E-14	3.56E-13	5.03E-38	3.39E-05	1.61E-04
11	310	3000	7.18E-02	1.64E-06	2.45E-03	1.28E-04	2.22E-13	2.78E-14	2.70E-13	4.60E-38	3.57E-05	1.60E-04

		Formula:	H2CO3	H3SiO4-	H4SiO4	H3AsO3	HAsO3--	As2S4--	HAs2S4-	O2	H2	H2S
		Type:	(a)	(a)	(a)	(a)	(a)	(a)	(a)	(a)	(a)	(a)
Cell	T (°C)	P(bar)	H2CO3 (aq)	H3SiO4-	H4SiO4 (aq)	H3AsO3 (aq)	HAsO3--	As2S4--	HAs2S4-	O2 (aq)	H2 (aq)	H2S (aq)
12	310	3000	6.50E-02	1.54E-06	2.46E-03	1.18E-04	1.83E-13	2.03E-14	2.06E-13	4.17E-38	3.77E-05	1.60E-04
13	310	3000	5.82E-02	1.47E-06	2.46E-03	1.08E-04	1.53E-13	1.48E-14	1.56E-13	3.74E-38	4.01E-05	1.59E-04
14	310	3000	5.14E-02	1.41E-06	2.47E-03	9.71E-05	1.29E-13	1.08E-14	1.17E-13	3.31E-38	4.29E-05	1.58E-04
15	310	3000	4.48E-02	1.36E-06	2.47E-03	8.66E-05	1.10E-13	7.79E-15	8.54E-14	2.89E-38	4.62E-05	1.56E-04
16	310	3000	3.84E-02	1.33E-06	2.48E-03	7.61E-05	9.26E-14	5.46E-15	6.07E-14	2.48E-38	5.01E-05	1.55E-04
17	310	3000	3.22E-02	1.30E-06	2.48E-03	6.57E-05	7.74E-14	3.71E-15	4.15E-14	2.08E-38	5.50E-05	1.53E-04
18	310	3000	2.63E-02	1.28E-06	2.48E-03	5.56E-05	6.39E-14	2.41E-15	2.72E-14	1.71E-38	6.11E-05	1.51E-04
Ore fluids	500	5000	2.80E-01	1.82E-02	1.17E-02	4.00E-05	2.95E-08	1.18E-08	1.62E-10	3.31E-28	4.77E-03	6.95E-03
1	280	3000	9.34E-02	1.69E-04	1.81E-03	6.67E-05	3.06E-09	1.24E-10	8.92E-12	6.51E-40	7.45E-06	6.79E-05
2	280	3000	9.10E-02	1.37E-04	1.83E-03	9.34E-05	2.56E-09	1.46E-10	1.42E-11	6.31E-40	7.64E-06	6.89E-05
3	280	3000	9.27E-02	8.60E-05	1.86E-03	1.20E-04	1.11E-09	8.00E-11	1.42E-11	6.40E-40	7.66E-06	6.93E-05
4	280	3000	9.84E-02	3.86E-05	1.88E-03	1.47E-04	2.24E-10	1.88E-11	8.98E-12	6.76E-40	7.52E-06	6.92E-05
5	280	3000	9.95E-02	7.51E-06	1.88E-03	1.74E-04	1.11E-11	1.10E-12	2.42E-12	6.85E-40	7.52E-06	6.94E-05
6	280	3000	9.40E-02	3.20E-06	1.89E-03	2.00E-04	2.54E-12	3.00E-13	1.43E-12	6.48E-40	7.77E-06	7.03E-05
7	280	3000	8.68E-02	2.15E-06	1.89E-03	2.27E-04	1.35E-12	1.90E-13	1.29E-12	5.99E-40	8.14E-06	7.16E-05
8	280	3000	7.91E-02	1.70E-06	1.90E-03	2.49E-04	9.59E-13	1.58E-13	1.31E-12	5.47E-40	8.58E-06	7.30E-05
9	280	3000	7.22E-02	1.46E-06	1.90E-03	2.30E-04	6.70E-13	1.00E-13	9.39E-13	5.00E-40	9.03E-06	7.31E-05
10	280	3000	6.53E-02	1.31E-06	1.91E-03	2.11E-04	5.09E-13	6.74E-14	6.86E-13	4.53E-40	9.55E-06	7.27E-05
11	280	3000	5.83E-02	1.22E-06	1.91E-03	1.92E-04	4.05E-13	4.68E-14	5.03E-13	4.05E-40	1.02E-05	7.23E-05
12	280	3000	5.13E-02	1.15E-06	1.92E-03	1.73E-04	3.30E-13	3.27E-14	3.65E-13	3.57E-40	1.09E-05	7.18E-05
13	280	3000	4.43E-02	1.10E-06	1.92E-03	1.53E-04	2.72E-13	2.26E-14	2.59E-13	3.09E-40	1.18E-05	7.11E-05
14	280	3000	3.74E-02	1.06E-06	1.92E-03	1.33E-04	2.23E-13	1.52E-14	1.77E-13	2.61E-40	1.29E-05	7.04E-05
15	280	3000	3.05E-02	1.03E-06	1.93E-03	1.12E-04	1.81E-13	9.64E-15	1.14E-13	2.14E-40	1.44E-05	6.94E-05

		Formula:	H2CO3	H3SiO4-	H4SiO4	H3AsO3	HAsO3--	As2S4--	HAs2S4-	O2	H2	H2S
		Type:	(a)	(a)	(a)	(a)	(a)	(a)	(a)	(a)	(a)	(a)
Cell	T (°C)	P(bar)	H2CO3 (aq)	H3SiO4-	H4SiO4 (aq)	H3AsO3 (aq)	HAsO3--	As2S4--	HAs2S4-	O2 (aq)	H2 (aq)	H2S (aq)
16	280	3000	2.38E-02	1.01E-06	1.93E-03	9.12E-05	1.42E-13	5.65E-15	6.73E-14	1.67E-40	1.64E-05	6.82E-05
17	280	3000	1.73E-02	9.91E-07	1.94E-03	7.00E-05	1.06E-13	2.91E-15	3.48E-14	1.22E-40	1.93E-05	6.66E-05
18	280	3000	1.14E-02	9.76E-07	1.94E-03	4.95E-05	7.39E-14	1.24E-15	1.48E-14	8.03E-41	2.39E-05	6.45E-05
Ore fluids	500	5000	2.80E-01	1.82E-02	1.17E-02	4.00E-05	2.95E-08	1.18E-08	1.62E-10	3.31E-28	4.77E-03	6.95E-03
1	250	3000	8.20E-02	7.37E-05	1.38E-03	6.67E-05	1.39E-09	5.57E-12	7.35E-13	3.73E-42	1.83E-06	1.81E-05
2	250	3000	8.45E-02	5.58E-05	1.39E-03	9.34E-05	1.00E-09	5.47E-12	1.05E-12	3.83E-42	1.83E-06	1.82E-05
3	250	3000	9.13E-02	3.12E-05	1.41E-03	1.20E-04	3.41E-10	2.25E-12	8.98E-13	4.11E-42	1.78E-06	1.81E-05
4	250	3000	9.72E-02	1.45E-05	1.43E-03	1.47E-04	7.43E-11	5.73E-13	5.87E-13	4.36E-42	1.74E-06	1.81E-05
5	250	3000	9.77E-02	4.11E-06	1.43E-03	1.74E-04	7.60E-12	6.90E-14	2.31E-13	4.39E-42	1.75E-06	1.81E-05
6	250	3000	9.24E-02	2.06E-06	1.44E-03	2.00E-04	2.37E-12	2.58E-14	1.60E-13	4.16E-42	1.81E-06	1.84E-05
7	250	3000	8.54E-02	1.46E-06	1.44E-03	2.27E-04	1.42E-12	1.84E-14	1.53E-13	3.84E-42	1.89E-06	1.87E-05
8	250	3000	7.78E-02	1.20E-06	1.44E-03	2.54E-04	1.10E-12	1.69E-14	1.66E-13	3.51E-42	1.99E-06	1.91E-05
9	250	3000	7.00E-02	1.05E-06	1.45E-03	2.80E-04	9.59E-13	1.76E-14	1.91E-13	3.16E-42	2.12E-06	1.95E-05
10	250	3000	6.21E-02	9.60E-07	1.45E-03	3.07E-04	8.99E-13	1.96E-14	2.26E-13	2.81E-42	2.26E-06	2.00E-05
11	250	3000	5.42E-02	9.00E-07	1.46E-03	3.34E-04	8.77E-13	2.27E-14	2.73E-13	2.45E-42	2.43E-06	2.06E-05
12	250	3000	4.62E-02	8.58E-07	1.46E-03	3.60E-04	8.77E-13	2.73E-14	3.37E-13	2.09E-42	2.65E-06	2.12E-05
13	250	3000	3.83E-02	8.27E-07	1.46E-03	3.33E-04	7.65E-13	2.49E-14	3.13E-13	1.74E-42	2.93E-06	2.20E-05
14	250	3000	3.04E-02	8.04E-07	1.47E-03	2.59E-04	5.72E-13	1.69E-14	2.15E-13	1.38E-42	3.31E-06	2.30E-05
15	250	3000	2.26E-02	7.86E-07	1.47E-03	1.88E-04	4.02E-13	1.05E-14	1.34E-13	1.03E-42	3.86E-06	2.43E-05
16	250	3000	1.49E-02	7.73E-07	1.47E-03	1.19E-04	2.50E-13	5.46E-15	6.98E-14	6.77E-43	4.79E-06	2.61E-05
17	250	3000	8.27E-03	7.62E-07	1.48E-03	6.84E-05	1.41E-13	1.90E-15	2.42E-14	3.78E-43	6.45E-06	2.67E-05
18	250	3000	2.95E-03	7.53E-07	1.48E-03	2.90E-05	5.94E-14	2.37E-16	3.02E-15	1.35E-43	1.09E-05	2.45E-05
Ore fluids	500	5000	2.80E-01	1.82E-02	1.17E-02	4.00E-05	2.95E-08	1.18E-08	1.62E-10	3.31E-28	4.77E-03	6.95E-03

		Formula:	H2CO3	H3SiO4-	H4SiO4	H3AsO3	HAsO3--	As2S4--	HAs2S4-	O2	H2	H2S
		Type:	(a)	(a)	(a)	(a)	(a)	(a)	(a)	(a)	(a)	(a)
Cell	T (°C)	P(bar)	H2CO3 (aq)	H3SiO4-	H4SiO4 (aq)	H3AsO3 (aq)	HAsO3--	As2S4--	HAs2S4-	O2 (aq)	H2 (aq)	H2S (aq)
1	220	3000	7.47E-02	2.89E-05	1.02E-03	6.67E-05	5.08E-10	1.64E-13	4.56E-14	1.21E-44	3.93E-07	4.24E-06
2	220	3000	8.21E-02	1.99E-05	1.04E-03	9.34E-05	3.02E-10	1.27E-13	5.66E-14	1.32E-44	3.79E-07	4.21E-06
3	220	3000	9.10E-02	1.06E-05	1.05E-03	1.20E-04	9.19E-11	4.60E-14	4.53E-14	1.46E-44	3.65E-07	4.18E-06
4	220	3000	9.66E-02	5.08E-06	1.06E-03	1.47E-04	2.20E-11	1.28E-14	3.08E-14	1.54E-44	3.58E-07	4.17E-06
5	220	3000	9.61E-02	2.05E-06	1.06E-03	1.74E-04	4.39E-12	3.04E-15	1.73E-14	1.53E-44	3.61E-07	4.20E-06
6	220	3000	9.06E-02	1.25E-06	1.07E-03	2.00E-04	2.01E-12	1.67E-15	1.46E-14	1.45E-44	3.73E-07	4.26E-06
7	220	3000	8.37E-02	9.62E-07	1.07E-03	2.27E-04	1.41E-12	1.41E-15	1.52E-14	1.34E-44	3.91E-07	4.33E-06
8	220	3000	7.63E-02	8.24E-07	1.07E-03	2.54E-04	1.20E-12	1.42E-15	1.73E-14	1.22E-44	4.12E-07	4.42E-06
9	220	3000	6.86E-02	7.46E-07	1.08E-03	2.80E-04	1.12E-12	1.57E-15	2.04E-14	1.10E-44	4.37E-07	4.52E-06
10	220	3000	6.08E-02	6.97E-07	1.08E-03	3.07E-04	1.10E-12	1.83E-15	2.47E-14	9.78E-45	4.67E-07	4.63E-06
11	220	3000	5.30E-02	6.64E-07	1.08E-03	3.34E-04	1.11E-12	2.20E-15	3.05E-14	8.53E-45	5.03E-07	4.76E-06
12	220	3000	4.51E-02	6.41E-07	1.08E-03	3.60E-04	1.14E-12	2.72E-15	3.81E-14	7.28E-45	5.49E-07	4.92E-06
13	220	3000	3.73E-02	6.25E-07	1.09E-03	3.87E-04	1.19E-12	3.45E-15	4.85E-14	6.02E-45	6.07E-07	5.10E-06
14	220	3000	2.94E-02	6.13E-07	1.09E-03	4.14E-04	1.24E-12	4.52E-15	6.34E-14	4.76E-45	6.88E-07	5.33E-06
15	220	3000	2.16E-02	6.04E-07	1.09E-03	4.40E-04	1.30E-12	6.21E-15	8.68E-14	3.50E-45	8.08E-07	5.64E-06
16	220	3000	1.39E-02	5.97E-07	1.10E-03	3.45E-04	1.02E-12	5.07E-15	7.05E-14	2.26E-45	1.01E-06	6.09E-06
17	220	3000	6.45E-03	5.93E-07	1.10E-03	1.50E-04	4.41E-13	1.60E-15	2.20E-14	1.05E-45	1.50E-06	6.96E-06
18	220	3000	9.17E-04	5.91E-07	1.10E-03	2.01E-05	5.96E-14	7.00E-17	9.49E-16	1.49E-46	3.99E-06	8.71E-06
Ore fluids	500	5000	2.80E-01	1.82E-02	1.17E-02	4.00E-05	2.95E-08	1.18E-08	1.62E-10	3.31E-28	4.77E-03	6.95E-03
1	190	3000	7.26E-02	9.77E-06	7.35E-04	6.67E-05	1.40E-10	2.80E-15	1.97E-15	2.03E-47	7.09E-08	8.50E-07
2	190	3000	8.16E-02	6.49E-06	7.45E-04	9.34E-05	7.72E-11	1.98E-15	2.32E-15	2.26E-47	6.77E-08	8.41E-07
3	190	3000	8.88E-02	3.48E-06	7.56E-04	1.20E-04	2.41E-11	7.43E-16	1.90E-15	2.45E-47	6.57E-08	8.38E-07
4	190	3000	8.95E-02	1.80E-06	7.66E-04	1.47E-04	6.68E-12	2.48E-16	1.42E-15	2.46E-47	6.63E-08	8.45E-07

		Formula:	H2CO3	H3SiO4-	H4SiO4	H3AsO3	HAsO3--	As2S4--	HAs2S4-	O2	H2	H2S
		Type:	(a)	(a)	(a)	(a)	(a)	(a)	(a)	(a)	(a)	(a)
Cell	T (°C)	P(bar)	H2CO3 (aq)	H3SiO4-	H4SiO4 (aq)	H3AsO3 (aq)	HAsO3--	As2S4--	HAs2S4-	O2 (aq)	H2 (aq)	H2S (aq)
5	190	3000	8.75E-02	9.83E-07	7.69E-04	1.74E-04	2.42E-12	1.08E-16	1.10E-15	2.40E-47	6.74E-08	8.52E-07
6	190	3000	8.16E-02	7.34E-07	7.70E-04	2.00E-04	1.64E-12	8.84E-17	1.14E-15	2.24E-47	7.02E-08	8.66E-07
7	190	3000	7.47E-02	6.25E-07	7.72E-04	2.27E-04	1.41E-12	9.10E-17	1.32E-15	2.06E-47	7.38E-08	8.83E-07
8	190	3000	6.73E-02	5.67E-07	7.74E-04	2.54E-04	1.34E-12	1.04E-16	1.60E-15	1.86E-47	7.82E-08	9.02E-07
9	190	3000	5.98E-02	5.33E-07	7.76E-04	2.80E-04	1.35E-12	1.25E-16	1.99E-15	1.65E-47	8.35E-08	9.25E-07
10	190	3000	5.22E-02	5.12E-07	7.79E-04	3.07E-04	1.40E-12	1.56E-16	2.50E-15	1.44E-47	8.99E-08	9.50E-07
11	190	3000	4.46E-02	4.98E-07	7.81E-04	3.34E-04	1.48E-12	1.99E-16	3.18E-15	1.24E-47	9.79E-08	9.80E-07
12	190	3000	3.70E-02	4.89E-07	7.83E-04	3.60E-04	1.57E-12	2.58E-16	4.12E-15	1.03E-47	1.08E-07	1.02E-06
13	190	3000	2.94E-02	4.83E-07	7.85E-04	3.87E-04	1.68E-12	3.46E-16	5.45E-15	8.17E-48	1.22E-07	1.06E-06
14	190	3000	2.19E-02	4.79E-07	7.87E-04	4.14E-04	1.80E-12	4.83E-16	7.51E-15	6.08E-48	1.42E-07	1.12E-06
15	190	3000	1.44E-02	4.77E-07	7.89E-04	4.40E-04	1.94E-12	7.32E-16	1.12E-14	4.00E-48	1.77E-07	1.21E-06
16	190	3000	6.93E-03	4.77E-07	7.91E-04	4.67E-04	2.09E-12	1.36E-15	2.04E-14	1.93E-48	2.56E-07	1.37E-06
17	190	3000	4.27E-04	4.81E-07	7.92E-04	2.60E-05	1.21E-13	2.81E-17	4.09E-16	1.19E-49	1.04E-06	2.19E-06
18	190	3000	2.79E-05	4.82E-07	7.89E-04	2.02E-06	9.68E-15	2.16E-19	3.06E-18	7.81E-51	4.06E-06	2.30E-06
Ore fluids	500	5000	2.80E-01	1.82E-02	1.17E-02	4.00E-05	2.95E-08	1.18E-08	1.62E-10	3.31E-28	4.77E-03	6.95E-03
1	160	3000	3.40E-02	6.51E-06	5.15E-04	6.67E-05	1.48E-10	2.26E-16	2.15E-16	6.76E-51	1.58E-08	1.64E-07
2	160	3000	3.44E-02	4.80E-06	5.24E-04	9.34E-05	9.96E-11	2.10E-16	3.01E-16	6.78E-51	1.60E-08	1.65E-07
3	160	3000	3.47E-02	2.78E-06	5.33E-04	1.20E-04	3.61E-11	9.60E-17	2.77E-16	6.79E-51	1.62E-08	1.67E-07
4	160	3000	3.50E-02	1.46E-06	5.40E-04	1.47E-04	1.05E-11	3.38E-17	2.12E-16	6.82E-51	1.63E-08	1.68E-07
5	160	3000	3.34E-02	8.28E-07	5.42E-04	1.74E-04	4.10E-12	1.60E-17	1.73E-16	6.51E-51	1.68E-08	1.70E-07
6	160	3000	2.81E-02	6.44E-07	5.43E-04	2.00E-04	3.02E-12	1.53E-17	2.00E-16	5.49E-51	1.84E-08	1.76E-07
7	160	3000	2.19E-02	5.63E-07	5.44E-04	2.27E-04	2.73E-12	1.85E-17	2.65E-16	4.28E-51	2.09E-08	1.84E-07
8	160	3000	1.54E-02	5.22E-07	5.45E-04	2.54E-04	2.73E-12	2.61E-17	3.88E-16	3.01E-51	2.51E-08	1.96E-07

		Formula:	H2CO3	H3SiO4-	H4SiO4	H3AsO3	HAsO3--	As2S4--	HAs2S4-	O2	H2	H2S
		Type:	(a)	(a)	(a)	(a)	(a)	(a)	(a)	(a)	(a)	(a)
Cell	T (°C)	P(bar)	H2CO3 (aq)	H3SiO4-	H4SiO4 (aq)	H3AsO3 (aq)	HAsO3--	As2S4--	HAs2S4-	O2 (aq)	H2 (aq)	H2S (aq)
9	160	3000	8.80E-03	5.01E-07	5.46E-04	2.80E-04	2.86E-12	4.40E-17	6.58E-16	1.73E-51	3.34E-08	2.16E-07
10	160	3000	2.28E-03	4.91E-07	5.48E-04	3.07E-04	3.12E-12	1.29E-16	1.90E-15	4.48E-52	6.61E-08	2.72E-07
11	160	3000	6.42E-06	4.91E-07	5.47E-04	1.11E-06	1.18E-14	5.23E-20	7.38E-19	1.26E-54	1.25E-06	6.35E-07
12	160	3000	2.27E-06	4.72E-07	5.45E-04	4.67E-07	4.75E-15	6.26E-21	8.90E-20	4.49E-55	2.10E-06	5.82E-07
13	160	3000	1.37E-06	4.56E-07	5.42E-04	3.07E-07	3.01E-15	2.20E-21	3.15E-20	2.73E-55	2.70E-06	5.58E-07
14	160	3000	9.82E-07	4.43E-07	5.40E-04	2.32E-07	2.21E-15	1.09E-21	1.57E-20	1.96E-55	3.19E-06	5.42E-07
15	160	3000	7.63E-07	4.32E-07	5.38E-04	1.87E-07	1.75E-15	6.47E-22	9.27E-21	1.53E-55	3.62E-06	5.31E-07
16	160	3000	6.23E-07	4.23E-07	5.36E-04	1.58E-07	1.45E-15	4.24E-22	6.07E-21	1.25E-55	4.01E-06	5.22E-07
17	160	3000	5.25E-07	4.15E-07	5.34E-04	1.37E-07	1.25E-15	2.99E-22	4.26E-21	1.06E-55	4.36E-06	5.14E-07
18	160	3000	4.54E-07	4.09E-07	5.32E-04	1.21E-07	1.09E-15	2.21E-22	3.14E-21	9.20E-56	4.70E-06	5.08E-07

		Formula:	HS-	S2--	S2O3--	SO2	SO3--	HSO3-	SO4--	HSO4-	Na+	NaOH
		Type:	(a)	(a)	(a)	(a)	(a)	(a)	(a)	(a)	(a)	(a)
Cell	T (°C)	P(bar)	HS-	S2--	S2O3--	SO2 (aq)	SO3--	HSO3-	SO4--	HSO4-	Na+	NaOH (aq)
Ore fluids	500	5000	7.07E-03	1.08E-08	5.78E-12	7.01E-11	2.04E-12	1.04E-09	1.33E-08	4.52E-11	1.03E-02	1.84E-03
1	400	3000	2.41E-03	1.55E-09	1.23E-12	1.76E-12	4.95E-13	1.03E-10	1.23E-08	3.46E-11	4.87E-03	2.19E-04
2	400	3000	1.84E-03	8.15E-10	6.13E-13	1.66E-12	2.51E-13	7.44E-11	6.01E-09	2.47E-11	4.60E-03	1.76E-04
3	400	3000	1.40E-03	4.35E-10	3.20E-13	1.63E-12	1.32E-13	5.56E-11	3.08E-09	1.84E-11	4.17E-03	1.34E-04
4	400	3000	8.94E-04	1.58E-10	1.14E-13	1.61E-12	4.76E-14	3.53E-11	1.07E-09	1.17E-11	2.57E-03	6.16E-05
5	400	3000	8.36E-05	1.38E-12	1.00E-15	1.62E-12	4.17E-16	3.32E-12	9.42E-12	1.10E-12	1.59E-05	3.56E-08
6	400	3000	1.52E-05	5.20E-14	3.64E-17	1.57E-12	1.54E-17	5.78E-13	3.55E-13	1.88E-13	1.16E-05	3.83E-09
7	400	3000	8.67E-06	1.74E-14	1.16E-17	1.50E-12	4.99E-18	3.12E-13	1.15E-13	9.97E-14	1.04E-05	1.80E-09

		Formula:	HS-	S2--	S2O3--	SO2	SO3--	HSO3-	SO4--	HSO4-	Na+	NaOH
		Type:	(a)	(a)	(a)	(a)	(a)	(a)	(a)	(a)	(a)	(a)
Cell	T (°C)	P(bar)	HS-	S2--	S2O3--	SO2 (aq)	SO3--	HSO3-	SO4--	HSO4-	Na+	NaOH (aq)
8	400	3000	6.35E-06	9.43E-15	6.01E-18	1.43E-12	2.63E-18	2.17E-13	6.04E-14	6.81E-14	9.61E-06	1.16E-09
9	400	3000	5.19E-06	6.33E-15	3.84E-18	1.37E-12	1.71E-18	1.68E-13	3.89E-14	5.18E-14	9.03E-06	8.54E-10
10	400	3000	4.50E-06	4.76E-15	2.74E-18	1.30E-12	1.25E-18	1.39E-13	2.81E-14	4.18E-14	8.56E-06	6.78E-10
11	400	3000	4.05E-06	3.85E-15	2.10E-18	1.24E-12	9.77E-19	1.18E-13	2.18E-14	3.50E-14	8.15E-06	5.63E-10
12	400	3000	3.73E-06	3.25E-15	1.69E-18	1.18E-12	8.01E-19	1.03E-13	1.76E-14	3.00E-14	7.79E-06	4.82E-10
13	400	3000	3.50E-06	2.84E-15	1.40E-18	1.12E-12	6.78E-19	9.16E-14	1.47E-14	2.61E-14	7.47E-06	4.22E-10
14	400	3000	3.32E-06	2.54E-15	1.19E-18	1.06E-12	5.87E-19	8.24E-14	1.26E-14	2.31E-14	7.19E-06	3.75E-10
15	400	3000	3.18E-06	2.32E-15	1.03E-18	1.01E-12	5.17E-19	7.47E-14	1.10E-14	2.05E-14	6.93E-06	3.39E-10
16	400	3000	3.07E-06	2.14E-15	8.97E-19	9.60E-13	4.62E-19	6.82E-14	9.66E-15	1.84E-14	6.70E-06	3.09E-10
17	400	3000	2.98E-06	1.99E-15	7.93E-19	9.11E-13	4.17E-19	6.26E-14	8.60E-15	1.66E-14	6.48E-06	2.84E-10
18	400	3000	2.90E-06	1.88E-15	7.07E-19	8.65E-13	3.80E-19	5.77E-14	7.72E-15	1.50E-14	6.28E-06	2.63E-10
Ore fluids	500	5000	7.07E-03	1.08E-08	5.78E-12	7.01E-11	2.04E-12	1.04E-09	1.33E-08	4.52E-11	1.03E-02	1.84E-03
1	370	3000	1.42E-03	7.45E-10	1.26E-12	7.29E-13	4.86E-13	6.95E-11	2.05E-08	4.28E-11	6.96E-03	1.68E-04
2	370	3000	1.11E-03	4.09E-10	6.44E-13	6.76E-13	2.55E-13	5.05E-11	1.03E-08	3.05E-11	6.46E-03	1.35E-04
3	370	3000	7.42E-04	1.61E-10	2.37E-13	6.31E-13	9.63E-14	3.18E-11	3.70E-09	1.89E-11	5.18E-03	8.40E-05
4	370	3000	3.74E-04	3.53E-11	5.18E-14	6.33E-13	2.10E-14	1.62E-11	7.84E-10	9.67E-12	3.47E-04	3.45E-06
5	370	3000	2.34E-05	1.58E-13	2.33E-16	6.38E-13	9.46E-17	1.00E-12	3.64E-12	5.96E-13	1.11E-05	5.61E-09
6	370	3000	8.43E-06	2.18E-14	3.02E-17	6.01E-13	1.26E-17	3.39E-13	4.84E-13	1.96E-13	9.12E-06	1.47E-09
7	370	3000	5.38E-06	8.96E-15	1.16E-17	5.60E-13	4.94E-18	2.00E-13	1.88E-13	1.13E-13	8.30E-06	8.06E-10
8	370	3000	4.13E-06	5.27E-15	6.30E-18	5.19E-13	2.77E-18	1.42E-13	1.04E-13	7.80E-14	7.72E-06	5.53E-10
9	370	3000	3.47E-06	3.68E-15	4.06E-18	4.80E-13	1.85E-18	1.10E-13	6.75E-14	5.86E-14	7.26E-06	4.21E-10
10	370	3000	3.06E-06	2.83E-15	2.87E-18	4.42E-13	1.35E-18	8.91E-14	4.83E-14	4.61E-14	6.88E-06	3.41E-10
11	370	3000	2.78E-06	2.31E-15	2.15E-18	4.06E-13	1.04E-18	7.44E-14	3.66E-14	3.74E-14	6.54E-06	2.87E-10

		Formula:	HS-	S2--	S2O3--	SO2	SO3--	HSO3-	SO4--	HSO4-	Na+	NaOH
		Type:	(a)	(a)	(a)	(a)	(a)	(a)	(a)	(a)	(a)	(a)
Cell	T (°C)	P(bar)	HS-	S2--	S2O3--	SO2 (aq)	SO3--	HSO3-	SO4--	HSO4-	Na+	NaOH (aq)
12	370	3000	2.59E-06	1.96E-15	1.68E-18	3.72E-13	8.41E-19	6.32E-14	2.88E-14	3.08E-14	6.25E-06	2.49E-10
13	370	3000	2.44E-06	1.71E-15	1.34E-18	3.40E-13	6.95E-19	5.45E-14	2.32E-14	2.57E-14	5.99E-06	2.19E-10
14	370	3000	2.33E-06	1.52E-15	1.09E-18	3.11E-13	5.85E-19	4.73E-14	1.90E-14	2.17E-14	5.75E-06	1.97E-10
15	370	3000	2.24E-06	1.38E-15	8.95E-19	2.83E-13	5.00E-19	4.14E-14	1.58E-14	1.83E-14	5.54E-06	1.78E-10
16	370	3000	2.16E-06	1.26E-15	7.44E-19	2.57E-13	4.31E-19	3.63E-14	1.33E-14	1.56E-14	5.34E-06	1.63E-10
17	370	3000	2.10E-06	1.16E-15	6.23E-19	2.33E-13	3.75E-19	3.20E-14	1.12E-14	1.33E-14	5.16E-06	1.51E-10
18	370	3000	2.05E-06	1.08E-15	5.24E-19	2.11E-13	3.28E-19	2.83E-14	9.54E-15	1.14E-14	5.00E-06	1.40E-10
Ore fluids	500	5000	7.07E-03	1.08E-08	5.78E-12	7.01E-11	2.04E-12	1.04E-09	1.33E-08	4.52E-11	1.03E-02	1.84E-03
1	340	3000	7.12E-04	2.86E-10	1.28E-12	3.31E-13	4.37E-13	4.67E-11	3.50E-08	5.90E-11	1.08E-02	1.17E-04
2	340	3000	5.66E-04	1.64E-10	6.75E-13	3.05E-13	2.38E-13	3.44E-11	1.82E-08	4.24E-11	9.80E-03	9.24E-05
3	340	3000	3.84E-04	6.67E-11	2.56E-13	2.84E-13	9.31E-14	2.19E-11	6.79E-09	2.66E-11	7.38E-03	5.43E-05
4	340	3000	1.84E-04	1.33E-11	5.25E-14	2.93E-13	1.89E-14	1.09E-11	1.35E-09	1.34E-11	4.53E-04	1.95E-06
5	340	3000	1.67E-05	1.25E-13	5.01E-16	2.99E-13	1.79E-16	9.97E-13	1.32E-11	1.23E-12	8.84E-06	2.87E-09
6	340	3000	6.03E-06	1.71E-14	6.37E-17	2.79E-13	2.34E-17	3.33E-13	1.72E-12	3.98E-13	7.14E-06	7.42E-10
7	340	3000	3.83E-06	6.92E-15	2.36E-17	2.55E-13	8.97E-18	1.93E-13	6.45E-13	2.23E-13	6.45E-06	4.04E-10
8	340	3000	2.95E-06	4.04E-15	1.24E-17	2.31E-13	4.92E-18	1.34E-13	3.45E-13	1.49E-13	5.98E-06	2.77E-10
9	340	3000	2.48E-06	2.80E-15	7.75E-18	2.07E-13	3.20E-18	1.01E-13	2.18E-13	1.08E-13	5.61E-06	2.11E-10
10	340	3000	2.19E-06	2.13E-15	5.27E-18	1.85E-13	2.27E-18	7.93E-14	1.50E-13	8.20E-14	5.29E-06	1.71E-10
11	340	3000	1.99E-06	1.72E-15	3.77E-18	1.63E-13	1.70E-18	6.39E-14	1.08E-13	6.33E-14	5.02E-06	1.45E-10
12	340	3000	1.85E-06	1.44E-15	2.78E-18	1.43E-13	1.32E-18	5.21E-14	8.09E-14	4.95E-14	4.78E-06	1.25E-10
13	340	3000	1.75E-06	1.24E-15	2.08E-18	1.25E-13	1.04E-18	4.28E-14	6.14E-14	3.88E-14	4.57E-06	1.11E-10
14	340	3000	1.67E-06	1.08E-15	1.57E-18	1.07E-13	8.34E-19	3.53E-14	4.70E-14	3.04E-14	4.38E-06	9.93E-11
15	340	3000	1.60E-06	9.58E-16	1.19E-18	9.17E-14	6.71E-19	2.90E-14	3.61E-14	2.37E-14	4.21E-06	9.02E-11

		Formula:	HS-	S2--	S2O3--	SO2	SO3--	HSO3-	SO4--	HSO4-	Na+	NaOH
		Type:	(a)	(a)	(a)	(a)	(a)	(a)	(a)	(a)	(a)	(a)
Cell	T (°C)	P(bar)	HS-	S2--	S2O3--	SO2 (aq)	SO3--	HSO3-	SO4--	HSO4-	Na+	NaOH (aq)
16	340	3000	1.55E-06	8.53E-16	9.01E-19	7.76E-14	5.41E-19	2.38E-14	2.77E-14	1.84E-14	4.06E-06	8.26E-11
17	340	3000	1.50E-06	7.64E-16	6.79E-19	6.50E-14	4.36E-19	1.94E-14	2.11E-14	1.42E-14	3.92E-06	7.64E-11
18	340	3000	1.46E-06	6.86E-16	5.10E-19	5.41E-14	3.51E-19	1.58E-14	1.61E-14	1.08E-14	3.79E-06	7.10E-11
Ore fluids	500	5000	7.07E-03	1.08E-08	5.78E-12	7.01E-11	2.04E-12	1.04E-09	1.33E-08	4.52E-11	1.03E-02	1.84E-03
1	310	3000	3.17E-04	9.35E-11	1.26E-12	1.49E-13	3.71E-13	3.03E-11	6.19E-08	8.60E-11	1.74E-02	7.40E-05
2	310	3000	2.54E-04	5.52E-11	6.94E-13	1.39E-13	2.10E-13	2.27E-11	3.36E-08	6.33E-11	1.53E-02	5.66E-05
3	310	3000	1.68E-04	2.17E-11	2.63E-13	1.34E-13	8.05E-14	1.46E-11	1.24E-08	4.04E-11	1.02E-02	2.88E-05
4	310	3000	7.60E-05	3.87E-12	4.99E-14	1.43E-13	1.49E-14	7.07E-12	2.28E-09	2.01E-11	6.60E-04	1.02E-06
5	310	3000	1.04E-05	8.05E-14	1.06E-15	1.47E-13	3.15E-16	9.81E-13	4.95E-11	2.80E-12	6.93E-06	1.25E-09
6	310	3000	4.00E-06	1.26E-14	1.54E-16	1.38E-13	4.70E-17	3.51E-13	7.36E-12	9.73E-13	5.42E-06	3.39E-10
7	310	3000	2.59E-06	5.27E-15	5.87E-17	1.25E-13	1.86E-17	2.06E-13	2.84E-12	5.51E-13	4.84E-06	1.86E-10
8	310	3000	2.02E-06	3.13E-15	3.12E-17	1.12E-13	1.03E-17	1.43E-13	1.54E-12	3.68E-13	4.45E-06	1.28E-10
9	310	3000	1.71E-06	2.20E-15	1.94E-17	9.87E-14	6.72E-18	1.07E-13	9.66E-13	2.64E-13	4.15E-06	9.78E-11
10	310	3000	1.52E-06	1.69E-15	1.31E-17	8.63E-14	4.76E-18	8.32E-14	6.59E-13	1.96E-13	3.89E-06	7.94E-11
11	310	3000	1.39E-06	1.37E-15	9.17E-18	7.46E-14	3.53E-18	6.60E-14	4.69E-13	1.48E-13	3.68E-06	6.71E-11
12	310	3000	1.30E-06	1.14E-15	6.56E-18	6.36E-14	2.69E-18	5.26E-14	3.40E-13	1.12E-13	3.49E-06	5.82E-11
13	310	3000	1.23E-06	9.76E-16	4.72E-18	5.34E-14	2.07E-18	4.19E-14	2.49E-13	8.42E-14	3.32E-06	5.15E-11
14	310	3000	1.17E-06	8.43E-16	3.37E-18	4.39E-14	1.59E-18	3.30E-14	1.80E-13	6.23E-14	3.18E-06	4.63E-11
15	310	3000	1.13E-06	7.32E-16	2.37E-18	3.53E-14	1.21E-18	2.57E-14	1.29E-13	4.50E-14	3.05E-06	4.21E-11
16	310	3000	1.09E-06	6.34E-16	1.62E-18	2.76E-14	9.10E-19	1.95E-14	8.95E-14	3.16E-14	2.93E-06	3.86E-11
17	310	3000	1.05E-06	5.47E-16	1.07E-18	2.09E-14	6.65E-19	1.44E-14	6.01E-14	2.13E-14	2.82E-06	3.58E-11
18	310	3000	1.02E-06	4.67E-16	6.71E-19	1.52E-14	4.72E-19	1.03E-14	3.86E-14	1.37E-14	2.72E-06	3.33E-11
Ore fluids	500	5000	7.07E-03	1.08E-08	5.78E-12	7.01E-11	2.04E-12	1.04E-09	1.33E-08	4.52E-11	1.03E-02	1.84E-03

		Formula:	HS-	S2--	S2O3--	SO2	SO3--	HSO3-	SO4--	HSO4-	Na+	NaOH
		Type:	(a)	(a)	(a)	(a)	(a)	(a)	(a)	(a)	(a)	(a)
Cell	T (°C)	P(bar)	HS-	S2--	S2O3--	SO2 (aq)	SO3--	HSO3-	SO4--	HSO4-	Na+	NaOH (aq)
1	280	3000	1.27E-04	2.58E-11	1.06E-12	5.33E-14	2.88E-13	1.66E-11	1.06E-07	1.12E-10	2.63E-02	4.38E-05
2	280	3000	1.02E-04	1.55E-11	6.04E-13	5.11E-14	1.66E-13	1.28E-11	5.91E-08	8.50E-11	2.18E-02	3.12E-05
3	280	3000	6.28E-05	5.27E-12	2.09E-13	5.20E-14	5.73E-14	8.04E-12	2.00E-08	5.41E-11	1.24E-02	1.24E-05
4	280	3000	2.74E-05	8.83E-13	3.79E-14	5.59E-14	1.02E-14	3.82E-12	3.54E-09	2.66E-11	9.44E-04	5.00E-07
5	280	3000	5.38E-06	3.72E-14	1.62E-15	5.67E-14	4.34E-16	7.56E-13	1.54E-10	5.26E-12	5.26E-06	4.86E-10
6	280	3000	2.34E-06	7.33E-15	2.91E-16	5.26E-14	7.96E-17	2.99E-13	2.79E-11	2.01E-12	3.93E-06	1.42E-10
7	280	3000	1.60E-06	3.40E-15	1.19E-16	4.73E-14	3.35E-17	1.80E-13	1.14E-11	1.16E-12	3.43E-06	7.91E-11
8	280	3000	1.30E-06	2.17E-15	6.58E-17	4.18E-14	1.91E-17	1.26E-13	6.23E-12	7.70E-13	3.11E-06	5.47E-11
9	280	3000	1.12E-06	1.56E-15	4.11E-17	3.64E-14	1.26E-17	9.38E-14	3.93E-12	5.46E-13	2.86E-06	4.20E-11
10	280	3000	1.00E-06	1.21E-15	2.72E-17	3.10E-14	8.83E-18	7.16E-14	2.64E-12	3.95E-13	2.66E-06	3.42E-11
11	280	3000	9.22E-07	9.83E-16	1.85E-17	2.59E-14	6.44E-18	5.53E-14	1.82E-12	2.87E-13	2.49E-06	2.89E-11
12	280	3000	8.64E-07	8.19E-16	1.27E-17	2.11E-14	4.76E-18	4.25E-14	1.27E-12	2.07E-13	2.35E-06	2.51E-11
13	280	3000	8.19E-07	6.91E-16	8.53E-18	1.67E-14	3.50E-18	3.21E-14	8.69E-13	1.45E-13	2.22E-06	2.22E-11
14	280	3000	7.83E-07	5.84E-16	5.55E-18	1.28E-14	2.52E-18	2.36E-14	5.77E-13	9.74E-14	2.11E-06	2.00E-11
15	280	3000	7.51E-07	4.90E-16	3.41E-18	9.26E-15	1.75E-18	1.66E-14	3.63E-13	6.17E-14	2.01E-06	1.82E-11
16	280	3000	7.22E-07	4.02E-16	1.92E-18	6.23E-15	1.14E-18	1.09E-14	2.09E-13	3.57E-14	1.92E-06	1.67E-11
17	280	3000	6.92E-07	3.17E-16	9.36E-19	3.77E-15	6.71E-19	6.45E-15	1.05E-13	1.80E-14	1.84E-06	1.55E-11
18	280	3000	6.61E-07	2.36E-16	3.71E-19	1.95E-15	3.40E-19	3.28E-15	4.34E-14	7.39E-15	1.77E-06	1.44E-11
Ore fluids	500	5000	7.07E-03	1.08E-08	5.78E-12	7.01E-11	2.04E-12	1.04E-09	1.33E-08	4.52E-11	1.03E-02	1.84E-03
1	250	3000	3.03E-05	2.69E-12	3.81E-13	1.17E-14	1.39E-13	5.66E-12	1.26E-07	9.96E-11	3.68E-02	2.17E-05
2	250	3000	2.25E-05	1.41E-12	2.05E-13	1.21E-14	7.45E-14	4.37E-12	6.69E-08	7.80E-11	2.80E-02	1.31E-05
3	250	3000	1.22E-05	3.79E-13	6.15E-14	1.33E-14	2.18E-14	2.65E-12	1.97E-08	4.93E-11	1.35E-02	3.91E-06
4	250	3000	5.50E-06	6.89E-14	1.21E-14	1.44E-14	4.22E-15	1.31E-12	3.81E-09	2.52E-11	1.45E-03	2.24E-07

		Formula:	HS-	S2--	S2O3--	SO2	SO3--	HSO3-	SO4--	HSO4-	Na+	NaOH
		Type:	(a)	(a)	(a)	(a)	(a)	(a)	(a)	(a)	(a)	(a)
Cell	T (°C)	P(bar)	HS-	S2--	S2O3--	SO2 (aq)	SO3--	HSO3-	SO4--	HSO4-	Na+	NaOH (aq)
5	250	3000	1.57E-06	5.98E-15	1.06E-15	1.45E-14	3.67E-16	3.74E-13	3.36E-10	7.20E-12	4.03E-06	1.65E-10
6	250	3000	8.04E-07	1.61E-15	2.60E-16	1.35E-14	9.22E-17	1.74E-13	8.31E-11	3.24E-12	2.81E-06	5.36E-11
7	250	3000	5.82E-07	8.39E-16	1.20E-16	1.21E-14	4.36E-17	1.11E-13	3.81E-11	1.97E-12	2.38E-06	3.07E-11
8	250	3000	4.87E-07	5.73E-16	7.06E-17	1.07E-14	2.66E-17	8.00E-14	2.23E-11	1.35E-12	2.10E-06	2.15E-11
9	250	3000	4.37E-07	4.48E-16	4.68E-17	9.30E-15	1.83E-17	6.08E-14	1.46E-11	9.73E-13	1.91E-06	1.66E-11
10	250	3000	4.10E-07	3.77E-16	3.27E-17	7.93E-15	1.33E-17	4.73E-14	1.01E-11	7.10E-13	1.75E-06	1.35E-11
11	250	3000	3.95E-07	3.32E-16	2.33E-17	6.61E-15	9.95E-18	3.68E-14	7.05E-12	5.15E-13	1.62E-06	1.15E-11
12	250	3000	3.89E-07	3.00E-16	1.65E-17	5.34E-15	7.44E-18	2.83E-14	4.88E-12	3.64E-13	1.51E-06	9.99E-12
13	250	3000	3.89E-07	2.76E-16	1.14E-17	4.16E-15	5.47E-18	2.12E-14	3.28E-12	2.47E-13	1.42E-06	8.87E-12
14	250	3000	3.94E-07	2.56E-16	7.42E-18	3.06E-15	3.86E-18	1.51E-14	2.07E-12	1.57E-13	1.33E-06	7.99E-12
15	250	3000	4.07E-07	2.37E-16	4.38E-18	2.06E-15	2.51E-18	9.92E-15	1.16E-12	8.83E-14	1.26E-06	7.28E-12
16	250	3000	4.31E-07	2.17E-16	2.13E-18	1.18E-15	1.41E-18	5.56E-15	5.29E-13	4.00E-14	1.20E-06	6.69E-12
17	250	3000	4.34E-07	1.65E-16	6.69E-19	4.97E-16	5.84E-19	2.31E-15	1.64E-13	1.24E-14	1.14E-06	6.20E-12
18	250	3000	3.94E-07	8.22E-17	7.05E-20	9.70E-17	1.13E-19	4.44E-16	1.90E-14	1.42E-15	1.09E-06	5.77E-12
Ore fluids	500	5000	7.07E-03	1.08E-08	5.78E-12	7.01E-11	2.04E-12	1.04E-09	1.33E-08	4.52E-11	1.03E-02	1.84E-03
1	220	3000	5.82E-06	1.92E-13	1.08E-13	2.24E-15	5.40E-14	1.63E-12	1.35E-07	8.34E-11	4.47E-02	8.01E-06
2	220	3000	3.89E-06	8.33E-14	5.32E-14	2.52E-15	2.59E-14	1.25E-12	6.66E-08	6.69E-11	3.12E-02	4.01E-06
3	220	3000	1.99E-06	2.02E-14	1.49E-14	2.87E-15	7.02E-15	7.42E-13	1.84E-08	4.20E-11	1.40E-02	1.05E-06
4	220	3000	9.32E-07	4.01E-15	3.20E-15	3.09E-15	1.48E-15	3.79E-13	3.88E-09	2.22E-11	1.82E-03	7.37E-08
5	220	3000	3.78E-07	6.80E-16	5.35E-16	3.07E-15	2.49E-16	1.51E-13	6.53E-10	8.79E-12	3.13E-06	4.89E-11
6	220	3000	2.35E-07	2.68E-16	1.92E-16	2.84E-15	9.13E-17	8.54E-14	2.35E-10	4.80E-12	2.01E-06	1.80E-11
7	220	3000	1.85E-07	1.65E-16	1.04E-16	2.55E-15	5.09E-17	5.91E-14	1.27E-10	3.18E-12	1.62E-06	1.07E-11
8	220	3000	1.62E-07	1.24E-16	6.77E-17	2.25E-15	3.41E-17	4.46E-14	8.18E-11	2.28E-12	1.39E-06	7.64E-12

		Formula:	HS-	S2--	S2O3--	SO2	SO3--	HSO3-	SO4--	HSO4-	Na+	NaOH
		Type:	(a)	(a)	(a)	(a)	(a)	(a)	(a)	(a)	(a)	(a)
Cell	T (°C)	P(bar)	HS-	S2--	S2O3--	SO2 (aq)	SO3--	HSO3-	SO4--	HSO4-	Na+	NaOH (aq)
9	220	3000	1.50E-07	1.03E-16	4.77E-17	1.96E-15	2.50E-17	3.50E-14	5.70E-11	1.69E-12	1.24E-06	5.95E-12
10	220	3000	1.44E-07	9.08E-17	3.49E-17	1.67E-15	1.90E-17	2.78E-14	4.11E-11	1.26E-12	1.11E-06	4.89E-12
11	220	3000	1.41E-07	8.27E-17	2.57E-17	1.39E-15	1.47E-17	2.20E-14	2.97E-11	9.25E-13	1.02E-06	4.17E-12
12	220	3000	1.40E-07	7.69E-17	1.87E-17	1.12E-15	1.13E-17	1.71E-14	2.11E-11	6.62E-13	9.39E-07	3.64E-12
13	220	3000	1.42E-07	7.23E-17	1.31E-17	8.68E-16	8.44E-18	1.29E-14	1.44E-11	4.51E-13	8.72E-07	3.23E-12
14	220	3000	1.45E-07	6.82E-17	8.62E-18	6.33E-16	6.02E-18	9.17E-15	9.16E-12	2.85E-13	8.15E-07	2.92E-12
15	220	3000	1.52E-07	6.42E-17	5.07E-18	4.19E-16	3.93E-18	5.97E-15	5.14E-12	1.58E-13	7.65E-07	2.66E-12
16	220	3000	1.62E-07	5.95E-17	2.42E-18	2.33E-16	2.17E-18	3.28E-15	2.28E-12	6.97E-14	7.22E-07	2.45E-12
17	220	3000	1.84E-07	5.25E-17	6.68E-19	8.37E-17	7.77E-19	1.16E-15	5.58E-13	1.68E-14	6.83E-07	2.27E-12
18	220	3000	2.29E-07	3.12E-17	2.11E-20	5.60E-18	5.23E-20	7.74E-17	1.42E-14	4.20E-16	6.46E-07	2.12E-12
Ore fluids	500	5000	7.07E-03	1.08E-08	5.78E-12	7.01E-11	2.04E-12	1.04E-09	1.33E-08	4.52E-11	1.03E-02	1.84E-03
1	190	3000	8.44E-07	8.41E-15	2.30E-14	3.70E-16	1.60E-14	3.87E-13	1.30E-07	6.56E-11	4.85E-02	2.16E-06
2	190	3000	5.42E-07	3.40E-15	1.09E-14	4.29E-16	7.32E-15	2.94E-13	6.17E-08	5.28E-11	3.29E-02	1.01E-06
3	190	3000	2.81E-07	8.42E-16	3.03E-15	4.76E-16	1.98E-15	1.72E-13	1.69E-08	3.24E-11	1.45E-02	2.59E-07
4	190	3000	1.42E-07	1.92E-16	6.93E-16	4.77E-16	4.54E-16	8.79E-14	3.77E-09	1.66E-11	1.86E-03	1.89E-08
5	190	3000	7.85E-08	5.90E-17	2.04E-16	4.63E-16	1.35E-16	4.65E-14	1.11E-09	8.67E-12	2.42E-06	1.31E-11
6	190	3000	5.98E-08	3.44E-17	1.06E-16	4.22E-16	7.21E-17	3.16E-14	5.79E-10	5.67E-12	1.42E-06	5.44E-12
7	190	3000	5.20E-08	2.57E-17	6.91E-17	3.75E-16	4.83E-17	2.39E-14	3.74E-10	4.07E-12	1.08E-06	3.39E-12
8	190	3000	4.83E-08	2.16E-17	4.96E-17	3.27E-16	3.59E-17	1.88E-14	2.65E-10	3.04E-12	8.92E-07	2.46E-12
9	190	3000	4.66E-08	1.94E-17	3.70E-17	2.79E-16	2.79E-17	1.51E-14	1.95E-10	2.29E-12	7.69E-07	1.94E-12
10	190	3000	4.60E-08	1.80E-17	2.79E-17	2.33E-16	2.20E-17	1.21E-14	1.45E-10	1.70E-12	6.80E-07	1.61E-12
11	190	3000	4.62E-08	1.71E-17	2.07E-17	1.89E-16	1.73E-17	9.49E-15	1.05E-10	1.23E-12	6.11E-07	1.38E-12
12	190	3000	4.70E-08	1.64E-17	1.49E-17	1.47E-16	1.33E-17	7.24E-15	7.39E-11	8.54E-13	5.56E-07	1.21E-12

		Formula:	HS-	S2--	S2O3--	SO2	SO3--	HSO3-	SO4--	HSO4-	Na+	NaOH
		Type:	(a)	(a)	(a)	(a)	(a)	(a)	(a)	(a)	(a)	(a)
Cell	T (°C)	P(bar)	HS-	S2--	S2O3--	SO2 (aq)	SO3--	HSO3-	SO4--	HSO4-	Na+	NaOH (aq)
13	190	3000	4.85E-08	1.57E-17	1.01E-17	1.08E-16	9.71E-18	5.25E-15	4.84E-11	5.51E-13	5.10E-07	1.08E-12
14	190	3000	5.08E-08	1.51E-17	6.17E-18	7.29E-17	6.55E-18	3.50E-15	2.82E-11	3.15E-13	4.72E-07	9.72E-13
15	190	3000	5.45E-08	1.42E-17	3.08E-18	4.16E-17	3.77E-18	1.98E-15	1.32E-11	1.45E-13	4.39E-07	8.89E-13
16	190	3000	6.18E-08	1.28E-17	9.27E-19	1.58E-17	1.45E-18	7.48E-16	3.53E-12	3.77E-14	4.10E-07	8.20E-13
17	190	3000	9.97E-08	8.41E-18	9.22E-21	3.83E-19	3.65E-20	1.83E-17	2.22E-14	2.28E-16	3.83E-07	7.63E-13
18	190	3000	1.06E-07	2.46E-18	4.49E-23	6.75E-21	6.61E-22	3.23E-19	1.03E-16	1.03E-18	3.57E-07	7.08E-13
Ore fluids	500	5000	7.07E-03	1.08E-08	5.78E-12	7.01E-11	2.04E-12	1.04E-09	1.33E-08	4.52E-11	1.03E-02	1.84E-03
1	160	3000	2.32E-07	9.63E-16	4.77E-15	1.72E-17	6.16E-15	5.65E-14	1.31E-07	2.46E-11	5.11E-02	1.04E-06
2	160	3000	1.68E-07	4.68E-16	2.32E-15	1.73E-17	2.99E-15	4.11E-14	6.25E-08	1.80E-11	3.43E-02	5.29E-07
3	160	3000	9.52E-08	1.33E-16	6.61E-16	1.73E-17	8.53E-16	2.34E-14	1.73E-08	1.03E-11	1.50E-02	1.43E-07
4	160	3000	4.93E-08	3.21E-17	1.59E-16	1.74E-17	2.05E-16	1.22E-14	4.08E-09	5.40E-12	1.77E-03	9.67E-09
5	160	3000	2.83E-08	1.05E-17	4.83E-17	1.63E-17	6.34E-17	6.48E-15	1.24E-09	2.79E-12	1.36E-06	4.11E-12
6	160	3000	2.28E-08	6.54E-18	2.31E-17	1.30E-17	3.21E-17	4.00E-15	5.79E-10	1.58E-12	7.65E-07	1.71E-12
7	160	3000	2.09E-08	5.02E-18	1.21E-17	9.30E-18	1.83E-17	2.51E-15	2.94E-10	8.67E-13	5.68E-07	1.07E-12
8	160	3000	2.07E-08	4.24E-18	6.00E-18	5.81E-18	1.02E-17	1.45E-15	1.38E-10	4.18E-13	4.60E-07	7.80E-13
9	160	3000	2.19E-08	3.69E-18	2.24E-18	2.76E-18	4.61E-18	6.58E-16	4.74E-11	1.43E-13	3.90E-07	6.16E-13
10	160	3000	2.71E-08	2.94E-18	2.34E-19	4.55E-19	7.55E-19	1.06E-16	3.97E-12	1.17E-14	3.38E-07	5.12E-13
11	160	3000	6.37E-08	8.85E-19	1.05E-23	1.59E-22	2.75E-22	3.72E-20	7.73E-17	2.17E-19	2.96E-07	4.39E-13
12	160	3000	5.65E-08	4.23E-19	1.06E-24	3.08E-23	5.07E-23	6.93E-21	8.53E-18	2.40E-20	2.69E-07	3.79E-13
13	160	3000	5.27E-08	2.91E-19	3.42E-25	1.39E-23	2.20E-23	3.03E-21	2.90E-18	8.17E-21	2.47E-07	3.33E-13
14	160	3000	5.00E-08	2.26E-19	1.61E-25	8.22E-24	1.26E-23	1.74E-21	1.41E-18	3.96E-21	2.29E-07	2.98E-13
15	160	3000	4.81E-08	1.87E-19	9.10E-26	5.53E-24	8.26E-24	1.14E-21	8.18E-19	2.29E-21	2.13E-07	2.69E-13
16	160	3000	4.66E-08	1.61E-19	5.77E-26	4.03E-24	5.90E-24	8.15E-22	5.30E-19	1.47E-21	1.99E-07	2.45E-13

		Formula:	HS-	S2--	S2O3--	SO2	SO3--	HSO3-	SO4--	HSO4-	Na+	NaOH
		Type:	(a)	(a)	(a)	(a)	(a)	(a)	(a)	(a)	(a)	(a)
Cell	T (°C)	P(bar)	HS-	S2--	S2O3--	SO2 (aq)	SO3--	HSO3-	SO4--	HSO4-	Na+	NaOH (aq)
17	160	3000	4.54E-08	1.42E-19	3.95E-26	3.09E-24	4.46E-24	6.15E-22	3.69E-19	1.02E-21	1.87E-07	2.25E-13
18	160	3000	4.43E-08	1.28E-19	2.86E-26	2.46E-24	3.52E-24	4.82E-22	2.71E-19	7.42E-22	1.76E-07	2.08E-13

		Formula:	NaCO3-	NaHCO3	NaSO4-	K+	KOH	KSO4-	KHSO4	Mg++	MgOH+	MgCO3
		Type:	(a)	(a)	(a)	(a)	(a)	(a)	(a)	(a)	(a)	(a)
Cell	T (°C)	P(bar)	NaCO3-	NaHCO3 (aq)	NaSO4-	K+	KOH (aq)	KSO4-	KHSO4 (aq)	Mg++	MgOH+	MgCO3 (aq)
Ore fluids	500	5000	1.80E-04	2.74E-03	5.07E-09	2.57E-02	2.14E-03	1.59E-07	1.76E-10	9.45E-12	1.39E-10	2.25E-12
1	400	3000	2.05E-04	3.05E-03	2.58E-09	2.06E-02	4.31E-04	8.84E-08	2.81E-11	6.15E-12	2.89E-11	4.57E-12
2	400	3000	1.22E-04	2.36E-03	1.47E-09	1.22E-02	2.21E-04	3.21E-08	1.33E-11	7.39E-12	2.95E-11	3.79E-12
3	400	3000	6.98E-05	1.77E-03	8.31E-10	6.27E-03	9.62E-05	1.04E-08	5.62E-12	8.72E-12	2.95E-11	3.11E-12
4	400	3000	2.04E-05	8.04E-04	2.40E-10	7.92E-04	9.19E-06	6.24E-10	5.24E-13	9.28E-12	2.37E-11	1.83E-12
5	400	3000	1.10E-09	4.66E-07	1.30E-14	1.62E-12	1.75E-15	1.12E-20	1.01E-22	7.40E-12	1.76E-12	1.27E-14
6	400	3000	2.07E-11	4.89E-08	2.38E-16	1.39E-14	2.17E-18	2.35E-24	1.19E-25	7.75E-11	2.68E-12	2.82E-15
7	400	3000	5.31E-12	2.23E-08	5.91E-17	2.74E-15	2.23E-19	1.28E-25	1.14E-26	1.70E-10	3.08E-12	1.66E-15
8	400	3000	2.42E-12	1.39E-08	2.59E-17	1.06E-15	5.94E-20	2.32E-26	2.85E-27	2.63E-10	3.31E-12	1.20E-15
9	400	3000	1.40E-12	9.91E-09	1.45E-17	5.40E-16	2.37E-20	7.02E-27	1.06E-27	3.49E-10	3.44E-12	9.55E-16
10	400	3000	9.29E-13	7.60E-09	9.27E-18	3.21E-16	1.18E-20	2.80E-27	4.90E-28	4.26E-10	3.53E-12	7.95E-16
11	400	3000	6.68E-13	6.09E-09	6.43E-18	2.11E-16	6.69E-21	1.33E-27	2.59E-28	4.95E-10	3.58E-12	6.81E-16
12	400	3000	5.08E-13	5.04E-09	4.70E-18	1.47E-16	4.18E-21	7.10E-28	1.50E-28	5.57E-10	3.60E-12	5.96E-16
13	400	3000	4.01E-13	4.26E-09	3.58E-18	1.08E-16	2.79E-21	4.12E-28	9.33E-29	6.12E-10	3.62E-12	5.29E-16
14	400	3000	3.27E-13	3.66E-09	2.80E-18	8.23E-17	1.96E-21	2.54E-28	6.09E-29	6.60E-10	3.62E-12	4.75E-16
15	400	3000	2.72E-13	3.19E-09	2.24E-18	6.44E-17	1.43E-21	1.65E-28	4.13E-29	7.04E-10	3.62E-12	4.30E-16

		Formula:	NaCO3-	NaHCO3	NaSO4-	K+	KOH	KSO4-	KHSO4	Mg++	MgOH+	MgCO3
		Type:	(a)	(a)	(a)	(a)	(a)	(a)	(a)	(a)	(a)	(a)
Cell	T (°C)	P(bar)	NaCO3-	NaHCO3 (aq)	NaSO4-	K+	KOH (aq)	KSO4-	KHSO4 (aq)	Mg++	MgOH+	MgCO3 (aq)
16	400	3000	2.30E-13	2.80E-09	1.83E-18	5.16E-17	1.08E-21	1.11E-28	2.89E-29	7.43E-10	3.61E-12	3.92E-16
17	400	3000	1.98E-13	2.49E-09	1.51E-18	4.22E-17	8.34E-22	7.73E-29	2.07E-29	7.78E-10	3.59E-12	3.59E-16
18	400	3000	1.72E-13	2.22E-09	1.26E-18	3.50E-17	6.59E-22	5.52E-29	1.52E-29	8.09E-10	3.58E-12	3.30E-16
Ore fluids	500	5000	1.80E-04	2.74E-03	5.07E-09	2.57E-02	2.14E-03	1.59E-07	1.76E-10	9.45E-12	1.39E-10	2.25E-12
1	370	3000	2.77E-04	4.38E-03	5.51E-09	1.97E-02	2.26E-04	1.11E-07	2.47E-11	1.56E-11	3.67E-11	1.08E-11
2	370	3000	1.65E-04	3.34E-03	3.12E-09	1.14E-02	1.14E-04	3.97E-08	1.13E-11	1.81E-11	3.68E-11	8.85E-12
3	370	3000	6.67E-05	1.99E-03	1.20E-09	3.45E-03	2.74E-05	5.84E-09	2.45E-12	2.18E-11	3.48E-11	6.15E-12
4	370	3000	1.39E-06	8.18E-05	2.50E-11	3.77E-07	1.87E-09	2.03E-13	1.67E-16	6.78E-12	6.82E-12	7.30E-13
5	370	3000	1.39E-10	1.33E-07	2.50E-15	3.23E-14	8.01E-18	5.34E-23	7.20E-25	3.68E-11	1.84E-12	1.01E-14
6	370	3000	1.25E-11	3.36E-08	2.15E-16	1.84E-15	1.43E-19	3.13E-25	1.19E-26	1.50E-10	2.36E-12	4.01E-15
7	370	3000	4.13E-12	1.75E-08	6.75E-17	5.01E-16	2.33E-20	2.93E-26	1.74E-27	2.77E-10	2.62E-12	2.57E-15
8	370	3000	2.06E-12	1.14E-08	3.19E-17	2.19E-16	7.49E-21	6.46E-27	5.03E-28	3.97E-10	2.77E-12	1.90E-15
9	370	3000	1.25E-12	8.25E-09	1.82E-17	1.20E-16	3.30E-21	2.13E-27	1.98E-28	5.04E-10	2.85E-12	1.51E-15
10	370	3000	8.43E-13	6.32E-09	1.16E-17	7.42E-17	1.74E-21	8.83E-28	9.32E-29	5.99E-10	2.90E-12	1.25E-15
11	370	3000	6.09E-13	5.03E-09	7.87E-18	4.99E-17	1.03E-21	4.23E-28	4.92E-29	6.81E-10	2.92E-12	1.06E-15
12	370	3000	4.62E-13	4.11E-09	5.60E-18	3.56E-17	6.65E-22	2.24E-28	2.80E-29	7.53E-10	2.93E-12	9.10E-16
13	370	3000	3.62E-13	3.41E-09	4.11E-18	2.65E-17	4.54E-22	1.27E-28	1.69E-29	8.16E-10	2.93E-12	7.92E-16
14	370	3000	2.91E-13	2.88E-09	3.09E-18	2.04E-17	3.25E-22	7.65E-29	1.07E-29	8.72E-10	2.92E-12	6.96E-16
15	370	3000	2.38E-13	2.45E-09	2.37E-18	1.61E-17	2.41E-22	4.79E-29	6.94E-30	9.20E-10	2.91E-12	6.15E-16
16	370	3000	1.98E-13	2.11E-09	1.84E-18	1.30E-17	1.84E-22	3.10E-29	4.64E-30	9.63E-10	2.89E-12	5.47E-16
17	370	3000	1.67E-13	1.82E-09	1.44E-18	1.07E-17	1.44E-22	2.06E-29	3.18E-30	1.00E-09	2.88E-12	4.88E-16
18	370	3000	1.42E-13	1.59E-09	1.14E-18	8.89E-18	1.15E-22	1.40E-29	2.21E-30	1.03E-09	2.86E-12	4.37E-16
Ore fluids	500	5000	1.80E-04	2.74E-03	5.07E-09	2.57E-02	2.14E-03	1.59E-07	1.76E-10	9.45E-12	1.39E-10	2.25E-12

		Formula:	NaCO3-	NaHCO3	NaSO4-	K+	KOH	KSO4-	KHSO4	Mg ⁺⁺	MgOH ⁺	MgCO3
		Type:	(a)	(a)	(a)	(a)	(a)	(a)	(a)	(a)	(a)	(a)
Cell	T (°C)	P(bar)	NaCO3-	NaHCO3 (aq)	NaSO4-	K+	KOH (aq)	KSO4-	KHSO4 (aq)	Mg ⁺⁺	MgOH ⁺	MgCO3 (aq)
1	340	3000	3.54E-04	6.68E-03	1.28E-08	1.78E-02	9.28E-05	1.32E-07	2.23E-11	5.09E-11	5.04E-11	2.86E-11
2	340	3000	2.12E-04	5.00E-03	7.23E-09	9.80E-03	4.53E-05	4.59E-08	9.71E-12	5.73E-11	4.96E-11	2.31E-11
3	340	3000	8.16E-05	2.81E-03	2.64E-09	2.46E-03	9.03E-06	5.70E-09	1.76E-12	6.59E-11	4.49E-11	1.54E-11
4	340	3000	1.44E-06	1.02E-04	4.75E-11	1.88E-07	4.11E-10	1.30E-13	8.30E-17	2.06E-11	8.42E-12	1.70E-12
5	340	3000	1.91E-10	1.52E-07	6.37E-15	8.05E-15	1.30E-18	3.75E-23	2.69E-25	4.79E-11	1.44E-12	2.23E-14
6	340	3000	1.68E-11	3.77E-08	5.34E-16	4.39E-16	2.25E-20	2.10E-25	4.21E-27	1.90E-10	1.82E-12	8.68E-15
7	340	3000	5.46E-12	1.93E-08	1.62E-16	1.18E-16	3.61E-21	1.88E-26	5.95E-28	3.49E-10	2.01E-12	5.47E-15
8	340	3000	2.69E-12	1.24E-08	7.42E-17	5.11E-17	1.15E-21	4.00E-27	1.65E-28	4.97E-10	2.11E-12	3.99E-15
9	340	3000	1.60E-12	8.79E-09	4.09E-17	2.78E-17	5.08E-22	1.28E-27	6.28E-29	6.27E-10	2.17E-12	3.12E-15
10	340	3000	1.06E-12	6.60E-09	2.50E-17	1.72E-17	2.69E-22	5.08E-28	2.83E-29	7.39E-10	2.20E-12	2.52E-15
11	340	3000	7.53E-13	5.13E-09	1.62E-17	1.15E-17	1.60E-22	2.33E-28	1.42E-29	8.35E-10	2.21E-12	2.08E-15
12	340	3000	5.57E-13	4.08E-09	1.09E-17	8.23E-18	1.03E-22	1.17E-28	7.69E-30	9.18E-10	2.21E-12	1.74E-15
13	340	3000	4.25E-13	3.29E-09	7.56E-18	6.12E-18	7.09E-23	6.27E-29	4.36E-30	9.88E-10	2.20E-12	1.47E-15
14	340	3000	3.31E-13	2.68E-09	5.30E-18	4.71E-18	5.09E-23	3.52E-29	2.56E-30	1.05E-09	2.19E-12	1.25E-15
15	340	3000	2.61E-13	2.20E-09	3.74E-18	3.72E-18	3.78E-23	2.03E-29	1.54E-30	1.10E-09	2.18E-12	1.06E-15
16	340	3000	2.08E-13	1.81E-09	2.65E-18	3.00E-18	2.90E-23	1.20E-29	9.37E-31	1.15E-09	2.16E-12	9.01E-16
17	340	3000	1.67E-13	1.49E-09	1.88E-18	2.46E-18	2.27E-23	7.24E-30	5.79E-31	1.19E-09	2.14E-12	7.65E-16
18	340	3000	1.35E-13	1.23E-09	1.33E-18	2.05E-18	1.82E-23	4.42E-30	3.61E-31	1.22E-09	2.13E-12	6.50E-16
Ore fluids	500	5000	1.80E-04	2.74E-03	5.07E-09	2.57E-02	2.14E-03	1.59E-07	1.76E-10	9.45E-12	1.39E-10	2.25E-12
1	310	3000	4.36E-04	1.03E-02	3.10E-08	1.44E-02	3.01E-05	1.43E-07	1.86E-11	1.92E-10	7.09E-11	8.06E-11
2	310	3000	2.57E-04	7.53E-03	1.74E-08	7.16E-03	1.33E-05	4.61E-08	7.42E-12	2.11E-10	6.81E-11	6.40E-11
3	310	3000	8.51E-05	3.74E-03	5.59E-09	1.21E-03	1.72E-06	3.79E-09	9.15E-13	2.34E-10	5.76E-11	3.96E-11
4	310	3000	1.43E-06	1.38E-04	9.80E-11	9.43E-08	7.54E-11	8.21E-14	4.36E-17	8.20E-11	1.14E-11	4.44E-12

		Formula:	NaCO3-	NaHCO3	NaSO4-	K+	KOH	KSO4-	KHSO4	Mg ⁺⁺	MgOH ⁺	MgCO3
		Type:	(a)	(a)	(a)	(a)	(a)	(a)	(a)	(a)	(a)	(a)
Cell	T (°C)	P(bar)	NaCO3-	NaHCO3 (aq)	NaSO4-	K+	KOH (aq)	KSO4-	KHSO4 (aq)	Mg ⁺⁺	MgOH ⁺	MgCO3 (aq)
5	310	3000	2.38E-10	1.72E-07	1.66E-14	1.50E-15	1.38E-19	2.08E-23	8.24E-26	7.03E-11	1.11E-12	5.18E-14
6	310	3000	2.35E-11	4.44E-08	1.56E-15	8.65E-17	2.72E-21	1.42E-25	1.48E-27	2.46E-10	1.34E-12	2.08E-14
7	310	3000	7.81E-12	2.28E-08	4.84E-16	2.32E-17	4.46E-22	1.32E-26	2.11E-28	4.38E-10	1.47E-12	1.31E-14
8	310	3000	3.87E-12	1.46E-08	2.21E-16	1.01E-17	1.44E-22	2.83E-27	5.85E-29	6.11E-10	1.53E-12	9.51E-15
9	310	3000	2.31E-12	1.03E-08	1.21E-16	5.47E-18	6.39E-23	8.97E-28	2.19E-29	7.58E-10	1.56E-12	7.36E-15
10	310	3000	1.53E-12	7.65E-09	7.28E-17	3.38E-18	3.40E-23	3.53E-28	9.71E-30	8.82E-10	1.57E-12	5.89E-15
11	310	3000	1.08E-12	5.87E-09	4.62E-17	2.26E-18	2.03E-23	1.59E-28	4.76E-30	9.86E-10	1.57E-12	4.81E-15
12	310	3000	7.89E-13	4.59E-09	3.02E-17	1.61E-18	1.32E-23	7.76E-29	2.48E-30	1.07E-09	1.56E-12	3.95E-15
13	310	3000	5.91E-13	3.63E-09	2.00E-17	1.20E-18	9.07E-24	3.99E-29	1.35E-30	1.14E-09	1.55E-12	3.26E-15
14	310	3000	4.49E-13	2.87E-09	1.33E-17	9.20E-19	6.53E-24	2.12E-29	7.45E-31	1.21E-09	1.54E-12	2.69E-15
15	310	3000	3.43E-13	2.27E-09	8.68E-18	7.26E-19	4.88E-24	1.14E-29	4.14E-31	1.26E-09	1.52E-12	2.20E-15
16	310	3000	2.61E-13	1.78E-09	5.57E-18	5.86E-19	3.75E-24	6.12E-30	2.29E-31	1.30E-09	1.51E-12	1.78E-15
17	310	3000	1.97E-13	1.37E-09	3.46E-18	4.81E-19	2.95E-24	3.24E-30	1.24E-31	1.34E-09	1.49E-12	1.42E-15
18	310	3000	1.47E-13	1.04E-09	2.07E-18	4.01E-19	2.37E-24	1.67E-30	6.49E-32	1.37E-09	1.47E-12	1.11E-15
Ore fluids	500	5000	1.80E-04	2.74E-03	5.07E-09	2.57E-02	2.14E-03	1.59E-07	1.76E-10	9.45E-12	1.39E-10	2.25E-12
1	280	3000	5.28E-04	1.52E-02	6.87E-08	9.80E-03	8.17E-06	1.29E-07	1.19E-11	6.66E-10	9.08E-11	2.24E-10
2	280	3000	2.91E-04	1.05E-02	3.68E-08	4.01E-03	2.90E-06	3.43E-08	3.96E-12	7.21E-10	8.47E-11	1.72E-10
3	280	3000	7.24E-05	4.21E-03	9.23E-09	3.48E-04	1.79E-07	1.34E-09	2.50E-13	7.95E-10	6.58E-11	9.32E-11
4	280	3000	1.37E-06	1.79E-04	1.82E-10	4.17E-08	1.16E-11	4.22E-14	1.77E-17	3.27E-10	1.48E-11	1.15E-11
5	280	3000	2.60E-10	1.75E-07	3.48E-14	2.21E-16	1.06E-20	7.62E-24	1.65E-26	1.07E-10	8.26E-13	1.14E-13
6	280	3000	3.05E-11	4.82E-08	3.88E-15	1.41E-17	2.62E-22	7.19E-26	3.65E-28	3.10E-10	9.28E-13	4.76E-14
7	280	3000	1.04E-11	2.47E-08	1.24E-15	3.82E-18	4.50E-23	7.07E-27	5.37E-29	5.18E-10	9.85E-13	2.97E-14
8	280	3000	5.18E-12	1.55E-08	5.68E-16	1.65E-18	1.48E-23	1.54E-27	1.48E-29	6.97E-10	1.01E-12	2.12E-14

		Formula:	NaCO3-	NaHCO3	NaSO4-	K+	KOH	KSO4-	KHSO4	Mg++	MgOH+	MgCO3
		Type:	(a)	(a)	(a)	(a)	(a)	(a)	(a)	(a)	(a)	(a)
Cell	T (°C)	P(bar)	NaCO3-	NaHCO3 (aq)	NaSO4-	K+	KOH (aq)	KSO4-	KHSO4 (aq)	Mg++	MgOH+	MgCO3 (aq)
9	280	3000	3.10E-12	1.08E-08	3.08E-16	8.91E-19	6.61E-24	4.87E-28	5.45E-30	8.43E-10	1.02E-12	1.62E-14
10	280	3000	2.04E-12	7.93E-09	1.81E-16	5.47E-19	3.54E-24	1.88E-28	2.34E-30	9.61E-10	1.01E-12	1.28E-14
11	280	3000	1.42E-12	5.97E-09	1.11E-16	3.65E-19	2.12E-24	8.16E-29	1.10E-30	1.05E-09	1.00E-12	1.02E-14
12	280	3000	1.02E-12	4.54E-09	6.88E-17	2.58E-19	1.38E-24	3.80E-29	5.45E-31	1.13E-09	9.91E-13	8.17E-15
13	280	3000	7.39E-13	3.47E-09	4.25E-17	1.91E-19	9.54E-25	1.83E-29	2.75E-31	1.19E-09	9.77E-13	6.51E-15
14	280	3000	5.38E-13	2.62E-09	2.57E-17	1.46E-19	6.89E-25	8.87E-30	1.38E-31	1.24E-09	9.62E-13	5.12E-15
15	280	3000	3.87E-13	1.94E-09	1.47E-17	1.15E-19	5.15E-25	4.19E-30	6.73E-32	1.28E-09	9.47E-13	3.92E-15
16	280	3000	2.69E-13	1.38E-09	7.80E-18	9.22E-20	3.97E-25	1.86E-30	3.06E-32	1.31E-09	9.33E-13	2.89E-15
17	280	3000	1.77E-13	9.29E-10	3.62E-18	7.54E-20	3.13E-25	7.34E-31	1.24E-32	1.33E-09	9.18E-13	2.00E-15
18	280	3000	1.07E-13	5.69E-10	1.38E-18	6.25E-20	2.51E-25	2.42E-31	4.14E-33	1.35E-09	9.03E-13	1.26E-15
Ore fluids	500	5000	1.80E-04	2.74E-03	5.07E-09	2.57E-02	2.14E-03	1.59E-07	1.76E-10	9.45E-12	1.39E-10	2.25E-12
1	250	3000	5.70E-04	2.07E-02	9.65E-08	4.48E-03	1.35E-06	5.38E-08	3.45E-12	2.36E-09	1.08E-10	6.16E-10
2	250	3000	2.62E-04	1.27E-02	4.52E-08	1.21E-03	2.90E-07	9.01E-09	7.73E-13	2.67E-09	9.78E-11	4.46E-10
3	250	3000	4.63E-05	4.08E-03	8.45E-09	4.98E-05	7.58E-09	1.48E-10	2.29E-14	3.07E-09	7.08E-11	2.12E-10
4	250	3000	1.28E-06	2.47E-04	2.45E-10	1.70E-08	1.40E-12	1.38E-14	4.69E-18	1.58E-09	1.99E-11	3.32E-11
5	250	3000	2.69E-10	1.82E-07	5.16E-14	2.58E-17	5.60E-22	1.57E-24	1.88E-27	1.86E-10	6.13E-13	2.73E-13
6	250	3000	4.12E-11	5.58E-08	7.51E-15	1.90E-18	1.90E-23	2.40E-26	5.74E-29	4.10E-10	6.21E-13	1.22E-13
7	250	3000	1.53E-11	2.94E-08	2.61E-15	5.25E-19	3.53E-24	2.71E-27	9.14E-30	6.20E-10	6.32E-13	7.75E-14
8	250	3000	7.95E-12	1.86E-08	1.25E-15	2.27E-19	1.20E-24	6.27E-28	2.60E-30	7.88E-10	6.31E-13	5.56E-14
9	250	3000	4.81E-12	1.29E-08	6.88E-16	1.22E-19	5.47E-25	2.05E-28	9.68E-31	9.15E-10	6.23E-13	4.21E-14
10	250	3000	3.17E-12	9.31E-09	4.09E-16	7.44E-20	2.96E-25	8.05E-29	4.17E-31	1.01E-09	6.12E-13	3.26E-14
11	250	3000	2.18E-12	6.86E-09	2.50E-16	4.93E-20	1.79E-25	3.52E-29	1.95E-31	1.08E-09	5.99E-13	2.55E-14
12	250	3000	1.53E-12	5.07E-09	1.53E-16	3.47E-20	1.17E-25	1.62E-29	9.46E-32	1.14E-09	5.85E-13	1.98E-14

		Formula:	NaCO3-	NaHCO3	NaSO4-	K+	KOH	KSO4-	KHSO4	Mg ⁺⁺	MgOH ⁺	MgCO3
		Type:	(a)	(a)	(a)	(a)	(a)	(a)	(a)	(a)	(a)	(a)
Cell	T (°C)	P(bar)	NaCO3-	NaHCO3 (aq)	NaSO4-	K+	KOH (aq)	KSO4-	KHSO4 (aq)	Mg ⁺⁺	MgOH ⁺	MgCO3 (aq)
13	250	3000	1.08E-12	3.71E-09	9.21E-17	2.55E-20	8.12E-26	7.60E-30	4.61E-32	1.18E-09	5.72E-13	1.51E-14
14	250	3000	7.46E-13	2.65E-09	5.24E-17	1.94E-20	5.89E-26	3.48E-30	2.18E-32	1.20E-09	5.59E-13	1.12E-14
15	250	3000	4.91E-13	1.78E-09	2.68E-17	1.52E-20	4.42E-26	1.47E-30	9.40E-33	1.22E-09	5.46E-13	7.82E-15
16	250	3000	2.90E-13	1.07E-09	1.11E-17	1.21E-20	3.41E-26	5.11E-31	3.34E-33	1.24E-09	5.34E-13	4.86E-15
17	250	3000	1.47E-13	5.53E-10	3.17E-18	9.87E-21	2.69E-26	1.24E-31	8.26E-34	1.25E-09	5.22E-13	2.57E-15
18	250	3000	4.79E-14	1.83E-10	3.37E-19	8.14E-21	2.16E-26	1.14E-32	7.67E-35	1.25E-09	5.10E-13	8.75E-16
Ore fluids	500	5000	1.80E-04	2.74E-03	5.07E-09	2.57E-02	2.14E-03	1.59E-07	1.76E-10	9.45E-12	1.39E-10	2.25E-12
1	220	3000	4.74E-04	2.33E-02	1.07E-07	1.00E-03	9.28E-08	1.02E-08	4.55E-13	8.68E-09	1.16E-10	1.57E-09
2	220	3000	1.76E-04	1.27E-02	4.28E-08	1.71E-04	1.15E-08	1.01E-09	6.59E-14	1.06E-08	1.02E-10	1.07E-09
3	220	3000	2.65E-05	3.67E-03	6.96E-09	5.08E-06	2.03E-10	1.11E-11	1.38E-15	1.26E-08	7.24E-11	4.79E-10
4	220	3000	9.33E-07	2.71E-04	2.56E-10	3.14E-09	6.88E-14	1.97E-15	5.17E-19	7.16E-09	2.29E-11	8.55E-11
5	220	3000	2.46E-10	1.78E-07	6.71E-14	2.38E-18	2.00E-23	2.26E-25	1.48E-28	3.71E-10	4.53E-13	6.47E-13
6	220	3000	5.21E-11	6.18E-08	1.35E-14	2.08E-19	9.96E-25	6.12E-27	6.57E-30	5.83E-10	4.05E-13	3.14E-13
7	220	3000	2.19E-11	3.38E-08	5.28E-15	5.92E-20	2.08E-25	8.43E-28	1.18E-30	7.65E-10	3.88E-13	2.05E-13
8	220	3000	1.21E-11	2.19E-08	2.69E-15	2.57E-20	7.45E-26	2.16E-28	3.53E-31	8.95E-10	3.74E-13	1.49E-13
9	220	3000	7.61E-12	1.52E-08	1.54E-15	1.38E-20	3.49E-26	7.45E-29	1.35E-31	9.85E-10	3.60E-13	1.13E-13
10	220	3000	5.14E-12	1.11E-08	9.42E-16	8.37E-21	1.92E-26	3.04E-29	5.93E-32	1.05E-09	3.47E-13	8.80E-14
11	220	3000	3.61E-12	8.18E-09	5.87E-16	5.52E-21	1.18E-26	1.37E-29	2.80E-32	1.09E-09	3.35E-13	6.89E-14
12	220	3000	2.58E-12	6.06E-09	3.65E-16	3.86E-21	7.77E-27	6.42E-30	1.37E-32	1.11E-09	3.23E-13	5.35E-14
13	220	3000	1.83E-12	4.43E-09	2.21E-16	2.82E-21	5.42E-27	3.04E-30	6.66E-33	1.13E-09	3.13E-13	4.09E-14
14	220	3000	1.27E-12	3.14E-09	1.25E-16	2.14E-21	3.95E-27	1.39E-30	3.12E-33	1.13E-09	3.03E-13	3.01E-14
15	220	3000	8.33E-13	2.10E-09	6.33E-17	1.66E-21	2.97E-27	5.81E-31	1.32E-33	1.13E-09	2.93E-13	2.08E-14
16	220	3000	4.86E-13	1.24E-09	2.55E-17	1.32E-21	2.30E-27	1.97E-31	4.55E-34	1.13E-09	2.85E-13	1.27E-14

		Formula:	NaCO3-	NaHCO3	NaSO4-	K+	KOH	KSO4-	KHSO4	Mg++	MgOH+	MgCO3
		Type:	(a)	(a)	(a)	(a)	(a)	(a)	(a)	(a)	(a)	(a)
Cell	T (°C)	P(bar)	NaCO3-	NaHCO3 (aq)	NaSO4-	K+	KOH (aq)	KSO4-	KHSO4 (aq)	Mg++	MgOH+	MgCO3 (aq)
17	220	3000	2.06E-13	5.31E-10	5.68E-18	1.07E-21	1.83E-27	3.75E-32	8.74E-35	1.12E-09	2.76E-13	5.58E-15
18	220	3000	2.71E-14	7.01E-11	1.32E-19	8.80E-22	1.47E-27	7.54E-34	1.77E-36	1.10E-09	2.68E-13	7.58E-16
Ore fluids	500	5000	1.80E-04	2.74E-03	5.07E-09	2.57E-02	2.14E-03	1.59E-07	1.76E-10	9.45E-12	1.39E-10	2.25E-12
1	190	3000	3.01E-04	2.23E-02	9.52E-08	1.10E-04	2.56E-09	8.63E-10	2.73E-14	3.54E-08	1.15E-10	3.81E-09
2	190	3000	1.02E-04	1.16E-02	3.54E-08	1.57E-05	2.55E-10	6.85E-11	3.31E-15	4.46E-08	1.01E-10	2.54E-09
3	190	3000	1.50E-05	3.21E-03	5.52E-09	4.40E-07	4.24E-12	6.93E-13	6.34E-17	5.24E-08	7.06E-11	1.10E-09
4	190	3000	5.56E-07	2.35E-04	2.05E-10	2.91E-10	1.62E-15	1.35E-16	2.43E-20	2.76E-08	2.17E-11	1.91E-10
5	190	3000	2.05E-10	1.58E-07	7.39E-14	1.81E-19	5.36E-25	2.31E-26	7.63E-30	7.72E-10	3.21E-13	1.46E-12
6	190	3000	5.89E-11	6.11E-08	2.00E-14	1.83E-20	3.81E-26	1.07E-27	4.74E-31	8.60E-10	2.51E-13	7.57E-13
7	190	3000	2.83E-11	3.47E-08	8.91E-15	5.37E-21	9.12E-27	1.84E-28	9.57E-32	9.45E-10	2.24E-13	5.05E-13
8	190	3000	1.68E-11	2.26E-08	4.82E-15	2.34E-21	3.48E-27	5.21E-29	3.00E-32	9.97E-10	2.06E-13	3.68E-13
9	190	3000	1.10E-11	1.58E-08	2.85E-15	1.25E-21	1.69E-27	1.90E-29	1.16E-32	1.02E-09	1.93E-13	2.79E-13
10	190	3000	7.56E-12	1.14E-08	1.75E-15	7.56E-22	9.52E-28	7.92E-30	5.08E-33	1.03E-09	1.81E-13	2.15E-13
11	190	3000	5.34E-12	8.28E-09	1.08E-15	4.95E-22	5.92E-28	3.55E-30	2.35E-33	1.03E-09	1.72E-13	1.65E-13
12	190	3000	3.79E-12	5.99E-09	6.52E-16	3.45E-22	3.95E-28	1.64E-30	1.10E-33	1.02E-09	1.63E-13	1.25E-13
13	190	3000	2.63E-12	4.23E-09	3.73E-16	2.51E-22	2.78E-28	7.39E-31	5.06E-34	1.01E-09	1.56E-13	9.23E-14
14	190	3000	1.74E-12	2.83E-09	1.93E-16	1.89E-22	2.04E-28	3.09E-31	2.14E-34	9.92E-10	1.49E-13	6.41E-14
15	190	3000	1.04E-12	1.69E-09	8.04E-17	1.46E-22	1.55E-28	1.07E-31	7.45E-35	9.72E-10	1.43E-13	3.96E-14
16	190	3000	4.58E-13	7.51E-10	1.93E-17	1.15E-22	1.20E-28	2.17E-32	1.51E-35	9.49E-10	1.38E-13	1.81E-14
17	190	3000	2.63E-14	4.29E-11	1.08E-19	9.29E-23	9.62E-29	1.05E-34	7.25E-38	9.13E-10	1.32E-13	1.06E-15
18	190	3000	1.60E-15	2.60E-12	4.53E-22	7.50E-23	7.70E-29	3.77E-37	2.60E-40	8.83E-10	1.26E-13	6.64E-17
Ore fluids	500	5000	1.80E-04	2.74E-03	5.07E-09	2.57E-02	2.14E-03	1.59E-07	1.76E-10	9.45E-12	1.39E-10	2.25E-12
1	160	3000	3.57E-04	1.99E-02	8.49E-08	3.65E-05	3.95E-10	2.35E-10	2.37E-15	5.74E-08	8.44E-11	7.17E-09

		Formula:	NaCO3-	NaHCO3	NaSO4-	K+	KOH	KSO4-	KHSO4	Mg++	MgOH+	MgCO3
		Type:	(a)	(a)	(a)	(a)	(a)	(a)	(a)	(a)	(a)	(a)
Cell	T (°C)	P(bar)	NaCO3-	NaHCO3 (aq)	NaSO4-	K+	KOH (aq)	KSO4-	KHSO4 (aq)	Mg++	MgOH+	MgCO3 (aq)
2	160	3000	1.32E-04	1.01E-02	3.13E-08	6.16E-06	5.11E-11	2.20E-11	3.07E-16	6.30E-08	7.12E-11	4.53E-09
3	160	3000	2.03E-05	2.74E-03	4.82E-09	1.90E-07	9.94E-13	2.44E-13	5.97E-18	6.72E-08	4.82E-11	1.88E-09
4	160	3000	7.11E-07	1.85E-04	1.69E-10	9.92E-11	3.02E-16	3.84E-17	1.81E-21	3.34E-08	1.41E-11	3.10E-10
5	160	3000	1.62E-10	7.48E-08	3.70E-14	1.37E-20	2.29E-26	1.50E-27	1.25E-31	6.25E-10	1.44E-13	1.67E-12
6	160	3000	4.41E-11	2.62E-08	8.68E-15	1.34E-21	1.66E-27	6.11E-29	6.57E-33	6.41E-10	1.08E-13	7.86E-13
7	160	3000	1.86E-11	1.27E-08	2.97E-15	3.87E-22	4.00E-28	8.08E-30	9.96E-34	6.67E-10	9.41E-14	4.47E-13
8	160	3000	8.79E-12	6.47E-09	1.04E-15	1.66E-22	1.53E-28	1.49E-30	1.98E-34	6.74E-10	8.48E-14	2.54E-13
9	160	3000	3.78E-12	2.91E-09	2.80E-16	8.77E-23	7.50E-29	2.49E-31	3.46E-35	6.66E-10	7.77E-14	1.24E-13
10	160	3000	7.94E-13	6.24E-10	1.90E-17	5.24E-23	4.27E-29	1.15E-32	1.64E-36	6.46E-10	7.18E-14	2.84E-14
11	160	3000	1.92E-15	1.50E-12	3.01E-22	3.38E-23	2.68E-29	1.34E-37	1.90E-41	6.10E-10	6.61E-14	7.25E-17
12	160	3000	5.66E-16	4.60E-13	2.88E-23	2.30E-23	1.73E-29	9.57E-39	1.41E-42	6.17E-10	6.31E-14	2.34E-17
13	160	3000	2.92E-16	2.45E-13	8.60E-24	1.64E-23	1.18E-29	2.21E-39	3.36E-43	6.21E-10	6.06E-14	1.31E-17
14	160	3000	1.82E-16	1.56E-13	3.72E-24	1.21E-23	8.38E-30	7.63E-40	1.19E-43	6.23E-10	5.84E-14	8.74E-18
15	160	3000	1.25E-16	1.10E-13	1.94E-24	9.24E-24	6.17E-30	3.25E-40	5.16E-44	6.21E-10	5.63E-14	6.38E-18
16	160	3000	9.13E-17	8.15E-14	1.14E-24	7.20E-24	4.67E-30	1.58E-40	2.56E-44	6.18E-10	5.44E-14	4.93E-18
17	160	3000	6.98E-17	6.32E-14	7.24E-25	5.72E-24	3.62E-30	8.49E-41	1.39E-44	6.14E-10	5.26E-14	3.95E-18
18	160	3000	5.51E-17	5.05E-14	4.88E-25	4.63E-24	2.86E-30	4.89E-41	8.12E-45	6.08E-10	5.09E-14	3.26E-18

		Formula:	MgHCO ₃ ⁺	MgSO ₄	Ca ⁺⁺	CaOH ⁺	CaCO ₃	CaHCO ₃ ⁺	CaSO ₄	Al ⁺⁺⁺	AlOH ⁺⁺	Al(OH) ₂ ⁺
		Type:	(a)	(a)	(a)	(a)	(a)	(a)	(a)	(a)	(a)	(a)
Cell	T (°C)	P(bar)	MgHCO ₃ ⁺	MgSO ₄ (aq)	Ca ⁺⁺	CaOH ⁺	CaCO ₃ (aq)	CaHCO ₃ ⁺	CaSO ₄ (aq)	Al ⁺⁺⁺	AlOH ⁺⁺	Al(OH) ₂ ⁺
Ore fluids	500	5000	1.42E-11	2.26E-16	2.09E-08	1.99E-07	1.74E-07	2.66E-08	1.61E-13	5.22E-26	1.42E-17	7.04E-12
1	400	3000	2.45E-11	1.86E-16	2.02E-08	5.39E-08	5.13E-07	7.22E-08	2.08E-13	1.10E-25	6.07E-18	2.53E-12
2	400	3000	2.42E-11	1.48E-16	2.82E-08	6.66E-08	5.15E-07	8.60E-08	2.01E-13	2.18E-25	9.74E-18	3.77E-12
3	400	3000	2.37E-11	1.20E-16	3.31E-08	6.85E-08	4.36E-07	8.71E-08	1.67E-13	4.67E-25	1.69E-17	6.00E-12
4	400	3000	1.89E-11	6.95E-17	2.58E-08	4.26E-08	1.97E-07	5.35E-08	7.47E-14	2.29E-24	5.99E-17	1.79E-11
5	400	3000	1.41E-12	4.86E-19	1.35E-10	2.08E-11	9.06E-12	2.63E-11	3.45E-18	4.91E-18	1.20E-11	3.35E-07
6	400	3000	2.10E-12	1.05E-19	2.36E-10	4.92E-12	3.12E-13	6.06E-12	1.15E-19	1.59E-14	6.02E-09	2.10E-05
7	400	3000	2.34E-12	5.97E-20	2.83E-10	2.99E-12	9.71E-14	3.58E-12	3.48E-20	2.44E-13	4.99E-08	8.57E-05
8	400	3000	2.43E-12	4.18E-20	3.07E-10	2.22E-12	4.86E-14	2.57E-12	1.68E-20	1.15E-12	1.67E-07	1.92E-04
9	400	3000	2.44E-12	3.20E-20	3.18E-10	1.78E-12	2.98E-14	1.99E-12	9.93E-21	3.29E-12	3.80E-07	3.32E-04
10	400	3000	2.42E-12	2.56E-20	3.23E-10	1.50E-12	2.03E-14	1.62E-12	6.53E-21	7.16E-12	7.04E-07	5.03E-04
11	400	3000	2.37E-12	2.12E-20	3.23E-10	1.29E-12	1.49E-14	1.35E-12	4.60E-21	1.32E-11	1.15E-06	6.97E-04
12	400	3000	2.30E-12	1.78E-20	3.21E-10	1.14E-12	1.14E-14	1.15E-12	3.39E-21	2.17E-11	1.71E-06	9.13E-04
13	400	3000	2.23E-12	1.52E-20	3.17E-10	1.02E-12	8.99E-15	9.93E-13	2.58E-21	3.29E-11	2.41E-06	1.15E-03
14	400	3000	2.16E-12	1.32E-20	3.12E-10	9.22E-13	7.29E-15	8.67E-13	2.01E-21	4.70E-11	3.22E-06	1.40E-03
15	400	3000	2.08E-12	1.15E-20	3.06E-10	8.42E-13	6.02E-15	7.63E-13	1.60E-21	6.42E-11	4.17E-06	1.66E-03
16	400	3000	2.00E-12	1.01E-20	3.00E-10	7.74E-13	5.06E-15	6.77E-13	1.29E-21	8.44E-11	5.23E-06	1.94E-03
17	400	3000	1.92E-12	8.86E-21	2.94E-10	7.15E-13	4.30E-15	6.04E-13	1.06E-21	1.08E-10	6.42E-06	2.23E-03
18	400	3000	1.85E-12	7.85E-21	2.87E-10	6.65E-13	3.70E-15	5.42E-13	8.75E-22	1.34E-10	7.73E-06	2.53E-03
Ore fluids	500	5000	1.42E-11	2.26E-16	2.09E-08	1.99E-07	1.74E-07	2.66E-08	1.61E-13	5.22E-26	1.42E-17	7.04E-12
1	370	3000	6.26E-11	6.03E-16	3.98E-08	4.82E-08	7.38E-07	1.46E-07	5.62E-13	7.09E-25	1.33E-17	3.09E-12
2	370	3000	5.99E-11	4.67E-16	5.47E-08	5.94E-08	7.40E-07	1.72E-07	5.35E-13	1.35E-24	2.09E-17	4.57E-12

		Formula:	MgHCO ₃ ⁺	MgSO ₄	Ca ⁺⁺	CaOH ⁺	CaCO ₃	CaHCO ₃ ⁺	CaSO ₄	Al ⁺⁺⁺	AlOH ⁺⁺	Al(OH) ₂ ⁺
		Type:	(a)	(a)	(a)	(a)	(a)	(a)	(a)	(a)	(a)	(a)
Cell	T (°C)	P(bar)	MgHCO ₃ ⁺	MgSO ₄ (aq)	Ca ⁺⁺	CaOH ⁺	CaCO ₃ (aq)	CaHCO ₃ ⁺	CaSO ₄ (aq)	Al ⁺⁺⁺	AlOH ⁺⁺	Al(OH) ₂ ⁺
3	370	3000	5.41E-11	3.09E-16	9.04E-08	8.10E-08	7.43E-07	2.24E-07	5.10E-13	4.36E-24	5.00E-17	9.62E-12
4	370	3000	1.06E-11	3.67E-17	9.62E-09	5.81E-09	3.22E-08	1.60E-08	2.21E-14	4.10E-22	2.81E-15	3.91E-10
5	370	3000	2.86E-12	5.10E-19	2.64E-10	7.40E-12	2.12E-12	2.04E-11	1.46E-18	2.18E-15	7.81E-10	4.70E-06
6	370	3000	3.52E-12	1.93E-19	3.65E-10	3.10E-12	2.73E-13	8.22E-12	1.80E-19	2.75E-13	3.25E-08	5.64E-05
7	370	3000	3.73E-12	1.17E-19	4.15E-10	2.07E-12	1.05E-13	5.24E-12	6.58E-20	2.37E-12	1.73E-07	1.72E-04
8	370	3000	3.74E-12	8.24E-20	4.39E-10	1.59E-12	5.68E-14	3.82E-12	3.36E-20	8.82E-12	4.81E-07	3.42E-04
9	370	3000	3.66E-12	6.18E-20	4.48E-10	1.30E-12	3.58E-14	2.96E-12	2.00E-20	2.21E-11	9.92E-07	5.55E-04
10	370	3000	3.52E-12	4.81E-20	4.49E-10	1.10E-12	2.47E-14	2.38E-12	1.30E-20	4.42E-11	1.72E-06	8.06E-04
11	370	3000	3.35E-12	3.82E-20	4.45E-10	9.59E-13	1.80E-14	1.95E-12	8.91E-21	7.67E-11	2.68E-06	1.09E-03
12	370	3000	3.17E-12	3.09E-20	4.38E-10	8.49E-13	1.37E-14	1.63E-12	6.35E-21	1.20E-10	3.87E-06	1.39E-03
13	370	3000	2.99E-12	2.52E-20	4.30E-10	7.61E-13	1.07E-14	1.38E-12	4.65E-21	1.76E-10	5.28E-06	1.72E-03
14	370	3000	2.80E-12	2.07E-20	4.20E-10	6.89E-13	8.52E-15	1.17E-12	3.47E-21	2.45E-10	6.91E-06	2.07E-03
15	370	3000	2.62E-12	1.71E-20	4.10E-10	6.30E-13	6.91E-15	1.01E-12	2.63E-21	3.26E-10	8.77E-06	2.43E-03
16	370	3000	2.45E-12	1.42E-20	4.00E-10	5.79E-13	5.68E-15	8.70E-13	2.02E-21	4.19E-10	1.08E-05	2.81E-03
17	370	3000	2.28E-12	1.18E-20	3.89E-10	5.36E-13	4.72E-15	7.55E-13	1.56E-21	5.26E-10	1.31E-05	3.20E-03
18	370	3000	2.12E-12	9.87E-21	3.79E-10	4.98E-13	3.96E-15	6.58E-13	1.22E-21	6.45E-10	1.56E-05	3.60E-03
Ore fluids	500	5000	1.42E-11	2.26E-16	2.09E-08	1.99E-07	1.74E-07	2.66E-08	1.61E-13	5.22E-26	1.42E-17	7.04E-12
1	340	3000	2.02E-10	2.50E-15	9.14E-08	4.16E-08	1.06E-06	3.35E-07	1.74E-12	7.56E-24	4.08E-17	4.47E-12
2	340	3000	1.88E-10	1.90E-15	1.24E-07	5.09E-08	1.06E-06	3.88E-07	1.65E-12	1.41E-23	6.38E-17	6.60E-12
3	340	3000	1.62E-10	1.20E-15	2.04E-07	6.92E-08	1.07E-06	5.04E-07	1.57E-12	4.83E-23	1.63E-16	1.47E-11
4	340	3000	3.10E-11	1.35E-16	3.39E-08	7.41E-09	6.71E-08	5.49E-08	1.01E-13	5.97E-21	1.15E-14	7.18E-10
5	340	3000	5.34E-12	1.80E-18	3.64E-10	5.50E-12	3.83E-12	4.12E-11	5.81E-18	1.08E-14	1.59E-09	6.46E-06

		Formula:	MgHCO ₃ ⁺	MgSO ₄	Ca ⁺⁺	CaOH ⁺	CaCO ₃	CaHCO ₃ ⁺	CaSO ₄	Al ⁺⁺⁺	AlOH ⁺⁺	Al(OH) ₂ ⁺
		Type:	(a)	(a)	(a)	(a)	(a)	(a)	(a)	(a)	(a)	(a)
Cell	T (°C)	P(bar)	MgHCO ₃ ⁺	MgSO ₄ (aq)	Ca ⁺⁺	CaOH ⁺	CaCO ₃ (aq)	CaHCO ₃ ⁺	CaSO ₄ (aq)	Al ⁺⁺⁺	AlOH ⁺⁺	Al(OH) ₂ ⁺
6	340	3000	6.44E-12	6.65E-19	4.85E-10	2.24E-12	4.81E-13	1.60E-11	6.94E-19	1.34E-12	6.57E-08	7.79E-05
7	340	3000	6.71E-12	3.92E-19	5.46E-10	1.49E-12	1.82E-13	1.00E-11	2.46E-19	1.16E-11	3.49E-07	2.39E-04
8	340	3000	6.60E-12	2.66E-19	5.73E-10	1.14E-12	9.65E-14	7.15E-12	1.21E-19	4.26E-11	9.66E-07	4.73E-04
9	340	3000	6.31E-12	1.92E-19	5.80E-10	9.27E-13	5.98E-14	5.43E-12	6.94E-20	1.06E-10	1.97E-06	7.67E-04
10	340	3000	5.92E-12	1.43E-19	5.78E-10	7.85E-13	4.04E-14	4.26E-12	4.32E-20	2.09E-10	3.40E-06	1.11E-03
11	340	3000	5.49E-12	1.08E-19	5.69E-10	6.81E-13	2.88E-14	3.41E-12	2.82E-20	3.57E-10	5.24E-06	1.49E-03
12	340	3000	5.04E-12	8.27E-20	5.57E-10	6.01E-13	2.13E-14	2.76E-12	1.90E-20	5.55E-10	7.49E-06	1.90E-03
13	340	3000	4.58E-12	6.32E-20	5.43E-10	5.38E-13	1.61E-14	2.26E-12	1.31E-20	8.03E-10	1.02E-05	2.34E-03
14	340	3000	4.14E-12	4.82E-20	5.28E-10	4.87E-13	1.24E-14	1.85E-12	9.06E-21	1.10E-09	1.32E-05	2.80E-03
15	340	3000	3.71E-12	3.67E-20	5.13E-10	4.44E-13	9.71E-15	1.52E-12	6.32E-21	1.45E-09	1.66E-05	3.28E-03
16	340	3000	3.30E-12	2.77E-20	4.98E-10	4.08E-13	7.64E-15	1.26E-12	4.42E-21	1.86E-09	2.04E-05	3.77E-03
17	340	3000	2.92E-12	2.08E-20	4.84E-10	3.77E-13	6.05E-15	1.04E-12	3.09E-21	2.31E-09	2.46E-05	4.29E-03
18	340	3000	2.57E-12	1.55E-20	4.69E-10	3.51E-13	4.81E-15	8.54E-13	2.16E-21	2.81E-09	2.90E-05	4.82E-03
Ore fluids	500	5000	1.42E-11	2.26E-16	2.09E-08	1.99E-07	1.74E-07	2.66E-08	1.61E-13	5.22E-26	1.42E-17	7.04E-12
1	310	3000	7.36E-10	1.19E-14	2.29E-07	3.43E-08	1.52E-06	8.19E-07	5.83E-12	1.11E-22	1.56E-16	7.20E-12
2	310	3000	6.73E-10	8.97E-15	3.08E-07	4.16E-08	1.52E-06	9.47E-07	5.56E-12	2.15E-22	2.54E-16	1.10E-11
3	310	3000	5.56E-10	5.40E-15	5.28E-07	5.71E-08	1.53E-06	1.27E-06	5.43E-12	9.32E-22	7.96E-16	2.91E-11
4	310	3000	1.15E-10	6.32E-16	1.57E-07	1.03E-08	1.56E-07	2.37E-07	5.78E-13	1.41E-19	6.40E-14	1.53E-09
5	310	3000	1.14E-11	7.51E-18	5.27E-10	3.74E-12	6.77E-12	8.80E-11	2.56E-17	8.08E-14	4.36E-09	1.07E-05
6	310	3000	1.31E-11	2.86E-18	6.43E-10	1.51E-12	9.11E-13	3.39E-11	3.27E-18	7.61E-12	1.47E-07	1.14E-04
7	310	3000	1.34E-11	1.68E-18	7.04E-10	9.96E-13	3.47E-13	2.09E-11	1.16E-18	6.15E-11	7.43E-07	3.40E-04
8	310	3000	1.29E-11	1.13E-18	7.25E-10	7.56E-13	1.83E-13	1.48E-11	5.66E-19	2.19E-10	2.00E-06	6.65E-04

Formula:		MgHCO ₃ ⁺	MgSO ₄	Ca ⁺⁺	CaOH ⁺	CaCO ₃	CaHCO ₃ ⁺	CaSO ₄	Al ⁺⁺⁺	AlOH ⁺⁺	Al(OH) ₂ ⁺	
Type:		(a)	(a)	(a)	(a)	(a)	(a)	(a)	(a)	(a)	(a)	
Cell	T (°C)	P(bar)	MgHCO ₃ ⁺	MgSO ₄ (aq)	Ca ⁺⁺	CaOH ⁺	CaCO ₃ (aq)	CaHCO ₃ ⁺	CaSO ₄ (aq)	Al ⁺⁺⁺	AlOH ⁺⁺	Al(OH) ₂ ⁺
9	310	3000	1.22E-11	7.99E-19	7.24E-10	6.13E-13	1.13E-13	1.10E-11	3.19E-19	5.26E-10	4.02E-06	1.07E-03
10	310	3000	1.12E-11	5.82E-19	7.13E-10	5.17E-13	7.57E-14	8.52E-12	1.95E-19	1.02E-09	6.81E-06	1.53E-03
11	310	3000	1.02E-11	4.28E-19	6.95E-10	4.47E-13	5.33E-14	6.69E-12	1.24E-19	1.71E-09	1.04E-05	2.03E-03
12	310	3000	9.16E-12	3.14E-19	6.74E-10	3.93E-13	3.88E-14	5.31E-12	8.03E-20	2.60E-09	1.46E-05	2.58E-03
13	310	3000	8.11E-12	2.29E-19	6.53E-10	3.51E-13	2.88E-14	4.23E-12	5.27E-20	3.71E-09	1.96E-05	3.16E-03
14	310	3000	7.09E-12	1.64E-19	6.31E-10	3.17E-13	2.16E-14	3.36E-12	3.44E-20	5.03E-09	2.53E-05	3.76E-03
15	310	3000	6.09E-12	1.15E-19	6.09E-10	2.89E-13	1.62E-14	2.66E-12	2.22E-20	6.54E-09	3.15E-05	4.38E-03
16	310	3000	5.15E-12	7.86E-20	5.88E-10	2.65E-13	1.22E-14	2.08E-12	1.40E-20	8.25E-09	3.84E-05	5.03E-03
17	310	3000	4.26E-12	5.15E-20	5.68E-10	2.45E-13	9.05E-15	1.61E-12	8.57E-21	1.02E-08	4.59E-05	5.69E-03
18	310	3000	3.43E-12	3.23E-20	5.49E-10	2.27E-13	6.63E-15	1.22E-12	5.04E-21	1.22E-08	5.39E-05	6.37E-03
Ore fluids	500	5000	1.42E-11	2.26E-16	2.09E-08	1.99E-07	1.74E-07	2.66E-08	1.61E-13	5.22E-26	1.42E-17	7.04E-12
1	280	3000	2.49E-09	5.16E-14	5.34E-07	2.59E-08	2.16E-06	1.88E-06	1.81E-11	1.56E-21	5.72E-16	1.11E-11
2	280	3000	2.24E-09	3.84E-14	7.37E-07	3.16E-08	2.17E-06	2.22E-06	1.76E-11	3.41E-21	1.04E-15	1.85E-11
3	280	3000	1.76E-09	2.10E-14	1.42E-06	4.54E-08	2.18E-06	3.22E-06	1.78E-11	2.39E-20	4.85E-15	6.81E-11
4	280	3000	4.16E-10	2.71E-15	7.33E-07	1.36E-08	3.60E-07	1.02E-06	3.08E-12	3.56E-18	3.71E-13	3.27E-09
5	280	3000	2.35E-11	2.71E-17	7.67E-10	2.35E-12	1.10E-11	1.77E-10	9.46E-17	7.49E-13	1.38E-08	1.92E-05
6	280	3000	2.48E-11	1.07E-17	8.22E-10	9.41E-13	1.63E-12	6.67E-11	1.34E-17	4.57E-11	3.38E-07	1.69E-04
7	280	3000	2.42E-11	6.26E-18	8.56E-10	6.10E-13	6.24E-13	3.98E-11	4.76E-18	3.27E-10	1.57E-06	4.78E-04
8	280	3000	2.25E-11	4.11E-18	8.55E-10	4.58E-13	3.25E-13	2.71E-11	2.29E-18	1.09E-09	4.04E-06	9.10E-04
9	280	3000	2.06E-11	2.85E-18	8.36E-10	3.68E-13	1.99E-13	1.98E-11	1.27E-18	2.51E-09	7.87E-06	1.43E-03
10	280	3000	1.85E-11	2.00E-18	8.07E-10	3.07E-13	1.31E-13	1.49E-11	7.47E-19	4.69E-09	1.30E-05	2.02E-03
11	280	3000	1.63E-11	1.41E-18	7.74E-10	2.63E-13	9.06E-14	1.14E-11	4.55E-19	7.65E-09	1.94E-05	2.67E-03

		Formula:	MgHCO ₃ ⁺	MgSO ₄	Ca ⁺⁺	CaOH ⁺	CaCO ₃	CaHCO ₃ ⁺	CaSO ₄	Al ⁺⁺⁺	AlOH ⁺⁺	Al(OH) ₂ ⁺
		Type:	(a)	(a)	(a)	(a)	(a)	(a)	(a)	(a)	(a)	(a)
Cell	T (°C)	P(bar)	MgHCO ₃ ⁺	MgSO ₄ (aq)	Ca ⁺⁺	CaOH ⁺	CaCO ₃ (aq)	CaHCO ₃ ⁺	CaSO ₄ (aq)	Al ⁺⁺⁺	AlOH ⁺⁺	Al(OH) ₂ ⁺
12	280	3000	1.41E-11	9.79E-19	7.40E-10	2.30E-13	6.43E-14	8.70E-12	2.80E-19	1.14E-08	2.70E-05	3.35E-03
13	280	3000	1.20E-11	6.63E-19	7.07E-10	2.04E-13	4.61E-14	6.65E-12	1.70E-19	1.59E-08	3.56E-05	4.06E-03
14	280	3000	9.93E-12	4.32E-19	6.76E-10	1.83E-13	3.30E-14	5.01E-12	1.01E-19	2.11E-08	4.52E-05	4.80E-03
15	280	3000	7.95E-12	2.65E-19	6.46E-10	1.66E-13	2.33E-14	3.69E-12	5.70E-20	2.70E-08	5.58E-05	5.56E-03
16	280	3000	6.08E-12	1.48E-19	6.18E-10	1.52E-13	1.59E-14	2.62E-12	2.96E-20	3.35E-08	6.72E-05	6.34E-03
17	280	3000	4.34E-12	7.24E-20	5.91E-10	1.39E-13	1.03E-14	1.75E-12	1.35E-20	4.06E-08	7.94E-05	7.13E-03
18	280	3000	2.81E-12	2.89E-20	5.66E-10	1.29E-13	6.06E-15	1.06E-12	5.05E-21	4.83E-08	9.24E-05	7.93E-03
Ore fluids	500	5000	1.42E-11	2.26E-16	2.09E-08	1.99E-07	1.74E-07	2.66E-08	1.61E-13	5.22E-26	1.42E-17	7.04E-12
1	250	3000	8.56E-09	1.56E-13	1.29E-06	1.81E-08	3.04E-06	4.44E-06	3.95E-11	2.93E-20	2.63E-15	1.99E-11
2	250	3000	7.91E-09	1.15E-13	1.96E-06	2.27E-08	3.05E-06	5.67E-06	4.03E-11	9.57E-20	6.58E-15	4.25E-11
3	250	3000	6.14E-09	5.81E-14	4.49E-06	3.46E-08	3.06E-06	9.28E-06	4.28E-11	1.26E-18	5.13E-14	2.35E-10
4	250	3000	1.82E-09	9.51E-15	4.15E-06	1.86E-08	9.14E-07	5.26E-06	1.34E-11	1.31E-16	2.76E-12	7.87E-09
5	250	3000	5.63E-11	7.83E-17	1.23E-09	1.40E-12	1.84E-11	3.98E-10	2.69E-16	1.02E-11	5.75E-08	4.04E-05
6	250	3000	5.38E-11	3.33E-17	1.09E-09	5.53E-13	3.20E-12	1.48E-10	4.46E-17	3.32E-10	8.84E-07	2.68E-04
7	250	3000	5.03E-11	1.97E-17	1.05E-09	3.52E-13	1.27E-12	8.65E-11	1.66E-17	1.94E-09	3.56E-06	6.96E-04
8	250	3000	4.56E-11	1.31E-17	9.98E-10	2.59E-13	6.74E-13	5.79E-11	8.09E-18	5.82E-09	8.52E-06	1.27E-03
9	250	3000	4.03E-11	9.03E-18	9.42E-10	2.05E-13	4.09E-13	4.11E-11	4.48E-18	1.25E-08	1.58E-05	1.94E-03
10	250	3000	3.50E-11	6.31E-18	8.85E-10	1.69E-13	2.67E-13	3.00E-11	2.63E-18	2.21E-08	2.52E-05	2.68E-03
11	250	3000	2.97E-11	4.38E-18	8.30E-10	1.44E-13	1.81E-13	2.21E-11	1.59E-18	3.47E-08	3.65E-05	3.48E-03
12	250	3000	2.47E-11	2.97E-18	7.80E-10	1.25E-13	1.24E-13	1.63E-11	9.54E-19	4.99E-08	4.96E-05	4.31E-03
13	250	3000	1.99E-11	1.94E-18	7.33E-10	1.10E-13	8.57E-14	1.18E-11	5.60E-19	6.77E-08	6.42E-05	5.17E-03
14	250	3000	1.54E-11	1.18E-18	6.90E-10	9.78E-14	5.79E-14	8.33E-12	3.11E-19	8.78E-08	8.02E-05	6.05E-03

		Formula:	MgHCO ₃ ⁺	MgSO ₄	Ca ⁺⁺	CaOH ⁺	CaCO ₃	CaHCO ₃ ⁺	CaSO ₄	Al ⁺⁺⁺	AlOH ⁺⁺	Al(OH) ₂ ⁺
		Type:	(a)	(a)	(a)	(a)	(a)	(a)	(a)	(a)	(a)	(a)
Cell	T (°C)	P(bar)	MgHCO ₃ ⁺	MgSO ₄ (aq)	Ca ⁺⁺	CaOH ⁺	CaCO ₃ (aq)	CaHCO ₃ ⁺	CaSO ₄ (aq)	Al ⁺⁺⁺	AlOH ⁺⁺	Al(OH) ₂ ⁺
15	250	3000	1.11E-11	6.40E-19	6.51E-10	8.80E-14	3.72E-14	5.55E-12	1.56E-19	1.10E-07	9.74E-05	6.94E-03
16	250	3000	7.13E-12	2.80E-19	6.16E-10	7.99E-14	2.15E-14	3.30E-12	6.31E-20	1.34E-07	1.16E-04	7.85E-03
17	250	3000	3.87E-12	8.36E-20	5.83E-10	7.30E-14	1.06E-14	1.67E-12	1.76E-20	1.59E-07	1.35E-04	8.76E-03
18	250	3000	1.34E-12	9.25E-21	5.52E-10	6.69E-14	3.39E-15	5.45E-13	1.83E-21	1.86E-07	1.55E-04	9.68E-03
Ore fluids	500	5000	1.42E-11	2.26E-16	2.09E-08	1.99E-07	1.74E-07	2.66E-08	1.61E-13	5.22E-26	1.42E-17	7.04E-12
1	220	3000	2.96E-08	4.46E-13	3.43E-06	1.21E-08	4.21E-06	1.13E-05	8.72E-11	9.57E-19	1.86E-14	4.89E-11
2	220	3000	2.85E-08	3.27E-13	5.94E-06	1.57E-08	4.22E-06	1.59E-05	9.39E-11	5.01E-18	6.76E-14	1.39E-10
3	220	3000	2.21E-08	1.58E-13	1.50E-05	2.49E-08	4.23E-06	2.77E-05	1.02E-10	9.02E-17	6.80E-13	9.32E-10
4	220	3000	7.38E-09	2.95E-14	1.85E-05	1.80E-08	1.72E-06	2.11E-05	4.34E-11	7.39E-15	2.94E-11	2.51E-08
5	220	3000	1.44E-10	2.22E-16	2.18E-09	7.94E-13	2.91E-11	9.25E-10	7.29E-16	2.04E-10	3.14E-07	9.88E-05
6	220	3000	1.21E-10	1.02E-16	1.53E-09	3.08E-13	6.13E-12	3.37E-10	1.46E-16	3.08E-09	2.76E-06	4.68E-04
7	220	3000	1.07E-10	6.22E-17	1.32E-09	1.91E-13	2.59E-12	1.92E-10	5.73E-17	1.34E-08	8.99E-06	1.07E-03
8	220	3000	9.36E-11	4.16E-17	1.17E-09	1.38E-13	1.41E-12	1.26E-10	2.87E-17	3.45E-08	1.93E-05	1.83E-03
9	220	3000	8.07E-11	2.89E-17	1.06E-09	1.07E-13	8.65E-13	8.77E-11	1.61E-17	6.71E-08	3.33E-05	2.69E-03
10	220	3000	6.87E-11	2.03E-17	9.59E-10	8.72E-14	5.69E-13	6.31E-11	9.55E-18	1.11E-07	5.07E-05	3.62E-03
11	220	3000	5.75E-11	1.41E-17	8.76E-10	7.32E-14	3.87E-13	4.59E-11	5.78E-18	1.64E-07	7.08E-05	4.59E-03
12	220	3000	4.71E-11	9.55E-18	8.04E-10	6.28E-14	2.68E-13	3.34E-11	3.48E-18	2.27E-07	9.35E-05	5.59E-03
13	220	3000	3.75E-11	6.19E-18	7.42E-10	5.48E-14	1.84E-13	2.40E-11	2.04E-18	2.97E-07	1.18E-04	6.61E-03
14	220	3000	2.85E-11	3.73E-18	6.87E-10	4.85E-14	1.24E-13	1.67E-11	1.12E-18	3.74E-07	1.45E-04	7.64E-03
15	220	3000	2.02E-11	1.98E-18	6.39E-10	4.33E-14	7.89E-14	1.09E-11	5.50E-19	4.56E-07	1.73E-04	8.68E-03
16	220	3000	1.26E-11	8.37E-19	5.96E-10	3.91E-14	4.47E-14	6.31E-12	2.15E-19	5.42E-07	2.02E-04	9.73E-03
17	220	3000	5.64E-12	1.93E-19	5.57E-10	3.55E-14	1.84E-14	2.64E-12	4.66E-20	6.30E-07	2.32E-04	1.08E-02

		Formula:	MgHCO ₃ ⁺	MgSO ₄	Ca ⁺⁺	CaOH ⁺	CaCO ₃	CaHCO ₃ ⁺	CaSO ₄	Al ⁺⁺⁺	AlOH ⁺⁺	Al(OH) ₂ ⁺
		Type:	(a)	(a)	(a)	(a)	(a)	(a)	(a)	(a)	(a)	(a)
Cell	T (°C)	P(bar)	MgHCO ₃ ⁺	MgSO ₄ (aq)	Ca ⁺⁺	CaOH ⁺	CaCO ₃ (aq)	CaHCO ₃ ⁺	CaSO ₄ (aq)	Al ⁺⁺⁺	AlOH ⁺⁺	Al(OH) ₂ ⁺
18	220	3000	7.74E-13	4.64E-21	5.19E-10	3.23E-14	2.35E-15	3.41E-13	1.05E-21	7.16E-07	2.62E-04	1.18E-02
Ore fluids	500	5000	1.42E-11	2.26E-16	2.09E-08	1.99E-07	1.74E-07	2.66E-08	1.61E-13	5.22E-26	1.42E-17	7.04E-12
1	190	3000	1.09E-07	1.26E-12	1.05E-05	7.65E-09	5.66E-06	3.18E-05	1.98E-10	6.06E-17	2.18E-13	1.73E-10
2	190	3000	1.07E-07	9.15E-13	1.94E-05	1.01E-08	5.68E-06	4.68E-05	2.18E-10	3.87E-16	9.32E-13	5.50E-10
3	190	3000	8.03E-08	4.22E-13	5.00E-05	1.63E-08	5.69E-06	8.16E-05	2.32E-10	7.11E-15	9.59E-12	3.77E-09
4	190	3000	2.47E-08	7.33E-14	6.25E-05	1.25E-08	2.46E-06	6.26E-05	1.01E-10	4.82E-13	3.63E-10	9.26E-08
5	190	3000	3.55E-10	5.48E-16	4.10E-09	4.29E-13	4.37E-11	2.09E-09	1.75E-15	4.81E-09	1.93E-06	2.53E-04
6	190	3000	2.59E-10	2.68E-16	2.23E-09	1.61E-13	1.09E-11	7.27E-10	4.08E-16	3.39E-08	9.75E-06	8.63E-04
7	190	3000	2.10E-10	1.65E-16	1.67E-09	9.62E-14	4.85E-12	3.96E-10	1.69E-16	1.04E-07	2.47E-05	1.70E-03
8	190	3000	1.74E-10	1.10E-16	1.37E-09	6.76E-14	2.70E-12	2.50E-10	8.58E-17	2.18E-07	4.60E-05	2.69E-03
9	190	3000	1.44E-10	7.54E-17	1.16E-09	5.15E-14	1.67E-12	1.69E-10	4.79E-17	3.74E-07	7.26E-05	3.75E-03
10	190	3000	1.18E-10	5.16E-17	1.01E-09	4.12E-14	1.09E-12	1.17E-10	2.79E-17	5.64E-07	1.04E-04	4.86E-03
11	190	3000	9.47E-11	3.47E-17	8.90E-10	3.41E-14	7.35E-13	8.27E-11	1.64E-17	7.82E-07	1.38E-04	6.00E-03
12	190	3000	7.44E-11	2.25E-17	7.94E-10	2.89E-14	4.97E-13	5.79E-11	9.48E-18	1.02E-06	1.76E-04	7.16E-03
13	190	3000	5.63E-11	1.36E-17	7.16E-10	2.50E-14	3.31E-13	3.96E-11	5.20E-18	1.28E-06	2.15E-04	8.32E-03
14	190	3000	3.99E-11	7.37E-18	6.49E-10	2.19E-14	2.11E-13	2.57E-11	2.57E-18	1.55E-06	2.57E-04	9.48E-03
15	190	3000	2.50E-11	3.20E-18	5.92E-10	1.94E-14	1.20E-13	1.49E-11	1.03E-18	1.83E-06	3.00E-04	1.06E-02
16	190	3000	1.16E-11	7.94E-19	5.42E-10	1.73E-14	5.11E-14	6.40E-12	2.38E-19	2.10E-06	3.42E-04	1.17E-02
17	190	3000	6.78E-13	4.55E-21	4.93E-10	1.55E-14	2.81E-15	3.52E-13	1.28E-21	2.32E-06	3.80E-04	1.27E-02
18	190	3000	4.24E-14	1.95E-23	4.50E-10	1.39E-14	1.65E-16	2.06E-14	5.14E-24	2.58E-06	4.23E-04	1.38E-02
Ore fluids	500	5000	1.42E-11	2.26E-16	2.09E-08	1.99E-07	1.74E-07	2.66E-08	1.61E-13	5.22E-26	1.42E-17	7.04E-12
1	160	3000	1.55E-07	1.44E-12	1.63E-05	4.46E-09	7.37E-06	4.40E-05	2.36E-10	2.73E-16	3.54E-13	1.60E-10

		Formula:	MgHCO ₃ ⁺	MgSO ₄	Ca ⁺⁺	CaOH ⁺	CaCO ₃	CaHCO ₃ ⁺	CaSO ₄	Al ⁺⁺⁺	AlOH ⁺⁺	Al(OH) ₂ ⁺
		Type:	(a)	(a)	(a)	(a)	(a)	(a)	(a)	(a)	(a)	(a)
Cell	T (°C)	P(bar)	MgHCO ₃ ⁺	MgSO ₄ (aq)	Ca ⁺⁺	CaOH ⁺	CaCO ₃ (aq)	CaHCO ₃ ⁺	CaSO ₄ (aq)	Al ⁺⁺⁺	AlOH ⁺⁺	Al(OH) ₂ ⁺
2	160	3000	1.31E-07	9.13E-13	2.75E-05	5.96E-09	7.39E-06	5.89E-05	2.36E-10	1.19E-15	1.14E-12	4.25E-10
3	160	3000	8.84E-08	3.79E-13	6.76E-05	9.75E-09	7.40E-06	9.63E-05	2.36E-10	1.71E-14	9.86E-12	2.59E-09
4	160	3000	2.58E-08	6.25E-14	1.31E-04	1.16E-08	4.99E-06	1.14E-04	1.59E-10	1.25E-12	4.05E-10	6.85E-08
5	160	3000	2.51E-10	3.23E-16	3.83E-09	1.83E-13	4.14E-11	1.72E-09	1.27E-15	1.82E-08	3.25E-06	2.95E-04
6	160	3000	1.58E-10	1.31E-16	1.93E-09	6.63E-14	9.36E-12	5.22E-10	2.48E-16	1.12E-07	1.50E-05	9.55E-04
7	160	3000	1.07E-10	6.04E-17	1.37E-09	3.87E-14	3.58E-12	2.36E-10	7.67E-17	3.14E-07	3.57E-05	1.83E-03
8	160	3000	6.73E-11	2.55E-17	1.07E-09	2.66E-14	1.56E-12	1.14E-10	2.47E-17	6.17E-07	6.37E-05	2.81E-03
9	160	3000	3.52E-11	7.80E-18	8.81E-10	2.00E-14	6.21E-13	4.86E-11	6.19E-18	9.95E-07	9.67E-05	3.84E-03
10	160	3000	8.37E-12	5.77E-19	7.38E-10	1.57E-14	1.21E-13	9.88E-12	3.90E-19	1.41E-06	1.32E-04	4.85E-03
11	160	3000	2.17E-14	9.64E-24	6.19E-10	1.27E-14	2.71E-16	2.24E-14	5.71E-24	1.78E-06	1.67E-04	5.77E-03
12	160	3000	7.33E-15	1.01E-24	5.57E-10	1.07E-14	7.72E-17	6.67E-15	5.27E-25	2.45E-06	2.19E-04	7.03E-03
13	160	3000	4.26E-15	3.27E-25	5.06E-10	9.17E-15	3.86E-17	3.47E-15	1.53E-25	3.23E-06	2.78E-04	8.34E-03
14	160	3000	2.93E-15	1.52E-25	4.63E-10	7.99E-15	2.33E-17	2.16E-15	6.42E-26	4.09E-06	3.42E-04	9.68E-03
15	160	3000	2.20E-15	8.42E-26	4.26E-10	7.05E-15	1.56E-17	1.48E-15	3.26E-26	5.03E-06	4.10E-04	1.10E-02
16	160	3000	1.73E-15	5.22E-26	3.93E-10	6.28E-15	1.11E-17	1.08E-15	1.86E-26	6.03E-06	4.83E-04	1.24E-02
17	160	3000	1.41E-15	3.48E-26	3.64E-10	5.63E-15	8.25E-18	8.15E-16	1.15E-26	7.10E-06	5.58E-04	1.38E-02
18	160	3000	1.18E-15	2.45E-26	3.38E-10	5.09E-15	6.35E-18	6.36E-16	7.57E-27	8.22E-06	6.37E-04	1.52E-02

		Formula:	Al(OH)3	Al(OH)4-	Zn ⁺⁺	ZnOH ⁺	Zn(OH)2	ZnHCO3 ⁺	Zn(HS)2	Au ⁺	AuOH	Au(OH)2-
		Type:	(a)	(a)	(a)	(a)	(a)	(a)	(a)	(a)	(a)	(a)
Cell	T (°C)	P(bar)	Al(OH)3 (aq)	Al(OH)4-	Zn ⁺⁺	ZnOH ⁺	Zn(OH)2 (aq)	ZnHCO3 ⁺	Zn(HS)2 (aq)	Au ⁺	AuOH (aq)	Au(OH)2-
Ore fluids	500	5000	6.25E-07	1.05E-04	0	0	0	0	0	4.03E-16	2.35E-08	2.91E-07
1	400	3000	1.82E-07	3.77E-05	1.10E-14	3.08E-09	6.51E-09	1.44E-13	2.20E-07	6.22E-18	1.00E-09	7.93E-09
2	400	3000	2.29E-07	3.67E-05	1.48E-14	3.67E-09	6.58E-09	1.66E-13	2.21E-07	7.33E-18	9.99E-10	6.08E-09
3	400	3000	3.05E-07	3.74E-05	2.04E-14	4.42E-09	6.64E-09	1.97E-13	2.22E-07	8.77E-18	1.00E-09	4.67E-09
4	400	3000	6.74E-07	5.34E-05	3.49E-14	6.03E-09	6.69E-09	2.65E-13	2.23E-07	1.19E-17	1.00E-09	3.03E-09
5	400	3000	1.18E-03	8.69E-03	4.01E-12	6.49E-08	6.72E-09	2.86E-12	2.24E-07	1.28E-16	1.01E-09	2.84E-10
6	400	3000	1.10E-02	1.45E-02	2.00E-10	4.37E-07	6.75E-09	1.88E-11	2.25E-07	8.57E-16	1.01E-09	5.05E-11
7	400	3000	2.36E-02	1.75E-02	7.52E-10	8.35E-07	6.79E-09	3.49E-11	2.25E-07	1.62E-15	1.00E-09	2.83E-11
8	400	3000	3.68E-02	1.98E-02	1.59E-09	1.20E-06	6.83E-09	4.87E-11	2.25E-07	2.32E-15	9.99E-10	2.05E-11
9	400	3000	5.02E-02	2.20E-02	2.62E-09	1.54E-06	6.87E-09	6.03E-11	2.25E-07	2.93E-15	9.94E-10	1.66E-11
10	400	3000	6.37E-02	2.40E-02	3.80E-09	1.85E-06	6.90E-09	6.98E-11	2.25E-07	3.48E-15	9.90E-10	1.42E-11
11	400	3000	7.71E-02	2.60E-02	5.07E-09	2.13E-06	6.94E-09	7.77E-11	2.25E-07	3.97E-15	9.85E-10	1.27E-11
12	400	3000	9.06E-02	2.80E-02	6.41E-09	2.39E-06	6.98E-09	8.42E-11	2.25E-07	4.41E-15	9.80E-10	1.16E-11
13	400	3000	1.04E-01	3.00E-02	7.79E-09	2.63E-06	7.02E-09	8.95E-11	2.25E-07	4.80E-15	9.76E-10	1.07E-11
14	400	3000	1.17E-01	3.20E-02	9.20E-09	2.85E-06	7.06E-09	9.37E-11	2.25E-07	5.15E-15	9.71E-10	1.01E-11
15	400	3000	1.31E-01	3.40E-02	1.06E-08	3.06E-06	7.10E-09	9.71E-11	2.24E-07	5.47E-15	9.66E-10	9.56E-12
16	400	3000	1.44E-01	3.60E-02	1.20E-08	3.26E-06	7.14E-09	9.97E-11	2.24E-07	5.76E-15	9.61E-10	9.14E-12
17	400	3000	1.58E-01	3.80E-02	1.35E-08	3.44E-06	7.18E-09	1.02E-10	2.24E-07	6.03E-15	9.55E-10	8.78E-12
18	400	3000	1.71E-01	4.00E-02	1.49E-08	3.62E-06	7.22E-09	1.03E-10	2.24E-07	6.27E-15	9.50E-10	8.48E-12
Ore fluids	500	5000	6.25E-07	1.05E-04	0	0	0	0	0	4.03E-16	2.35E-08	2.91E-07
1	370	3000	1.28E-07	2.19E-05	2.36E-14	2.43E-09	3.69E-09	2.94E-13	1.33E-07	2.09E-18	3.53E-10	2.51E-09
2	370	3000	1.62E-07	2.19E-05	3.10E-14	2.86E-09	3.73E-09	3.30E-13	1.34E-07	2.41E-18	3.50E-10	1.96E-09

		Formula:	Al(OH)3	Al(OH)4-	Zn ⁺⁺	ZnOH ⁺	Zn(OH)2	ZnHCO3 ⁺	Zn(HS)2	Au ⁺	AuOH	Au(OH)2-
		Type:	(a)	(a)	(a)	(a)	(a)	(a)	(a)	(a)	(a)	(a)
Cell	T (°C)	P(bar)	Al(OH)3 (aq)	Al(OH)4-	Zn ⁺⁺	ZnOH ⁺	Zn(OH)2 (aq)	ZnHCO3 ⁺	Zn(HS)2 (aq)	Au ⁺	AuOH (aq)	Au(OH)2-
3	370	3000	2.63E-07	2.42E-05	4.91E-14	3.74E-09	3.77E-09	4.12E-13	1.34E-07	3.10E-18	3.48E-10	1.33E-09
4	370	3000	6.50E-06	3.05E-04	1.21E-13	6.20E-09	3.80E-09	6.83E-13	1.35E-07	5.14E-18	3.50E-10	6.81E-10
5	370	3000	4.02E-03	1.15E-02	5.08E-11	1.21E-07	3.81E-09	1.33E-11	1.35E-07	1.00E-16	3.52E-10	4.19E-11
6	370	3000	1.54E-02	1.57E-02	5.28E-10	3.80E-07	3.84E-09	4.03E-11	1.35E-07	3.12E-16	3.50E-10	1.48E-11
7	370	3000	2.84E-02	1.83E-02	1.50E-09	6.35E-07	3.86E-09	6.41E-11	1.35E-07	5.12E-16	3.47E-10	9.30E-12
8	370	3000	4.16E-02	2.06E-02	2.81E-09	8.67E-07	3.89E-09	8.31E-11	1.35E-07	6.88E-16	3.44E-10	7.05E-12
9	370	3000	5.49E-02	2.27E-02	4.36E-09	1.08E-06	3.93E-09	9.78E-11	1.35E-07	8.40E-16	3.41E-10	5.84E-12
10	370	3000	6.83E-02	2.48E-02	6.06E-09	1.27E-06	3.96E-09	1.09E-10	1.35E-07	9.71E-16	3.38E-10	5.08E-12
11	370	3000	8.16E-02	2.68E-02	7.86E-09	1.44E-06	3.99E-09	1.17E-10	1.35E-07	1.08E-15	3.34E-10	4.56E-12
12	370	3000	9.49E-02	2.89E-02	9.71E-09	1.60E-06	4.02E-09	1.23E-10	1.34E-07	1.18E-15	3.31E-10	4.18E-12
13	370	3000	1.08E-01	3.10E-02	1.16E-08	1.75E-06	4.05E-09	1.26E-10	1.34E-07	1.27E-15	3.27E-10	3.89E-12
14	370	3000	1.21E-01	3.31E-02	1.35E-08	1.89E-06	4.08E-09	1.28E-10	1.34E-07	1.34E-15	3.24E-10	3.66E-12
15	370	3000	1.35E-01	3.52E-02	1.54E-08	2.02E-06	4.12E-09	1.29E-10	1.33E-07	1.41E-15	3.20E-10	3.47E-12
16	370	3000	1.48E-01	3.73E-02	1.74E-08	2.14E-06	4.15E-09	1.28E-10	1.33E-07	1.46E-15	3.16E-10	3.31E-12
17	370	3000	1.61E-01	3.94E-02	1.93E-08	2.26E-06	4.18E-09	1.27E-10	1.33E-07	1.51E-15	3.12E-10	3.17E-12
18	370	3000	1.74E-01	4.15E-02	2.12E-08	2.37E-06	4.22E-09	1.25E-10	1.32E-07	1.55E-15	3.08E-10	3.05E-12
Ore fluids	500	5000	6.25E-07	1.05E-04	0	0	0	0	0	4.03E-16	2.35E-08	2.91E-07
1	340	3000	9.05E-08	1.12E-05	6.53E-14	2.09E-09	1.93E-09	7.51E-13	7.63E-08	7.06E-19	1.13E-10	6.35E-10
2	340	3000	1.16E-07	1.15E-05	8.41E-14	2.43E-09	1.96E-09	8.27E-13	7.66E-08	8.05E-19	1.12E-10	5.06E-10
3	340	3000	2.01E-07	1.37E-05	1.33E-13	3.17E-09	1.98E-09	1.03E-12	7.69E-08	1.03E-18	1.12E-10	3.46E-10
4	340	3000	5.68E-06	1.88E-04	3.58E-13	5.49E-09	1.99E-09	1.82E-12	7.75E-08	1.80E-18	1.13E-10	1.70E-10
5	340	3000	3.88E-03	1.14E-02	6.84E-11	7.25E-08	2.00E-09	2.42E-11	7.78E-08	2.38E-17	1.14E-10	1.52E-11

		Formula:	Al(OH)3	Al(OH)4-	Zn ⁺⁺	ZnOH ⁺	Zn(OH)2	ZnHCO3 ⁺	Zn(HS)2	Au ⁺	AuOH	Au(OH)2-
		Type:	(a)	(a)	(a)	(a)	(a)	(a)	(a)	(a)	(a)	(a)
Cell	T (°C)	P(bar)	Al(OH)3 (aq)	Al(OH)4-	Zn ⁺⁺	ZnOH ⁺	Zn(OH)2 (aq)	ZnHCO3 ⁺	Zn(HS)2 (aq)	Au ⁺	AuOH (aq)	Au(OH)2-
6	340	3000	1.51E-02	1.58E-02	6.98E-10	2.27E-07	2.01E-09	7.23E-11	7.78E-08	7.33E-17	1.13E-10	5.37E-12
7	340	3000	2.79E-02	1.85E-02	1.98E-09	3.78E-07	2.03E-09	1.14E-10	7.77E-08	1.20E-16	1.12E-10	3.36E-12
8	340	3000	4.10E-02	2.08E-02	3.70E-09	5.16E-07	2.05E-09	1.45E-10	7.75E-08	1.60E-16	1.10E-10	2.54E-12
9	340	3000	5.42E-02	2.30E-02	5.70E-09	6.39E-07	2.07E-09	1.67E-10	7.73E-08	1.94E-16	1.09E-10	2.10E-12
10	340	3000	6.73E-02	2.52E-02	7.87E-09	7.50E-07	2.09E-09	1.82E-10	7.71E-08	2.22E-16	1.07E-10	1.83E-12
11	340	3000	8.04E-02	2.74E-02	1.01E-08	8.52E-07	2.11E-09	1.90E-10	7.69E-08	2.46E-16	1.06E-10	1.64E-12
12	340	3000	9.34E-02	2.96E-02	1.25E-08	9.46E-07	2.13E-09	1.94E-10	7.66E-08	2.65E-16	1.04E-10	1.49E-12
13	340	3000	1.06E-01	3.18E-02	1.48E-08	1.03E-06	2.16E-09	1.93E-10	7.63E-08	2.81E-16	1.02E-10	1.38E-12
14	340	3000	1.19E-01	3.40E-02	1.72E-08	1.12E-06	2.18E-09	1.89E-10	7.59E-08	2.94E-16	9.98E-11	1.29E-12
15	340	3000	1.32E-01	3.63E-02	1.96E-08	1.19E-06	2.21E-09	1.83E-10	7.55E-08	3.05E-16	9.77E-11	1.22E-12
16	340	3000	1.45E-01	3.85E-02	2.20E-08	1.27E-06	2.24E-09	1.74E-10	7.50E-08	3.12E-16	9.55E-11	1.15E-12
17	340	3000	1.58E-01	4.08E-02	2.44E-08	1.34E-06	2.27E-09	1.64E-10	7.45E-08	3.18E-16	9.32E-11	1.09E-12
18	340	3000	1.71E-01	4.31E-02	2.69E-08	1.41E-06	2.29E-09	1.53E-10	7.39E-08	3.22E-16	9.07E-11	1.04E-12
Ore fluids	500	5000	6.25E-07	1.05E-04	0	0	0	0	0	4.03E-16	2.35E-08	2.91E-07
1	310	3000	6.50E-08	5.28E-06	2.08E-13	1.85E-09	9.47E-10	2.16E-12	4.10E-08	2.19E-19	3.25E-11	1.33E-10
2	310	3000	8.63E-08	5.68E-06	2.68E-13	2.15E-09	9.59E-10	2.40E-12	4.11E-08	2.50E-19	3.23E-11	1.07E-10
3	310	3000	1.72E-07	7.60E-06	4.50E-13	2.88E-09	9.68E-10	3.13E-12	4.14E-08	3.32E-19	3.22E-11	7.19E-11
4	310	3000	4.93E-06	9.93E-05	1.37E-12	5.30E-09	9.72E-10	6.01E-12	4.18E-08	6.18E-19	3.28E-11	3.33E-11
5	310	3000	4.05E-03	1.09E-02	1.08E-10	4.53E-08	9.73E-10	5.21E-11	4.20E-08	5.31E-18	3.30E-11	4.49E-12
6	310	3000	1.50E-02	1.55E-02	9.41E-10	1.31E-07	9.81E-10	1.44E-10	4.20E-08	1.51E-17	3.28E-11	1.70E-12
7	310	3000	2.76E-02	1.83E-02	2.56E-09	2.15E-07	9.90E-10	2.21E-10	4.19E-08	2.43E-17	3.24E-11	1.08E-12
8	310	3000	4.05E-02	2.08E-02	4.69E-09	2.90E-07	1.00E-09	2.77E-10	4.18E-08	3.20E-17	3.19E-11	8.28E-13

		Formula:	Al(OH)3	Al(OH)4-	Zn ⁺⁺	ZnOH ⁺	Zn(OH)2	ZnHCO3 ⁺	Zn(HS)2	Au ⁺	AuOH	Au(OH)2-
		Type:	(a)	(a)	(a)	(a)	(a)	(a)	(a)	(a)	(a)	(a)
Cell	T (°C)	P(bar)	Al(OH)3 (aq)	Al(OH)4-	Zn ⁺⁺	ZnOH ⁺	Zn(OH)2 (aq)	ZnHCO3 ⁺	Zn(HS)2 (aq)	Au ⁺	AuOH (aq)	Au(OH)2-
9	310	3000	5.34E-02	2.32E-02	7.10E-09	3.56E-07	1.01E-09	3.14E-10	4.17E-08	3.83E-17	3.14E-11	6.89E-13
10	310	3000	6.62E-02	2.55E-02	9.68E-09	4.16E-07	1.02E-09	3.35E-10	4.15E-08	4.34E-17	3.09E-11	6.02E-13
11	310	3000	7.90E-02	2.79E-02	1.23E-08	4.70E-07	1.03E-09	3.45E-10	4.13E-08	4.76E-17	3.03E-11	5.40E-13
12	310	3000	9.17E-02	3.03E-02	1.50E-08	5.19E-07	1.05E-09	3.43E-10	4.11E-08	5.09E-17	2.97E-11	4.94E-13
13	310	3000	1.04E-01	3.27E-02	1.78E-08	5.66E-07	1.06E-09	3.34E-10	4.09E-08	5.34E-17	2.90E-11	4.57E-13
14	310	3000	1.17E-01	3.51E-02	2.05E-08	6.10E-07	1.08E-09	3.17E-10	4.06E-08	5.52E-17	2.82E-11	4.26E-13
15	310	3000	1.30E-01	3.75E-02	2.33E-08	6.52E-07	1.09E-09	2.94E-10	4.03E-08	5.64E-17	2.73E-11	3.99E-13
16	310	3000	1.42E-01	3.99E-02	2.60E-08	6.94E-07	1.11E-09	2.67E-10	3.99E-08	5.69E-17	2.64E-11	3.74E-13
17	310	3000	1.55E-01	4.24E-02	2.89E-08	7.35E-07	1.13E-09	2.36E-10	3.94E-08	5.68E-17	2.53E-11	3.50E-13
18	310	3000	1.67E-01	4.49E-02	3.18E-08	7.77E-07	1.16E-09	2.04E-10	3.88E-08	5.61E-17	2.42E-11	3.27E-13
Ore fluids	500	5000	6.25E-07	1.05E-04	0	0	0	0	0	4.03E-16	2.35E-08	2.91E-07
1	280	3000	4.62E-08	2.47E-06	6.41E-13	1.58E-09	4.61E-10	6.04E-12	1.90E-08	5.23E-20	7.96E-12	2.43E-11
2	280	3000	6.61E-08	2.84E-06	8.49E-13	1.86E-09	4.62E-10	6.84E-12	1.93E-08	6.10E-20	7.93E-12	1.95E-11
3	280	3000	1.69E-07	4.53E-06	1.66E-12	2.70E-09	4.67E-10	1.01E-11	1.94E-08	8.84E-20	8.00E-12	1.22E-11
4	280	3000	4.25E-06	5.08E-05	5.52E-12	5.22E-09	4.74E-10	2.05E-11	1.94E-08	1.72E-19	8.15E-12	5.56E-12
5	280	3000	4.40E-03	1.02E-02	1.92E-10	2.99E-08	4.76E-10	1.18E-10	1.94E-08	9.83E-19	8.20E-12	1.08E-12
6	280	3000	1.52E-02	1.49E-02	1.30E-09	7.55E-08	4.73E-10	2.81E-10	1.97E-08	2.48E-18	8.11E-12	4.56E-13
7	280	3000	2.74E-02	1.80E-02	3.22E-09	1.17E-07	4.69E-10	4.01E-10	2.00E-08	3.81E-18	7.98E-12	3.00E-13
8	280	3000	3.99E-02	2.07E-02	5.54E-09	1.51E-07	4.63E-10	4.70E-10	2.04E-08	4.88E-18	7.83E-12	2.32E-13
9	280	3000	5.25E-02	2.33E-02	8.14E-09	1.82E-07	4.66E-10	5.16E-10	2.04E-08	5.74E-18	7.68E-12	1.95E-13
10	280	3000	6.50E-02	2.59E-02	1.09E-08	2.11E-07	4.72E-10	5.37E-10	2.03E-08	6.41E-18	7.52E-12	1.71E-13
11	280	3000	7.75E-02	2.84E-02	1.36E-08	2.36E-07	4.79E-10	5.35E-10	2.02E-08	6.92E-18	7.33E-12	1.54E-13

		Formula:	Al(OH)3	Al(OH)4-	Zn ⁺⁺	ZnOH ⁺	Zn(OH)2	ZnHCO3 ⁺	Zn(HS)2	Au ⁺	AuOH	Au(OH)2-
		Type:	(a)	(a)	(a)	(a)	(a)	(a)	(a)	(a)	(a)	(a)
Cell	T (°C)	P(bar)	Al(OH)3 (aq)	Al(OH)4-	Zn ⁺⁺	ZnOH ⁺	Zn(OH)2 (aq)	ZnHCO3 ⁺	Zn(HS)2 (aq)	Au ⁺	AuOH (aq)	Au(OH)2-
12	280	3000	8.99E-02	3.10E-02	1.64E-08	2.60E-07	4.86E-10	5.16E-10	2.01E-08	7.28E-18	7.13E-12	1.40E-13
13	280	3000	1.02E-01	3.36E-02	1.91E-08	2.81E-07	4.94E-10	4.81E-10	1.99E-08	7.51E-18	6.90E-12	1.30E-13
14	280	3000	1.15E-01	3.62E-02	2.19E-08	3.02E-07	5.04E-10	4.35E-10	1.97E-08	7.62E-18	6.64E-12	1.20E-13
15	280	3000	1.27E-01	3.88E-02	2.47E-08	3.23E-07	5.14E-10	3.78E-10	1.94E-08	7.61E-18	6.33E-12	1.11E-13
16	280	3000	1.39E-01	4.15E-02	2.76E-08	3.44E-07	5.27E-10	3.13E-10	1.91E-08	7.45E-18	5.97E-12	1.02E-13
17	280	3000	1.51E-01	4.41E-02	3.06E-08	3.67E-07	5.44E-10	2.42E-10	1.86E-08	7.15E-18	5.53E-12	9.23E-14
18	280	3000	1.63E-01	4.68E-02	3.40E-08	3.93E-07	5.65E-10	1.70E-10	1.80E-08	6.65E-18	5.00E-12	8.19E-14
Ore fluids	500	5000	6.25E-07	1.05E-04	0	0	0	0	0	4.03E-16	2.35E-08	2.91E-07
1	250	3000	3.61E-08	1.18E-06	3.15E-12	1.99E-09	3.09E-10	2.68E-11	5.33E-09	1.03E-20	1.66E-12	3.62E-12
2	250	3000	6.08E-08	1.50E-06	4.92E-12	2.55E-09	3.13E-10	3.51E-11	5.35E-09	1.32E-20	1.68E-12	2.75E-12
3	250	3000	2.07E-07	2.84E-06	1.22E-11	4.22E-09	3.19E-10	6.23E-11	5.33E-09	2.19E-20	1.72E-12	1.56E-12
4	250	3000	3.67E-06	2.31E-05	4.04E-11	8.12E-09	3.24E-10	1.27E-10	5.32E-09	4.22E-20	1.75E-12	7.31E-13
5	250	3000	5.01E-03	8.93E-03	6.01E-10	3.07E-08	3.26E-10	4.80E-10	5.34E-09	1.60E-19	1.76E-12	2.08E-13
6	250	3000	1.55E-02	1.38E-02	2.86E-09	6.53E-08	3.23E-10	9.61E-10	5.41E-09	3.38E-19	1.74E-12	1.03E-13
7	250	3000	2.74E-02	1.72E-02	6.33E-09	9.52E-08	3.20E-10	1.29E-09	5.51E-09	4.90E-19	1.71E-12	7.15E-14
8	250	3000	3.95E-02	2.02E-02	1.02E-08	1.19E-07	3.16E-10	1.46E-09	5.62E-09	6.08E-19	1.68E-12	5.71E-14
9	250	3000	5.16E-02	2.31E-02	1.41E-08	1.37E-07	3.12E-10	1.51E-09	5.75E-09	6.96E-19	1.64E-12	4.88E-14
10	250	3000	6.36E-02	2.60E-02	1.76E-08	1.51E-07	3.07E-10	1.47E-09	5.89E-09	7.60E-19	1.60E-12	4.33E-14
11	250	3000	7.56E-02	2.88E-02	2.08E-08	1.62E-07	3.01E-10	1.37E-09	6.06E-09	8.03E-19	1.55E-12	3.92E-14
12	250	3000	8.76E-02	3.17E-02	2.36E-08	1.69E-07	2.94E-10	1.21E-09	6.25E-09	8.29E-19	1.49E-12	3.59E-14
13	250	3000	9.95E-02	3.45E-02	2.59E-08	1.74E-07	2.86E-10	1.03E-09	6.48E-09	8.38E-19	1.43E-12	3.30E-14
14	250	3000	1.11E-01	3.74E-02	2.76E-08	1.75E-07	2.76E-10	8.22E-10	6.77E-09	8.30E-19	1.36E-12	3.03E-14

		Formula:	Al(OH)3	Al(OH)4-	Zn ⁺⁺	ZnOH ⁺	Zn(OH)2	ZnHCO3 ⁺	Zn(HS)2	Au ⁺	AuOH	Au(OH)2-
		Type:	(a)	(a)	(a)	(a)	(a)	(a)	(a)	(a)	(a)	(a)
Cell	T (°C)	P(bar)	Al(OH)3 (aq)	Al(OH)4-	Zn ⁺⁺	ZnOH ⁺	Zn(OH)2 (aq)	ZnHCO3 ⁺	Zn(HS)2 (aq)	Au ⁺	AuOH (aq)	Au(OH)2-
15	250	3000	1.23E-01	4.03E-02	2.87E-08	1.74E-07	2.64E-10	6.02E-10	7.14E-09	8.03E-19	1.26E-12	2.75E-14
16	250	3000	1.35E-01	4.33E-02	2.88E-08	1.68E-07	2.47E-10	3.81E-10	7.69E-09	7.48E-19	1.14E-12	2.43E-14
17	250	3000	1.47E-01	4.62E-02	3.03E-08	1.70E-07	2.43E-10	2.14E-10	7.85E-09	6.66E-19	9.90E-13	2.07E-14
18	250	3000	1.59E-01	4.92E-02	3.50E-08	1.90E-07	2.67E-10	8.52E-11	7.21E-09	5.28E-19	7.67E-13	1.58E-14
Ore fluids	500	5000	6.25E-07	1.05E-04	0	0	0	0	0	4.03E-16	2.35E-08	2.91E-07
1	220	3000	3.46E-08	6.23E-07	1.89E-11	2.68E-09	1.98E-10	1.40E-10	1.26E-09	1.69E-21	2.86E-13	4.12E-13
2	220	3000	7.03E-08	8.64E-07	3.60E-11	3.84E-09	2.03E-10	2.19E-10	1.25E-09	2.43E-21	2.94E-13	2.89E-13
3	220	3000	2.73E-07	1.76E-06	1.02E-10	6.80E-09	2.08E-10	4.26E-10	1.24E-09	4.32E-21	3.02E-13	1.57E-13
4	220	3000	3.95E-06	1.22E-05	3.29E-10	1.29E-08	2.11E-10	8.49E-10	1.24E-09	8.19E-21	3.08E-13	7.63E-14
5	220	3000	6.00E-03	7.44E-03	2.27E-09	3.34E-08	2.12E-10	2.18E-09	1.25E-09	2.12E-20	3.09E-13	3.07E-14
6	220	3000	1.64E-02	1.24E-02	7.07E-09	5.75E-08	2.10E-10	3.54E-09	1.26E-09	3.65E-20	3.05E-13	1.85E-14
7	220	3000	2.77E-02	1.61E-02	1.32E-08	7.70E-08	2.08E-10	4.36E-09	1.29E-09	4.85E-20	3.00E-13	1.39E-14
8	220	3000	3.93E-02	1.94E-02	1.94E-08	9.18E-08	2.06E-10	4.71E-09	1.31E-09	5.74E-20	2.95E-13	1.17E-14
9	220	3000	5.08E-02	2.26E-02	2.51E-08	1.03E-07	2.03E-10	4.72E-09	1.34E-09	6.37E-20	2.88E-13	1.03E-14
10	220	3000	6.23E-02	2.58E-02	3.02E-08	1.11E-07	2.00E-10	4.50E-09	1.38E-09	6.80E-20	2.81E-13	9.31E-15
11	220	3000	7.38E-02	2.90E-02	3.45E-08	1.16E-07	1.96E-10	4.10E-09	1.41E-09	7.06E-20	2.72E-13	8.57E-15
12	220	3000	8.53E-02	3.22E-02	3.80E-08	1.20E-07	1.91E-10	3.58E-09	1.46E-09	7.18E-20	2.62E-13	7.94E-15
13	220	3000	9.66E-02	3.55E-02	4.08E-08	1.22E-07	1.86E-10	2.99E-09	1.51E-09	7.17E-20	2.51E-13	7.37E-15
14	220	3000	1.08E-01	3.87E-02	4.26E-08	1.21E-07	1.79E-10	2.35E-09	1.58E-09	7.02E-20	2.37E-13	6.82E-15
15	220	3000	1.19E-01	4.20E-02	4.34E-08	1.19E-07	1.71E-10	1.68E-09	1.67E-09	6.71E-20	2.21E-13	6.22E-15
16	220	3000	1.31E-01	4.53E-02	4.29E-08	1.13E-07	1.59E-10	1.03E-09	1.81E-09	6.17E-20	1.98E-13	5.51E-15
17	220	3000	1.42E-01	4.86E-02	3.96E-08	1.02E-07	1.41E-10	4.27E-10	2.07E-09	5.20E-20	1.64E-13	4.51E-15

		Formula:	Al(OH)3	Al(OH)4-	Zn ⁺⁺	ZnOH ⁺	Zn(OH)2	ZnHCO3 ⁺	Zn(HS)2	Au ⁺	AuOH	Au(OH)2-
		Type:	(a)	(a)	(a)	(a)	(a)	(a)	(a)	(a)	(a)	(a)
Cell	T (°C)	P(bar)	Al(OH)3 (aq)	Al(OH)4-	Zn ⁺⁺	ZnOH ⁺	Zn(OH)2 (aq)	ZnHCO3 ⁺	Zn(HS)2 (aq)	Au ⁺	AuOH (aq)	Au(OH)2-
18	220	3000	1.53E-01	5.21E-02	3.31E-08	8.30E-08	1.13E-10	4.93E-11	2.59E-09	3.25E-20	1.01E-13	2.76E-15
Ore fluids	500	5000	6.25E-07	1.05E-04	0	0	0	0	0	4.03E-16	2.35E-08	2.91E-07
1	190	3000	4.11E-08	3.47E-07	1.48E-10	4.00E-09	1.22E-10	9.26E-10	2.41E-10	2.27E-22	3.96E-14	3.39E-14
2	190	3000	8.97E-08	4.99E-07	3.09E-10	6.00E-09	1.25E-10	1.55E-09	2.38E-10	3.42E-22	4.09E-14	2.30E-14
3	190	3000	3.55E-07	1.05E-06	8.72E-10	1.06E-08	1.28E-10	2.95E-09	2.37E-10	6.06E-22	4.19E-14	1.26E-14
4	190	3000	4.95E-06	7.49E-06	2.53E-09	1.88E-08	1.29E-10	5.24E-09	2.39E-10	1.08E-21	4.22E-14	6.47E-15
5	190	3000	7.20E-03	5.94E-03	9.10E-09	3.54E-08	1.29E-10	9.60E-09	2.41E-10	2.02E-21	4.21E-14	3.52E-15
6	190	3000	1.75E-02	1.07E-02	1.84E-08	4.93E-08	1.28E-10	1.24E-08	2.45E-10	2.79E-21	4.15E-14	2.58E-15
7	190	3000	2.83E-02	1.47E-02	2.78E-08	5.95E-08	1.26E-10	1.37E-08	2.50E-10	3.35E-21	4.07E-14	2.15E-15
8	190	3000	3.92E-02	1.84E-02	3.63E-08	6.66E-08	1.24E-10	1.37E-08	2.56E-10	3.72E-21	3.98E-14	1.90E-15
9	190	3000	5.01E-02	2.21E-02	4.34E-08	7.16E-08	1.22E-10	1.31E-08	2.62E-10	3.96E-21	3.88E-14	1.73E-15
10	190	3000	6.10E-02	2.57E-02	4.92E-08	7.48E-08	1.20E-10	1.19E-08	2.69E-10	4.09E-21	3.76E-14	1.61E-15
11	190	3000	7.19E-02	2.93E-02	5.37E-08	7.67E-08	1.17E-10	1.03E-08	2.78E-10	4.14E-21	3.63E-14	1.50E-15
12	190	3000	8.27E-02	3.30E-02	5.70E-08	7.73E-08	1.14E-10	8.62E-09	2.88E-10	4.11E-21	3.48E-14	1.41E-15
13	190	3000	9.35E-02	3.67E-02	5.91E-08	7.67E-08	1.10E-10	6.78E-09	3.00E-10	4.00E-21	3.30E-14	1.31E-15
14	190	3000	1.04E-01	4.04E-02	5.97E-08	7.49E-08	1.05E-10	4.90E-09	3.17E-10	3.81E-21	3.07E-14	1.21E-15
15	190	3000	1.15E-01	4.42E-02	5.84E-08	7.12E-08	9.84E-11	3.05E-09	3.42E-10	3.50E-21	2.78E-14	1.08E-15
16	190	3000	1.26E-01	4.81E-02	5.38E-08	6.40E-08	8.75E-11	1.32E-09	3.88E-10	2.96E-21	2.32E-14	9.02E-16
17	190	3000	1.36E-01	5.23E-02	3.44E-08	4.04E-08	5.51E-11	5.09E-11	6.19E-10	1.48E-21	1.16E-14	4.53E-16
18	190	3000	1.46E-01	5.64E-02	3.34E-08	3.85E-08	5.24E-11	3.17E-12	6.52E-10	7.54E-22	5.88E-15	2.30E-16
Ore fluids	500	5000	6.25E-07	1.05E-04	0	0	0	0	0	4.03E-16	2.35E-08	2.91E-07
1	160	3000	2.50E-08	1.90E-07	2.65E-10	2.55E-09	6.23E-11	1.35E-09	4.11E-11	8.42E-24	3.44E-15	3.58E-15

		Formula:	Al(OH) ₃	Al(OH) ₄ ⁻	Zn ⁺⁺	ZnOH ⁺	Zn(OH) ₂	ZnHCO ₃ ⁺	Zn(HS) ₂	Au ⁺	AuOH	Au(OH) ₂ ⁻
		Type:	(a)	(a)	(a)	(a)	(a)	(a)	(a)	(a)	(a)	(a)
Cell	T (°C)	P(bar)	Al(OH) ₃ (aq)	Al(OH) ₄ ⁻	Zn ⁺⁺	ZnOH ⁺	Zn(OH) ₂ (aq)	ZnHCO ₃ ⁺	Zn(HS) ₂ (aq)	Au ⁺	AuOH (aq)	Au(OH) ₂ ⁻
2	160	3000	5.01E-08	2.78E-07	4.47E-10	3.41E-09	6.29E-11	1.80E-09	4.15E-11	1.12E-23	3.46E-15	2.63E-15
3	160	3000	1.88E-07	6.00E-07	1.10E-09	5.58E-09	6.35E-11	2.95E-09	4.19E-11	1.83E-23	3.48E-15	1.51E-15
4	160	3000	2.84E-06	4.71E-06	3.17E-09	9.88E-09	6.41E-11	5.22E-09	4.23E-11	3.23E-23	3.50E-15	7.95E-16
5	160	3000	6.73E-03	6.31E-03	1.06E-08	1.78E-08	6.38E-11	8.95E-09	4.28E-11	5.80E-23	3.47E-15	4.45E-16
6	160	3000	1.62E-02	1.18E-02	1.92E-08	2.33E-08	6.22E-11	9.84E-09	4.42E-11	7.50E-23	3.34E-15	3.32E-16
7	160	3000	2.62E-02	1.66E-02	2.67E-08	2.66E-08	5.98E-11	8.71E-09	4.63E-11	8.38E-23	3.15E-15	2.72E-16
8	160	3000	3.63E-02	2.12E-02	3.20E-08	2.80E-08	5.66E-11	6.40E-09	4.93E-11	8.55E-23	2.89E-15	2.31E-16
9	160	3000	4.62E-02	2.58E-02	3.43E-08	2.74E-08	5.17E-11	3.57E-09	5.44E-11	7.99E-23	2.52E-15	1.93E-16
10	160	3000	5.61E-02	3.06E-02	3.04E-08	2.29E-08	4.14E-11	7.69E-10	6.84E-11	5.96E-23	1.81E-15	1.35E-16
11	160	3000	6.56E-02	3.58E-02	1.39E-08	1.00E-08	1.78E-11	9.45E-13	1.60E-10	1.40E-23	4.17E-16	3.11E-17
12	160	3000	7.59E-02	3.98E-02	1.70E-08	1.15E-08	1.94E-11	3.84E-13	1.46E-10	1.14E-23	3.23E-16	2.31E-17
13	160	3000	8.63E-02	4.37E-02	1.96E-08	1.25E-08	2.03E-11	2.53E-13	1.40E-10	1.05E-23	2.85E-16	1.97E-17
14	160	3000	9.67E-02	4.75E-02	2.19E-08	1.33E-08	2.09E-11	1.93E-13	1.36E-10	1.00E-23	2.63E-16	1.76E-17
15	160	3000	1.07E-01	5.14E-02	2.40E-08	1.40E-08	2.13E-11	1.58E-13	1.33E-10	9.72E-24	2.47E-16	1.62E-17
16	160	3000	1.18E-01	5.52E-02	2.59E-08	1.46E-08	2.17E-11	1.34E-13	1.31E-10	9.49E-24	2.35E-16	1.51E-17
17	160	3000	1.28E-01	5.90E-02	2.77E-08	1.51E-08	2.20E-11	1.17E-13	1.29E-10	9.30E-24	2.26E-16	1.42E-17
18	160	3000	1.38E-01	6.27E-02	2.94E-08	1.56E-08	2.23E-11	1.04E-13	1.28E-10	9.15E-24	2.18E-16	1.35E-17

Formula:		AuHS	Au(HS)2-	Au2(HS)2 S--	Au+++	Mn++	MnOH+	MnHCO3+	MnSO4	MnO4-	MnO4--	
Type:		(a)	(a)	(a)	(a)	(a)	(a)	(a)	(a)	(a)	(a)	
Cell	T (°C)	P(bar)	AuHS (aq)	Au(HS)2-	Au2(HS)2 S--	Au+++	Mn++	MnOH+	MnHCO3+	MnSO4 (aq)	MnO4-	MnO4--
Ore fluids	500	5000	2.35E-07	7.76E-06	3.58E-08	2.68E-53	2.68E-05	3.68E-03	3.84E-04	1.99E-10	2.09E-30	7.83E-27
1	400	3000	3.11E-08	1.02E-06	1.60E-09	2.29E-57	5.47E-05	2.79E-03	2.09E-03	9.59E-10	1.36E-35	5.76E-31
2	400	3000	3.08E-08	7.79E-07	8.43E-10	2.79E-57	7.34E-05	3.32E-03	2.39E-03	8.89E-10	9.89E-36	2.99E-31
3	400	3000	3.09E-08	5.97E-07	4.51E-10	3.65E-57	9.65E-05	3.82E-03	2.71E-03	8.28E-10	7.07E-36	1.52E-31
4	400	3000	3.09E-08	3.86E-07	1.64E-10	6.03E-57	1.37E-04	4.31E-03	3.02E-03	6.73E-10	3.70E-36	4.56E-32
5	400	3000	3.11E-08	3.62E-08	1.43E-12	7.43E-54	1.38E-03	4.07E-03	2.87E-03	5.98E-11	3.05E-38	3.49E-35
6	400	3000	3.10E-08	6.42E-09	5.37E-14	3.77E-51	5.48E-03	2.18E-03	1.50E-03	4.56E-12	4.31E-40	1.04E-37
7	400	3000	3.08E-08	3.58E-09	1.79E-14	3.09E-50	7.48E-03	1.52E-03	1.01E-03	1.57E-12	8.63E-41	1.26E-38
8	400	3000	3.06E-08	2.58E-09	9.65E-15	1.01E-49	8.84E-03	1.22E-03	7.90E-04	8.25E-13	3.42E-41	3.79E-39
9	400	3000	3.03E-08	2.07E-09	6.45E-15	2.24E-49	9.97E-03	1.07E-03	6.66E-04	5.29E-13	1.84E-41	1.72E-39
10	400	3000	3.01E-08	1.77E-09	4.83E-15	4.03E-49	1.10E-02	9.75E-04	5.88E-04	3.78E-13	1.17E-41	9.77E-40
11	400	3000	2.99E-08	1.57E-09	3.88E-15	6.37E-49	1.19E-02	9.15E-04	5.33E-04	2.89E-13	8.29E-42	6.37E-40
12	400	3000	2.97E-08	1.42E-09	3.26E-15	9.21E-49	1.29E-02	8.75E-04	4.92E-04	2.31E-13	6.28E-42	4.56E-40
13	400	3000	2.94E-08	1.31E-09	2.84E-15	1.25E-48	1.38E-02	8.48E-04	4.61E-04	1.91E-13	5.00E-42	3.48E-40
14	400	3000	2.92E-08	1.22E-09	2.52E-15	1.62E-48	1.47E-02	8.30E-04	4.35E-04	1.61E-13	4.12E-42	2.78E-40
15	400	3000	2.90E-08	1.15E-09	2.29E-15	2.03E-48	1.55E-02	8.18E-04	4.14E-04	1.38E-13	3.49E-42	2.30E-40
16	400	3000	2.87E-08	1.10E-09	2.10E-15	2.47E-48	1.64E-02	8.10E-04	3.95E-04	1.20E-13	3.02E-42	1.96E-40
17	400	3000	2.85E-08	1.05E-09	1.95E-15	2.93E-48	1.73E-02	8.06E-04	3.80E-04	1.06E-13	2.66E-42	1.71E-40
18	400	3000	2.82E-08	1.01E-09	1.82E-15	3.41E-48	1.81E-02	8.04E-04	3.65E-04	9.40E-14	2.37E-42	1.51E-40
Ore fluids	500	5000	2.35E-07	7.76E-06	3.58E-08	2.68E-53	2.68E-05	3.68E-03	3.84E-04	1.99E-10	2.09E-30	7.83E-27
1	370	3000	1.72E-08	5.25E-07	9.51E-10	5.35E-58	8.45E-05	2.07E-03	2.78E-03	2.09E-09	9.06E-38	8.46E-33
2	370	3000	1.71E-08	4.07E-07	5.21E-10	6.31E-58	1.13E-04	2.49E-03	3.18E-03	1.94E-09	6.79E-38	4.68E-33

		Formula:	AuHS	Au(HS)2-	Au2(HS)2 S--	Au+++	Mn++	MnOH+	MnHCO3+	MnSO4	MnO4-	MnO4--
		Type:	(a)	(a)	(a)	(a)	(a)	(a)	(a)	(a)	(a)	(a)
Cell	T (°C)	P(bar)	AuHS (aq)	Au(HS)2-	Au2(HS)2 S--	Au+++	Mn++	MnOH+	MnHCO3+	MnSO4 (aq)	MnO4-	MnO4--
3	370	3000	1.69E-08	2.73E-07	2.06E-10	9.10E-58	1.60E-04	2.91E-03	3.55E-03	1.58E-09	3.87E-38	1.63E-33
4	370	3000	1.70E-08	1.40E-07	4.51E-11	2.42E-57	2.65E-04	3.25E-03	3.96E-03	1.07E-09	1.31E-38	2.40E-34
5	370	3000	1.70E-08	8.60E-09	2.02E-13	3.01E-53	3.68E-03	2.09E-03	2.55E-03	3.56E-11	2.70E-41	3.55E-38
6	370	3000	1.69E-08	3.02E-09	2.77E-14	1.22E-51	6.67E-03	1.15E-03	1.34E-03	5.75E-12	1.63E-42	8.46E-40
7	370	3000	1.67E-08	1.88E-09	1.13E-14	6.23E-51	8.24E-03	8.34E-04	9.32E-04	2.29E-12	4.30E-43	1.50E-40
8	370	3000	1.65E-08	1.41E-09	6.62E-15	1.66E-50	9.43E-03	6.93E-04	7.35E-04	1.26E-12	1.90E-43	5.29E-41
9	370	3000	1.63E-08	1.16E-09	4.59E-15	3.25E-50	1.05E-02	6.16E-04	6.20E-04	8.18E-13	1.08E-43	2.61E-41
10	370	3000	1.60E-08	1.00E-09	3.51E-15	5.36E-50	1.14E-02	5.70E-04	5.42E-04	5.79E-13	7.08E-44	1.56E-41
11	370	3000	1.58E-08	8.90E-10	2.84E-15	7.92E-50	1.24E-02	5.40E-04	4.86E-04	4.33E-13	5.06E-44	1.05E-41
12	370	3000	1.56E-08	8.08E-10	2.40E-15	1.08E-49	1.33E-02	5.21E-04	4.43E-04	3.37E-13	3.84E-44	7.60E-42
13	370	3000	1.53E-08	7.44E-10	2.08E-15	1.40E-49	1.42E-02	5.09E-04	4.07E-04	2.68E-13	3.04E-44	5.84E-42
14	370	3000	1.51E-08	6.93E-10	1.84E-15	1.74E-49	1.51E-02	5.01E-04	3.77E-04	2.18E-13	2.47E-44	4.67E-42
15	370	3000	1.48E-08	6.50E-10	1.65E-15	2.08E-49	1.59E-02	4.96E-04	3.51E-04	1.79E-13	2.06E-44	3.85E-42
16	370	3000	1.45E-08	6.13E-10	1.49E-15	2.43E-49	1.68E-02	4.94E-04	3.28E-04	1.49E-13	1.75E-44	3.25E-42
17	370	3000	1.43E-08	5.81E-10	1.37E-15	2.78E-49	1.77E-02	4.93E-04	3.07E-04	1.24E-13	1.50E-44	2.80E-42
18	370	3000	1.40E-08	5.53E-10	1.26E-15	3.12E-49	1.85E-02	4.94E-04	2.88E-04	1.05E-13	1.31E-44	2.44E-42
Ore fluids	500	5000	2.35E-07	7.76E-06	3.58E-08	2.68E-53	2.68E-05	3.68E-03	3.84E-04	1.99E-10	2.09E-30	7.83E-27
1	340	3000	9.04E-09	2.24E-07	4.20E-10	1.59E-58	1.29E-04	1.27E-03	3.54E-03	4.47E-09	2.89E-40	5.59E-35
2	340	3000	8.93E-09	1.77E-07	2.41E-10	1.84E-58	1.73E-04	1.54E-03	4.06E-03	4.20E-09	2.25E-40	3.30E-35
3	340	3000	8.84E-09	1.20E-07	9.81E-11	2.69E-58	2.46E-04	1.81E-03	4.57E-03	3.46E-09	1.31E-40	1.20E-35
4	340	3000	8.94E-09	5.91E-08	1.97E-11	8.26E-58	4.18E-04	1.98E-03	5.07E-03	2.27E-09	4.03E-41	1.51E-36
5	340	3000	9.00E-09	5.30E-09	1.85E-13	3.07E-54	3.82E-03	1.25E-03	3.24E-03	1.11E-10	1.77E-43	6.82E-40

		Formula:	AuHS	Au(HS)2-	Au2(HS)2 S--	Au+++	Mn++	MnOH+	MnHCO3+	MnSO4	MnO4-	MnO4--
		Type:	(a)	(a)	(a)	(a)	(a)	(a)	(a)	(a)	(a)	(a)
Cell	T (°C)	P(bar)	AuHS (aq)	Au(HS)2-	Au2(HS)2 S--	Au+++	Mn++	MnOH+	MnHCO3+	MnSO4 (aq)	MnO4-	MnO4--
6	340	3000	8.90E-09	1.86E-09	2.51E-14	1.19E-52	6.80E-03	6.82E-04	1.68E-03	1.78E-11	1.06E-44	1.60E-41
7	340	3000	8.76E-09	1.15E-09	1.01E-14	5.95E-52	8.36E-03	4.95E-04	1.15E-03	6.87E-12	2.74E-45	2.78E-42
8	340	3000	8.61E-09	8.61E-10	5.84E-15	1.54E-51	9.55E-03	4.12E-04	8.94E-04	3.69E-12	1.20E-45	9.75E-43
9	340	3000	8.44E-09	7.03E-10	4.02E-15	2.95E-51	1.06E-02	3.67E-04	7.42E-04	2.31E-12	6.71E-46	4.78E-43
10	340	3000	8.27E-09	6.03E-10	3.04E-15	4.72E-51	1.16E-02	3.41E-04	6.39E-04	1.58E-12	4.32E-46	2.83E-43
11	340	3000	8.08E-09	5.33E-10	2.43E-15	6.75E-51	1.25E-02	3.25E-04	5.61E-04	1.13E-12	3.03E-46	1.88E-43
12	340	3000	7.89E-09	4.80E-10	2.02E-15	8.93E-51	1.34E-02	3.15E-04	4.99E-04	8.37E-13	2.24E-46	1.34E-43
13	340	3000	7.69E-09	4.37E-10	1.72E-15	1.12E-50	1.43E-02	3.08E-04	4.46E-04	6.29E-13	1.72E-46	1.01E-43
14	340	3000	7.47E-09	4.02E-10	1.49E-15	1.33E-50	1.52E-02	3.04E-04	4.00E-04	4.77E-13	1.35E-46	7.91E-44
15	340	3000	7.25E-09	3.72E-10	1.30E-15	1.53E-50	1.61E-02	3.03E-04	3.59E-04	3.62E-13	1.08E-46	6.33E-44
16	340	3000	7.02E-09	3.45E-10	1.15E-15	1.72E-50	1.70E-02	3.02E-04	3.21E-04	2.75E-13	8.74E-47	5.16E-44
17	340	3000	6.78E-09	3.21E-10	1.01E-15	1.87E-50	1.79E-02	3.03E-04	2.87E-04	2.09E-13	7.11E-47	4.26E-44
18	340	3000	6.54E-09	3.00E-10	8.99E-16	2.00E-50	1.88E-02	3.04E-04	2.56E-04	1.58E-13	5.81E-47	3.55E-44
Ore fluids	500	5000	2.35E-07	7.76E-06	3.58E-08	2.68E-53	2.68E-05	3.68E-03	3.84E-04	1.99E-10	2.09E-30	7.83E-27
1	310	3000	4.35E-09	8.18E-08	1.47E-10	4.59E-59	1.83E-04	6.45E-04	4.11E-03	9.02E-09	4.39E-43	1.79E-37
2	310	3000	4.30E-09	6.53E-08	8.67E-11	5.44E-59	2.46E-04	7.83E-04	4.75E-03	8.60E-09	3.49E-43	1.09E-37
3	310	3000	4.29E-09	4.36E-08	3.42E-11	8.90E-59	3.57E-04	9.07E-04	5.36E-03	7.08E-09	1.94E-43	3.68E-38
4	310	3000	4.37E-09	2.03E-08	6.14E-12	3.32E-58	6.22E-04	9.56E-04	5.89E-03	4.42E-09	5.23E-44	3.80E-39
5	310	3000	4.41E-09	2.75E-09	1.27E-13	3.11E-55	3.76E-03	6.27E-04	3.93E-03	3.52E-10	5.57E-46	6.10E-42
6	310	3000	4.36E-09	1.03E-09	1.98E-14	9.41E-54	6.61E-03	3.65E-04	2.18E-03	6.49E-11	4.12E-47	1.89E-43
7	310	3000	4.29E-09	6.51E-10	8.24E-15	4.41E-53	8.21E-03	2.73E-04	1.53E-03	2.61E-11	1.14E-47	3.56E-44
8	310	3000	4.20E-09	4.91E-10	4.86E-15	1.10E-52	9.42E-03	2.31E-04	1.20E-03	1.42E-11	5.12E-48	1.31E-44

		Formula:	AuHS	Au(HS)2-	Au2(HS)2 S--	Au+++	Mn++	MnOH+	MnHCO3+	MnSO4	MnO4-	MnO4--
		Type:	(a)	(a)	(a)	(a)	(a)	(a)	(a)	(a)	(a)	(a)
Cell	T (°C)	P(bar)	AuHS (aq)	Au(HS)2-	Au2(HS)2 S--	Au+++	Mn++	MnOH+	MnHCO3+	MnSO4 (aq)	MnO4-	MnO4--
9	310	3000	4.11E-09	4.04E-10	3.38E-15	2.03E-52	1.05E-02	2.09E-04	1.00E-03	8.93E-12	2.92E-48	6.59E-45
10	310	3000	4.01E-09	3.47E-10	2.57E-15	3.16E-52	1.15E-02	1.96E-04	8.59E-04	6.05E-12	1.90E-48	3.98E-45
11	310	3000	3.90E-09	3.07E-10	2.06E-15	4.39E-52	1.25E-02	1.88E-04	7.51E-04	4.28E-12	1.34E-48	2.68E-45
12	310	3000	3.79E-09	2.76E-10	1.71E-15	5.63E-52	1.34E-02	1.83E-04	6.60E-04	3.08E-12	9.84E-49	1.93E-45
13	310	3000	3.66E-09	2.50E-10	1.44E-15	6.81E-52	1.43E-02	1.81E-04	5.81E-04	2.23E-12	7.46E-49	1.45E-45
14	310	3000	3.52E-09	2.28E-10	1.23E-15	7.86E-52	1.52E-02	1.80E-04	5.08E-04	1.60E-12	5.73E-49	1.12E-45
15	310	3000	3.38E-09	2.09E-10	1.05E-15	8.69E-52	1.62E-02	1.80E-04	4.41E-04	1.14E-12	4.42E-49	8.76E-46
16	310	3000	3.22E-09	1.90E-10	8.99E-16	9.26E-52	1.71E-02	1.80E-04	3.78E-04	7.85E-13	3.40E-49	6.89E-46
17	310	3000	3.04E-09	1.73E-10	7.62E-16	9.54E-52	1.80E-02	1.81E-04	3.18E-04	5.23E-13	2.57E-49	5.40E-46
18	310	3000	2.85E-09	1.56E-10	6.39E-16	9.49E-52	1.89E-02	1.83E-04	2.61E-04	3.34E-13	1.91E-49	4.18E-46
Ore fluids	500	5000	2.35E-07	7.76E-06	3.58E-08	2.68E-53	2.68E-05	3.68E-03	3.84E-04	1.99E-10	2.09E-30	7.83E-27
1	280	3000	1.73E-09	2.33E-08	3.72E-11	7.83E-60	2.40E-04	2.99E-04	4.39E-03	1.68E-08	3.56E-46	3.56E-40
2	280	3000	1.73E-09	1.90E-08	2.25E-11	9.99E-60	3.25E-04	3.59E-04	5.10E-03	1.61E-08	2.77E-46	2.11E-40
3	280	3000	1.74E-09	1.19E-08	7.71E-12	2.09E-59	4.88E-04	4.00E-04	5.74E-03	1.27E-08	1.32E-46	5.57E-41
4	280	3000	1.76E-09	5.29E-09	1.29E-12	8.92E-59	8.60E-04	4.11E-04	6.20E-03	7.48E-09	3.31E-47	5.21E-42
5	280	3000	1.77E-09	1.03E-09	5.41E-14	2.28E-56	3.65E-03	2.88E-04	4.38E-03	9.34E-10	8.07E-49	2.71E-44
6	280	3000	1.77E-09	4.42E-10	1.07E-14	4.68E-55	6.31E-03	1.86E-04	2.66E-03	2.13E-10	8.18E-50	1.28E-45
7	280	3000	1.76E-09	2.98E-10	5.04E-15	1.95E-54	7.94E-03	1.46E-04	1.92E-03	9.16E-11	2.48E-50	2.77E-46
8	280	3000	1.76E-09	2.38E-10	3.27E-15	4.50E-54	9.21E-03	1.27E-04	1.52E-03	5.12E-11	1.16E-50	1.09E-46
9	280	3000	1.72E-09	1.99E-10	2.34E-15	7.91E-54	1.03E-02	1.17E-04	1.27E-03	3.25E-11	6.83E-51	5.73E-47
10	280	3000	1.67E-09	1.71E-10	1.79E-15	1.18E-53	1.13E-02	1.11E-04	1.09E-03	2.18E-11	4.51E-51	3.56E-47
11	280	3000	1.61E-09	1.51E-10	1.44E-15	1.57E-53	1.23E-02	1.08E-04	9.42E-04	1.50E-11	3.18E-51	2.44E-47

		Formula:	AuHS	Au(HS)2-	Au2(HS)2 S--	Au+++	Mn++	MnOH+	MnHCO3+	MnSO4	MnO4-	MnO4--
		Type:	(a)	(a)	(a)	(a)	(a)	(a)	(a)	(a)	(a)	(a)
Cell	T (°C)	P(bar)	AuHS (aq)	Au(HS)2-	Au2(HS)2 S--	Au+++	Mn++	MnOH+	MnHCO3+	MnSO4 (aq)	MnO4-	MnO4--
12	280	3000	1.55E-09	1.35E-10	1.18E-15	1.93E-53	1.33E-02	1.07E-04	8.14E-04	1.04E-11	2.32E-51	1.76E-47
13	280	3000	1.48E-09	1.21E-10	9.85E-16	2.22E-53	1.43E-02	1.06E-04	6.98E-04	7.14E-12	1.72E-51	1.32E-47
14	280	3000	1.40E-09	1.09E-10	8.19E-16	2.43E-53	1.52E-02	1.06E-04	5.88E-04	4.73E-12	1.27E-51	9.95E-48
15	280	3000	1.31E-09	9.73E-11	6.74E-16	2.52E-53	1.62E-02	1.07E-04	4.81E-04	2.96E-12	9.20E-52	7.47E-48
16	280	3000	1.21E-09	8.57E-11	5.40E-16	2.46E-53	1.71E-02	1.08E-04	3.78E-04	1.70E-12	6.38E-52	5.46E-48
17	280	3000	1.09E-09	7.36E-11	4.14E-16	2.25E-53	1.81E-02	1.10E-04	2.78E-04	8.56E-13	4.11E-52	3.79E-48
18	280	3000	9.54E-10	6.08E-11	2.97E-16	1.87E-53	1.90E-02	1.11E-04	1.85E-04	3.52E-13	2.36E-52	2.41E-48
Ore fluids	500	5000	2.35E-07	7.76E-06	3.58E-08	2.68E-53	2.68E-05	3.68E-03	3.84E-04	1.99E-10	2.09E-30	7.83E-27
1	250	3000	4.02E-10	2.47E-09	2.17E-12	9.81E-61	3.04E-04	1.23E-04	4.51E-03	2.12E-08	1.26E-49	3.31E-43
2	250	3000	4.05E-10	1.86E-09	1.14E-12	1.64E-60	4.20E-04	1.39E-04	5.22E-03	1.96E-08	8.53E-50	1.56E-43
3	250	3000	4.09E-10	1.03E-09	3.05E-13	4.95E-60	6.57E-04	1.45E-04	5.82E-03	1.42E-08	3.23E-50	2.84E-44
4	250	3000	4.13E-10	4.76E-10	5.51E-14	2.18E-59	1.14E-03	1.46E-04	6.19E-03	8.32E-09	8.29E-51	2.85E-45
5	250	3000	4.15E-10	1.35E-10	4.78E-15	1.45E-57	3.44E-03	1.12E-04	4.77E-03	1.71E-09	4.85E-52	5.05E-47
6	250	3000	4.15E-10	6.82E-11	1.30E-15	1.72E-56	5.73E-03	8.34E-05	3.35E-03	5.34E-10	7.90E-53	4.48E-48
7	250	3000	4.14E-10	4.88E-11	6.84E-16	6.02E-56	7.34E-03	7.04E-05	2.60E-03	2.63E-10	2.91E-53	1.24E-48
8	250	3000	4.12E-10	4.02E-11	4.75E-16	1.27E-55	8.64E-03	6.42E-05	2.15E-03	1.59E-10	1.52E-53	5.64E-49
9	250	3000	4.11E-10	3.57E-11	3.77E-16	2.08E-55	9.80E-03	6.11E-05	1.84E-03	1.06E-10	9.49E-54	3.25E-49
10	250	3000	4.08E-10	3.30E-11	3.24E-16	2.91E-55	1.09E-02	5.97E-05	1.59E-03	7.37E-11	6.49E-54	2.14E-49
11	250	3000	4.06E-10	3.13E-11	2.91E-16	3.67E-55	1.20E-02	5.93E-05	1.37E-03	5.19E-11	4.65E-54	1.52E-49
12	250	3000	4.02E-10	3.03E-11	2.70E-16	4.28E-55	1.30E-02	5.95E-05	1.17E-03	3.62E-11	3.39E-54	1.12E-49
13	250	3000	3.97E-10	2.97E-11	2.56E-16	4.66E-55	1.41E-02	6.02E-05	9.72E-04	2.44E-11	2.47E-54	8.39E-50
14	250	3000	3.92E-10	2.94E-11	2.47E-16	4.76E-55	1.51E-02	6.12E-05	7.82E-04	1.55E-11	1.74E-54	6.19E-50

		Formula:	AuHS	Au(HS)2-	Au2(HS)2 S--	Au+++	Mn++	MnOH+	MnHCO3+	MnSO4	MnO4-	MnO4--
		Type:	(a)	(a)	(a)	(a)	(a)	(a)	(a)	(a)	(a)	(a)
Cell	T (°C)	P(bar)	AuHS (aq)	Au(HS)2-	Au2(HS)2 S--	Au+++	Mn++	MnOH+	MnHCO3+	MnSO4 (aq)	MnO4-	MnO4--
15	250	3000	3.84E-10	2.95E-11	2.40E-16	4.50E-55	1.61E-02	6.24E-05	5.90E-04	8.75E-12	1.15E-54	4.37E-50
16	250	3000	3.72E-10	3.01E-11	2.36E-16	3.81E-55	1.72E-02	6.37E-05	3.95E-04	4.00E-12	6.59E-55	2.78E-50
17	250	3000	3.28E-10	2.65E-11	1.82E-16	2.79E-55	1.82E-02	6.51E-05	2.24E-04	1.25E-12	3.10E-55	1.51E-50
18	250	3000	2.33E-10	1.70E-11	8.28E-17	1.45E-55	1.92E-02	6.65E-05	8.13E-05	1.44E-13	8.41E-56	5.31E-51
Ore fluids	500	5000	2.35E-07	7.76E-06	3.58E-08	2.68E-53	2.68E-05	3.68E-03	3.84E-04	1.99E-10	2.09E-30	7.83E-27
1	220	3000	7.61E-11	1.85E-10	7.47E-14	9.22E-62	3.90E-04	4.45E-05	4.50E-03	2.51E-08	1.58E-53	1.14E-46
2	220	3000	7.71E-11	1.26E-10	3.21E-14	2.13E-61	5.50E-04	4.70E-05	5.18E-03	2.21E-08	8.93E-54	3.97E-47
3	220	3000	7.81E-11	6.63E-11	7.72E-15	7.91E-61	8.79E-04	4.71E-05	5.70E-03	1.51E-08	2.99E-54	5.98E-48
4	220	3000	7.89E-11	3.17E-11	1.53E-15	3.47E-60	1.48E-03	4.66E-05	5.94E-03	8.81E-09	7.94E-55	6.55E-49
5	220	3000	7.92E-11	1.28E-11	2.59E-16	6.89E-59	3.32E-03	3.92E-05	4.95E-03	2.82E-09	1.03E-55	3.56E-50
6	220	3000	7.91E-11	7.85E-12	1.03E-16	4.21E-58	5.14E-03	3.35E-05	3.99E-03	1.24E-09	2.89E-56	6.57E-51
7	220	3000	7.89E-11	6.09E-12	6.41E-17	1.14E-57	6.60E-03	3.09E-05	3.38E-03	7.28E-10	1.37E-56	2.56E-51
8	220	3000	7.87E-11	5.27E-12	4.89E-17	2.09E-57	7.86E-03	2.99E-05	2.96E-03	4.88E-10	8.34E-57	1.41E-51
9	220	3000	7.83E-11	4.81E-12	4.13E-17	3.13E-57	9.04E-03	2.97E-05	2.64E-03	3.49E-10	5.76E-57	9.34E-52
10	220	3000	7.79E-11	4.55E-12	3.71E-17	4.12E-57	1.02E-02	2.99E-05	2.35E-03	2.57E-10	4.25E-57	6.80E-52
11	220	3000	7.73E-11	4.39E-12	3.46E-17	4.95E-57	1.13E-02	3.05E-05	2.08E-03	1.89E-10	3.23E-57	5.22E-52
12	220	3000	7.66E-11	4.30E-12	3.30E-17	5.56E-57	1.24E-02	3.14E-05	1.81E-03	1.36E-10	2.48E-57	4.10E-52
13	220	3000	7.58E-11	4.26E-12	3.20E-17	5.86E-57	1.35E-02	3.23E-05	1.54E-03	9.41E-11	1.87E-57	3.23E-52
14	220	3000	7.46E-11	4.26E-12	3.14E-17	5.80E-57	1.46E-02	3.35E-05	1.25E-03	6.06E-11	1.36E-57	2.48E-52
15	220	3000	7.30E-11	4.32E-12	3.11E-17	5.31E-57	1.58E-02	3.47E-05	9.47E-04	3.45E-11	9.14E-58	1.81E-52
16	220	3000	7.07E-11	4.43E-12	3.10E-17	4.33E-57	1.70E-02	3.60E-05	6.32E-04	1.55E-11	5.27E-58	1.17E-52
17	220	3000	6.66E-11	4.70E-12	3.10E-17	2.71E-57	1.81E-02	3.74E-05	3.03E-04	3.85E-12	2.03E-58	5.51E-53

Formula:		AuHS	Au(HS)2-	Au2(HS)2 S--	Au+++	Mn++	MnOH+	MnHCO3+	MnSO4	MnO4-	MnO4--	
Type:		(a)	(a)	(a)	(a)	(a)	(a)	(a)	(a)	(a)	(a)	
Cell	T (°C)	P(bar)	AuHS (aq)	Au(HS)2-	Au2(HS)2 S--	Au+++	Mn++	MnOH+	MnHCO3+	MnSO4 (aq)	MnO4-	MnO4--
18	220	3000	5.12E-11	4.48E-12	2.29E-17	6.88E-58	1.92E-02	3.87E-05	4.44E-05	9.87E-14	1.80E-59	8.05E-54
Ore fluids	500	5000	2.35E-07	7.76E-06	3.58E-08	2.68E-53	2.68E-05	3.68E-03	3.84E-04	1.99E-10	2.09E-30	7.83E-27
1	190	3000	1.13E-11	8.96E-12	1.32E-15	6.55E-63	5.13E-04	1.39E-05	4.41E-03	2.79E-08	5.72E-58	1.15E-50
2	190	3000	1.15E-11	5.88E-12	5.28E-16	1.75E-62	7.33E-04	1.43E-05	5.03E-03	2.37E-08	2.97E-58	3.52E-51
3	190	3000	1.16E-11	3.13E-12	1.30E-16	6.49E-62	1.17E-03	1.43E-05	5.44E-03	1.57E-08	9.82E-59	5.34E-52
4	190	3000	1.17E-11	1.61E-12	2.99E-17	2.43E-61	1.94E-03	1.45E-05	5.52E-03	8.99E-09	2.84E-59	6.97E-53
5	190	3000	1.17E-11	8.83E-13	9.19E-18	1.74E-60	3.39E-03	1.33E-05	4.91E-03	4.17E-09	7.29E-60	1.01E-53
6	190	3000	1.17E-11	6.64E-13	5.42E-18	5.39E-60	4.75E-03	1.28E-05	4.40E-03	2.50E-09	3.42E-60	3.79E-54
7	190	3000	1.17E-11	5.69E-13	4.10E-18	1.05E-59	5.97E-03	1.28E-05	4.02E-03	1.74E-09	2.14E-60	2.14E-54
8	190	3000	1.16E-11	5.22E-13	3.51E-18	1.61E-59	7.13E-03	1.32E-05	3.71E-03	1.29E-09	1.54E-60	1.49E-54
9	190	3000	1.15E-11	4.96E-13	3.21E-18	2.12E-59	8.27E-03	1.37E-05	3.41E-03	9.85E-10	1.18E-60	1.14E-54
10	190	3000	1.15E-11	4.82E-13	3.05E-18	2.55E-59	9.42E-03	1.44E-05	3.12E-03	7.52E-10	9.42E-61	9.27E-55
11	190	3000	1.14E-11	4.76E-13	2.96E-18	2.84E-59	1.06E-02	1.52E-05	2.80E-03	5.63E-10	7.54E-61	7.69E-55
12	190	3000	1.12E-11	4.75E-13	2.93E-18	2.97E-59	1.18E-02	1.60E-05	2.44E-03	4.05E-10	5.95E-61	6.39E-55
13	190	3000	1.11E-11	4.79E-13	2.92E-18	2.92E-59	1.30E-02	1.70E-05	2.05E-03	2.73E-10	4.53E-61	5.19E-55
14	190	3000	1.09E-11	4.87E-13	2.94E-18	2.67E-59	1.43E-02	1.80E-05	1.61E-03	1.63E-10	3.21E-61	4.00E-55
15	190	3000	1.05E-11	5.03E-13	2.98E-18	2.19E-59	1.56E-02	1.91E-05	1.12E-03	7.86E-11	1.97E-61	2.76E-55
16	190	3000	9.94E-12	5.35E-13	3.03E-18	1.39E-59	1.70E-02	2.04E-05	5.71E-04	2.16E-11	8.27E-62	1.42E-55
17	190	3000	7.92E-12	6.81E-13	3.15E-18	1.84E-60	1.84E-02	2.17E-05	3.74E-05	1.38E-13	2.71E-63	9.61E-57
18	190	3000	4.22E-12	3.83E-13	9.66E-19	2.56E-61	1.93E-02	2.23E-05	2.51E-06	6.36E-16	9.26E-65	6.63E-58
Ore fluids	500	5000	2.35E-07	7.76E-06	3.58E-08	2.68E-53	2.68E-05	3.68E-03	3.84E-04	1.99E-10	2.09E-30	7.83E-27
1	160	3000	1.18E-12	6.41E-13	5.79E-17	1.49E-65	6.92E-04	8.35E-06	4.23E-03	3.34E-08	2.00E-62	3.28E-54

Formula:		AuHS	Au(HS)2-	Au2(HS)2 S--	Au+++	Mn++	MnOH+	MnHCO3+	MnSO4	MnO4-	MnO4--	
Type:		(a)	(a)	(a)	(a)	(a)	(a)	(a)	(a)	(a)	(a)	
Cell	T (°C)	P(bar)	AuHS (aq)	Au(HS)2-	Au2(HS)2 S--	Au+++	Mn++	MnOH+	MnHCO3+	MnSO4 (aq)	MnO4-	MnO4--
2	160	3000	1.18E-12	4.71E-13	2.84E-17	2.75E-65	9.87E-04	9.43E-06	4.78E-03	2.83E-08	1.22E-62	1.35E-54
3	160	3000	1.19E-12	2.71E-13	8.14E-18	8.08E-65	1.56E-03	9.96E-06	5.05E-03	1.83E-08	4.44E-63	2.48E-55
4	160	3000	1.20E-12	1.42E-13	1.97E-18	3.10E-64	2.51E-03	9.77E-06	4.96E-03	1.02E-08	1.27E-63	3.30E-56
5	160	3000	1.20E-12	8.11E-14	6.50E-19	1.94E-63	4.11E-03	8.70E-06	4.19E-03	4.56E-09	3.32E-64	5.08E-57
6	160	3000	1.18E-12	6.40E-14	4.15E-19	4.89E-63	5.67E-03	8.62E-06	3.49E-03	2.44E-09	1.53E-64	2.00E-57
7	160	3000	1.17E-12	5.72E-14	3.32E-19	7.78E-63	7.19E-03	8.96E-06	2.81E-03	1.34E-09	8.60E-65	1.09E-57
8	160	3000	1.14E-12	5.47E-14	2.98E-19	9.26E-63	8.74E-03	9.58E-06	2.10E-03	6.73E-10	4.92E-65	6.54E-58
9	160	3000	1.09E-12	5.50E-14	2.84E-19	8.35E-63	1.04E-02	1.04E-05	1.30E-03	2.44E-10	2.37E-65	3.59E-58
10	160	3000	9.78E-13	6.04E-14	2.82E-19	3.81E-63	1.22E-02	1.14E-05	3.69E-04	2.15E-11	4.53E-66	9.73E-59
11	160	3000	5.26E-13	7.57E-14	1.98E-19	5.48E-65	1.34E-02	1.21E-05	1.10E-06	4.13E-16	3.07E-69	2.97E-61
12	160	3000	3.72E-13	4.72E-14	8.62E-20	3.15E-65	1.42E-02	1.20E-05	3.87E-07	4.50E-17	7.71E-70	9.53E-62
13	160	3000	3.15E-13	3.70E-14	5.66E-20	2.62E-65	1.51E-02	1.21E-05	2.34E-07	1.52E-17	3.85E-70	5.33E-62
14	160	3000	2.83E-13	3.13E-14	4.26E-20	2.41E-65	1.59E-02	1.21E-05	1.69E-07	7.37E-18	2.41E-70	3.60E-62
15	160	3000	2.60E-13	2.75E-14	3.44E-20	2.30E-65	1.68E-02	1.23E-05	1.32E-07	4.29E-18	1.69E-70	2.69E-62
16	160	3000	2.44E-13	2.48E-14	2.89E-20	2.24E-65	1.76E-02	1.24E-05	1.09E-07	2.79E-18	1.28E-70	2.14E-62
17	160	3000	2.31E-13	2.27E-14	2.51E-20	2.21E-65	1.85E-02	1.26E-05	9.37E-08	1.95E-18	1.02E-70	1.78E-62
18	160	3000	2.20E-13	2.10E-14	2.22E-20	2.18E-65	1.93E-02	1.28E-05	8.23E-08	1.44E-18	8.41E-71	1.52E-62

		Formula:	Fe ⁺⁺	FeOH ⁺	Fe(OH) ₂	Fe(OH) ₃ ⁻	FeSO ₄	Fe ⁺⁺⁺	FeOH ₂ ⁺⁺	Fe(OH) ₂ ⁺	Fe(OH) ₃	Fe(OH) ₄ ⁻
		Type:	(a)	(a)	(a)	(a)	(a)	(a)	(a)	(a)	(a)	(a)
Cell	T (°C)	P(bar)	Fe ⁺⁺	FeOH ⁺	Fe(OH) ₂ (aq)	Fe(OH) ₃ ⁻	FeSO ₄ (aq)	Fe ⁺⁺⁺	FeOH ₂ ⁺⁺	Fe(OH) ₂ ⁺	Fe(OH) ₃ (aq)	Fe(OH) ₄ ⁻
Ore fluids	500	5000	7.42E-12	4.05E-09	4.36E-07	4.67E-07	2.45E-15	2.26E-26	1.43E-18	1.05E-11	1.07E-07	3.00E-07
1	400	3000	1.07E-11	2.47E-09	9.21E-08	2.99E-08	4.19E-15	1.17E-26	7.83E-19	5.03E-12	4.57E-08	4.28E-08
2	400	3000	1.44E-11	2.96E-09	9.33E-08	2.33E-08	3.92E-15	1.47E-26	1.00E-18	5.99E-12	4.59E-08	3.31E-08
3	400	3000	1.98E-11	3.57E-09	9.42E-08	1.80E-08	3.82E-15	1.94E-26	1.32E-18	7.20E-12	4.62E-08	2.56E-08
4	400	3000	3.39E-11	4.87E-09	9.50E-08	1.18E-08	3.75E-15	3.23E-26	2.12E-18	9.81E-12	4.66E-08	1.66E-08
5	400	3000	3.91E-09	5.24E-08	9.54E-08	1.10E-09	3.80E-15	3.97E-23	2.45E-16	1.06E-10	4.68E-08	1.56E-09
6	400	3000	1.95E-07	3.54E-07	9.61E-08	1.98E-10	3.65E-15	2.05E-20	1.32E-14	7.08E-10	4.68E-08	2.78E-10
7	400	3000	7.35E-07	6.78E-07	9.68E-08	1.12E-10	3.45E-15	1.72E-19	5.07E-14	1.34E-09	4.68E-08	1.56E-10
8	400	3000	1.56E-06	9.80E-07	9.77E-08	8.22E-11	3.26E-15	5.73E-19	1.09E-13	1.93E-09	4.67E-08	1.14E-10
9	400	3000	2.58E-06	1.26E-06	9.85E-08	6.73E-11	3.07E-15	1.30E-18	1.81E-13	2.45E-09	4.67E-08	9.21E-11
10	400	3000	3.75E-06	1.51E-06	9.93E-08	5.86E-11	2.89E-15	2.39E-18	2.65E-13	2.92E-09	4.66E-08	7.93E-11
11	400	3000	5.02E-06	1.75E-06	1.00E-07	5.28E-11	2.72E-15	3.86E-18	3.56E-13	3.34E-09	4.66E-08	7.09E-11
12	400	3000	6.36E-06	1.97E-06	1.01E-07	4.89E-11	2.56E-15	5.72E-18	4.52E-13	3.71E-09	4.65E-08	6.49E-11
13	400	3000	7.75E-06	2.17E-06	1.02E-07	4.60E-11	2.41E-15	7.96E-18	5.52E-13	4.06E-09	4.64E-08	6.05E-11
14	400	3000	9.17E-06	2.36E-06	1.03E-07	4.38E-11	2.26E-15	1.06E-17	6.54E-13	4.37E-09	4.64E-08	5.70E-11
15	400	3000	1.06E-05	2.54E-06	1.04E-07	4.21E-11	2.12E-15	1.35E-17	7.57E-13	4.66E-09	4.63E-08	5.43E-11
16	400	3000	1.21E-05	2.71E-06	1.05E-07	4.08E-11	1.99E-15	1.69E-17	8.61E-13	4.92E-09	4.62E-08	5.21E-11
17	400	3000	1.36E-05	2.88E-06	1.05E-07	3.97E-11	1.87E-15	2.05E-17	9.65E-13	5.17E-09	4.61E-08	5.02E-11
18	400	3000	1.50E-05	3.03E-06	1.06E-07	3.89E-11	1.75E-15	2.45E-17	1.07E-12	5.39E-09	4.60E-08	4.86E-11
Ore fluids	500	5000	7.42E-12	4.05E-09	4.36E-07	4.67E-07	2.45E-15	2.26E-26	1.43E-18	1.05E-11	1.07E-07	3.00E-07
1	370	3000	3.27E-11	3.73E-09	6.60E-08	1.28E-08	1.32E-14	5.01E-26	1.50E-18	4.58E-12	3.07E-08	1.74E-08
2	370	3000	4.32E-11	4.42E-09	6.71E-08	1.02E-08	1.20E-14	6.12E-26	1.88E-18	5.36E-12	3.08E-08	1.38E-08
3	370	3000	6.87E-11	5.80E-09	6.81E-08	7.04E-09	1.11E-14	9.09E-26	2.78E-18	6.98E-12	3.10E-08	9.41E-09

		Formula:	Fe ⁺⁺	FeOH ⁺	Fe(OH) ₂	Fe(OH) ₃ ⁻	FeSO ₄	Fe ⁺⁺⁺	FeOH ⁺⁺	Fe(OH) ₂ ⁺	Fe(OH) ₃	Fe(OH) ₄ ⁻
		Type:	(a)	(a)	(a)	(a)	(a)	(a)	(a)	(a)	(a)	(a)
Cell	T (°C)	P(bar)	Fe ⁺⁺	FeOH ⁺	Fe(OH) ₂ (aq)	Fe(OH) ₃ ⁻	FeSO ₄ (aq)	Fe ⁺⁺⁺	FeOH ⁺⁺	Fe(OH) ₂ ⁺	Fe(OH) ₃ (aq)	Fe(OH) ₄ ⁻
4	370	3000	1.69E-10	9.62E-09	6.86E-08	3.62E-09	1.11E-14	2.42E-25	6.37E-18	1.16E-11	3.13E-08	4.84E-09
5	370	3000	7.10E-08	1.88E-07	6.88E-08	2.22E-10	1.12E-14	3.00E-21	2.87E-15	2.26E-10	3.14E-08	2.97E-10
6	370	3000	7.40E-07	5.92E-07	6.95E-08	7.97E-11	1.04E-14	1.25E-19	3.12E-14	7.04E-10	3.13E-08	1.06E-10
7	370	3000	2.11E-06	9.92E-07	7.03E-08	5.11E-11	9.53E-15	6.60E-19	8.97E-14	1.17E-09	3.13E-08	6.67E-11
8	370	3000	3.98E-06	1.36E-06	7.11E-08	3.95E-11	8.69E-15	1.82E-18	1.70E-13	1.58E-09	3.12E-08	5.09E-11
9	370	3000	6.20E-06	1.70E-06	7.20E-08	3.34E-11	7.89E-15	3.69E-18	2.65E-13	1.94E-09	3.12E-08	4.24E-11
10	370	3000	8.65E-06	2.00E-06	7.29E-08	2.97E-11	7.13E-15	6.32E-18	3.69E-13	2.25E-09	3.11E-08	3.72E-11
11	370	3000	1.13E-05	2.29E-06	7.38E-08	2.73E-11	6.43E-15	9.68E-18	4.80E-13	2.54E-09	3.10E-08	3.37E-11
12	370	3000	1.40E-05	2.56E-06	7.48E-08	2.56E-11	5.78E-15	1.38E-17	5.93E-13	2.79E-09	3.09E-08	3.11E-11
13	370	3000	1.68E-05	2.81E-06	7.57E-08	2.44E-11	5.18E-15	1.85E-17	7.08E-13	3.01E-09	3.08E-08	2.91E-11
14	370	3000	1.97E-05	3.04E-06	7.67E-08	2.35E-11	4.63E-15	2.39E-17	8.24E-13	3.21E-09	3.07E-08	2.76E-11
15	370	3000	2.26E-05	3.27E-06	7.77E-08	2.29E-11	4.13E-15	2.99E-17	9.39E-13	3.40E-09	3.06E-08	2.64E-11
16	370	3000	2.55E-05	3.49E-06	7.88E-08	2.24E-11	3.68E-15	3.65E-17	1.05E-12	3.56E-09	3.05E-08	2.54E-11
17	370	3000	2.85E-05	3.70E-06	7.98E-08	2.20E-11	3.26E-15	4.35E-17	1.17E-12	3.71E-09	3.04E-08	2.45E-11
18	370	3000	3.15E-05	3.90E-06	8.09E-08	2.17E-11	2.89E-15	5.10E-17	1.28E-12	3.85E-09	3.02E-08	2.38E-11
Ore fluids	500	5000	7.42E-12	4.05E-09	4.36E-07	4.67E-07	2.45E-15	2.26E-26	1.43E-18	1.05E-11	1.07E-07	3.00E-07
1	340	3000	1.33E-10	6.26E-09	4.42E-08	4.32E-09	5.37E-14	3.37E-25	3.85E-18	4.77E-12	2.05E-08	6.01E-09
2	340	3000	1.72E-10	7.32E-09	4.50E-08	3.53E-09	4.85E-14	4.05E-25	4.72E-18	5.51E-12	2.06E-08	4.86E-09
3	340	3000	2.72E-10	9.59E-09	4.57E-08	2.47E-09	4.45E-14	6.11E-25	7.02E-18	7.15E-12	2.08E-08	3.36E-09
4	340	3000	7.33E-10	1.66E-08	4.59E-08	1.20E-09	4.62E-14	1.85E-24	1.76E-17	1.25E-11	2.10E-08	1.65E-09
5	340	3000	1.40E-07	2.19E-07	4.60E-08	1.07E-10	4.74E-14	6.84E-21	3.60E-15	1.65E-10	2.11E-08	1.47E-10
6	340	3000	1.43E-06	6.87E-07	4.65E-08	3.86E-11	4.35E-14	2.74E-19	3.81E-14	5.09E-10	2.10E-08	5.23E-11
7	340	3000	4.08E-06	1.15E-06	4.71E-08	2.47E-11	3.90E-14	1.43E-18	1.09E-13	8.42E-10	2.10E-08	3.30E-11

		Formula:	Fe ⁺⁺	FeOH ⁺	Fe(OH) ₂	Fe(OH) ₃ ⁻	FeSO ₄	Fe ⁺⁺⁺	FeOH ⁺⁺	Fe(OH) ₂ ⁺	Fe(OH) ₃	Fe(OH) ₄ ⁻
		Type:	(a)	(a)	(a)	(a)	(a)	(a)	(a)	(a)	(a)	(a)
Cell	T (°C)	P(bar)	Fe ⁺⁺	FeOH ⁺	Fe(OH) ₂ (aq)	Fe(OH) ₃ ⁻	FeSO ₄ (aq)	Fe ⁺⁺⁺	FeOH ⁺⁺	Fe(OH) ₂ ⁺	Fe(OH) ₃ (aq)	Fe(OH) ₄ ⁻
8	340	3000	7.67E-06	1.58E-06	4.78E-08	1.92E-11	3.45E-14	3.87E-18	2.05E-13	1.13E-09	2.09E-08	2.52E-11
9	340	3000	1.19E-05	1.97E-06	4.86E-08	1.64E-11	3.02E-14	7.74E-18	3.17E-13	1.39E-09	2.09E-08	2.10E-11
10	340	3000	1.65E-05	2.33E-06	4.94E-08	1.47E-11	2.62E-14	1.30E-17	4.37E-13	1.61E-09	2.08E-08	1.85E-11
11	340	3000	2.14E-05	2.66E-06	5.02E-08	1.36E-11	2.26E-14	1.97E-17	5.62E-13	1.80E-09	2.07E-08	1.68E-11
12	340	3000	2.66E-05	2.97E-06	5.11E-08	1.28E-11	1.93E-14	2.76E-17	6.88E-13	1.96E-09	2.06E-08	1.55E-11
13	340	3000	3.18E-05	3.27E-06	5.21E-08	1.23E-11	1.62E-14	3.66E-17	8.14E-13	2.11E-09	2.05E-08	1.45E-11
14	340	3000	3.72E-05	3.56E-06	5.31E-08	1.20E-11	1.36E-14	4.66E-17	9.38E-13	2.24E-09	2.04E-08	1.38E-11
15	340	3000	4.28E-05	3.84E-06	5.42E-08	1.18E-11	1.12E-14	5.75E-17	1.06E-12	2.35E-09	2.02E-08	1.32E-11
16	340	3000	4.85E-05	4.12E-06	5.54E-08	1.16E-11	9.13E-15	6.92E-17	1.18E-12	2.45E-09	2.01E-08	1.27E-11
17	340	3000	5.43E-05	4.39E-06	5.66E-08	1.16E-11	7.37E-15	8.15E-17	1.29E-12	2.54E-09	2.00E-08	1.22E-11
18	340	3000	6.02E-05	4.67E-06	5.79E-08	1.16E-11	5.88E-15	9.44E-17	1.40E-12	2.62E-09	1.98E-08	1.18E-11
Ore fluids	500	5000	7.42E-12	4.05E-09	4.36E-07	4.67E-07	2.45E-15	2.26E-26	1.43E-18	1.05E-11	1.07E-07	3.00E-07
1	310	3000	6.39E-10	1.11E-08	2.80E-08	1.25E-09	2.56E-13	2.97E-24	1.17E-17	5.33E-12	1.37E-08	1.87E-09
2	310	3000	8.26E-10	1.30E-08	2.84E-08	1.03E-09	2.35E-13	3.63E-24	1.44E-17	6.16E-12	1.38E-08	1.53E-09
3	310	3000	1.39E-09	1.74E-08	2.88E-08	6.98E-10	2.24E-13	6.04E-24	2.27E-17	8.24E-12	1.39E-08	1.03E-09
4	310	3000	4.21E-09	3.19E-08	2.88E-08	3.18E-10	2.43E-13	2.20E-23	6.46E-17	1.53E-11	1.41E-08	4.77E-10
5	310	3000	3.31E-07	2.72E-07	2.88E-08	4.25E-11	2.52E-13	2.03E-20	5.38E-15	1.31E-10	1.41E-08	6.40E-11
6	310	3000	2.90E-06	7.91E-07	2.91E-08	1.64E-11	2.32E-13	6.34E-19	4.86E-14	3.76E-10	1.41E-08	2.44E-11
7	310	3000	7.94E-06	1.30E-06	2.95E-08	1.08E-11	2.05E-13	3.11E-18	1.34E-13	6.08E-10	1.41E-08	1.57E-11
8	310	3000	1.46E-05	1.77E-06	3.00E-08	8.47E-12	1.79E-13	8.14E-18	2.46E-13	8.09E-10	1.40E-08	1.21E-11
9	310	3000	2.23E-05	2.19E-06	3.06E-08	7.28E-12	1.54E-13	1.59E-17	3.73E-13	9.81E-10	1.40E-08	1.02E-11
10	310	3000	3.06E-05	2.57E-06	3.11E-08	6.59E-12	1.31E-13	2.61E-17	5.06E-13	1.13E-09	1.39E-08	9.03E-12
11	310	3000	3.93E-05	2.93E-06	3.17E-08	6.15E-12	1.10E-13	3.87E-17	6.42E-13	1.25E-09	1.38E-08	8.23E-12

		Formula:	Fe ⁺⁺	FeOH ⁺	Fe(OH) ₂	Fe(OH) ₃ ⁻	FeSO ₄	Fe ⁺⁺⁺	FeOH ⁺⁺	Fe(OH) ₂ ⁺	Fe(OH) ₃	Fe(OH) ₄ ⁻
		Type:	(a)	(a)	(a)	(a)	(a)	(a)	(a)	(a)	(a)	(a)
Cell	T (°C)	P(bar)	Fe ⁺⁺	FeOH ⁺	Fe(OH) ₂ (aq)	Fe(OH) ₃ ⁻	FeSO ₄ (aq)	Fe ⁺⁺⁺	FeOH ⁺⁺	Fe(OH) ₂ ⁺	Fe(OH) ₃ (aq)	Fe(OH) ₄ ⁻
12	310	3000	4.84E-05	3.27E-06	3.24E-08	5.87E-12	9.05E-14	5.33E-17	7.78E-13	1.36E-09	1.38E-08	7.65E-12
13	310	3000	5.76E-05	3.59E-06	3.32E-08	5.69E-12	7.30E-14	6.95E-17	9.09E-13	1.45E-09	1.37E-08	7.20E-12
14	310	3000	6.72E-05	3.91E-06	3.40E-08	5.59E-12	5.76E-14	8.72E-17	1.04E-12	1.53E-09	1.36E-08	6.84E-12
15	310	3000	7.71E-05	4.24E-06	3.49E-08	5.55E-12	4.42E-14	1.06E-16	1.16E-12	1.60E-09	1.34E-08	6.55E-12
16	310	3000	8.75E-05	4.56E-06	3.60E-08	5.55E-12	3.27E-14	1.26E-16	1.27E-12	1.65E-09	1.33E-08	6.29E-12
17	310	3000	9.84E-05	4.91E-06	3.72E-08	5.60E-12	2.33E-14	1.46E-16	1.38E-12	1.70E-09	1.31E-08	6.06E-12
18	310	3000	1.10E-04	5.27E-06	3.86E-08	5.69E-12	1.59E-14	1.66E-16	1.48E-12	1.73E-09	1.29E-08	5.85E-12
Ore fluids	500	5000	7.42E-12	4.05E-09	4.36E-07	4.67E-07	2.45E-15	2.26E-26	1.43E-18	1.05E-11	1.07E-07	3.00E-07
1	280	3000	2.92E-09	1.87E-08	1.69E-08	3.37E-10	1.14E-12	2.33E-23	3.22E-17	5.57E-12	9.02E-09	5.68E-10
2	280	3000	3.91E-09	2.21E-08	1.71E-08	2.75E-10	1.08E-12	3.04E-23	4.14E-17	6.57E-12	9.09E-09	4.61E-10
3	280	3000	7.61E-09	3.20E-08	1.73E-08	1.73E-10	1.10E-12	6.31E-23	7.63E-17	9.57E-12	9.20E-09	2.91E-10
4	280	3000	2.49E-08	6.10E-08	1.72E-08	7.68E-11	1.20E-12	2.60E-22	2.35E-16	1.85E-11	9.33E-09	1.31E-10
5	280	3000	8.61E-07	3.48E-07	1.73E-08	1.49E-11	1.22E-12	6.63E-20	8.51E-15	1.06E-10	9.36E-09	2.55E-11
6	280	3000	5.94E-06	8.97E-07	1.75E-08	6.43E-12	1.11E-12	1.41E-18	6.00E-14	2.68E-10	9.34E-09	1.08E-11
7	280	3000	1.52E-05	1.43E-06	1.78E-08	4.37E-12	9.73E-13	6.22E-18	1.54E-13	4.18E-10	9.30E-09	7.20E-12
8	280	3000	2.70E-05	1.91E-06	1.82E-08	3.52E-12	8.33E-13	1.54E-17	2.70E-13	5.43E-10	9.26E-09	5.66E-12
9	280	3000	4.01E-05	2.33E-06	1.85E-08	3.07E-12	7.01E-13	2.88E-17	3.99E-13	6.48E-10	9.21E-09	4.82E-12
10	280	3000	5.40E-05	2.72E-06	1.89E-08	2.81E-12	5.76E-13	4.59E-17	5.29E-13	7.35E-10	9.16E-09	4.29E-12
11	280	3000	6.84E-05	3.07E-06	1.94E-08	2.65E-12	4.63E-13	6.60E-17	6.58E-13	8.07E-10	9.10E-09	3.93E-12
12	280	3000	8.31E-05	3.41E-06	1.99E-08	2.56E-12	3.62E-13	8.86E-17	7.82E-13	8.67E-10	9.03E-09	3.67E-12
13	280	3000	9.83E-05	3.75E-06	2.05E-08	2.51E-12	2.73E-13	1.13E-16	9.00E-13	9.16E-10	8.95E-09	3.46E-12
14	280	3000	1.14E-04	4.08E-06	2.12E-08	2.50E-12	1.96E-13	1.39E-16	1.01E-12	9.55E-10	8.84E-09	3.29E-12
15	280	3000	1.31E-04	4.44E-06	2.20E-08	2.51E-12	1.33E-13	1.65E-16	1.11E-12	9.85E-10	8.72E-09	3.15E-12

		Formula:	Fe ⁺⁺	FeOH ⁺	Fe(OH) ₂	Fe(OH) ₃ ⁻	FeSO ₄	Fe ⁺⁺⁺	FeOH ⁺⁺	Fe(OH) ₂ ⁺	Fe(OH) ₃	Fe(OH) ₄ ⁻
		Type:	(a)	(a)	(a)	(a)	(a)	(a)	(a)	(a)	(a)	(a)
Cell	T (°C)	P(bar)	Fe ⁺⁺	FeOH ⁺	Fe(OH) ₂ (aq)	Fe(OH) ₃ ⁻	FeSO ₄ (aq)	Fe ⁺⁺⁺	FeOH ⁺⁺	Fe(OH) ₂ ⁺	Fe(OH) ₃ (aq)	Fe(OH) ₄ ⁻
16	280	3000	1.49E-04	4.83E-06	2.30E-08	2.56E-12	8.23E-14	1.91E-16	1.19E-12	1.01E-09	8.56E-09	3.01E-12
17	280	3000	1.70E-04	5.29E-06	2.44E-08	2.66E-12	4.47E-14	2.16E-16	1.27E-12	1.02E-09	8.36E-09	2.88E-12
18	280	3000	1.95E-04	5.86E-06	2.62E-08	2.80E-12	2.01E-14	2.38E-16	1.32E-12	1.01E-09	8.09E-09	2.73E-12
Ore fluids	500	5000	7.42E-12	4.05E-09	4.36E-07	4.67E-07	2.45E-15	2.26E-26	1.43E-18	1.05E-11	1.07E-07	3.00E-07
1	250	3000	1.48E-08	3.21E-08	9.58E-09	7.84E-11	3.79E-12	2.07E-22	9.58E-17	5.95E-12	5.87E-09	1.57E-10
2	250	3000	2.29E-08	4.08E-08	9.63E-09	5.92E-11	3.94E-12	3.42E-22	1.44E-16	7.63E-12	5.95E-09	1.19E-10
3	250	3000	5.58E-08	6.60E-08	9.60E-09	3.27E-11	4.44E-12	9.86E-22	3.35E-16	1.26E-11	6.05E-09	6.74E-11
4	250	3000	1.81E-07	1.25E-07	9.58E-09	1.50E-11	4.88E-12	4.18E-21	1.03E-15	2.42E-11	6.14E-09	3.14E-11
5	250	3000	2.69E-06	4.71E-07	9.61E-09	4.27E-12	4.92E-12	2.78E-19	1.58E-14	9.12E-11	6.15E-09	8.93E-12
6	250	3000	1.31E-05	1.02E-06	9.74E-09	2.16E-12	4.48E-12	3.44E-18	7.82E-14	1.95E-10	6.14E-09	4.45E-12
7	250	3000	2.97E-05	1.53E-06	9.91E-09	1.55E-12	3.92E-12	1.27E-17	1.78E-13	2.86E-10	6.12E-09	3.13E-12
8	250	3000	4.95E-05	1.98E-06	1.01E-08	1.29E-12	3.35E-12	2.86E-17	2.94E-13	3.60E-10	6.09E-09	2.54E-12
9	250	3000	7.07E-05	2.37E-06	1.03E-08	1.16E-12	2.81E-12	5.03E-17	4.15E-13	4.19E-10	6.05E-09	2.21E-12
10	250	3000	9.24E-05	2.72E-06	1.06E-08	1.08E-12	2.30E-12	7.64E-17	5.33E-13	4.66E-10	6.01E-09	2.00E-12
11	250	3000	1.14E-04	3.05E-06	1.09E-08	1.03E-12	1.83E-12	1.06E-16	6.44E-13	5.04E-10	5.96E-09	1.85E-12
12	250	3000	1.37E-04	3.36E-06	1.12E-08	1.01E-12	1.40E-12	1.38E-16	7.48E-13	5.34E-10	5.90E-09	1.74E-12
13	250	3000	1.60E-04	3.68E-06	1.17E-08	1.01E-12	1.02E-12	1.71E-16	8.42E-13	5.57E-10	5.83E-09	1.65E-12
14	250	3000	1.85E-04	4.02E-06	1.22E-08	1.02E-12	6.95E-13	2.04E-16	9.24E-13	5.73E-10	5.73E-09	1.57E-12
15	250	3000	2.12E-04	4.40E-06	1.29E-08	1.05E-12	4.23E-13	2.35E-16	9.93E-13	5.81E-10	5.61E-09	1.49E-12
16	250	3000	2.45E-04	4.89E-06	1.38E-08	1.11E-12	2.10E-13	2.64E-16	1.04E-12	5.81E-10	5.43E-09	1.42E-12
17	250	3000	2.89E-04	5.56E-06	1.53E-08	1.20E-12	7.29E-14	2.87E-16	1.07E-12	5.69E-10	5.19E-09	1.33E-12
18	250	3000	3.64E-04	6.78E-06	1.83E-08	1.41E-12	1.01E-14	2.96E-16	1.05E-12	5.35E-10	4.77E-09	1.20E-12
Ore fluids	500	5000	7.42E-12	4.05E-09	4.36E-07	4.67E-07	2.45E-15	2.26E-26	1.43E-18	1.05E-11	1.07E-07	3.00E-07

		Formula:	Fe ⁺⁺	FeOH ⁺	Fe(OH) ₂	Fe(OH) ₃ ⁻	FeSO ₄	Fe ⁺⁺⁺	FeOH ⁺⁺	Fe(OH) ₂ ⁺	Fe(OH) ₃	Fe(OH) ₄ ⁻
		Type:	(a)	(a)	(a)	(a)	(a)	(a)	(a)	(a)	(a)	(a)
Cell	T (°C)	P(bar)	Fe ⁺⁺	FeOH ⁺	Fe(OH) ₂ (aq)	Fe(OH) ₃ ⁻	FeSO ₄ (aq)	Fe ⁺⁺⁺	FeOH ⁺⁺	Fe(OH) ₂ ⁺	Fe(OH) ₃ (aq)	Fe(OH) ₄ ⁻
1	220	3000	9.16E-08	5.92E-08	5.06E-09	1.49E-11	1.39E-11	2.32E-21	3.31E-16	6.76E-12	3.77E-09	3.76E-11
2	220	3000	1.70E-07	8.24E-08	5.02E-09	1.01E-11	1.60E-11	5.07E-21	6.05E-16	9.64E-12	3.84E-09	2.62E-11
3	220	3000	4.66E-07	1.41E-07	4.99E-09	5.28E-12	1.88E-11	1.76E-20	1.60E-15	1.70E-11	3.91E-09	1.41E-11
4	220	3000	1.48E-06	2.63E-07	4.98E-09	2.52E-12	2.06E-11	7.47E-20	4.84E-15	3.20E-11	3.96E-09	6.81E-12
5	220	3000	1.03E-05	6.84E-07	5.01E-09	1.02E-12	2.04E-11	1.49E-18	3.41E-14	8.32E-11	3.97E-09	2.74E-12
6	220	3000	3.26E-05	1.20E-06	5.08E-09	6.27E-13	1.85E-11	9.49E-18	1.10E-13	1.44E-10	3.97E-09	1.66E-12
7	220	3000	6.24E-05	1.66E-06	5.17E-09	4.90E-13	1.62E-11	2.71E-17	2.10E-13	1.94E-10	3.95E-09	1.27E-12
8	220	3000	9.48E-05	2.04E-06	5.27E-09	4.26E-13	1.38E-11	5.32E-17	3.17E-13	2.33E-10	3.93E-09	1.08E-12
9	220	3000	1.27E-04	2.37E-06	5.39E-09	3.93E-13	1.16E-11	8.57E-17	4.20E-13	2.63E-10	3.91E-09	9.67E-13
10	220	3000	1.60E-04	2.66E-06	5.53E-09	3.75E-13	9.47E-12	1.23E-16	5.17E-13	2.86E-10	3.88E-09	8.94E-13
11	220	3000	1.91E-04	2.93E-06	5.68E-09	3.66E-13	7.51E-12	1.62E-16	6.05E-13	3.04E-10	3.85E-09	8.41E-13
12	220	3000	2.23E-04	3.19E-06	5.87E-09	3.63E-13	5.74E-12	2.03E-16	6.84E-13	3.17E-10	3.81E-09	8.00E-13
13	220	3000	2.55E-04	3.45E-06	6.08E-09	3.65E-13	4.17E-12	2.43E-16	7.53E-13	3.27E-10	3.76E-09	7.67E-13
14	220	3000	2.88E-04	3.73E-06	6.36E-09	3.73E-13	2.81E-12	2.83E-16	8.12E-13	3.33E-10	3.70E-09	7.36E-13
15	220	3000	3.26E-04	4.06E-06	6.73E-09	3.87E-13	1.67E-12	3.19E-16	8.57E-13	3.34E-10	3.62E-09	7.07E-13
16	220	3000	3.73E-04	4.49E-06	7.27E-09	4.12E-13	8.05E-13	3.50E-16	8.85E-13	3.31E-10	3.50E-09	6.73E-13
17	220	3000	4.47E-04	5.22E-06	8.30E-09	4.66E-13	2.23E-13	3.67E-16	8.80E-13	3.17E-10	3.29E-09	6.26E-13
18	220	3000	6.44E-04	7.35E-06	1.15E-08	6.43E-13	7.77E-15	3.43E-16	7.84E-13	2.73E-10	2.80E-09	5.30E-13
Ore fluids	500	5000	7.42E-12	4.05E-09	4.36E-07	4.67E-07	2.45E-15	2.26E-26	1.43E-18	1.05E-11	1.07E-07	3.00E-07
1	190	3000	7.38E-07	1.21E-07	2.45E-09	2.18E-12	5.80E-11	3.58E-20	1.41E-15	8.41E-12	2.38E-09	7.53E-12
2	190	3000	1.49E-06	1.75E-07	2.42E-09	1.42E-12	6.96E-11	8.89E-20	2.81E-15	1.25E-11	2.42E-09	5.06E-12
3	190	3000	4.09E-06	3.01E-07	2.41E-09	7.54E-13	7.92E-11	3.13E-19	7.44E-15	2.21E-11	2.47E-09	2.74E-12
4	190	3000	1.18E-05	5.35E-07	2.43E-09	3.89E-13	7.95E-11	1.17E-18	2.04E-14	3.94E-11	2.50E-09	1.42E-12

		Formula:	Fe ⁺⁺	FeOH ⁺	Fe(OH) ₂	Fe(OH) ₃ ⁻	FeSO ₄	Fe ⁺⁺⁺	FeOH ⁺⁺	Fe(OH) ₂ ⁺	Fe(OH) ₃	Fe(OH) ₄ ⁻
		Type:	(a)	(a)	(a)	(a)	(a)	(a)	(a)	(a)	(a)	(a)
Cell	T (°C)	P(bar)	Fe ⁺⁺	FeOH ⁺	Fe(OH) ₂ (aq)	Fe(OH) ₃ ⁻	FeSO ₄ (aq)	Fe ⁺⁺⁺	FeOH ⁺⁺	Fe(OH) ₂ ⁺	Fe(OH) ₃ (aq)	Fe(OH) ₄ ⁻
5	190	3000	4.31E-05	1.02E-06	2.45E-09	2.14E-13	7.64E-11	8.54E-18	7.47E-14	7.41E-11	2.50E-09	7.74E-13
6	190	3000	8.92E-05	1.45E-06	2.49E-09	1.62E-13	6.80E-11	2.78E-17	1.55E-13	1.04E-10	2.49E-09	5.74E-13
7	190	3000	1.39E-04	1.80E-06	2.54E-09	1.40E-13	5.86E-11	5.78E-17	2.42E-13	1.26E-10	2.48E-09	4.84E-13
8	190	3000	1.88E-04	2.09E-06	2.60E-09	1.29E-13	4.92E-11	9.48E-17	3.23E-13	1.42E-10	2.47E-09	4.35E-13
9	190	3000	2.34E-04	2.34E-06	2.66E-09	1.24E-13	4.04E-11	1.36E-16	3.96E-13	1.54E-10	2.45E-09	4.05E-13
10	190	3000	2.78E-04	2.56E-06	2.74E-09	1.22E-13	3.21E-11	1.79E-16	4.61E-13	1.63E-10	2.43E-09	3.84E-13
11	190	3000	3.21E-04	2.77E-06	2.82E-09	1.22E-13	2.47E-11	2.22E-16	5.17E-13	1.69E-10	2.40E-09	3.68E-13
12	190	3000	3.63E-04	2.98E-06	2.93E-09	1.23E-13	1.81E-11	2.64E-16	5.64E-13	1.73E-10	2.37E-09	3.56E-13
13	190	3000	4.06E-04	3.20E-06	3.05E-09	1.27E-13	1.23E-11	3.04E-16	6.02E-13	1.75E-10	2.34E-09	3.44E-13
14	190	3000	4.54E-04	3.45E-06	3.22E-09	1.32E-13	7.50E-12	3.39E-16	6.30E-13	1.75E-10	2.29E-09	3.33E-13
15	190	3000	5.12E-04	3.78E-06	3.47E-09	1.41E-13	3.72E-12	3.68E-16	6.45E-13	1.73E-10	2.21E-09	3.20E-13
16	190	3000	6.01E-04	4.34E-06	3.94E-09	1.59E-13	1.10E-12	3.82E-16	6.37E-13	1.65E-10	2.09E-09	3.00E-13
17	190	3000	9.76E-04	6.94E-06	6.30E-09	2.56E-13	1.06E-14	3.25E-16	5.19E-13	1.31E-10	1.66E-09	2.40E-13
18	190	3000	1.57E-03	1.10E-05	9.93E-09	4.04E-13	7.50E-17	2.79E-16	4.26E-13	1.05E-10	1.32E-09	1.91E-13
Ore fluids	500	5000	7.42E-12	4.05E-09	4.36E-07	4.67E-07	2.45E-15	2.26E-26	1.43E-18	1.05E-11	1.07E-07	3.00E-07
1	160	3000	1.77E-06	1.39E-07	1.24E-09	6.33E-13	7.26E-11	6.32E-20	1.37E-15	4.73E-12	1.39E-09	2.66E-12
2	160	3000	2.99E-06	1.86E-07	1.25E-09	4.67E-13	7.28E-11	1.17E-19	2.24E-15	6.35E-12	1.41E-09	1.97E-12
3	160	3000	7.33E-06	3.03E-07	1.26E-09	2.70E-13	7.29E-11	3.43E-19	5.20E-15	1.04E-11	1.42E-09	1.14E-12
4	160	3000	2.12E-05	5.37E-07	1.27E-09	1.42E-13	7.32E-11	1.31E-18	1.43E-14	1.85E-11	1.44E-09	6.02E-13
5	160	3000	7.17E-05	9.85E-07	1.29E-09	8.12E-14	6.76E-11	8.53E-18	4.84E-14	3.35E-11	1.44E-09	3.40E-13
6	160	3000	1.39E-04	1.37E-06	1.33E-09	6.50E-14	5.07E-11	2.42E-17	9.15E-14	4.45E-11	1.42E-09	2.60E-13
7	160	3000	2.10E-04	1.70E-06	1.40E-09	5.93E-14	3.34E-11	4.55E-17	1.33E-13	5.18E-11	1.40E-09	2.23E-13
8	160	3000	2.83E-04	2.01E-06	1.49E-09	5.84E-14	1.85E-11	6.87E-17	1.66E-13	5.61E-11	1.36E-09	2.00E-13

		Formula:	Fe ⁺⁺	FeOH ⁺	Fe(OH) ₂	Fe(OH) ₃ ⁻	FeSO ₄	Fe ⁺⁺⁺	FeOH ⁺⁺	Fe(OH) ₂ ⁺	Fe(OH) ₃	Fe(OH) ₄ ⁻
		Type:	(a)	(a)	(a)	(a)	(a)	(a)	(a)	(a)	(a)	(a)
Cell	T (°C)	P(bar)	Fe ⁺⁺	FeOH ⁺	Fe(OH) ₂ (aq)	Fe(OH) ₃ ⁻	FeSO ₄ (aq)	Fe ⁺⁺⁺	FeOH ⁺⁺	Fe(OH) ₂ ⁺	Fe(OH) ₃ (aq)	Fe(OH) ₄ ⁻
9	160	3000	3.65E-04	2.37E-06	1.64E-09	6.14E-14	7.29E-12	9.01E-17	1.90E-13	5.75E-11	1.30E-09	1.83E-13
10	160	3000	5.09E-04	3.11E-06	2.06E-09	7.55E-14	7.66E-13	1.02E-16	1.92E-13	5.37E-11	1.17E-09	1.60E-13
11	160	3000	1.44E-03	8.44E-06	5.50E-09	2.01E-13	3.77E-17	7.33E-17	1.27E-13	3.35E-11	7.14E-10	9.81E-14
12	160	3000	1.92E-03	1.06E-05	6.54E-09	2.30E-13	5.17E-18	8.42E-17	1.32E-13	3.22E-11	6.54E-10	8.63E-14
13	160	3000	2.30E-03	1.20E-05	7.11E-09	2.41E-13	1.98E-18	9.80E-17	1.41E-13	3.22E-11	6.26E-10	7.97E-14
14	160	3000	2.65E-03	1.31E-05	7.52E-09	2.48E-13	1.04E-18	1.12E-16	1.50E-13	3.23E-11	6.07E-10	7.51E-14
15	160	3000	2.97E-03	1.41E-05	7.84E-09	2.52E-13	6.46E-19	1.27E-16	1.58E-13	3.25E-11	5.94E-10	7.16E-14
16	160	3000	3.26E-03	1.50E-05	8.11E-09	2.56E-13	4.39E-19	1.42E-16	1.67E-13	3.27E-11	5.82E-10	6.88E-14
17	160	3000	3.54E-03	1.57E-05	8.35E-09	2.58E-13	3.18E-19	1.56E-16	1.74E-13	3.29E-11	5.73E-10	6.65E-14
18	160	3000	3.80E-03	1.64E-05	8.55E-09	2.60E-13	2.41E-19	1.71E-16	1.81E-13	3.30E-11	5.65E-10	6.45E-14

		Formula:	CH ₄	C ₂ H ₆	HCOOH	HCOO ⁻	CH ₃ COO ⁻ H	CH ₃ COO ⁻		
		Type:	(a)	(a)	(a)	(a)	(a)	(a)		
Cell	T (°C)	P(bar)	CH ₄ (aq)	C ₂ H ₆ (aq)	HCOOH (aq)	HCOO ⁻	CH ₃ COO ⁻ H (aq)	CH ₃ COO ⁻	pH	Eh(V)
Ore fluids	500	5000	1.21E-01	1.89E-05	9.63E-06	2.36E-03	9.02E-07	9.99E-06	6.950431	-1.167
1	400	3000	5.32E-02	5.73E-06	4.66E-06	1.55E-03	7.07E-07	1.38E-05	7.083514	-0.98413
2	400	3000	5.58E-02	6.14E-06	4.60E-06	1.18E-03	7.14E-07	1.07E-05	6.988764	-0.97212
3	400	3000	5.72E-02	6.36E-06	4.60E-06	9.01E-04	7.21E-07	8.25E-06	6.89138	-0.95941
4	400	3000	5.84E-02	6.55E-06	4.61E-06	5.81E-04	7.28E-07	5.37E-06	6.729954	-0.93809
5	400	3000	5.84E-02	6.54E-06	4.64E-06	5.45E-05	7.32E-07	5.03E-07	5.699416	-0.8004
6	400	3000	5.99E-02	6.78E-06	4.59E-06	9.65E-06	7.32E-07	8.99E-08	4.912785	-0.69562

Formula:		CH4	C2H6	HCOOH	HCOO-	CH3COO H	CH3COO-			
Type:		(a)	(a)	(a)	(a)	(a)	(a)			
Cell	T (°C)	P(bar)	CH4 (aq)	C2H6 (aq)	HCOOH (aq)	HCOO-	CH3COO H (aq)	CH3COO-	pH	Eh(V)
7	400	3000	6.18E-02	7.09E-06	4.54E-06	5.38E-06	7.33E-07	5.08E-08	4.649529	-0.66085
8	400	3000	6.39E-02	7.43E-06	4.48E-06	3.87E-06	7.33E-07	3.70E-08	4.503009	-0.64169
9	400	3000	6.62E-02	7.80E-06	4.41E-06	3.10E-06	7.34E-07	3.01E-08	4.406536	-0.62922
10	400	3000	6.85E-02	8.20E-06	4.35E-06	2.64E-06	7.34E-07	2.61E-08	4.337177	-0.62038
11	400	3000	7.09E-02	8.62E-06	4.29E-06	2.34E-06	7.34E-07	2.34E-08	4.284509	-0.61378
12	400	3000	7.35E-02	9.06E-06	4.23E-06	2.12E-06	7.35E-07	2.15E-08	4.242981	-0.60867
13	400	3000	7.61E-02	9.53E-06	4.17E-06	1.95E-06	7.35E-07	2.01E-08	4.209322	-0.60462
14	400	3000	7.89E-02	1.00E-05	4.10E-06	1.82E-06	7.35E-07	1.90E-08	4.181458	-0.60134
15	400	3000	8.17E-02	1.06E-05	4.04E-06	1.71E-06	7.35E-07	1.82E-08	4.158001	-0.59865
16	400	3000	8.47E-02	1.11E-05	3.98E-06	1.62E-06	7.35E-07	1.75E-08	4.137984	-0.59642
17	400	3000	8.78E-02	1.17E-05	3.92E-06	1.55E-06	7.35E-07	1.70E-08	4.120707	-0.59457
18	400	3000	9.10E-02	1.23E-05	3.86E-06	1.48E-06	7.35E-07	1.65E-08	4.105655	-0.59301
Ore fluids	500	5000	1.21E-01	1.89E-05	9.63E-06	2.36E-03	9.02E-07	9.99E-06	6.950431	-1.167
1	370	3000	1.94E-02	1.17E-06	2.88E-06	9.57E-04	3.37E-07	7.15E-06	6.947518	-0.90531
2	370	3000	2.06E-02	1.28E-06	2.83E-06	7.37E-04	3.41E-07	5.67E-06	6.860601	-0.89502
3	370	3000	2.19E-02	1.39E-06	2.79E-06	4.91E-04	3.45E-07	3.88E-06	6.719125	-0.87772
4	370	3000	2.21E-02	1.41E-06	2.81E-06	2.52E-04	3.49E-07	2.00E-06	6.463467	-0.84518
5	370	3000	2.21E-02	1.41E-06	2.82E-06	1.55E-05	3.49E-07	1.23E-07	5.213114	-0.68556
6	370	3000	2.30E-02	1.50E-06	2.77E-06	5.43E-06	3.50E-07	4.37E-08	4.742059	-0.62595
7	370	3000	2.42E-02	1.61E-06	2.72E-06	3.37E-06	3.50E-07	2.78E-08	4.534075	-0.60002
8	370	3000	2.55E-02	1.74E-06	2.66E-06	2.53E-06	3.51E-07	2.13E-08	4.410723	-0.58493
9	370	3000	2.69E-02	1.88E-06	2.59E-06	2.07E-06	3.51E-07	1.79E-08	4.3273	-0.57497

		Formula:	CH4	C2H6	HCOOH	HCOO-	CH3COO H	CH3COO-		
		Type:	(a)	(a)	(a)	(a)	(a)	(a)		
Cell	T (°C)	P(bar)	CH4 (aq)	C2H6 (aq)	HCOOH (aq)	HCOO-	CH3COO H (aq)	CH3COO-	pH	Eh(V)
10	370	3000	2.85E-02	2.04E-06	2.53E-06	1.78E-06	3.52E-07	1.57E-08	4.266507	-0.56792
11	370	3000	3.02E-02	2.22E-06	2.47E-06	1.57E-06	3.52E-07	1.43E-08	4.220006	-0.56271
12	370	3000	3.20E-02	2.42E-06	2.41E-06	1.42E-06	3.52E-07	1.33E-08	4.183195	-0.55876
13	370	3000	3.40E-02	2.64E-06	2.34E-06	1.31E-06	3.52E-07	1.26E-08	4.1533	-0.55571
14	370	3000	3.62E-02	2.89E-06	2.28E-06	1.21E-06	3.53E-07	1.20E-08	4.128535	-0.55334
15	370	3000	3.85E-02	3.17E-06	2.21E-06	1.13E-06	3.53E-07	1.15E-08	4.107689	-0.55148
16	370	3000	4.10E-02	3.47E-06	2.15E-06	1.06E-06	3.53E-07	1.11E-08	4.089916	-0.55003
17	370	3000	4.38E-02	3.82E-06	2.09E-06	1.00E-06	3.53E-07	1.08E-08	4.074599	-0.5489
18	370	3000	4.67E-02	4.20E-06	2.02E-06	9.51E-07	3.53E-07	1.06E-08	4.06128	-0.54804
Ore fluids	500	5000	1.21E-01	1.89E-05	9.63E-06	2.36E-03	9.02E-07	9.99E-06	6.950431	-1.167
1	340	3000	5.82E-03	1.75E-07	1.77E-06	5.23E-04	1.47E-07	3.03E-06	6.765011	-0.82076
2	340	3000	6.23E-03	1.93E-07	1.73E-06	4.10E-04	1.49E-07	2.46E-06	6.685275	-0.8119
3	340	3000	6.60E-03	2.11E-07	1.71E-06	2.77E-04	1.50E-07	1.70E-06	6.547011	-0.79581
4	340	3000	6.56E-03	2.08E-07	1.73E-06	1.36E-04	1.52E-07	8.33E-07	6.270447	-0.76202
5	340	3000	6.50E-03	2.05E-07	1.75E-06	1.22E-05	1.52E-07	7.43E-08	5.185731	-0.62987
6	340	3000	6.82E-03	2.20E-07	1.71E-06	4.27E-06	1.52E-07	2.65E-08	4.716531	-0.57336
7	340	3000	7.26E-03	2.41E-07	1.67E-06	2.64E-06	1.53E-07	1.68E-08	4.508296	-0.54878
8	340	3000	7.78E-03	2.66E-07	1.62E-06	1.96E-06	1.53E-07	1.29E-08	4.385895	-0.53473
9	340	3000	8.37E-03	2.96E-07	1.57E-06	1.59E-06	1.53E-07	1.09E-08	4.303836	-0.52564
10	340	3000	9.05E-03	3.32E-07	1.51E-06	1.36E-06	1.54E-07	9.63E-09	4.24451	-0.51939
11	340	3000	9.83E-03	3.75E-07	1.46E-06	1.20E-06	1.54E-07	8.80E-09	4.199452	-0.51493
12	340	3000	1.07E-02	4.27E-07	1.40E-06	1.07E-06	1.54E-07	8.20E-09	4.16401	-0.5117

Formula:		CH4	C2H6	HCOOH	HCOO-	CH3COO H	CH3COO-			
Type:		(a)	(a)	(a)	(a)	(a)	(a)			
Cell	T (°C)	P(bar)	CH4 (aq)	C2H6 (aq)	HCOOH (aq)	HCOO-	CH3COO H (aq)	CH3COO-	pH	Eh(V)
13	340	3000	1.18E-02	4.89E-07	1.35E-06	9.69E-07	1.54E-07	7.77E-09	4.13539	-0.50938
14	340	3000	1.30E-02	5.66E-07	1.29E-06	8.85E-07	1.55E-07	7.43E-09	4.111803	-0.50774
15	340	3000	1.44E-02	6.60E-07	1.23E-06	8.13E-07	1.55E-07	7.17E-09	4.092043	-0.50664
16	340	3000	1.61E-02	7.76E-07	1.16E-06	7.49E-07	1.55E-07	6.96E-09	4.075272	-0.50598
17	340	3000	1.81E-02	9.20E-07	1.10E-06	6.91E-07	1.55E-07	6.79E-09	4.060883	-0.50569
18	340	3000	2.04E-02	1.10E-06	1.04E-06	6.39E-07	1.55E-07	6.64E-09	4.048428	-0.5057
Ore fluids	500	5000	1.21E-01	1.89E-05	9.63E-06	2.36E-03	9.02E-07	9.99E-06	6.950431	-1.167
1	310	3000	1.52E-03	2.08E-08	1.04E-06	2.62E-04	5.82E-08	1.12E-06	6.562562	-0.73541
2	310	3000	1.62E-03	2.27E-08	1.03E-06	2.08E-04	5.90E-08	9.14E-07	6.485091	-0.72716
3	310	3000	1.68E-03	2.40E-08	1.02E-06	1.38E-04	5.97E-08	6.18E-07	6.334704	-0.7102
4	310	3000	1.63E-03	2.29E-08	1.05E-06	6.46E-05	6.04E-08	2.83E-07	6.030995	-0.67463
5	310	3000	1.60E-03	2.23E-08	1.06E-06	8.76E-06	6.04E-08	3.80E-08	5.129485	-0.57007
6	310	3000	1.68E-03	2.39E-08	1.04E-06	3.28E-06	6.05E-08	1.46E-08	4.692022	-0.52
7	310	3000	1.80E-03	2.64E-08	1.01E-06	2.06E-06	6.07E-08	9.43E-09	4.492304	-0.49767
8	310	3000	1.94E-03	2.95E-08	9.77E-07	1.55E-06	6.08E-08	7.34E-09	4.374893	-0.48497
9	310	3000	2.11E-03	3.34E-08	9.42E-07	1.26E-06	6.09E-08	6.23E-09	4.2966	-0.47689
10	310	3000	2.31E-03	3.81E-08	9.05E-07	1.08E-06	6.11E-08	5.55E-09	4.240376	-0.47145
11	310	3000	2.55E-03	4.40E-08	8.66E-07	9.47E-07	6.12E-08	5.10E-09	4.197962	-0.4677
12	310	3000	2.83E-03	5.14E-08	8.26E-07	8.44E-07	6.13E-08	4.79E-09	4.164814	-0.46513
13	310	3000	3.18E-03	6.11E-08	7.83E-07	7.60E-07	6.15E-08	4.55E-09	4.138204	-0.46345
14	310	3000	3.62E-03	7.39E-08	7.37E-07	6.87E-07	6.16E-08	4.38E-09	4.116391	-0.46247
15	310	3000	4.18E-03	9.13E-08	6.90E-07	6.21E-07	6.17E-08	4.24E-09	4.098207	-0.4621

Formula:		CH4	C2H6	HCOOH	HCOO-	CH3COO H	CH3COO-			
Type:		(a)	(a)	(a)	(a)	(a)	(a)			
Cell	T (°C)	P(bar)	CH4 (aq)	C2H6 (aq)	HCOOH (aq)	HCOO-	CH3COO H (aq)	CH3COO-	pH	Eh(V)
16	310	3000	4.91E-03	1.16E-07	6.39E-07	5.60E-07	6.18E-08	4.13E-09	4.082841	-0.46228
17	310	3000	5.88E-03	1.52E-07	5.86E-07	5.02E-07	6.19E-08	4.05E-09	4.069714	-0.46297
18	310	3000	7.22E-03	2.06E-07	5.31E-07	4.46E-07	6.20E-08	3.97E-09	4.058402	-0.46417
Ore fluids	500	5000	1.21E-01	1.89E-05	9.63E-06	2.36E-03	9.02E-07	9.99E-06	6.950431	-1.167
1	280	3000	3.78E-04	2.21E-09	5.61E-07	1.25E-04	2.09E-08	3.89E-07	6.387771	-0.65613
2	280	3000	3.96E-04	2.37E-09	5.56E-07	9.93E-05	2.12E-08	3.16E-07	6.304578	-0.64754
3	280	3000	3.97E-04	2.38E-09	5.63E-07	6.23E-05	2.15E-08	1.98E-07	6.120299	-0.62731
4	280	3000	3.81E-04	2.23E-09	5.83E-07	2.86E-05	2.18E-08	8.89E-08	5.803136	-0.59197
5	280	3000	3.79E-04	2.21E-09	5.87E-07	5.59E-06	2.18E-08	1.73E-08	5.069863	-0.51136
6	280	3000	4.03E-04	2.42E-09	5.71E-07	2.32E-06	2.18E-08	7.38E-09	4.682044	-0.46947
7	280	3000	4.40E-04	2.74E-09	5.50E-07	1.49E-06	2.19E-08	4.94E-09	4.497618	-0.4502
8	280	3000	4.85E-04	3.18E-09	5.26E-07	1.13E-06	2.19E-08	3.92E-09	4.38877	-0.43937
9	280	3000	5.35E-04	3.66E-09	5.04E-07	9.26E-07	2.20E-08	3.36E-09	4.316215	-0.4325
10	280	3000	5.96E-04	4.29E-09	4.80E-07	7.92E-07	2.20E-08	3.03E-09	4.264537	-0.42804
11	280	3000	6.71E-04	5.12E-09	4.54E-07	6.93E-07	2.21E-08	2.80E-09	4.225895	-0.42516
12	280	3000	7.67E-04	6.24E-09	4.27E-07	6.13E-07	2.22E-08	2.65E-09	4.195963	-0.4234
13	280	3000	8.94E-04	7.82E-09	3.98E-07	5.45E-07	2.22E-08	2.53E-09	4.172148	-0.42254
14	280	3000	1.07E-03	1.02E-08	3.66E-07	4.83E-07	2.23E-08	2.44E-09	4.152801	-0.42245
15	280	3000	1.31E-03	1.39E-08	3.31E-07	4.24E-07	2.23E-08	2.38E-09	4.136822	-0.42312
16	280	3000	1.69E-03	2.03E-08	2.93E-07	3.66E-07	2.24E-08	2.32E-09	4.123452	-0.42463
17	280	3000	2.34E-03	3.28E-08	2.51E-07	3.07E-07	2.24E-08	2.28E-09	4.112157	-0.42718
18	280	3000	3.56E-03	6.15E-08	2.04E-07	2.45E-07	2.24E-08	2.25E-09	4.102558	-0.43108

		Formula:	CH4	C2H6	HCOOH	HCOO-	CH3COO H	CH3COO-		
		Type:	(a)	(a)	(a)	(a)	(a)	(a)		
Cell	T (°C)	P(bar)	CH4 (aq)	C2H6 (aq)	HCOOH (aq)	HCOO-	CH3COO H (aq)	CH3COO-	pH	Eh(V)
Ore fluids	500	5000	1.21E-01	1.89E-05	9.63E-06	2.36E-03	9.02E-07	9.99E-06	6.950431	-1.167
1	250	3000	8.22E-05	1.87E-10	2.81E-07	5.45E-05	6.71E-09	1.18E-07	6.209345	-0.57836
2	250	3000	8.16E-05	1.84E-10	2.87E-07	4.15E-05	6.81E-09	8.93E-08	6.093363	-0.56619
3	250	3000	7.72E-05	1.70E-10	2.99E-07	2.39E-05	6.90E-09	5.00E-08	5.857907	-0.5411
4	250	3000	7.39E-05	1.58E-10	3.10E-07	1.14E-05	6.98E-09	2.32E-08	5.549385	-0.50854
5	250	3000	7.39E-05	1.58E-10	3.11E-07	3.23E-06	6.99E-09	6.59E-09	4.988018	-0.45022
6	250	3000	7.86E-05	1.73E-10	3.03E-07	1.58E-06	7.01E-09	3.30E-09	4.672705	-0.41813
7	250	3000	8.56E-05	1.96E-10	2.92E-07	1.07E-06	7.03E-09	2.34E-09	4.513767	-0.40253
8	250	3000	9.46E-05	2.27E-10	2.79E-07	8.37E-07	7.05E-09	1.91E-09	4.418914	-0.39375
9	250	3000	1.06E-04	2.68E-10	2.65E-07	6.97E-07	7.06E-09	1.68E-09	4.356062	-0.38843
10	250	3000	1.20E-04	3.23E-10	2.51E-07	6.00E-07	7.08E-09	1.54E-09	4.311529	-0.38517
11	250	3000	1.39E-04	4.00E-10	2.34E-07	5.25E-07	7.10E-09	1.44E-09	4.278475	-0.3833
12	250	3000	1.64E-04	5.12E-10	2.17E-07	4.61E-07	7.12E-09	1.37E-09	4.253097	-0.38247
13	250	3000	1.99E-04	6.83E-10	1.98E-07	4.05E-07	7.14E-09	1.32E-09	4.233089	-0.38253
14	250	3000	2.52E-04	9.72E-10	1.77E-07	3.50E-07	7.16E-09	1.29E-09	4.217008	-0.38347
15	250	3000	3.41E-04	1.53E-09	1.53E-07	2.95E-07	7.18E-09	1.26E-09	4.203913	-0.38548
16	250	3000	5.23E-04	2.89E-09	1.24E-07	2.35E-07	7.20E-09	1.24E-09	4.193169	-0.3891
17	250	3000	9.44E-04	6.99E-09	9.27E-08	1.73E-07	7.21E-09	1.22E-09	4.184151	-0.39476
18	250	3000	2.66E-03	3.30E-08	5.54E-08	1.02E-07	7.22E-09	1.21E-09	4.176901	-0.40563
Ore fluids	500	5000	1.21E-01	1.89E-05	9.63E-06	2.36E-03	9.02E-07	9.99E-06	6.950431	-1.167
1	220	3000	1.54E-05	1.21E-11	1.30E-07	2.08E-05	1.89E-09	2.97E-08	6.010465	-0.5005
2	220	3000	1.43E-05	1.08E-11	1.37E-07	1.49E-05	1.91E-09	2.05E-08	5.852578	-0.48426

Formula:		CH4	C2H6	HCOOH	HCOO-	CH3COO H	CH3COO-			
Type:		(a)	(a)	(a)	(a)	(a)	(a)			
Cell	T (°C)	P(bar)	CH4 (aq)	C2H6 (aq)	HCOOH (aq)	HCOO-	CH3COO H (aq)	CH3COO-	pH	Eh(V)
3	220	3000	1.32E-05	9.57E-12	1.45E-07	8.23E-06	1.94E-09	1.09E-08	5.591594	-0.45784
4	220	3000	1.27E-05	8.97E-12	1.49E-07	4.05E-06	1.96E-09	5.23E-09	5.294736	-0.42832
5	220	3000	1.28E-05	9.11E-12	1.49E-07	1.63E-06	1.97E-09	2.11E-09	4.890136	-0.3888
6	220	3000	1.37E-05	1.00E-11	1.45E-07	9.64E-07	1.97E-09	1.29E-09	4.663309	-0.36723
7	220	3000	1.49E-05	1.14E-11	1.40E-07	7.13E-07	1.98E-09	9.90E-10	4.540809	-0.3561
8	220	3000	1.65E-05	1.32E-11	1.34E-07	5.83E-07	1.98E-09	8.48E-10	4.466269	-0.34981
9	220	3000	1.84E-05	1.55E-11	1.27E-07	5.00E-07	1.99E-09	7.68E-10	4.416743	-0.34611
10	220	3000	2.09E-05	1.87E-11	1.20E-07	4.39E-07	1.99E-09	7.17E-10	4.381798	-0.34398
11	220	3000	2.42E-05	2.32E-11	1.12E-07	3.91E-07	2.00E-09	6.83E-10	4.356073	-0.34294
12	220	3000	2.86E-05	2.98E-11	1.04E-07	3.48E-07	2.00E-09	6.60E-10	4.336547	-0.34275
13	220	3000	3.48E-05	3.99E-11	9.45E-08	3.08E-07	2.01E-09	6.43E-10	4.321393	-0.34331
14	220	3000	4.44E-05	5.73E-11	8.42E-08	2.68E-07	2.01E-09	6.30E-10	4.309454	-0.34467
15	220	3000	6.09E-05	9.19E-11	7.22E-08	2.26E-07	2.02E-09	6.21E-10	4.299974	-0.34704
16	220	3000	9.51E-05	1.79E-10	5.81E-08	1.80E-07	2.02E-09	6.15E-10	4.292413	-0.35098
17	220	3000	2.07E-04	5.71E-10	3.96E-08	1.21E-07	2.03E-09	6.10E-10	4.28663	-0.3586
18	220	3000	1.46E-03	1.07E-08	1.50E-08	4.56E-08	2.03E-09	6.08E-10	4.283154	-0.37898
Ore fluids	500	5000	1.21E-01	1.89E-05	9.63E-06	2.36E-03	9.02E-07	9.99E-06	6.950431	-1.167
1	190	3000	2.37E-06	5.50E-13	5.48E-08	6.70E-06	4.53E-10	5.87E-09	5.780509	-0.42177
2	190	3000	2.16E-06	4.77E-13	5.83E-08	4.67E-06	4.59E-10	3.90E-09	5.605015	-0.40468
3	190	3000	2.03E-06	4.35E-13	6.11E-08	2.58E-06	4.66E-10	2.09E-09	5.346235	-0.38027
4	190	3000	2.05E-06	4.43E-13	6.16E-08	1.33E-06	4.72E-10	1.08E-09	5.075525	-0.35549
5	190	3000	2.12E-06	4.62E-13	6.10E-08	7.17E-07	4.74E-10	5.91E-10	4.806804	-0.33105

Formula:		CH4	C2H6	HCOOH	HCOO-	CH3COO H	CH3COO-			
Type:		(a)	(a)	(a)	(a)	(a)	(a)			
Cell	T (°C)	P(bar)	CH4 (aq)	C2H6 (aq)	HCOOH (aq)	HCOO-	CH3COO H (aq)	CH3COO-	pH	Eh(V)
6	190	3000	2.28E-06	5.16E-13	5.91E-08	5.17E-07	4.75E-10	4.41E-10	4.669558	-0.31914
7	190	3000	2.51E-06	5.94E-13	5.66E-08	4.21E-07	4.76E-10	3.75E-10	4.590971	-0.31281
8	190	3000	2.80E-06	6.99E-13	5.39E-08	3.62E-07	4.77E-10	3.41E-10	4.541986	-0.30935
9	190	3000	3.18E-06	8.40E-13	5.09E-08	3.21E-07	4.78E-10	3.20E-10	4.509303	-0.30754
10	190	3000	3.66E-06	1.04E-12	4.76E-08	2.88E-07	4.80E-10	3.08E-10	4.486435	-0.30681
11	190	3000	4.32E-06	1.32E-12	4.41E-08	2.59E-07	4.81E-10	2.99E-10	4.469917	-0.30687
12	190	3000	5.24E-06	1.77E-12	4.02E-08	2.31E-07	4.82E-10	2.94E-10	4.457752	-0.30763
13	190	3000	6.63E-06	2.51E-12	3.60E-08	2.03E-07	4.83E-10	2.90E-10	4.448726	-0.30911
14	190	3000	8.98E-06	3.94E-12	3.11E-08	1.74E-07	4.85E-10	2.88E-10	4.442078	-0.31147
15	190	3000	1.38E-05	7.46E-12	2.52E-08	1.40E-07	4.86E-10	2.87E-10	4.437353	-0.31524
16	190	3000	2.87E-05	2.24E-11	1.76E-08	9.73E-08	4.87E-10	2.86E-10	4.434469	-0.32226
17	190	3000	4.69E-04	1.48E-09	4.36E-09	2.43E-08	4.88E-10	2.89E-10	4.436082	-0.35023
18	190	3000	7.16E-03	8.79E-08	1.11E-09	6.25E-09	4.86E-10	2.89E-10	4.436863	-0.37745
Ore fluids	500	5000	1.21E-01	1.89E-05	9.63E-06	2.36E-03	9.02E-07	9.99E-06	6.950431	-1.167
1	160	3000	6.66E-07	5.82E-14	1.38E-08	2.71E-06	9.12E-11	2.03E-09	5.876018	-0.38115
2	160	3000	6.78E-07	5.96E-14	1.40E-08	1.98E-06	9.28E-11	1.50E-09	5.74331	-0.36988
3	160	3000	6.90E-07	6.12E-14	1.41E-08	1.14E-06	9.45E-11	8.65E-10	5.514129	-0.35034
4	160	3000	6.99E-07	6.23E-14	1.42E-08	5.95E-07	9.57E-11	4.55E-10	5.248491	-0.32759
5	160	3000	7.37E-07	6.73E-14	1.39E-08	3.29E-07	9.60E-11	2.58E-10	4.995856	-0.30634
6	160	3000	8.81E-07	8.77E-14	1.28E-08	2.35E-07	9.62E-11	2.01E-10	4.876819	-0.29772
7	160	3000	1.14E-06	1.28E-13	1.13E-08	1.81E-07	9.64E-11	1.75E-10	4.810532	-0.29436
8	160	3000	1.63E-06	2.19E-13	9.50E-09	1.41E-07	9.66E-11	1.63E-10	4.771092	-0.29427

		Formula:	CH ₄	C ₂ H ₆	HCOOH	HCOO-	CH ₃ COO H	CH ₃ COO-		
		Type:	(a)	(a)	(a)	(a)	(a)	(a)		
Cell	T (°C)	P(bar)	CH ₄ (aq)	C ₂ H ₆ (aq)	HCOOH (aq)	HCOO-	CH ₃ COO H (aq)	CH ₃ COO-	pH	Eh(V)
9	160	3000	2.87E-06	5.10E-13	7.20E-09	1.02E-07	9.69E-11	1.56E-10	4.74691	-0.29741
10	160	3000	1.11E-05	3.90E-12	3.67E-09	5.09E-08	9.71E-11	1.53E-10	4.733588	-0.30888
11	160	3000	3.95E-03	2.60E-08	1.95E-10	2.71E-09	9.69E-11	1.53E-10	4.731084	-0.36342
12	160	3000	1.11E-02	1.23E-07	1.16E-10	1.55E-09	9.65E-11	1.47E-10	4.713357	-0.37151
13	160	3000	1.83E-02	2.58E-07	9.02E-11	1.17E-09	9.61E-11	1.42E-10	4.698294	-0.37483
14	160	3000	2.55E-02	4.24E-07	7.62E-11	9.67E-10	9.57E-11	1.38E-10	4.686053	-0.37683
15	160	3000	3.27E-02	6.15E-07	6.72E-11	8.35E-10	9.54E-11	1.35E-10	4.676063	-0.37826
16	160	3000	3.99E-02	8.27E-07	6.07E-11	7.41E-10	9.50E-11	1.32E-10	4.667834	-0.37937
17	160	3000	4.71E-02	1.06E-06	5.58E-11	6.71E-10	9.46E-11	1.29E-10	4.660997	-0.38029
18	160	3000	5.44E-02	1.31E-06	5.18E-11	6.16E-10	9.42E-11	1.27E-10	4.655278	-0.38109

Notes s: solid; a: aqueous solution; the unit is mol.

Table B3-2 The comparison of time-integrated fluid infiltration with different instantaneous fluid:rock ratio at 220 °C. The time integrated fluid:rock is 1:1 by mass.

(1) Results of one fluid infiltration with instantaneous f:r = 1 (by mass).

		Formula:	Au	C	SiO ₂	Fe ₃ O ₄	FeS ₂	Fe.877S	ZnS	FeAsS	CaCO ₃	KAl ₃ Si ₃ O ₁₀ (OH) ₂
		Type:	(s)	(s)	(s)	(s)	(s)	(s)	(s)	(s)	(s)	(s)
Cell	T (°C)	P (bar)	Gold	Graphite	Quartz	Magnetite	Pyrite	Pyrrhotite	Sphalerite	Arsenopyrite	Calcite	Muscovite
Ore fluids	500	5000	0	0	0	0	0	0	0	0	0	0
1	220	3000	8.38E-06	2.64E-01	5.18E-01	1.55E-02	8.97E-03	0	1.54E-04	0	7.47E-03	8.35E-02
2	220	3000	5.79E-11	1.66E-02	3.33E-01	1.78E-02	1.96E-03	0	1.54E-04	0	7.48E-03	5.75E-02
3	220	3000	5.92E-11	1.66E-02	3.29E-01	1.78E-02	1.96E-03	0	1.54E-04	0	7.47E-03	5.69E-02
4	220	3000	3.39E-11	1.66E-02	3.51E-01	1.78E-02	1.96E-03	0	1.54E-04	0	0	5.67E-02
5	220	3000	1.87E-11	1.66E-02	3.91E-01	1.78E-02	1.96E-03	0	1.54E-04	0	0	5.67E-02
6	220	3000	5.00E-12	1.66E-02	3.98E-01	1.78E-02	1.96E-03	0	1.54E-04	0	0	5.67E-02
7	220	3000	1.94E-12	1.66E-02	3.98E-01	1.78E-02	1.96E-03	0	1.54E-04	0	0	5.67E-02
8	220	3000	1.10E-12	1.66E-02	3.98E-01	1.78E-02	1.96E-03	0	1.54E-04	0	0	5.67E-02
9	220	3000	8.08E-13	1.66E-02	3.98E-01	1.78E-02	1.96E-03	0	1.54E-04	0	0	5.67E-02
10	220	3000	7.14E-13	1.66E-02	3.98E-01	1.78E-02	1.96E-03	0	1.54E-04	0	0	5.67E-02
11	220	3000	7.19E-13	1.66E-02	3.98E-01	1.78E-02	1.96E-03	0	1.54E-04	0	0	5.67E-02
12	220	3000	7.92E-13	1.66E-02	3.98E-01	1.78E-02	1.96E-03	0	1.54E-04	0	0	5.67E-02
13	220	3000	9.33E-13	1.66E-02	3.98E-01	1.78E-02	1.96E-03	0	1.54E-04	0	0	5.67E-02
14	220	3000	1.16E-12	1.66E-02	3.98E-01	1.78E-02	1.96E-03	0	1.54E-04	0	0	5.67E-02
15	220	3000	1.55E-12	1.66E-02	3.98E-01	1.78E-02	1.96E-03	0	1.54E-04	0	0	5.67E-02
16	220	3000	2.22E-12	1.64E-02	3.98E-01	1.78E-02	1.90E-03	0	1.54E-04	1.22E-04	0	5.67E-02
17	220	3000	3.88E-12	1.61E-02	3.98E-01	1.77E-02	1.85E-03	0	1.54E-04	2.22E-04	0	5.67E-02
18	220	3000	1.57E-11	1.29E-02	3.98E-01	1.72E-02	0	3.75E-03	1.54E-04	1.56E-04	0	5.67E-02

		Formula:	Ca ₂ Al ₃ Si 3O ₁₂ (OH)	Ca ₂ FeAl ₂ Si ₃ O ₁₂ O H	Mg _{4.5} Al 3Si _{2.5} O ₁ 0(OH) ₈	Na(AlSi ₃ O ₈)	H ₂ O	H ⁺	OH ⁻	CO ₃ ⁻⁻	HCO ₃ ⁻	H ₂ CO ₃
		Type:	(s)	(s)	(s)	(s)	(a)	(a)	(a)	(a)	(a)	(a)
Cell	T (°C)	P (bar)	Zoisite	Epidote	Chlorite	Albite	H ₂ O	H ⁺	OH ⁻	CO ₃ ⁻⁻	HCO ₃ ⁻	H ₂ CO ₃ (aq)
Ore fluids	500	5000	0	0	0	0	4.86E+00	1.66E-08	2.62E-03	3.42E-05	9.52E-03	2.80E-01
1	220	3000	0	0	1.02E-02	8.86E-02	5.36E+00	1.29E-07	1.13E-05	1.26E-04	5.02E-02	7.47E-02
2	220	3000	0	0	1.02E-02	1.66E-01	5.40E+00	1.86E-07	7.66E-06	5.90E-05	3.74E-02	8.21E-02
3	220	3000	0	0	1.02E-02	1.68E-01	5.45E+00	3.36E-07	3.97E-06	1.55E-05	2.15E-02	9.10E-02
4	220	3000	3.75E-03	0	1.02E-02	1.58E-01	5.49E+00	6.51E-07	1.88E-06	3.21E-06	1.08E-02	9.66E-02
5	220	3000	3.77E-03	0	1.02E-02	1.44E-01	5.51E+00	1.67E-06	7.61E-07	5.40E-07	4.32E-03	9.61E-02
6	220	3000	3.74E-03	0	1.02E-02	1.42E-01	5.53E+00	2.87E-06	4.68E-07	2.02E-07	2.49E-03	9.06E-02
7	220	3000	3.74E-03	0	1.02E-02	1.42E-01	5.55E+00	3.85E-06	3.63E-07	1.16E-07	1.77E-03	8.37E-02
8	220	3000	3.74E-03	0	1.02E-02	1.42E-01	5.57E+00	4.62E-06	3.13E-07	8.04E-08	1.38E-03	7.63E-02
9	220	3000	3.74E-03	0	1.02E-02	1.42E-01	5.59E+00	5.22E-06	2.85E-07	6.10E-08	1.12E-03	6.86E-02
10	220	3000	3.74E-03	0	1.02E-02	1.42E-01	5.62E+00	5.70E-06	2.67E-07	4.85E-08	9.30E-04	6.08E-02
11	220	3000	3.74E-03	0	1.02E-02	1.42E-01	5.64E+00	6.09E-06	2.56E-07	3.92E-08	7.71E-04	5.30E-02
12	220	3000	3.74E-03	0	1.02E-02	1.42E-01	5.66E+00	6.41E-06	2.48E-07	3.18E-08	6.34E-04	4.51E-02
13	220	3000	3.74E-03	0	1.02E-02	1.42E-01	5.68E+00	6.68E-06	2.43E-07	2.54E-08	5.09E-04	3.73E-02
14	220	3000	3.74E-03	0	1.02E-02	1.42E-01	5.71E+00	6.90E-06	2.39E-07	1.96E-08	3.94E-04	2.94E-02
15	220	3000	3.74E-03	0	1.02E-02	1.42E-01	5.73E+00	7.09E-06	2.36E-07	1.42E-08	2.84E-04	2.16E-02
16	220	3000	3.74E-03	0	1.02E-02	1.42E-01	5.75E+00	7.25E-06	2.35E-07	9.11E-09	1.81E-04	1.39E-02
17	220	3000	3.74E-03	0	1.02E-02	1.42E-01	5.78E+00	7.38E-06	2.34E-07	4.22E-09	8.32E-05	6.45E-03
18	220	3000	3.74E-03	0	1.02E-02	1.42E-01	5.79E+00	7.47E-06	2.34E-07	6.05E-10	1.18E-05	9.17E-04

		Formula:	H3SiO4-	H4SiO4	H3AsO3	HAsO3--	As2S4--	HAs2S4-	O2	H2	H2S	HS-
		Type:	(a)	(a)	(a)	(a)	(a)	(a)	(a)	(a)	(a)	(a)
Cell	T (°C)	P (bar)	H3SiO4-	H4SiO4 (aq)	H3AsO3 (aq)	HAsO3--	As2S4--	HAs2S4-	O2 (aq)	H2 (aq)	H2S (aq)	HS-
Ore fluids	500	5000	1.82E-02	1.17E-02	4.00E-05	2.95E-08	1.18E-08	1.62E-10	3.31E-28	4.77E-03	6.95E-03	7.07E-03
1	220	3000	2.89E-05	1.02E-03	6.67E-05	5.08E-10	1.64E-13	4.56E-14	1.21E-44	3.93E-07	4.24E-06	5.82E-06
2	220	3000	1.99E-05	1.04E-03	9.34E-05	3.02E-10	1.27E-13	5.66E-14	1.32E-44	3.79E-07	4.21E-06	3.89E-06
3	220	3000	1.06E-05	1.05E-03	1.20E-04	9.19E-11	4.60E-14	4.53E-14	1.46E-44	3.65E-07	4.18E-06	1.99E-06
4	220	3000	5.08E-06	1.06E-03	1.47E-04	2.20E-11	1.28E-14	3.08E-14	1.54E-44	3.58E-07	4.17E-06	9.32E-07
5	220	3000	2.05E-06	1.06E-03	1.74E-04	4.39E-12	3.04E-15	1.73E-14	1.53E-44	3.61E-07	4.20E-06	3.78E-07
6	220	3000	1.25E-06	1.07E-03	2.00E-04	2.01E-12	1.67E-15	1.46E-14	1.45E-44	3.73E-07	4.26E-06	2.35E-07
7	220	3000	9.62E-07	1.07E-03	2.27E-04	1.41E-12	1.41E-15	1.52E-14	1.34E-44	3.91E-07	4.33E-06	1.85E-07
8	220	3000	8.24E-07	1.07E-03	2.54E-04	1.20E-12	1.42E-15	1.73E-14	1.22E-44	4.12E-07	4.42E-06	1.62E-07
9	220	3000	7.46E-07	1.08E-03	2.80E-04	1.12E-12	1.57E-15	2.04E-14	1.10E-44	4.37E-07	4.52E-06	1.50E-07
10	220	3000	6.97E-07	1.08E-03	3.07E-04	1.10E-12	1.83E-15	2.47E-14	9.78E-45	4.67E-07	4.63E-06	1.44E-07
11	220	3000	6.64E-07	1.08E-03	3.34E-04	1.11E-12	2.20E-15	3.05E-14	8.53E-45	5.03E-07	4.76E-06	1.41E-07
12	220	3000	6.41E-07	1.08E-03	3.60E-04	1.14E-12	2.72E-15	3.81E-14	7.28E-45	5.49E-07	4.92E-06	1.40E-07
13	220	3000	6.25E-07	1.09E-03	3.87E-04	1.19E-12	3.45E-15	4.85E-14	6.02E-45	6.07E-07	5.10E-06	1.42E-07
14	220	3000	6.13E-07	1.09E-03	4.14E-04	1.24E-12	4.52E-15	6.34E-14	4.76E-45	6.88E-07	5.33E-06	1.45E-07
15	220	3000	6.04E-07	1.09E-03	4.40E-04	1.30E-12	6.21E-15	8.68E-14	3.50E-45	8.08E-07	5.64E-06	1.52E-07
16	220	3000	5.97E-07	1.10E-03	3.45E-04	1.02E-12	5.07E-15	7.05E-14	2.26E-45	1.01E-06	6.09E-06	1.62E-07
17	220	3000	5.93E-07	1.10E-03	1.50E-04	4.41E-13	1.60E-15	2.20E-14	1.05E-45	1.50E-06	6.96E-06	1.84E-07
18	220	3000	5.91E-07	1.10E-03	2.01E-05	5.96E-14	7.00E-17	9.49E-16	1.49E-46	3.99E-06	8.71E-06	2.29E-07

		Formula:	S2--	S2O3--	SO2	SO3--	HSO3-	SO4--	HSO4-	Na+	NaOH	NaCO3-
		Type:	(a)	(a)	(a)	(a)	(a)	(a)	(a)	(a)	(a)	(a)
Cell	T (°C)	P (bar)	S2--	S2O3--	SO2 (aq)	SO3--	HSO3-	SO4--	HSO4-	Na+	NaOH (aq)	NaCO3-
Ore fluids	500	5000	1.08E-08	5.78E-12	7.01E-11	2.04E-12	1.04E-09	1.33E-08	4.52E-11	1.03E-02	1.84E-03	1.80E-04
1	220	3000	1.92E-13	1.08E-13	2.24E-15	5.40E-14	1.63E-12	1.35E-07	8.34E-11	4.47E-02	8.01E-06	4.74E-04
2	220	3000	8.33E-14	5.32E-14	2.52E-15	2.59E-14	1.25E-12	6.66E-08	6.69E-11	3.12E-02	4.01E-06	1.76E-04
3	220	3000	2.02E-14	1.49E-14	2.87E-15	7.02E-15	7.42E-13	1.84E-08	4.20E-11	1.40E-02	1.05E-06	2.65E-05
4	220	3000	4.01E-15	3.20E-15	3.09E-15	1.48E-15	3.79E-13	3.88E-09	2.22E-11	1.82E-03	7.37E-08	9.33E-07
5	220	3000	6.80E-16	5.35E-16	3.07E-15	2.49E-16	1.51E-13	6.53E-10	8.79E-12	3.13E-06	4.89E-11	2.46E-10
6	220	3000	2.68E-16	1.92E-16	2.84E-15	9.13E-17	8.54E-14	2.35E-10	4.80E-12	2.01E-06	1.80E-11	5.21E-11
7	220	3000	1.65E-16	1.04E-16	2.55E-15	5.09E-17	5.91E-14	1.27E-10	3.18E-12	1.62E-06	1.07E-11	2.19E-11
8	220	3000	1.24E-16	6.77E-17	2.25E-15	3.41E-17	4.46E-14	8.18E-11	2.28E-12	1.39E-06	7.64E-12	1.21E-11
9	220	3000	1.03E-16	4.77E-17	1.96E-15	2.50E-17	3.50E-14	5.70E-11	1.69E-12	1.24E-06	5.95E-12	7.61E-12
10	220	3000	9.08E-17	3.49E-17	1.67E-15	1.90E-17	2.78E-14	4.11E-11	1.26E-12	1.11E-06	4.89E-12	5.14E-12
11	220	3000	8.27E-17	2.57E-17	1.39E-15	1.47E-17	2.20E-14	2.97E-11	9.25E-13	1.02E-06	4.17E-12	3.61E-12
12	220	3000	7.69E-17	1.87E-17	1.12E-15	1.13E-17	1.71E-14	2.11E-11	6.62E-13	9.39E-07	3.64E-12	2.58E-12
13	220	3000	7.23E-17	1.31E-17	8.68E-16	8.44E-18	1.29E-14	1.44E-11	4.51E-13	8.72E-07	3.23E-12	1.83E-12
14	220	3000	6.82E-17	8.62E-18	6.33E-16	6.02E-18	9.17E-15	9.16E-12	2.85E-13	8.15E-07	2.92E-12	1.27E-12
15	220	3000	6.42E-17	5.07E-18	4.19E-16	3.93E-18	5.97E-15	5.14E-12	1.58E-13	7.65E-07	2.66E-12	8.33E-13
16	220	3000	5.95E-17	2.42E-18	2.33E-16	2.17E-18	3.28E-15	2.28E-12	6.97E-14	7.22E-07	2.45E-12	4.86E-13
17	220	3000	5.25E-17	6.68E-19	8.37E-17	7.77E-19	1.16E-15	5.58E-13	1.68E-14	6.83E-07	2.27E-12	2.06E-13
18	220	3000	3.12E-17	2.11E-20	5.60E-18	5.23E-20	7.74E-17	1.42E-14	4.20E-16	6.46E-07	2.12E-12	2.71E-14

		Formula:	NaHCO3	NaSO4-	K+	KOH	KSO4-	KHSO4	Mg ⁺⁺	MgOH+	MgCO3	MgHCO3 +
		Type:	(a)	(a)	(a)	(a)	(a)	(a)	(a)	(a)	(a)	(a)
Cell	T (°C)	P (bar)	NaHCO3 (aq)	NaSO4-	K+	KOH (aq)	KSO4-	KHSO4 (aq)	Mg ⁺⁺	MgOH+	MgCO3 (aq)	MgHCO3 +
Ore fluids	500	5000	2.74E-03	5.07E-09	2.57E-02	2.14E-03	1.59E-07	1.76E-10	9.45E-12	1.39E-10	2.25E-12	1.42E-11
1	220	3000	2.33E-02	1.07E-07	1.00E-03	9.28E-08	1.02E-08	4.55E-13	8.68E-09	1.16E-10	1.57E-09	2.96E-08
2	220	3000	1.27E-02	4.28E-08	1.71E-04	1.15E-08	1.01E-09	6.59E-14	1.06E-08	1.02E-10	1.07E-09	2.85E-08
3	220	3000	3.67E-03	6.96E-09	5.08E-06	2.03E-10	1.11E-11	1.38E-15	1.26E-08	7.24E-11	4.79E-10	2.21E-08
4	220	3000	2.71E-04	2.56E-10	3.14E-09	6.88E-14	1.97E-15	5.17E-19	7.16E-09	2.29E-11	8.55E-11	7.38E-09
5	220	3000	1.78E-07	6.71E-14	2.38E-18	2.00E-23	2.26E-25	1.48E-28	3.71E-10	4.53E-13	6.47E-13	1.44E-10
6	220	3000	6.18E-08	1.35E-14	2.08E-19	9.96E-25	6.12E-27	6.57E-30	5.83E-10	4.05E-13	3.14E-13	1.21E-10
7	220	3000	3.38E-08	5.28E-15	5.92E-20	2.08E-25	8.43E-28	1.18E-30	7.65E-10	3.88E-13	2.05E-13	1.07E-10
8	220	3000	2.19E-08	2.69E-15	2.57E-20	7.45E-26	2.16E-28	3.53E-31	8.95E-10	3.74E-13	1.49E-13	9.36E-11
9	220	3000	1.52E-08	1.54E-15	1.38E-20	3.49E-26	7.45E-29	1.35E-31	9.85E-10	3.60E-13	1.13E-13	8.07E-11
10	220	3000	1.11E-08	9.42E-16	8.37E-21	1.92E-26	3.04E-29	5.93E-32	1.05E-09	3.47E-13	8.80E-14	6.87E-11
11	220	3000	8.18E-09	5.87E-16	5.52E-21	1.18E-26	1.37E-29	2.80E-32	1.09E-09	3.35E-13	6.89E-14	5.75E-11
12	220	3000	6.06E-09	3.65E-16	3.86E-21	7.77E-27	6.42E-30	1.37E-32	1.11E-09	3.23E-13	5.35E-14	4.71E-11
13	220	3000	4.43E-09	2.21E-16	2.82E-21	5.42E-27	3.04E-30	6.66E-33	1.13E-09	3.13E-13	4.09E-14	3.75E-11
14	220	3000	3.14E-09	1.25E-16	2.14E-21	3.95E-27	1.39E-30	3.12E-33	1.13E-09	3.03E-13	3.01E-14	2.85E-11
15	220	3000	2.10E-09	6.33E-17	1.66E-21	2.97E-27	5.81E-31	1.32E-33	1.13E-09	2.93E-13	2.08E-14	2.02E-11
16	220	3000	1.24E-09	2.55E-17	1.32E-21	2.30E-27	1.97E-31	4.55E-34	1.13E-09	2.85E-13	1.27E-14	1.26E-11
17	220	3000	5.31E-10	5.68E-18	1.07E-21	1.83E-27	3.75E-32	8.74E-35	1.12E-09	2.76E-13	5.58E-15	5.64E-12
18	220	3000	7.01E-11	1.32E-19	8.80E-22	1.47E-27	7.54E-34	1.77E-36	1.10E-09	2.68E-13	7.58E-16	7.74E-13

		Formula:	MgSO4	Ca ⁺⁺	CaOH ⁺	CaCO3	CaHCO3 +	CaSO4	Al ⁺⁺⁺	AlOH ⁺⁺	Al(OH)2 ⁺	Al(OH)3
		Type:	(a)	(a)	(a)	(a)	(a)	(a)	(a)	(a)	(a)	(a)
Cell	T (°C)	P (bar)	MgSO4 (aq)	Ca ⁺⁺	CaOH ⁺	CaCO3 (aq)	CaHCO3 +	CaSO4 (aq)	Al ⁺⁺⁺	AlOH ⁺⁺	Al(OH)2 ⁺	Al(OH)3 (aq)
Ore fluids	500	5000	2.26E-16	2.09E-08	1.99E-07	1.74E-07	2.66E-08	1.61E-13	5.22E-26	1.42E-17	7.04E-12	6.25E-07
1	220	3000	4.46E-13	3.43E-06	1.21E-08	4.21E-06	1.13E-05	8.72E-11	9.57E-19	1.86E-14	4.89E-11	3.46E-08
2	220	3000	3.27E-13	5.94E-06	1.57E-08	4.22E-06	1.59E-05	9.39E-11	5.01E-18	6.76E-14	1.39E-10	7.03E-08
3	220	3000	1.58E-13	1.50E-05	2.49E-08	4.23E-06	2.77E-05	1.02E-10	9.02E-17	6.80E-13	9.32E-10	2.73E-07
4	220	3000	2.95E-14	1.85E-05	1.80E-08	1.72E-06	2.11E-05	4.34E-11	7.39E-15	2.94E-11	2.51E-08	3.95E-06
5	220	3000	2.22E-16	2.18E-09	7.94E-13	2.91E-11	9.25E-10	7.29E-16	2.04E-10	3.14E-07	9.88E-05	6.00E-03
6	220	3000	1.02E-16	1.53E-09	3.08E-13	6.13E-12	3.37E-10	1.46E-16	3.08E-09	2.76E-06	4.68E-04	1.64E-02
7	220	3000	6.22E-17	1.32E-09	1.91E-13	2.59E-12	1.92E-10	5.73E-17	1.34E-08	8.99E-06	1.07E-03	2.77E-02
8	220	3000	4.16E-17	1.17E-09	1.38E-13	1.41E-12	1.26E-10	2.87E-17	3.45E-08	1.93E-05	1.83E-03	3.93E-02
9	220	3000	2.89E-17	1.06E-09	1.07E-13	8.65E-13	8.77E-11	1.61E-17	6.71E-08	3.33E-05	2.69E-03	5.08E-02
10	220	3000	2.03E-17	9.59E-10	8.72E-14	5.69E-13	6.31E-11	9.55E-18	1.11E-07	5.07E-05	3.62E-03	6.23E-02
11	220	3000	1.41E-17	8.76E-10	7.32E-14	3.87E-13	4.59E-11	5.78E-18	1.64E-07	7.08E-05	4.59E-03	7.38E-02
12	220	3000	9.55E-18	8.04E-10	6.28E-14	2.68E-13	3.34E-11	3.48E-18	2.27E-07	9.35E-05	5.59E-03	8.53E-02
13	220	3000	6.19E-18	7.42E-10	5.48E-14	1.84E-13	2.40E-11	2.04E-18	2.97E-07	1.18E-04	6.61E-03	9.66E-02
14	220	3000	3.73E-18	6.87E-10	4.85E-14	1.24E-13	1.67E-11	1.12E-18	3.74E-07	1.45E-04	7.64E-03	1.08E-01
15	220	3000	1.98E-18	6.39E-10	4.33E-14	7.89E-14	1.09E-11	5.50E-19	4.56E-07	1.73E-04	8.68E-03	1.19E-01
16	220	3000	8.37E-19	5.96E-10	3.91E-14	4.47E-14	6.31E-12	2.15E-19	5.42E-07	2.02E-04	9.73E-03	1.31E-01
17	220	3000	1.93E-19	5.57E-10	3.55E-14	1.84E-14	2.64E-12	4.66E-20	6.30E-07	2.32E-04	1.08E-02	1.42E-01
18	220	3000	4.64E-21	5.19E-10	3.23E-14	2.35E-15	3.41E-13	1.05E-21	7.16E-07	2.62E-04	1.18E-02	1.53E-01

		Formula:	Al(OH) ₄ ⁻	Zn ⁺⁺	ZnOH ⁺	Zn(OH) ₂	ZnHCO ₃ ⁺	Zn(HS) ₂	Au ⁺	AuOH	Au(OH) ₂ ⁻	AuHS
		Type:	(a)	(a)	(a)	(a)	(a)	(a)	(a)	(a)	(a)	(a)
Cell	T (°C)	P (bar)	Al(OH) ₄ ⁻	Zn ⁺⁺	ZnOH ⁺	Zn(OH) ₂ (aq)	ZnHCO ₃ ⁺	Zn(HS) ₂ (aq)	Au ⁺	AuOH (aq)	Au(OH) ₂ ⁻	AuHS (aq)
Ore fluids	500	5000	1.05E-04	0	0	0	0	0	4.03E-16	2.35E-08	2.91E-07	2.35E-07
1	220	3000	6.23E-07	1.89E-11	2.68E-09	1.98E-10	1.40E-10	1.26E-09	1.69E-21	2.86E-13	4.12E-13	7.61E-11
2	220	3000	8.64E-07	3.60E-11	3.84E-09	2.03E-10	2.19E-10	1.25E-09	2.43E-21	2.94E-13	2.89E-13	7.71E-11
3	220	3000	1.76E-06	1.02E-10	6.80E-09	2.08E-10	4.26E-10	1.24E-09	4.32E-21	3.02E-13	1.57E-13	7.81E-11
4	220	3000	1.22E-05	3.29E-10	1.29E-08	2.11E-10	8.49E-10	1.24E-09	8.19E-21	3.08E-13	7.63E-14	7.89E-11
5	220	3000	7.44E-03	2.27E-09	3.34E-08	2.12E-10	2.18E-09	1.25E-09	2.12E-20	3.09E-13	3.07E-14	7.92E-11
6	220	3000	1.24E-02	7.07E-09	5.75E-08	2.10E-10	3.54E-09	1.26E-09	3.65E-20	3.05E-13	1.85E-14	7.91E-11
7	220	3000	1.61E-02	1.32E-08	7.70E-08	2.08E-10	4.36E-09	1.29E-09	4.85E-20	3.00E-13	1.39E-14	7.89E-11
8	220	3000	1.94E-02	1.94E-08	9.18E-08	2.06E-10	4.71E-09	1.31E-09	5.74E-20	2.95E-13	1.17E-14	7.87E-11
9	220	3000	2.26E-02	2.51E-08	1.03E-07	2.03E-10	4.72E-09	1.34E-09	6.37E-20	2.88E-13	1.03E-14	7.83E-11
10	220	3000	2.58E-02	3.02E-08	1.11E-07	2.00E-10	4.50E-09	1.38E-09	6.80E-20	2.81E-13	9.31E-15	7.79E-11
11	220	3000	2.90E-02	3.45E-08	1.16E-07	1.96E-10	4.10E-09	1.41E-09	7.06E-20	2.72E-13	8.57E-15	7.73E-11
12	220	3000	3.22E-02	3.80E-08	1.20E-07	1.91E-10	3.58E-09	1.46E-09	7.18E-20	2.62E-13	7.94E-15	7.66E-11
13	220	3000	3.55E-02	4.08E-08	1.22E-07	1.86E-10	2.99E-09	1.51E-09	7.17E-20	2.51E-13	7.37E-15	7.58E-11
14	220	3000	3.87E-02	4.26E-08	1.21E-07	1.79E-10	2.35E-09	1.58E-09	7.02E-20	2.37E-13	6.82E-15	7.46E-11
15	220	3000	4.20E-02	4.34E-08	1.19E-07	1.71E-10	1.68E-09	1.67E-09	6.71E-20	2.21E-13	6.22E-15	7.30E-11
16	220	3000	4.53E-02	4.29E-08	1.13E-07	1.59E-10	1.03E-09	1.81E-09	6.17E-20	1.98E-13	5.51E-15	7.07E-11
17	220	3000	4.86E-02	3.96E-08	1.02E-07	1.41E-10	4.27E-10	2.07E-09	5.20E-20	1.64E-13	4.51E-15	6.66E-11
18	220	3000	5.21E-02	3.31E-08	8.30E-08	1.13E-10	4.93E-11	2.59E-09	3.25E-20	1.01E-13	2.76E-15	5.12E-11

		Formula:	Au(HS)2-	Au ₂ (HS) 2S ⁻⁻	Au ⁺⁺⁺	Mn ⁺⁺	MnOH ⁺	MnHCO ₃ +	MnSO ₄	MnO ₄ ⁻	MnO ₄ ⁻⁻	Fe ⁺⁺
		Type:	(a)	(a)	(a)	(a)	(a)	(a)	(a)	(a)	(a)	(a)
Cell	T (°C)	P (bar)	Au(HS)2-	Au ₂ (HS) 2S ⁻⁻	Au ⁺⁺⁺	Mn ⁺⁺	MnOH ⁺	MnHCO ₃ +	MnSO ₄ (aq)	MnO ₄ ⁻	MnO ₄ ⁻⁻	Fe ⁺⁺
Ore fluids	500	5000	7.76E-06	3.58E-08	2.68E-53	2.68E-05	3.68E-03	3.84E-04	1.99E-10	2.09E-30	7.83E-27	7.42E-12
1	220	3000	1.85E-10	7.47E-14	9.22E-62	3.90E-04	4.45E-05	4.50E-03	2.51E-08	1.58E-53	1.14E-46	9.16E-08
2	220	3000	1.26E-10	3.21E-14	2.13E-61	5.50E-04	4.70E-05	5.18E-03	2.21E-08	8.93E-54	3.97E-47	1.70E-07
3	220	3000	6.63E-11	7.72E-15	7.91E-61	8.79E-04	4.71E-05	5.70E-03	1.51E-08	2.99E-54	5.98E-48	4.66E-07
4	220	3000	3.17E-11	1.53E-15	3.47E-60	1.48E-03	4.66E-05	5.94E-03	8.81E-09	7.94E-55	6.55E-49	1.48E-06
5	220	3000	1.28E-11	2.59E-16	6.89E-59	3.32E-03	3.92E-05	4.95E-03	2.82E-09	1.03E-55	3.56E-50	1.03E-05
6	220	3000	7.85E-12	1.03E-16	4.21E-58	5.14E-03	3.35E-05	3.99E-03	1.24E-09	2.89E-56	6.57E-51	3.26E-05
7	220	3000	6.09E-12	6.41E-17	1.14E-57	6.60E-03	3.09E-05	3.38E-03	7.28E-10	1.37E-56	2.56E-51	6.24E-05
8	220	3000	5.27E-12	4.89E-17	2.09E-57	7.86E-03	2.99E-05	2.96E-03	4.88E-10	8.34E-57	1.41E-51	9.48E-05
9	220	3000	4.81E-12	4.13E-17	3.13E-57	9.04E-03	2.97E-05	2.64E-03	3.49E-10	5.76E-57	9.34E-52	1.27E-04
10	220	3000	4.55E-12	3.71E-17	4.12E-57	1.02E-02	2.99E-05	2.35E-03	2.57E-10	4.25E-57	6.80E-52	1.60E-04
11	220	3000	4.39E-12	3.46E-17	4.95E-57	1.13E-02	3.05E-05	2.08E-03	1.89E-10	3.23E-57	5.22E-52	1.91E-04
12	220	3000	4.30E-12	3.30E-17	5.56E-57	1.24E-02	3.14E-05	1.81E-03	1.36E-10	2.48E-57	4.10E-52	2.23E-04
13	220	3000	4.26E-12	3.20E-17	5.86E-57	1.35E-02	3.23E-05	1.54E-03	9.41E-11	1.87E-57	3.23E-52	2.55E-04
14	220	3000	4.26E-12	3.14E-17	5.80E-57	1.46E-02	3.35E-05	1.25E-03	6.06E-11	1.36E-57	2.48E-52	2.88E-04
15	220	3000	4.32E-12	3.11E-17	5.31E-57	1.58E-02	3.47E-05	9.47E-04	3.45E-11	9.14E-58	1.81E-52	3.26E-04
16	220	3000	4.43E-12	3.10E-17	4.33E-57	1.70E-02	3.60E-05	6.32E-04	1.55E-11	5.27E-58	1.17E-52	3.73E-04
17	220	3000	4.70E-12	3.10E-17	2.71E-57	1.81E-02	3.74E-05	3.03E-04	3.85E-12	2.03E-58	5.51E-53	4.47E-04
18	220	3000	4.48E-12	2.29E-17	6.88E-58	1.92E-02	3.87E-05	4.44E-05	9.87E-14	1.80E-59	8.05E-54	6.44E-04

		Formula:	FeOH+	Fe(OH)2	Fe(OH)3-	FeSO4	Fe+++	FeOH++	Fe(OH)2+	Fe(OH)3	Fe(OH)4-	CH4
		Type:	(a)	(a)	(a)	(a)	(a)	(a)	(a)	(a)	(a)	(a)
Cell	T (°C)	P (bar)	FeOH+	Fe(OH)2 (aq)	Fe(OH)3-	FeSO4 (aq)	Fe+++	FeOH++	Fe(OH)2+	Fe(OH)3 (aq)	Fe(OH)4-	CH4 (aq)
Ore fluids	500	5000	4.05E-09	4.36E-07	4.67E-07	2.45E-15	2.26E-26	1.43E-18	1.05E-11	1.07E-07	3.00E-07	1.21E-01
1	220	3000	5.92E-08	5.06E-09	1.49E-11	1.39E-11	2.32E-21	3.31E-16	6.76E-12	3.77E-09	3.76E-11	1.54E-05
2	220	3000	8.24E-08	5.02E-09	1.01E-11	1.60E-11	5.07E-21	6.05E-16	9.64E-12	3.84E-09	2.62E-11	1.43E-05
3	220	3000	1.41E-07	4.99E-09	5.28E-12	1.88E-11	1.76E-20	1.60E-15	1.70E-11	3.91E-09	1.41E-11	1.32E-05
4	220	3000	2.63E-07	4.98E-09	2.52E-12	2.06E-11	7.47E-20	4.84E-15	3.20E-11	3.96E-09	6.81E-12	1.27E-05
5	220	3000	6.84E-07	5.01E-09	1.02E-12	2.04E-11	1.49E-18	3.41E-14	8.32E-11	3.97E-09	2.74E-12	1.28E-05
6	220	3000	1.20E-06	5.08E-09	6.27E-13	1.85E-11	9.49E-18	1.10E-13	1.44E-10	3.97E-09	1.66E-12	1.37E-05
7	220	3000	1.66E-06	5.17E-09	4.90E-13	1.62E-11	2.71E-17	2.10E-13	1.94E-10	3.95E-09	1.27E-12	1.49E-05
8	220	3000	2.04E-06	5.27E-09	4.26E-13	1.38E-11	5.32E-17	3.17E-13	2.33E-10	3.93E-09	1.08E-12	1.65E-05
9	220	3000	2.37E-06	5.39E-09	3.93E-13	1.16E-11	8.57E-17	4.20E-13	2.63E-10	3.91E-09	9.67E-13	1.84E-05
10	220	3000	2.66E-06	5.53E-09	3.75E-13	9.47E-12	1.23E-16	5.17E-13	2.86E-10	3.88E-09	8.94E-13	2.09E-05
11	220	3000	2.93E-06	5.68E-09	3.66E-13	7.51E-12	1.62E-16	6.05E-13	3.04E-10	3.85E-09	8.41E-13	2.42E-05
12	220	3000	3.19E-06	5.87E-09	3.63E-13	5.74E-12	2.03E-16	6.84E-13	3.17E-10	3.81E-09	8.00E-13	2.86E-05
13	220	3000	3.45E-06	6.08E-09	3.65E-13	4.17E-12	2.43E-16	7.53E-13	3.27E-10	3.76E-09	7.67E-13	3.48E-05
14	220	3000	3.73E-06	6.36E-09	3.73E-13	2.81E-12	2.83E-16	8.12E-13	3.33E-10	3.70E-09	7.36E-13	4.44E-05
15	220	3000	4.06E-06	6.73E-09	3.87E-13	1.67E-12	3.19E-16	8.57E-13	3.34E-10	3.62E-09	7.07E-13	6.09E-05
16	220	3000	4.49E-06	7.27E-09	4.12E-13	8.05E-13	3.50E-16	8.85E-13	3.31E-10	3.50E-09	6.73E-13	9.51E-05
17	220	3000	5.22E-06	8.30E-09	4.66E-13	2.23E-13	3.67E-16	8.80E-13	3.17E-10	3.29E-09	6.26E-13	2.07E-04
18	220	3000	7.35E-06	1.15E-08	6.43E-13	7.77E-15	3.43E-16	7.84E-13	2.73E-10	2.80E-09	5.30E-13	1.46E-03

		Formula:	C2H6	HCOOH	HCOO-	CH3COO H	CH3COO -		
		Type:	(a)	(a)	(a)	(a)	(a)		
Cell	T (°C)	P (bar)	C2H6 (aq)	HCOOH (aq)	HCOO-	CH3COO H (aq)	CH3COO -	pH	Eh(V)
Ore fluids	500	5000	1.89E-05	9.63E-06	2.36E-03	9.02E-07	9.99E-06	6.950431	-1.167
1	220	3000	1.21E-11	1.30E-07	2.08E-05	1.89E-09	2.97E-08	6.010465	-0.5005
2	220	3000	1.08E-11	1.37E-07	1.49E-05	1.91E-09	2.05E-08	5.852578	-0.48426
3	220	3000	9.57E-12	1.45E-07	8.23E-06	1.94E-09	1.09E-08	5.591594	-0.45784
4	220	3000	8.97E-12	1.49E-07	4.05E-06	1.96E-09	5.23E-09	5.294736	-0.42832
5	220	3000	9.11E-12	1.49E-07	1.63E-06	1.97E-09	2.11E-09	4.890136	-0.3888
6	220	3000	1.00E-11	1.45E-07	9.64E-07	1.97E-09	1.29E-09	4.663309	-0.36723
7	220	3000	1.14E-11	1.40E-07	7.13E-07	1.98E-09	9.90E-10	4.540809	-0.3561
8	220	3000	1.32E-11	1.34E-07	5.83E-07	1.98E-09	8.48E-10	4.466269	-0.34981
9	220	3000	1.55E-11	1.27E-07	5.00E-07	1.99E-09	7.68E-10	4.416743	-0.34611
10	220	3000	1.87E-11	1.20E-07	4.39E-07	1.99E-09	7.17E-10	4.381798	-0.34398
11	220	3000	2.32E-11	1.12E-07	3.91E-07	2.00E-09	6.83E-10	4.356073	-0.34294
12	220	3000	2.98E-11	1.04E-07	3.48E-07	2.00E-09	6.60E-10	4.336547	-0.34275
13	220	3000	3.99E-11	9.45E-08	3.08E-07	2.01E-09	6.43E-10	4.321393	-0.34331
14	220	3000	5.73E-11	8.42E-08	2.68E-07	2.01E-09	6.30E-10	4.309454	-0.34467
15	220	3000	9.19E-11	7.22E-08	2.26E-07	2.02E-09	6.21E-10	4.299974	-0.34704
16	220	3000	1.79E-10	5.81E-08	1.80E-07	2.02E-09	6.15E-10	4.292413	-0.35098
17	220	3000	5.71E-10	3.96E-08	1.21E-07	2.03E-09	6.10E-10	4.28663	-0.3586
18	220	3000	1.07E-08	1.50E-08	4.56E-08	2.03E-09	6.08E-10	4.283154	-0.37898

Notes s: solid; a: aqueous solution; f:r, fluid:rock; the unit is mol.

(2) Results of 10 fluid infiltration increments with instantaneous f:r = 0.1 (by mass).

		Formula:	Au	C	SiO2	Fe3O4	FeS2	Fe.877S	ZnS	FeAsS	CaCO3	KAl3Si3O10(OH)2
		Type:	(s)	(s)	(s)	(s)	(s)	(s)	(s)	(s)	(s)	(s)
Cell	T (°C)	P (bar)	Gold	Graphite	Quartz	Magnetite	Pyrite	Pyrrhotite	Sphalerite	Arsenopyrite	Calcite	Muscovite
Ore fluids	500	5000	0	0	0	0	0	0	0	0	0	0
1	220	3000	0	0	1.02E-02	8.65E-02	5.31E-01	1.01E-08	1.46E-06	2.09E-05	6.08E-03	6.97E-03
2	220	3000	0	0	1.02E-02	1.52E-01	5.31E-01	1.01E-08	1.46E-06	2.09E-05	6.08E-03	6.97E-03
3	220	3000	0	0	1.02E-02	1.52E-01	5.31E-01	1.01E-08	1.46E-06	2.09E-05	6.08E-03	6.97E-03
4	220	3000	0	0	1.02E-02	1.52E-01	5.31E-01	1.01E-08	1.46E-06	2.09E-05	6.08E-03	6.97E-03
5	220	3000	0	0	1.02E-02	1.52E-01	5.31E-01	1.01E-08	1.46E-06	2.09E-05	6.08E-03	6.97E-03
6	220	3000	0	0	1.02E-02	1.52E-01	5.31E-01	1.01E-08	1.46E-06	2.09E-05	6.08E-03	6.97E-03
7	220	3000	0	0	1.02E-02	1.52E-01	5.33E-01	1.15E-08	1.26E-06	1.43E-05	5.05E-03	6.70E-03
8	220	3000	0	2.05E-03	1.02E-02	1.49E-01	5.34E-01	7.20E-08	1.57E-07	2.31E-07	9.35E-04	9.74E-03
9	220	3000	3.54E-03	2.03E-04	1.02E-02	1.42E-01	5.34E-01	8.40E-08	1.31E-07	1.61E-07	7.98E-04	9.89E-03
10	220	3000	3.71E-03	3.44E-05	1.02E-02	1.42E-01	5.34E-01	8.40E-08	1.31E-07	1.61E-07	7.98E-04	9.89E-03
11	220	3000	3.71E-03	3.74E-05	1.02E-02	1.42E-01	5.34E-01	8.40E-08	1.31E-07	1.61E-07	7.98E-04	9.89E-03
12	220	3000	3.70E-03	4.27E-05	1.02E-02	1.42E-01	5.34E-01	8.40E-08	1.31E-07	1.61E-07	7.98E-04	9.89E-03
13	220	3000	3.70E-03	4.82E-05	1.02E-02	1.42E-01	5.34E-01	8.40E-08	1.31E-07	1.61E-07	7.98E-04	9.89E-03
14	220	3000	3.72E-03	2.59E-05	1.02E-02	1.42E-01	5.34E-01	8.40E-08	1.31E-07	1.61E-07	7.98E-04	9.89E-03
15	220	3000	3.72E-03	2.67E-05	1.02E-02	1.42E-01	5.34E-01	8.40E-08	1.31E-07	1.61E-07	7.98E-04	9.89E-03
16	220	3000	3.72E-03	2.75E-05	1.02E-02	1.42E-01	5.34E-01	8.40E-08	1.31E-07	1.61E-07	7.98E-04	9.89E-03
17	220	3000	3.72E-03	2.85E-05	1.02E-02	1.42E-01	5.34E-01	8.40E-08	1.31E-07	1.61E-07	7.98E-04	9.89E-03
18	220	3000	3.72E-03	2.97E-05	1.02E-02	1.42E-01	5.34E-01	8.40E-08	1.31E-07	1.61E-07	7.98E-04	9.89E-03

		Formula:	H3SiO4-	H4SiO4	H3AsO3	HAsO3--	As2S4--	HAs2S4-	O2	H2	H2S	HS-
		Type:	(a)	(a)	(a)	(a)	(a)	(a)	(a)	(a)	(a)	(a)
Cell	T (°C)	P (bar)	H3SiO4-	H4SiO4 (aq)	H3AsO3 (aq)	HAsO3--	As2S4--	HAs2S4-	O2 (aq)	H2 (aq)	H2S (aq)	HS-
Ore fluids	500	5000	1.82E-03	1.17E-03	4.00E-06	2.95E-09	1.18E-09	1.62E-11	3.31E-29	4.77E-04	6.95E-04	7.07E-04
1	220	3000	3.68E-06	1.01E-04	4.00E-06	5.41E-11	1.11E-14	2.24E-15	1.14E-45	4.01E-08	4.25E-07	7.59E-07
2	220	3000	3.68E-06	1.01E-04	4.00E-06	5.41E-11	1.11E-14	2.24E-15	1.14E-45	4.01E-08	4.25E-07	7.59E-07
3	220	3000	3.68E-06	1.01E-04	4.00E-06	5.41E-11	1.11E-14	2.24E-15	1.14E-45	4.01E-08	4.25E-07	7.59E-07
4	220	3000	3.68E-06	1.01E-04	4.00E-06	5.41E-11	1.11E-14	2.24E-15	1.14E-45	4.01E-08	4.25E-07	7.59E-07
5	220	3000	3.68E-06	1.01E-04	4.00E-06	5.41E-11	1.11E-14	2.24E-15	1.14E-45	4.01E-08	4.25E-07	7.59E-07
6	220	3000	3.68E-06	1.01E-04	4.00E-06	5.41E-11	1.11E-14	2.24E-15	1.14E-45	4.01E-08	4.25E-07	7.59E-07
7	220	3000	3.22E-06	1.02E-04	4.00E-06	3.83E-11	7.98E-15	1.98E-15	1.08E-45	4.11E-08	4.29E-07	6.59E-07
8	220	3000	4.25E-07	1.03E-04	4.00E-06	4.28E-13	6.84E-17	1.98E-16	1.55E-45	3.42E-08	4.04E-07	7.73E-08
9	220	3000	3.57E-07	1.03E-04	4.00E-06	2.93E-13	4.64E-17	1.64E-16	1.58E-45	3.39E-08	4.03E-07	6.47E-08
10	220	3000	3.57E-07	1.03E-04	4.00E-06	2.93E-13	4.64E-17	1.64E-16	1.58E-45	3.39E-08	4.03E-07	6.47E-08
11	220	3000	3.57E-07	1.03E-04	4.00E-06	2.93E-13	4.64E-17	1.64E-16	1.58E-45	3.39E-08	4.03E-07	6.47E-08
12	220	3000	3.57E-07	1.03E-04	4.00E-06	2.93E-13	4.64E-17	1.64E-16	1.58E-45	3.39E-08	4.03E-07	6.47E-08
13	220	3000	3.57E-07	1.03E-04	4.00E-06	2.93E-13	4.64E-17	1.64E-16	1.58E-45	3.39E-08	4.03E-07	6.47E-08
14	220	3000	3.57E-07	1.03E-04	4.00E-06	2.93E-13	4.64E-17	1.64E-16	1.58E-45	3.39E-08	4.03E-07	6.47E-08
15	220	3000	3.57E-07	1.03E-04	4.00E-06	2.93E-13	4.64E-17	1.64E-16	1.58E-45	3.39E-08	4.03E-07	6.47E-08
16	220	3000	3.57E-07	1.03E-04	4.00E-06	2.93E-13	4.64E-17	1.64E-16	1.58E-45	3.39E-08	4.03E-07	6.47E-08
17	220	3000	3.57E-07	1.03E-04	4.00E-06	2.93E-13	4.64E-17	1.64E-16	1.58E-45	3.39E-08	4.03E-07	6.47E-08
18	220	3000	3.57E-07	1.03E-04	4.00E-06	2.93E-13	4.64E-17	1.64E-16	1.58E-45	3.39E-08	4.03E-07	6.47E-08

		Formula:	S2--	S2O3--	SO2	SO3--	HSO3-	SO4--	HSO4-	Na+	NaOH	NaCO3-
		Type:	(a)	(a)	(a)	(a)	(a)	(a)	(a)	(a)	(a)	(a)
Cell	T (°C)	P (bar)	S2--	S2O3--	SO2 (aq)	SO3--	HSO3-	SO4--	HSO4-	Na+	NaOH (aq)	NaCO3-
Ore fluids	500	5000	1.08E-09	5.78E-13	7.01E-12	2.04E-13	1.04E-10	1.33E-09	4.52E-12	1.03E-03	1.84E-04	1.80E-05
1	220	3000	3.34E-14	1.71E-14	2.06E-16	8.76E-15	1.94E-13	2.16E-08	9.56E-12	5.48E-03	1.23E-06	8.86E-05
2	220	3000	3.34E-14	1.71E-14	2.06E-16	8.76E-15	1.94E-13	2.16E-08	9.56E-12	5.48E-03	1.23E-06	8.86E-05
3	220	3000	3.34E-14	1.71E-14	2.06E-16	8.76E-15	1.94E-13	2.16E-08	9.56E-12	5.48E-03	1.23E-06	8.86E-05
4	220	3000	3.34E-14	1.71E-14	2.06E-16	8.76E-15	1.94E-13	2.16E-08	9.56E-12	5.48E-03	1.23E-06	8.86E-05
5	220	3000	3.34E-14	1.71E-14	2.06E-16	8.76E-15	1.94E-13	2.16E-08	9.56E-12	5.48E-03	1.23E-06	8.86E-05
6	220	3000	3.34E-14	1.71E-14	2.06E-16	8.76E-15	1.94E-13	2.16E-08	9.56E-12	5.48E-03	1.23E-06	8.86E-05
7	220	3000	2.36E-14	1.13E-14	1.94E-16	5.89E-15	1.58E-13	1.40E-08	7.69E-12	4.56E-03	9.15E-07	5.47E-05
8	220	3000	2.81E-16	2.36E-16	3.15E-16	1.08E-16	3.32E-14	2.86E-10	1.98E-12	4.26E-04	1.53E-08	1.73E-07
9	220	3000	1.93E-16	1.66E-16	3.22E-16	7.56E-17	2.85E-14	2.01E-10	1.71E-12	2.85E-04	8.85E-09	8.52E-08
10	220	3000	1.93E-16	1.66E-16	3.22E-16	7.56E-17	2.85E-14	2.01E-10	1.71E-12	2.85E-04	8.85E-09	8.52E-08
11	220	3000	1.93E-16	1.66E-16	3.22E-16	7.56E-17	2.85E-14	2.01E-10	1.71E-12	2.85E-04	8.85E-09	8.52E-08
12	220	3000	1.93E-16	1.66E-16	3.22E-16	7.56E-17	2.85E-14	2.01E-10	1.71E-12	2.85E-04	8.85E-09	8.52E-08
13	220	3000	1.93E-16	1.66E-16	3.22E-16	7.56E-17	2.85E-14	2.01E-10	1.71E-12	2.85E-04	8.85E-09	8.52E-08
14	220	3000	1.93E-16	1.66E-16	3.22E-16	7.56E-17	2.85E-14	2.01E-10	1.71E-12	2.85E-04	8.85E-09	8.52E-08
15	220	3000	1.93E-16	1.66E-16	3.22E-16	7.56E-17	2.85E-14	2.01E-10	1.71E-12	2.85E-04	8.85E-09	8.52E-08
16	220	3000	1.93E-16	1.66E-16	3.22E-16	7.56E-17	2.85E-14	2.01E-10	1.71E-12	2.85E-04	8.85E-09	8.52E-08
17	220	3000	1.93E-16	1.66E-16	3.22E-16	7.56E-17	2.85E-14	2.01E-10	1.71E-12	2.85E-04	8.85E-09	8.52E-08
18	220	3000	1.93E-16	1.66E-16	3.22E-16	7.56E-17	2.85E-14	2.01E-10	1.71E-12	2.85E-04	8.85E-09	8.52E-08

		Formula:	NaHCO3	NaSO4-	K+	KOH	KSO4-	KHSO4	Mg ⁺⁺	MgOH+	MgCO3	MgHCO3 +
		Type:	(a)	(a)	(a)	(a)	(a)	(a)	(a)	(a)	(a)	(a)
Cell	T (°C)	P (bar)	NaHCO3 (aq)	NaSO4-	K+	KOH (aq)	KSO4-	KHSO4 (aq)	Mg ⁺⁺	MgOH+	MgCO3 (aq)	MgHCO3 +
Ore fluids	500	5000	2.74E-04	5.07E-10	2.57E-03	2.14E-04	1.59E-08	1.76E-11	9.45E-13	1.39E-11	2.25E-13	1.42E-12
1	220	3000	3.37E-03	1.90E-08	2.98E-04	3.42E-08	4.35E-09	1.50E-13	7.41E-10	1.23E-11	1.98E-10	2.95E-09
2	220	3000	3.37E-03	1.90E-08	2.98E-04	3.42E-08	4.35E-09	1.50E-13	7.41E-10	1.23E-11	1.98E-10	2.95E-09
3	220	3000	3.37E-03	1.90E-08	2.98E-04	3.42E-08	4.35E-09	1.50E-13	7.41E-10	1.23E-11	1.98E-10	2.95E-09
4	220	3000	3.37E-03	1.90E-08	2.98E-04	3.42E-08	4.35E-09	1.50E-13	7.41E-10	1.23E-11	1.98E-10	2.95E-09
5	220	3000	3.37E-03	1.90E-08	2.98E-04	3.42E-08	4.35E-09	1.50E-13	7.41E-10	1.23E-11	1.98E-10	2.95E-09
6	220	3000	3.37E-03	1.90E-08	2.98E-04	3.42E-08	4.35E-09	1.50E-13	7.41E-10	1.23E-11	1.98E-10	2.95E-09
7	220	3000	2.40E-03	1.13E-08	1.35E-04	1.39E-08	1.42E-09	5.66E-14	7.56E-10	1.13E-11	1.54E-10	2.60E-09
8	220	3000	5.84E-05	4.89E-11	3.35E-09	6.55E-14	1.72E-15	5.25E-19	1.46E-09	4.18E-12	1.43E-11	1.39E-09
9	220	3000	3.43E-05	2.44E-11	7.46E-10	1.26E-14	2.86E-16	1.04E-19	1.35E-09	3.36E-12	1.01E-11	1.14E-09
10	220	3000	3.43E-05	2.44E-11	7.46E-10	1.26E-14	2.86E-16	1.04E-19	1.35E-09	3.36E-12	1.01E-11	1.14E-09
11	220	3000	3.43E-05	2.44E-11	7.46E-10	1.26E-14	2.86E-16	1.04E-19	1.35E-09	3.36E-12	1.01E-11	1.14E-09
12	220	3000	3.43E-05	2.44E-11	7.46E-10	1.26E-14	2.86E-16	1.04E-19	1.35E-09	3.36E-12	1.01E-11	1.14E-09
13	220	3000	3.43E-05	2.44E-11	7.46E-10	1.26E-14	2.86E-16	1.04E-19	1.35E-09	3.36E-12	1.01E-11	1.14E-09
14	220	3000	3.43E-05	2.44E-11	7.46E-10	1.26E-14	2.86E-16	1.04E-19	1.35E-09	3.36E-12	1.01E-11	1.14E-09
15	220	3000	3.43E-05	2.44E-11	7.46E-10	1.26E-14	2.86E-16	1.04E-19	1.35E-09	3.36E-12	1.01E-11	1.14E-09
16	220	3000	3.43E-05	2.44E-11	7.46E-10	1.26E-14	2.86E-16	1.04E-19	1.35E-09	3.36E-12	1.01E-11	1.14E-09
17	220	3000	3.43E-05	2.44E-11	7.46E-10	1.26E-14	2.86E-16	1.04E-19	1.35E-09	3.36E-12	1.01E-11	1.14E-09
18	220	3000	3.43E-05	2.44E-11	7.46E-10	1.26E-14	2.86E-16	1.04E-19	1.35E-09	3.36E-12	1.01E-11	1.14E-09

		Formula:	MgSO4	Ca ⁺⁺	CaOH ⁺	CaCO3	CaHCO3 ⁺	CaSO4	Al ⁺⁺⁺	AlOH ⁺⁺	Al(OH)2 ⁺	Al(OH)3
		Type:	(a)	(a)	(a)	(a)	(a)	(a)	(a)	(a)	(a)	(a)
Cell	T (°C)	P (bar)	MgSO4 (aq)	Ca ⁺⁺	CaOH ⁺	CaCO3 (aq)	CaHCO3 ⁺	CaSO4 (aq)	Al ⁺⁺⁺	AlOH ⁺⁺	Al(OH)2 ⁺	Al(OH)3 (aq)
Ore fluids	500	5000	2.26E-17	2.09E-09	1.99E-08	1.74E-08	2.66E-09	1.61E-14	5.22E-27	1.42E-18	7.04E-13	6.25E-08
1	220	3000	5.34E-14	2.37E-07	1.02E-09	4.19E-07	8.91E-07	8.27E-12	3.23E-20	8.00E-16	2.50E-12	2.22E-09
2	220	3000	5.34E-14	2.37E-07	1.02E-09	4.19E-07	8.91E-07	8.27E-12	3.23E-20	8.00E-16	2.50E-12	2.22E-09
3	220	3000	5.34E-14	2.37E-07	1.02E-09	4.19E-07	8.91E-07	8.27E-12	3.23E-20	8.00E-16	2.50E-12	2.22E-09
4	220	3000	5.34E-14	2.37E-07	1.02E-09	4.19E-07	8.91E-07	8.27E-12	3.23E-20	8.00E-16	2.50E-12	2.22E-09
5	220	3000	5.34E-14	2.37E-07	1.02E-09	4.19E-07	8.91E-07	8.27E-12	3.23E-20	8.00E-16	2.50E-12	2.22E-09
6	220	3000	5.34E-14	2.37E-07	1.02E-09	4.19E-07	8.91E-07	8.27E-12	3.23E-20	8.00E-16	2.50E-12	2.22E-09
7	220	3000	4.02E-14	3.03E-07	1.19E-09	4.18E-07	1.00E-06	7.96E-12	5.94E-20	1.29E-15	3.79E-12	3.00E-09
8	220	3000	5.09E-15	5.34E-06	4.69E-09	4.13E-07	5.71E-06	1.07E-11	4.67E-16	1.65E-12	1.29E-09	1.80E-07
9	220	3000	3.63E-15	4.06E-06	3.14E-09	2.42E-07	3.88E-06	6.36E-12	1.22E-15	3.71E-12	2.59E-09	3.11E-07
10	220	3000	3.63E-15	4.06E-06	3.14E-09	2.42E-07	3.88E-06	6.36E-12	1.22E-15	3.71E-12	2.59E-09	3.11E-07
11	220	3000	3.63E-15	4.06E-06	3.14E-09	2.42E-07	3.88E-06	6.36E-12	1.22E-15	3.71E-12	2.59E-09	3.11E-07
12	220	3000	3.63E-15	4.06E-06	3.14E-09	2.42E-07	3.88E-06	6.36E-12	1.22E-15	3.71E-12	2.59E-09	3.11E-07
13	220	3000	3.63E-15	4.06E-06	3.14E-09	2.42E-07	3.88E-06	6.36E-12	1.22E-15	3.71E-12	2.59E-09	3.11E-07
14	220	3000	3.63E-15	4.06E-06	3.14E-09	2.42E-07	3.88E-06	6.36E-12	1.22E-15	3.71E-12	2.59E-09	3.11E-07
15	220	3000	3.63E-15	4.06E-06	3.14E-09	2.42E-07	3.88E-06	6.36E-12	1.22E-15	3.71E-12	2.59E-09	3.11E-07
16	220	3000	3.63E-15	4.06E-06	3.14E-09	2.42E-07	3.88E-06	6.36E-12	1.22E-15	3.71E-12	2.59E-09	3.11E-07
17	220	3000	3.63E-15	4.06E-06	3.14E-09	2.42E-07	3.88E-06	6.36E-12	1.22E-15	3.71E-12	2.59E-09	3.11E-07
18	220	3000	3.63E-15	4.06E-06	3.14E-09	2.42E-07	3.88E-06	6.36E-12	1.22E-15	3.71E-12	2.59E-09	3.11E-07

		Formula:	Al(OH) ₄ ⁻	Zn ⁺⁺	ZnOH ⁺	Zn(OH) ₂	ZnHCO ₃ ⁺	Zn(HS) ₂	Au ⁺	AuOH	Au(OH) ₂ ⁻	AuHS
		Type:	(a)	(a)	(a)	(a)	(a)	(a)	(a)	(a)	(a)	(a)
Cell	T (°C)	P (bar)	Al(OH) ₄ ⁻	Zn ⁺⁺	ZnOH ⁺	Zn(OH) ₂ (aq)	ZnHCO ₃ ⁺	Zn(HS) ₂ (aq)	Au ⁺	AuOH (aq)	Au(OH) ₂ ⁻	AuHS (aq)
Ore fluids	500	5000	1.05E-05	0	0	0	0	0	4.03E-17	2.35E-09	2.91E-08	2.35E-08
1	220	3000	5.13E-08	1.21E-12	2.10E-10	1.95E-11	1.03E-11	1.26E-10	1.32E-22	2.80E-14	5.19E-14	7.53E-12
2	220	3000	5.13E-08	1.21E-12	2.10E-10	1.95E-11	1.03E-11	1.26E-10	1.32E-22	2.80E-14	5.19E-14	7.53E-12
3	220	3000	5.13E-08	1.21E-12	2.10E-10	1.95E-11	1.03E-11	1.26E-10	1.32E-22	2.80E-14	5.19E-14	7.53E-12
4	220	3000	5.13E-08	1.21E-12	2.10E-10	1.95E-11	1.03E-11	1.26E-10	1.32E-22	2.80E-14	5.19E-14	7.53E-12
5	220	3000	5.13E-08	1.21E-12	2.10E-10	1.95E-11	1.03E-11	1.26E-10	1.32E-22	2.80E-14	5.19E-14	7.53E-12
6	220	3000	5.13E-08	1.21E-12	2.10E-10	1.95E-11	1.03E-11	1.26E-10	1.32E-22	2.80E-14	5.19E-14	7.53E-12
7	220	3000	6.05E-08	1.48E-12	2.34E-10	1.94E-11	1.11E-11	1.27E-10	1.46E-22	2.77E-14	4.47E-14	7.51E-12
8	220	3000	4.78E-07	4.01E-11	1.42E-09	2.07E-11	9.72E-11	1.20E-10	9.08E-22	3.03E-14	6.44E-15	7.70E-12
9	220	3000	6.96E-07	5.30E-11	1.65E-09	2.07E-11	1.15E-10	1.20E-10	1.06E-21	3.04E-14	5.44E-15	7.71E-12
10	220	3000	6.96E-07	5.30E-11	1.65E-09	2.07E-11	1.15E-10	1.20E-10	1.06E-21	3.04E-14	5.44E-15	7.71E-12
11	220	3000	6.96E-07	5.30E-11	1.65E-09	2.07E-11	1.15E-10	1.20E-10	1.06E-21	3.04E-14	5.44E-15	7.71E-12
12	220	3000	6.96E-07	5.30E-11	1.65E-09	2.07E-11	1.15E-10	1.20E-10	1.06E-21	3.04E-14	5.44E-15	7.71E-12
13	220	3000	6.96E-07	5.30E-11	1.65E-09	2.07E-11	1.15E-10	1.20E-10	1.06E-21	3.04E-14	5.44E-15	7.71E-12
14	220	3000	6.96E-07	5.30E-11	1.65E-09	2.07E-11	1.15E-10	1.20E-10	1.06E-21	3.04E-14	5.44E-15	7.71E-12
15	220	3000	6.96E-07	5.30E-11	1.65E-09	2.07E-11	1.15E-10	1.20E-10	1.06E-21	3.04E-14	5.44E-15	7.71E-12
16	220	3000	6.96E-07	5.30E-11	1.65E-09	2.07E-11	1.15E-10	1.20E-10	1.06E-21	3.04E-14	5.44E-15	7.71E-12
17	220	3000	6.96E-07	5.30E-11	1.65E-09	2.07E-11	1.15E-10	1.20E-10	1.06E-21	3.04E-14	5.44E-15	7.71E-12
18	220	3000	6.96E-07	5.30E-11	1.65E-09	2.07E-11	1.15E-10	1.20E-10	1.06E-21	3.04E-14	5.44E-15	7.71E-12

		Formula:	Au(HS)2-	Au ₂ (HS) 2S--	Au+++	Mn++	MnOH+	MnHCO ₃ +	MnSO ₄	MnO ₄ -	MnO ₄ --	Fe++
		Type:	(a)	(a)	(a)	(a)	(a)	(a)	(a)	(a)	(a)	(a)
Cell	T (°C)	P (bar)	Au(HS)2-	Au ₂ (HS) 2S--	Au+++	Mn++	MnOH+	MnHCO ₃ +	MnSO ₄ (aq)	MnO ₄ -	MnO ₄ --	Fe++
Ore fluids	500	5000	7.76E-07	3.58E-09	2.68E-54	2.68E-06	3.68E-04	3.84E-05	1.99E-11	2.09E-31	7.83E-28	7.42E-13
1	220	3000	2.38E-11	1.31E-14	5.20E-63	2.85E-05	3.96E-06	3.76E-04	2.52E-09	2.14E-54	2.12E-47	6.01E-09
2	220	3000	2.38E-11	1.31E-14	5.20E-63	2.85E-05	3.96E-06	3.76E-04	2.52E-09	2.14E-54	2.12E-47	6.01E-09
3	220	3000	2.38E-11	1.31E-14	5.20E-63	2.85E-05	3.96E-06	3.76E-04	2.52E-09	2.14E-54	2.12E-47	6.01E-09
4	220	3000	2.38E-11	1.31E-14	5.20E-63	2.85E-05	3.96E-06	3.76E-04	2.52E-09	2.14E-54	2.12E-47	6.01E-09
5	220	3000	2.38E-11	1.31E-14	5.20E-63	2.85E-05	3.96E-06	3.76E-04	2.52E-09	2.14E-54	2.12E-47	6.01E-09
6	220	3000	2.38E-11	1.31E-14	5.20E-63	2.85E-05	3.96E-06	3.76E-04	2.52E-09	2.14E-54	2.12E-47	6.01E-09
7	220	3000	2.08E-11	9.35E-15	6.12E-63	3.21E-05	4.09E-06	3.73E-04	2.13E-09	1.60E-54	1.32E-47	7.42E-09
8	220	3000	2.64E-12	1.06E-16	4.49E-61	8.54E-05	2.43E-06	3.21E-04	4.34E-10	3.29E-56	2.24E-50	1.78E-07
9	220	3000	2.22E-12	7.26E-17	6.47E-61	9.33E-05	2.33E-06	3.13E-04	3.70E-10	2.33E-56	1.29E-50	2.34E-07
10	220	3000	2.22E-12	7.26E-17	6.47E-61	9.33E-05	2.33E-06	3.13E-04	3.70E-10	2.33E-56	1.29E-50	2.34E-07
11	220	3000	2.22E-12	7.26E-17	6.47E-61	9.33E-05	2.33E-06	3.13E-04	3.70E-10	2.33E-56	1.29E-50	2.34E-07
12	220	3000	2.22E-12	7.26E-17	6.47E-61	9.33E-05	2.33E-06	3.13E-04	3.70E-10	2.33E-56	1.29E-50	2.34E-07
13	220	3000	2.22E-12	7.26E-17	6.47E-61	9.33E-05	2.33E-06	3.13E-04	3.70E-10	2.33E-56	1.29E-50	2.34E-07
14	220	3000	2.22E-12	7.26E-17	6.47E-61	9.33E-05	2.33E-06	3.13E-04	3.70E-10	2.33E-56	1.29E-50	2.34E-07
15	220	3000	2.22E-12	7.26E-17	6.47E-61	9.33E-05	2.33E-06	3.13E-04	3.70E-10	2.33E-56	1.29E-50	2.34E-07
16	220	3000	2.22E-12	7.26E-17	6.47E-61	9.33E-05	2.33E-06	3.13E-04	3.70E-10	2.33E-56	1.29E-50	2.34E-07
17	220	3000	2.22E-12	7.26E-17	6.47E-61	9.33E-05	2.33E-06	3.13E-04	3.70E-10	2.33E-56	1.29E-50	2.34E-07
18	220	3000	2.22E-12	7.26E-17	6.47E-61	9.33E-05	2.33E-06	3.13E-04	3.70E-10	2.33E-56	1.29E-50	2.34E-07

		Formula:	FeOH+	Fe(OH)2	Fe(OH)3-	FeSO4	Fe+++	FeOH++	Fe(OH)2+	Fe(OH)3	Fe(OH)4-	CH4
		Type:	(a)	(a)	(a)	(a)	(a)	(a)	(a)	(a)	(a)	(a)
Cell	T (°C)	P (bar)	FeOH+	Fe(OH)2 (aq)	Fe(OH)3-	FeSO4 (aq)	Fe+++	FeOH++	Fe(OH)2+	Fe(OH)3 (aq)	Fe(OH)4-	CH4 (aq)
Ore fluids	500	5000	4.05E-10	4.36E-08	4.67E-08	2.45E-16	2.26E-27	1.43E-19	1.05E-12	1.07E-08	3.00E-08	1.21E-02
1	220	3000	4.73E-09	5.06E-10	1.92E-12	1.25E-12	1.36E-22	2.19E-17	5.30E-13	3.71E-10	4.76E-12	1.61E-06
2	220	3000	4.73E-09	5.06E-10	1.92E-12	1.25E-12	1.36E-22	2.19E-17	5.30E-13	3.71E-10	4.76E-12	1.61E-06
3	220	3000	4.73E-09	5.06E-10	1.92E-12	1.25E-12	1.36E-22	2.19E-17	5.30E-13	3.71E-10	4.76E-12	1.61E-06
4	220	3000	4.73E-09	5.06E-10	1.92E-12	1.25E-12	1.36E-22	2.19E-17	5.30E-13	3.71E-10	4.76E-12	1.61E-06
5	220	3000	4.73E-09	5.06E-10	1.92E-12	1.25E-12	1.36E-22	2.19E-17	5.30E-13	3.71E-10	4.76E-12	1.61E-06
6	220	3000	4.73E-09	5.06E-10	1.92E-12	1.25E-12	1.36E-22	2.19E-17	5.30E-13	3.71E-10	4.76E-12	1.61E-06
7	220	3000	5.36E-09	5.12E-10	1.69E-12	1.16E-12	1.65E-22	2.62E-17	5.97E-13	3.72E-10	4.16E-12	1.70E-06
8	220	3000	2.87E-08	4.82E-10	2.10E-13	2.13E-12	9.44E-21	5.80E-16	3.53E-12	3.87E-10	5.71E-13	1.19E-06
9	220	3000	3.32E-08	4.80E-10	1.76E-13	2.19E-12	1.35E-20	7.58E-16	4.10E-12	3.87E-10	4.81E-13	1.17E-06
10	220	3000	3.32E-08	4.80E-10	1.76E-13	2.19E-12	1.35E-20	7.58E-16	4.10E-12	3.87E-10	4.81E-13	1.17E-06
11	220	3000	3.32E-08	4.80E-10	1.76E-13	2.19E-12	1.35E-20	7.58E-16	4.10E-12	3.87E-10	4.81E-13	1.17E-06
12	220	3000	3.32E-08	4.80E-10	1.76E-13	2.19E-12	1.35E-20	7.58E-16	4.10E-12	3.87E-10	4.81E-13	1.17E-06
13	220	3000	3.32E-08	4.80E-10	1.76E-13	2.19E-12	1.35E-20	7.58E-16	4.10E-12	3.87E-10	4.81E-13	1.17E-06
14	220	3000	3.32E-08	4.80E-10	1.76E-13	2.19E-12	1.35E-20	7.58E-16	4.10E-12	3.87E-10	4.81E-13	1.17E-06
15	220	3000	3.32E-08	4.80E-10	1.76E-13	2.19E-12	1.35E-20	7.58E-16	4.10E-12	3.87E-10	4.81E-13	1.17E-06
16	220	3000	3.32E-08	4.80E-10	1.76E-13	2.19E-12	1.35E-20	7.58E-16	4.10E-12	3.87E-10	4.81E-13	1.17E-06
17	220	3000	3.32E-08	4.80E-10	1.76E-13	2.19E-12	1.35E-20	7.58E-16	4.10E-12	3.87E-10	4.81E-13	1.17E-06
18	220	3000	3.32E-08	4.80E-10	1.76E-13	2.19E-12	1.35E-20	7.58E-16	4.10E-12	3.87E-10	4.81E-13	1.17E-06

		Formula:	C2H6	HCOOH	HCOO-	CH3COO H	CH3COO-		
		Type:	(a)	(a)	(a)	(a)	(a)		
Cell	T (°C)	P (bar)	C2H6 (aq)	HCOOH (aq)	HCOO-	CH3COO H (aq)	CH3COO-	pH	Eh(V)
Ore fluids	500	5000	1.89E-06	9.63E-07	2.36E-04	9.02E-08	9.99E-07	6.950431	-1.167
1	220	3000	1.30E-12	1.25E-08	2.59E-06	1.86E-10	3.79E-09	6.116838	-0.51144
2	220	3000	1.30E-12	1.25E-08	2.59E-06	1.86E-10	3.79E-09	6.116838	-0.51144
3	220	3000	1.30E-12	1.25E-08	2.59E-06	1.86E-10	3.79E-09	6.116838	-0.51144
4	220	3000	1.30E-12	1.25E-08	2.59E-06	1.86E-10	3.79E-09	6.116838	-0.51144
5	220	3000	1.30E-12	1.25E-08	2.59E-06	1.86E-10	3.79E-09	6.116838	-0.51144
6	220	3000	1.30E-12	1.25E-08	2.59E-06	1.86E-10	3.79E-09	6.116838	-0.51144
7	220	3000	1.40E-12	1.23E-08	2.20E-06	1.88E-10	3.31E-09	6.059115	-0.50638
8	220	3000	8.28E-13	1.48E-08	3.45E-07	1.91E-10	4.37E-10	5.235773	-0.42217
9	220	3000	8.08E-13	1.49E-08	2.92E-07	1.91E-10	3.68E-10	5.165887	-0.41516
10	220	3000	8.08E-13	1.49E-08	2.92E-07	1.91E-10	3.68E-10	5.165887	-0.41516
11	220	3000	8.08E-13	1.49E-08	2.92E-07	1.91E-10	3.68E-10	5.165887	-0.41516
12	220	3000	8.08E-13	1.49E-08	2.92E-07	1.91E-10	3.68E-10	5.165887	-0.41516
13	220	3000	8.08E-13	1.49E-08	2.92E-07	1.91E-10	3.68E-10	5.165887	-0.41516
14	220	3000	8.08E-13	1.49E-08	2.92E-07	1.91E-10	3.68E-10	5.165887	-0.41516
15	220	3000	8.08E-13	1.49E-08	2.92E-07	1.91E-10	3.68E-10	5.165887	-0.41516
16	220	3000	8.08E-13	1.49E-08	2.92E-07	1.91E-10	3.68E-10	5.165887	-0.41516
17	220	3000	8.08E-13	1.49E-08	2.92E-07	1.91E-10	3.68E-10	5.165887	-0.41516
18	220	3000	8.08E-13	1.49E-08	2.92E-07	1.91E-10	3.68E-10	5.165887	-0.41516

Notes s: solid; a: aqueous solution; f:r, fluid:rock; the unit is mol.

(3) Results of 20 fluid infiltration increments with instantaneous f:r = 0.05 (by mass).

		Formula:	Au	C	SiO2	Fe3O4	FeS2	Fe.877S	ZnS	FeAsS	CaCO3	KAl3Si3O 10(OH)2
		Type:	(s)	(s)	(s)	(s)	(s)	(s)	(s)	(s)	(s)	(s)
Cell	T (°C)	P (bar)	Gold	Graphite	Quartz	Magnetite	Pyrite	Pyrrhotite	Sphalerite	Arsenopyrite	Calcite	Muscovite
Ore fluids	500	5000	0	0	0	0	0	0	0	0	0	0
1	220	3000	8.38E-06	2.64E-01	5.41E-01	1.54E-02	8.97E-03	0	1.54E-04	0	7.47E-03	8.21E-02
2	220	3000	2.82E-11	2.57E-03	3.77E-01	1.78E-02	1.96E-03	0	1.54E-04	0	7.49E-03	5.70E-02
3	220	3000	2.57E-11	2.08E-03	3.77E-01	1.78E-02	1.96E-03	0	1.54E-04	0	7.48E-03	5.70E-02
4	220	3000	2.40E-11	2.08E-03	3.78E-01	1.78E-02	1.96E-03	0	1.54E-04	0	7.48E-03	5.71E-02
5	220	3000	2.56E-11	2.07E-03	3.77E-01	1.78E-02	1.96E-03	0	1.54E-04	0	7.48E-03	5.70E-02
6	220	3000	2.53E-11	2.07E-03	3.77E-01	1.78E-02	1.96E-03	0	1.54E-04	0	7.48E-03	5.70E-02
7	220	3000	2.41E-11	2.07E-03	3.78E-01	1.78E-02	1.96E-03	0	1.54E-04	0	7.48E-03	5.71E-02
8	220	3000	2.57E-11	2.01E-03	3.77E-01	1.78E-02	1.96E-03	0	1.54E-04	0	7.48E-03	5.70E-02
9	220	3000	3.20E-12	2.13E-03	3.95E-01	1.75E-02	1.96E-03	0	1.54E-04	0	0	5.67E-02
10	220	3000	0	2.07E-03	3.98E-01	1.78E-02	1.96E-03	0	1.54E-04	0	0	5.67E-02
11	220	3000	0	2.07E-03	3.98E-01	1.78E-02	1.96E-03	0	1.54E-04	0	0	5.67E-02
12	220	3000	0	1.99E-03	3.98E-01	1.78E-02	1.96E-03	0	1.54E-04	0	0	5.67E-02
13	220	3000	0	2.07E-03	3.98E-01	1.78E-02	1.96E-03	0	1.54E-04	0	0	5.67E-02
14	220	3000	0	2.07E-03	3.98E-01	1.78E-02	1.96E-03	0	1.54E-04	0	0	5.67E-02
15	220	3000	0	2.07E-03	3.98E-01	1.78E-02	1.96E-03	0	1.54E-04	0	0	5.67E-02
16	220	3000	0	2.07E-03	3.98E-01	1.78E-02	1.96E-03	0	1.54E-04	0	0	5.67E-02
17	220	3000	0	2.07E-03	3.98E-01	1.78E-02	1.96E-03	0	1.54E-04	0	0	5.67E-02
18	220	3000	0	1.99E-03	3.98E-01	1.78E-02	1.96E-03	0	1.54E-04	0	0	5.67E-02

			Ca ₂ Al ₃ Si ₃ O ₁₂ (OH)	Ca ₂ FeAl ₂ Si ₃ O ₁₂ H	Mg _{4.5} Al ₃ Si _{2.5} O ₁₀ (OH) ₈	Na(AlSi ₃ O ₈)	H ₂ O	H ⁺	OH ⁻	CO ₃ ⁻⁻	HCO ₃ ⁻	H ₂ CO ₃
			Type: (s)	(s)	(s)	(s)	(a)	(a)	(a)	(a)	(a)	(a)
Cell	T (°C)	P (bar)	Zoisite	Epidote	Chlorite	Albite	H ₂ O	H ⁺	OH ⁻	CO ₃ ⁻⁻	HCO ₃ ⁻	H ₂ CO ₃ (aq)
Ore fluids	500	5000	0	0	0	0	2.43E-01	8.31E-10	1.31E-04	1.71E-06	4.76E-04	1.40E-02
1	220	3000	0	0	1.02E-02	8.21E-02	2.66E-01	5.03E-09	7.28E-07	1.05E-05	3.04E-03	3.49E-03
2	220	3000	0	0	1.02E-02	1.52E-01	2.66E-01	5.03E-09	7.28E-07	1.05E-05	3.04E-03	3.49E-03
3	220	3000	0	0	1.02E-02	1.52E-01	2.66E-01	5.03E-09	7.28E-07	1.05E-05	3.04E-03	3.49E-03
4	220	3000	0	0	1.02E-02	1.52E-01	2.66E-01	5.03E-09	7.28E-07	1.05E-05	3.04E-03	3.49E-03
5	220	3000	0	0	1.02E-02	1.52E-01	2.66E-01	5.03E-09	7.28E-07	1.05E-05	3.04E-03	3.49E-03
6	220	3000	0	0	1.02E-02	1.52E-01	2.66E-01	5.03E-09	7.28E-07	1.05E-05	3.04E-03	3.49E-03
7	220	3000	0	0	1.02E-02	1.52E-01	2.66E-01	5.03E-09	7.28E-07	1.05E-05	3.04E-03	3.49E-03
8	220	3000	0	0	1.02E-02	1.52E-01	2.68E-01	1.28E-08	2.50E-07	9.00E-07	9.96E-04	3.30E-03
9	220	3000	2.79E-03	9.51E-04	1.02E-02	1.43E-01	2.68E-01	3.59E-08	7.67E-08	8.81E-08	3.79E-04	4.04E-03
10	220	3000	3.71E-03	3.19E-05	1.02E-02	1.42E-01	2.68E-01	3.59E-08	7.67E-08	8.81E-08	3.79E-04	4.04E-03
11	220	3000	3.71E-03	3.68E-05	1.02E-02	1.42E-01	2.68E-01	3.59E-08	7.67E-08	8.81E-08	3.79E-04	4.04E-03
12	220	3000	3.70E-03	4.34E-05	1.02E-02	1.42E-01	2.68E-01	3.59E-08	7.67E-08	8.81E-08	3.79E-04	4.04E-03
13	220	3000	3.72E-03	2.53E-05	1.02E-02	1.42E-01	2.68E-01	3.59E-08	7.67E-08	8.81E-08	3.79E-04	4.04E-03
14	220	3000	3.72E-03	2.66E-05	1.02E-02	1.42E-01	2.68E-01	3.59E-08	7.67E-08	8.81E-08	3.79E-04	4.04E-03
15	220	3000	3.72E-03	2.84E-05	1.02E-02	1.42E-01	2.68E-01	3.59E-08	7.67E-08	8.81E-08	3.79E-04	4.04E-03
16	220	3000	3.71E-03	3.11E-05	1.02E-02	1.42E-01	2.68E-01	3.59E-08	7.67E-08	8.81E-08	3.79E-04	4.04E-03
17	220	3000	3.71E-03	3.55E-05	1.02E-02	1.42E-01	2.68E-01	3.59E-08	7.67E-08	8.81E-08	3.79E-04	4.04E-03
18	220	3000	3.70E-03	4.66E-05	1.02E-02	1.42E-01	2.68E-01	3.59E-08	7.67E-08	8.81E-08	3.79E-04	4.04E-03

		Formula:	H3SiO4-	H4SiO4	H3AsO3	HAsO3--	As2S4--	HAs2S4-	O2	H2	H2S	HS-
		Type:	(a)	(a)	(a)	(a)	(a)	(a)	(a)	(a)	(a)	(a)
Cell	T (°C)	P (bar)	H3SiO4-	H4SiO4 (aq)	H3AsO3 (aq)	HAsO3--	As2S4--	HAs2S4-	O2 (aq)	H2 (aq)	H2S (aq)	HS-
Ore fluids	500	5000	9.08E-04	5.87E-04	2.00E-06	1.48E-09	5.91E-10	8.12E-12	1.66E-29	2.38E-04	3.48E-04	3.53E-04
1	220	3000	1.84E-06	5.03E-05	2.00E-06	2.70E-11	5.53E-15	1.12E-15	5.68E-46	2.01E-08	2.12E-07	3.79E-07
2	220	3000	1.84E-06	5.03E-05	2.00E-06	2.70E-11	5.53E-15	1.12E-15	5.68E-46	2.01E-08	2.12E-07	3.79E-07
3	220	3000	1.84E-06	5.03E-05	2.00E-06	2.70E-11	5.53E-15	1.12E-15	5.68E-46	2.01E-08	2.12E-07	3.79E-07
4	220	3000	1.84E-06	5.03E-05	2.00E-06	2.70E-11	5.53E-15	1.12E-15	5.68E-46	2.01E-08	2.12E-07	3.79E-07
5	220	3000	1.84E-06	5.03E-05	2.00E-06	2.70E-11	5.53E-15	1.12E-15	5.68E-46	2.01E-08	2.12E-07	3.79E-07
6	220	3000	1.84E-06	5.03E-05	2.00E-06	2.70E-11	5.53E-15	1.12E-15	5.68E-46	2.01E-08	2.12E-07	3.79E-07
7	220	3000	1.84E-06	5.03E-05	2.00E-06	2.70E-11	5.53E-15	1.12E-15	5.68E-46	2.01E-08	2.12E-07	3.79E-07
8	220	3000	6.68E-07	5.20E-05	2.00E-06	2.46E-12	5.08E-16	3.99E-16	5.25E-46	2.10E-08	2.17E-07	1.32E-07
9	220	3000	2.09E-07	5.21E-05	2.00E-06	1.96E-13	3.53E-17	1.09E-16	6.43E-46	1.89E-08	2.09E-07	3.91E-08
10	220	3000	2.09E-07	5.21E-05	2.00E-06	1.96E-13	3.53E-17	1.09E-16	6.43E-46	1.89E-08	2.09E-07	3.91E-08
11	220	3000	2.09E-07	5.21E-05	2.00E-06	1.96E-13	3.53E-17	1.09E-16	6.43E-46	1.89E-08	2.09E-07	3.91E-08
12	220	3000	2.09E-07	5.21E-05	2.00E-06	1.96E-13	3.53E-17	1.09E-16	6.43E-46	1.89E-08	2.09E-07	3.91E-08
13	220	3000	2.09E-07	5.21E-05	2.00E-06	1.96E-13	3.53E-17	1.09E-16	6.43E-46	1.89E-08	2.09E-07	3.91E-08
14	220	3000	2.09E-07	5.21E-05	2.00E-06	1.96E-13	3.53E-17	1.09E-16	6.43E-46	1.89E-08	2.09E-07	3.91E-08
15	220	3000	2.09E-07	5.21E-05	2.00E-06	1.96E-13	3.53E-17	1.09E-16	6.43E-46	1.89E-08	2.09E-07	3.91E-08
16	220	3000	2.09E-07	5.21E-05	2.00E-06	1.96E-13	3.53E-17	1.09E-16	6.43E-46	1.89E-08	2.09E-07	3.91E-08
17	220	3000	2.09E-07	5.21E-05	2.00E-06	1.96E-13	3.53E-17	1.09E-16	6.43E-46	1.89E-08	2.09E-07	3.91E-08
18	220	3000	2.09E-07	5.21E-05	2.00E-06	1.96E-13	3.53E-17	1.09E-16	6.43E-46	1.89E-08	2.09E-07	3.91E-08

		Formula:	S2--	S2O3--	SO2	SO3--	HSO3-	SO4--	HSO4-	Na+	NaOH	NaCO3-
		Type:	(a)	(a)	(a)	(a)	(a)	(a)	(a)	(a)	(a)	(a)
Cell	T (°C)	P (bar)	S2--	S2O3--	SO2 (aq)	SO3--	HSO3-	SO4--	HSO4-	Na+	NaOH (aq)	NaCO3-
Ore fluids	500	5000	5.40E-10	2.89E-13	3.50E-12	1.02E-13	5.21E-11	6.63E-10	2.26E-12	5.16E-04	9.18E-05	9.01E-06
1	220	3000	1.67E-14	8.57E-15	1.03E-16	4.38E-15	9.68E-14	1.08E-08	4.78E-12	2.74E-03	6.15E-07	4.43E-05
2	220	3000	1.67E-14	8.57E-15	1.03E-16	4.38E-15	9.68E-14	1.08E-08	4.78E-12	2.74E-03	6.15E-07	4.43E-05
3	220	3000	1.67E-14	8.57E-15	1.03E-16	4.38E-15	9.68E-14	1.08E-08	4.78E-12	2.74E-03	6.15E-07	4.43E-05
4	220	3000	1.67E-14	8.57E-15	1.03E-16	4.38E-15	9.68E-14	1.08E-08	4.78E-12	2.74E-03	6.15E-07	4.43E-05
5	220	3000	1.67E-14	8.57E-15	1.03E-16	4.38E-15	9.68E-14	1.08E-08	4.78E-12	2.74E-03	6.15E-07	4.43E-05
6	220	3000	1.67E-14	8.57E-15	1.03E-16	4.38E-15	9.68E-14	1.08E-08	4.78E-12	2.74E-03	6.15E-07	4.43E-05
7	220	3000	1.67E-14	8.57E-15	1.03E-16	4.38E-15	9.68E-14	1.08E-08	4.78E-12	2.74E-03	6.15E-07	4.43E-05
8	220	3000	1.52E-15	7.05E-16	9.34E-17	3.68E-16	3.10E-14	8.24E-10	1.51E-12	7.66E-04	7.48E-08	1.77E-06
9	220	3000	1.25E-16	7.92E-17	1.22E-16	3.86E-17	1.26E-14	9.26E-11	6.86E-13	1.23E-04	4.51E-09	4.12E-08
10	220	3000	1.25E-16	7.92E-17	1.22E-16	3.86E-17	1.26E-14	9.26E-11	6.86E-13	1.23E-04	4.51E-09	4.12E-08
11	220	3000	1.25E-16	7.92E-17	1.22E-16	3.86E-17	1.26E-14	9.26E-11	6.86E-13	1.23E-04	4.51E-09	4.12E-08
12	220	3000	1.25E-16	7.92E-17	1.22E-16	3.86E-17	1.26E-14	9.26E-11	6.86E-13	1.23E-04	4.51E-09	4.12E-08
13	220	3000	1.25E-16	7.92E-17	1.22E-16	3.86E-17	1.26E-14	9.26E-11	6.86E-13	1.23E-04	4.51E-09	4.12E-08
14	220	3000	1.25E-16	7.92E-17	1.22E-16	3.86E-17	1.26E-14	9.26E-11	6.86E-13	1.23E-04	4.51E-09	4.12E-08
15	220	3000	1.25E-16	7.92E-17	1.22E-16	3.86E-17	1.26E-14	9.26E-11	6.86E-13	1.23E-04	4.51E-09	4.12E-08
16	220	3000	1.25E-16	7.92E-17	1.22E-16	3.86E-17	1.26E-14	9.26E-11	6.86E-13	1.23E-04	4.51E-09	4.12E-08
17	220	3000	1.25E-16	7.92E-17	1.22E-16	3.86E-17	1.26E-14	9.26E-11	6.86E-13	1.23E-04	4.51E-09	4.12E-08
18	220	3000	1.25E-16	7.92E-17	1.22E-16	3.86E-17	1.26E-14	9.26E-11	6.86E-13	1.23E-04	4.51E-09	4.12E-08

		Formula:	NaHCO3	NaSO4-	K+	KOH	KSO4-	KHSO4	Mg ⁺⁺	MgOH+	MgCO3	MgHCO3 ₊
		Type:	(a)	(a)	(a)	(a)	(a)	(a)	(a)	(a)	(a)	(a)
Cell	T (°C)	P (bar)	NaHCO3 (aq)	NaSO4-	K+	KOH (aq)	KSO4-	KHSO4 (aq)	Mg ⁺⁺	MgOH+	MgCO3 (aq)	MgHCO3 ₊
Ore fluids	500	5000	1.37E-04	2.53E-10	1.28E-03	1.07E-04	7.97E-09	8.79E-12	4.73E-13	6.97E-12	1.12E-13	7.10E-13
1	220	3000	1.69E-03	9.52E-09	1.49E-04	1.71E-08	2.18E-09	7.49E-14	3.70E-10	6.16E-12	9.88E-11	1.48E-09
2	220	3000	1.69E-03	9.52E-09	1.49E-04	1.71E-08	2.18E-09	7.49E-14	3.70E-10	6.16E-12	9.88E-11	1.48E-09
3	220	3000	1.69E-03	9.52E-09	1.49E-04	1.71E-08	2.18E-09	7.49E-14	3.70E-10	6.16E-12	9.88E-11	1.48E-09
4	220	3000	1.69E-03	9.52E-09	1.49E-04	1.71E-08	2.18E-09	7.49E-14	3.70E-10	6.16E-12	9.88E-11	1.48E-09
5	220	3000	1.69E-03	9.52E-09	1.49E-04	1.71E-08	2.18E-09	7.49E-14	3.70E-10	6.16E-12	9.88E-11	1.48E-09
6	220	3000	1.69E-03	9.52E-09	1.49E-04	1.71E-08	2.18E-09	7.49E-14	3.70E-10	6.16E-12	9.88E-11	1.48E-09
7	220	3000	1.69E-03	9.52E-09	1.49E-04	1.71E-08	2.18E-09	7.49E-14	3.70E-10	6.16E-12	9.88E-11	1.48E-09
8	220	3000	1.92E-04	3.61E-10	5.78E-07	3.01E-11	1.19E-12	1.17E-16	4.64E-10	3.49E-12	2.20E-11	7.84E-10
9	220	3000	1.42E-05	9.93E-12	3.33E-10	6.63E-15	1.20E-16	3.75E-20	4.91E-10	1.44E-12	4.14E-12	3.98E-10
10	220	3000	1.42E-05	9.93E-12	3.33E-10	6.63E-15	1.20E-16	3.75E-20	4.91E-10	1.44E-12	4.14E-12	3.98E-10
11	220	3000	1.42E-05	9.93E-12	3.33E-10	6.63E-15	1.20E-16	3.75E-20	4.91E-10	1.44E-12	4.14E-12	3.98E-10
12	220	3000	1.42E-05	9.93E-12	3.33E-10	6.63E-15	1.20E-16	3.75E-20	4.91E-10	1.44E-12	4.14E-12	3.98E-10
13	220	3000	1.42E-05	9.93E-12	3.33E-10	6.63E-15	1.20E-16	3.75E-20	4.91E-10	1.44E-12	4.14E-12	3.98E-10
14	220	3000	1.42E-05	9.93E-12	3.33E-10	6.63E-15	1.20E-16	3.75E-20	4.91E-10	1.44E-12	4.14E-12	3.98E-10
15	220	3000	1.42E-05	9.93E-12	3.33E-10	6.63E-15	1.20E-16	3.75E-20	4.91E-10	1.44E-12	4.14E-12	3.98E-10
16	220	3000	1.42E-05	9.93E-12	3.33E-10	6.63E-15	1.20E-16	3.75E-20	4.91E-10	1.44E-12	4.14E-12	3.98E-10
17	220	3000	1.42E-05	9.93E-12	3.33E-10	6.63E-15	1.20E-16	3.75E-20	4.91E-10	1.44E-12	4.14E-12	3.98E-10
18	220	3000	1.42E-05	9.93E-12	3.33E-10	6.63E-15	1.20E-16	3.75E-20	4.91E-10	1.44E-12	4.14E-12	3.98E-10

		Formula:	MgSO4	Ca ⁺⁺	CaOH ⁺	CaCO3	CaHCO3 ⁺	CaSO4	Al ⁺⁺⁺	AlOH ⁺⁺	Al(OH) ₂ ⁺	Al(OH) ₃
		Type:	(a)	(a)	(a)	(a)	(a)	(a)	(a)	(a)	(a)	(a)
Cell	T (°C)	P (bar)	MgSO4 (aq)	Ca ⁺⁺	CaOH ⁺	CaCO3 (aq)	CaHCO3 ⁺	CaSO4 (aq)	Al ⁺⁺⁺	AlOH ⁺⁺	Al(OH) ₂ ⁺	Al(OH) ₃ (aq)
Ore fluids	500	5000	1.13E-17	1.04E-09	9.93E-09	8.71E-09	1.33E-09	8.07E-15	2.61E-27	7.11E-19	3.52E-13	3.13E-08
1	220	3000	2.67E-14	1.19E-07	5.08E-10	2.10E-07	4.45E-07	4.13E-12	1.61E-20	4.00E-16	1.25E-12	1.11E-09
2	220	3000	2.67E-14	1.19E-07	5.08E-10	2.10E-07	4.45E-07	4.13E-12	1.61E-20	4.00E-16	1.25E-12	1.11E-09
3	220	3000	2.67E-14	1.19E-07	5.08E-10	2.10E-07	4.45E-07	4.13E-12	1.61E-20	4.00E-16	1.25E-12	1.11E-09
4	220	3000	2.67E-14	1.19E-07	5.08E-10	2.10E-07	4.45E-07	4.13E-12	1.61E-20	4.00E-16	1.25E-12	1.11E-09
5	220	3000	2.67E-14	1.19E-07	5.08E-10	2.10E-07	4.45E-07	4.13E-12	1.61E-20	4.00E-16	1.25E-12	1.11E-09
6	220	3000	2.67E-14	1.19E-07	5.08E-10	2.10E-07	4.45E-07	4.13E-12	1.61E-20	4.00E-16	1.25E-12	1.11E-09
7	220	3000	2.67E-14	1.19E-07	5.08E-10	2.10E-07	4.45E-07	4.13E-12	1.61E-20	4.00E-16	1.25E-12	1.11E-09
8	220	3000	5.63E-15	5.88E-07	1.28E-09	2.07E-07	1.05E-06	3.87E-12	1.37E-18	1.34E-14	2.44E-11	9.31E-09
9	220	3000	1.26E-15	1.50E-06	1.37E-09	1.01E-07	1.38E-06	2.24E-12	3.65E-16	1.31E-12	1.09E-09	1.54E-07
10	220	3000	1.26E-15	1.50E-06	1.37E-09	1.01E-07	1.38E-06	2.24E-12	3.65E-16	1.31E-12	1.09E-09	1.54E-07
11	220	3000	1.26E-15	1.50E-06	1.37E-09	1.01E-07	1.38E-06	2.24E-12	3.65E-16	1.31E-12	1.09E-09	1.54E-07
12	220	3000	1.26E-15	1.50E-06	1.37E-09	1.01E-07	1.38E-06	2.24E-12	3.65E-16	1.31E-12	1.09E-09	1.54E-07
13	220	3000	1.26E-15	1.50E-06	1.37E-09	1.01E-07	1.38E-06	2.24E-12	3.65E-16	1.31E-12	1.09E-09	1.54E-07
14	220	3000	1.26E-15	1.50E-06	1.37E-09	1.01E-07	1.38E-06	2.24E-12	3.65E-16	1.31E-12	1.09E-09	1.54E-07
15	220	3000	1.26E-15	1.50E-06	1.37E-09	1.01E-07	1.38E-06	2.24E-12	3.65E-16	1.31E-12	1.09E-09	1.54E-07
16	220	3000	1.26E-15	1.50E-06	1.37E-09	1.01E-07	1.38E-06	2.24E-12	3.65E-16	1.31E-12	1.09E-09	1.54E-07
17	220	3000	1.26E-15	1.50E-06	1.37E-09	1.01E-07	1.38E-06	2.24E-12	3.65E-16	1.31E-12	1.09E-09	1.54E-07
18	220	3000	1.26E-15	1.50E-06	1.37E-09	1.01E-07	1.38E-06	2.24E-12	3.65E-16	1.31E-12	1.09E-09	1.54E-07

		Formula:	Al(OH) ₄ ⁻	Zn ⁺⁺	ZnOH ⁺	Zn(OH) ₂	ZnHCO ₃ ⁺	Zn(HS) ₂	Au ⁺	AuOH	Au(OH) ₂ -	AuHS
		Type:	(a)	(a)	(a)	(a)	(a)	(a)	(a)	(a)	(a)	(a)
Cell	T (°C)	P (bar)	Al(OH) ₄ ⁻	Zn ⁺⁺	ZnOH ⁺	Zn(OH) ₂ (aq)	ZnHCO ₃ ⁺	Zn(HS) ₂ (aq)	Au ⁺	AuOH (aq)	Au(OH) ₂ -	AuHS (aq)
Ore fluids	500	5000	5.26E-06	0	0	0	0	0	2.01E-17	1.18E-09	1.45E-08	1.18E-08
1	220	3000	2.56E-08	6.06E-13	1.05E-10	9.74E-12	5.16E-12	6.30E-11	6.58E-23	1.40E-14	2.59E-14	3.77E-12
2	220	3000	2.56E-08	6.06E-13	1.05E-10	9.74E-12	5.16E-12	6.30E-11	6.58E-23	1.40E-14	2.59E-14	3.77E-12
3	220	3000	2.56E-08	6.06E-13	1.05E-10	9.74E-12	5.16E-12	6.30E-11	6.58E-23	1.40E-14	2.59E-14	3.77E-12
4	220	3000	2.56E-08	6.06E-13	1.05E-10	9.74E-12	5.16E-12	6.30E-11	6.58E-23	1.40E-14	2.59E-14	3.77E-12
5	220	3000	2.56E-08	6.06E-13	1.05E-10	9.74E-12	5.16E-12	6.30E-11	6.58E-23	1.40E-14	2.59E-14	3.77E-12
6	220	3000	2.56E-08	6.06E-13	1.05E-10	9.74E-12	5.16E-12	6.30E-11	6.58E-23	1.40E-14	2.59E-14	3.77E-12
7	220	3000	2.56E-08	6.06E-13	1.05E-10	9.74E-12	5.16E-12	6.30E-11	6.58E-23	1.40E-14	2.59E-14	3.77E-12
8	220	3000	7.74E-08	2.78E-12	2.44E-10	9.74E-12	1.13E-11	6.44E-11	1.51E-22	1.38E-14	9.17E-15	3.74E-12
9	220	3000	4.01E-07	1.84E-11	6.80E-10	1.01E-11	3.85E-11	6.21E-11	4.27E-22	1.45E-14	3.02E-15	3.80E-12
10	220	3000	4.01E-07	1.84E-11	6.80E-10	1.01E-11	3.85E-11	6.21E-11	4.27E-22	1.45E-14	3.02E-15	3.80E-12
11	220	3000	4.01E-07	1.84E-11	6.80E-10	1.01E-11	3.85E-11	6.21E-11	4.27E-22	1.45E-14	3.02E-15	3.80E-12
12	220	3000	4.01E-07	1.84E-11	6.80E-10	1.01E-11	3.85E-11	6.21E-11	4.27E-22	1.45E-14	3.02E-15	3.80E-12
13	220	3000	4.01E-07	1.84E-11	6.80E-10	1.01E-11	3.85E-11	6.21E-11	4.27E-22	1.45E-14	3.02E-15	3.80E-12
14	220	3000	4.01E-07	1.84E-11	6.80E-10	1.01E-11	3.85E-11	6.21E-11	4.27E-22	1.45E-14	3.02E-15	3.80E-12
15	220	3000	4.01E-07	1.84E-11	6.80E-10	1.01E-11	3.85E-11	6.21E-11	4.27E-22	1.45E-14	3.02E-15	3.80E-12
16	220	3000	4.01E-07	1.84E-11	6.80E-10	1.01E-11	3.85E-11	6.21E-11	4.27E-22	1.45E-14	3.02E-15	3.80E-12
17	220	3000	4.01E-07	1.84E-11	6.80E-10	1.01E-11	3.85E-11	6.21E-11	4.27E-22	1.45E-14	3.02E-15	3.80E-12
18	220	3000	4.01E-07	1.84E-11	6.80E-10	1.01E-11	3.85E-11	6.21E-11	4.27E-22	1.45E-14	3.02E-15	3.80E-12

		Formula:	Au(HS)2-	Au ₂ (HS) 2S ⁻⁻	Au ⁺⁺⁺	Mn ⁺⁺	MnOH ⁺	MnHCO ₃ +	MnSO ₄	MnO ₄ ⁻	MnO ₄ ⁻⁻	Fe ⁺⁺
		Type:	(a)	(a)	(a)	(a)	(a)	(a)	(a)	(a)	(a)	(a)
Cell	T (°C)	P (bar)	Au(HS)2-	Au ₂ (HS) 2S ⁻⁻	Au ⁺⁺⁺	Mn ⁺⁺	MnOH ⁺	MnHCO ₃ +	MnSO ₄ (aq)	MnO ₄ ⁻	MnO ₄ ⁻⁻	Fe ⁺⁺
Ore fluids	500	5000	3.88E-07	1.79E-09	1.34E-54	1.34E-06	1.84E-04	1.92E-05	9.95E-12	1.04E-31	3.91E-28	3.71E-13
1	220	3000	1.19E-11	6.54E-15	2.60E-63	1.43E-05	1.98E-06	1.88E-04	1.26E-09	1.07E-54	1.06E-47	3.01E-09
2	220	3000	1.19E-11	6.54E-15	2.60E-63	1.43E-05	1.98E-06	1.88E-04	1.26E-09	1.07E-54	1.06E-47	3.01E-09
3	220	3000	1.19E-11	6.54E-15	2.60E-63	1.43E-05	1.98E-06	1.88E-04	1.26E-09	1.07E-54	1.06E-47	3.01E-09
4	220	3000	1.19E-11	6.54E-15	2.60E-63	1.43E-05	1.98E-06	1.88E-04	1.26E-09	1.07E-54	1.06E-47	3.01E-09
5	220	3000	1.19E-11	6.54E-15	2.60E-63	1.43E-05	1.98E-06	1.88E-04	1.26E-09	1.07E-54	1.06E-47	3.01E-09
6	220	3000	1.19E-11	6.54E-15	2.60E-63	1.43E-05	1.98E-06	1.88E-04	1.26E-09	1.07E-54	1.06E-47	3.01E-09
7	220	3000	1.19E-11	6.54E-15	2.60E-63	1.43E-05	1.98E-06	1.88E-04	1.26E-09	1.07E-54	1.06E-47	3.01E-09
8	220	3000	4.29E-12	6.13E-16	1.33E-62	2.78E-05	1.96E-06	1.75E-04	4.64E-10	1.40E-55	3.83E-49	1.41E-08
9	220	3000	1.32E-12	4.90E-17	1.66E-61	4.79E-05	1.42E-06	1.55E-04	1.81E-10	1.50E-56	1.01E-50	8.72E-08
10	220	3000	1.32E-12	4.90E-17	1.66E-61	4.79E-05	1.42E-06	1.55E-04	1.81E-10	1.50E-56	1.01E-50	8.72E-08
11	220	3000	1.32E-12	4.90E-17	1.66E-61	4.79E-05	1.42E-06	1.55E-04	1.81E-10	1.50E-56	1.01E-50	8.72E-08
12	220	3000	1.32E-12	4.90E-17	1.66E-61	4.79E-05	1.42E-06	1.55E-04	1.81E-10	1.50E-56	1.01E-50	8.72E-08
13	220	3000	1.32E-12	4.90E-17	1.66E-61	4.79E-05	1.42E-06	1.55E-04	1.81E-10	1.50E-56	1.01E-50	8.72E-08
14	220	3000	1.32E-12	4.90E-17	1.66E-61	4.79E-05	1.42E-06	1.55E-04	1.81E-10	1.50E-56	1.01E-50	8.72E-08
15	220	3000	1.32E-12	4.90E-17	1.66E-61	4.79E-05	1.42E-06	1.55E-04	1.81E-10	1.50E-56	1.01E-50	8.72E-08
16	220	3000	1.32E-12	4.90E-17	1.66E-61	4.79E-05	1.42E-06	1.55E-04	1.81E-10	1.50E-56	1.01E-50	8.72E-08
17	220	3000	1.32E-12	4.90E-17	1.66E-61	4.79E-05	1.42E-06	1.55E-04	1.81E-10	1.50E-56	1.01E-50	8.72E-08
18	220	3000	1.32E-12	4.90E-17	1.66E-61	4.79E-05	1.42E-06	1.55E-04	1.81E-10	1.50E-56	1.01E-50	8.72E-08

		Formula:	FeOH+	Fe(OH)2	Fe(OH)3-	FeSO4	Fe+++	FeOH++	Fe(OH)2+	Fe(OH)3	Fe(OH)4	CH4
		Type:	(a)	(a)	(a)	(a)	(a)	(a)	(a)	(a)	(a)	(a)
Cell	T (°C)	P (bar)	FeOH+	Fe(OH)2 (aq)	Fe(OH)3-	FeSO4 (aq)	Fe+++	FeOH++	Fe(OH)2+	Fe(OH)3 (aq)	Fe(OH)4 -	CH4 (aq)
Ore fluids	500	5000	2.02E-10	2.18E-08	2.34E-08	1.22E-16	1.13E-27	7.17E-20	5.24E-13	5.35E-09	1.50E-08	6.03E-03
1	220	3000	2.36E-09	2.53E-10	9.58E-13	6.25E-13	6.81E-23	1.10E-17	2.65E-13	1.85E-10	2.38E-12	8.06E-07
2	220	3000	2.36E-09	2.53E-10	9.58E-13	6.25E-13	6.81E-23	1.10E-17	2.65E-13	1.85E-10	2.38E-12	8.06E-07
3	220	3000	2.36E-09	2.53E-10	9.58E-13	6.25E-13	6.81E-23	1.10E-17	2.65E-13	1.85E-10	2.38E-12	8.06E-07
4	220	3000	2.36E-09	2.53E-10	9.58E-13	6.25E-13	6.81E-23	1.10E-17	2.65E-13	1.85E-10	2.38E-12	8.06E-07
5	220	3000	2.36E-09	2.53E-10	9.58E-13	6.25E-13	6.81E-23	1.10E-17	2.65E-13	1.85E-10	2.38E-12	8.06E-07
6	220	3000	2.36E-09	2.53E-10	9.58E-13	6.25E-13	6.81E-23	1.10E-17	2.65E-13	1.85E-10	2.38E-12	8.06E-07
7	220	3000	2.36E-09	2.53E-10	9.58E-13	6.25E-13	6.81E-23	1.10E-17	2.65E-13	1.85E-10	2.38E-12	8.06E-07
8	220	3000	5.63E-09	2.59E-10	3.52E-13	5.53E-13	3.64E-22	4.45E-17	6.28E-13	1.88E-10	8.70E-13	8.90E-07
9	220	3000	1.46E-08	2.50E-10	1.07E-13	7.77E-13	3.95E-21	2.67E-16	1.72E-12	1.92E-10	2.78E-13	7.25E-07
10	220	3000	1.46E-08	2.50E-10	1.07E-13	7.77E-13	3.95E-21	2.67E-16	1.72E-12	1.92E-10	2.78E-13	7.25E-07
11	220	3000	1.46E-08	2.50E-10	1.07E-13	7.77E-13	3.95E-21	2.67E-16	1.72E-12	1.92E-10	2.78E-13	7.25E-07
12	220	3000	1.46E-08	2.50E-10	1.07E-13	7.77E-13	3.95E-21	2.67E-16	1.72E-12	1.92E-10	2.78E-13	7.25E-07
13	220	3000	1.46E-08	2.50E-10	1.07E-13	7.77E-13	3.95E-21	2.67E-16	1.72E-12	1.92E-10	2.78E-13	7.25E-07
14	220	3000	1.46E-08	2.50E-10	1.07E-13	7.77E-13	3.95E-21	2.67E-16	1.72E-12	1.92E-10	2.78E-13	7.25E-07
15	220	3000	1.46E-08	2.50E-10	1.07E-13	7.77E-13	3.95E-21	2.67E-16	1.72E-12	1.92E-10	2.78E-13	7.25E-07
16	220	3000	1.46E-08	2.50E-10	1.07E-13	7.77E-13	3.95E-21	2.67E-16	1.72E-12	1.92E-10	2.78E-13	7.25E-07
17	220	3000	1.46E-08	2.50E-10	1.07E-13	7.77E-13	3.95E-21	2.67E-16	1.72E-12	1.92E-10	2.78E-13	7.25E-07
18	220	3000	1.46E-08	2.50E-10	1.07E-13	7.77E-13	3.95E-21	2.67E-16	1.72E-12	1.92E-10	2.78E-13	7.25E-07

		Formula:	C2H6	HCOOH	HCOO-	CH3COO H	CH3COO-		
		Type:	(a)	(a)	(a)	(a)	(a)		
Cell	T (°C)	P (bar)	C2H6 (aq)	HCOOH (aq)	HCOO-	CH3COO H (aq)	CH3COO-	pH	Eh(V)
Ore fluids	500	5000	9.44E-07	4.82E-07	1.18E-04	4.51E-08	4.99E-07	6.950431	-1.167
1	220	3000	6.48E-13	6.25E-09	1.29E-06	9.30E-11	1.89E-09	6.116838	-0.51144
2	220	3000	6.48E-13	6.25E-09	1.29E-06	9.30E-11	1.89E-09	6.116838	-0.51144
3	220	3000	6.48E-13	6.25E-09	1.29E-06	9.30E-11	1.89E-09	6.116838	-0.51144
4	220	3000	6.48E-13	6.25E-09	1.29E-06	9.30E-11	1.89E-09	6.116838	-0.51144
5	220	3000	6.48E-13	6.25E-09	1.29E-06	9.30E-11	1.89E-09	6.116838	-0.51144
6	220	3000	6.48E-13	6.25E-09	1.29E-06	9.30E-11	1.89E-09	6.116838	-0.51144
7	220	3000	6.48E-13	6.25E-09	1.29E-06	9.30E-11	1.89E-09	6.116838	-0.51144
8	220	3000	7.55E-13	6.11E-09	4.45E-07	9.61E-11	6.88E-10	5.70127	-0.47194
9	220	3000	5.57E-13	6.76E-09	1.54E-07	9.62E-11	2.16E-10	5.233453	-0.42403
10	220	3000	5.57E-13	6.76E-09	1.54E-07	9.62E-11	2.16E-10	5.233453	-0.42403
11	220	3000	5.57E-13	6.76E-09	1.54E-07	9.62E-11	2.16E-10	5.233453	-0.42403
12	220	3000	5.57E-13	6.76E-09	1.54E-07	9.62E-11	2.16E-10	5.233453	-0.42403
13	220	3000	5.57E-13	6.76E-09	1.54E-07	9.62E-11	2.16E-10	5.233453	-0.42403
14	220	3000	5.57E-13	6.76E-09	1.54E-07	9.62E-11	2.16E-10	5.233453	-0.42403
15	220	3000	5.57E-13	6.76E-09	1.54E-07	9.62E-11	2.16E-10	5.233453	-0.42403
16	220	3000	5.57E-13	6.76E-09	1.54E-07	9.62E-11	2.16E-10	5.233453	-0.42403
17	220	3000	5.57E-13	6.76E-09	1.54E-07	9.62E-11	2.16E-10	5.233453	-0.42403
18	220	3000	5.57E-13	6.76E-09	1.54E-07	9.62E-11	2.16E-10	5.233453	-0.42403

Notes s: solid; a: aqueous solution; f:r, fluid:rock; the unit is mol.

Appendix C Statements of contribution by others

To Whom It May Concern,

I, Si-Yu Hu, contributed to all aspects of research including, but not limited to, sample collection, processing and analysis, data processing, and manuscripting preparation to the publication entitled :

Manuscript 1

“Raman characterization of carbonaceous material in the Macraes orogenic gold deposit and metasedimentary host rocks, New Zealand.”

Manuscript 2

“Associations between sulfides, carbonaceous material, gold and other trace elements in polyframboids: Implications for the source of orogenic gold deposits, Otago Schist, New Zealand.”

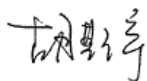
Manuscript 3

“A new look at mixed sphalerite-pyrite framboids and the sequestration of Zn into framboids as a key process of Zn cycling in the ocean.”

Manuscript 4

“Resolving the Role of Carbonaceous Materials in Gold Precipitation in Metasediment-hosted Orogenic Gold Deposits.”

Si-Yu Hu



Date: 07/09/2016

A realistic breakdown of the contribution by co-authors is as follows:

Manuscript 1:

Author	Si-Yu Hu	Katy Evans	Dave Craw	Kirsten Rempel	Julien Bourdet	Jeffrey Dick	Kliti Grice
Percentage	60%	12%	8%	8%	5%	4%	3%

Manuscript 2:

Author	Si-Yu Hu	Katy Evans	Louise Fisher	Kirsten Rempel	Dave Craw	Noreen J. Evans	Susan Cumberland	Aileen Robert	Kliti Grice
Percentage	65%	12%	8%	5%	2%	2%	2%	2%	2%







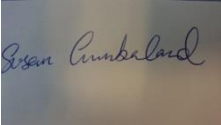


Manuscript 3:

Author	Si-Yu Hu	Katy Evans	Kirsten Rempel	Paul Guagliardo	Matt Kilburn	Dave Craw	Kliti Grice
Percentage	65%	10%	8%	8%	3%	3%	3%

Manuscript 4:

Author	Si-Yu Hu	Katy Evans	Dave Craw	Kirsten Rempel	Kliti Grice
Percentage	70%	15%	7%	5%	3%

I, as a one of the co-authors, endorse that this level of contribution by the candidate indicated above is appropriate.

Name	Signature
Katy Evans	
Kirsten Rempel	
Kliti Grice	See attached email
Dave Crow	
Jeffrey Dick	
Louise Fisher	
Noreen J. Evans	
Susan Cumberland	
Paul Guagliardo	
Matt Kilburn	

Approve email from Kliti Grice

Dear Shirley,
Congratulations.
I agree on all the %.
I can't send an electronic signature- against university policy but I can send you this email as evidence.
best wishes,
Kliti

Professor Kliti Grice FRACI CChem, FGSEAG
Founding Director of WA-Organic and Isotope Geochemistry Centre
Department of Chemistry
Chemistry and Resources Precinct
Curtin University
Perth, WA
Australia
6845
Tele +61 (0)8 9266 2474
K.Grice@curtin.edu.au

The level of contribution from those who are not contactable at the time of submission of this thesis (Julien Bourdet and Aileen Robert) is endorsed by Katy Evans.



07/09/2016

Appendix D Permission of copyright from third parties

The following pages are the rights granted by Elsevier to the publications that form **Chapter 3** and **Chapter 4** of this thesis, to allow the reproduction of the full article in a thesis.

**ELSEVIER LICENSE
TERMS AND CONDITIONS**

Aug 31, 2016

This Agreement between Siyu Hu ("You") and Elsevier ("Elsevier") consists of your license details and the terms and conditions provided by Elsevier and Copyright Clearance Center.

License Number	3939681086975
License date	Aug 31, 2016
Licensed Content Publisher	Elsevier
Licensed Content Publication	Ore Geology Reviews
Licensed Content Title	Raman characterization of carbonaceous material in the Macraes orogenic gold deposit and metasedimentary host rocks, New Zealand
Licensed Content Author	Siyu Hu,Katy Evans,Dave Craw,Kirsten Rempel,Julien Bourdet,Jeffrey Dick,Kliti Grice
Licensed Content Date	October 2015
Licensed Content Volume Number	70
Licensed Content Issue Number	n/a
Licensed Content Pages	16
Start Page	80
End Page	95
Type of Use	reuse in a thesis/dissertation
Intended publisher of new work	other
Portion	full article
Format	both print and electronic
Are you the author of this Elsevier article?	Yes
Will you be translating?	No
Order reference number	
Title of your thesis/dissertation	The Role of Carbonaceous Material in the Formation of Macraes Orogenic Gold Deposit, New Zealand
Expected completion date	Sep 2016
Estimated size (number of pages)	200
Elsevier VAT number	GB 494 6272 12
Requestor Location	Siyu Hu Applied Geology, Curtin University kent Street Bentley, Western Australia 6101 Australia Attn: Siyu Hu
Total	0.00 USD
Terms and Conditions	

INTRODUCTION

1. The publisher for this copyrighted material is Elsevier. By clicking "accept" in connection with completing this licensing transaction, you agree that the following terms and conditions apply to this transaction (along with the Billing and Payment terms and conditions established by Copyright Clearance Center, Inc. ("CCC"), at the time that you opened your Rightslink account and that are available at any time at <http://myaccount.copyright.com>).

GENERAL TERMS

2. Elsevier hereby grants you permission to reproduce the aforementioned material subject to the terms and conditions indicated.

3. Acknowledgement: If any part of the material to be used (for example, figures) has appeared in our publication with credit or acknowledgement to another source, permission must also be sought from that source. If such permission is not obtained then that material may not be included in your publication/copies. Suitable acknowledgement to the source must be made, either as a footnote or in a reference list at the end of your publication, as follows:

"Reprinted from Publication title, Vol /edition number, Author(s), Title of article / title of chapter, Pages No., Copyright (Year), with permission from Elsevier [OR APPLICABLE SOCIETY COPYRIGHT OWNER]." Also Lancet special credit - "Reprinted from The Lancet, Vol. number, Author(s), Title of article, Pages No., Copyright (Year), with permission from Elsevier."

4. Reproduction of this material is confined to the purpose and/or media for which permission is hereby given.

5. Altering/Modifying Material: Not Permitted. However figures and illustrations may be altered/adapted minimally to serve your work. Any other abbreviations, additions, deletions and/or any other alterations shall be made only with prior written authorization of Elsevier Ltd. (Please contact Elsevier at permissions@elsevier.com)

6. If the permission fee for the requested use of our material is waived in this instance, please be advised that your future requests for Elsevier materials may attract a fee.

7. Reservation of Rights: Publisher reserves all rights not specifically granted in the combination of (i) the license details provided by you and accepted in the course of this licensing transaction, (ii) these terms and conditions and (iii) CCC's Billing and Payment terms and conditions.

8. License Contingent Upon Payment: While you may exercise the rights licensed immediately upon issuance of the license at the end of the licensing process for the transaction, provided that you have disclosed complete and accurate details of your proposed use, no license is finally effective unless and until full payment is received from you (either by publisher or by CCC) as provided in CCC's Billing and Payment terms and conditions. If full payment is not received on a timely basis, then any license preliminarily granted shall be deemed automatically revoked and shall be void as if never granted. Further, in the event that you breach any of these terms and conditions or any of CCC's Billing and Payment terms and conditions, the license is automatically revoked and shall be void as if never granted. Use of materials as described in a revoked license, as well as any use of the materials beyond the scope of an unrevoked license, may constitute copyright infringement and publisher reserves the right to take any and all action to protect its copyright in the materials.

9. Warranties: Publisher makes no representations or warranties with respect to the licensed material.

10. Indemnity: You hereby indemnify and agree to hold harmless publisher and CCC, and their respective officers, directors, employees and agents, from and against any and all claims arising out of your use of the licensed material other than as specifically authorized pursuant to this license.

11. No Transfer of License: This license is personal to you and may not be sublicensed, assigned, or transferred by you to any other person without publisher's written permission.

12. No Amendment Except in Writing: This license may not be amended except in a writing signed by both parties (or, in the case of publisher, by CCC on publisher's behalf).

13. Objection to Contrary Terms: Publisher hereby objects to any terms contained in any purchase order, acknowledgment, check endorsement or other writing prepared by you, which terms are inconsistent with these terms and conditions or CCC's Billing and Payment

terms and conditions. These terms and conditions, together with CCC's Billing and Payment terms and conditions (which are incorporated herein), comprise the entire agreement between you and publisher (and CCC) concerning this licensing transaction. In the event of any conflict between your obligations established by these terms and conditions and those established by CCC's Billing and Payment terms and conditions, these terms and conditions shall control.

14. **Revocation:** Elsevier or Copyright Clearance Center may deny the permissions described in this License at their sole discretion, for any reason or no reason, with a full refund payable to you. Notice of such denial will be made using the contact information provided by you. Failure to receive such notice will not alter or invalidate the denial. In no event will Elsevier or Copyright Clearance Center be responsible or liable for any costs, expenses or damage incurred by you as a result of a denial of your permission request, other than a refund of the amount(s) paid by you to Elsevier and/or Copyright Clearance Center for denied permissions.

LIMITED LICENSE

The following terms and conditions apply only to specific license types:

15. **Translation:** This permission is granted for non-exclusive world English rights only unless your license was granted for translation rights. If you licensed translation rights you may only translate this content into the languages you requested. A professional translator must perform all translations and reproduce the content word for word preserving the integrity of the article.

16. **Posting licensed content on any Website:** The following terms and conditions apply as follows: Licensing material from an Elsevier journal: All content posted to the web site must maintain the copyright information line on the bottom of each image; A hyper-text must be included to the Homepage of the journal from which you are licensing at <http://www.sciencedirect.com/science/journal/xxxxx> or the Elsevier homepage for books at <http://www.elsevier.com>; Central Storage: This license does not include permission for a scanned version of the material to be stored in a central repository such as that provided by Heron/XanEdu.

Licensing material from an Elsevier book: A hyper-text link must be included to the Elsevier homepage at <http://www.elsevier.com>. All content posted to the web site must maintain the copyright information line on the bottom of each image.

Posting licensed content on Electronic reserve: In addition to the above the following clauses are applicable: The web site must be password-protected and made available only to bona fide students registered on a relevant course. This permission is granted for 1 year only. You may obtain a new license for future website posting.

17. **For journal authors:** the following clauses are applicable in addition to the above:

Preprints:

A preprint is an author's own write-up of research results and analysis, it has not been peer-reviewed, nor has it had any other value added to it by a publisher (such as formatting, copyright, technical enhancement etc.).

Authors can share their preprints anywhere at any time. Preprints should not be added to or enhanced in any way in order to appear more like, or to substitute for, the final versions of articles however authors can update their preprints on arXiv or RePEc with their Accepted Author Manuscript (see below).

If accepted for publication, we encourage authors to link from the preprint to their formal publication via its DOI. Millions of researchers have access to the formal publications on ScienceDirect, and so links will help users to find, access, cite and use the best available version. Please note that Cell Press, The Lancet and some society-owned have different preprint policies. Information on these policies is available on the journal homepage.

Accepted Author Manuscripts: An accepted author manuscript is the manuscript of an article that has been accepted for publication and which typically includes author-incorporated changes suggested during submission, peer review and editor-author communications.

Authors can share their accepted author manuscript:

- immediately
 - o via their non-commercial person homepage or blog
 - o by updating a preprint in arXiv or RePEc with the accepted manuscript
 - o via their research institute or institutional repository for internal institutional uses or as part of an invitation-only research collaboration work-group
 - o directly by providing copies to their students or to research collaborators for their personal use
 - o for private scholarly sharing as part of an invitation-only work group on commercial sites with which Elsevier has an agreement
- after the embargo period
 - o via non-commercial hosting platforms such as their institutional repository
 - o via commercial sites with which Elsevier has an agreement

In all cases accepted manuscripts should:

- link to the formal publication via its DOI
- bear a CC-BY-NC-ND license - this is easy to do
- if aggregated with other manuscripts, for example in a repository or other site, be shared in alignment with our hosting policy not be added to or enhanced in any way to appear more like, or to substitute for, the published journal article.

Published journal article (JPA): A published journal article (PJA) is the definitive final record of published research that appears or will appear in the journal and embodies all value-adding publishing activities including peer review co-ordination, copy-editing, formatting, (if relevant) pagination and online enrichment.

Policies for sharing publishing journal articles differ for subscription and gold open access articles:

Subscription Articles: If you are an author, please share a link to your article rather than the full-text. Millions of researchers have access to the formal publications on ScienceDirect, and so links will help your users to find, access, cite, and use the best available version. Theses and dissertations which contain embedded PJAs as part of the formal submission can be posted publicly by the awarding institution with DOI links back to the formal publications on ScienceDirect.

If you are affiliated with a library that subscribes to ScienceDirect you have additional private sharing rights for others' research accessed under that agreement. This includes use for classroom teaching and internal training at the institution (including use in course packs and courseware programs), and inclusion of the article for grant funding purposes.

Gold Open Access Articles: May be shared according to the author-selected end-user license and should contain a [CrossMark logo](#), the end user license, and a DOI link to the formal publication on ScienceDirect.

Please refer to Elsevier's [posting policy](#) for further information.

18. For book authors the following clauses are applicable in addition to the above:

Authors are permitted to place a brief summary of their work online only. You are not allowed to download and post the published electronic version of your chapter, nor may you scan the printed edition to create an electronic version. **Posting to a repository:** Authors are permitted to post a summary of their chapter only in their institution's repository.

19. **Thesis/Dissertation:** If your license is for use in a thesis/dissertation your thesis may be submitted to your institution in either print or electronic form. Should your thesis be published commercially, please reapply for permission. These requirements include permission for the Library and Archives of Canada to supply single copies, on demand, of the complete thesis and include permission for Proquest/UMI to supply single copies, on demand, of the complete thesis. Should your thesis be published commercially, please reapply for permission. Theses and dissertations which contain embedded PJAs as part of the formal submission can be posted publicly by the awarding institution with DOI links back to the formal publications on ScienceDirect.

Elsevier Open Access Terms and Conditions

You can publish open access with Elsevier in hundreds of open access journals or in nearly 2000 established subscription journals that support open access publishing. Permitted third party re-use of these open access articles is defined by the author's choice of Creative Commons user license. See our [open access license policy](#) for more information.

Terms & Conditions applicable to all Open Access articles published with Elsevier:

Any reuse of the article must not represent the author as endorsing the adaptation of the article nor should the article be modified in such a way as to damage the author's honour or reputation. If any changes have been made, such changes must be clearly indicated.

The author(s) must be appropriately credited and we ask that you include the end user license and a DOI link to the formal publication on ScienceDirect.

If any part of the material to be used (for example, figures) has appeared in our publication with credit or acknowledgement to another source it is the responsibility of the user to ensure their reuse complies with the terms and conditions determined by the rights holder.

Additional Terms & Conditions applicable to each Creative Commons user license:

CC BY: The CC-BY license allows users to copy, to create extracts, abstracts and new works from the Article, to alter and revise the Article and to make commercial use of the Article (including reuse and/or resale of the Article by commercial entities), provided the user gives appropriate credit (with a link to the formal publication through the relevant DOI), provides a link to the license, indicates if changes were made and the licensor is not represented as endorsing the use made of the work. The full details of the license are available at <http://creativecommons.org/licenses/by/4.0>.

CC BY NC SA: The CC BY-NC-SA license allows users to copy, to create extracts, abstracts and new works from the Article, to alter and revise the Article, provided this is not done for commercial purposes, and that the user gives appropriate credit (with a link to the formal publication through the relevant DOI), provides a link to the license, indicates if changes were made and the licensor is not represented as endorsing the use made of the work. Further, any new works must be made available on the same conditions. The full details of the license are available at <http://creativecommons.org/licenses/by-nc-sa/4.0>.

CC BY NC ND: The CC BY-NC-ND license allows users to copy and distribute the Article, provided this is not done for commercial purposes and further does not permit distribution of the Article if it is changed or edited in any way, and provided the user gives appropriate credit (with a link to the formal publication through the relevant DOI), provides a link to the license, and that the licensor is not represented as endorsing the use made of the work. The full details of the license are available at <http://creativecommons.org/licenses/by-nc-nd/4.0>.

Any commercial reuse of Open Access articles published with a CC BY NC SA or CC BY NC ND license requires permission from Elsevier and will be subject to a fee.

Commercial reuse includes:

- Associating advertising with the full text of the Article
- Charging fees for document delivery or access
- Article aggregation
- Systematic distribution via e-mail lists or share buttons

Posting or linking by commercial companies for use by customers of those companies.

20. Other Conditions:

v1.8

Questions? customercare@copyright.com or +1-855-239-3415 (toll free in the US) or +1-978-646-2777.

**ELSEVIER LICENSE
TERMS AND CONDITIONS**

Aug 31, 2016

This Agreement between Siyu Hu ("You") and Elsevier ("Elsevier") consists of your license details and the terms and conditions provided by Elsevier and Copyright Clearance Center.

License Number	3939690051374
License date	Aug 31, 2016
Licensed Content Publisher	Elsevier
Licensed Content Publication	Geochimica et Cosmochimica Acta
Licensed Content Title	Associations between sulfides, carbonaceous material, gold and other trace elements in polyframboids: Implications for the source of orogenic gold deposits, Otago Schist, New Zealand
Licensed Content Author	Si-Yu Hu,Katy Evans,Louise Fisher,Kirsten Rempel,Dave Craw,Noreen J. Evans,Susan Cumberland,Aileen Robert,Kliti Grice
Licensed Content Date	1 May 2016
Licensed Content Volume Number	180
Licensed Content Issue Number	n/a
Licensed Content Pages	17
Start Page	197
End Page	213
Type of Use	reuse in a thesis/dissertation
Intended publisher of new work	other
Portion	full article
Format	both print and electronic
Are you the author of this Elsevier article?	Yes
Will you be translating?	No
Order reference number	
Title of your thesis/dissertation	The Role of Carbonaceous Material in the Formation of Macraes Orogenic Gold Deposit, New Zealand
Expected completion date	Sep 2016
Estimated size (number of pages)	200
Elsevier VAT number	GB 494 6272 12
Requestor Location	Siyu Hu Applied Geology, Curtin University kent Street Bentley, Western Australia 6101 Australia Attn: Siyu Hu
Total	0.00 USD
Terms and Conditions	

INTRODUCTION

1. The publisher for this copyrighted material is Elsevier. By clicking "accept" in connection with completing this licensing transaction, you agree that the following terms and conditions apply to this transaction (along with the Billing and Payment terms and conditions established by Copyright Clearance Center, Inc. ("CCC"), at the time that you opened your Rightslink account and that are available at any time at <http://myaccount.copyright.com>).

GENERAL TERMS

2. Elsevier hereby grants you permission to reproduce the aforementioned material subject to the terms and conditions indicated.

3. Acknowledgement: If any part of the material to be used (for example, figures) has appeared in our publication with credit or acknowledgement to another source, permission must also be sought from that source. If such permission is not obtained then that material may not be included in your publication/copies. Suitable acknowledgement to the source must be made, either as a footnote or in a reference list at the end of your publication, as follows:

"Reprinted from Publication title, Vol /edition number, Author(s), Title of article / title of chapter, Pages No., Copyright (Year), with permission from Elsevier [OR APPLICABLE SOCIETY COPYRIGHT OWNER]." Also Lancet special credit - "Reprinted from The Lancet, Vol. number, Author(s), Title of article, Pages No., Copyright (Year), with permission from Elsevier."

4. Reproduction of this material is confined to the purpose and/or media for which permission is hereby given.

5. Altering/Modifying Material: Not Permitted. However figures and illustrations may be altered/adapted minimally to serve your work. Any other abbreviations, additions, deletions and/or any other alterations shall be made only with prior written authorization of Elsevier Ltd. (Please contact Elsevier at permissions@elsevier.com)

6. If the permission fee for the requested use of our material is waived in this instance, please be advised that your future requests for Elsevier materials may attract a fee.

7. Reservation of Rights: Publisher reserves all rights not specifically granted in the combination of (i) the license details provided by you and accepted in the course of this licensing transaction, (ii) these terms and conditions and (iii) CCC's Billing and Payment terms and conditions.

8. License Contingent Upon Payment: While you may exercise the rights licensed immediately upon issuance of the license at the end of the licensing process for the transaction, provided that you have disclosed complete and accurate details of your proposed use, no license is finally effective unless and until full payment is received from you (either by publisher or by CCC) as provided in CCC's Billing and Payment terms and conditions. If full payment is not received on a timely basis, then any license preliminarily granted shall be deemed automatically revoked and shall be void as if never granted. Further, in the event that you breach any of these terms and conditions or any of CCC's Billing and Payment terms and conditions, the license is automatically revoked and shall be void as if never granted. Use of materials as described in a revoked license, as well as any use of the materials beyond the scope of an unrevoked license, may constitute copyright infringement and publisher reserves the right to take any and all action to protect its copyright in the materials.

9. Warranties: Publisher makes no representations or warranties with respect to the licensed material.

10. Indemnity: You hereby indemnify and agree to hold harmless publisher and CCC, and their respective officers, directors, employees and agents, from and against any and all claims arising out of your use of the licensed material other than as specifically authorized pursuant to this license.

11. No Transfer of License: This license is personal to you and may not be sublicensed, assigned, or transferred by you to any other person without publisher's written permission.

12. No Amendment Except in Writing: This license may not be amended except in a writing signed by both parties (or, in the case of publisher, by CCC on publisher's behalf).

13. Objection to Contrary Terms: Publisher hereby objects to any terms contained in any purchase order, acknowledgment, check endorsement or other writing prepared by you, which terms are inconsistent with these terms and conditions or CCC's Billing and Payment

terms and conditions. These terms and conditions, together with CCC's Billing and Payment terms and conditions (which are incorporated herein), comprise the entire agreement between you and publisher (and CCC) concerning this licensing transaction. In the event of any conflict between your obligations established by these terms and conditions and those established by CCC's Billing and Payment terms and conditions, these terms and conditions shall control.

14. **Revocation:** Elsevier or Copyright Clearance Center may deny the permissions described in this License at their sole discretion, for any reason or no reason, with a full refund payable to you. Notice of such denial will be made using the contact information provided by you. Failure to receive such notice will not alter or invalidate the denial. In no event will Elsevier or Copyright Clearance Center be responsible or liable for any costs, expenses or damage incurred by you as a result of a denial of your permission request, other than a refund of the amount(s) paid by you to Elsevier and/or Copyright Clearance Center for denied permissions.

LIMITED LICENSE

The following terms and conditions apply only to specific license types:

15. **Translation:** This permission is granted for non-exclusive world **English** rights only unless your license was granted for translation rights. If you licensed translation rights you may only translate this content into the languages you requested. A professional translator must perform all translations and reproduce the content word for word preserving the integrity of the article.

16. **Posting licensed content on any Website:** The following terms and conditions apply as follows: Licensing material from an Elsevier journal: All content posted to the web site must maintain the copyright information line on the bottom of each image; A hyper-text must be included to the Homepage of the journal from which you are licensing at <http://www.sciencedirect.com/science/journal/xxxxx> or the Elsevier homepage for books at <http://www.elsevier.com>; Central Storage: This license does not include permission for a scanned version of the material to be stored in a central repository such as that provided by Heron/XanEdu.

Licensing material from an Elsevier book: A hyper-text link must be included to the Elsevier homepage at <http://www.elsevier.com>. All content posted to the web site must maintain the copyright information line on the bottom of each image.

Posting licensed content on Electronic reserve: In addition to the above the following clauses are applicable: The web site must be password-protected and made available only to bona fide students registered on a relevant course. This permission is granted for 1 year only. You may obtain a new license for future website posting.

17. **For journal authors:** the following clauses are applicable in addition to the above:

Preprints:

A preprint is an author's own write-up of research results and analysis, it has not been peer-reviewed, nor has it had any other value added to it by a publisher (such as formatting, copyright, technical enhancement etc.).

Authors can share their preprints anywhere at any time. Preprints should not be added to or enhanced in any way in order to appear more like, or to substitute for, the final versions of articles however authors can update their preprints on arXiv or RePEc with their Accepted Author Manuscript (see below).

If accepted for publication, we encourage authors to link from the preprint to their formal publication via its DOI. Millions of researchers have access to the formal publications on ScienceDirect, and so links will help users to find, access, cite and use the best available version. Please note that Cell Press, The Lancet and some society-owned have different preprint policies. Information on these policies is available on the journal homepage.

Accepted Author Manuscripts: An accepted author manuscript is the manuscript of an article that has been accepted for publication and which typically includes author-incorporated changes suggested during submission, peer review and editor-author communications.

Authors can share their accepted author manuscript:

- immediately
 - o via their non-commercial person homepage or blog
 - o by updating a preprint in arXiv or RePEc with the accepted manuscript
 - o via their research institute or institutional repository for internal institutional uses or as part of an invitation-only research collaboration work-group
 - o directly by providing copies to their students or to research collaborators for their personal use
 - o for private scholarly sharing as part of an invitation-only work group on commercial sites with which Elsevier has an agreement
- after the embargo period
 - o via non-commercial hosting platforms such as their institutional repository
 - o via commercial sites with which Elsevier has an agreement

In all cases accepted manuscripts should:

- link to the formal publication via its DOI
- bear a CC-BY-NC-ND license - this is easy to do
- if aggregated with other manuscripts, for example in a repository or other site, be shared in alignment with our hosting policy not be added to or enhanced in any way to appear more like, or to substitute for, the published journal article.

Published journal article (JPA): A published journal article (PJA) is the definitive final record of published research that appears or will appear in the journal and embodies all value-adding publishing activities including peer review co-ordination, copy-editing, formatting, (if relevant) pagination and online enrichment.

Policies for sharing publishing journal articles differ for subscription and gold open access articles:

Subscription Articles: If you are an author, please share a link to your article rather than the full-text. Millions of researchers have access to the formal publications on ScienceDirect, and so links will help your users to find, access, cite, and use the best available version. Theses and dissertations which contain embedded PJAs as part of the formal submission can be posted publicly by the awarding institution with DOI links back to the formal publications on ScienceDirect.

If you are affiliated with a library that subscribes to ScienceDirect you have additional private sharing rights for others' research accessed under that agreement. This includes use for classroom teaching and internal training at the institution (including use in course packs and courseware programs), and inclusion of the article for grant funding purposes.

Gold Open Access Articles: May be shared according to the author-selected end-user license and should contain a [CrossMark logo](#), the end user license, and a DOI link to the formal publication on ScienceDirect.

Please refer to Elsevier's [posting policy](#) for further information.

18. For book authors the following clauses are applicable in addition to the above:

Authors are permitted to place a brief summary of their work online only. You are not allowed to download and post the published electronic version of your chapter, nor may you scan the printed edition to create an electronic version. **Posting to a repository:** Authors are permitted to post a summary of their chapter only in their institution's repository.

19. **Thesis/Dissertation:** If your license is for use in a thesis/dissertation your thesis may be submitted to your institution in either print or electronic form. Should your thesis be published commercially, please reapply for permission. These requirements include permission for the Library and Archives of Canada to supply single copies, on demand, of the complete thesis and include permission for Proquest/UMI to supply single copies, on demand, of the complete thesis. Should your thesis be published commercially, please reapply for permission. Theses and dissertations which contain embedded PJAs as part of the formal submission can be posted publicly by the awarding institution with DOI links back to the formal publications on ScienceDirect.

Elsevier Open Access Terms and Conditions

You can publish open access with Elsevier in hundreds of open access journals or in nearly 2000 established subscription journals that support open access publishing. Permitted third party re-use of these open access articles is defined by the author's choice of Creative Commons user license. See our [open access license policy](#) for more information.

Terms & Conditions applicable to all Open Access articles published with Elsevier:

Any reuse of the article must not represent the author as endorsing the adaptation of the article nor should the article be modified in such a way as to damage the author's honour or reputation. If any changes have been made, such changes must be clearly indicated.

The author(s) must be appropriately credited and we ask that you include the end user license and a DOI link to the formal publication on ScienceDirect.

If any part of the material to be used (for example, figures) has appeared in our publication with credit or acknowledgement to another source it is the responsibility of the user to ensure their reuse complies with the terms and conditions determined by the rights holder.

Additional Terms & Conditions applicable to each Creative Commons user license:

CC BY: The CC-BY license allows users to copy, to create extracts, abstracts and new works from the Article, to alter and revise the Article and to make commercial use of the Article (including reuse and/or resale of the Article by commercial entities), provided the user gives appropriate credit (with a link to the formal publication through the relevant DOI), provides a link to the license, indicates if changes were made and the licensor is not represented as endorsing the use made of the work. The full details of the license are available at <http://creativecommons.org/licenses/by/4.0>.

CC BY NC SA: The CC BY-NC-SA license allows users to copy, to create extracts, abstracts and new works from the Article, to alter and revise the Article, provided this is not done for commercial purposes, and that the user gives appropriate credit (with a link to the formal publication through the relevant DOI), provides a link to the license, indicates if changes were made and the licensor is not represented as endorsing the use made of the work. Further, any new works must be made available on the same conditions. The full details of the license are available at <http://creativecommons.org/licenses/by-nc-sa/4.0>.

CC BY NC ND: The CC BY-NC-ND license allows users to copy and distribute the Article, provided this is not done for commercial purposes and further does not permit distribution of the Article if it is changed or edited in any way, and provided the user gives appropriate credit (with a link to the formal publication through the relevant DOI), provides a link to the license, and that the licensor is not represented as endorsing the use made of the work. The full details of the license are available at <http://creativecommons.org/licenses/by-nc-nd/4.0>.

Any commercial reuse of Open Access articles published with a CC BY NC SA or CC BY NC ND license requires permission from Elsevier and will be subject to a fee.

Commercial reuse includes:

- Associating advertising with the full text of the Article
- Charging fees for document delivery or access
- Article aggregation
- Systematic distribution via e-mail lists or share buttons

Posting or linking by commercial companies for use by customers of those companies.

20. Other Conditions:

v1.8

Questions? customercare@copyright.com or +1-855-239-3415 (toll free in the US) or +1-978-646-2777.